Iridium-Catalyzed CH-Functionalization : Development and Applications of Innovative Strategies for Hydrogen Isotope Exchange on Small Molecules and Biotherapeutic Drugs for Drug Discovery

Mégane Valero

université PARIS-SACLAY

Iridium-Catalyzed CH-Functionalization: Development and Applications of Innovative Strategies for Hydrogen Isotope Exchange on Small Molecules and Biotherapeutic Drugs for Drug Discovery

Thèse de doctorat de l'université Paris-Saclay

École doctorale n° ED n°571 2MIB | Sciences chimiques : molécules, matériaux, instrumentation et biosystèmes
Spécialité de doctorat: Chimie
Unité de recherche : Service de Chimie Bioorganique et de Marquage
Référent : Faculté des sciences

Thèse présentée et soutenue à Gif-sur-Yvette, le 17 Janvier 2020, par

Mégane Valero

Composition du Jury

Giang Vo-Thanh Professeur, Université Paris-Saclay	Président & Examinateur
Joanna Wencel-Delord Associate Professor, Université de Strasbourg	Rapporteur & Examinatrice
Luc Demange Professeur, Université de Paris	Rapporteur & Examinateur
Michael Schnürch Associate Professor, Technische Universität Wien	Examinateur
Christophe Dugave Docteur, CEA-Saclay	Directeur de thèse
Volker Derdau Doctor, Sanofi Germany	Co-Encadrant
Jens Atzrodt Doctor, Sanofi Germany	Invité

Thèse de doctorat

NNT : 2020UPASS009

“Everything will be alright in the end. If it is not alright, it is because it is not yet the end.”
Oscar Wilde

Acknowledgements

My first thanks go to *Christophe*. Thank you for your guidance and advise even though being far from each other. In particular during the heavy task of writing up the PhD, these months were pretty intense, and this actual manuscript would have not been possible without your constant help. I am very thankful I had the opportunity to become part of the ISOTOPICS network. It was great three years meeting all together in different countries. This whole came to life because before being my PhD director, you were the coordinator of the project, so I want to thank you for that too.

I would like to thank the four jury members who have accepted to take the huge responsibility of evaluating my work at the end of these intense three years! Prof. Giang Vo-Thanh, Dr. Joanna Wencel-Delord, Prof. Michael Schnürch and Prof. Luc Demange, I hope you will enjoy reading this heavy thesis.

Of course, thanks to my *German bodyguards*. So many anecdotes, already from the first time we have met for the interview. Apparently, I had put on too much perfume… Thank you for the supervision over the 3 years, for all these group meeting where I had so much fun and learned a lot. I think from the "you have to change office" to today, a lot have been achieved.

Jens, first of all thank you for picking me up for this position. I still remember the phone call in October 2016 and how happy I was. No beginning is easy, and definitely not the one of my PhD (three slides in 2 weeks!), but what an adventure! You have been always very kind and available for any help. Thank you for all the scientific discussions, training, input over these three years. When you have changed position, this was hard to accept for me, but I am thankful you have not just left. Indeed, you have stayed around and involved in my PhD when other would have stopped caring. I have enjoyed a lot our Wednesday lunch as well, always waiting for you because YOU were the one late, yes! Seeing you eating salad for three years and discussing about science, dog, cat, holidays, German/French fun facts, people we don´t like, Game of Thrones *etc*. We also had good time during the different Isotopics meeting, I will never forget the driving to Liege sitting at the back like a little kid! I am also glad I met someone as competitive as me haha I hope life will allow us to meet again in the future!

Volker, I don´t even know where to start! You are an incredible person. I have no problem to write down here how much I feared you in the beginning. Such a cold and tough German man. I was even exchanging with your former PhD student, asking for advice and if my situation would improve or stay as it was for three years... Luckily Romain was right: "He will make your first months very tough, but it is for the best you will see, it will get better". I did not believe a word at that time! Six month later (yes that was relatively long) indeed it started to improve. Your training to make me become a scientist finally worked out, you

stopped putting up this horrible “face-to-face Friday meeting” just before leaving for the weekend, we started to talk more, and this enabled me to become more self-confident. Thank you for always be available anytime I have entered your office to present you new results, exchange new ideas, ask for help (PhD related or German Bürokratie related…) or just complain about everything, but more specifically the LCMS machine which does not work properly! “I can´t work like this!”. In any circumstances you always had the ability to calm me down when I was stressed, so be prepared to get phone call in the future if I am not able to do it myself wherever I will be. You made me grow up so much during these years, professionally and personally. I have enjoyed and learned so much during our long discussions about life at coffee breaks and during our Tuesday lunch. I needed time in the beginning to notice and understand that everything you have done or advised me to change/do was for myself. I hope I brought you enough unexpected fun over these three years, you don´t know it yet, but you are going to miss the Easter and Christmas decorations in the lab, I know it! The blinking lights on the windows and the Christmas balls on your plant! I count on you to put at least your red Pompom on your lab coat, I will wait for a proof picture every 1st of December! Overall, I feel now ready to live the rest of my life, and this is mainly thanks to you. There are not enough words to express how much I am thankful that life has mixed our routes.

Remo, to work with a colleague like you, I could have not wish for better! Even busy with tritiation you were always there to help me, answering chemistry questions, training me with the manifolds etc. You made things so easy, never change that. I know anytime a new student came in the lab, you always said to Volker this was not a good choice, even with me, “The Queen of France”. But I heard I am the last one for who you would say it was not a good choice, as you always ended up being wrong, which I am happy about. Thank you for your kindness and patience, in particular in moments I was overstressed. Of course, I am also happy about the different memories we had, going eating with the team in restaurant and playing bowling!

How would I have survived my PhD without you *Helena*? From our first meeting thanks to Werngard, where I was impressed by you (god knows why...) to our first lunch asking already too private questions! I would not be the person I am today if I have not met you. You have always been present, being so patient, dealing with my moods when everything was wrong. I will never thank you enough for that. I don´t think I have ever met someone as patient, as kind, as flexible, as available, as good listener, as funny, as spontaneous, as positive, as….everything! People like you are not that common out there. Thank you for all the hours you kept listening to my drama, because there were indeed so many! Nevertheless, and for the best, there were also plenty of happy stories! You initiated me to travelling (and trained me to pack light!): from Sheffield (yes that one was the first, your beloved University…and country!) to Barcelona, from Dubrovnik to Paris (thanks again for visiting me during my secondment), from Corfu to Koblenz (yes sometimes there is no need to go far). Travelling with you was amazing, but simple things can be as good: there is no best partner than you for a “Netflix and chill” day (official…or not…). Laughing out loud with Grace and Frankie,

getting depressed with The Crown, (you) crying watching what I call “funny” movie, getting Christmas mood watching Love Actually for the 467th times and so many others! Thank you for always feeding me with good food and filling up my glass of wine (even though during writing I was filling it up myself...). I am enjoying right now our last month’s together until I move for a new adventure but even after I am not worried, we just need to decide which new country we want to visit (Island…)! ¡T’estimo!

Marion Champignon! You have been my lovely French bubble here in Germany. I am so glad you were around when I started my PhD. We have so many funny stories about my beginning with my huge need of sleeping and you, Helena and Prisca keeping asking me for a social life! I am happy I have stopped (reduced....) being stubborn as a donkey and started hanging out with you. So many nice memories we have built together, all these nights at your place talking and eating Aroma like piggies! All these Sunday brunch at Hollycross getting food for free and about to get my statue until we changed for Sugar Mama! And these delicious cooking from you which I miss (no one on earth can make the Rhubapaaa pie as good as you do!). Yes....most of these memories are food related....and??! Is that so bad?! But that is not true! There were also great trips around Europe. Konstance and my Easter enigma, Warsaw and Nemo following us everywhere! Thank you for all this great time together over the last 3 years! Thank you as well for keeping contact even when you decided to leave to speak Swissy. I am looking forward to our next trip! Also with *Guillhem*, the very tall patata! It is always fun to be with you guys!

Marta, my polish lady! I can just smile now when I remember Marion informing us about her new roommate. I did not want to meet you or even worse, like you, I did not want a new person in our girls’ group…I needed just one dinner to start asking you (not directly of course) to join anytime. Thank you for your support, always listening to this Chemistry which sounded like coming from another world. So many dinners, so many trips as well! Our guide to Warsaw, taking us for Vodka shot from 17h on, moving from one bar to another because indeed, we had to test all of them! What is life for if not, right? It feels always so warm to discuss with you, you are so generous, giving anything you can from yourself. Dziękuję Ci!

Prisca, even though our shared time was short, thank you for being by my side! Another Frenchie in Town, I enjoyed spending time with you, and I am happy even after 3 years we keep contact in the group and still share any good new or complain about any annoying thing!

Angel and *Mario*, you have also been great support for me and it was always a lot of fun to hang out with you both! Spanish and German style at the same time. I think we should organize a date between our cats!

Marta and *Dave*, another wonderful couple with who I always have good time! Thank you, *Dave*, for always calling me “The World’s Famous Scientist”! It was always fun to compete with you, even at The king of Tokio! I mean, any game is made for winning! We always agreed on that, even if Marta and Helena used to make fun of us! *Marta*, so much energy in

such a small body! Thank you both and I wish you full happiness with the new coming little girl!

Thank you to *Martin S*., always available to help with my analytics or to solve any problems with the LCMS and the NMR machine. Our Friday lunch were always great, and I think we have waiting too long to meet outside from brunch on weekend!

Thank you to the other members of my working group in Sanofi, there from the beginning, gone already, or new: *Annina*, *Jennifer*, *Fabien*, *Thomas*, *Wolfgang*, *Claudia*, *Christian*, *Gerald*, *Armin*, *Anurag*. I have enjoyed working with you and playing bowling!

Thank you *Alleyn*, you always have been such a positive, friendly and open person! Any time I achieved a success, you always took the time to send me an email to congratulate me. Wherever I go I hope we will keep in touch!

Giang, I remember how much I wanted to do my PhD with you at the end of my Master internship, I could not be happier today to have you in my jury now. When I knew I had to pick up someone from the university Paris-Saclay, I did not need a second to decide who! You have been a mentor for me from the first moment we met. I miss our long discussions in your office, but I am happy we had the opportunity to meet again during these three years. Thank you to always find time slot for me to discuss my concerns. I hope this thesis makes you proud of me, I have no doubt we will keep in touch for a lot of years, and I cannot wait to go again to the restaurant with you.

Of course, some of my PhD projects were done in collaboration and for this I would like to thank the different partners:

Thank you to *Stefan G*., my favorite DFT expert in Sanofi! I have learned a lot about DFT with you and our group meeting were always fun.

Thank you to *Matthias T*., *Daniel B*. and *Thomas B*. for the work on the phenylacetic acids. *Daniel*, I spent such a great time with you in my lab, listening to Taylor Swift, you making fun of me “dealing” with my NMR spectra. I have enjoyed coming few days to Braunschweig and visiting your lab, drinking the hazelnut liquor, playing at night with the whole group, and you showing me a nice view of the Town from the roof of the institute! I will never forget how much fun I had with this game about bunnies, carrots and salads in this bar, and our nice last brunch before I travelled back to Frankfurt.

Thank you to *Bruno C*., *Simon T*. and *Donia B*. from Toulouse; and *Grégory P*., *Sophie F*., *Christophe D*. in Paris, for our collaboration on the nanoparticles. I have enjoyed both of my secondments and learned a lot during this time.

Thank you to the fourteen Isotopics students with who I always had good time during our different meeting. Thank you in particular to *Laura*, *Malvika*, *Francesco*, *Mateusz* and *Alexandra*! You were the highlight of all!

Thank you to the entire Isotopics network, PI, advisory board. All this adventure within this Marie Curie fellowship was unbelievable and I have enriched my knowledges so much spending time with all of you.

Julien, *Albane* and *Guillaume*, thank you guys for keeping in touch over these years. I will never get bored of our stupid group discussions!

Moushou, even being separated physically after the Magistère, we always kept contact and I am happy we exchanged so much about our PhD stories. It was so good to see you again in Toulouse two years ago! All the best for the future and of course we will meet again!

Guillermo, we have met too late but our common sense of humor makes every moment with you totally hilarious! I hope you will have a lot of fun with your PhD. I hope to see you soon again.

Joséphine, what an encounter! Cousin by blood but no contact over years, when you came in Frankfurt it was like a fresh bubble of air and of you. I have discovered you (again) and I hope we won't wait that long before meeting again.

I would like to thank to amazing assistants at Sanofi which took care of all the travelling plans over the three years: *Andrea G*. and *Marion G*. Also, all the Sanofi coworkers from the different departments I had the pleasure to work with.

Thank you to *Corinne R*., woman who I met too late! I enjoyed so much discussing with you and I am looking forward to visit you in Collioure when the house will be ready!

Thank you to my *parents*, thank you to my *mother* who was always supportive and kept believing in me doing this PhD even in time I did not. Thank you for having listening to all this chemistry you were not always understanding!

Pumpkin, my hairy and chubby cat! Thank you for always sleeping by my side and showing me month after month that I am not such a bad mummy. You provide me all the tenderness I need when I feel lonely.

Finally, my last thank goes to the country which has adopted me for three years! Beloved *Germany*, your culture is unbelievable, and you made me feel home every single day!

Résumé de thèse – Français

Fonctionnalisation de liaisons C-H par catalyse à l'iridium : Développement de nouvelles méthodes pour l'échange d'isotopes d'hydrogène sur des petites molécules et des composés biothérapeutiques

Mégane Valero

Le développement de nouvelles méthodes, efficaces, rapides et facile à mettre en œuvre pour le marquage avec du deutérium ou du tritium de composés organiques tels que des médicaments est indispensable dans les secteurs industriels comme académique. Ces composés isotopiquement marqués sont essentiels lors des études précliniques. En effet, ces méthodes de marquages permettent d'obtenir plus rapidement les données nécessaires concernant la métabolisation et le profil de sécurité d'un candidat médicament, ce qui permet de réduire le temps investit dans cette recherche. Les méthodes classiques de marquages sont basées sur la synthèse d'un précurseur qui est ensuite marqué isotopiquement puis modifié jusqu'à l'obtention de la structure finale du candidat médicament. Ces anciennes méthodes, coûteuses en temps et en argent et génératrices d'effluents radioactifs, peuvent être évitées par en utilisant directement le composé d'intérêt, en particulier par échange d'isotopes d'hydrogène (HIE).

Dans un premier temps, nous avons utilisé une nouvelle génération de catalyseur d'iridium avec ligand P,N-bidentate. Ce catalyseur élaboré par l'équipe du professeur Tamm, a montré son efficacité pour la réaction d'échange d'isotopes d'hydrogène et sur divers substrats. Son utilisationa été étendue par l'évaluation de son activité dans les réactions d'échange d'isotopes d'hydrogène avec les sulphonamides (1), les N-oxydes (2) et les phosphonamides (3) qui sont des motifs présents dans des molécules d'intérêt pharmaceutique. Après optimisation des conditions de réaction, la réaction HIE a pu être réalisée dans des conditions très douces, et a fourni une très bonne incorporation de deutérium dans les positions ortho des sulphonamides DG1 jusqu'à 92% D, des phosphonamides DG2 jusqu'à 99% D et des N-oxydes DG3 jusqu'à 100% D (schéma 1).[1]

Schéma 1: *Réaction d'échange d'isotopes d'hydrogène à l'aide d'un catalyseur d'iridium sur des composés contenant les groupements directeurs suivant : sulphonamide, phosphonamide et N-oxydes* [1]

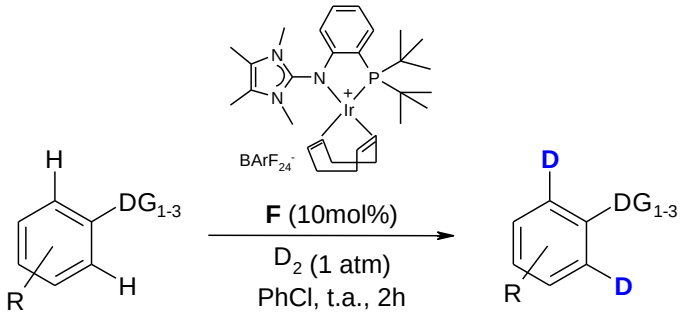

DG_1 = sulphonamides
DG_2 = phosphonamides
DG_3 = N-oxydes

DG_1 : **43-92 %D**
DG_2 : **60-99 %D**
DG_3 : **45-100 %D**

Exemples sélectionnés:

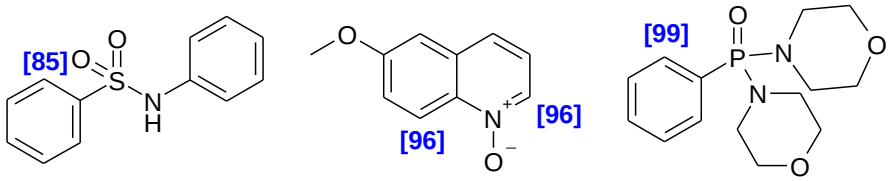

1 **2** **3**

Au cours de ces travaux de thèse, nous avons développé la première méthode de marquage catalytique à l'iridium dans des conditions douces (température ambiante) sur les motifs dérivés d'acides phenylacetiques tels que esters et amides, motifs également très présents dans les structures pharmacologiques. Cette méthode a permis d'introduire du deutérium ou du tritium en position *ortho* du groupement directeur de façon sélective avec des rendements satisfaisants à très bons (schéma 2). Cette méthode a été appliquée avec sucès au marquage de plusieurs composés pharmaceutiques (schéma 2)[2]

Schéma 2: *Réaction d'échange d'isotopes d'hydrogène sur des dérivés d'acides phénylacétiques avec un catalyseur à l'iridium* [2]

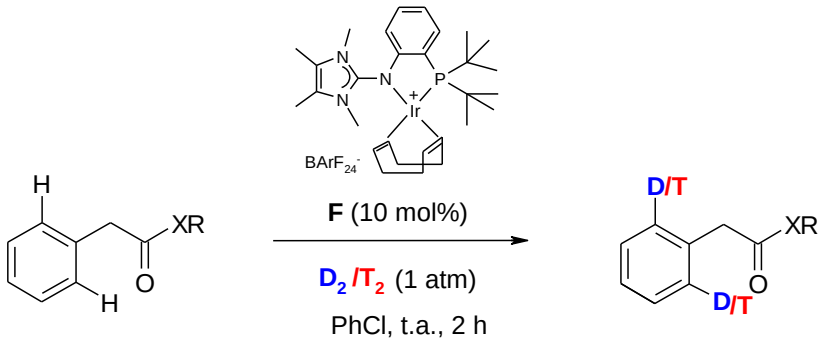

Exemples sélectionnés:

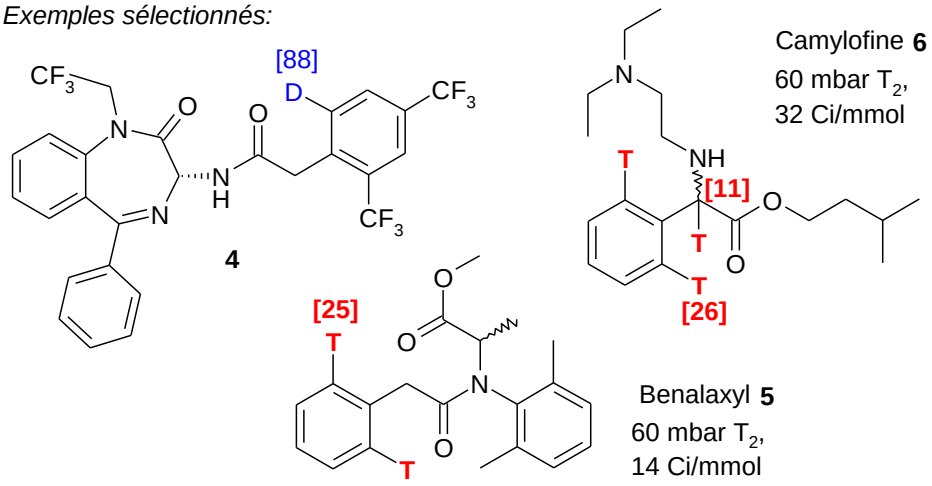

Lors d'un autre projet, nous avons mis en évidence que la position de marquage au sein d'une molécule avec plusieurs groupements directeurs peut être modulée en fonction du catalyseur d'iridium utilisé ainsi que de la température réactionnelle (de -60°C à +130°C) (schéma 3).[3]

Schéma 3: *Contrôle de la régio-sélectivité de la réaction d'échange d'isotopes d'hydrogène en fonction de la température et du catalyseur utilisé* [3]

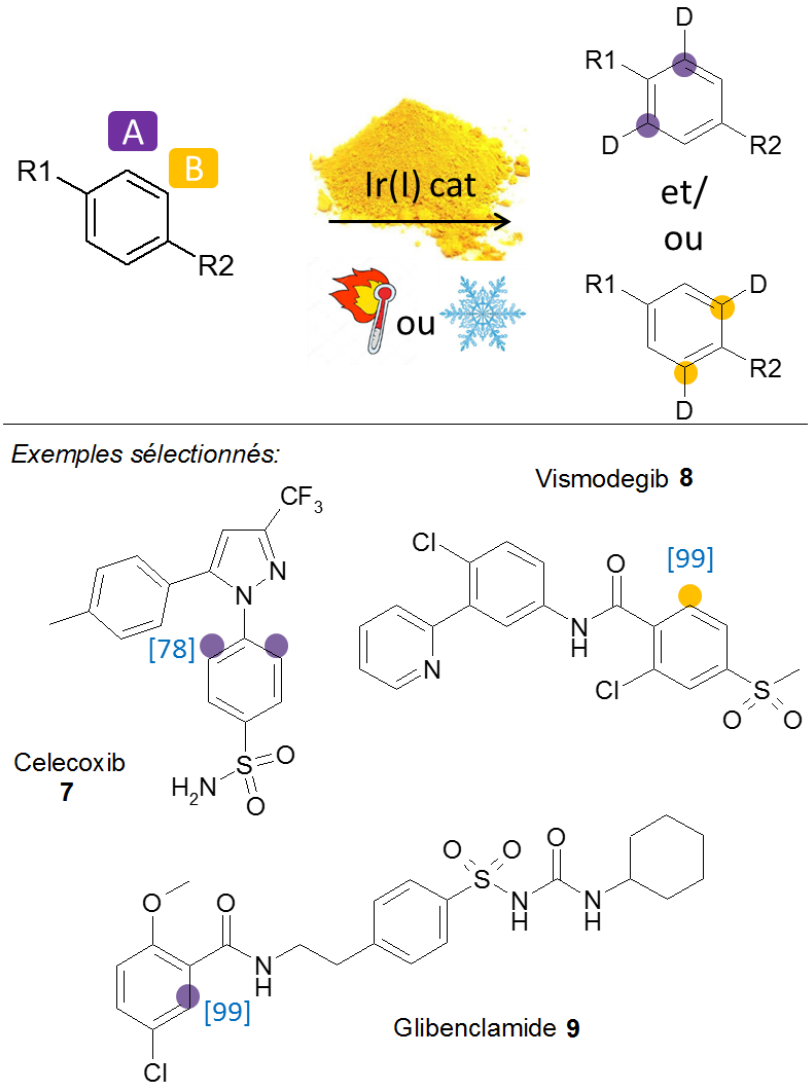

L'utilisation de calculs de DFT nous a permis de postuler un ordre de préférence classifiant différents groupements directeurs par rapport à leur réactivité vis-à-vis de la réaction d'HIE en situation de compétition (deux substrats et un catalyseur d'iridium). Ces données théoriques ont été confirmées par les données expérimentales (schéma 4) sur des molécules modèles mais aussi sur des médicaments.[4]

Schéma 4: *Prédiction de la régio-selectivité de la réaction d'échange d'isotopes d'hydrogène en situation de compétition entre deux différents groupements directeurs au sein d'un même substrat* [4]

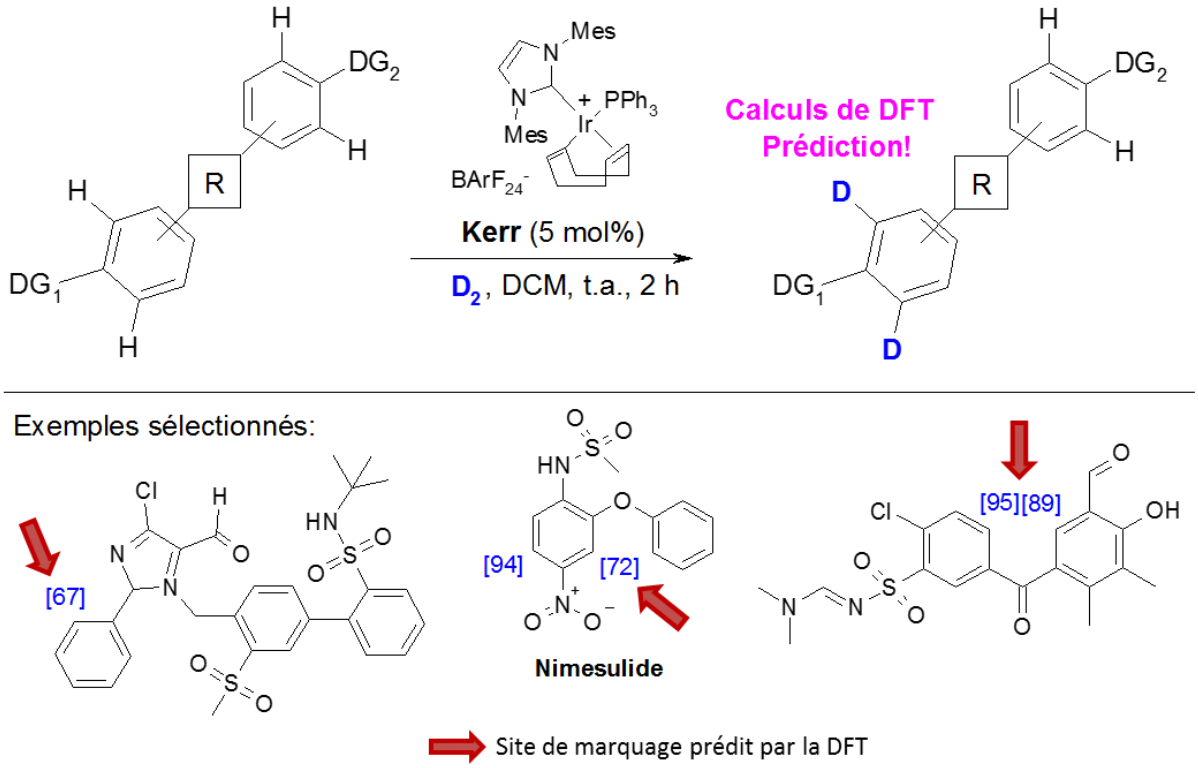

Lors d'un autre projet, le marquage sélectif au tritium d'une structure complexe tel qu'un médicament cytotoxique (maytansine DM4) a débouché sur le marquage de différentes chaînes latérales employées dans des méthodes de conjugaison aux anticorps. Ces données ont permis d'étendre cette méthodologie au marquage au deutérium d'acides aminés et de di-tri et tétra-peptide, sélectivement sur le carbone alpha d'un résidu glycine (schéma 5).[5]

Schéma 5: Réaction d'échange d'isotopes d'hydrogène sur *des Carbones(sp3)-H à l'aide de catalyse à l'iridium* [5]

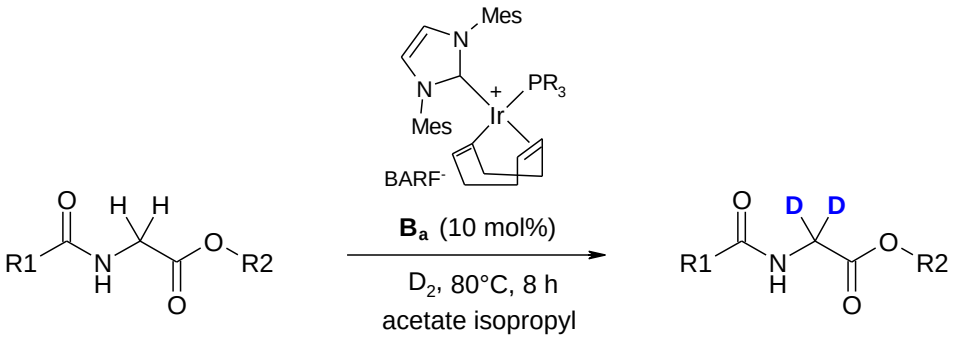

R1= N-groupement protecteur ou acide aminé

R2= Me ou acide aminé

28 exemples
1 exemple complexe tritium
haute sélectivité
jusqu'à 99% D incorporation

Exemples sélectionnés:

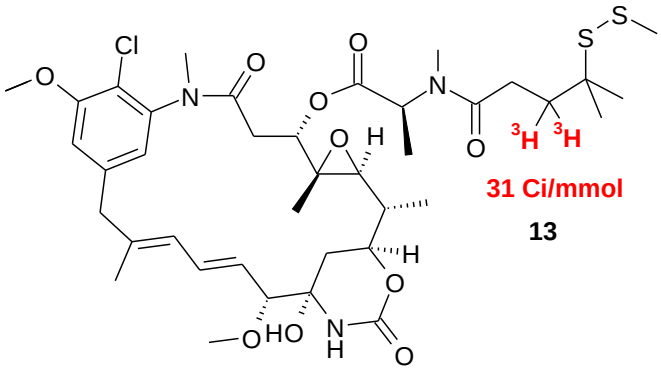

31 Ci/mmol

13

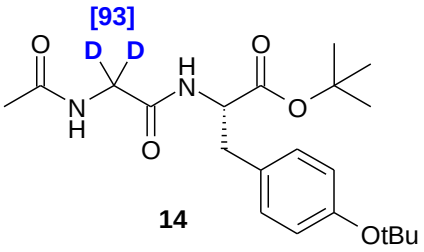

14

(L)-Ac-Gly-Tyr(OtBu)-OtBu

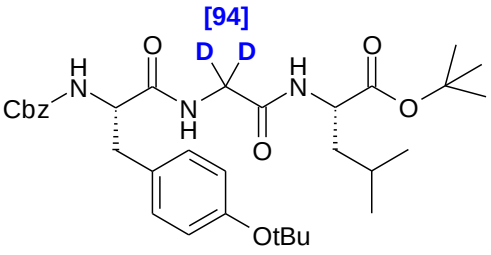

15

(L)-Cbz-Tyr(OtBu)-Gly-Leu-OtBu

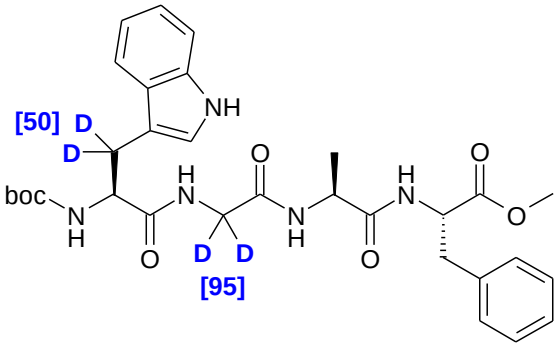

16

(L)-Boc-Trp-Gly-Ala-Phe-OMe

Finalement, en collaboration avec le CEA-Saclay et le CNRS, nous avons développé les premières nanoparticules d'iridium stables à l'air et actives vis-à-vis de l'échange d'isotopes d'hydrogène sur des anilines (schéma 6).[6]

Schéma 6: Réaction d'échange d'isotopes d'hydrogène sur des composés organiques avec un groupement directeur aniline à l'aide de nanoparticules d'iridium stabilisées par des ligands NHC [6]

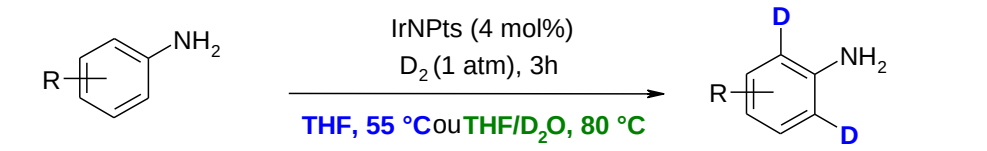

R = alcane, arène, halogène

32 exemples, Jusqu'à 99%D
1 example complexe tritium

Exemples sélectionnés:

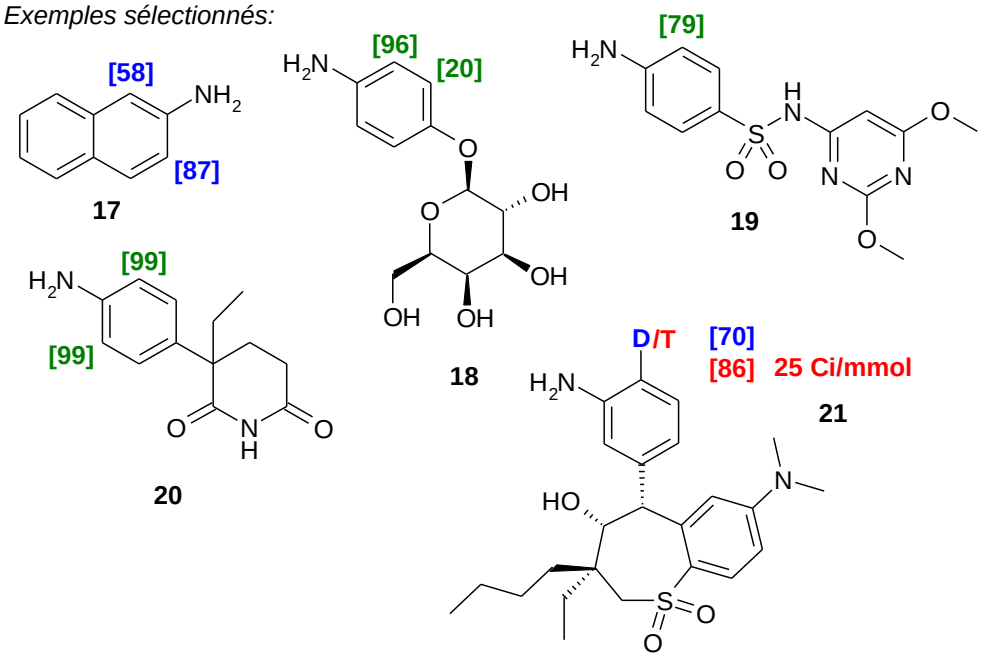

L'ensemble des travaux réalisés pendant cette thèse a permis le marquage au tritium de composés médicamenteux tels que le DM4, le Benalaxyl, ou encore le pharmacophore du Volixibat.

En conlusion, l'introduction de deutérium ou de tritium dans la molécule finale a été effectuée en utilisant la catalyse de l'iridium homogène et hétérogène et nous avons vu au cours des différentes parties de la thèse comment ces méthodes ont été développées d'abord sur de petites molécules modèles et appliquées avec succès ensuite sur des composés médicamenteux.

Sur la base des travaux élaborés dans la thèse, il reste quelques défis à relever et certains projets scientifiques qui n'ont pas pu être achevés par manque de temps :

• Nous avons développé une nouvelle méthode de marquage C-(sp3) des petits peptides (jusqu'à quatre acides aminés). Cependant, la méthode ne fonctionne qu'avec des groupes protecteurs sur les fonctions azotées ou oxygénées. Il serait utile de développer une méthode

sélective pour des peptides plus gros sans avoir besoin de groupes protecteurs. Par conséquent, de nouveaux catalyseurs avec une stabilité élevée et une meilleure solubilité dans les solvants polaires sont nécessaires.

• Nous avons découvert une nouvelle façon de prédire l'influence des différents groupements directeur dans les réactions d'échange d'isotopes d'hydrogène en situation de compétition. C'est le cas normal d'une approche de fonctionnalisation à un stade avancé. Il serait donc intéressant de rapprocher les observations obtenues avec d'autres réactions de couplage catalysées par les métaux de transition C-C et C-X.

• Nous avons étudié les IrNPts dans les réactions d'HIE. C'est la première fois que ces nanoparticules sont utilisées en catalyse et il serait très intéressant d'élargir leur champ d'application et d'étudier ces nanoparticules dans d'autres réactions comme dans les hydrogénations ou les réductions.

• Le dernier sujet à traiter serait basé sur les conjugués d'anticorps monoclonaux, comme discuté dans la partie sur les ADC. Il serait important non seulement de pouvoir marquer radioactivement le médicament, mais également de développer des méthodes permettant de marquer l'anticorps et de suivre sa distribution.

---

[1] M. Valero, A. Burhop, R. Weck, K. Jess, M. Tamm, V. Derdau, J. Atzrodt, *JLCR*, **2017**, *61*(*4*), 380-385.
[2] M. Valero, D. Becker, K. Jess, R. Weck, J. Atzrodt, T. Bannenberg, V. Derdau, M. Tamm, *Chem. Eur. J.* **2019**, *25(26)*, 6517-6522.
[3] M. Valero, A. Mishra, J. Blass, R. Weck, V. Derdau, *ChemistryOpen, **2019**, 8(9)*, 1183-1189.
[4] M. Valero, T. Kruissink, J. Blass, R. Weck, S. Güssregen, A. T. Plowright, V. Derdau, *manuscript in preparation*.
[5] M. Valero, R. Weck, S. Güssregen, J. Atzrodt, V. Derdau, *Angew. Chem. Int. Ed.* **2018**, *57*(*27*), 8159-8163.
[6] M. Valero, D. Bouzouita, A. Palazzolo, J. Atzrodt, C. Dugave, S. Tricard, S. Feuillastre, G. Pieters, B. Chaudret, V. Derdau, *Angew. Chem. Int. Ed.,* accepted manuscript.

Abbreviations and Symbols

Ala	Alanine
ADC	Antibody-Drug-Conjugate
ADME	Adsorption, distribution, metabolism, excretion
AMS	Accelerator Mass Spectroscopy
Arg	Arginine
Asp	Aspartate
Atm	Atmosphere
Au	Gold
AUC	Area under curve
β^+	Positron
β^-	Electron
Bn	Benzyl
Bq	Bequerel
Boc	Tert-butyl-carbonate
C-H	Carbon-Hydrogen
CF_3	Trifluoromethyl
Ci	Curie
CO	Carbon monoxide
COD	1,5-cyclooctadiene
Cy	Cyclohexyl
D_2O	Deuterated water
DBU	1,8-Diazabicyclo[5 .4.0] undec-7 -ene.
DCC	N,N' –Dicyclohexyl carbodiimide
DCM	Dichloromethane
DDD	Drug Discovery & Development
DFT	Density functional theory
DG	Directing Group
DIPEA	N,N-Diisopropylethylamine
DMAP	N,N-Dimethylpyridin-4-amine
DMPK	Drug metabolism and pharmacokinetics
DMF	N, N-Dimethylformamide
DMSO	Dimethyl sulfoxide
EMEA	European Medicines Evaluation Agency
Equiv./ Eq.	Equivalents
EW	Electron withdrawing
FDA	Food and Drug Association
Fmoc	Fluorenylmethyloxycarbonyl protecting group
h	Hours
HAT	Hydrogen atom transfer
H/D/T	Hydrogen/Deuterium/Tritium
HIE	Hydrogen Isotope Exchange
HMDS	Hexamethyl disilazane
HOBt	1-Hydroxybenzotriazole
HPLC	High-Performance Liquid Chromatography
HTS	High-throughput screening
Ir	Iridium
KOtBu	Potasium tert-butylhydroxylate
LCMS	Liquid Chromatography-Mass Spectrometry
$LiAlD_4$	Lithium aluminum deuteride
LSF	Late stage Functionalization

Lys	Lysine
MeV	Mega electron volt
mL	Milliliter
MPa	Megapascal
MS	Mass spectrometry
MRI	Magnetic Resonance Imaging
MW	Microwave
n-Bu	n-Butyl
NDA	New Drug Application
NHC	N-heterocyclic carbene
Ni	Nickel
NMP	N-methylpyrrolidone
NMR	Nuclear magnetic Resonance
NP	Nanoparticles
NSAIDs	Nonsteroida1 anti-inflammatory drugs
P	Pressure
Pd	Palladium
PET	Positron Emission Tomography
PG	Protecting group
Ph	Phenyl
PK	Pharmacokinetic
PK-PD	Pharmacokinetic-Pharmcodynamic
Pt	Platinum
ppm	Parts-per-million
PPB	Plasma Protein Binding
PVP	Polyvinylpyrrolidone
QWBA	Quantitative whole bodyautoradiography
R	Ideal gas constant
RCC	Radiochemical Conversion
RCP	Radiochemical Purity
RCY	Radiochemical Yield
R&D	Research & Development
Rh	Rhodium
RT	Room temperature (22-25°C)
Ru	Ruthenium
SA	Specific Activity
SIL	Stable isotopically labelled
T	Temperature
t	Time
tBu	*tert*-Butyl
TEA	Triethylamine
TEM	Transmission Electron Microscopy
Tf	Triflate
TFA	Trifluoroacetic acid
THF	Tetrahydrofuran
TON	Turn-over-numbers
V	Volume
w	Watt
Xantphos	4,5-Bis(diphenylphosphino)-9 ,9-dimethylxanthene
XRD	X-Ray detection
Z (or Cbz)	Carboxybenzyl

Definitions and Descriptions[1]

1. Radioactivity: is defined as the property of certain nuclei to spontaneous fragment or rearrange, resulting in the emission of radiation.

2. Activity (A): the quantitative measure of radioactivity. The number of nuclear decays, occurring in a given quantity of material over a certain time interval, divided by that time interval.

3. Becquerel (Bq): the agreed SI derived unit for the quantity of activity, equal to one disintegration per second. Pre-SI units can also be found (e.g. Ci: 1 Ci = 3.7 GBq).

4. Specific Activity: (SA) the measured activity per gram of compound, measured in Bq/g or GBq/mg. Previously reported in Ci.

5. Molar Activity: (MA) the measured radioactivity per mol of compound, measured in Bq/mol or GBq/mol. Previously reported in Ci.

6. Radiochemical Yield (RCY): is the amount of activity in the product expressed as the percentage (%) of starting activity used in the considered procedure. In this thesis, RCY is attributed only on the values of radioactivity after synthesis, purification and evaluation of chemical purity at the very end of the process.

7. Radiochemical Purity (RCP): Ratio of the activity of a radionuclide in a stated chemical species in a material over the total activity of all species containing that radionuclide in that material: the absence of other radiochemical compounds/species, measured by radio-HPLC.

Table 1: *Characteristics of the hydrogen isotopes*

Hydrogen isotopes	Symbol	Protons	Neutrons	Atomic mass	Radioactivity	Discovery
Hydrogen	1H	1	0	1.00782504	no	1766 H. Cavendish
Deuterium	2H or D	1	1	2.01410178	no	1931 H. Clayton Urey
Tritium	3H or T	1	2	3.0160492	- half-life: 12.3 y - 1T=29.2Ci/mmol	1934 E. Rutherford

[1] Coenen, H.H., Gee, A.D., Adam, M., Antoni, G., Cutler, C.S., Fujibayashi, Y., Jeong, J.M., Mach, R.H., Mindt, T.L., Pike, V.W., Windhorst, A.D., *Nucl. Med. Biol* **2017**, *55*, v-xi.

Table of content

Part V

Part VI

Appendix

Part I

Introduction

I.1 Drug Discovery and Development

The ultimate target of pharmaceutical companies is to develop new drugs and to improve the life of patients. This is of great ethical importance and a high benefit for human society in general as diseases are generating costs in billions. Mostly big pharmaceutical companies are investing high levels of time and money in drug research. Indeed, the Drug Discovery and Development (DDD) process is extremely risky because most of the drug candidates fail.
When looking at the number of compounds (*figure I.1*), the first screenings involve thousands of molecules which are evaluated in each step of the DDD process. This procedure can be considered to work in principle as a funnel and will provide finally one drug compound. The overall DDD process takes between 15 and 20 years, and cost an average between 1 to 2.5 billion €, sometimes more than 5-6 billion € in some cases.

Figure I. 1: Drug discovery and Development process

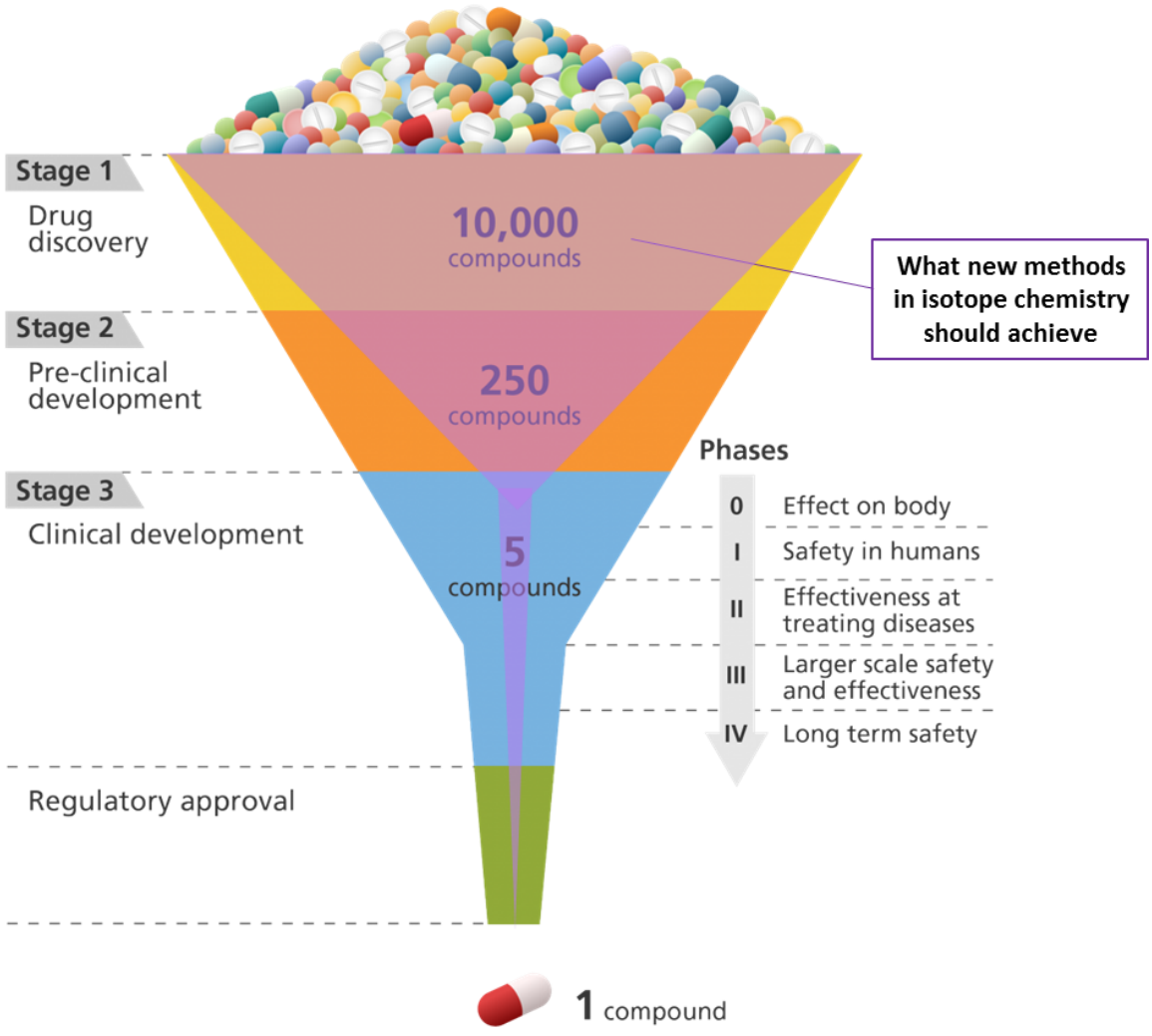

In a cost and time driven efficient organization, it is a constant duty to further optimize the whole process towards operational excellence. Therefore, there is a continuous need to identify and develop new methods to make the process faster and less elaborated. One of these methods is the faster supply and easier application of isotopically labelled compounds in the DDD process. It is envisioned that with these new achievements in isotope chemistry, better drug candidates can be identified in a much shorter time frame.

The Drug Discovery & Development (DDD) process involves globally seven major steps (*figure I.1*). The first one is the identification of the disease or disorder the company wants to cure or treat, in connection with the related target which needs to be identified. It can be for example a membrane, a membrane receptor, an enzyme, an ion channel, or a protein-protein interaction. The second step is the identification of one to three lead molecules by biological assay evaluation with high-throughput screening (HTS). The numbers of tested molecules are differing strongly depending of the project and disease model, but can reach millions of compounds in the primary assay (activity related). In the secondary assay, which is more selectivity based normally, numbers up to 10000 (see *Figure I.1*) are tested. During this optimization process, the different lead series are optimized in iterative cycles to improve several parameters. These steps are called Drug Discovery and are ending with the nomination of a drug candidate. After this important decision there is no further change of the chemical structure of the compound possible and the Drug Development is starting.

The third step concerns the preclinical studies of the identified drug candidate. Different pathways to synthesize and analyze the compound are explored to end up with the most efficient and easy-to-handle synthesis. The pharmacokinetic (PK) parameters of the compound is evaluated by profiling absorption, distribution, metabolism and excretion (ADME) studies as well as toxicology evaluation. The preclinical studies are done *in vitro* (e.g. hepatocytes, S9 fractions) and *in vivo* (in animal models). When all collected and analyzed pharmocokinetic and toxicologic data allow the progression of the drug candidate, the fourth step is starting: the clinical studies in humans which involve four phases.

The Phase 0, first try in healthy volunteers (10-15 subjects) on a very short duration (≤7 days), consists of collecting the first PK-PD data (e.g.: bioavailability, clearance time. etc.) prior the Phase 1. It can be done via conventional methods by extrapolation from animal models or by microdosing studies using radiolabeled isotopes. The analysis by Accelerator Mass Spectroscopy will mostly employ ^{14}C whereas Positron Emission Tomography will mostly use ^{11}C.

The Phase 1 enables to determine the safety, dosing and formulation. The drug candidate is tested in total on 60 to 90 healthy human volunteers, by single dose followed by repeated dose in order to assess safety and side-effects and to find the correct drug dosage.

The Phase 2 is the first try in patients to demonstrate the effectiveness of the new treatment and to continue safety studies. This clinical evaluation which shows how the drug works lasts several years and is done with cohorts of 100 to 500 patients. The Phase 2 represents the highest risk of failure in the whole DDD process with almost 70% of drug attrition (even more for molecules targeting the central nervous system). This partly results from

insufficient preliminary PK/PD evaluation, a problem which could be overcome by an early extensive use of (radio)labeled drug candidates.

It is followed by the Phase 3, which consists of testing the drug candidate on a higher number of patients, up to 10000 in various conditions including different populations, different dosages, sex/age effects and drug combinations. The effect, the tolerance and the side effects will be further investigated during this phase and usually permits to detect potential drug interactions. From the start of the Phase 3, the probability of success is increasing. Finally, the last step consists of the constitution of the Marketing Authorization dossier for the approval from the authorities in the different countries, e.g. Food and Drug Administration (FDA) or European Medicines Evaluation Agency (EMEA).[1]

Phase 4 clinical trial is the post-marketing follow-up of the drug in order to track long-term drug side-effects and drug interaction on a real population after prolonged time of use. This phase may also lead to the withdrawal of the drug from the market in case serious issues and drawbacks are detected.

I.2 Limitations of Drug Discovery and Development

The pharmaceutical industry is facing huge challenges like reduced Research and Development (R&D) efficiency, stagnant success rate, patent expirations for key drugs, price competition from generics, sanitary scandals, high regulatory hurdles, and the industry's perceived tarnished image in the public.[1] Despite major scientific and technical advances in DDD and unprecedented investment in pharmaceutical R&D,[2] the number of new drugs approved by the EMEA or FDA was dramatically low in the years 2005-2010.[3]

Figure I. 2: Novel FDA approvals since 1993. Annual numbers of new molecular entities (NMEs) and biologics license applications (BLAs) approved by the Center for Drug Evaluation and Research (CDER) [5]

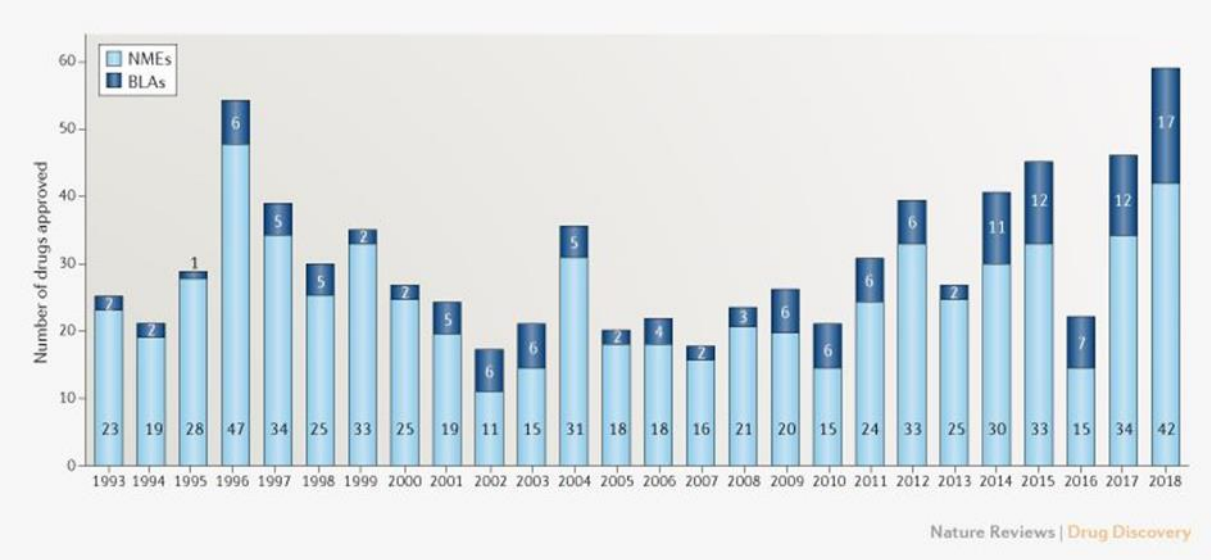

By comparison to 1995-2000, it took at least twice more drug candidates coming out of preclinical trials for one product to reach final launch.[4] However, in 2018 the FDA registered a record of novel drug approvals (59) indicating that the changes in R&D management in the last years are making impact (*figure I.2*).[5] This is in part due to the emerging of new methods for (radio)labeling drug candidates.

The regulatory authorities only accept non-altering (radio)labelling such as deuterium, tritium, carbon-14, carbon-11, fluorine-18 etc., except in the case of large biologics for which slight modifications are accepted. However, it is known that their common way of synthesis (labelling of the first building block and carrying the radioactivity over the whole synthesis providing the drug structure) can be time-consuming, expensive and far from trivial especially for short half-life isotopes. Indeed, there is a clear lack of effective methods for isotopic labelling of drug molecules and for this reason, we need to development innovative labelling strategies, applicable to large sets of small molecules, biomolecules and drug candidates, without affecting their molecular properties.[3]

I.3. Isotopically labelled compounds in DDD

The choice of isotope label which is being used in an application of a labelled compound depends on several parameters. There are on one hand commercial reasons, like availability or costs. Another general point is time-dependent, either how fast potential isotopically labelled precursors can be delivered or how fast these compounds can be synthetically introduced into the final labelled target molecule. In this context, it is always beneficial if direct labelling methods, e.g. hydrogen or carbon isotope exchange, are known and can be applied immediately. In all applications, the isotope label must be stable under the used experiment conditions, the use as internal MS standard under aqueous conditions with low pH or metabolic or chemical stability in *in-vivo* experiments with long- or short-lived radioisotopes (e.g. ^{14}C or ^{11}C).

For radioactive isotopes, there are additional parameters to be considered which can differ depending on the followed experiment. Mostly the isotope label should not change the chemical and physical properties of the target molecule, and therefore for most organic drug candidates labelling with isotopes of hydrogen, carbon, nitrogen, sulphur and phosphorus are beneficial. Based on the parameters mentioned above and the half-life, specific activity or emitted energy of the isotope, the best isotope label for the experiment is chosen. Finally, all chemical methods used should be handled safely without any risk to the operating chemist or the environment.

In Figure I.3, the applications of isotopically labelled compounds in DDD is described. For early research mainly tritium (^{3}H) is used for e.g. protein binding, receptor occupancy or receptor identification *in-vitro* studies. This is mostly due to the low cost, minimal compound needs and limited synthesis efforts. As the ^{3}H label can be in principle metabolically cleaved, generally ^{14}C labelling is preferred for *in-vivo* studies, like tissue distribution or animal PK studies. Short-lived isotopes like fluor-18 or carbon-11 with a half-life of just 110 and 20 min, respectively, can be applied in non-invasive imaging experiments by Positron Emission Tomography (PET). Stable labelled compounds (e.g. labelled with deuterium, carbon-13 or nitrogen-15) are mostly applied to generate isotopically labelled MS standards mainly during the preclinical and clinical time frame. Recently they are also applied in deuterated drugs, which is discussed later.

Figure I. 3: *Applications of isotopically compounds in DDD*

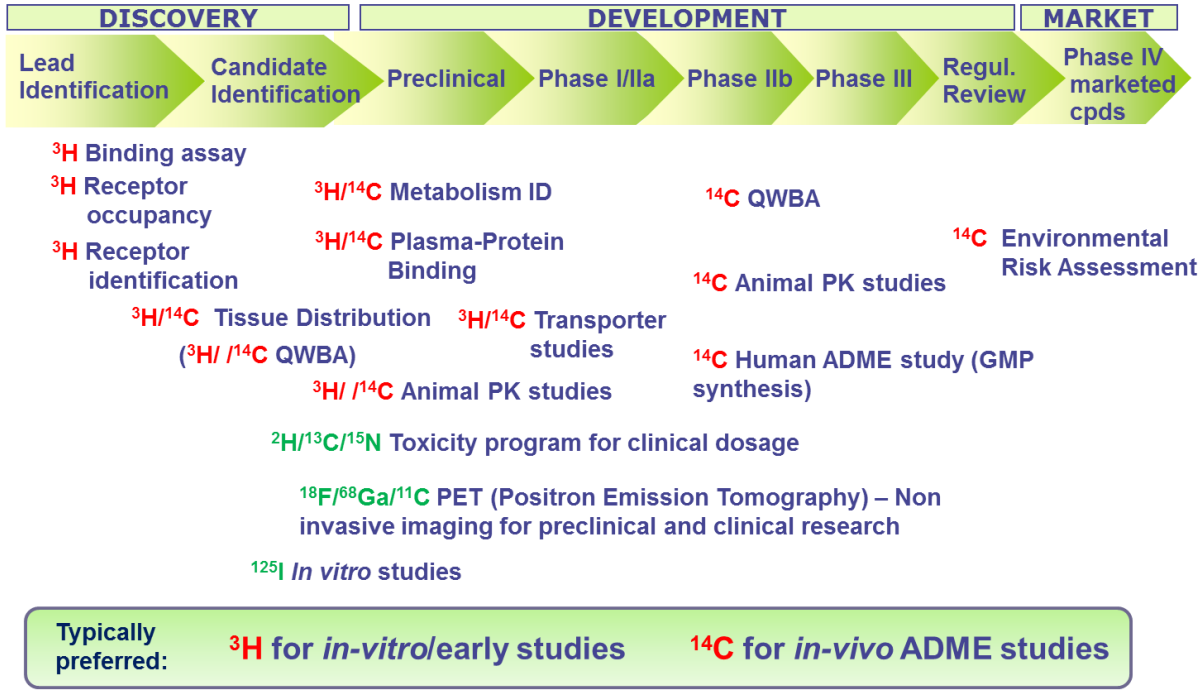

Herein the connection with whole ISOTOPICS consortium can be easily identified bridging the needs for new and innovative methods in all discussed areas of isotopically stable-, long- and short-lived (radio)isotopes.

I.4 Hydrogen isotopes in DDD and life sciences

The popularity of hydrogen isotopes in the life sciences is due to their ability to be incorporated into the target molecule without changing its chemical structure, physical properties or biological activity.[6] Therefore, hydrogen isotopes are unique tools for identifying and understanding biological and chemical processes (*figure I.4)*. They have many properties of ideal tracer nuclides and can be detected with very high sensitivity. In

comparison to ^{13}C or ^{14}C, hydrogen isotope labelling is easier, quicker and much cheaper.[7] However a disadvantage can be the lack of metabolic stability prediction of deuterated and tritiated compounds. The main risk with tritium is to form *in vivo* tritiated water $^{3}H_2O$ which can be distributed in the whole body and due to the radioactive emission may cause cancer.[8,6] After incorporation tritated water stays inside the human body for 7-14 days.[9]

Figure I. 4: *Applications of hydrogen isotopes in life sciences* [6]

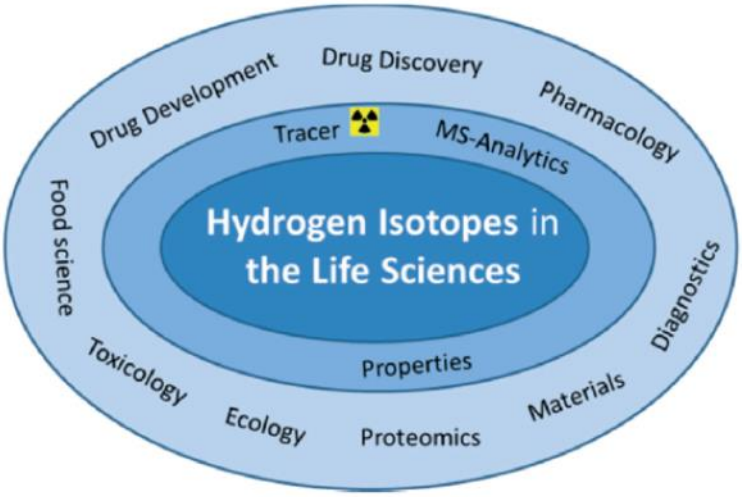

I.4.1. Applications of deuterium in DDD

Overall, we can classify deuterium applications in four general topics:

- Absolute quantification through internal standardization for quantitative MS analysis (see **I.4.1.a**)
- Kinetic and equilibrium isotope effects for mechanism studies (see **I.4.1.b**)
- Deuterated PET tracers (see **I.4.1.c**)
- Para-hydrogen for induced polarization MRI [10]

I.4.1.a) Deuterium labelled internal MS standards

Liquid chromatography coupled with tandem mass spectrometry detection (LC-MS/MS) has become the most efficient bioanalytical tool for the investigation of samples coming from environmental, animal, and human studies.[11] Internal standards are essential for a quantitative LC-MS/MS analysis of an analyte in complex solutions (e.g. blood, urine, or bile). Deuterium labelled internal standards are advantageous due to their close physical and chemical properties with the analyte and its standard and the suppression of the matrix effect (*figure I.5*).[6,14] The compound of interest can be then measured relatively to the added internal standard by correlating a response ratio with a concentration ratio.[12]

Figure I. 5: *LC/MS of the internal standard* [6]

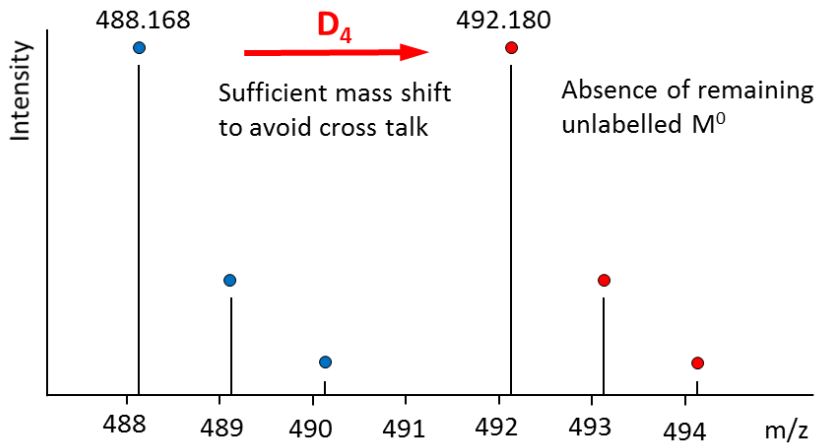

Stable Isotope labeled internal standards need to have a sufficient mass difference (typically, for small molecules without chlorine, bromine or sulfur-containing functionalities, an incorporation of 3 to 5 deuterium atoms) to avoid cross signal overlapping and negligible remaining M_0.

I.4.1.b) Kinetic Isotope Effect and deuterated drugs

After the administration of the drug in the body, it has to face metabolic transformation to facilitate elimination by increased hydrosolubility.[13] The main metabolizing enzymes in human are from the cytochrome P450 enzyme family, which provided them much attention by the pharmaceutical industry.[14] Significant kinetic isotope effects (KIE) were observed for several P450-catalyzed reactions: specific deuteration incorporation has the potential to impact the rate of metabolic transformations, provided that the rate-limiting step involves cleavage of a C–H bond (figure *I.6*).[15,6]

Figure I. 6: *Kinetic isotope effects of C-H and C-D bonds cleavage* [6]

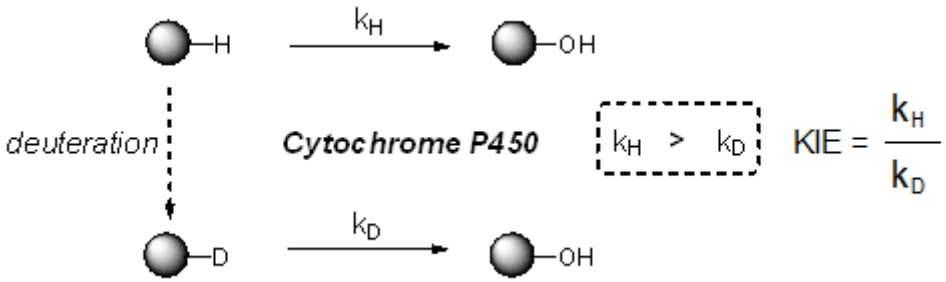

Depending on the enzymes involved and, therefore, the mechanism of the rate-determining step, another consequence can be a different metabolic turnover of drug molecules when

replacing hydrogen for deuterium.[16] Thus, the alteration of ADME properties by selective deuterium incorporation has recently received much attention.[17,6] The kinetic isotope effect lowers the rates of metabolism reactions and thus notably prolongs the biologic half-life of deuterated drugs. Thanks to this property, we can obtain a reduced systemic clearance and higher systemic exposure, as well as reduced formation of toxic or reactive metabolites, while retaining the potency of the original drug (*figure I.7*).

Consequently, potential drug benefits could include a smaller dosage, a lower risk for drug-drug interactions, and fewer side effects, resulting overall in an improved PK and safety profile, and an optimized effectiveness.[6]

Figure I. 7: *Potential pharmacological effects of specific drug deuteration* [6]

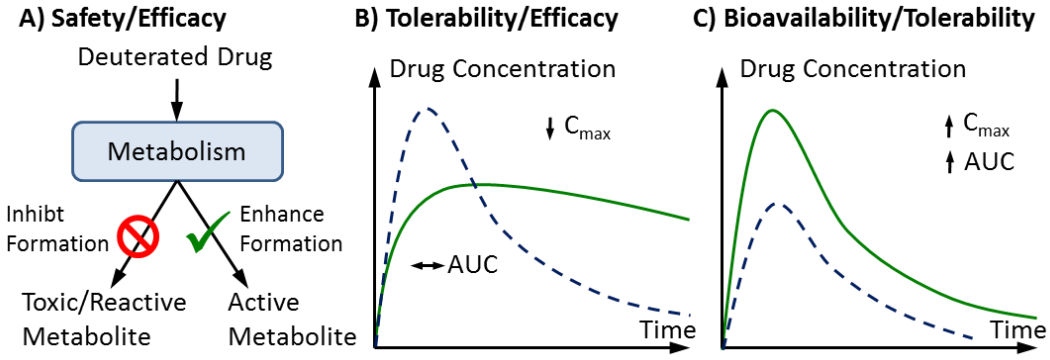

A: Metabolic shunting resulting in reduced exposure to undesirable metabolites (e.g. toxic or reactive). **B:** Reduced systemic clearance resulting in increased half-life. **C:** Decreased pre-systemic metabolism resulting in higher bioavailability of unmetabolised drug.

C_{max}: maximum drug concentration achieved
AUC (area under curve): total drug exposure across time

Significant clinical progress has been made in recent years regarding the use of deuterated drugs.[18] The FDA has accepted the New Drug Application (NDA) for Tetrabenazine **1** (Austedo®),[19] for the treatment of chorea associated with Huntington disease, based on successful Phase 3 clinical trials.[20] Other examples of deuterated drugs, such as CTP-499 **2** (deuterated pentoxifylline)[21] or AVP-786 **3** (deuterated dextromethorphane),[22] are currently in advanced clinical testing[23] or have demonstrated improved *in vivo* PK properties (*scheme I.1*).[24,6] These deuterium properties could also be an opportunity to reconsider old drugs which were abandoned due to side-effects related to chemical or metabolic instability. This is true for tetrabenazine which was metabolically more stable with deuterium, and deuterated thalidomide which was chemically more stable.

Scheme I. 1: *Selected deuterated clinical drug development candidates and corresponding unlabeled original drugs* [6]

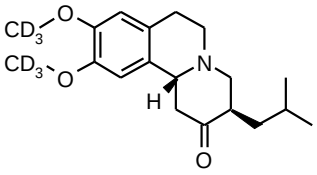

1
Tetrabenazine (Xenazine)
SD-809

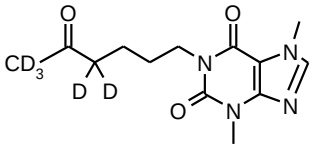

2
Pentoxifylline
CTP-499

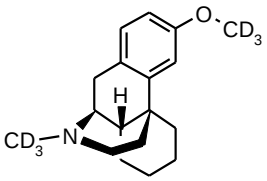

3
Dextromethorphan-$_6$
AVP-786

I.4.1.c) Deuterium PET tracers

Deuterated PET tracers have the properties to improved metabolic stability and sensitivity. The isotope ^{18}F is preferably employed in PET due to its longer half-life (109.8 min) compare to ^{11}C (20.4 min). However, the insertion of deuterium in the tracer in plus of the ^{18}F had showed to increase metabolic stability. Indeed, ^{18}F-D_4-Fluoromethylcholine **4** has proven to be a better PET tracer, with a favorable radiation dosimetry profile for clinical imaging compared to the non-deuterated ^{18}F -Fluoromethylcholine (*scheme I.2*).[25]

Scheme I. 2: *Structure of the 18F-D4-Fluoromethylcholine*

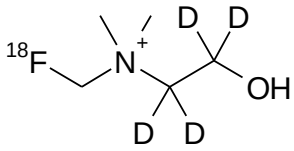

4
^{18}F-D$_4$- Fluoromethylcholine

I.4.2. Applications of tritium in DDD

I.4.2.a) Tritium in Quantitative Whole Body Audioradiography

A convenient *in vivo* imaging method is the Quantitative Whole Body Audioradiography (QWBA). This experiment provides qualitative and quantitative information on drug distribution and PK, by measuring drug-related radioactivity from body slices or organ sections (*figure I.8*).[26] These data are important to assess whether the drug reaches the target organ or accumulates in tissues associated with potential safety issues. QWBA studies are routinely conducted for small molecule drug candidates, to determine the maximum radioactive dose that can be administered to humans in the following radiolabelled human

ADME study.[27] This technique has also been increasingly used to figure out the biodistribution of biotherapeutic drugs, such as antibody-drug conjugates, oligonucleotides, fusion proteins, and peptides.[28,6]

Figure I. 8: *Quantitative Whole Body Audioradiography (QWBA) following subcutaneous administration of a tritium labeled drug development candidate* [6]

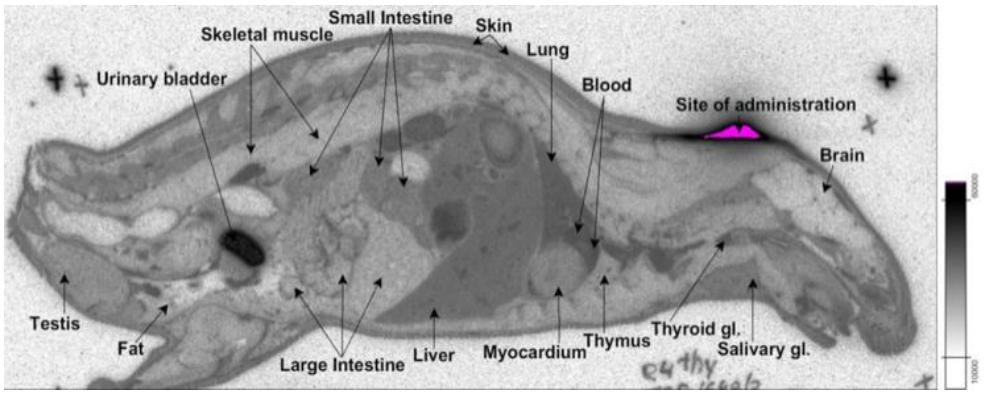

In relation with tritium, the short path length of the emitted β^--particles provides a high spatial resolution and tissue distribution information at the cellular level.[29,6]

I.4.2.b) Tritium in scintillation proximity assay

Tritium allows radioligand binding assays or scintillation proximity assay (figure I.9), which are widely used to characterize receptors, to study receptor dynamics and localization, to monitor enzyme reactions, to identify novel chemical structures that interact with receptors, and to define ligand activity and selectivity in normal and diseased tissues.[30] The selection of the radioligand is based on the stability, selectivity, and a high specific activity, in the range of 50-100 Ci/mmol which typically requires the introduction of 2-4 tritium atoms (considering the ^3H specific radioactivity of 29 Ci/mmol). In addition to this, radioligands should have a high affinity and low non-specific binding.[6]

Figure I. 9: Principle of the scintillation proximity assay [6]

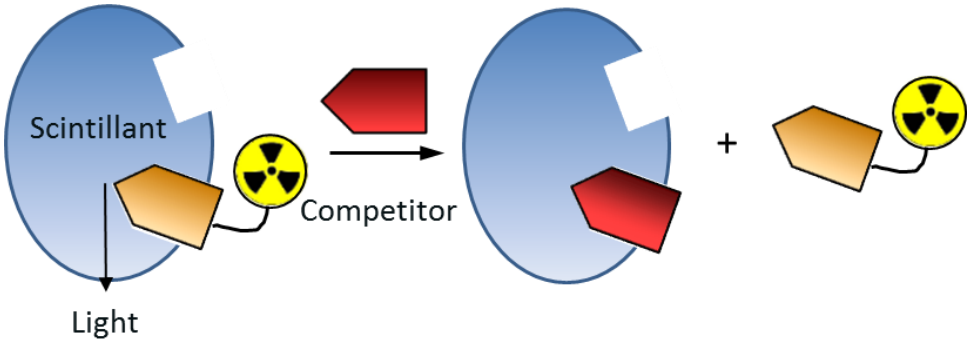

I.4.2.c) Tritium in plasma protein binding

Besides receptor binding, another important PK/PD parameter that can impact the efficiency of a drug is Plasma Protein Binding (PPB).[31] Plasma proteins prevent membrane insertion of hydrophobic drugs, help in drug transport and protect drugs against metabolization. Interspecies differences in PPB may affect drug-safety margins and thus, a careful assessment of unbound drug concentration in human and animal plasma is fairly requested by authorities before starting any clinical trials. Due to their relatively low costs and more straightforward access, tritium labelled compounds are able to provide a valuable tool which allows early assessment of reactive metabolite formation[32,6] (*figure I.10*).

Figure I. 10: *Plasma Protein Binding (PPB) assay based on equilibrium dialysis* [6]

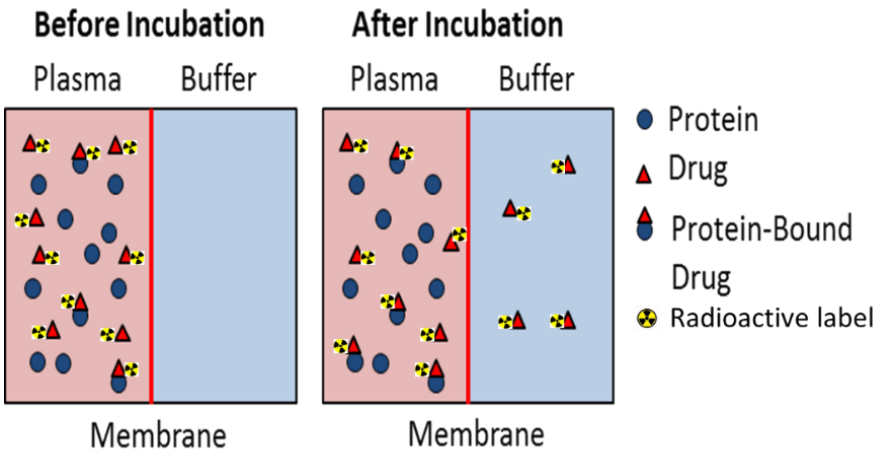

1.5. Hydrogen isotopes labelling methods

The incorporation of deuterium or tritium into an organic molecule can be achieved by two main routes: either by a conventional multistep synthesis with a radioactive building block or by a late-stage functionalization (LSF) approach. A classical synthesis starting from appropriate commercially available labelled precursor is less and less considered, as it can be very time and resource consuming, depending on the complexity of the chemistry, the chemical structure of the target molecule, or the labelling position. Therefore, in the recent years, the development of methods for fast and convenient LSF with deuterium or tritium into organic molecules was highly investigated.[33] However, all the traditional LSF pathways need a sometimes long-lasting precursor synthesis.[34] As described in the ^{3}H-synthesis of galantamin **6**, the brominated precursor **5** was needed to perform the reaction (*scheme I.3,* **A**). The halogen/tritium exchange was carried out with palladium on charcoal as catalyst at room temperature to yield ^{3}H-galantamin **6**.[35] In the example of ^{3}H-mecillinam **8** synthesis, the unsaturated precursor **7** was synthesized in 6 steps and finally hydrogenated with tritium gas and palladium on charcoal catalysis (*scheme I.3,* **B**).[36]

Scheme I. 3: *Traditional approaches to introduce tritium into complex molecules* [34,35,36,37]

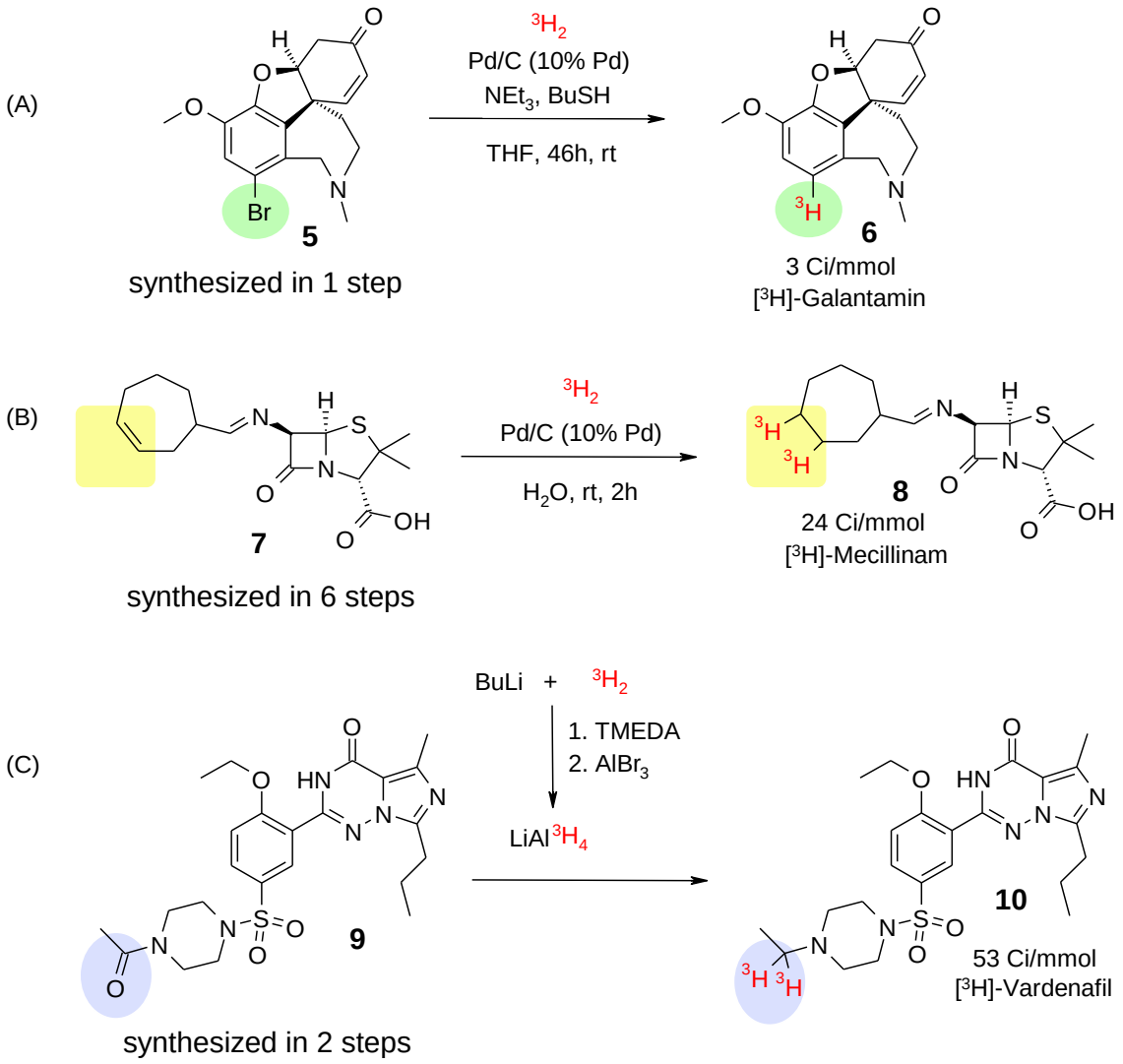

Another very common method is based on the use of metal tritides, which need to be synthesized freshly from tritium gas prior use in the reduction of carbonyl or imine moieties. In the example(*scheme I.3,* **C**) ^{3}H-vardenafil **10** was synthesised by reduction of the amide carbonyl function with lithium aluminium tritide.[37] While all these methods have proven their usefulness in many reported examples, the precursor synthesis remains the key to a fast delivery of the tritiated compound.

Another approach to apply the principles of chemical modification of complex molecules at the latest possible time point (LSF) is the hydrogen isotope exchange (HIE). It enables a selective installation of C–D[38] and C–T[39] bonds in the target molecule by exchange of a C-H bond.[40] Especially for the synthesis of tritium labelled substances, a labelling procedure at the latest possible reaction step is minimizing radioactive waste and decreases the handling time with the radioactive products. Numerous HIE protocols utilizing homogeneous or heterogeneous catalysts have already been described.[41] In scheme I.4, the tritiation of

valsartan **11** under classical HIE conditions with an iridium catalyst is described.[42] Furthermore, with the HIE method only a minimum amount of starting material is necessary, which is especially for early projects a great advantage for the fast compound supply. The principles of this reaction will be discussed in more detail below.

Scheme I. 4: *typical HIE reaction with iridium catalysis of valsartan*

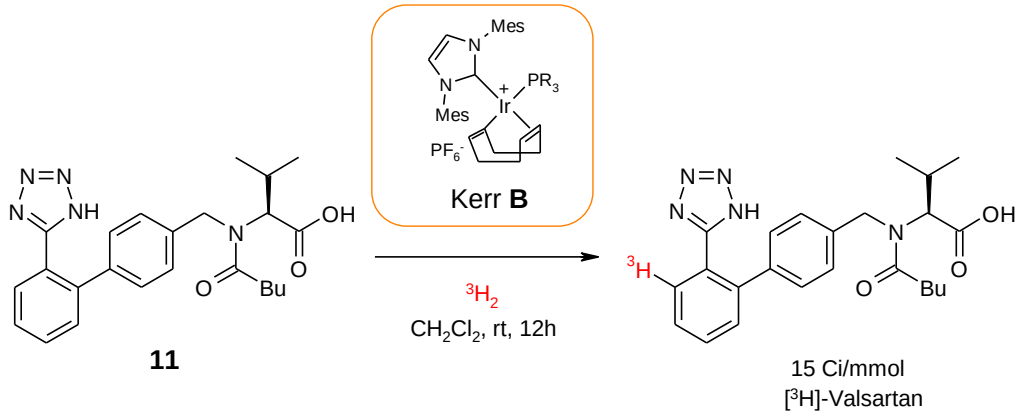

HIE reactions can be performed under acid/base, heterogeneous and homogeneous catalysis (*scheme I.5*). Typically, heterogeneous metal-catalyzed HIE generally results in relatively unspecific incorporation of numerous deuterium atoms into a molecular substrate (*scheme I.5, left*). Accordingly, heterogeneous metal-catalyzed H/D exchange is typically the method of choice for preparation of stable isotopically-labeled internal standards for LC-MS/MS investigations. In contrast, homogeneous metal catalysed HIE methods are typically much more selective incorporating deuterium only at specific positions in the molecule, e.g. next to a directing group (*scheme I.5, middle*). Therefore, these methods are of particular importance for tritium incorporation via H/T exchange.[6] Acid/base-mediated labeling methods are still used, even though they are among the oldest methods, there are still new examples being reported. The selectivity of these methods largely depends on innate electronic activation within the target molecule (*scheme I.5, right*).

Scheme I. 5: *Illustration of various selectivities available by distinct HIE methods.*

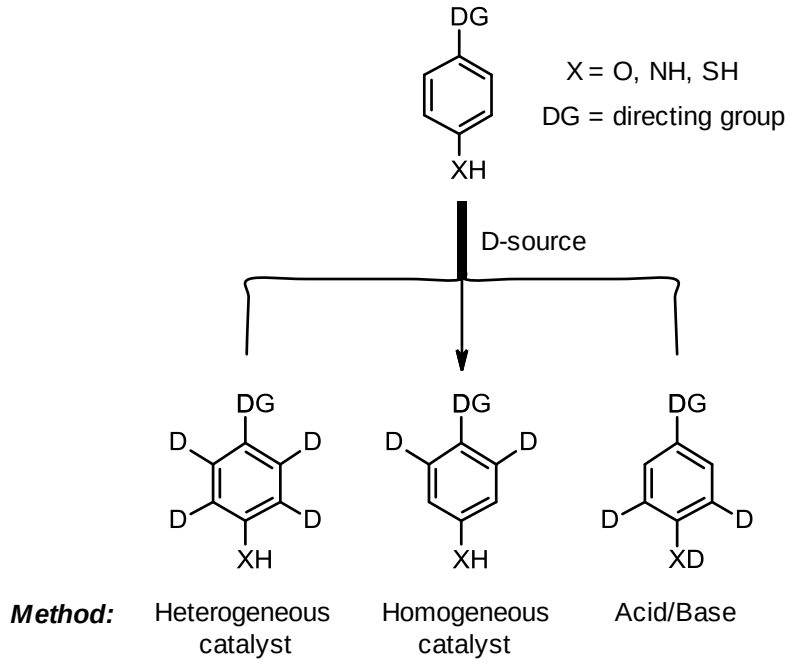

I.5.1. Hydrogen isotope exchange acid-mediated labelling

Acid or base-catalyzed HIE methods are in principle the easiest protocols to perform as long as there is no issue with stability, solubility or selectivity. At temperatures above 100°C generally a very efficient but unselective hydrogen deuterium exchange takes place. Most of these examples are of older provenance, with no new application having been reported in the last ten years, most probably due to the development of more effective alternative methods. While simple Brönsted acids such as DCl[43] or D_2SO_4[44] are mostly used to introduce deuterium into activated aromatic compounds, bases like $NaOD/D_2O$,[45] $DMAP/D_2O$,[46] Na_2CO_3/D_2O[47] or even near-critical D_2O[48] are convenient reagents for introducing the hydrogen isotope into aliphatic CH-positions. Due to the fact that the isotope source is used in high excess there are only a few acid/base-catalyzed protocols known to introduce tritium.[6]

As peptides have become more and more important in pharmaceutical research, a significant increase of reported methods to prepare deuterium-labeled amino acids or peptides has been observed. For example, Hashimoto *et al.* reported the deuteration of α-amino acids derivatives by triflic acid (trifluoromethanesulfonic acid) with high deuterium content (*scheme I.6,* ***12,13 =>14,15***).[49] In one example, a pentapeptide was deuterated at room temperature in 9 hours with up to 8 deuterium atoms introduced at the aromatic positions.[50]

Scheme I.6: *Acid-mediated labeling of amino acid derivatives*

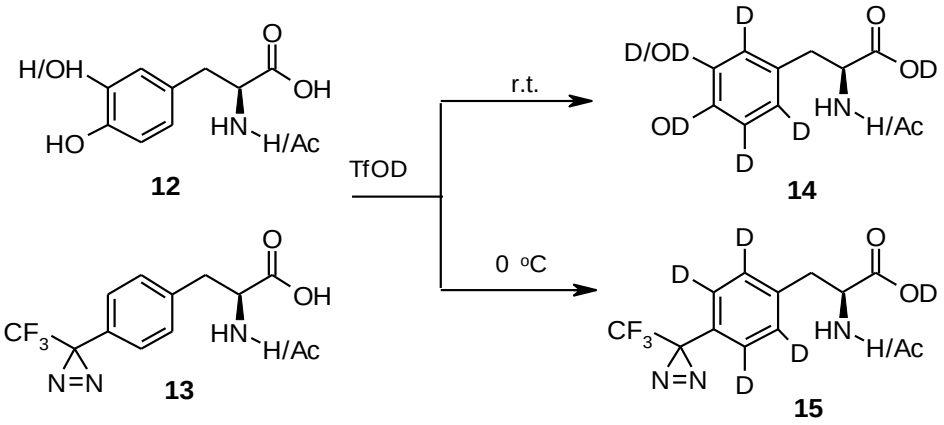

Chen and Yin *et. al*. demonstrated, by Brønsted acid-catalyzed deuteration at the methyl group of N-heteroarylmethanes, the deuteration of complex molecules like tropicamide **17** or papaverine **19**, under mild reaction conditions (*scheme I.7*).[51] Quinolines, pyridines, benzo[d]thiazoles, indoles and imines were all deuterated at the methyl groups with high (>90%D) deuterium incorporation.

Scheme I.7: *Bronsted acid-assisted labeling in benzylic position of heteroarenes.*

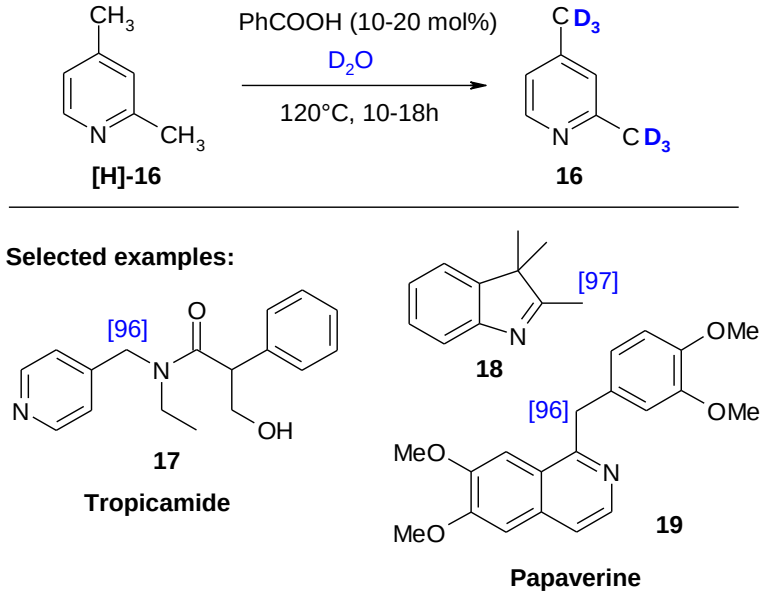

I.5.2. Hydrogen isotope exchange base-mediated labelling

A convenient way to synthesize deuterium labeled amines and nitrogen-containing heterocycles was reported by Zhang and Yan *et al.* (*scheme I.8*).[52] They used KOtBu and [D_6]DMSO and postulated a free radical deuteration mechanism initiated by deprotonation of [D_6]DMSO. With this method, exceptionally high deuterium incorporations of up to 99%D in the benzylic positions (**20-22**) have been observed. However, in some examples (e.g. **23**, **26**, *scheme I.8*) exchange was also seen at C(sp^2)-carbons.

Scheme I.8: *Base-mediated labeling of benzylamines*

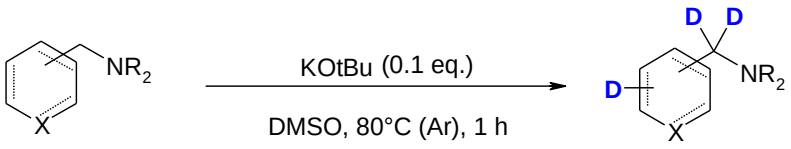

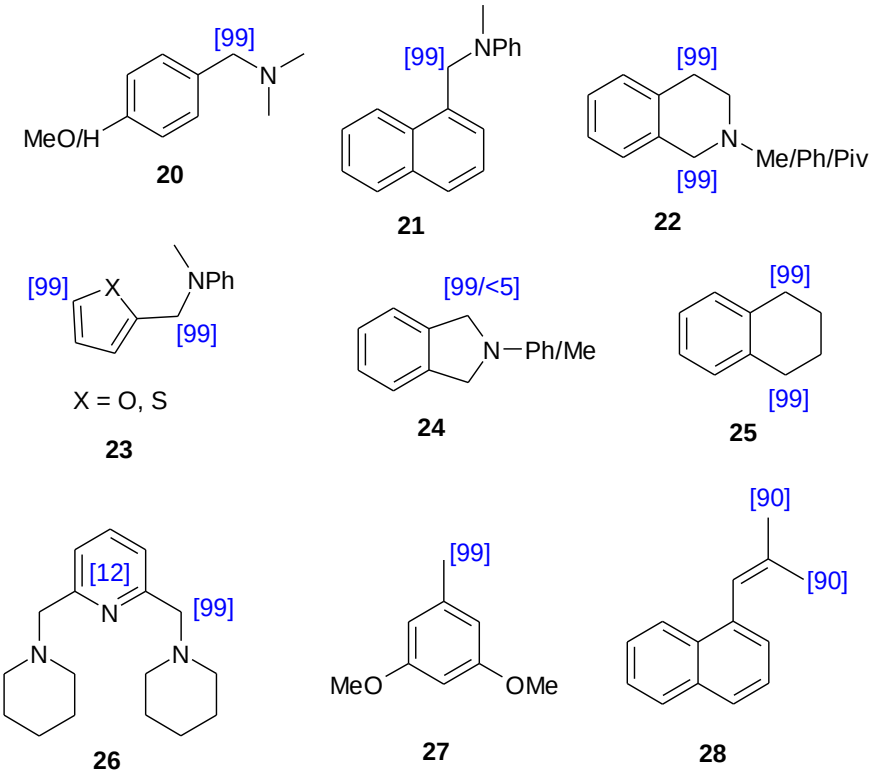

Xie and Chen *et al.* developed a highly effective method using NaOH as a catalyst and D_2O as the deuterium source under microwave irradiation at 180 °C (*scheme I.9*).[53] High degrees of both, regioselectivity and deuterium incorporation, for the *ortho*- and/or *para*-hydrogens relative to the oxygen atom was achieved. The method showed a relatively high functional

group tolerance and allowed the deuteration of complex pharmaceutically interesting substrates, such as Desvenlafaxine **34**.

Scheme I.9: *Base-medated HIE with Phenols*

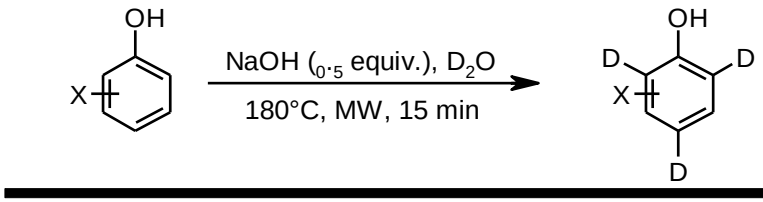

Selected Examples:

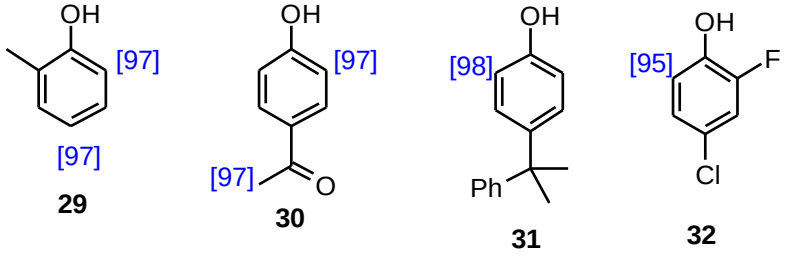

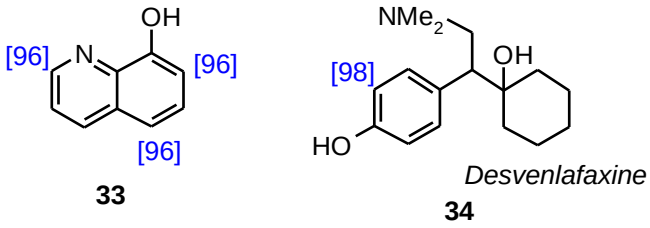

Finally, it can be summarized that the field of acid/base-catalyzed H/D exchange is slowly progressing with some very convenient new approaches and methods emerging.

I.5.3. Hydrogen isotope exchange with heterogeneous metal catalysis

One of the technical advantages of heterogeneous catalysis is the possibility to remove the catalyst by simple filtration on reaction completion. Moreover, in exchange processes that occur without side reactions or decomposition, no further purification step is necessary. Catalysts are also often more stable and much less expensive than homogeneous catalysts. However, due to the generally low levels of selectivity there is always the possibility of unwanted dehalogenation, hydrogenation, hydrolysis, or, under more harsh conditions, racemization. High catalytic activity for H/D exchange by heterogeneous approaches has been found with palladium, platinum, rhodium, nickel, cobalt, and, more recently, ruthenium catalysts. On the other hand, no particular exchange activity has been observed in heterogeneous reaction procedures with either iridium or iron, which are used with

success in homogeneous catalysis (see next section). Regarding the isotope source, gaseous deuterium or tritium, deuterium- or tritium-oxide, and deuterated protic solvents that transfer their labile deuterium to the substrate have all been used as isotopic hydrogen sources.[Error! Bookmark not defined.,Error! Bookmark not defined.] A selection of the most recent method developments and trends of heterogeneously catalyzed HIE reactions is described below.

I.5.3.a) Transition metal-catalyzed HIE reactions

Palladium is amongst the most common transition metals applied in C–H functionalization, and there are many recent applications of such heterogeneously catalyzed HIE reactions reported.[8e,54,55,56,57,58,59,60] In principle, Pd/C is one of the most widely used heterogeneous catalyst in organic synthesis, as typically applied in hydrogenation reactions. Many different catalyst variations are commercially available, generating a complex portfolio of hydrogenation reactivity measured in turn-over-numbers of different model reactions. Pd/C has also proven its usefulness in HIE reactions.

Pd/C has been widely applied to introduce tritium into molecules.[15,58,59] In addition to palladium, platinum also plays an appreciable role in heterogeneous catalyzed HIE reactions. Platinum has especially proven to be very efficient for aromatic C–H positions, with much higher deuterium incorporation compared to aliphatic C–H positions. Recently, a method for deuteration of several arenes under Pt/C-^{i}PrOH-D_2O conditions was reported (*scheme I.10*). Remarkably, the activation of the metal surface was performed by *in situ* generated hydrogen/deuterium through transfer hydrogenation from *iso*-propanol. This developed external hydrogen gas-free method could, therefore, be used on process scale or for substrates where undesired Pt/H_2-reductions were otherwise likely.[61]

Scheme I.10: *Global deuteration using Pt/C*

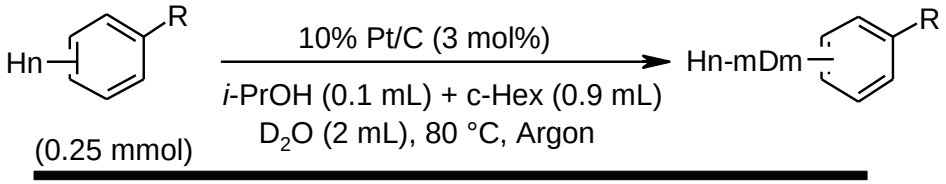

Selected Examples:

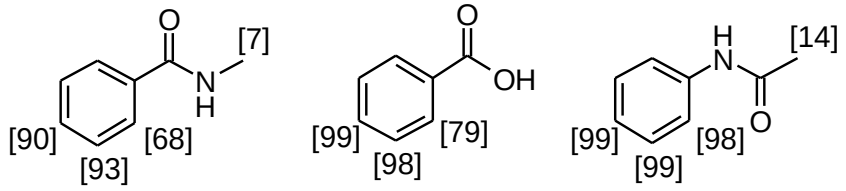

35 **36** **37**

One of the major improvements in this general field over the past 10 years has been the application of ruthenium in the heterogeneous catalyzed HIE reaction. While ruthenium catalysts have been used in selective homogeneous HIE reactions for many years,

heterogeneous ruthenium catalysts on support have been neglected. In a first example, a regioselective deuteration of carbinol carbons (**38-40**, *scheme I.11*) was achieved by the combination of ruthenium on carbon (Ru/C), hydrogen gas, and deuterium oxide (D_2O). The reaction proceeded with high deuterium efficiency and regioselectivity at the α-position relative to the hydroxy unit, with hydrogen exchange of either one deuterium atom for secondary alcohols or two deuterium atoms for primary alcohols, respectively.

Scheme I.11: *Heterogeneous Ru-catalyzed α-deuteration of alcohols*

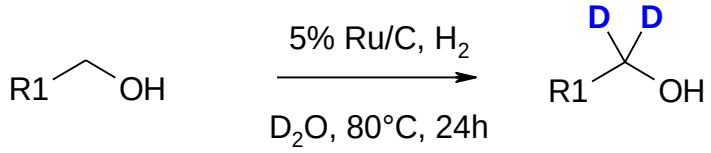

R1 = alkyl, branched alkyl, cyclohexyl

6 examples, D-content 81-100 %, 78-100% yield

Selected examples:

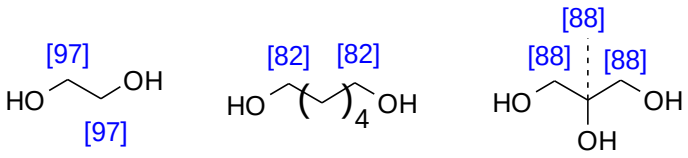

38 **39** **40**

I.5.3.b) HIE reactions with catalyst mixtures

In 2006, Sajiki *et al.* made the first report of a synergistic effect when using catalyst mixtures of Pd/C and Pt/C for H/D exchange reactions (Pd-Pt-D_2O-H_2).[62] Since then this principle has been demonstrated successfully on several occasions (scheme I.12).

Scheme I.12: *Synergic Pd/Pt-catalyzed HIE with bisanilines*

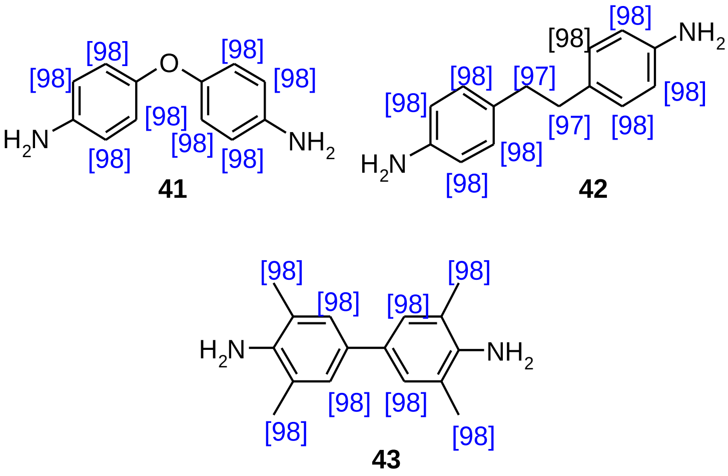

Conditions: 10% Pd/C, 5% Pt/C, D_2O, H_2, 180 °C, 24 h

In a specific example, Pd/C and Pt/C catalyst mixtures revealed an almost quantitative deuteration of a number of bisanilines (**41-43**). With this method, benzylic and aromatic positions were deuterated very effectively (*scheme I.12*).[63]

In another example reported by Derdau and Atzrodt, the synergistic effect was proven after $NaBD_4$-activation of the catalyst mixture resulting in significantly higher deuterium incorporations compared to those obtained with the single catalysts induced H/D exchange of heterocycles (*scheme I.13*).[64] More specifically, a significant synergistic effect could be observed for quinoline-2-carboxylic acid **44**, aminonaphthalene **45**, and 5-amino-benzothiophene **46**. For 8-methylquinoline **47**, an almost complete deuteration was achieved with the Pd/Pt/C catalyst mixture and, in contrast to Pd/C alone, a representative mass peak at M+9 could also be identified and, thus, the material could be used as precursor for internal MS standard preparation.

Scheme I.13: *Synergistic effect in the $NaBD_4$ activated microwave-induced H/D exchange.*

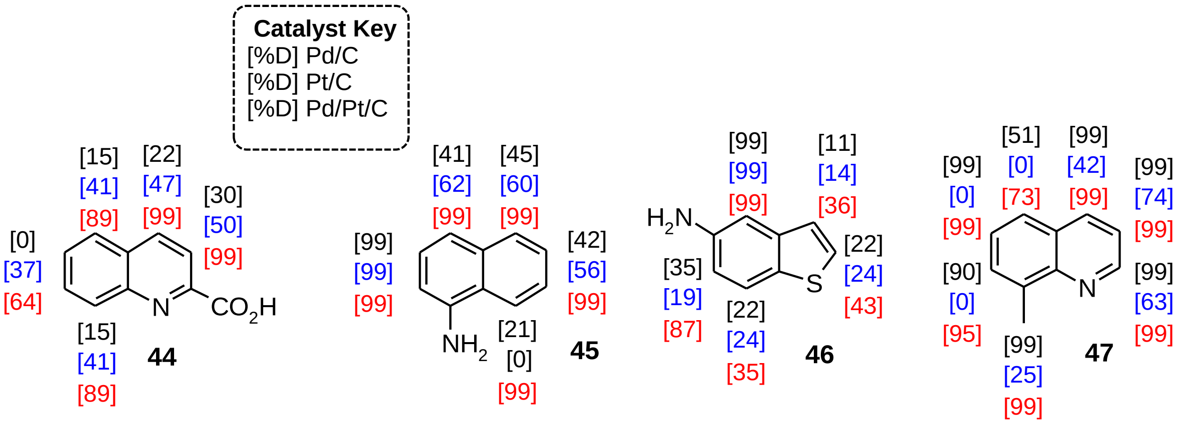

I.5.3.c) HIE reactions with nanoparticles

Another cutting-edge catalyst application is the use of nanoparticles.[65] These heterogeneous particles are fully dispersed in an aqueous or organic solvent and invisible to the human eye, and may be considered homogeneous in contrast with heterogeneous catalysts which are made of metal nanoparticles supported on an inorganic matrix. Therefore, the critical reaction parameter continues to be the surface of the activated catalyst with an exceptionally huge surface/volume ratio.

Nevertheless, nanoparticles have shown very interesting reactivities and selectivities in a number of HIE reactions. For example, Pieters *et al.* reported an efficient H/D exchange in the presence of ruthenium nanoparticles of pyridines, quinolines, indoles, and alkyl amines allowing selective deuteration α to the nitrogen atom position (**48→49**, *scheme I.14*). At stereogenic centers the reaction proceeded under full retention of stereo information.[18] Under the described reaction conditions there was no difference in reported C(sp^2)- or C(sp^3)-labeling selectivity as long as a stereoscopic proximity to a nitrogen atom was present.

Scheme I.14: *Ru-nanoparticle-mediated HIE of amines.*

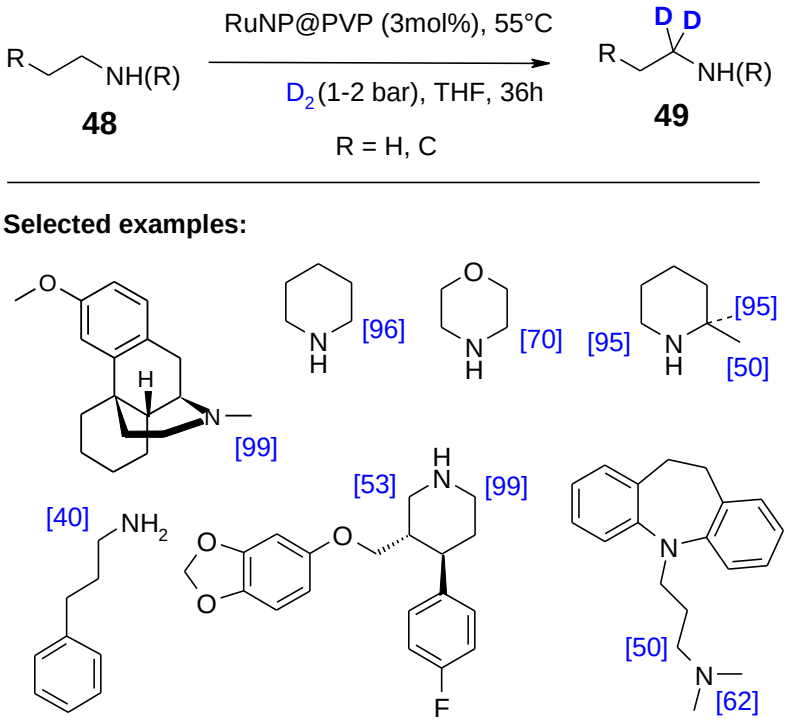

The same Ru nanoparticles were applied in the selective deuteration of amino acids and peptides (**50→51**, *scheme I.15*).[66] An enantiospecific CH-activation reaction followed by deuterium incorporation at stereogenic centers was demonstrated. Deeper insights into the mechanism of the process suggested that the key intermediate is probably a four membered dimetallacycle which is triggering the selectivity in the HIE reaction for the α-position of the

directing heteroatom. These results clearly demonstrate the potential of nanoparticles for the effective catalysis of CH bond activation and pave the way for new enantiospecific CH-functionalization reactions.

Scheme I.15: *Ru-nanoparticle-mediated HIE of amino acids and small peptides.*

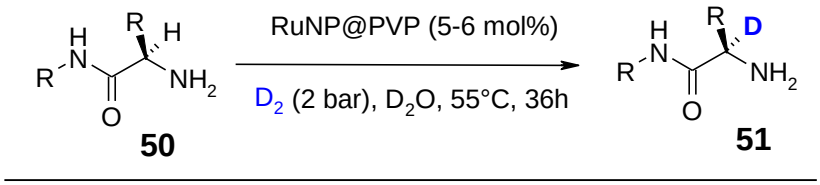

Selected examples:

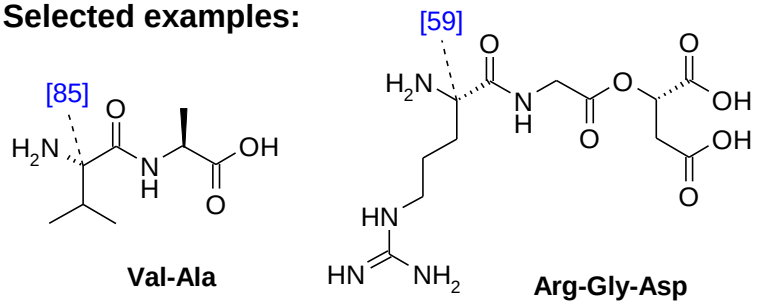

Val-Ala **Arg-Gly-Asp**

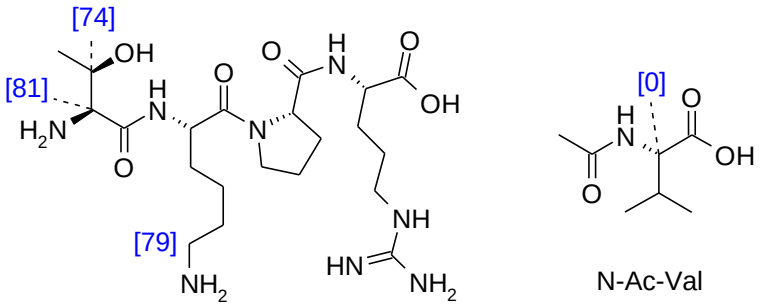

Thr-Lys-Pro-Arg

Generally, the applications of nanoparticles show different reactivity or selectivity compared to the already known homogeneous or heterogeneous HIE reaction systems. It is, therefore, anticipated that advances in material science will also enrich the armory of HIE reaction methods in the future.

Currently known techniques for heterogeneous labeling with deuterium/tritium atoms use the following representative combinations of catalyst and hydrogen isotope sources: Pd/C–D_2 or Pd/C–T_2, Pd/C–(H_2/D_2)-D_2O(DCl), Pd/C-Et_3SiD-*i*PrOH-D_8, Pd/C(en)-D_2, Pd/PVP-D_2, Pt/C–D_2, PtO_2–D_2–D_2O, Rh/C, or Rh black-D_2, Ru/C–D_2, and, more rarely, cobalt or nickel metal. Generally, significant improvements have been made by applying the synergistic effect of catalyst mixtures to deliver higher deuterium contents. As a new and emerging field, nanoparticles are promising for further improvements in deuteration efficiency and selectivity.

I.5.4. Hydrogen isotope exchange with homogeneous metal catalysis

Homogeneous catalysts generally constitute a transition metal core and different surrounding organic ligands. As these can be conveniently modified the catalytic properties of the catalyst can be tuned easily. Furthermore, homogeneous catalysis can be performed under very mild, widely applicable reaction conditions. Therefore, parallel to advances in pH-mediated HIE and heterogeneous catalysis, the homogeneous catalysed HIE reaction dominates modern isotope labelling.[67] Interestingly, mostly iridium and ruthenium catalysts have been studied in HIE reactions in the past. While iridium catalysts (see **1.6**) have been known for many years to catalyse HIE reactions at aromatic positions, the field of iridium catalysed aliphatic HIE applications stayed a rather orphaned field of research. However, very successful homogeneous catalysed deuteration protocols with ruthenium catalysts have been reported since 2012.

Beller *et. al.* were able to exploit the bimetal containing Shvo catalyst,[68] **52**, in the α,β-deuteration of complex tertiary amines (*scheme I.16*).[69] Above 120°C the Shvo catalyst dimer breaks down into two distinct, catalytically active monomers: one the dehydrogenated form **53**, and the other the hydrogenated form **54.** It was proposed that both species are involved in the catalytic cycle of the reaction of **55** to **56** using deuterated *iso*-propanol (IPA-d_8) as the isotope source. This method was applied to several different drug molecules, including lidocaine **57** and metoclopramide **58**.

Scheme I.16: *Ru-catalyzed α,β-deuteration of biologically-relevant amines*

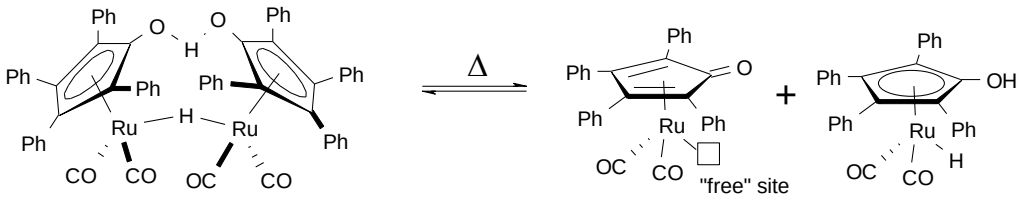

Shvo catalyst 52 **53** **54**

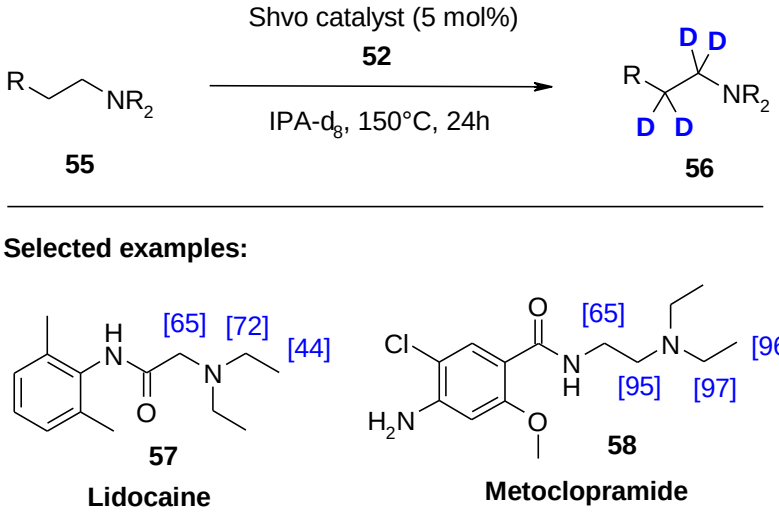

Schnürch *et. al*. reported in 2012 the regioselective deuteration of *N*-heterocycles using the $Ru_3(CO)_{12}$ and ^tBuOD as the deuterium source (*scheme I.17*).[70] In some substrates, deuteration occurred at aromatic and benzylic positions, postulated to react via a nitrogen coordination directed intermediate **61**, favoring the C(sp^3)-carbon for H/D exchange when both were available.

Scheme I.17: *Ru-catalyzed directed HIE with N-heterocycles*

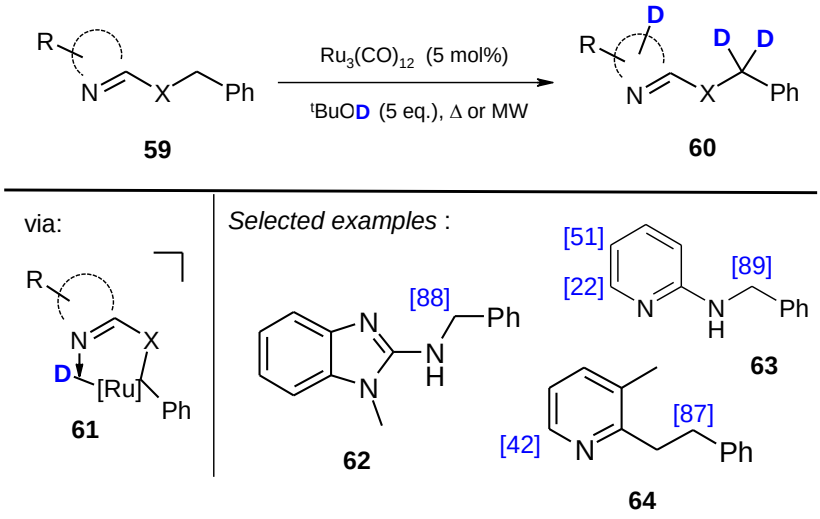

In 2017, MacMillan and Hesk *et al.* reported the first example of direct installation of tritium at α-amino C(sp^3)-H bonds, utilizing a photo redox-mediated (catalyst **67**) hydrogen atom transfer (HAT) protocol with D_2O/T_2O as isotope source (*scheme I.18*). [38]

Scheme I.18: *Photo redox-mediated hydrogen isotope exchange with D_2O/T_2O*

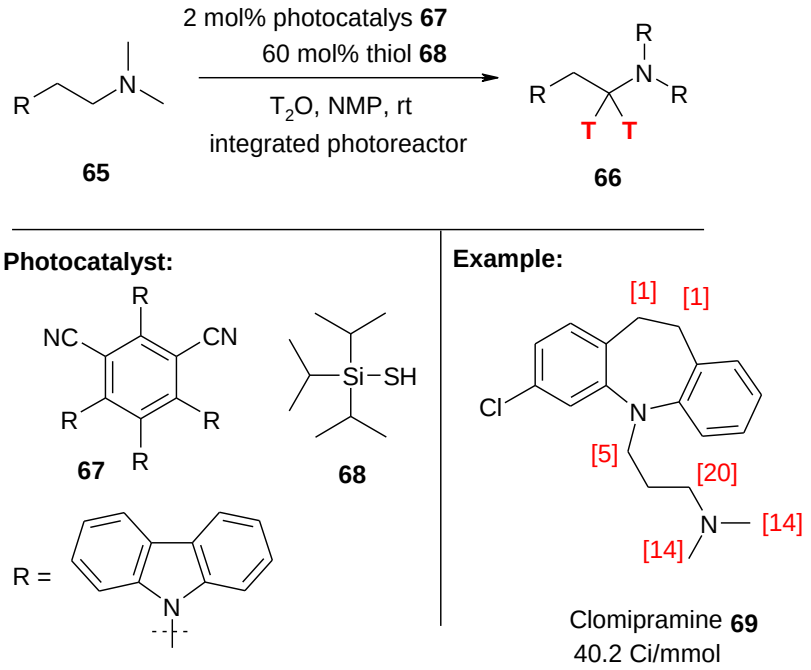

While the underlying mechanism is complex due to the photochemical activation and the following redox process, the observed exchange regioselectivities and deuterium/tritium values were remarkably high. However, a more preferred tritium source is tritium gas as it is both less toxic than T_2O, routinely handled with modern manifold systems and higher specific activities can be more easily achieved.[71]

Homogeneous metal-catalyzed HIE dominates current efforts to achieve labeling in complex molecules by late-stage C–H functionalization. Indeed, a broad range of directing groups and functionalities are now amenable to these selective labeling methods, and often by more than one class of catalyst or metal. Associated with this, the most attractive methods remain those where conditions are mild and most practicable, and where catalysts are readily handled within routine preparative reaction protocols. Accordingly, as researchers strive to establish more advanced methods, air and moisture stable techniques for broad adoption should be the target of future developments in the field. For directed labeling techniques, broadening the drug-like functionalities that can be used as directing groups should remain an additional and prominent focus. Among all transition metals employed in homogeneous HIE methods, iridium is arguably the most widely studied.

I.6. Directed iridium-catalyzed HIE reactions

Scheme I.19: *Homogeneous iridium(I) catalysts*

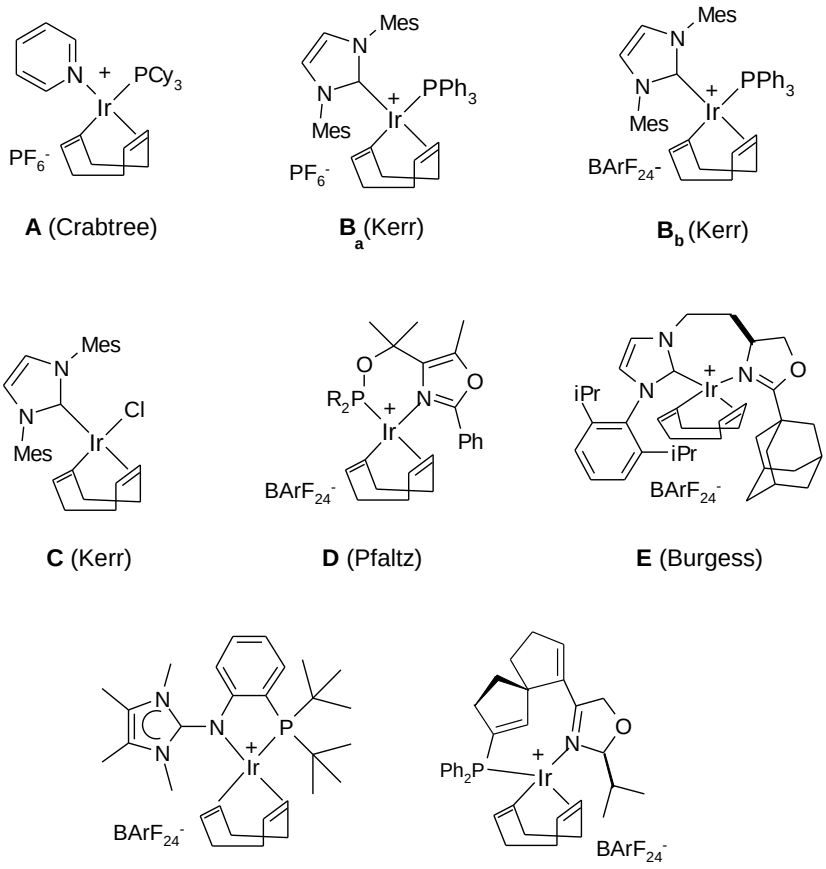

A (Crabtree) **B$_a$** (Kerr) **B$_b$** (Kerr)

C (Kerr) **D** (Pfaltz) **E** (Burgess)

F (Tamm) **G** (Ding), Spinphox

Iridium catalysts have been notably successful in the chemoselective and enantioselective hydrogenation of C-N and non-functionalized C-C bonds, and are a significant alternative to asymmetric hydrogenation reactions catalysed with rhodium- or ruthenium–complexes.[33] Due to the increasing significance of the HIE reactions, there are recently published methods utilizing metals like iron[72], cobalt[73] or ruthenium[74,75,76] which were optimized for this reaction type. However, the state-of-the-art-procedure for HIE reactions remains dominated by iridium catalysts such as those explored by Crabtree **A**[77,78], Kerr **B$_a$** (counter anion PF_6-), **B$_b$** (counter anion $BArF_{24}$-) and **C** (chlorine instead of PPh_3),[79,80] Pfaltz **D**[81], Burgess **E**[82], Tamm **F**[83] or Ding **G**[84] (*scheme I.19)*. Most of these catalysts are commercially available and are nowadays applied regularly in HIE reactions within industry laboratories.[33]

The iridium catalyst by coordinating to a directing group (DG) followed by a CH-functionalization process is able to catalyze the exchange of the hydrogen with its isotopes, deuterium or tritium. In the aromatic HIE reactions on sp^2-carbons the two ortho-positions of the DG are affected, while in the directed aliphatic exchange only the two hydrogens at one sp^3-carbon are exchanged (*scheme I.20*). In both cases, the general isotope source is deuterium or tritium gas. While reaction types look quite similar, the activation energies and

geometries in the transition states of the HIE reaction are quite different and are catalyst-dependent which will be outlined and explored in the later chapters of the thesis.

Scheme I.20: *Principle of directed-iridium catalysed HIE reaction*

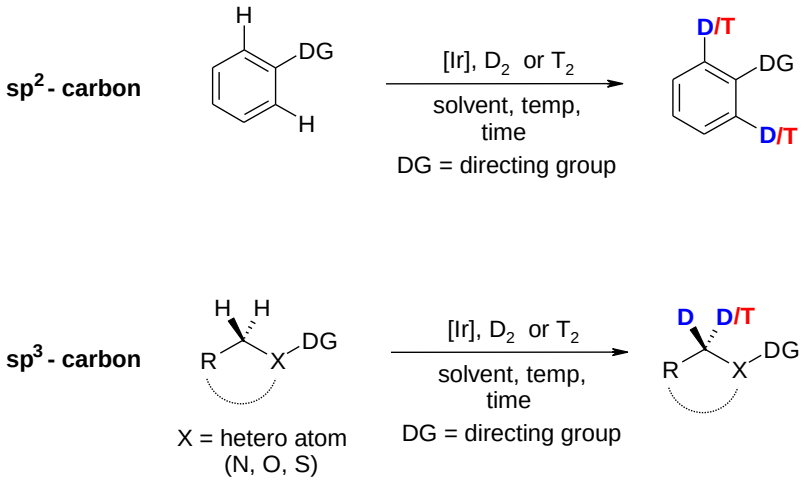

The first mechanism proposal of the iridium-catalyzed HIE reaction was done by Heys *et al*. in 1996,[85] and further improved by Kerr *et al*. in 2014.[79c] Following the exposure to deuterium gas, the iridium complex $\mathbf{B_a}$ loses the hydrogenated COD ligand as D_4-cyclooctane (*scheme I.21*). The resulting Ir specie needs to be stabilized by coordination of the substrate as the Ir is coordinately unsaturated. In this example, the substrate **70** is coordinating to the Ir catalyst and delivers to **71**. Next, the metal inserts into the CH-bond by a sigma-complex assisted metathesis process, and the hydrogen atom is bound in the coordination sphere of the iridium(I) metal (oxidative addition, **72a**). In the following step, there are several equilibria wherein H-D and D-D bonds are broken in the ligand sphere of the iridium metal, and in equilibrium with the gaseous deuterium atmosphere (**72a**↔**72b**). When the deuterium atom from the Ir complex is inserting into the Ir-C bond, the H/D exchange occurs (**72c**). Finally, the product **73** is eliminated from the iridium complex by reductive elimination.

Scheme I.21: *Proposed mechanism of directed-iridium catalysed HIE reaction*

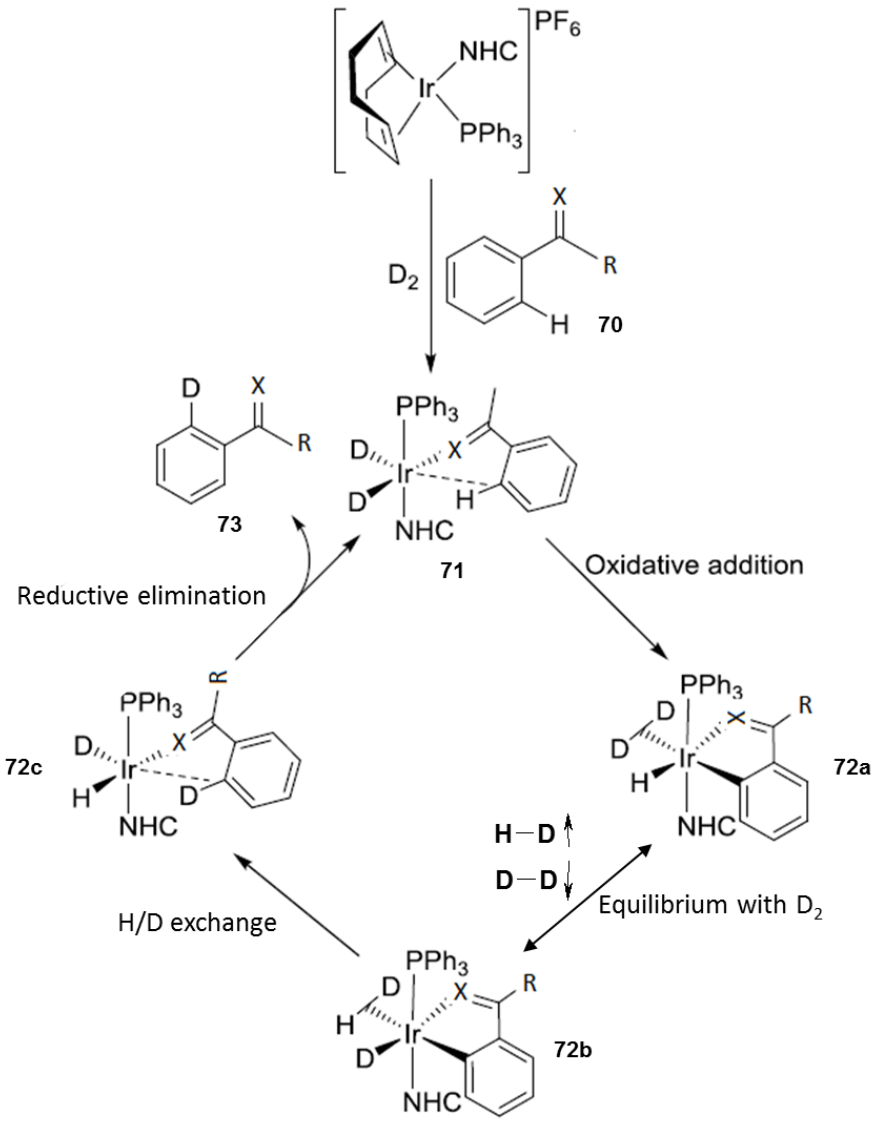

A broad range of directing groups and functionalities are now described for these selective labeling methods, and often by more than one class of catalyst. Accordingly, air and moisture stable catalysts should be the target of future developments in the field. Also, broadening the chemical functionalities usable as directing groups should remain an additional and prominent focus, in particular for functional groups frequently found in drug molecules.[33]

HIE on carbon-sp^2 centers are already for some cases described in the literature, using Kerr catalyst $\mathbf{B_a}$ and providing a broad range of functionalities employable for the exchange, like ketones **74**, esters **75**, amides **76** or **77**, acetanilide **78**, nitro **79** and heterocycles **80-83** (*scheme I.22*).[86] More challenging, there were some examples of primary sulfonamides **84**

catalyzed by chloro-Kerr catalyst **C**,[87] and only one example of secondary sulfonamide **85** catalyzed by Pfaltz catalyst **D**.[88]

Scheme I.22: *Scope of directing groups described in C(sp²)-H Iridium catalysed ortho-directed HIE*

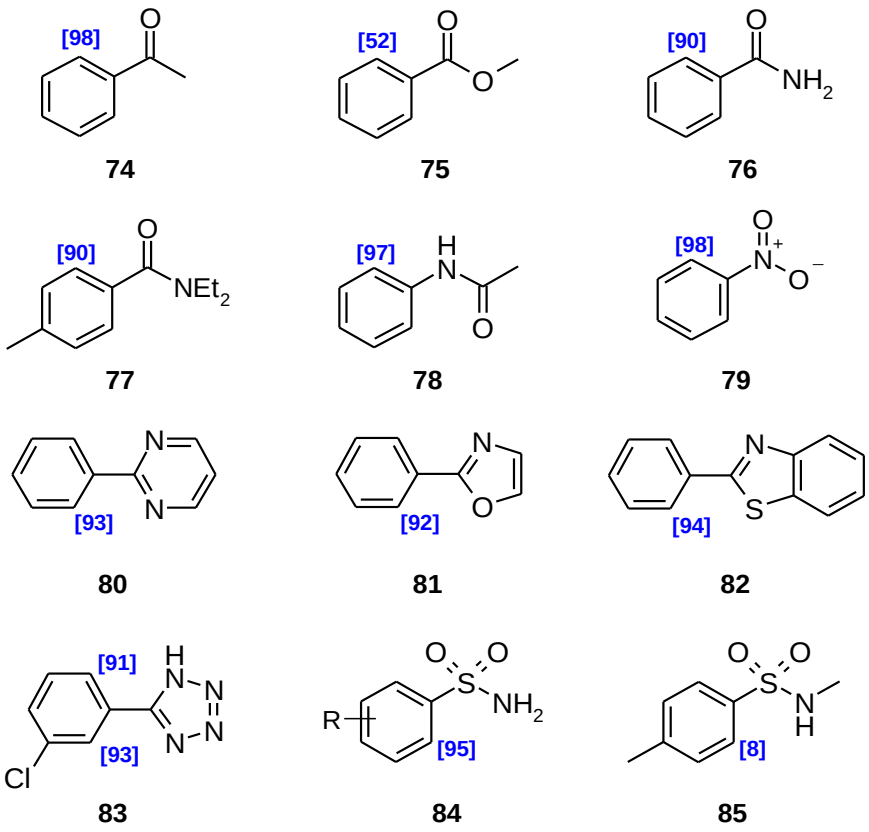

Some applications on carbon-sp³ centers are also described even with tritium labelling on more complex structures like **86**, **87** and **88** (*scheme I.23*).[33]

Scheme I.23: *C(sp³)-H Iridium catalysed HIE on complex structures*

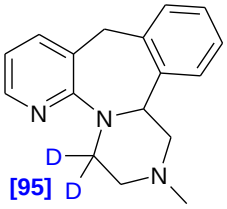

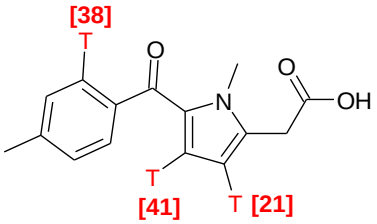

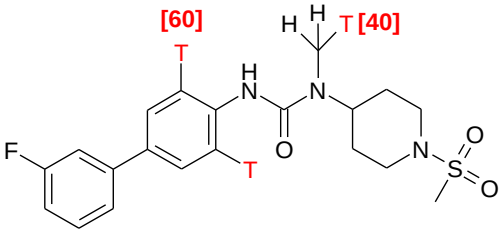

Mirtazapine **86** **87** **88**

Nevertheless, some key functionalities present in drug compounds are still not applicable for known HIE reactions, or the conditions are not fulfilling the requirements of the tritium chemistry. Furthermore, sometimes the labelling positions are not metabolically or chemically stable or the obtained specific activity is not suitable for the followed biological experiment and request other positions of the molecule to be radiolabelled.

I.7. CH functionalization

Generally, the overall process CH functionalization can be understood as catalytic replacement of a C–H bond (mainly by transition metals) followed by a substitution either by carbon, halogen, oxygen or nitrogen atoms, or hydrogen isotopes (*scheme I.24*). Therefore, the HIE reaction can be considered as the most fundamental of all CH functionalization processes. The catalytic activation of C–H bonds has been in the spotlight of research for several decades.[89,90] There are numerous investigations on CH functionalization towards C–C,[91] C–X,[92] C–N,[93] or C–O[94] bond formation, wherein in some cases also HIE reactions were studied to get insights into the mechanism. Nevertheless, it should be stated that there is a strong connection between the HIE reaction and CH functionalization reactions to form C-C, C-N or C-X bonds.

Scheme I.24: *A principle method of CH functionalization to form C-D/T or C-X (C, N, O) bonds.*

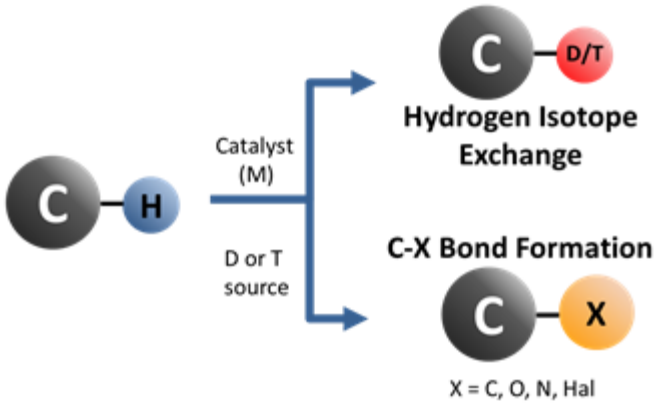

Consequently, CH activation, in the broad context of late stage functionalization, has become a strong tool in lead optimization of bioactive molecules in the life science academia and industry.[95]

I.8. Objectives of the thesis

The objective of this PhD thesis is to develop efficient, selective, fast and safe methods for the labelling of pharmaceutical relevant molecules by HIE applying iridium catalysis. Even though there has been a renaissance in HIE method development in the last ten years, there are still some synthetic challenges which involve both biological and small molecules. In the biologicals field particularly the labelling of compound classes such as peptides, proteins and sugars proved to be highly challenging. In spite of recent progress, known methods for directed aromatic *ortho*-selective HIE reactions usually do not give reasonable incorporation levels for some specific molecule classes such as sulphonamides (e.g. sildenafil **89**), phenylacetic acid derivatives (e.g. diclofenac **90**), amino acids (e.g. lisinopril diester **91**), alkaloids (e.g. DM4 **92**), anilines (e.g. volixibat pharmacophore **93**), which is why the HIE labelling of these drugs still poses significant challenges.

Scheme I.25: Challenging drug structures

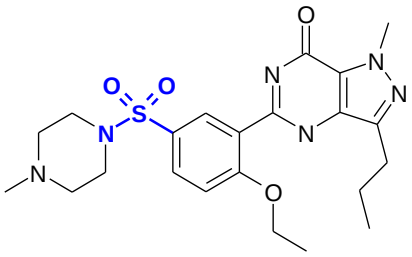

Sildenafil **89**

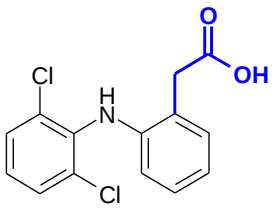

Diclofenac **90**

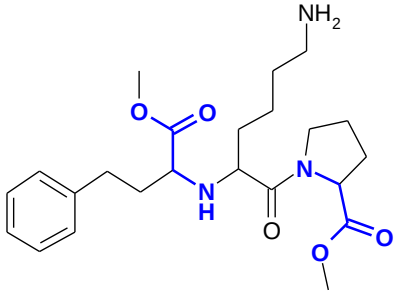

Lisinopril (diester) **91**

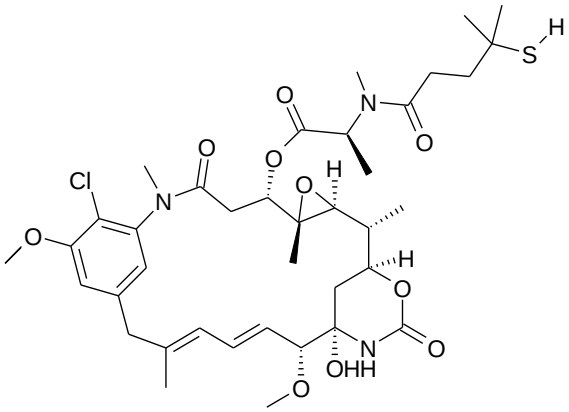

DM4 **92**

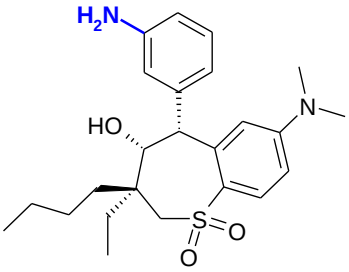

Volixibat pharmacophore
93

These methods should allow the direct deuteration or tritiation of the desired target molecule, at a selective and hopefully metabolically stable position in a single reaction step. Deuterated compounds with a high deuterium content at a specific position are especially interesting from the perspective of deuterated drugs, where the metabolism at one specific position should be blocked or at least minimized. For tritiations, the reaction conditions and results have to comply with specific requirements:

I. 0.5-2.0 tritium atoms added into the target molecule
II. 5-20 mol% catalyst
III. Room temperature (if possible)
IV. Reduced pressure of tritium gas T_2 (50-200 mbar, 1-3 Ci T_2 gas)
V. Can be used safely on the tritium manifold
VI. Safe waste management: easy and safe workup without volatile radioactive side-products

These specifications allow on the one hand to generate radioactive material which fulfils the requirements for the prior discussed biological experiments, like protein binding, QWBA studies or RIA assays, on the other hand allow the safe and efficient supply of these compounds in a cost- and resource-driven industry environment.

We intended to develop new methods by using deuterium (1 atmosphere). As a stable isotope, deuterium can be handled under standard laboratory conditions without special

permissions, handling licenses, or radiation safety measures. We were particularly interested to get the deuterated molecules and to test them later in biologic assays or in hepatocyte metabolism studies. Furthermore, we wanted to select the catalysts and procedures based on the list of specifications compatible with tritium labelling (see above).

However, due to the high kinetic isotope effect H > D > T and the necessary reduced pressure it was planned to add a final adaption of every optimized deuteration method to a tritium application. Furthermore we were interested to get more insights in the parameters driving selectivity and reactivity of HIE reactions with complex structures, which occurs for most drug compounds.

In the first project of the PhD it was envisioned to study sulphonamides (e.g. sildenafil **89**, *scheme I.25*) which are still a challenging DG for HIE. This project should also include two other not reported DG in this context: phosphonamides and N-oxides (**Part II-Chapter 1**).

The following chapter will be devoted to an old challenge in HIE which are the phenylacetic acid derivatives often present in drug compounds, like diclofenac **90** (*scheme I.25*), and still not available as a DG in mild and easy to handle conditions (**Part II-Chapter 2**).

In the third part, we want to look experimentally and theoretically at the influence of the reaction condition parameters on the selectivity and reactivity of HIE reactions (**Part III-Chapter 1 and 2**).

The fourth part of the manuscript will be focusing on HIE on carbon-C(sp^3) centers, describing a new method for the labelling of amino acids and small peptides (e.g. lisinopril diester **91** , this being included in an Antibody-Drug-Conjugate (ADC) Sanofi project involving DM4 **92** (**Part IV**).

As this previous parts were describing only homogeneous iridium catalysis, we will present in the fifth part a heterogeneous iridium catalysis method using newly reported iridium nanoparticles, applied in HIE on anilines such as Volixibat pharmacophore **93** (**Part V**).

Finally we will conclude this PhD work and have a look on our future prospects and perspectives (**Part VI**).

As working in a strong scientific network is one of the major parameters in a ITN European Scholarship network, parts of this work should be done in collaboration with other groups and universities. It was planned to collaborate especially with the group of Prof Bruno Chaudret (INSA, Toulouse, France) and Dr. Gregory Pieters (CEA Saclay, Paris, France) on nanoparticle development. Furthermore, a collaboration with the University of Braunschweig and Prof. Matthias Tamm was envisioned to elaborate homogeneous iridium catalysis.

[1] M. Abou-Gharbia and W. E. Childers, *J. Med. Chem.* **2014**, *57*, 5525-5553.

[2] Hay M *et al. Nature Biotechnol.* **2014**, *32*, 40-51.

[3] C. Dugave, ISOTOPICS (Isotopic labelling for drug innovation)-ETN .

[4] Scannell J W *et al. Nature Rev. Drug Discov.* **2012**, *11*, 191.

[5] Asher Mullard, *Nature Reviews Drug Discovery* **2019**, *18*, 85-89, *doi: 10.1038/d41573-019-00014-x.*

[6] J. Atzrodt, V. Derdau, WJ. Kerr, M. Reid. *Angew. Chem. Int. Ed.* **2018**, *57*, 1758-1784.

[7] R. Voges, R. Heys, T. Moenius, Preparation of Compounds labeled with Tritium and Carbon-14, Wiley **2009**, Chichester, UK.

[8] J. Atzrodt, J. Allen "Synthesis of radiolabelled compounds for clinical studies" in Drug Discovery and Evaluation; Methods in clinical Pharmacology ed. H.-G. Vogel, J. Maas, A. Gebauer, Springer Verlag, Heidelberg **2010**, 105-118.

[9] a) Fact Sheet on Tritium, Radiation Protection Limits, and Drinking Water Standards, U.S. Nuclear Regulatory Commission b) Singh, V. P.; Pai, R. K.; Veerender, D. D.; Vishnu, M. S.; Vijayan, P.; Managanvi, S. S.; Badiger, N. M.; Bhat, H. R. *Radiation Protection Dosimetry*. **2010**, *142*, 153–159.

[10] T. Ratajczyk *et al. Solid State Nuclear Magnetic Resonance*, **2012**, (43–44), 14–21.

[11] a) E. Stovkis, H. Rosing, J.H. Beijnen, Rapid Commun. Mass. Spectrom. 2005, 19, 401-407; b) A.K. Hewavitharana, J. Chromatogr. A 2011, 1218, 359-361.

[12] a) M. Jemal, Y.-Q. Xia, Curr. Drug. Metabolism 2006, 7, 491-502; b) R.H. Liu, D.-L. Lin, W.-T. Chang, C. Liu, W.-I. Tsay, J.-H. Li, T.-L. Kuo, Anal. Chem. 2002, 74, 618A-626A.

[13] F.P. Guengerich, Chem. Res. Toxicol. 2008, 21(1), 70-83.

[14] A. Dudda, G.-U. Kürzel, In Drug Discovery and Evaluation Safety and Pharmacokinetic Assays; H. Vogel, F. Hock; J. Maas, D. Mayer, Eds.; Springer: Berlin, Heidelberg, New York, 2006, pp 151-193.

[15] a) S.D. Nelson, W.F. Trager, Drug Metab. Dispos. 2003, 31(12), 1481-1498; b) F.P. Guengerich, Chem. Res. Toxicol. 2001, 14(6), 611-650; c) G. Chowdhury, M.W. Calcutt, L.D. Nagy, F.P. Geungerich, Biochemistry 2012, 51, 9995-10007.

[16] a) L. Shao, M.C. Hewitt, Drug News Persp. 2010, 23(6), 398-404; b) D.J. Kushner, A. Baker, T.G. Dunstall, Can. J. Physiol. Pharmacol. 1999, 77(2), 79-88.

[17] a) B. Halford, Chem. Eng. News 2016, 94(27), 32-36; b) The Economist 2015, Septmber 5th; c) R.H. Howland, J. Psychosoc. Nurs. Men. 2015, 53(9), 13-16; d) A. Katsnelson, Nat. Med. 2013, 19(6), 656; e) R. Schillerstrom, Drug Disc. Dev. 2009, 12(5), 6-8; f) K. Sanderson, Nature 2009, 458, 269; g-) A.T. Yarnell, Chem. Eng. News 2009, 87(25), 36-39.

[18] R.D. Tung, Future Med. Chem. 2016, 8(5), 491-494.

[19] A. Mullard, Rev. Drug Discov. 2017, 16, 305.

[20] Teva Pharmaceutical Industries Ltd. Press Release 2016, October 20, http://www.tevapharm.com/news

[21] a) Concert Pharmaceuticals Inc Press Release 2014, July 08: http://ir.concertpharma.com/releasedetail.cfm?releaseid=858155. b) L.A. Sabounjian, P. Graham, L.Wu, V. Braman, C. Cheng, J. Liu, J. Shipley, J. Neutel, M Dao, Clin. Pharmacol. Drug Dev. 2016, 5, 1-12. c) V. Braman, P. Graham, C. Cheng, D. Turnquist, M. Harnett, L.A. Sabounjian, J. Shipley, Clin. Pharmacol. Drug Dev. 2013, 2(1), 53-66. d) X. Tanga, G. Bridsonb, J. Kea, L. Wub, H. Erol, P. Grahamb, C.H. Lina, V. Bramanb, H. Zhaoa, J.F. Liub, Z. Lina, C. Cheng, J. Chromatogr. B, 2014, 963, 1-9.

[22] Avanir Pharmacuticals. Inc. Press Release 2015, November 16, http://www.avanir.com/press/

[23] a) http://ir.concertpharma.com/releases.cfm. b)http://investor.auspexpharma.com/releases.cfm.

[24] a) F. Maltais, Y.C. Jung, M. Chen, J. Tanoury, R.B. Perni, N. Mani, L. Laitinen, H. Huang, S. Liao, H. Gao, H. Tsao, E. Block, C. Ma, R.S. Shawgo, C. Town, C.L. Brummel, D. Howe, S. Pazhanisamy, S. Raybuck, M. Namchuk, Y.L. Bennani, J. Med. Chem. 2009, 52, 7993-8001; b) G. Xu, B. Lv, J.Y. Roberge, B. Xu, J. Du, J. Dong, Y. Chen, K. Peng, L. Zhang, X. Tang, Y. Feng, M. Xu, W. Fu, W. Zhang, L. Zhu, Z. Deng, Z. Sheng, A. Welihinda, X. Sun, J. Med. Chem. 2014, 57, 1236-1251; c) F. Schneider, M. Hillgenberg, R. Koytchev, R.G. Alken, Drug Res. 2006, 56, 295-300; d) F. Schneider, E. Mattern-Dogru, M. Hillgenberg, and R.G. Alken, Drug Res. 2007, 57, 293-298.

[25] E. O. Aboagye *et al*., *JNM*, **2014**, *55*, 256-263.

[26] a) E.G. Solon, Chem. Res. Toxicol. 2012, 25, 543-555; c) L. Wang, H. Hong, D. Zhang, Application of quantitative whole body autoradiography (QWBA) in drug discovery and development in ADME. in D. Zhang and S. Surapanemi, Eds. Enabling technologies in drug design and development. J Wiley & Sons Publishers, Hoboken, NJ, 2012, 419-434; d) A.W. Harrell, C. Sychterz, M.Y. Ho, A. Weber, K. Valko, K. Negash, Pharma Res. Per. 2015, 3(5), e00173.

[27] a) N. Penner, L.J. Klunk, C. Prakash, Biopharm. Drug Dispos. 2009, 30, 185-203; b) S.J. Roffey, R.S. Obach, J.I. Gedge, D.A, Smith, Drug Metab. Rev. 2007, 39, 17-43; c) J.H. Beumer, J.H. Beijnen, J.H.M. Schellens, Clin. Pharmacokin. 2006, 45(1), 33-58; d) J.G. Dain, J.M. Collins, W.T. Robinson, Pharm. Res. 1994, 11, 925.

[28] a) S.C. Alley, X. Zhang, N.M. Okeley, J. Pharmacol. Exp. Ther. 2009, 330, 932-938; b) E. Herzog, S. Harris, C. Henson, Thromb. Res. 2014, 133, 900-907.

[29] a) E.G. Solon, Expert Opin. Drug Discov. 2007, 2(4) 503-514; b) A. McEwen, C. Henson, Bioanalysis 2015, 7(5), 557-568; b) M.J. Potchoiba, M.R. Nocerini, Drug. Metab. Dispos. 2004, 32, 1190-1198.

[30] a) P. Hein, M.C. Michel, K. Leineweber, T. Wieland, N. Wettschureck, S. Offermanns, Receptor and binding studies, in: Practical Methods in Cardiovascular Research, S. Dhein, F. Mohr, M. Delmar (Eds.), Springer, Berlin Heidelberg, 2005, 723-783; b) M. McKinney, R. Raddatz, Curr. Prot. Pharmacol. 2006, 33, 1.3.1-1.3.42.

[31] a) T. Bohnert, L.-S. Gan, J. Pharm. Sci. 2013, 102(9), 2953-2994; b) G.L. Trainor, Expert Opin. Drug Discov. 2007, 2(1), 51-64.

[32] B.K. Park, A. Boobis, S. Clarke, C. E. P. Goldring, D. Jones, J. G. Kenna, C. Lambert, H.G. Laverty, D.J. Naisbitt, S. Nelson, D. A. Nicoll-Griffith, R.S. Obach, P. Routledge, D.A. Smith, D.J. Tweedie, N. Vermeulen, D.P. Williams, I.D. Wilson, T.A. Baillie, Nat. Rev. Drug Disc. 2011, 10, 292-306.

[33] J. Atzrodt, V. Derdau, WJ. Kerr, M. Reid. *Angew. Chem. Int. Ed.* **2018**; *57*: 3022-3047.

[34] Radioaktive Isotope des Wasserstoffs, Kohlenstoffs und Iods – strahlende Stecknadeln im Heuhaufen, V. Derdau, Chem. Unserer Zeit 2019, 53, 2-9.

[35] C. G. M. Janssen, J. B. A. Thijssen, W. L. M. Verluyten *J. Label Compd. Radiopharm.* **2003**, *46*, 1117–1125.

[36] S. M. Frederiksen, G. Grue-Sorensen, *J. Label Compd. Radiopharm.* **2003**, *46*, 773-779.

[37] U. Pleiss, *J. Label. Compd. Radiopharm.* **2003**, *46*, 1241-1247.

[38] a) M. Hatano, T. Nishimura, H. Yorimitsu, Org. Lett. 2016, 18(15), 3674–3677; b) W. Bai, K. H. Lee, S. K. S. Tse, K. W. Chan, Z. Lin, G. Jia, Organometallics 2015, 34, 3686-3698; c) S. Ma, G. Villa, P. S. Thuy-Boun, A. Homs, J.-Q. Yu, Angew. Chem. Int. Ed. 2014, 53, 734-737; d); N. Modutlwa, T. Maegawa, Y. Monguchi, H. Sajiki, J. Label. Compd. Radiopharm. 2010, 53, 686-692.

[39] a) D. Hesk, C.F. Lavey, P. McNamara, J. Label. Compd. Radiopharm. 2010, 53, 722-730; b) M.R. Chappelle, C.R. Hawes, J. Label. Compd. Radiopharm. 2010, 53, 745-751; c) C.N. Filer, J. Label. Compd. Radiopharm. 2010, 53, 739-744; d) S.R. Pollack, D.J. Schenk, J. Label Compd. Radiopharm. 2015, 58 433–441; e) V.P. Shevchenko, I.Y. Nagaev, N.F. Myasoedov, J. Label. Compd. Radiopharm. 2010, 53, 693-703.

[40] a) J. Atzrodt, V. Derdau, M. Reid, WJ. Kerr. *Angew. Chem. Int. Ed.* **2018**; *57*: 3022–3047. b) J. Atzrodt, V. Derdau, T. Fey, J. Zimmermann. *Angew. Chem., Int. Ed.* **2007**; *46*: 7744–7765.

[41] For selected reviews, see: a) JR. Heys. *J. Label. Compd. Radiopharm.* **2007**; *50*: 770-778. b) GN. Nilsson, WJ. Kerr. *J. Label. Compd. Radiopharm.* **2010**; *53*: 662-667. c) R. Salter. *J. Label. Compd. Radiopharm.* **2010**; *53*: 645-657. d) PH. Allen, MJ. Hickey, LP. Kingston, DJ. Wilkinson. *J. Label. Compd. Radiopharm.* **2010**; *53*: 731-738. e) J. Atzrodt, V. Derdau. *J. Label. Compd. Radiopharm.* **2010**; *53*: 674-685.

[42] W. J. Kerr, D.M. Lindsay, M. Reid, J. Atzrodt, V. Derdau, P. Rojahn and R. Weck, *Chem Commun*. **2016**, *52*, 6669 - 6672, e) J. Atzrodt, V. Derdau, M. Reid, W. J. Kerr, *Angew. Chem. Int. Ed.* **2018**, *57*, 3022 – 3047

[43] a) L. Zhou, X. Bian, S. Yang, B. Mu, *J. Label. Compd. Radiopharm.* **2012**, *55*, 158-160; b) M. Mackova, M. Himl, L. Minarova, J. Lang, P. Lhotak, *Tetrahedron Lett.* **2011**, *52*, 2543-2546; c) U. Hakala, K. Waehaelae, *J. Org. Chem.* **2007**, *72*, 5817-5819; d) A. Martins, M. Lautens, *Org. Lett.* **2008,** *10*, 4351-4353.

[44] K. Mueller, A. Seubert, Isotopes Environ. Health Stud. 2014, 50, 88-93.

[45] a) S. J. Rozze, M. J. Fray, J. Label. Compd. Radiopharm. 2009, 52, 435-442; b) F. Li, Q. Chen, C.-C. Liu, Y.-H. Wu, X.-P. Liu, G.-F. Yang, Appl. Magn. Reson. 2012, 42, 169-177; c) N. Backstrom, C. I. F. Watt, Tetrahedron Lett. 2009, 50, 3234-3236; d) J. R. Mohrig, N. J. Reiter, R. Kirk, M. R. Zawadski, V.N. Lamarre, J. Am. Chem. Soc. 2011, 133, 5124-5128.

[46] X. Ariza, G. Asins, J. Garcia, F. G. Fausto, K. Makowski, D. Serra, J. Velasco, J. Label. Compd. Radiopharm. 2010, 53, 556-558.

[47] A. Miyazawa, H. Shimodaira, Y. Kawanishi, *Bull. Chem. Soc. Jpn.* **2011**, *84*, 1368-1370.

[48] B. Kerler, J. Pol, K. Hartonen, M. T. Soederstroem, H. T. Koskela, M.-L. Riekkola, J. Supercritical Fluids 2007, 39, 381-388.

[49] L. Wang, Y. Murai, T. Yoshida, M. Okamoto, K. Masuda, Y. Sakihama, Y. Hashidoko, Y. Hatanaka, M. Hashimoto, *Biosci. Biotechnol. Biochem.* **2014**, *78*, 1129-1134.

[50] Y. Murai, L. Wang, K. Masuda, Y. Sakihama,Y. Hashidoko,Y. Hatanaka, M. Hashimoto, Eur. J. Org. Chem. 2013, 5111-5116.

[51] Liu M, Chen X, Chen T, Yin SF. A facile and general acid-catalyzed deuteration at methyl groups of N-heteroarylmethanes. *Org. Biomol. Chem*. **2017**; *15*: 2507.

[52] Y. Hu, L. Liang, W. Wei, X. Sun, X. Zhang, M. Yan, Tetrahedron 2015, 71, 1425-1430.

[53] M. Zhan, R. Xu, Y. Tian, H. Jiang, L. Zhao, Y. Xie, Y. Chen, Eur. J. Org. Chem. 2015, 3370-3373.

[54] H. Esaki, R. Ohtaki, T. Maegawa, Y. Monguchi, H. Sajiki, J. Org. Chem. 2007, 72, 2143-2150.

[55] a) T. Kurita, F. Aoki, T. Mizumoto, T. Maejima, H. Esaki, T. Maegawa, Y. Monguchi, H. Sajiki, Chem. Eur. J. 2008, 14, 3371-3379.

[56] a) V. Derdau, J. Atzrodt, Ger. Offen. (**2007**), **DE 102005056856 A1**; b) V. Derdau, J. Atzrodt, W. Holla, *J. Label. Compd. Radiopharm* **2007**, *50*, 295-299.

[57] J. Kang, A. Vonderheide, V. V. Guliants, *ChemSusChem* **2015**, *8*, 3044-3047.

[58] V. P. Shevchenko, G.A. Badun, I.A. Razzhivina, I.Y.Nagaev, K.V. Shevchenko, N.F. Myasoedov, *Dokl. Phys. Chem.* **2015**, *463*, 182-187.

[59] V. P. Shevchenko, I. A. Razzhivina, M. G. Chernysheva, G.A. Badun, I. Y. Nagaev, K. V. Shevchenko, N. F. Myasoedov, Radiochemistry 2015, 57, 312-320.

[60] T. Kurita, K. Hattori, S. Seki, T. Mizumoto, F. Aoki, Y. Yamada, K. Ikawa, T. Maegawa, Y. Monguchi, H. Sajiki, *Chem. Eur. J.* **2008**, *14*, 664-673.

[61] Y. Sawama, T. Yamada, Y. Yabe, K. Morita, K. Shibata, M. Shigetsura, Y. Monguchi, H. Sajiki, Adv. Synth.Catal. 2013, 355, 1529-1534.

[62] H. Esaki, R. Ohtaki, T. Maegawa, T. Monguchi, H. Sajiki, J. Org. Chem. 2007, 72, 2143-2150.

[63] N. Ito, T. Watahaki, T. Maesawa, T. Maegawa, H. Sajiki, Synthesis 2008, 1467-1478.

[64] V. Derdau, J. Atzrodt, J. Zimmermann, C. Kroll, F. Brückner, Chem. Eur. J. 2009, 15, 10397-10404.

[65] For review on particles, see: a) Nanoparticles and Catalysis (Volume 1) edited by D. Astruc, Wiley-VCH, **2008**, Weinheim. b) The Nano-Micro Interface: Bridging the Micro and Nano Worlds edited by M. Van de Voorde, M. Werner, H.-J. Fecht; Wiley-VCH, **2015**, Weinheim.

[66] Taglang C, Martinez-Prieto LM, Del Rosal I, Maron L, Poteau R, Philippot K, Chaudret B, Perato S, Sam Lone A, Puente C, Dugave C, Rousseau B, Pieters G. Enantiospecific C-H Activation Using Ruthenium Nanocatalysts. *Angew. Chem., Int. Ed.* **2015**; *54*: 10474-10477.

[67] a) Lockley WJS, Hesk D. Rhodium- and ruthenium-catalysed hydrogen isotope exchange. *J. Label. Compd. Radiopharm.* **2010**; *53*: 704-715. b) Nilsson GN, Kerr WJ. The development and use of novel iridium complexes as catalysts for *ortho*-directed hydrogen isotope exchange reactions. *J. Label. Compd. Radiopharm.* **2010**; *53*: 662-667. c) Allen PH, Hickey MJ, Kingston LP, Wilkinson DJ. Metal-catalysed isotopic exchange labelling: 30 years of experience in pharmaceutical R&D. *J. Label. Compd. Radiopharm.* **2010**; *53*: 731-738. d) Lockley WJS. Hydrogen isotope labelling using iridium(I) dionates. *J. Label. Compd. Radiopharm.* **2010**; *53*: 668-673. e) Heys JR. Organoiridium complexes for hydrogen isotope exchange Labeling. *J. Label. Compd. Radiopharm.* **2007**; *50*: 770-778. f) Hesk D, McNamara P. Synthesis of isotopically labelled compounds at ScheringPlough, an historical perspective. *J. Label. Compd. Radiopharm.* **2007**; *50*: 875-887.

[68] Conley BL, Pennington-Boggio MK, Boz E, Williams TJ. Discovery, Applications, and Catalytic Mechanisms of Shvo's Catalyst. *Chem. Rev.* **2010**; *110*: 2294-2312.

[69] Neubert L, Michalik D, Bähn S, Imm S, Neumann H, Atzrodt J, Derdau V, Holla W, Beller M. Ruthenium-Catalyzed Selective α,β-Deuteration of Bioactive Amines. *J. Am. Chem. Soc.* **2012**; *134*: 12239-12244.

[70] Gröll B, Schnürch M, Mihovilovic MD. Selective Ru(0)-Catalyzed Deuteration of Electron-Rich and Electron-Poor Nitrogen-Containing Heterocycles. *J. Org. Chem*. **2012**; *77*: 4432-4437.

[71] Yang H, Dormer PG, Rivera NR, Hoover AJ. Palladium(II)-Mediated C-H Tritiation of Complex Pharmaceuticals. *Angew. Chem. Int. Ed.* **2018**; *57:* 1883-1887.

[72] RP. Yu, D. Hesk, N. Rivera, I. Pelczer, PJ. Chirik. *Nature* **2016**; *529*: 195-199.

[73] WN. Palmer, PJ. Chirik. *ACS Catal*. **2017**; *7*: 5674–5678.

[74] L. Neubert, D. Michalik, S. Bähn, S. Imm, H. Neumann, J. Atzrodt, V. Derdau, W. Holla, M. Beller. *J. Am. Chem. Soc.* **2012**; *134*: 12239-12244.

[75] C. Taglang, LM. Martinez-Prieto, I. Del Rosal, L. Maron, R. Poteau, K. Philippot, B. Chaudret, S. Perato, A. Sam Lone, C. Puente, C. Dugave, B. Rousseau, G. Pieters. *Angew. Chem., Int. Ed.* **2015**; *54*: 10474-10477.

[76] L. Gao, S. Perato, S. Garcia-Argote, C. Taglang, LM. Martinez-Prieto, C. Chollet, DA. Buisson, V. Dauvois, P. Lesot, B. Chaudret, B. Rousseau, S. Feuillastre, G. Pieters. *Chem. Commun.* **2018**; *54*: 2986-2989.

[77] RH. Crabtree. *Acc. Chem. Res.* **1979**; *12*: 331-337.

[78] For applications of Crabtree's catalyst in hydrogen isotope exchange see: a) D. Hesk, PR. Das, B. Evans. *J. Labelled Compd. Radiopharm.* **1995**; *36*: 497-502. b) GJ. Ellames, JS. Gibson, JM. Herbert, AH. McNeill. *Tetrahedron* **2001**; *57*: 9487-9497. c) N. Bushby, DA. Killick. *J. Labelled Compd. Radiopharm.* **2007**; *50*: 519-520. d) SC. Schou. *J. Labelled Compd. Radiopharm.* **2009**; *52*: 376-381. e) D. Hesk, CF. Lavey, P. McNamara. *J. Labelled Compd. Radiopharm.* **2010**; *53*: 722-730. f) M. Vliegen, P. Haspeslagh, W. Verluyten. *J. Labelled Compd. Radiopharm.* **2012**; *55*: 155-157.

[79] a) JA. Brown, S. Irvine, AR. Kennedy, WJ. Kerr, S. Andersson, GN. Nilsson. *Chem. Commun.* **2008**; 1115-1117. b) AR. Cochrane, C. Idziak, WJ. Kerr, B. Mondal, LC. Paterson, T. Tuttle, S. Andersson, GN. Nilsson. *Org. Biomol. Chem.* **2014**; *12*: 3598-3603. c) JA. Brown, AR. Cochrane, S. Irvine, WJ. Kerr, B. Mondal, JA. Parkinson, LC. Paterson, M. Reid, T. Tuttle, S. Andersson, GN. Nilsson. *Adv. Synth. Catal.* **2014**; *356*: 3551-3562. d) AR. Kennedy, WJ. Kerr, R. Moir, M. Reid. *Org. Biomol. Chem.* **2014**; *12*: 7927-7931. e). WJ. Kerr, RJ. Mudd, LC. Paterson, JA. Brown. *Chem. Eur. J.* **2014**; *20*: 14604-14607. f) J. Atzrodt, V. Derdau, WJ. Kerr, M. Reid, P. Rojahn, R. Weck. *Tetrahedron* **2015**; *71*: 1924-1929. g) WJ. Kerr, DM. Lindsay, M. Reid, J. Atzrodt, V. Derdau, P. Rojahn, R. Weck. *Chem. Commun.* **2016**; *52*: 6669-6672. h) WJ. Kerr, RJ. Mudd, PK. Owens, M. Reid, JA. Brown, S. Campos. *J. Label. Compd. Radiopharm.* **2016**; *59*: 601-603. i) WJ. Kerr, DM. Lindsay, PK. Owens, M. Reid, T. Tuttle, S. Campos. *ACS Catal.* **2017**; *7*: 7182-7186.

[80] WJ. Kerr, RJ. Mudd, M. Reid, J. Atzrodt, V. Derdau. *ACS Catal*. **2018**; *8*: 11, 10895-10900.

[81] M. Parmentier, Hartung, AT. Pfaltz, D. Muri. *Chem. Eur. J.* **2014**; *20*: 11496-11504.

[82] a) A. Burhop, R. Weck, J. Atzrodt, V. Derdau. *Eur. J. Org. Chem.* **2017**; *11*: 1418–1424. b) A. Burhop, R. Prohaska, R. Weck, J. Atzrodt, V. Derdau. *J. Label. Compd. Radiopharm.* **2017**; *60*: 343-348.

[83] a) K. Jess, V. Derdau, R. Weck, J. Atzrodt, M. Freytag, PG. Jones, M. Tamm. *Adv. Synth. Catal*. **2017**; *359*: 629-638. b) M. Valero, A. Burhop, K. Jess, R. Weck, M. Tamm, J. Atzrodt, V. Derdau. *J. Label. Compd. Radiopharm.* **2018**; *61*: 380-385.

[84] Z. Han, Z. Wang, X. Zhang, K. Ding. *Angew. Chem., Int. Ed.*, **2009**; **48**: 5345-5349. b) please note that to our knowledge this catalyst has never been used in HIE reactions before.

[85] A. Y. L. Shu, W. Chen, J. R. Heys, *J. Organomet. Chem*. **1996**, *524*, 87-93.

[86] a) W. J. Kerr, M. Reid et al. Adv. Synth. Catal. **2014**, *356*, 3551-3562. b) W. J. Kerr, M. Reid, T. Tuttle et al. *Molecules* **2015**, *20*, 11676-11698. c) W. J. Kerr, M. Reid et al. *J. Label Compd. Radiopharm* **2016**, *59,* 601–603. d) J. Atzrodt, V. Derdau, W.J. Kerr, et al. *Tetrahedron* **2015**, *71*, 1924-1924. e) W.J. Kerr, J. Atzrodt, V. Derdau, et al. *Chem. Commun.* **2016**, *52*, 6669-6672.

[87] *ACS Catal.* **2015**, *5*, 402–410.

[88] *Chem. Eur. J.*, **2014**, *20*,11496–11504.

[89] a) J. K. Kim, K. Shin, S. Chang in Topics in Organometallic Chemistry (Eds.: P. H. Dixneuf, H. Doucet), Springer, Cham, 2016; b) C–H Bond Activation in Organic Synthesis, ed. L. J. Jack, CRC Press, Boca Raton, 2015; c) C–H Activation, ed. J.-Q. Yu and Z. Shi, Topics in Current Chemistry, Springer, New York, 2010, vol. 26.

[90] a) T. Cernak, K. D. Dykstra, S. Tyagarajan, P. Vachal, S. W. Krska, Chem. Soc. Rev. 2016, 45, 546–576; b) T. Gensch, M. N. Hopkinson, F. Glorius, J. Wencel-Delord, Chem. Soc. Rev. 2016, 45, 2900-2936; c) C. Borie, L. Ackermann, M. Nechab, Chem. Soc. Rev. 2016, 45, 1368-1386; d) W. Liu, L. Ackermann, ACS Catal. 2016, 6, 3743-3752; e) Y. Segawa, T. Maekawa, K. Itami, Angew. Chem. Int. Ed. 2015, 54, 66-81; f) J. Li, L. Ackermann, Nat. Chem. 2015, 7, 686-687; g) G. Song, X. Li, Acc. Chem. Res. 2015, 48, 1007-1020; h) N. Kuhl, N. Schroeder, F. Glorius, Adv. Synth. Catal. 2014, 356, 1443-1460; i) S. A. Girard, T. Knauber, C.-J. Li, Angew. Chem. Int. Ed. 2014, 53, 74-100; j) G. Rouquet, N. Chatani, Angew. Chem. Int. Ed. 2013, 52, 11726-11743; k) C. S. Yeung, V. M. Dong, Chem. Rev. 2011, 111, 1215-1292; l) T. Satoh, M. Miura, Chem. Eur. J. 2010, 16, 11212-11222; m) T. W. Lyons, M. S. Sanford, Chem. Rev. 2010, 110, 1147; n) I. A. I. Mkhalid, J. H. Barnard, T. B. Marder, J. M. Murphy, J. F. Hartwig, Chem. Rev. 2010, 110, 890-931; o) C. Coperet, Chem. Rev. 2010, 110, 656-680; p) D. A. Colby, R. G. Bergman, J. A. Ellman, Chem. Rev. 2010, 110, 624-655; q) C.-L. Sun, B.-J. Li, Z.-J. Shi, Chem. Commun. 2010, 46, 677-685.

[91] a) Y. Lu, D.-H. Wang, K.M. Engle, J.-Q. Yu, J. Am. Chem. Soc. 2010, 132, 5916-5921; b) J. A. Schiffner, T. Wöste, H. M. Oestreich, Eur. J. Org. Chem. 2010, 174-182; c) B. Xiao, Y. Fu, J. Xu, T.-J. Gong, J.-J. Dai, J. Yi, L. Liu, J. Am. Chem. Soc. 2010, 132, 468-469; d) F.W. Patureau, F. Glorius, J. Am. Chem. Soc. 2010, 132, 9982-9983; e) D.-H. Wang, K. M. Engle, B.-F. Shi, J.-Q. Yu, Science 2010, 327, 315-319; f) M. Wasa, K. M. Engle, J.-Q. Yu, J. Am. Chem. Soc. 2010, 132, 3680-3681; g) F. Wang, G. Song, X. Li, Org. Lett. 2010, 12, 5430-5433; h) K. Muralirajan, K. Parthasarathy, C.-H. Cheng, Angew. Chem. Int. Ed. 2011, 50, 4169-4172; h) S. Rakshit, F. W. Patureau, F. Glorius, J. Am. Chem. Soc. 2010, 132, 9585-9587; i) N. Guimond, C. Gouliaras, K. Fagnou, J.

Am. Chem. Soc. 2010, 132, 6908-6909; j) K. Morimoto, K. Hirano, T. Satoh, M. Miura, Org. Lett. 2010, 12, 2068-2071.

[92] a) X. Zhao, C.E. Dimitrijevi, V. M. Dong, J. Am. Chem. Soc. 2009, 131, 3466-3467; b) X. Wang, T.-S. Mei, J.-Q. Yu, J. Am. Chem. Soc. 2009, 131, 7520-7521; c) T.-S. Mei, R. Giri, N. Maugel, J.-Q. Yu, Angew. Chem. Int. Ed. 2008, 47, 5215-5219; d) J.-J. Li, T.-S. Mei, J.-Q. Yu, Angew.Chem. Int. Ed. 2008, 47, 6452-6455; e) K. L. Hull, W. Q. Anani, M. S. Sanford, J. Am. Chem. Soc. 2006, 128, 7134-7135.

[93] a) L. Ackermann, A. V. Lygin, N. Hofmann, Org. Lett. 2011, 13, 3278-3281; b) S. H. Cho, J. Yoon, S. Chang, J. Am. Chem. Soc. 2011, 133, 5996-6005; c) Q. Shuai, G. Deng, J. Chua, D. S. Bohle, C.-J. Li, Adv. Synth. Catal. 2010, 352, 632-636; d) T.-S. Mei, X. Wang, J.-Q. Yu, J. Am. Chem. Soc. 2009, 131, 10806-10807; e) Q. Wang, S. L. Schreiber, Org. Lett. 2009, 11, 5178-5180; f) D. Monguchi, T. Fujiwara, H. Furukawa, A. Mori, Org. Lett. 2009, 11, 1607-1610.

[94] a) X. Wang, Y. Lu, H.-X. Dai, J.-Q. Yu, J. Am. Chem. Soc. 2010, 132, 12203-12205; b) Y.-H. Zhang, J.-Q. Yu, J. Am. Chem. Soc. 2009, 131, 14654-14655; c) D. C. Powers, M. A. L. Geibel, J. E. M. N. Klein, T. Ritter, J. Am. Chem. Soc. 2009, 131,17050-17051; d) L. V. Desai, K. J. Stowers, M. S. Sanford, J. Am. Chem. Soc. 2008, 130, 13285-13293.

[95] T. Cernak, K. D. Dykstra, S. Tyagarajan, P. Vachal, S. W. Krska. *Chem. Soc. Rev.* **2016**; *45:* 546-576.

Part II

Homogeneous iridium catalysis on $C(sp^2)$-H centers

<u>Chapter 1:</u> Performance and analysis of iridium(I)-catalyzed hydrogen isotope exchange reactions of aryl- and heteroaryl compounds

In 2014 catalyst **F** was synthesized by the working group of Prof. Tamm for the first time and in collaboration with Sanofi tested in HIE reactions. Based on this initial work which showed HIE reactivity for N-Boc indoles (**1**), N-Boc anilines (**2**) and anisoles (**3**, *scheme II.1.1*),[1] we became interested in the broader scope and limitations of this catalyst.

Scheme II.1. 1: *Previous work with catalyst **F** in the HIE reactions of N-Boc anilines and anisoles* [1]

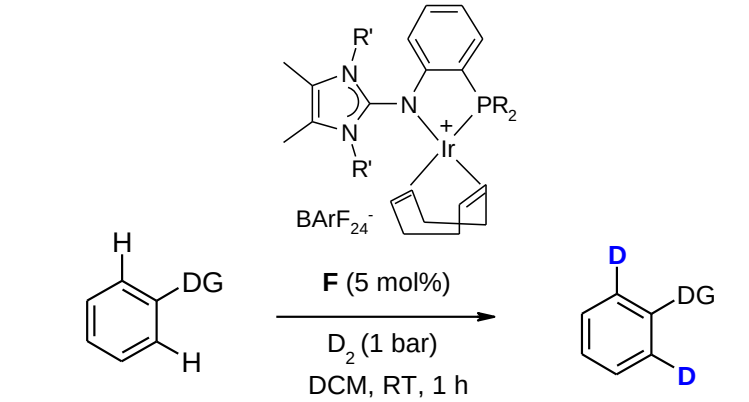

Selected examples:

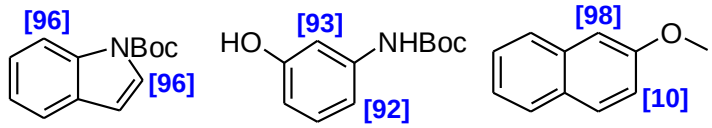

1 **2** **3**

II.1.1. Sulphonamides, N-oxides and phosphonamides – unexplored directing groups in HIE reactions

As mentioned in the introduction, Kerr's catalysts **B** and **C** are widely applied for mild and selective *ortho*-labelling employing a broad range of directing groups.[2] Despite recent progresses, a number of interesting functionalities still present significant challenges in HIE protocols, such as secondary and tertiary sulphonamides (also sulphonyl ureas), which are important structural moieties in several groups of drugs called sulpha drugs. These groups include sulphonamide antibiotics like sulfamethoxazole **4**,[3] protease inhibitors for HIV treatment like Darunavir **5**,[4] PDE5 inhibitors for treatment of erectile dysfunction like

Sildenafil (Viagra) **6**,[5] sulphonyl ureas for treatment of diabetes mellitus like Glibenclamide **7**[6] (*scheme II.1.2*).[7]

Scheme II.1. 2: *Secondary and tertiary sulphonamide (urea) drugs* [7]

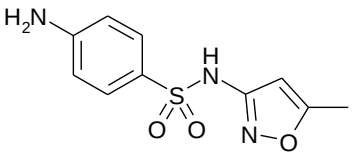

Sulfamethoxazole **4**

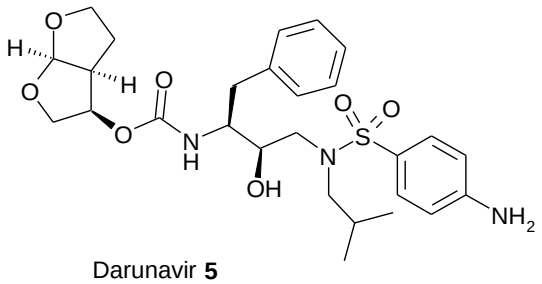

Darunavir **5**

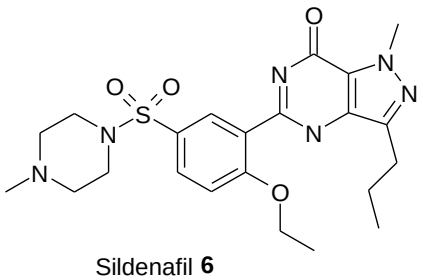

Sildenafil **6**

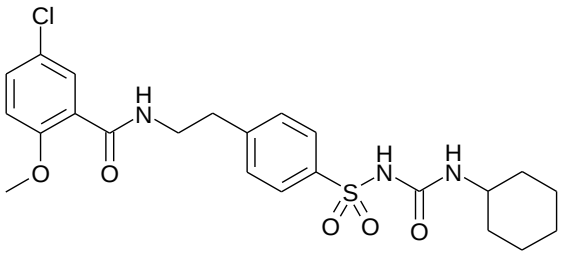

Glibenclamide **7**

The highly air- and moisture-sensitive, non-commercial catalysts **D** with phosphine-oxazoline P,N ligands, originally developed by Pfaltz for asymmetric hydrogenation of olefins, proved efficiency also in the HIE reaction of weakly coordinating substrates such as secondary sulphonamide **[H]-8** (*scheme II.1.3*, A).[8] However this single example was the only one reported so far showing good deuterium incorporation. Based on a comprehensive screening of readily available Ir-catalysts, Derdau and Atzrodt *et al* have identified another hydrogenation catalyst which has also an appreciable HIE capacity: the commercial air-stable Burgess catalyst **E**.[9] With this catalyst, they have developed the first practical HIE protocol for selective *ortho*-deuteration of various secondary and tertiary sulphonamides **[H]-9**, the best results being obtained on tertiary sulphonamides (*scheme II.1.3*, B).[7] They have also showed a similar reactivity by using monodentate Kerr catalyst **C**,[10] which proved to be even more efficient in the HIE reaction of secondary sulphonamides **[H]-10** (*scheme II.1.3*, C).[7] They also applied their method to sulpha drugs and even adapted to the special conditions required for selective tritium labelling (5–10 eq. of T_2 gas, low pressure). However, the need of elevated temperatures (100–120°C) to obtain reasonable deuterium incorporation (up to 78%), still remain an important limitation of this method.[7]

***Scheme II.1. 3**: Previous established HIE methods for selective ortho-deuteration of secondary and tertiary sulphonamides [7,8]*

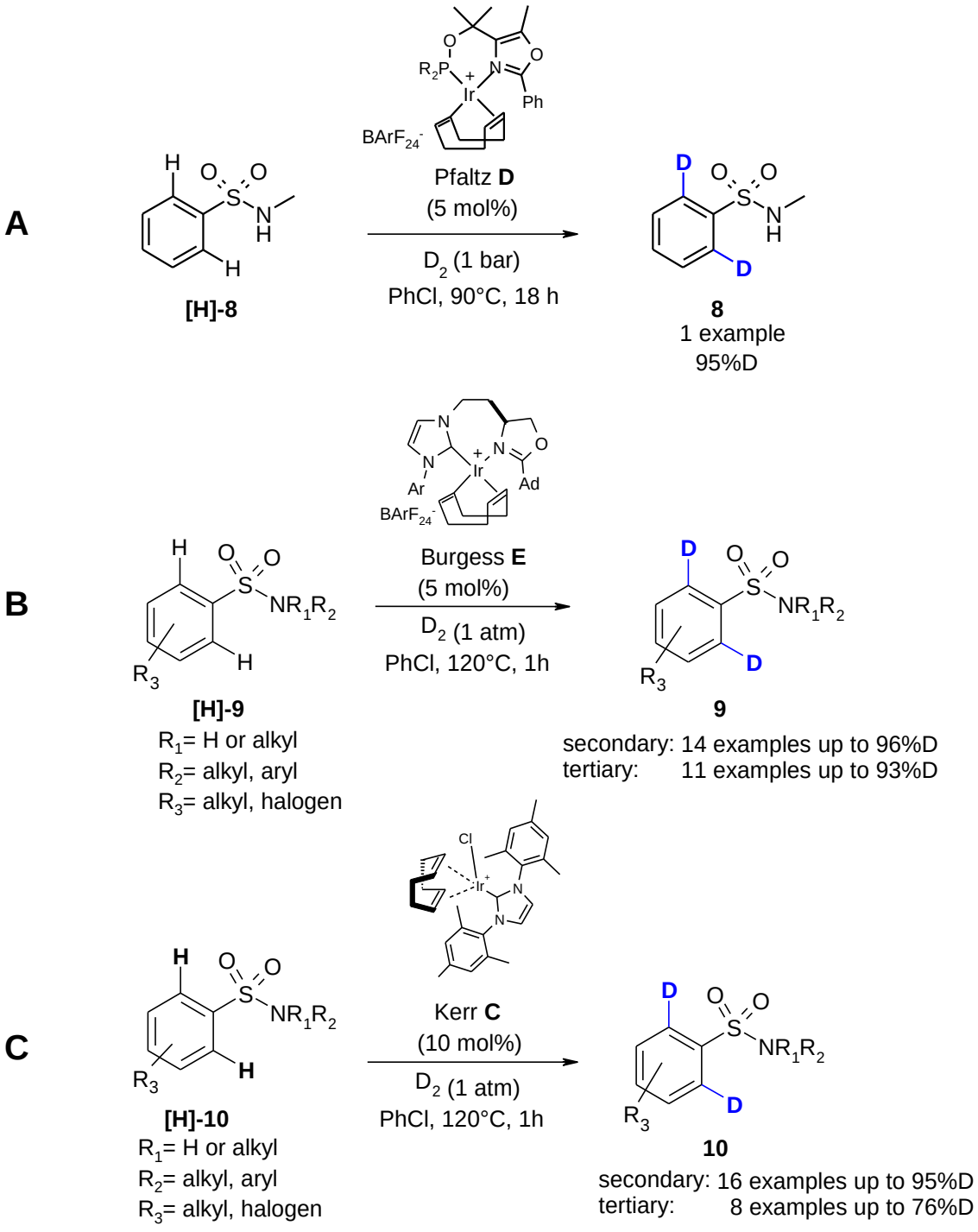

An evaluation of N-oxides as substrates for the directed HIE reaction with catalyst **F** was also of our interest. Heterocyclic *N*-oxides have emerged as potent compounds with anticancer, antibacterial, antihypertensive, antiparasitic, anti-HIV, anti-inflammatory, herbicidal, neuroprotective, and precognitive properties.[11] They can also be employed as sedative medication such as Chloradiazepoxide **11** and anticoagulant such as Otamixaban **12** (*scheme II.1.4*).[12] *N*-Oxides have rarely been described as directing groups in HIE reactions,[13] which would in principle enable the labeling of pyridines or quinolines after reductive cleavage of the N-O bond. This HIE approach can be convenient if direct labeling in the *ortho*-positions of the heterocyclic nitrogen atom (Rh black, D_2O[14] or Rh black, THF-D_2O[15]) cannot be accomplished or if higher specific activities in the case of tritium introduction are required.

Scheme II.1. 4: *N-oxide containing drugs*

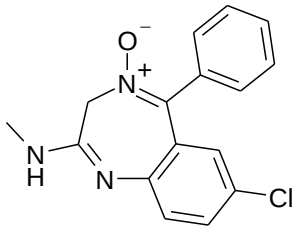

Chloradiazepoxide **11**

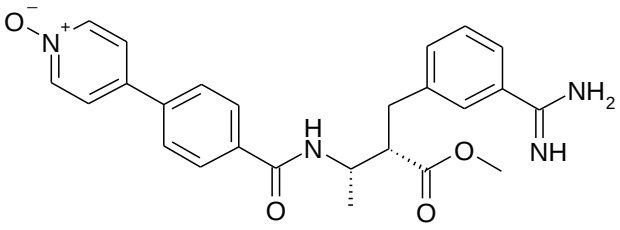

Otamixaban **12**

Furthermore, we have examined phosphonamides as they have never been applied in *ortho*-directed HIE reactions before. Phosphorus-containing drugs are still very rarely approved. One actual example is the phosphoric ester Sofosbufir **13**, used against hepatitis C (*scheme II.1.5*). However due to the limited chemical stability of phosphoric esters, it was decided to explore the family of phosphonamides first.

Scheme II.1. 5: *Phosphorus-containing drugs – Sofosbuvir* ***13***

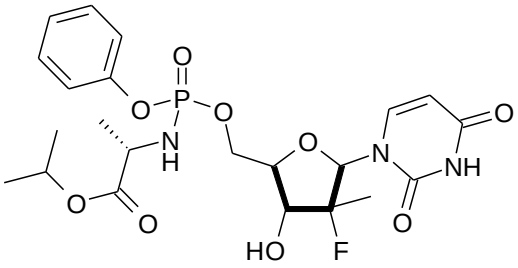

Sofosbuvir **13**

II.1.2. Explanation of the HIE reaction process at Sanofi laboratories

The general reaction optimization process to establish a tritium method is structured into three main parts: the reactions in a parallel synthesizer with atmospheric deuterium gas (D_2), the optimization in the deuterium manifold with low D_2 pressure and finally the application on the tritium manifold (*scheme II.1.6 and see Annexes 1 & 2 for details*).

Scheme II.1. 6: *General HIE reaction process and materials*

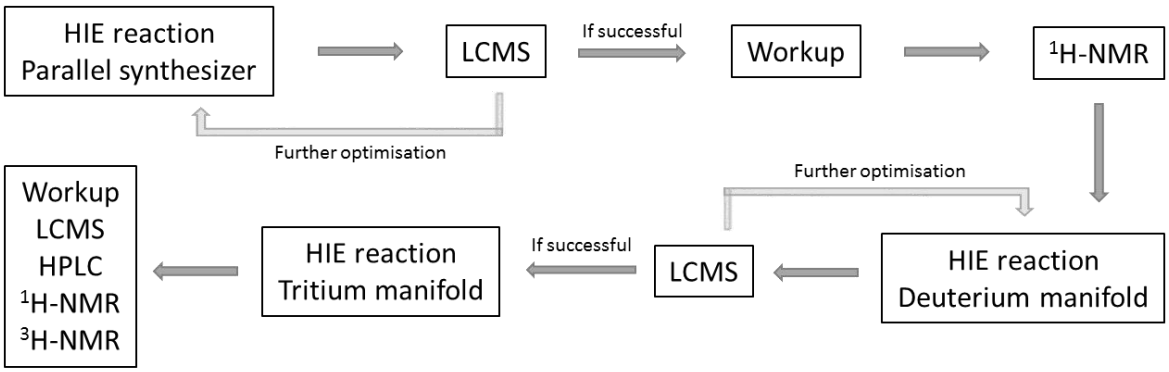

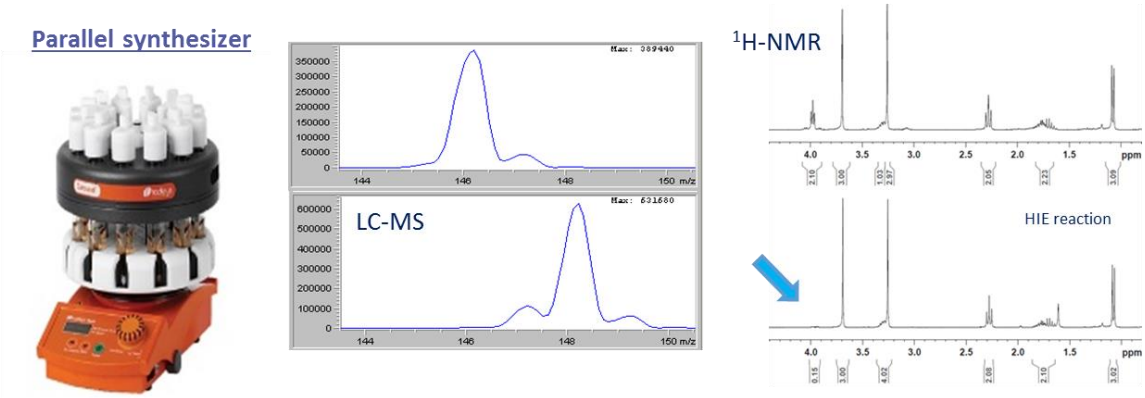

Deuterium Manifold

Tritium Manifold

- **HIE reaction on the parallel synthesizer:** the substrate is reacted under several conditions such as different solvents, temperatures, reaction times and catalyst amounts. All reactions are first analyzed by LC-MS and only if the success of the HIE reaction can be stated by shift of the M_0 peak, the reaction mixture is worked up and analyzed by ^{1}H NMR. The comparison of the ^{1}H NMR of the starting material and the product provides the following information: position of the labelling, degree of deuterium incorporation and overall purity.

- **HIE reaction on the deuterium manifold:** after identification of the optimum reaction conditions with the parallel synthesizer, the substrate is run at lower pressure of D_2. The reaction is analyzed by LC-MS, and the conditions are further optimized as long as no acceptable deuterium incorporation is observed (at least 70% D) with as reduced D_2 pressure as possible.

- **HIE reaction on the tritium manifold:** after successful HIE reaction on the deuterium manifold, the same conditions are applied on the tritium manifold. After workup, an aliquot is transferred and analysed by LC-MS. If the reaction is successful, purification and isolation *via* HPLC are done to provide the tritiated product which is then analysed by radio-HPLC, ^{1}H/ ^{3}H NMR and MS.

II.1.3. Optimization of the HIE reaction conditions on the model sulphonamide compound

We started to evaluate Tamm's catalyst **F** for the HIE reaction of tertiary sulphonamide **[H]-14** in different solvents at room temperature. Sulphonamide **[H]-14** was chosen as model compound due to its tertiary sulphonamide directing group (DG),. Moreover, it is a currently available product, iprompt to ionization and UV-detectable to be easily seen in LC-MS. Results are summarized in *table II.1*).

The catalytic HIE reaction with our model substrate **[H]-14** was strongly influenced by the solvent. In most solvents, none or only poor deuterium exchange was observed; however, high deuterium incorporation was found in chlorobenzene (entry 9). The strong influence of chlorobenzene in HIE reactions has been observed earlier,[8,7] however the effect is still not understood.

Table II.1. 1: Solvent screening of catalyst **F** in the HIE reaction with tertiary sulphonamide **[H]-14.**[a]

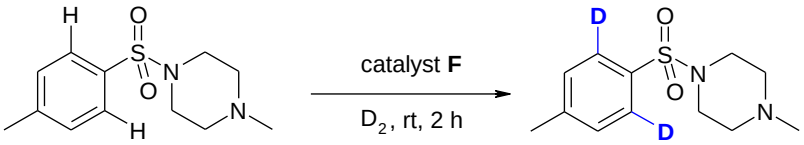

[H]-14 **14**

Entry	Solvent	%D 14[b]
1	dichloromethane	22
2	chloroform	12
3	MTBE	11
4	ethanol	0
5	cyclohexane	15
6	MeTHF	0
7	isopropylacetate	0
8	1-butanol	0
9	chlorobenzene	82
10	fluorobenzene	16

[a] Conditions: substrate **[H]-14** (10 µmol, 2.5 mg), catalyst **F** (1.0 µmol, 1.5 mg, 10 mol%), solvent (2 mL), D_2 (1 atm), rt, 2 h . [b] Percentage of deuterium incorporation determined by LC-MS.

In the next step, we tried to find optimized conditions for a subsequent broader substrate screening (*table II.1.2*). We modified catalyst content and reaction time and found that generally 10 mol% catalyst **F** are needed to obtain high deuterium introduction for substrate **[H]-14** within two hours (entry 9). Even though higher excess of deuterium was used in the optimization reactions, the deuteration reached a plateau after 30 min (entry 7) not proceeding significantly by longer reaction times up to 6h (entry 10).

Table II.1. 2: *Optimization of catalyst content and reaction time in the HIE reaction of tertiary sulphonamide* ***[H]-14.***[a]

Entry	Catalyst F (mol%)	Time (min)	%D 14[b]
1	3	300	0
2	5	300	0
3	7,5	120	32
4	10	5	15
5	10	10	44
6	10	15	69
7	10	30	80
8	10	60	82
9	10	120	85
10	10	300	89

[a] Conditions: substrate **[H]-14** (2.5 mg, 10 µmol), catalyst **F** (0.5-1.5 mg, 0.3-1 µmol, 3-10 mol%, 0.03-0.1 eq.), chlorobenzene (2 mL), D_2 (1 atm), rt. [b] Percentage of deuterium incorporation determined by LC-MS.

II.1.4. Application of the optimized conditions on aryl-sulphonamides, N-oxides and aryl-phosphonamides

We then studied the HIE reaction of various sulphonamides under the optimized reaction conditions (*scheme II.1.7*). Even though the labelling was not significantly higher after 120 min than after 30 min, we chose a reaction time of 2h for all further substrate screening. The catalyst revealed high reactivity and deuterium incorporation in the HIE reactions of primary, secondary and even tertiary sulphonamides. In the case of the primary sulphonamide **15**, catalyst **F** at room temperature showed similar amount of deuterium incorporation as compared to the results reported by Kerr with catalyst **C** done at higher temperature (120°C).[10] Interestingly, with catalyst **F**, secondary (**16**–**18**) and tertiary (**14**, **19**–**21**) sulphonamides underwent successful HIE reactions at room temperature as well, whereas the deuteration only proceeded at elevated temperatures (> 80–120°C) with catalysts **C** and **E**.[7] A temperature sensitive Sanofi drug candidate was therefore deuterated and later on tritiated, a reaction which was completely out of reach with the former reaction protocol.

Scheme II.1. 7: *HIE reactions of aryl-sulphonamides* ***14-21*** *catalyzed by* ***F****.*[a,b]

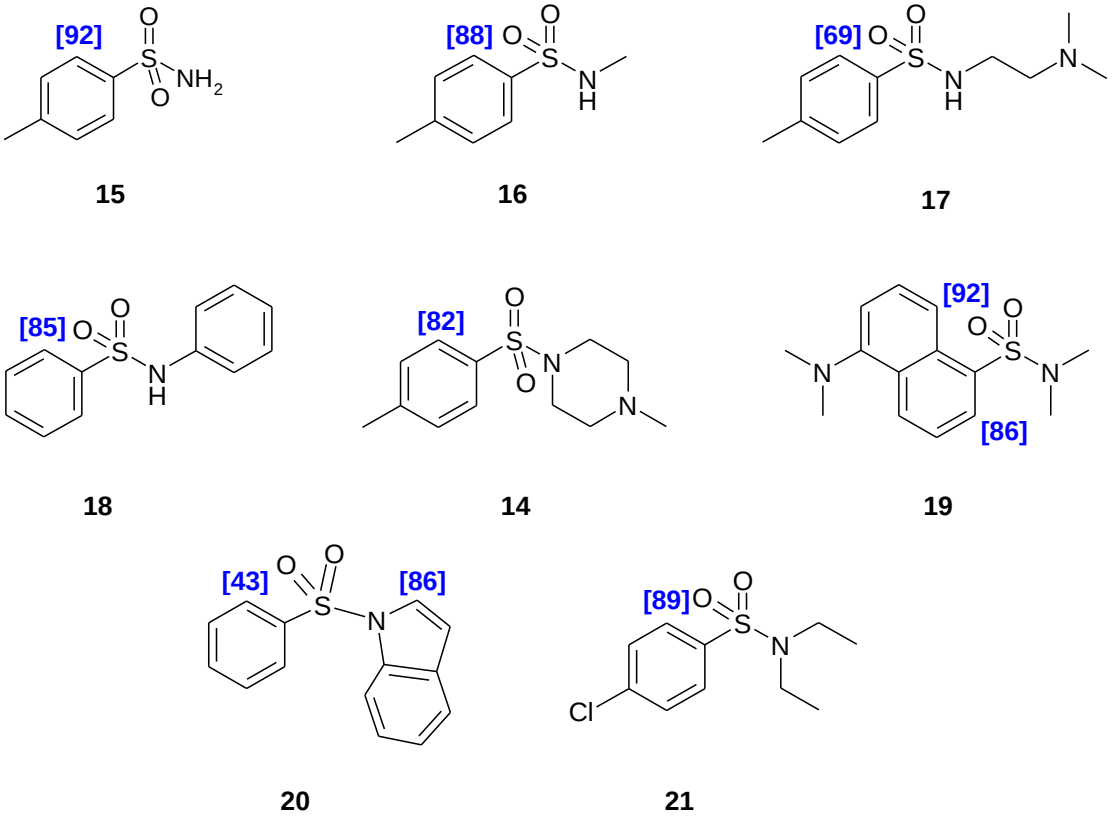

[a] Conditions: substrate (22 µmol), catalyst **F** (10 mol%), chlorobenzene (2 mL), D_2 (1atm), rt, 2 h. [b]Positions and percentage of deuterium incorporation determined by ^{1}H NMR.

In our study, the deuteration of the quinolone moiety in substrates **22–27** proceeded with moderate to very good and selective incorporation, independently of other aromatic substituents (*scheme II.1.8*). The 2- and 8-positions of 3-methylquinoline *N*-oxide **22** were deuterated in 73% and 100%, respectively. Similar results were obtained for 3-bromoquinoline *N*-oxide **23** and 6-methoxyquinoline *N*-oxide **24** with deuterium incorporation in these positions higher than 80%. Interestingly, the level of deuterium introduction dropped to approx. 50% at the 3-position in isoquinoline *N*-oxide **25** and in simple pyridine *N*-oxides **26** and **27** Since position 1 of isoquinoline *N*-oxide **25** was still exchanged by deuterium in 93%, a significant electronic effect can be considered as the steric differences between the 1- and 3-position are comparatively small. Indeed, as 1-position 1 of isoquinoline *N*-oxide **25** is a benzylic position, it is electronically more enriched than the quinoline 3-position.

Scheme II.1. 8: *HIE reactions of N-oxides* ***22-27*** *catalyzed by* ***F****.*[a,b]

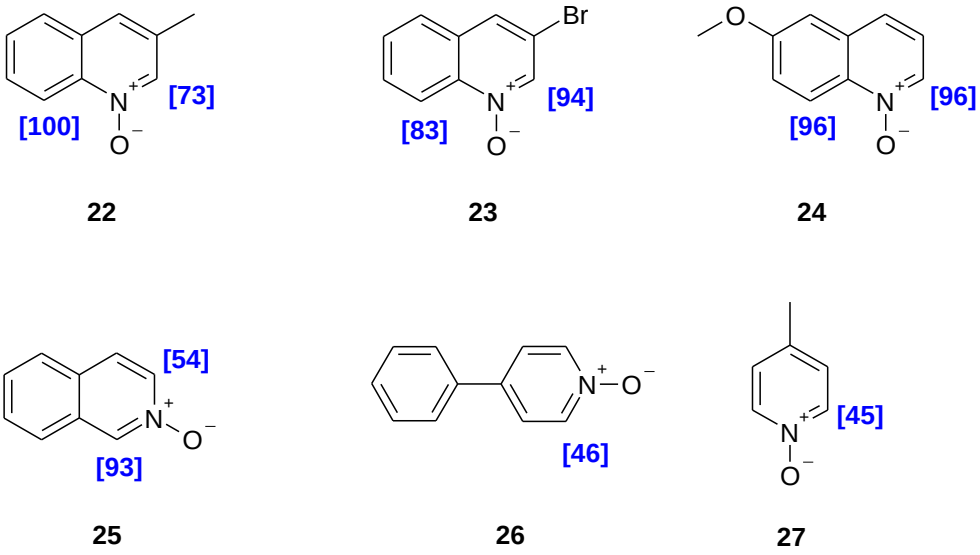

22 **23** **24**

25 **26** **27**

[a]Conditions: substrate (5 µmol), catalyst **F** (10 mol%), chlorobenzene (2 mL), D_2 (1atm), rt, 2 h. [b]Positions and percentage of deuterium incorporation determined by ^{1}H NMR.

Concerning the HIE reactions of aryl-phosphonamides with catalyst **F**, we have found good to excellent H/D exchange in the reaction of primary phosphonamide **28** (82%D), secondary phosphonamide **39** (70%D), and tertiary phosphonamides **30**–**33** (60–99%D) (*scheme II.1.9*).

Scheme II.1. 9: *HIE reactions of aryl-phosphonamides* ***28-33*** *catalyzed by* ***F****.*[a,b]

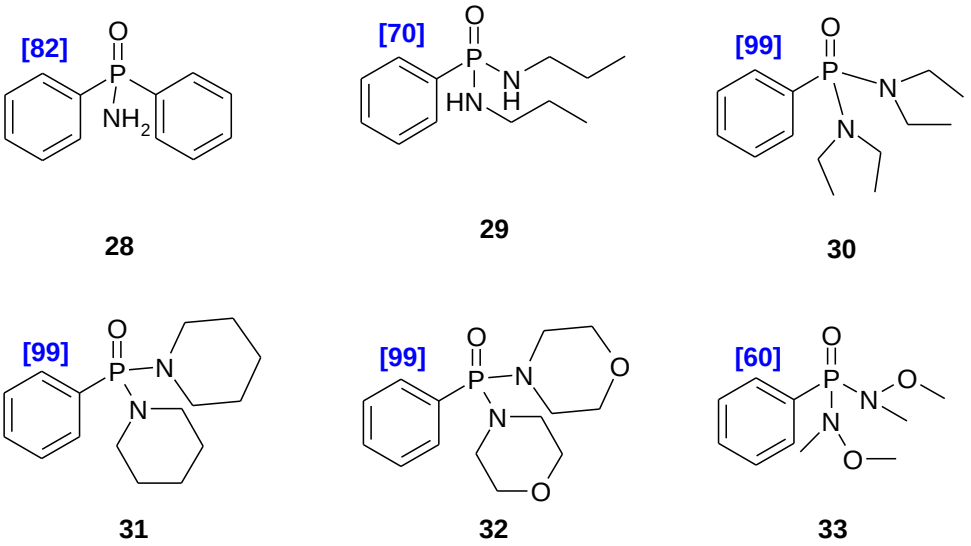

28 **29** **30**

31 **32** **33**

[a] Conditions: substrate (10 µmol), catalyst **F** (10 mol%), chlorobenzene (1 mL), D_2 (1atm), rt, 2 h. [b] Positions and percentage of deuterium incorporation determined by ^{1}H NMR.

Unfortunately, the application of these reaction conditions in HIE reactions with Sildenafil **6**, Otamixaban **12** and Sofosbuvir **13** did not enable the incorporation of deuterium.

II.1.5. Conclusion

In this scientific project, we have extended the use of the newly discovered catalyst **F** by evaluation of its activity in HIE reaction with aryl-sulphonamides, N-oxides and aryl-phosphonamides. After optimization we were able to run the HIE reaction under very mild reaction conditions which permitted very high deuterium incorporation (up to 99%D). The results emphasize the usefulness of this air-stable catalyst and, in the case of the sulphonamides, catalyst **F** seems to be more active than other commercially available iridium catalysts.

During this preliminary phase of my PhD, I became familiar of standard HIE procedures and associated analysis. I also became aware of the limits of model compounds we are working on, as observed when transferring our developed method on drug molecules.

---

1 K. Jess, V. Derdau, R. Weck, J. Atzrodt, M. Freytag, P. G. Jones, M. Tamm, *Adv. Synth. Catal.* **2017**, *359*, 629 – 638.

2 a) J. Atzrodt, V. Derdau, W. J. Kerr, M. Reid, P. Rojahn, R. Weck, *Tetrahedron* **2015**, *71*, 1924–1929; b) J. A. Brown, A. R. Cochrane, S. Irvine, W. J. Kerr, B. Mondal, J. A. Parkinson, L. C. Paterson, M. Reid, T. Tuttle, S. Andersson, G. N. Nilsson, *Adv. Synth. Catal.* **2014**, *356*, 3551–3562; c) A. R. Cochrane, S. Irvine, W. J. Kerr, M. Reid, S. Andersson, G. N. Nilsson, *J. Labelled Compd. Radiopharm.* **2013**, *56*, 451–454; d) P. W. C. Cross, J. M. Herbert, W. J. Kerr, A. H. McNeill, L. C. Paterson, *Synlett* **2016**, *27*, 111–115.

3 R. Gleckman, S. Alvarez, D.W. Joubert, *Am. J. Hosp. Pharm*., 1979, 36, 893-906.

4 A.K. Ghosh, Z.L. Dawson, H. Mitsuya, *Bioorg. Med. Chem.*, 2007, **15**, 7576-7580.

5 N. K. Terrett, A. S. Bell, D. Brown, P. Ellis, *Bioorg. Med. Chem.*, 1996, **6**, 1819-1824.

6 L. Luzi, G. Pozza, *Acta Diabetol*., 1997, **34**, 239-244.

7 a) A. Burhop, R. Weck, J. Atzrodt, V. Derdau, *Eur. J. Org. Chem*. **2017**, 1418–1424; b) A. Burhop, R. Prohaska, R. Weck, J. Atzrodt and V. Derdau, *J. Label. Compd. Radiopharm*. **2017**, *60*, 343-348.

8 M. Parmentier, T. Hartung, A. Pfaltz, D. Muri, *Chem. Eur. J.* **2014**, *20*, 11496–11504.

9 a) M. C. Perry, X. Cui, M. T. Powell, D. R. Hou, J. H. Reibenspies, K. Burgess, *J. Am. Chem. Soc.* **2003**, *125*, 113-123; b) S. Khumsubdee, Y. Fan, K. Burgess, *J. Org. Chem.* **2013**, 9969-9974; c) Y. Zhu, Y. Fan, K. Burgess, *J. Am. Chem. Soc.* **2010**, *132*, 6249-6253.

10 W. J. Kerr, M. Reid, T. Tuttle, *ACS Catal.* **2015**, *5*, 402–410.

11 A. M. Mfuh and O. V. Larionov, Curr Med Chem. **2015**, *22*, 2819–2857.

12 A. M. Mfuh, O. V. Larionov, *Curr Med Chem*. 2015 ; 22(24): 2819–2857.

13 a) S. Chen, G. Song, X. Li, *Tetrahedron Letters* **2008**, *49*, 6929-6932; b) J. W. Pavlik, S. Laohhasurayotin, *J. Heterocycl. Chem.* **2005**, 42, 73-76.

14 a) V. Derdau, J. Atzrodt, W. Holla, *J. Label. Compd. Radiopharm.* **2007**, *50*, 295-298; b) V. Derdau, J. Atzrodt, J. Zimmermann, C. Kroll, F. Brückner, *Chem. Eur. J.* **2009**, *15*, 10397-10404; c) W. J. S. Lockley, *J. Label. Compd. Radiopharm.***2010**, *53*, 668-673.

15 E. Alexakis, J. R. Jones, W.J.S. Lockley, *Tetrahedron Lett.* **2006**, *47*, 5025-5028.

Supporting information Part II – Chapter 1

Materials and General deuteration procedure: see Annex 1.

Solvent screening of catalyst F in the HIE reaction with tertiary sulfonamide [H]-14 (*table II.1.1*)

For the screening of different solvents, 1-methyl-4-[(4-methylphenyl)sulfonyl]-piperazine **[H]-14** in solvent (10 µmol, 500 µL, 1 eq.), the catalyst **F** (1.5 mg, 1 µmol, 10 mol%, 0.1 eq.) and the different solvents were used. All reactions were performed according to the general deuteration procedure at rt for 2 h. Deuterium incorporation was determined by LC-MS and labelling position was by ^{1}H-NMR.

Optimization of catalyst content and reaction time in the HIE reaction of tertiary sulfonamide [H]-14 (*table II.1.2*)

1-methyl-4-[(4-methylphenyl)sulfonyl]-piperazine **[H]-14** in chlorobenzene (2.5 mg, 10 µmol, 500 µL, 1 eq.) and catalyst **F** indicated in table 2 (0.5-1.5 mg, 0.3-1 µmol, 3-10 mol%, 0.03-0.1 eq.) were used for the optimization of the HIE reaction. The reaction was stirred for the declared time and at the stated temperature under D_2 atmosphere.

General procedure for the synthesis of the phosphonamides 29-33

(*Organic letters*, **2013**, *15(17*), 4504-4507)

To a solution of the corresponding amine (40.0 mmol, 2 eq.) and a catalytic amount of DMAP (0.2 mmol, 0.01 eq.) in dichloromethane (180 mL) was added dropwise a solution of dichlorophenylphosphine (20.0 mmol, 1 eq.) and trimethylamine (40.0 mmol, 2 eq.) in dichloromethane at 0°C. The mixture was stirred at 0°C for 1h, allowed to warm at RT and stirred overnight. The solvent was evaporated and diethylether (200 mL) to yield a salt. The salt was removed by filtration and washed with diethylether. After removal of the solvent the residue was purified by silica gel chromatography (DCM/Acetone 1/1).

- **Phosphonic diamide, *P*-phenyl-N,N'-dipropyl (29)**

Propylamine (2.365 g, 40.0 mmol, 2 eq.), DMAP (25.0 mg, 0.2 mmol, 0.01 eq), dichlorophenylphosphine (2.6 mL, 20.0 mmol, 1 eq.), trimethylamine (5.6 mL, 40.0 mmol, 2 eq.).

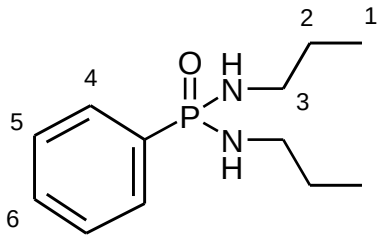

29

Molecular Weight =240.2878
Molecular Formula =C12H21N2OP

Yield=60%

^{1}H-NMR ($CDCl_3$; 300MHz): (δ ppm) 7.83 (m, 2H, H_4), 7.59 - 7.41 (massif, 3H, H_5 and H_6), 2.95 (q, J = 7.0 Hz, 4H, H_3), 2.38 (s large, 2H, NH), 1.50 (sx, J = 7.0 Hz, 4H, H_2), 0.92 (t, , J = 7.0 Hz, 6H, H_1).

^{13}C-NMR ($CDCl_3$; 300MHz): (δ ppm) 133.14 (C_6), 131.34 (C_4), 128.38 (C_5), 42.55 (C_3), 25.27 (C_2), 11.24 (C_1).

- **Phosphonic diamide, *P*-phenyl *N*,*N*,*N*',*N*'-tetraethyl (30)**

Diethylamine (2.900 g, 40.0 mmol, 2 eq), DMAP (25.0 mg, 0.2 mmol, 0.01 eq), dichlorophenylphosphine (2.6 mL, 20.0 mmol, 1 eq.), trimethylamine (5.6 mL, 40.0 mmol, 2 eq.).

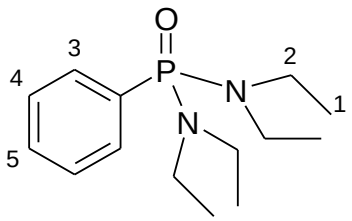

Molecular Weight =268.3420
Molecular Formula =C14H25N2OP

30

Yield=57%

^{1}H-NMR (DMSO-d_6; 300MHz): (δ ppm) 7.68 (m, 2H, H_3), 7.59 - 7.41 (massif, 3H, H_4 and H_5), 2.95 (m, 8H, H_2), 0.95 (t, J = 7.0 Hz,12H, H_1).

^{13}C-NMR (DMSO-d_6; 300MHz): (δ ppm) 131.94 (C_3), 130.85 (C_5), 128.11 (C_4), 38.36 (C_2), 13.62 (C_1).

- **Piperidine, 1,1'-(phenylphosphinylidene)bis (31)**

Piperidine (3.410 g, 40.0 mmol, 2 eq), DMAP (25.0 mg, 0.2 mmol, 0.01 eq), dichlorophenylphosphine (2.6 mL, 20.0 mmol, 1 eq.), trimethylamine (5.6 mL, 40.0 mmol, 2 eq.).

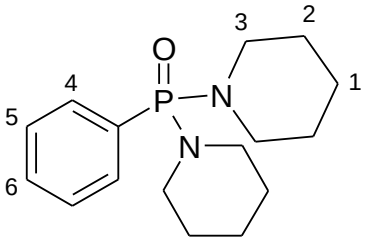

Molecular Weight =292.3642
Molecular Formula =C16H25N2OP

31

Yield=65%

^{1}H-NMR (DMSO-d_6; 300MHz): (δ ppm) 7.67 (m, 2H, H_4), 7.57 - 7.41 (massif, 3H, H_5 and H_6), 2.90 (m, 8H, H_3), 1.58-1.29 (m, 12H, H_1 and H_2).

^{13}C-NMR (DMSO-d_6; 300MHz): (δ ppm) 131.83 (C_4), 130.97 (C_6), 128.34 (C_5), 45.03 (C_3), 26.13 (C_2), 24.75 (C_1).

- **Morpholine, 4,4'-(phenylphosphinylidene)bis (32)**

Morpholine (3.490 g, 40.0 mmol, 2 eq), DMAP (25.0 mg, 0.2 mmol, 0.01 eq), dichlorophenylphosphine (2.6 mL, 20.0 mmol, 1 eq.), trimethylamine (5.6 mL, 40.0 mmol, 2 eq.).

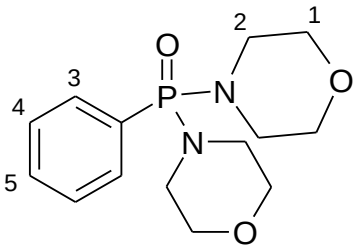

Molecular Weight =296.3089
Molecular Formula =C14H21N2O3P

32

Yield=61%
^{1}H-NMR (DMSO-d_6; 300MHz): (δ ppm) 7.70 (m, 2H, H_3), 7.64 - 7.47 (massif, 3H, H_4 and H_5), 3.65-3.45 (massif, 8H, H_1), 3.10-2.87 (massif, 8H, H_2).
NMR ^{13}C (DMSO-d_6; 300MHz): (δ ppm) 132.12 (C_3), 131.80 (C_5), 128.62 (C_4), 67.08 (C_1), 44.45 (C_2).

- **Phosphonic diamide, *P*-phenyl *N*,*N*'-methoxy, *N*,*N*'-methyl (33)**

Methanamine-*N*-methoxy,hydrochloride (3.900 g, 40.0 mmol, 2 eq), DMAP (25.0 mg, 0.2 mmol, 0.01 eq), dichlorophenylphosphine (2.6 mL, 20.0 mmol, 1 eq.), trimethylamine (5.6 mL, 40.0 mmol, 2 eq.).

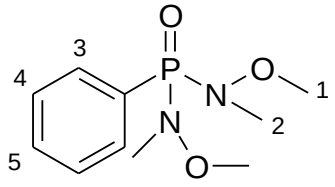

Molecular Weight =244.2324
Molecular Formula =C10H17N2O3P

33

Yield=56%
^{1}H-NMR (CDCl3; 300MHz): (δ ppm) 7.92 (m, 2H, H_3), 7.55 - 7.48 (massif, 3H, H_4 and H_5), 3.45 (s, 6H, H_1), 2.95 (ds, 6H, H_2).
^{13}C-NMR (CDCl3; 300MHz): (δ ppm) 131.40 (C_5), 130.92 (C_3), 128.20 (C_4), 61.47 (C_1), 35.39 (C_2).

HIE reactions of sulphonamides 14-21catalyzed by F (*scheme II.1.7*)

Conditions: substrate (22.0 µmol, 1 eq.), catalyst **F** (3.4 mg, 2.2 µmol, 10 mol%, 0.1 eq.), PhCl (2 mL), D_2 (1 atm), rt, 2 h.

Sulphonamide **15**

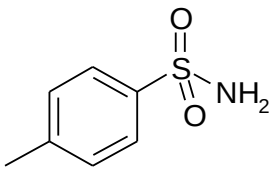

15

Molecular Weight =171.2193
Molecular Formula =C7H9NO2S

^{1}H NMR (300 MHz, DMSO-d_6): δ 7.71 (d, ^3J = 8.2 Hz, 2H, 2 CH *ortho*-SO_2NH_2), 7.35 (d, ^3J = 8.2 Hz, 2H, 2 CH *ortho*-CH_3), 2.38 (s, 3H, CH_3) ppm. Incorporation expected at δ 7.71 (red arrow). Determined against integral at δ 2.38 (blue arrow).

Yield: 83%.

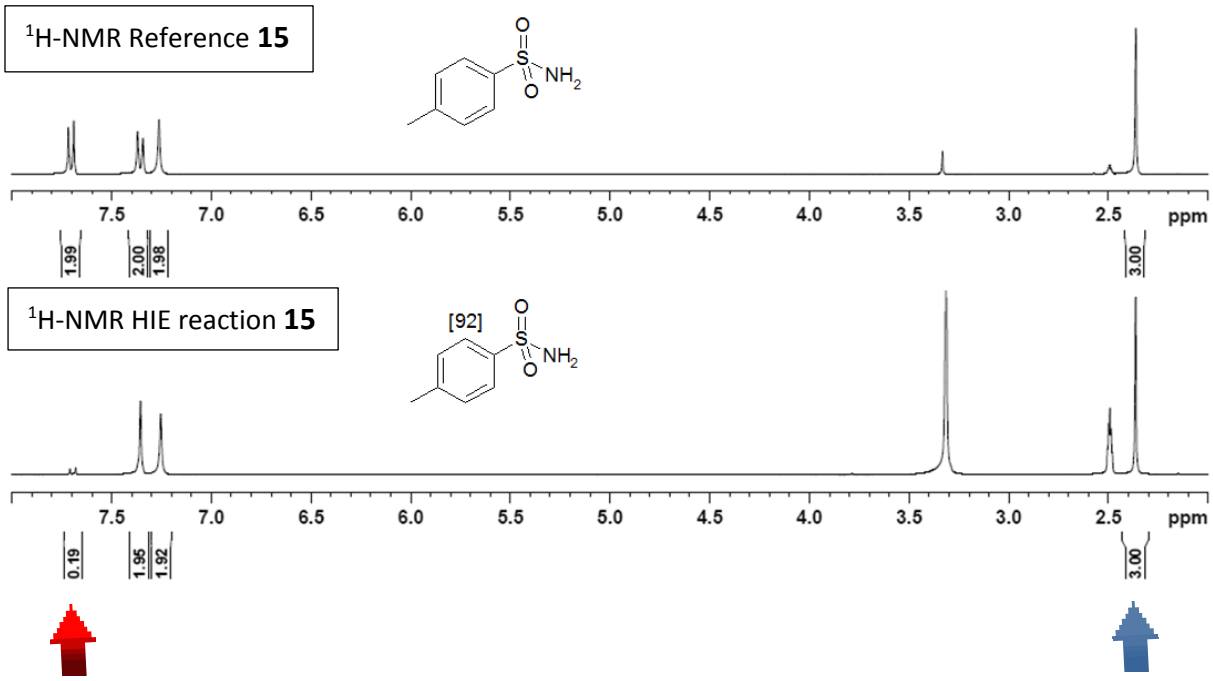

Sulphonamide **16**

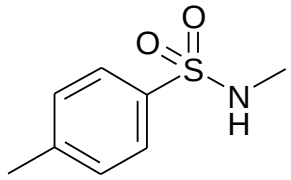

Molecular Weight =185.2464
Molecular Formula =C8H11NO2S

16

^{1}H NMR (300 MHz, DMSO-d_6): δ 7.65 (d, ^3J = 8.0 Hz, 2H, 2 CH *ortho*-SO_2NH_2), 7.40 (d, ^3J = 8.0 Hz, 2H, 2 CH *ortho*-CH_3), 7.33 (s large, 1H, NH), 2.38 (s, 3H, CH_3) ppm. Incorporation expected at δ 7.65 (red arrow). Determined against integral at δ 2.38 (blue arrow).

Yield: 80%.

^{1}H-NMR Reference **16**

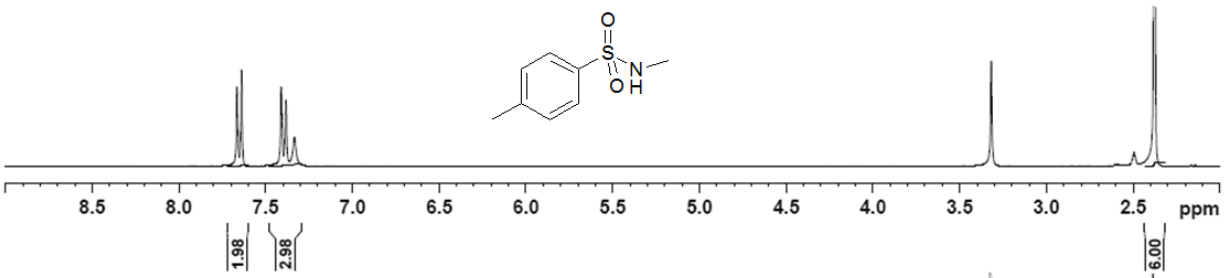

^{1}H-NMR HIE reaction **16**

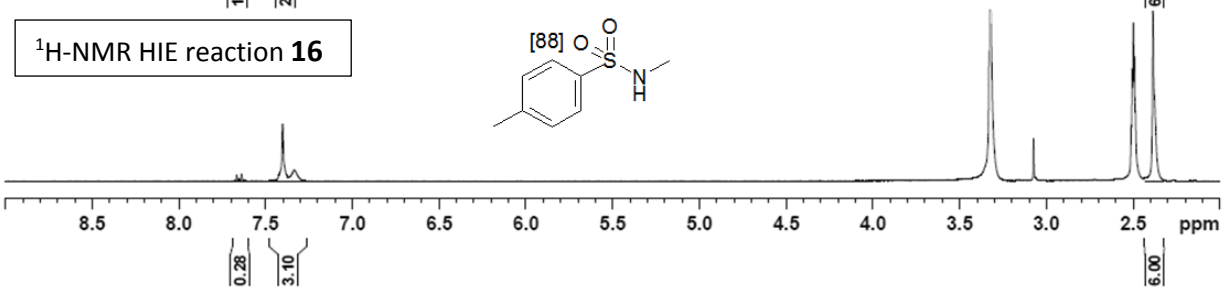

Sulphonamide **17**

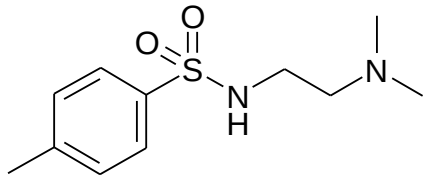

17

Molecular Weight =242.3423
Molecular Formula =C11H18N2O2S

^{1}H NMR (300 MHz, DMSO-d_6): δ 7.69 (d, ^3J = 8.5 Hz, 2H, 2 CH *ortho*-SO_2NH_2), 7.42 (s large, 1H, NH), 7.38 (d, ^3J = 8.5 Hz, 2H, 2 CH *ortho*-CH_3), 2.80 (m, 2H, CH_2), 2.40 (s, 3H, CH_3), 2.25 (m, 2H, CH_2), 2.05 (s, 6H, 2 CH_3) ppm. Incorporation expected at δ 7.69 (red arrow). Determined against integral at δ 2.05 (blue arrow).

Yield: 75%.

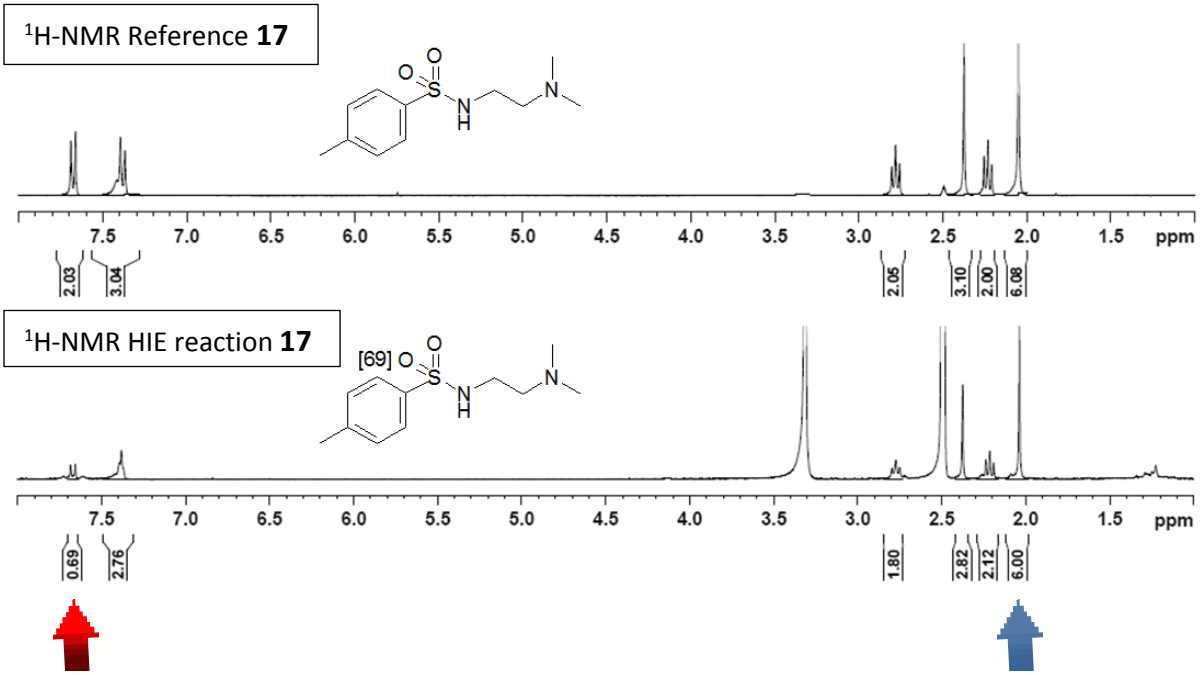

Sulphonamide **18**

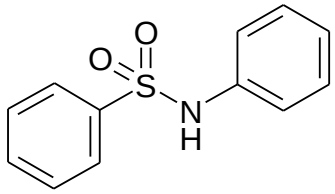

18

Molecular Weight =233.2910
Molecular Formula =C12H11NO2S

^{1}H NMR (300 MHz, DMSO-d$_6$): δ 7.75 (d, ^{3}J = 8.6 Hz, 2H, 2 CH *ortho*-SO_2NH_2), 7.55 (m, 3H, 3 CH phenyl), 7.20 (m, 2H, 2 CH phenyl), 7.08 (d, ^{3}J = 8.6 Hz, 2H, 2 CH *meta*-SO_2NH_2), 7.00 (m, 1H, CH phenyl) ppm. Incorporation expected at δ 7.75 (red arrow). Determined against integral at δ 7.00 (blue arrow).

Yield: 88%.

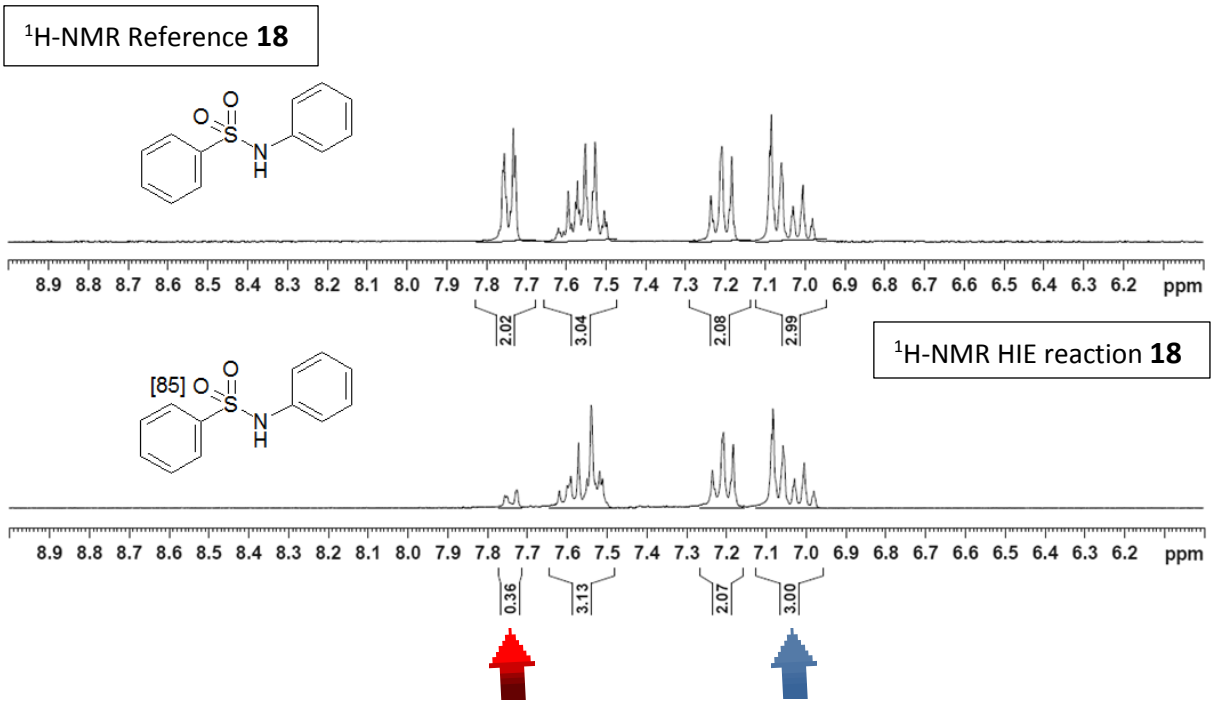

Sulphonamide **14**

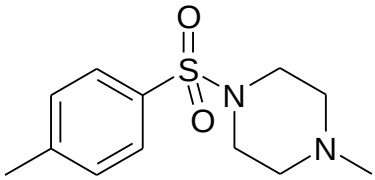

Molecular Weight =254.3535
Molecular Formula =C12H18N2O2S

14

^{1}H NMR (300 MHz, DMSO-d$_6$): δ 7.62 (d, ^3J = 8.2 Hz, 2H, 2 CH *ortho*-SO_2NH_2), 7.45 (d, ^3J = 8.2 Hz, 2H, 2 CH *ortho*-CH_3), 2.85 (m, 4H, 2 CH_2), 2.40 (s, 3H, CH_3), 2.35 (m, 4H, 2 CH_2), 2.40 (s, 3H, CH_3) ppm. Incorporation expected at δ 7.62 (red arrow). Determined against integral at δ 2.85 (blue arrow).

Yield: 87%.

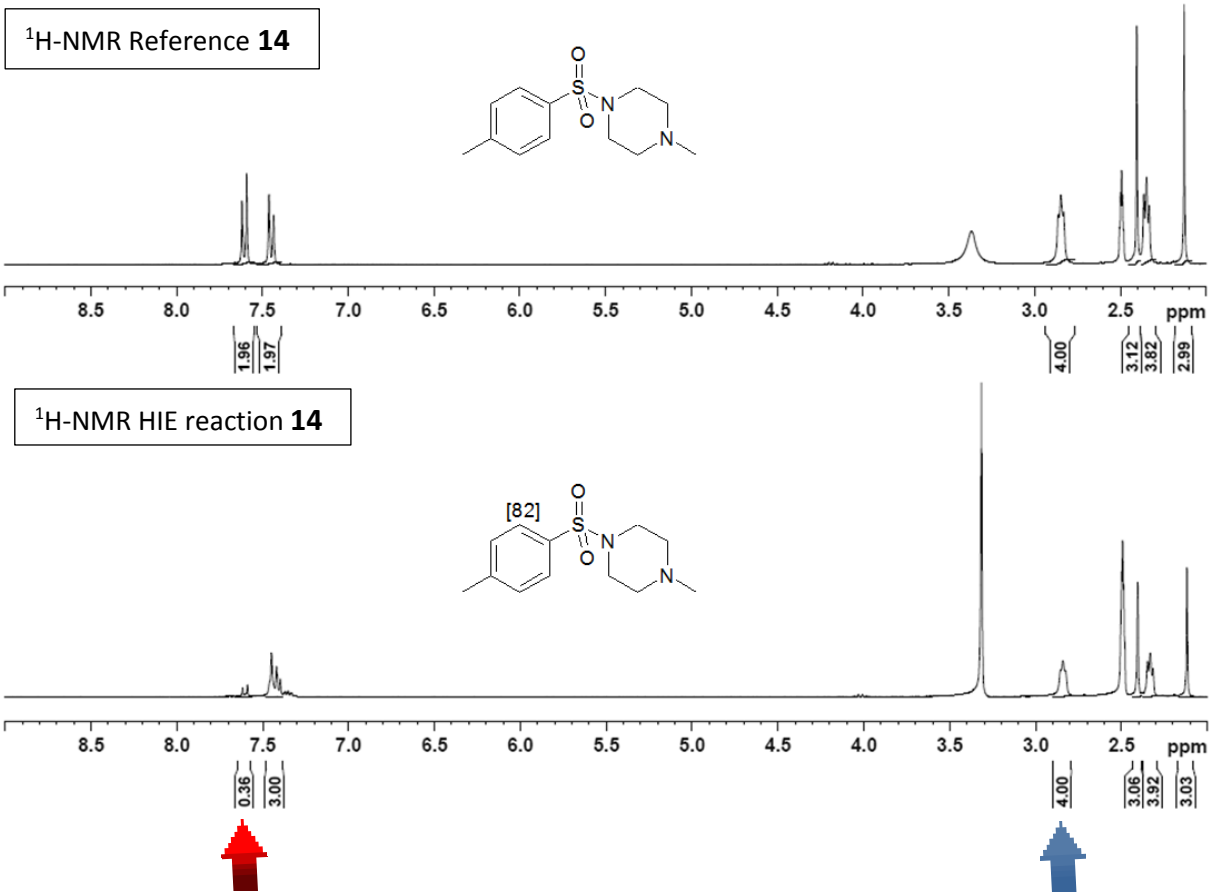

Sulphonamide **19**

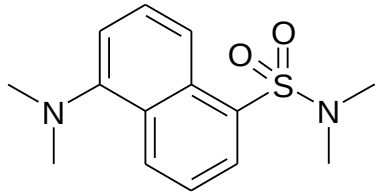

Molecular Weight =278.3758
Molecular Formula =C14H18N2O2S

19

^{1}H NMR (300 MHz, DMSO-d_6): δ 8.50 (m, 1H, CH *ortho*-SO_2NH_2), 8.30 (m, 1H, CH), 8.08 (m, 1H, CH *ortho*-SO_2NH_2), 7.63 (m, 2H, 2 CH), 7.25 (m, 1H, CH), 2.85 (s, 6H, 2 CH_3), 2.75 (s, 6H, 2 CH_3) ppm. Incorporation expected at δ 8.50 and/or 8.08 (red arrow). Determined against integral at δ 2.75 (blue arrow).

Yield: 76%.

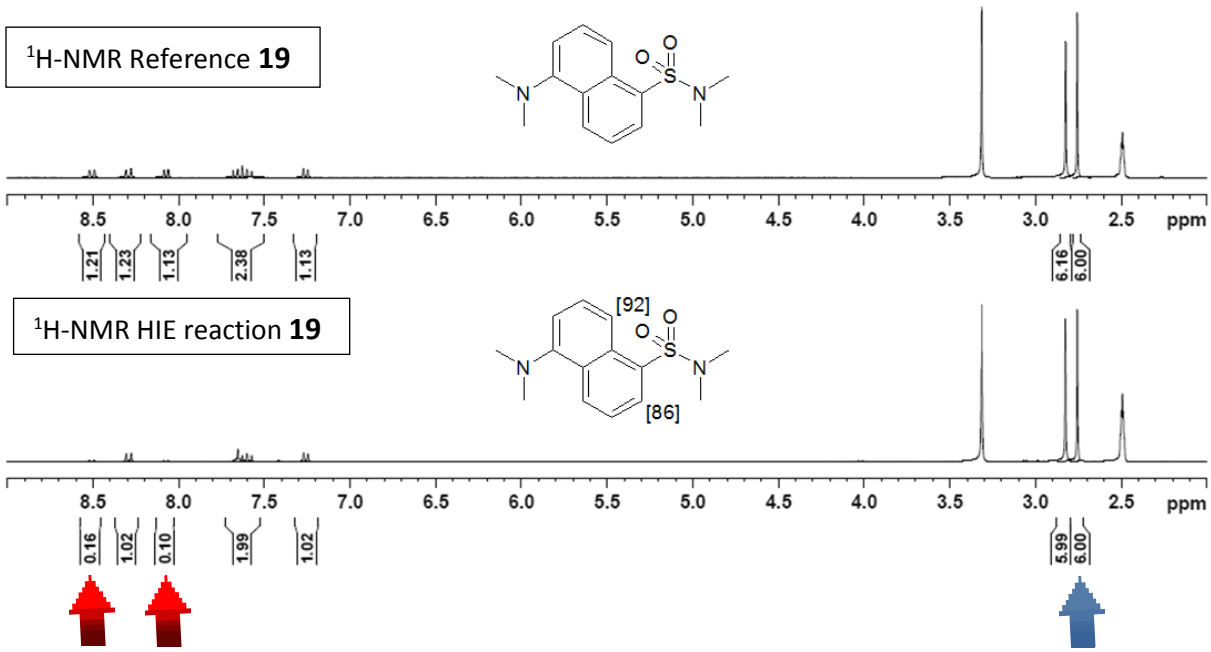

Sulphonamide **20**

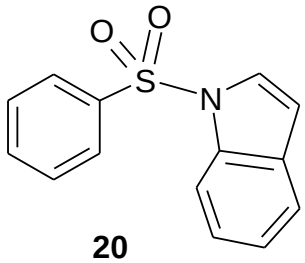

20

Molecular Weight =257.3133
Molecular Formula =C14H11NO2S

^{1}H NMR (300 MHz, DMSO-d_6): δ 7.95 (m, 3H, 3 CH), 7.80 (m, 1H, CH), 7.67 (m, 1H, CH), 7.59 (m, 3H, 3 CH), 7.35 (m, 1H, CH), 7.25 (m, 1H, CH), 6.85 (m, 1H, CH) ppm. Incorporation expected at δ 7.95 and/or 7.80 (red arrow). Determined against integral at δ 7.25 (blue arrow).

Yield: 73%.

^{1}H-NMR Reference **20**

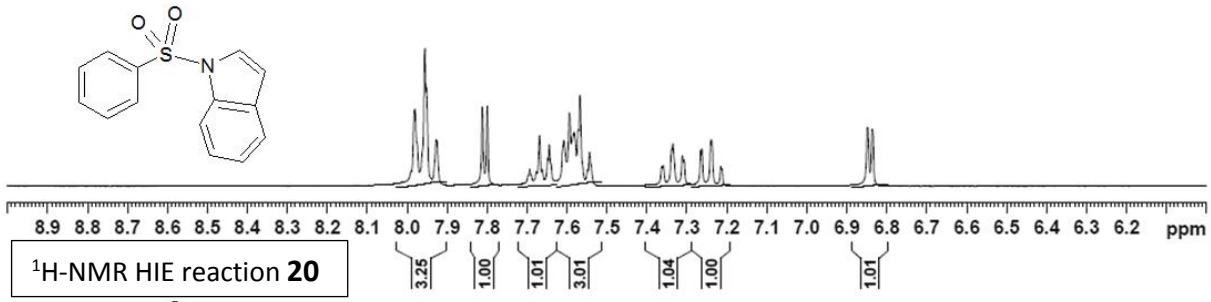

^{1}H-NMR HIE reaction **20**

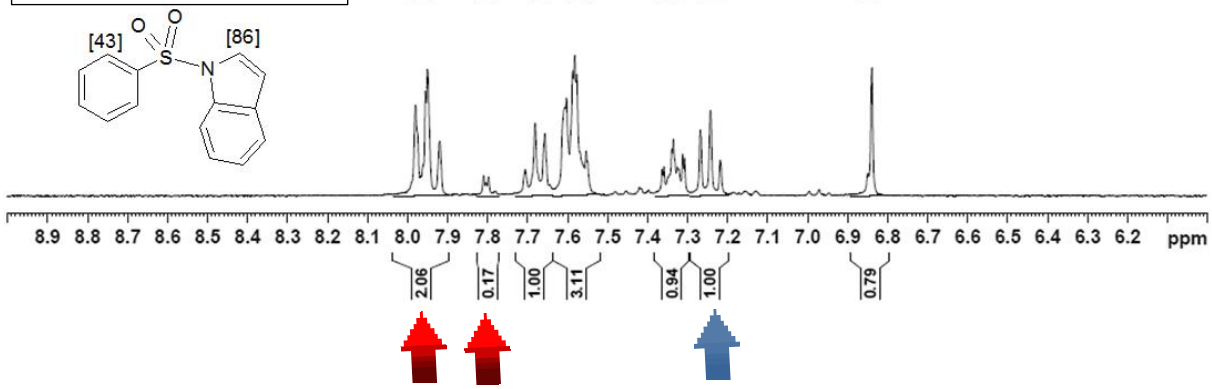

Sulphonamide **21**

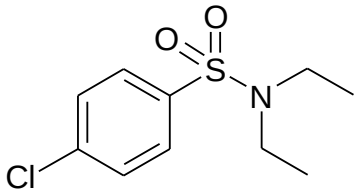

21

Molecular Weight =247.7456
Molecular Formula =C10H14ClNO2S

^{1}H NMR (300 MHz, DMSO-d_6): δ 7.82 (d, ^3J = 7.9 Hz, 2H, 2 CH *ortho*-SO_2N), 7.65 (d, ^3J = 7.9 Hz, 2H, 2 CH *ortho*-Cl), 3.15 (m, 4H, 2 CH_2), 1.02 (m, 6H, 2 CH_3) ppm. Incorporation expected at δ 7.82 (red arrow). Determined against integral at δ 1.02 (blue arrow).

Yield: 82%.

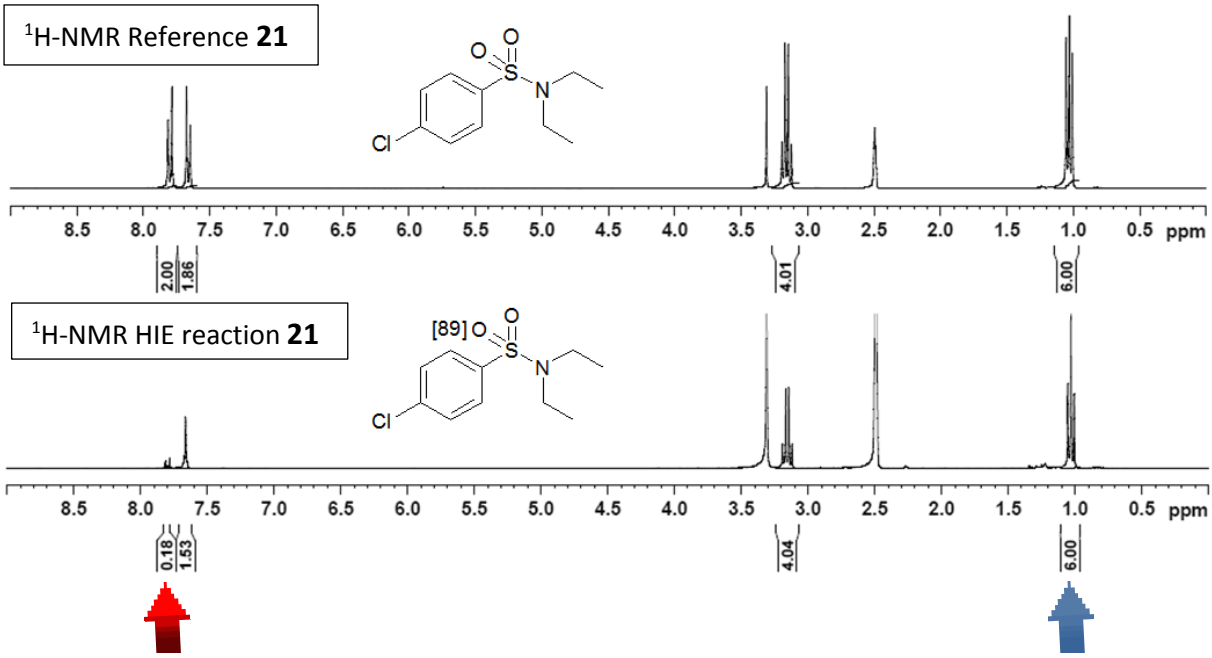

HIE reactions of N-oxides 22-27 catalyzed by F (*scheme II.1.8*)

Conditions: substrate (5 µmol, 1 eq.), catalyst **F** (0.8 mg, 0.5 µmol, 10 mol%, 0.1 eq.), PhCl (2 mL), D_2 (1 atm), rt, 2 h.

N-oxide **22**

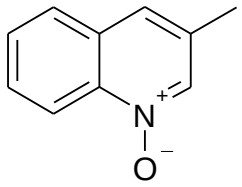

22

Molecular Weight =159.1893
Molecular Formula =C10H9NO

Yield: 72%.

^{1}H-NMR Reference **22**

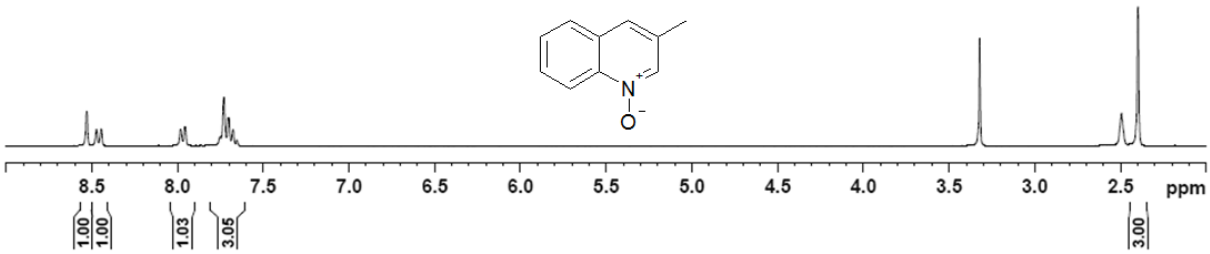

^{1}H-NMR HIE reaction **22**

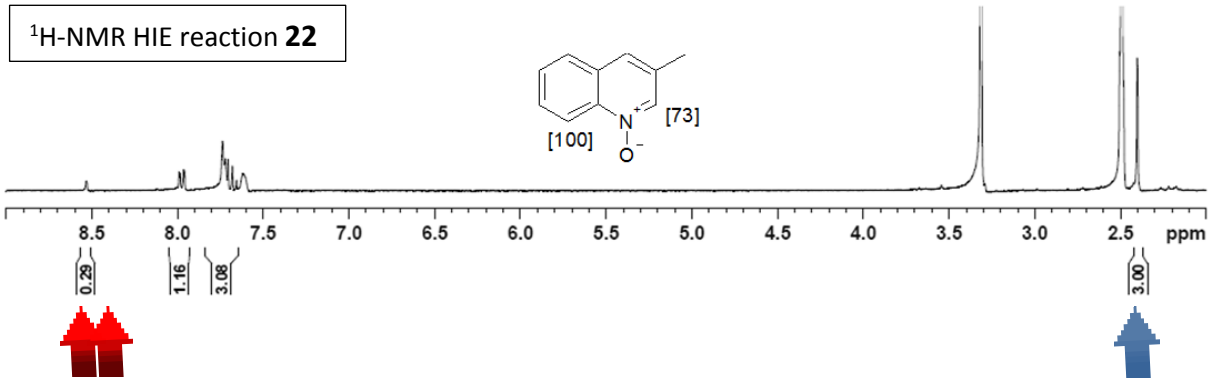

N-oxide **23**

Yield: 77%.

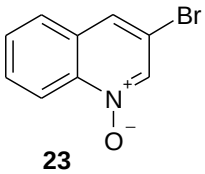

23

Molecular Weight =224.0583
Molecular Formula =C9H6BrNO

^{1}H-NMR Reference **23**

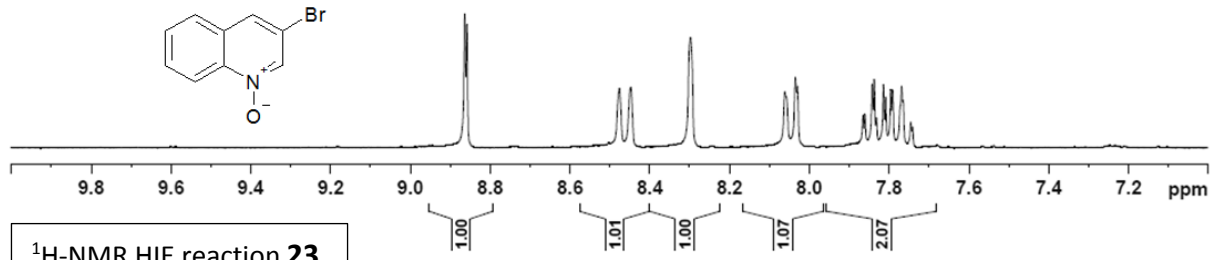

^{1}H-NMR HIE reaction **23**

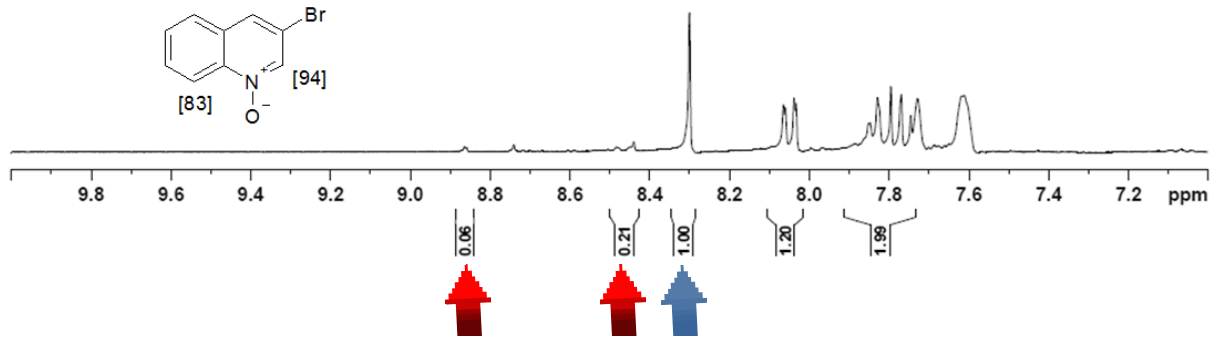

N-oxide **24**

Yield: 81%.

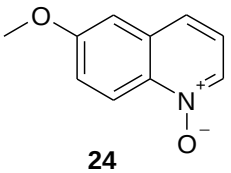

24

Molecular Weight =175.1887
Molecular Formula =C10H9NO2

^{1}H-NMR Reference **24**

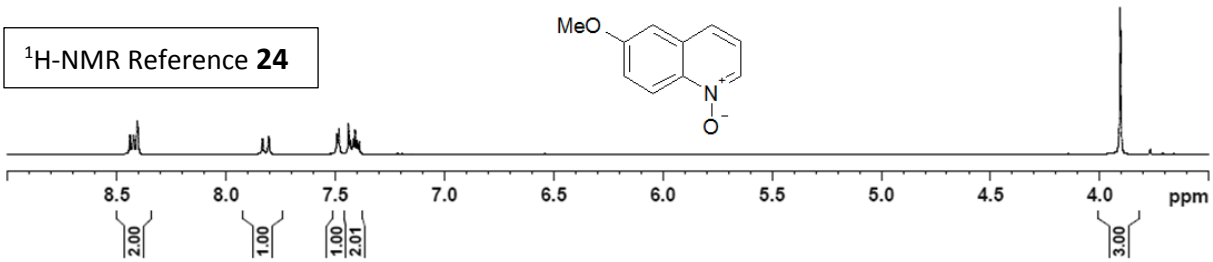

^{1}H-NMR HIE reaction **24**

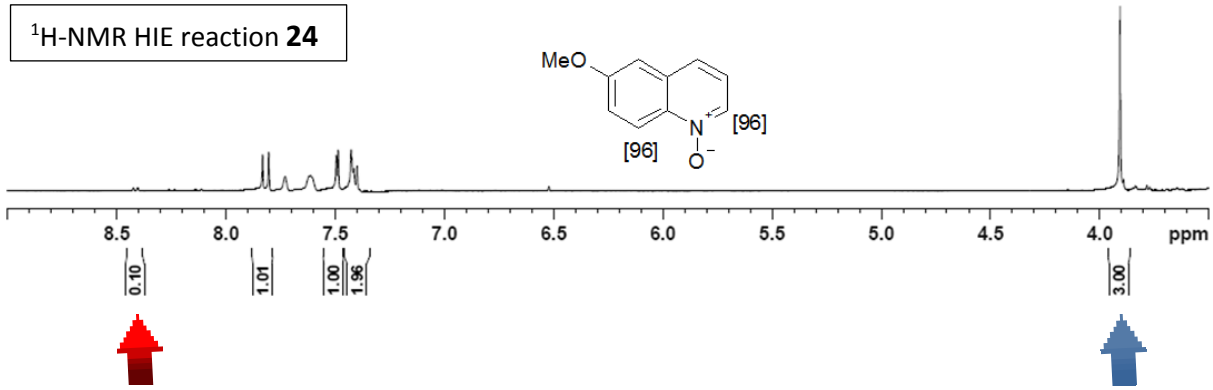

N-oxide **25**

Yield: 75%.

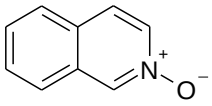

25

Molecular Weight =145.1622
Molecular Formula =C9H7NO

^{1}H-NMR Reference **25**

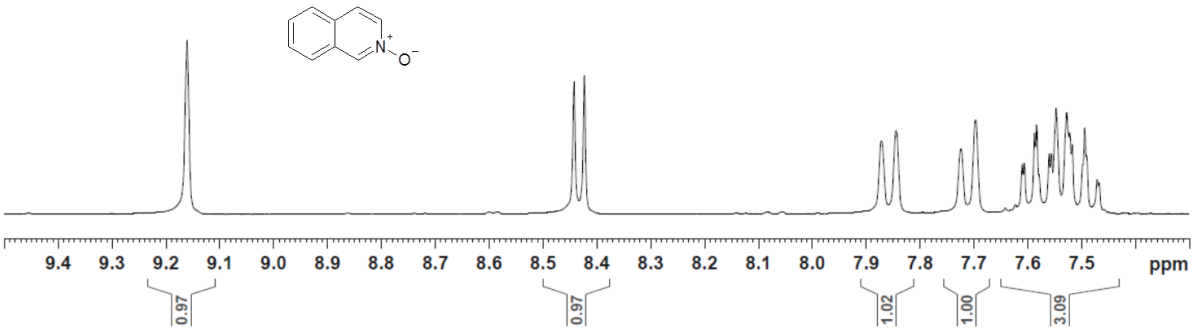

^{1}H-NMR HIE reaction **25**

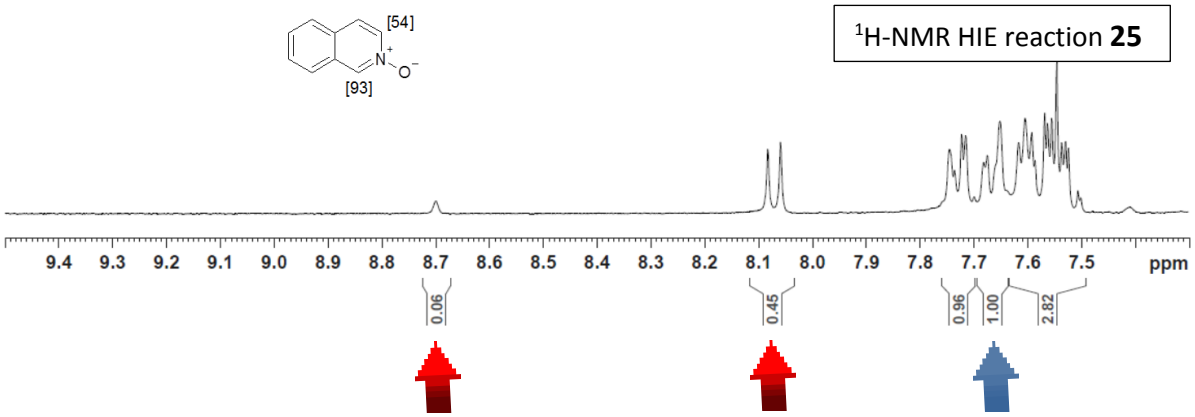

N-oxide **26**

Yield: 71%.

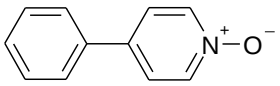

26

Molecular Weight =171.2005
Molecular Formula =C11H9NO

^{1}H-NMR Reference **26**

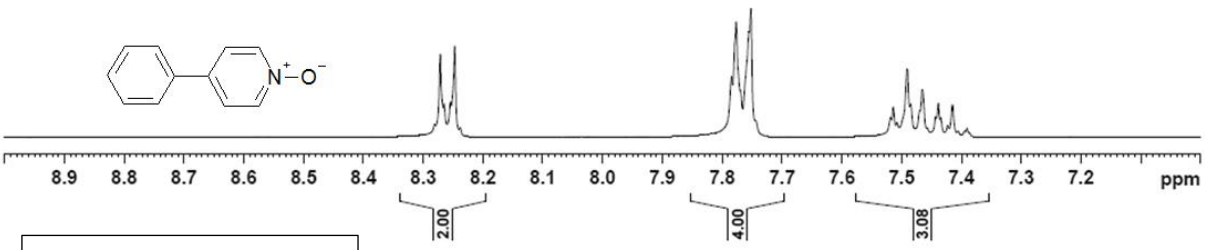

^{1}H-NMR HIE reaction **26**

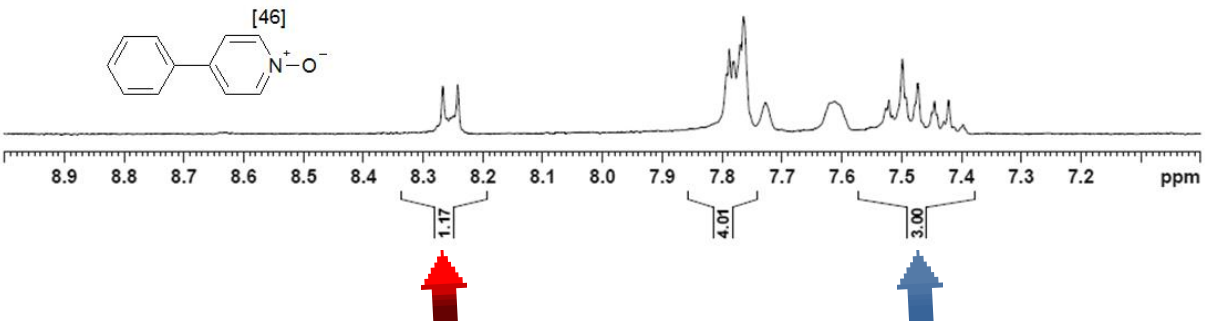

N-oxide **27**

Yield: 89%.

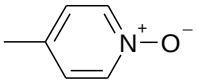

Molecular Weight =109.1288
Molecular Formula =C6H7NO

27

^{1}H-NMR Reference **27**

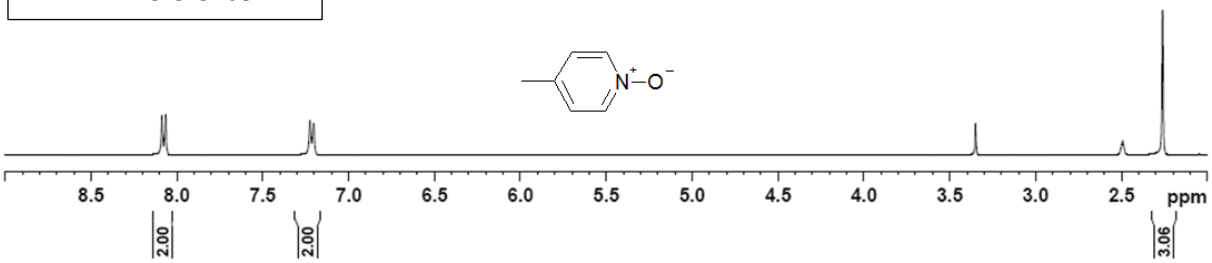

^{1}H-NMR HIE reaction **27**

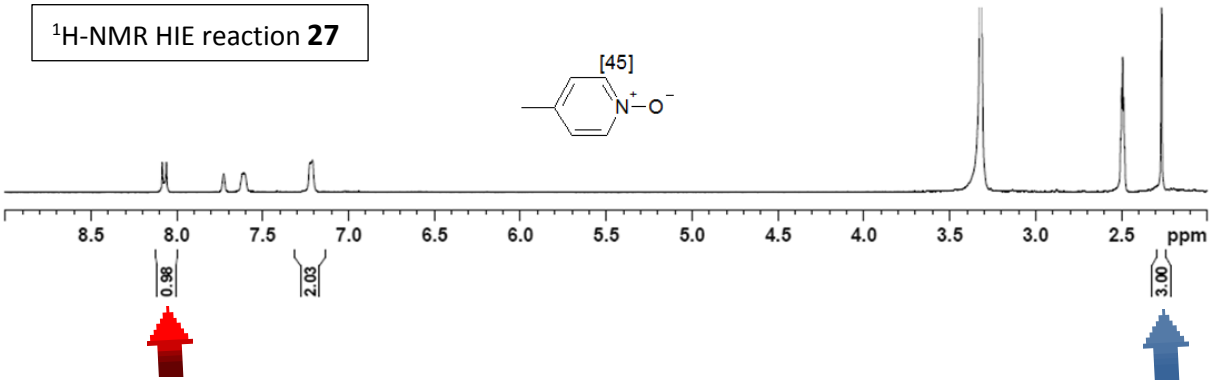

HIE reactions of phosphonamides 28-33 catalyzed by F (*scheme II.1.9*)

Conditions: substrate (10 µmol, 1 eq.), catalyst **F** (1.5 mg, 1.0 µmol, 10 mol%, 0.1 eq.), PhCl (1 mL), D_2 (1 atm), rt, 2 h.

^{1}H-NMR described previously pages 53-54.

Phosphonamide **28**
Yield: 89%.

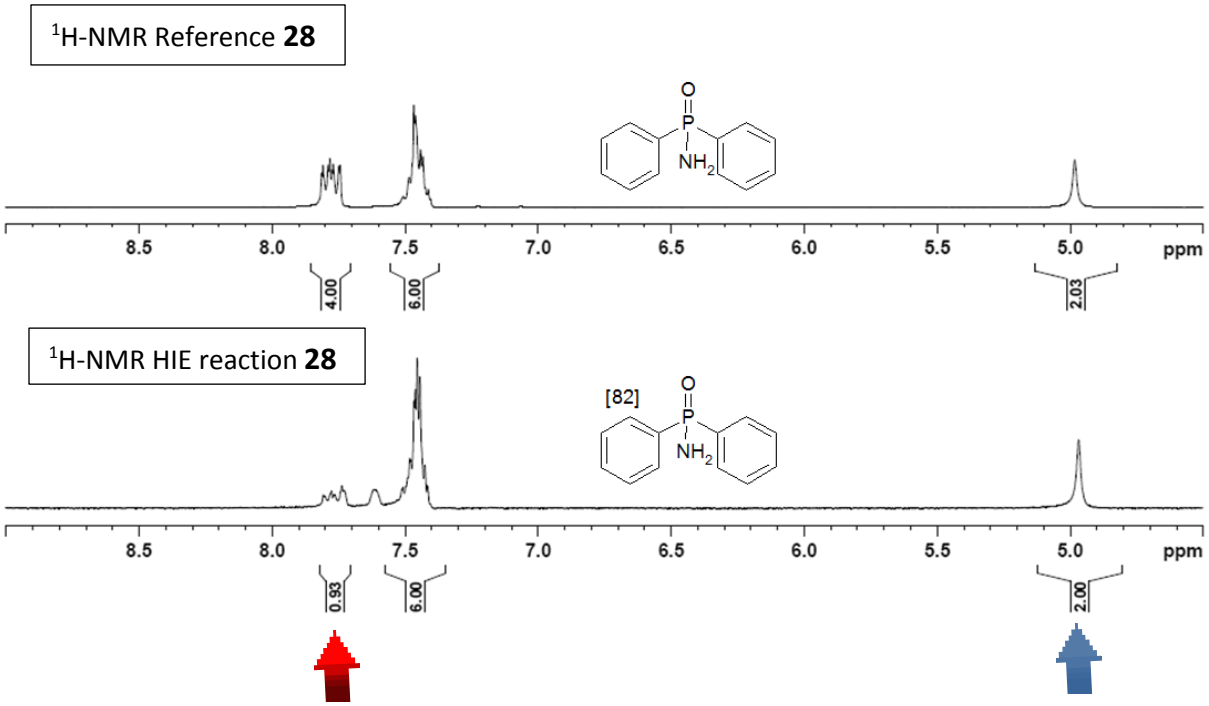

Phosphonamide **29**
Yield: 99%.

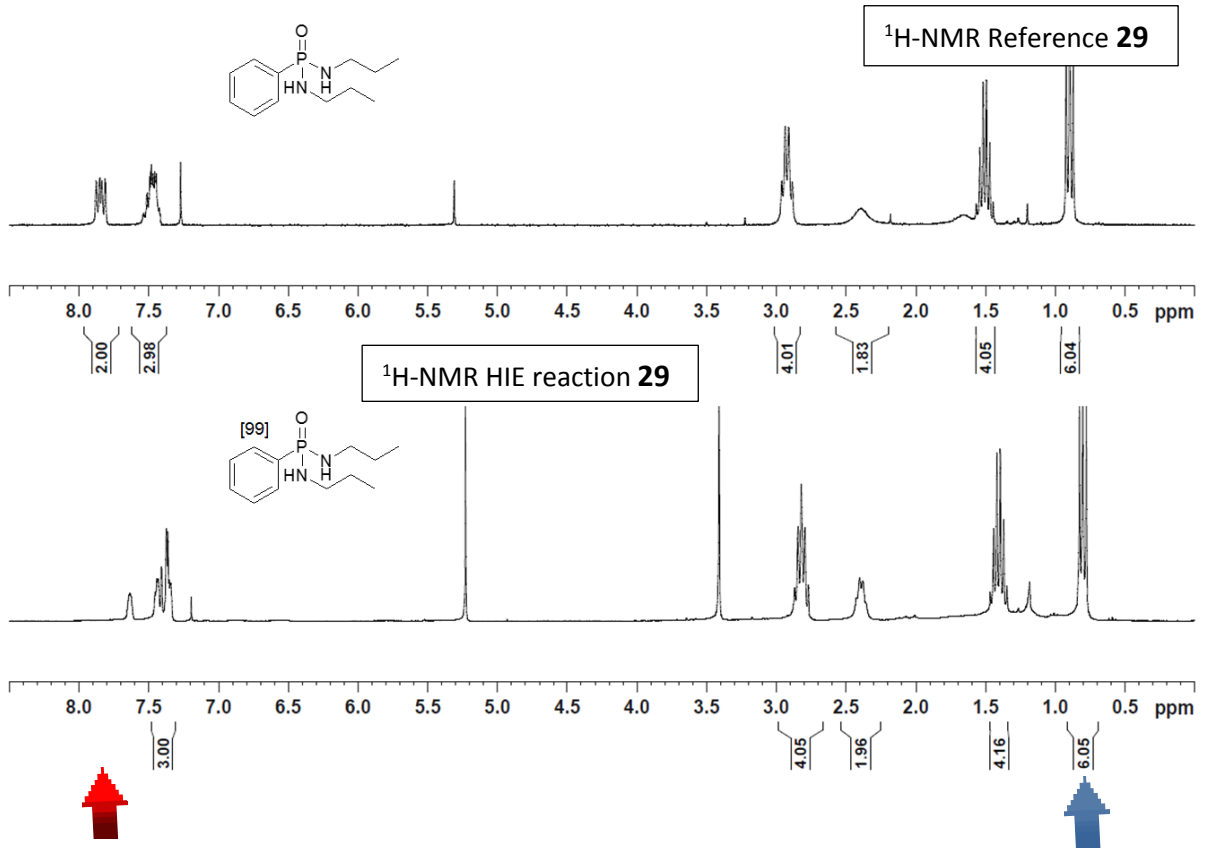

Phosphonamide **30**

Yield: 67%.

^{1}H-NMR Reference **30**

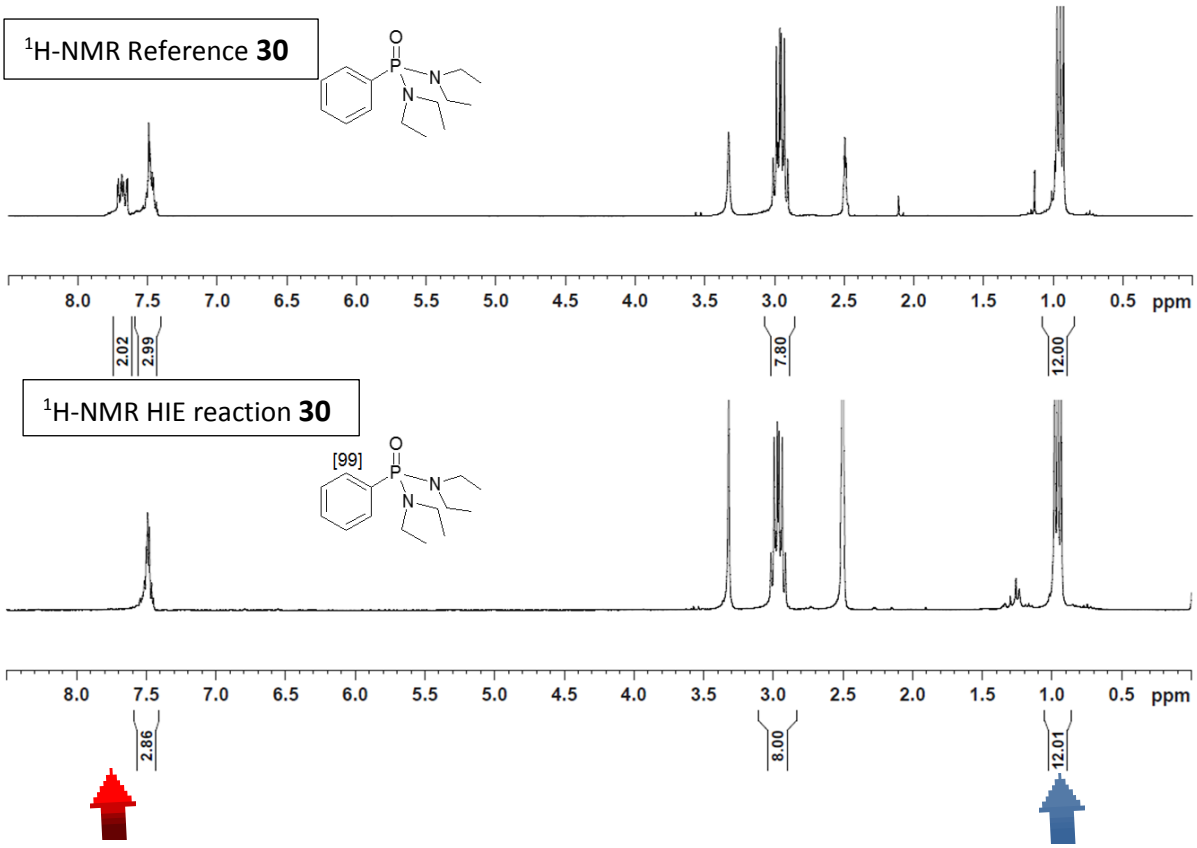

^{1}H-NMR HIE reaction **30**

[99]

Phosphonamide **31**

Yield: 99%.

^{1}H-NMR Reference **31**

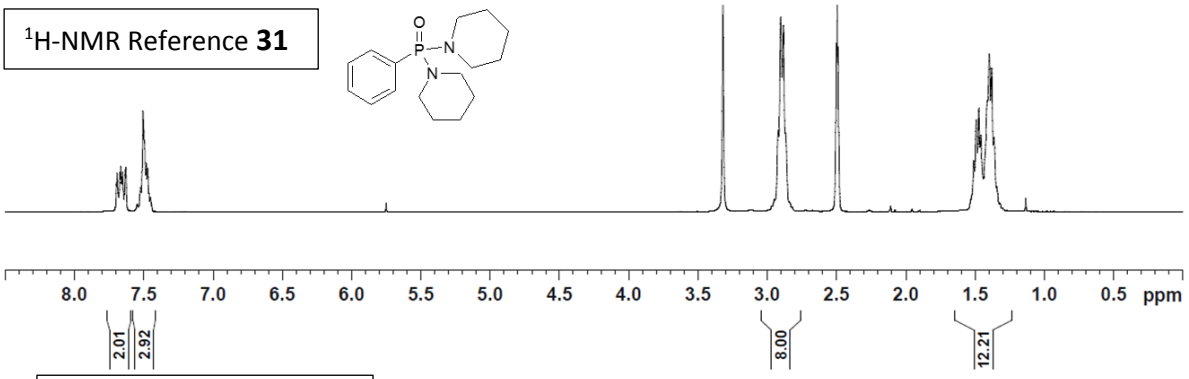

^{1}H-NMR HIE reaction **31**

[99]

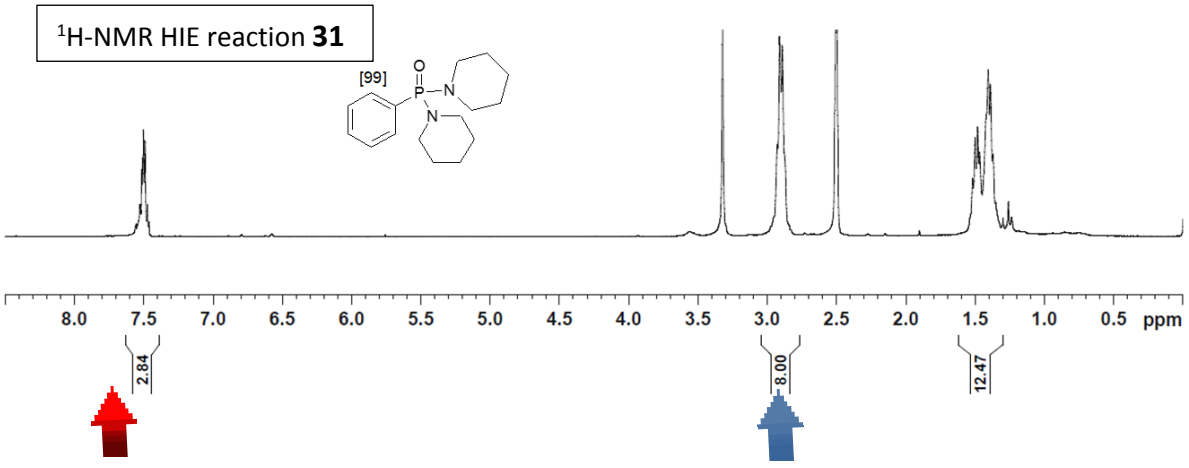

Phosphonamide **32**

Yield: 70%.

^{1}H-NMR Reference **32**

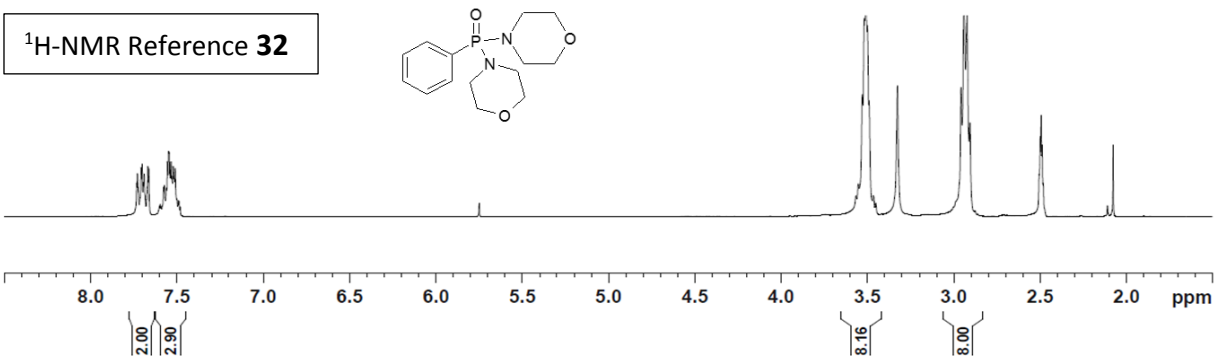

^{1}H-NMR HIE reaction **32**

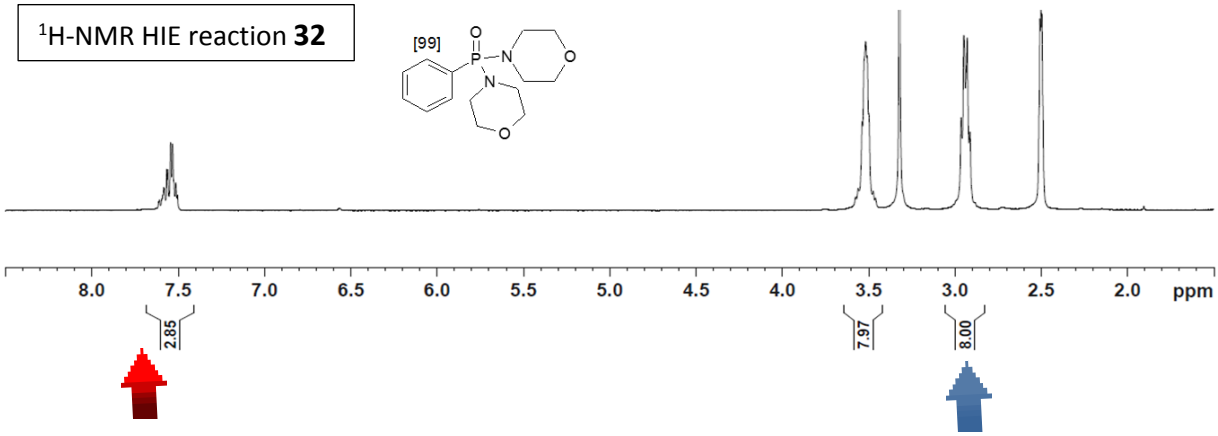

Phosphonamide **33**

Yield: 71%.

^{1}H-NMR Reference **33**

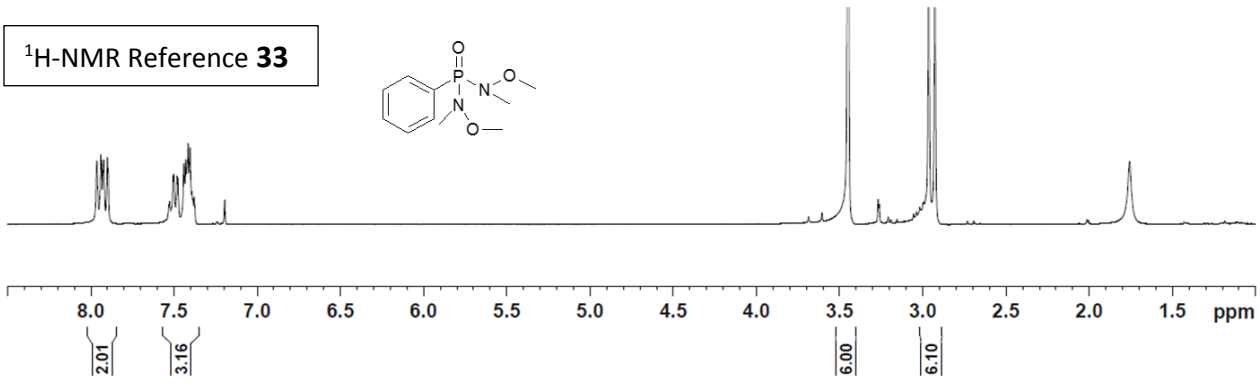

^{1}H-NMR HIE reaction **33**

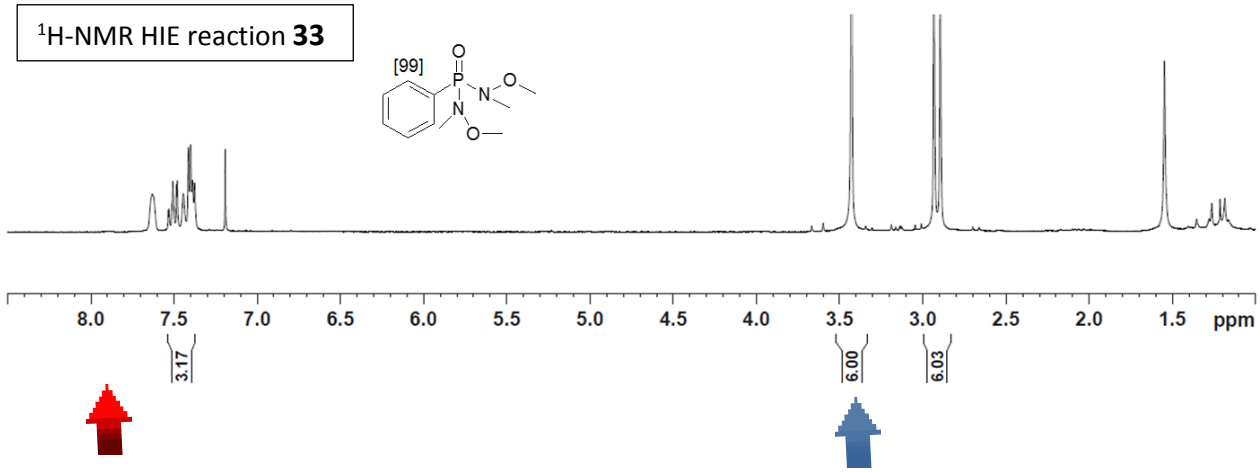

Chapter 2: Overcoming an old challenge in directed iridium-catalyzed hydrogen isotope exchange reactions - Phenylacetic acid derivatives

II.2.1. Introduction

II.2.1.1. The phenylacetic acid derivatives moiety in life sciences

The phenylacetic acid derivatives are present in many life science products such as pharmaceutical drugs such as Ibuprofen **1**, Diclofenac **2,** Penicillin G **3**, Clopidogrel **4**, Camylofine **5**, Fexofenadine **6**, Naproxen **7,** Loperamide **8**, and Lorcainide **9**. The phenylacetic acid moiety is also present in fungicides like e.g. Benalaxyl **10** which is used in crop protections (*scheme II.2.1*).

Scheme II.2. 1: *Phenylacetic acid derivative drugs*

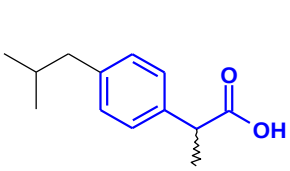

Ibuprofen**1**

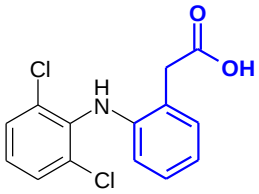

Diclofenac **2**

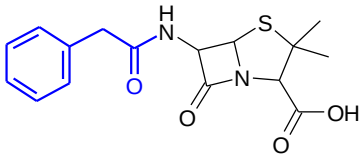

Penicillin G **3**

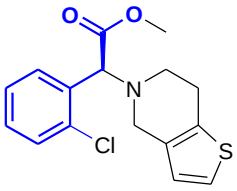

Clopidogrel **4**

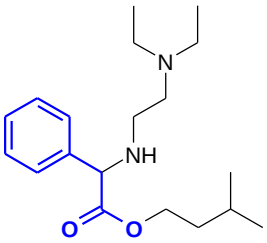

Camylofine **5**

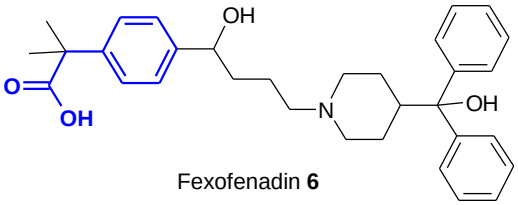

Fexofenadin **6**

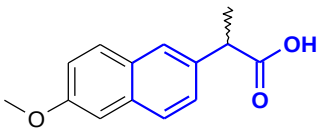

Naproxen **7**

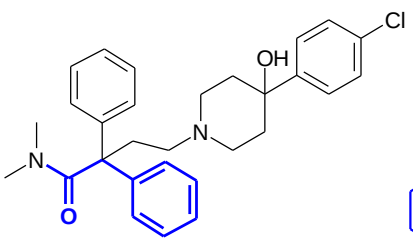

Loperamide **8**

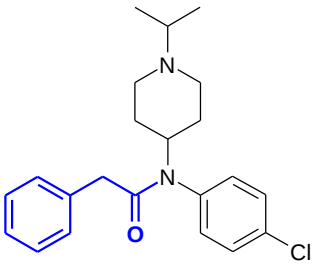

Lorcainide **9**

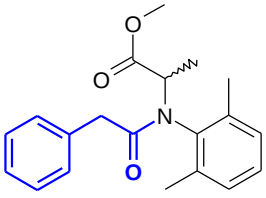

Benalaxyl **10**

II.2.1.2. Literature background of HIE reactions on phenylacetic acid derivatives

In 1996, Heys *et al.* studied the HIE performance of several iridium(I) complexes such as Crabtree's catalyst **A**, $[Ir(COD)(PPh_3)_2]BF_4$ **18** and $[Ir(COD)(dppe)]BF_4$ **19**. A very low deuterium incorporation of only up to ca. 7% (**11**) was found for ethyl phenylacetate **[H]-11** (*scheme II.2.2,* A).[1] Sajiki *et al.* developed an unselective method based on heterogeneous catalysis for labeling of all aromatic protons (**12**) with palladium and platinum on charcoal at 180 °C in D_2O (*scheme II.2.2,* B).[2]

Scheme II.2. 2: *Known aromatic HIE reactions for CH-activation/deuteration in phenylacetic acid derivatives* ***[H]-11-14*** [1,2,4,5]

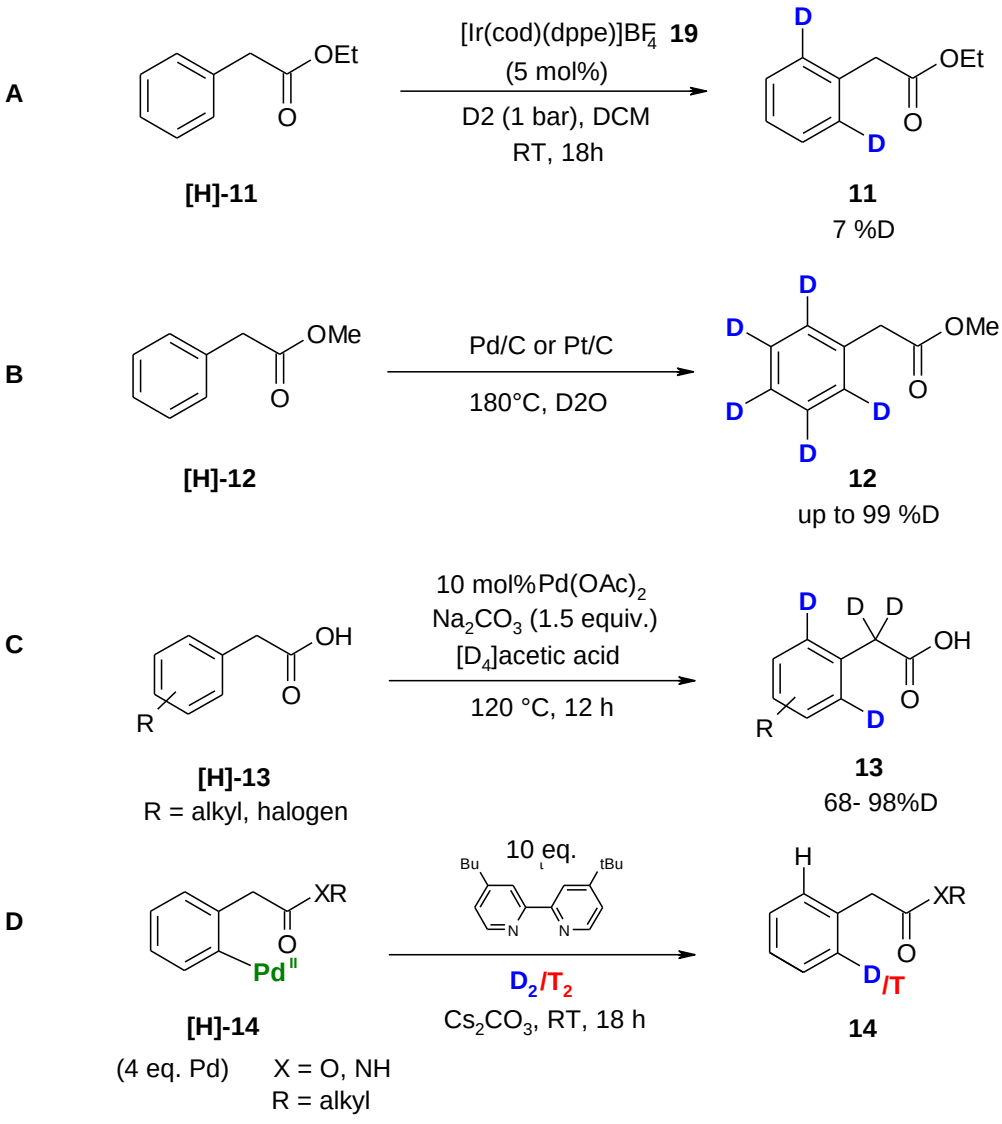

Even though the deuterium incorporation was high (up to 99 %D), the harsh conditions at 180°C, the low selectivity and the large excess of D_2O were limiting the general usefulness of the method. The high excess of the isotope source (D_2O) made the transfer to tritium chemistry impractical.[3] The first *ortho*-selective HIE method was reported by Yu *et al.* in 2014. They discovered a palladium-catalyzed HIE reaction of phenylacetic acids **[H]-13** with deuterated acetic acid as deuterium source and *ortho*-deuteration up to 99 %D (*scheme II.2.2,* C).[4] However high temperature and low pH limit the applicability of the method. Moreover, due to the high excess of the deuterium source (used as solvent), the method was not transferable to the tritium requirements.

Recently, the approach was adapted to tritium chemistry by Hoover *et al.*[5] They generated substrate-palladium complexes **[H]-14**, which were isolated and purified, and then in a second step, were reduced subsequently by deuterium or tritium (*scheme II.2.2*, D). However, Hoover's protocol is non-catalytic and requires a potentially troublesome precursor synthesis, together with tedious removal of excess palladium and ligand.

In order to circumvent these shortcomings, we became interested in developing an improved catalytic HIE method under very mild reaction conditions with D_2/T_2 as hydrogen isotope source.

II.2.1.3. What makes phenylacetic acid derivatives such a challenge?

As described above, phenylacetic acid derivatives have remained a challenge in direct HIE methodology for tritium applications. For iridium catalyzed HIE reactions, the comparison of the activation energies $\Delta\Delta H$ for different aromatic substrates **[H]-12, [H]-15-17** might help in understanding why some DG are more challenging than others. In *figure II.2.1*, these activation energies $\Delta\Delta H$ have been calculated (in the gas phase) for the HIE reactions with catalyst **F** at 25°C). The high-energy barriers which are needed for a successful HIE reaction of phenylacetic esters **[H]-12** and ketones **[H]-15** is suggesting that only a very efficient catalyst must be used if mild reaction conditions (low temperatures) can be applied. Interestingly, the compounds **[H]-12, [H]-15-17** are passing through a six-membered ring transition state, however due to their additional lone pairs in the aromatic substituting oxygen and nitrogen atoms, the possible mesomeric structures can lower the whole activation energy significantly. For this reason, there are some literature reports on successful iridium catalyzed HIE reactions of acetanilides **[H]-17** with up to 97%D and fewer for acetylphenol **[H]-16** (up to 69%D) known already.[6]
As the P,N-ligated iridium catalyst **F** had demonstrated unique reactivity features and an unprecedented HIE transition-state flexibility involving 5-, 6- and even 4-membered rings,[7] we wanted to investigate its activity towards phenylacetic acid derivatives.

Figure II.2. 1: *Potential energy profile for ortho-deuteration of* ***12, 15-17*** *with iridium catalyst* ***F*** *scaled to Gibbs free energy (ΔG^0).*

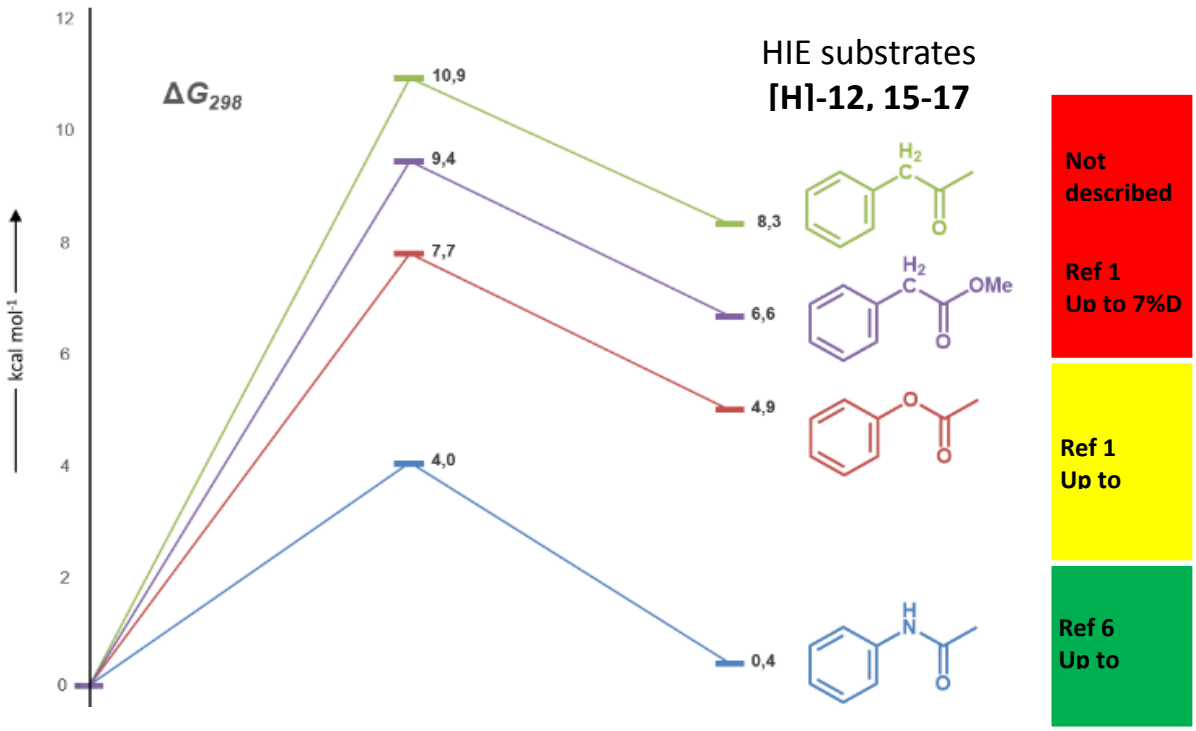

II.2.2. Optimization of the model compound

II.2.2.1. Catalyst screening

The HIE study was initiated by examining the deuteration of methyl phenylacetate **[H]-12** as model substrate under 1 bar of D_2 with different commercially available iridium(I) catalyst (globally noted Ir-cat) and catalyst **F**. Catalyst **F** can be synthesized in five reaction steps according the procedure described by Tamm *et al.*[7]

The reaction was run at room temperature in chlorobenzene for 2h (*table II.2.1*). The results clearly demonstrated the high activity of catalyst **F** (entry 8) with incorporation of 1.8 deuterium atoms into the molecule. Especially compared to the other tested catalysts **A-E**, **18-20** (entry 1-7) which could incorporate 0.13 deuterium atoms at the maximum under the described reaction conditions. [1]

Table II.2. 1: *Comparison of different commercially available iridium(I) catalysts and catalyst* ***F*** *in HIE reactions of methyl phenylacetate* ***[H]-12***

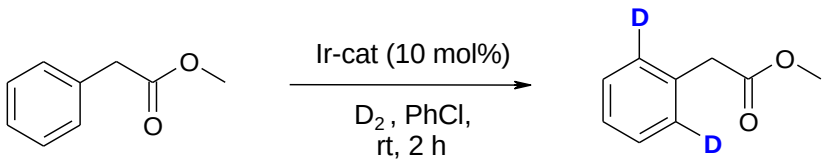

[H]-12 **12**

Entry	Catalyst	Loading (mol%)	D/molecule (12)[c]
1[a]	[Ir COD(PPh_3)$_2$]BF_4 (18)	100	<0.02[a]
2[a]	[Ir COD(dppe)]BF_4 (19)	5	0.13[a]
3[b]	Pfaltz catalyst D	10	0
4[b]	1,5-COD(F_6-acac)iridium(I) (20)	10	0.01
5[b]	Burgess catalyst E	10	0.06
6[b]	Kerr catalyst B_a	10	0.01
7[b]	Crabtree catalyst A	10	0.02
8[b]	Tamm catalyst F	10	1.8

[a]Literature data; [b]Conditions: substrate **[H]-12** (1.5 mg, 10 µmol, 1 eq.), D_2 (1 atm), chlorobenzene (1 mL), rt, 2h. [c]determined by LC-MS

II.2.2.2. Time screening

A reaction advancement (deuterium incorporation) was studied versus time on model compound **[H]-12** with catalyst **F** in chlorobenzene at room temperature. Samples of the on-going reaction were taken off at different time points, from 15 min to 24 h, and analysed by LC-MS. A maximum plateau corresponding to 1.8 deuterium/molecule was reached after 105 min (*figure II.2.2*). Consequently, an optimal reaction time of two hours was kept for the entire project.

Figure II.2. 2: *Kinetic study of the HIE reaction of methylphenylacetate ester* ***[H]-12*** *with catalyst* ***F****.* [a,b]

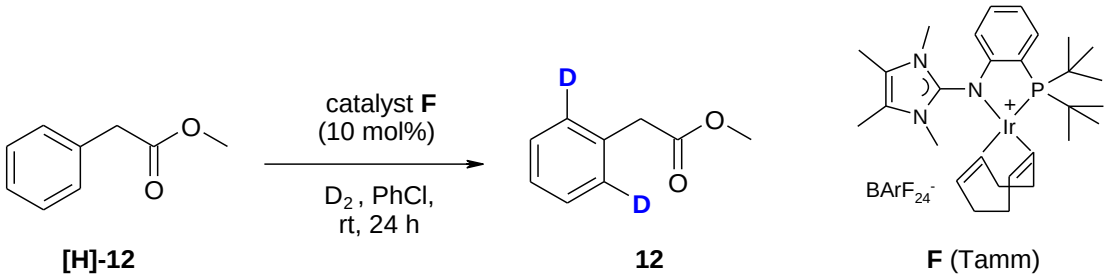

[H]-12 **12** **F** (Tamm)

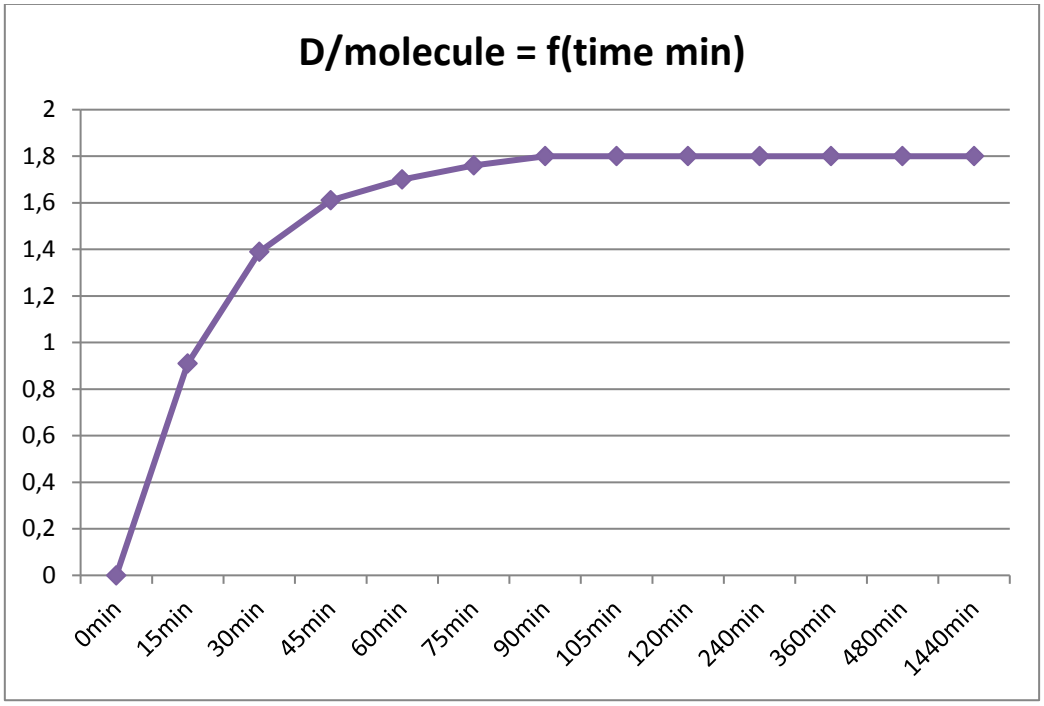

[a]Conditions: substrate **[H]-12** (1.5 mg, 10 µmol, 1 eq.), catalyst **F** (1.5 mg, 1.0 µmol, 10 mol%), chlorobenzene (1 mL), D_2 (1atm), rt. [b]Position determined by 1H NMR and percentage of deuterium incorporation analysed by LC-MS.

II.2.2.3. Solvent and temperature screening

Furthermore, we evaluated the impact of the solvent and temperature in HIE reactions of methyl phenylacetate **[H]-12** with catalyst **F** (*table II.2.2*). The highest deuterium incorporation was obtained in chlorobenzene with 1.80 D/molecule at room temperature (entry 6). A small decrease was observed at 110°C with 1.71 D/molecule (entry 17). Use of solvents like chloroform (entry 1 & 12), isopropylacetate (entry 4 & 15), dichloromethane (entry 5 & 16), cyclohexane (entry 7 and 18), methylcyclohexane (entry 8 & 19), and toluene (entry 10) provided a deuterium enrichment going from 0.90 to 1.10 D/molecule. In MTBE (entry 2 & 13), ethanol (entry 3 & 14), 1-butanol (entry 9 & 20) and dioxane (entry 11 & 22) the HIE proceeded in a much lower isotopic enrichment going from 0.40 to 0.83 D/molecule.

Table II.2. 2: *Solvent and temperature screening of catalyst* ***F*** *in the HIE reaction of methylphenylacetate ester* ***[H]-12****.* [a,b]

Entry	Solvent	Temp.	D/molecule
1	chloroform	RT	0.9
2	MTBE	RT	0.77
3	ethanol	RT	0.65
4	isopropylacetate	RT	0.9
5	dichloromethane	RT	1.06
6	chlorobenzene	RT	1.8
7	cyclohexane	RT	1.05
8	methylcyclohexane	RT	0.9
9	1-butanol	RT	0.72
10	toluene	RT	1.02
11	dioxane	RT	0.4
12	chloroform	55°C	1.06
13	MTBE	50°C	0.68
14	ethanol	70°C	0.41
15	isopropylacetate	85°C	0.93
16	dichloromethane	35°C	1.03
17	chlorobenzene	110°C	1.71
18	cyclohexane	75°C	0.99
19	methylcyclohexane	95°C	0.99
20	1-butanol	110C	0.83
21	toluene	105°C	0.94
22	dioxane	95°C	0.52

[a]Conditions: substrate **[H]-12** (1.5 mg, 10 µmol, 1 eq.), catalyst **F** (1.5 mg, 1.0 µmol, 10 mol%), solvent (1 mL), D_2 (1atm), 2 h. [b]Position determined by ^{1}H NMR and percentage of deuterium incorporation analysed by LC-MS.

II.2.2.4. Catalyst loading screening

We have also investigated the catalyst loading of **F** (*table II.2.3*) in order to optimize the labelling conditions. A loading of 5 mol% resulted in 1.5 added deuterium atoms in the substrate (entry 1) whereas with 10-15-20 mol%, as before, the same maximum isotopic enrichment was 1.80 D/molecule. Consequently, we used 10 mol% of catalyst **F** for the project.

Table II.2. 3: *Evaluation of catalyst **F** loading in the HIE reaction of **[H]-12**.*[a,b]

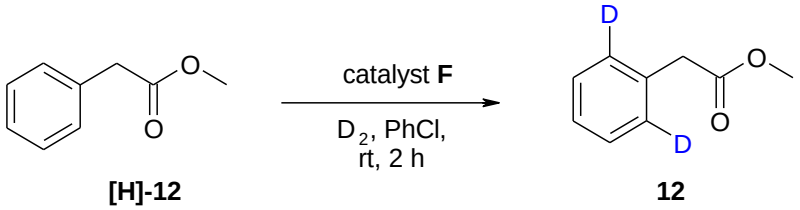

[H]-12 **12**

Entry	Catalyst ratio	D/molecule
1	**5 mol%**	**1.49**
2	**10 mol%**	**1.8**
3	**15 mol%**	**1.79**
4	**20 mol%**	**1.8**

[a]Conditions: substrate **[H]-12** (1.5 mg, 10 µmol, 1 eq.), catalyst **F** (1.5 mg, 1.0 µmol, 10 mol%), chlorobenzene (1 mL), D_2 (1atm), rt, 2 h. [b]Position determined by 1H NMR and percentage of deuterium incorporation analysed by LC-MS.

By varying the reaction parameters, such as catalyst amount, solvent, temperature and time, optimal conditions were identified to be 10 mol% catalyst **F** in chlorobenzene at room temperature for 2 h. Under these conditions, we have pursued our study on a series of phenylacetic acid derivatives.

II.2.3. Scope and limitation of catalyst F in HIE of phenylacetic acid derivatives

II.2.3.1. HIE reactions with catalyst F on phenylacetic ester derivatives

Catalyst **F** has promoted *ortho*-directed deuteration of a variety of phenylacetic acid esters (**11, 12, 18–27**) with high yields, good selectivity and good to high deuterium incorporation of up to 95 %D (*scheme II.2.3*).

Scheme II.2. 3: *HIE reactions of phenylacetic acid esters* ***11, 12, 21–37*** *with catalyst* ***F***[a,b]

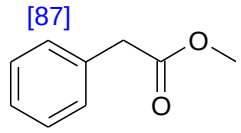

12, 83%

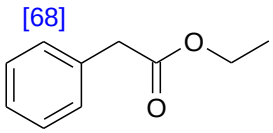

11, 78%

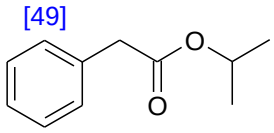

21, 81%

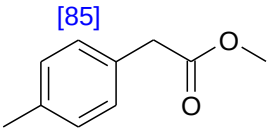

22, 87%

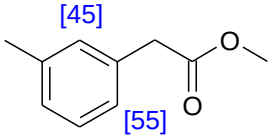

23, 91%

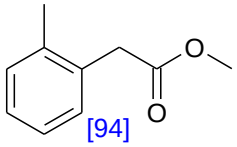

24, 82%

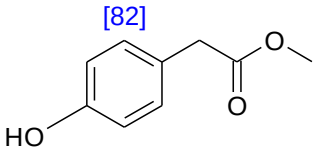

25, 89%

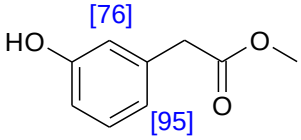

26, 91%

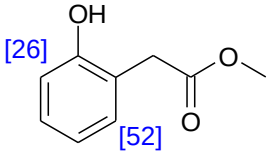

27, 91%

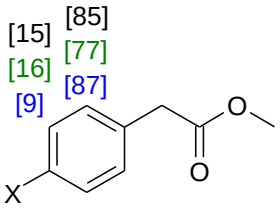

28a (X=F), 32%
28b (X=Cl), 90%
28c (X=Br), 88%

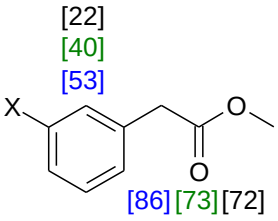

29a (X=F), 75%
29b (X=Cl), 89%
29c (X=Br), 95%

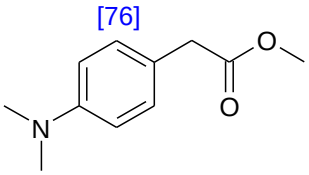

30, 82%

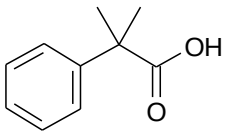

31 [0]

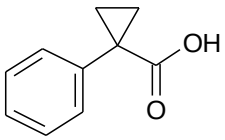

32 [0]

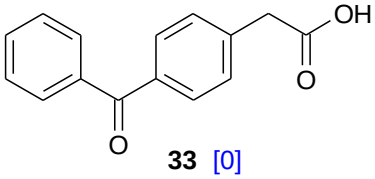

33 [0]

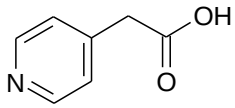

34 [0]

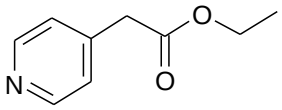

35 [0]

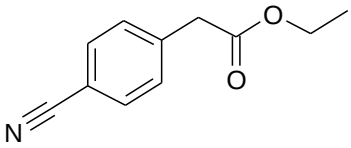

36 [0]

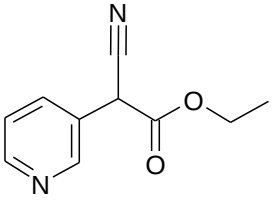

37 [0]

[a]Conditions: substrate (1 eq.), catalyst **F** (10 mol%), chlorobenzene (1 mL), D_2 (1atm), rt, 2 h. [b]Position and percentage of deuterium incorporation determined by ^{1}H NMR.

Interestingly, the efficiency of the HIE reaction depended strongly on the size of the ester function, resulting in decreasing deuterium incorporation levels in the order methyl (**12**, 87%D) > ethyl (**11**, 68%D) > isopropyl (**21**, 49%D). Additionally, the HIE reaction was somewhat sensitive towards the substitution pattern at the aryl ring. While *meta*-substitution in 3-tolylacetic acid methyl ester **23** gave 45 %D and 55 %D, respectively, the corresponding *para*- (**22**) or *ortho*-substituted (**24**) analogues gave better deuterium incorporation (85 %D and 94 %D). This was also observed in the halogenated substrates **28** and **29**. Interestingly, this trend was not observed for the hydroxyl-substituted esters **25–27**, indicating that not only steric but also electronic factors, like electron density or mesomeric resonance structures, exert influence on the outcome of the HIE reaction.
Even though the kinetic study shown previously had demonstrated that after 2 h, the reaction reached its maximum of deuterium incorporation, the reaction time for compounds with lower deuterium incorporation like **21**, **23** or **27** was thus increased to 24 h. However, this had no positive effect on the final deuteration results. Probably this is due to the inactivation of the catalyst as no decomposition was detected and still large excess of D_2 remained in the reaction system. Unfortunately, the HIE reactions on free phenylacetic acids like **31-34** were not successful at all. A possible reason could be that the acidic proton of the carboxylic acid is coordinating to the iridium(I) metal and inhibiting any further activity. In addition, compounds containing nitrile function directly on the phenyl ring (**36**) or in the benzylic position (**37**) did not work at all either. The triple C-N bond being extremely rich in electrons and the iridium(I) being a transition metal looking for stabilization of his electronic environment, the iridium might directly coordinate with the N-atom of the cyanide, and therefore due to the rigidity too distant from the aromatic ring to catalyse a successful HIE reaction. Moreover, the absence of reactivity of **37** can also be due to the steric environment at the benzylic position.

The influence of the pyridine functionalities was investigated, first with the free phenylacetic acid (**34**) but as we already observed with compounds **31-33**, free acids are not providing successful results. Consequently, the ester derivatives **34, 35** containing the pyridine were also run under our reaction conditions. However, no deuterium incorporation has been observed. This is probably due to the N-heteroatom in the pyridine moiety as a competing directing group. As the pyridine is a much better metal ligand in comparison to the carboxylic acid functional group (see Part III Chapter 2) the resulting coordinated catalyst is unable to perform the HIE reaction.

II.2.3.2. HIE reactions with catalyst F on phenylacetic amide derivatives

Under the general reaction conditions, *ortho*-directed deuteration of a variety of phenylacetic amides (**38**–**49**) was also achieved with high yields, good selectivity and high to excellent deuterium incorporation up to 99%D (*scheme II.2.4*). In nearly all reactions of the *N*-methyl amides **38**, **39**, **41**, **42**, **44** and **45**, we observed additional deuteration at the

N-methyl group with 13–33 %D (**39**, 63 %D). Interestingly, these aliphatic labelling side reactions could be completely avoided by introduction of larger *N*-substituents like in amides **40**, **43**, **46** and **47**, indicating that excellent selectivity and deuterium incorporation can be achieved. Unfortunately, we observed no HIE reaction with primary amides like **48** and **49** under these reaction conditions. We propose that the primary amide chelates to the iridium(I) atom similar to the carboxylates and therefore a more stable complex is being formed making a HIE reaction impossible.

Scheme II.2. 4: *HIE reaction on various phenylacetic amides* ***38-49*** *with catalyst* ***F****.* [a,b]

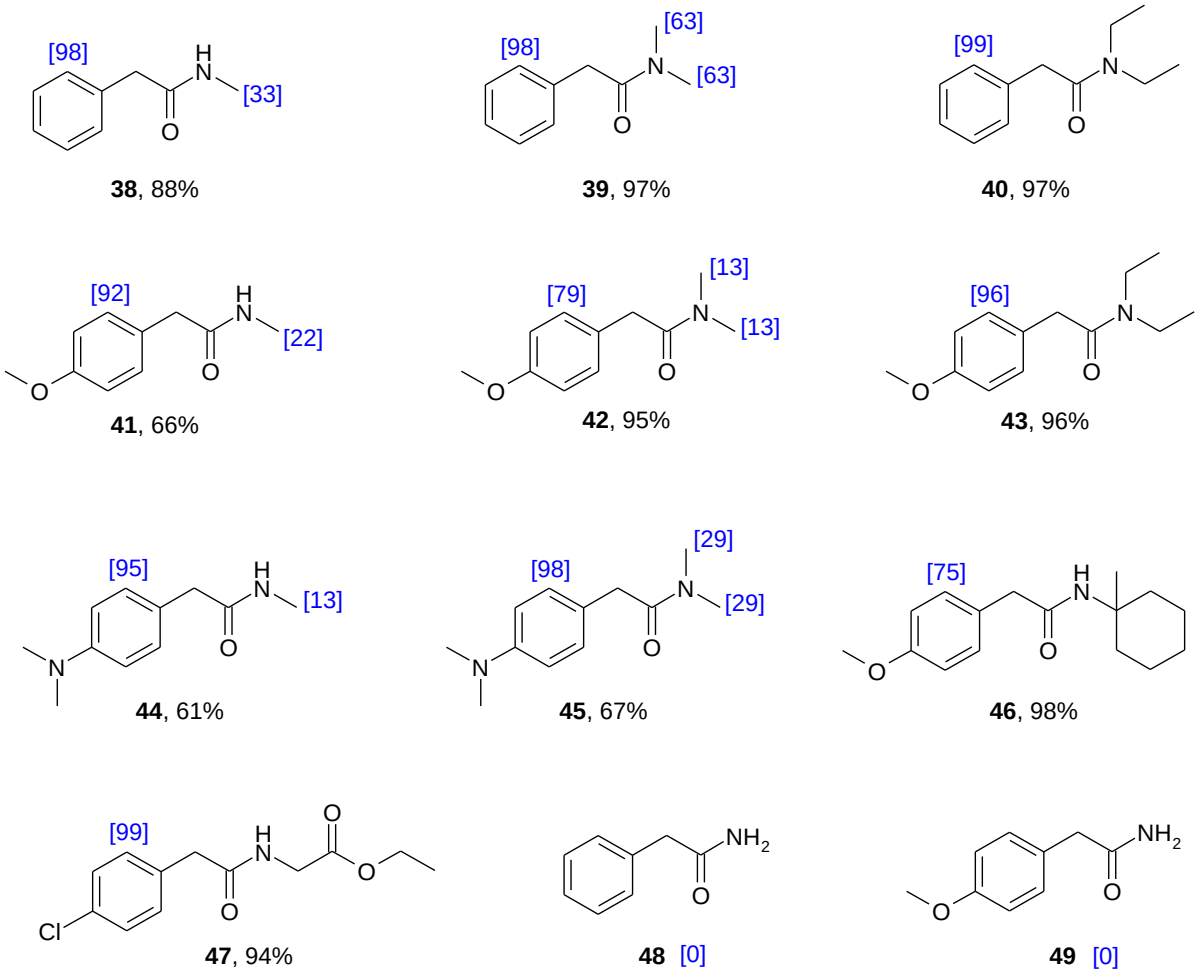

[a]Conditions: substrate (1 eq.), catalyst **F** (10 mol%), chlorobenzene (1 mL), D_2 (1atm), rt, 2 h. [b]Position and percentage of deuterium incorporation determined by ^{1}H NMR.

II.2.3.3. Application on phenylacetic acid derivatives drug molecules

II.2.3.3.a) HIE reactions on drugs with excess of deuterium gas

We further applied our method to more complex and multi-functionalized drug-like molecules bearing a phenyl acetyl moiety **5**, **10**, **50**–**53** at atmospheric deuterium pressure (*scheme II.2.5*).

Scheme II.2. 5: *HIE reaction with various drug-like phenylacetic acid esters and amides.* [a,b]

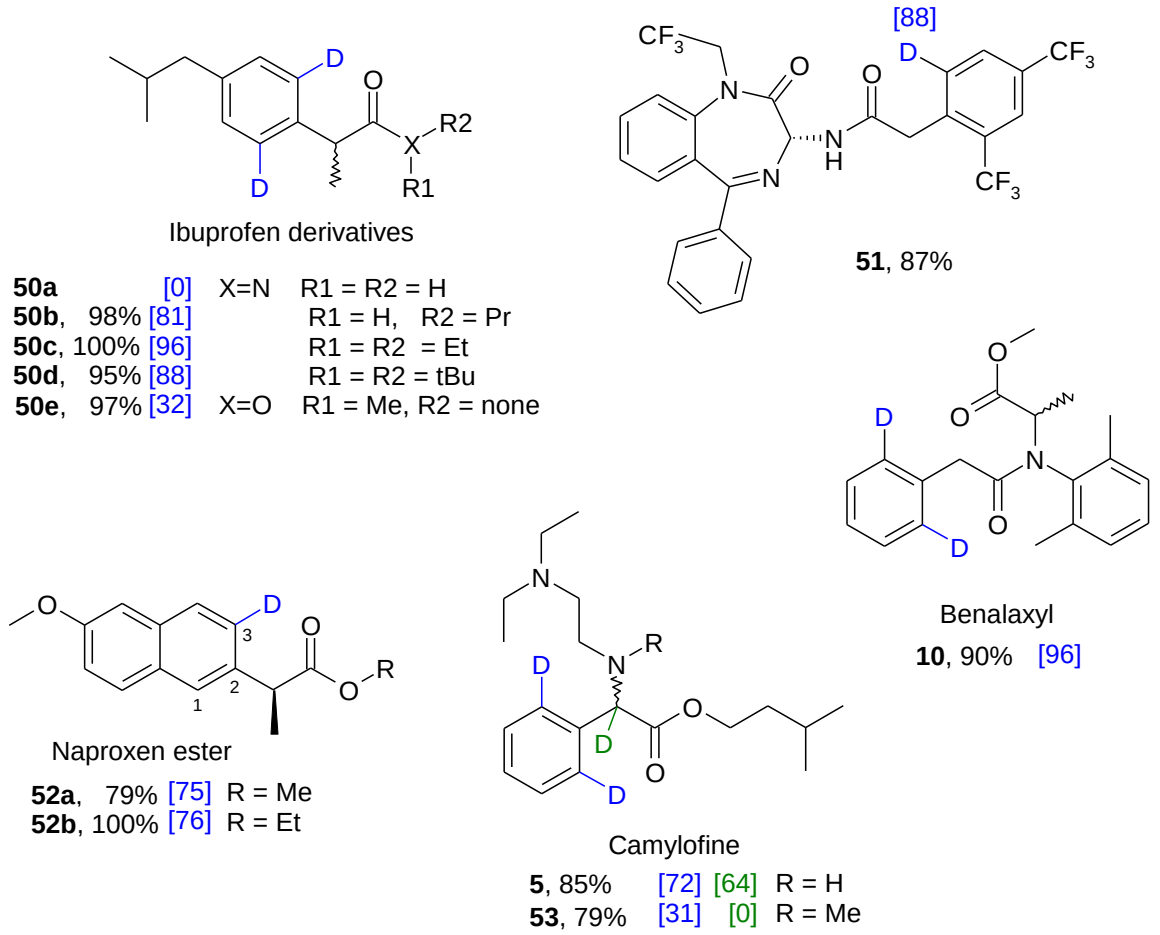

[a]Conditions: substrate (1 eq.), catalyst **F** (10 mol%), chlorobenzene (1 mL), D_2 (1atm), rt, 2 h. [b]Position and percentage of deuterium incorporation determined by 1H NMR.

For the ibuprofen derivatives **50a–e**, no HIE product has been observed for the primary amide **50a**, thus confirming the negative impact of this chemical function on the iridium-catalyzed HIE. However, good to excellent deuterium introduction were obtained for secondary and tertiary amides **50b–d** (81–96 %D). The corresponding ester **50e** (32 %D) afforded lower deuteration efficiency compared to the amides **50b–d**. A remarkable selectivity and deuterium incorporation of 99%D was achieved for drug-like compound **48**[8]

without side labelling of the other aromatic ring systems. For both naproxen esters **52a** (75 %D) and **52b** (76 %D), deuteration results are identical, but interestingly, only the 3-position has reacted. Ester **52b** was also converted into the corresponding acid (naproxen **7**) under basic conditions without significant loss of deuterium. Surprisingly, next to the expected aromatic labeling (72 %D), we have also observed deuteration in the benzylic position (64 %D) of camylofine **5**. Deuteration of the benzyl CH_2 was completely abolished by methylation of the secondary amine function in **53**, indicating that free NH groups have a significant effect on activity and selectivity of catalyst **F**. Finally, the HIE product of benalaxyl **10** have afforded a deuterium incorporation of 96 %D selectively in the *ortho*-position.

Scheme II.2. 6: *Unsuccesful drug structures used in HIE reactions with catalyst* ***F****.* [a,b]

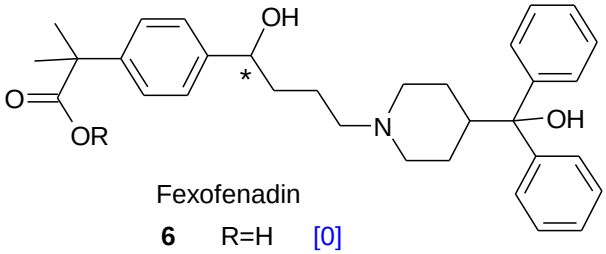

Fexofenadin

6 R=H [0]
54 R=Me [0]

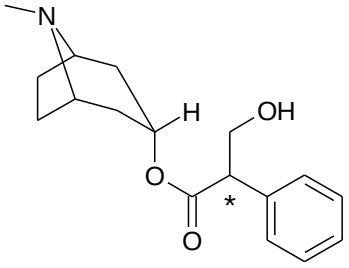

Atropine **55** [0]

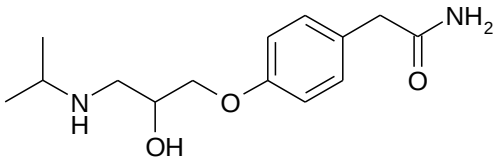

Atenolol **56** [0]

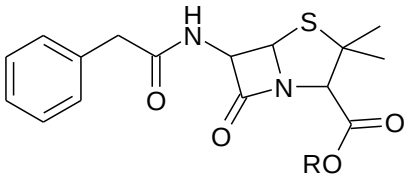

Penicillin G

3 R=H [0]
57 R=Me [0]

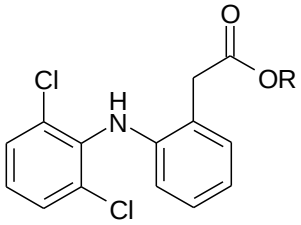

Diclofenac

58 R=H [0]
59 R=Me [0]

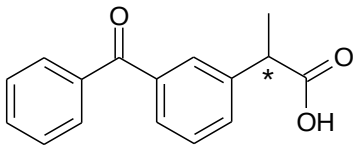

Ketoprofen **60** [0]

[a]Conditions: substrate (1 eq.), catalyst **F** (10 mol%), chlorobenzene (1 mL), D_2 (1atm), rt, 2 h. [b]Deuterium incorporation analysed by LC-MS.

Even though we had success in the HIE reactions of drugs **5**, **10**, **50–53**, we obtained no deuteration for the compounds presented in scheme II.2.6. Fexofenadine **6**, either as a free acid (**6**) or as the methyl ester (**54**), Penicillin G **3** and Diclofenac **58**, both of them investigated as free acid (**3** and **58**) and as methylated ester (**57** and **59**) did not react at all.

As expected, the free acid Ketoprofen **60** was not successful either in the HIE reaction. Also, Atropine **55** did not provide a good result. Finally, atenolol **56** containing a primary amide group could not be labelled with deuterium.

II.2.3.3.b) Transfer of the procedure to the deuterium manifold

Finally, we intended to test our developed method for tritiation of drug-like compounds. This implies that the reaction procedure is preliminarily adapted to the deuterium manifold. Camylofine **5** and Benalaxyl **10** have been selected to investigate conditions at lower deuterium pressures (<200 mbar) (*table II.2.4*).

For comparison, we run the HIE reaction of Camylofine **5** in the manifold under atmospheric deuterium pressure first and obtained the deuterated product with 1.5 D/molecule (entry 1). In the HIE reaction with 10 (entry 2), 20 (entry 3) and 30 (entry 4) equivalents of D_2, rather similar deuterium introduction was observed (1.1 - 1.3). As Benalaxyl **10** was deuterated with 96 %D at 1 bar of D_2 gas (entry 5), the equivalents window was in this case reduced down to 2.5 to 10 eq. of D_2. A very good result of 1.7 D/molecule (85 %D) was obtained with 5 eq. of D_2 (entry 7), the same as with 10 eq. of D_2 (entry 8).

Table II.2. 4: *Optimization of the deuterium pressure on the deuterium manifold*

Entry	Substrate	P1 D_2 (mbar)	P2 D_2 (mbar)	Eq D_2	D/molecule
1	Camylofine 5	1013	1013	n.d.	1.5
2	Camylofine 5	248	166	10	1.1
3	Camylofine 5	422	270	20	1.2
4	Camylofine 5	642	407	30	1.3
5	Benalaxyl 10	1013	1013	n.d.	1.9
6	Benalaxyl 10	125	107	2.5	1.2
7	Benalaxyl 10	155	119	5	1.7
8	Benalaxyl 10	180	107	10	1.7

[a]Conditions: substrate (1 eq.), catalyst **F** (10 mol%), chlorobenzene (1 mL), rt, 2 h. [b]Percentage of deuterium incorporation determined by LC-MS.

II.2.3.3.c) Transfer of the procedure to the tritium manifold

Finally, we performed the HIE reactions of Camylofine **5** and Benalaxyl **10** under the optimized conditions in the tritium manifold (s*cheme II.2. 7)*. We observed that the HIE

reaction of Camylofine **5**, performed with 10 eq. of tritium, led to a 26 %T incorporation in the *ortho*-position and 11 %T incorporation in the benzylic position. In total, we obtained a specific activity of 32 Ci/mmol for this molecule.

Benalaxyl **10** was deuterated selectively in the *ortho*-position with 96 %D as we have seen earlier. Despite an anticipated kinetic isotope effect (D vs. T) and a much lower tritium pressure (60 mbar, 7 equivalents vs. atmospheric deuterium pressure), a specific activity of 14 Ci/mmol (25 %T) was obtained in **10**, which was more than sufficient for the planned *in-vitro* studies with ^{3}H-benalaxyl.

Scheme II.2. 8: *Tritiation of drug compounds with catalyst **F***

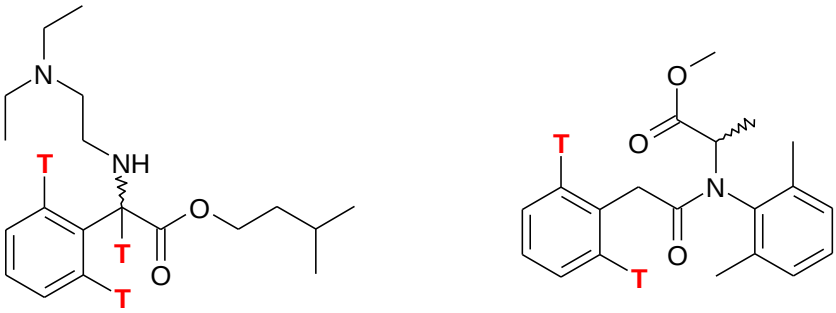

Camylofine

5 [26] [11] 60 mbar T_2, 32 Ci/mmol

Benalaxyl

10 [25] 60 mbar T_2, 14 Ci/mmol

II.2.4. Insights in the mechanism

Density functional theory (DFT) calculations were performed by Thomas Bannenberg to rationalise the experimentally observed high activity of (pre-)catalyst **F** in the deuteration of phenylacetic acid derivatives.

Methyl phenylacetate (**[H]-12**) and its binding to a cationic iridium(I) complex fragment $[(P,N)IrD_2]^+$ afforded complex **IN1** as the first stationary point on the potential energy surface (*Figure II.2.3,* left). Substrate binding in intermediate **IN1** involves the carbonyl oxygen atom and an agostic *ortho*-C–H bond, which adopts an axial position *trans* to the phosphorus atom and points between the two equatorial deuterium atoms.

In analogy to other mechanistic studies,[6,9] C–H activation represents the rate-determining step and leads to the HD complex **IN2** through σ-bond metathesis via transition state **TS1**. **IN2** is destabilized by only 6.6 kcal mol^{-1} relative to **IN1** despite the formation of a less favourable six-membered metallacycle.[1] Hydride fluxionality[10] involving **TS2** gives **IN3** with a rotated HD ligand, which allows elimination and C–D bond formation through **TS3** to furnish **IN4**, which contains the *ortho*-deuterated substrate **12**-*d* (*Figure II.2.3,* right). To confirm that

C–H activation represents the rate-determining step, the kinetic isotope effect (KIE)[11] was studied theoretically and experimentally for the deuteration of **12** and for the hydrogenation of bis-deuterated (2,6-$C_6H_3D_2$)C(O)OMe (**12**-d_2), respectively. The calculated and experimental KIE values of 3.5 and 3.5(3) are identical within the experimental error and also in good agreement with the values derived from related reactions.[9] These findings substantiate our mechanistic proposal, and the low activation barriers associated with the C–H and C–D activation steps confirm the observed high catalytic activtiy of **F**. While Heys *et al.* have shown that arylacetates resisted efficient iridium-catalyzed HIE, the related substrates N-phenylacetamide, MeC(O)NHPh, and phenyl acetate, MeC(O)OPh, gave markedly better results, indicating that replacing the bridging unit CH_2 by NH or O is favourable to achieve *ortho*-deuteration via the formation of a six-membered metallcycle.[1]

Figure II.2. 3: *Potential energy profile for ortho-deuteration of phenyl acetic methylester (**[H]-12**) with iridium catalyst **F**, scaled to Gibbs free energy (ΔG^0).*[a]

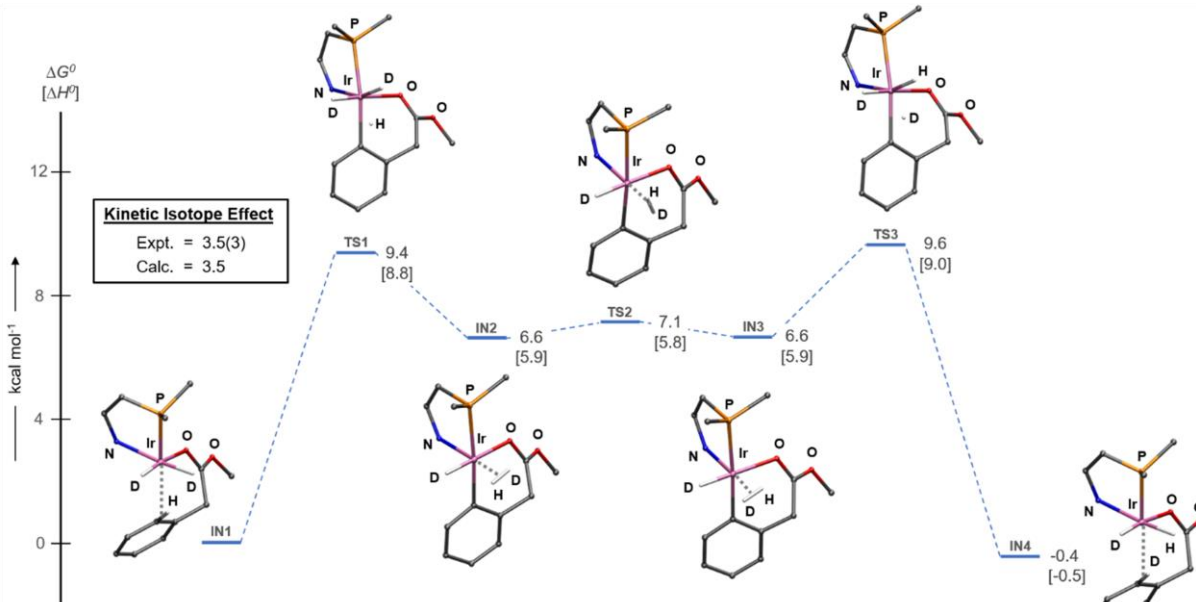

[a]All theoretical calculations were performed according to the Density Functional Theory (DFT) method M06/6-311G(d,p) for all main group elements and a "Stuttgart 1997 ECP" – double-ξ basis set with an effective core potential – for the 5d transition metal iridium. For the stationary points, all hydrogen atoms, except for those involved in the reaction pathway, were omitted for clarity, and only a rudimentary N–C–C–P–C2 skeleton of the P,N ligand is shown.

Therefore, the profile for the C–H activation step (**IN1**→**TS1**→**IN2**) was also calculated for these substrates. This has revealed the expected lower activation barriers and significant stabilization of the corresponding intermediates, especially for the acetamide (NH) derivative, which can be ascribed to conjugation within the NH- and O-bridged metallacycles.[12]

Occasionally, a color change from deep orange to dark blue of the solution was observed under the HIE reaction conditions described above, hinting at the formation of a new iridium species. In Braunschweig, a dark blue complex was isolated by stirring a solution of **F** in CH_2Cl_2 and toluene under dihydrogen atmosphere. Single crystals of this species were obtained by slow diffusion of hexane into a saturated dichloromethane solution, and X-ray diffraction analysis afforded the molecular structure of the dicationic diiridium complex $[(P,N)_2Ir_2H_4][BArF_{24}]_2$ (**61**, *Figure II.2.4*).

Figure II.2. 4: *ORTEP diagram of the dication in the complex* $[(P,N)_2Ir_2H_4][BArF_{24}]_2$ (**61**) [a]

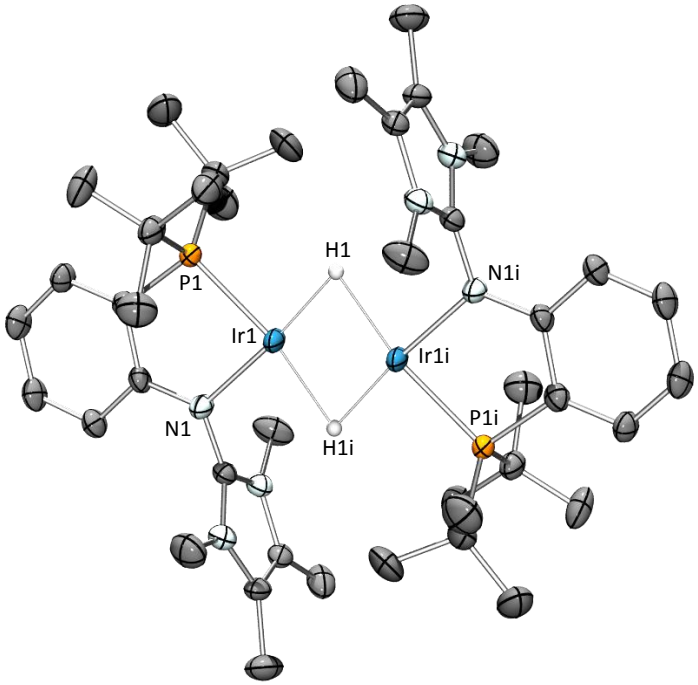

[a)]All hydrogen atoms except for the bridging ones have been omitted for clarity; the positions of the expected terminal hydrides could not be refined.

Interestingly, attempts to perform HIE on substrate **[H]-12** in the presence of complex **61** in chlorobenzene at room temperature afforded only marginal deuterium incorporation, indicating that this complex is not part of the catalytic cycle, but represents a deactivated form or an overly stabilized resting-state, respectively.[12]

II.2.5. Conclusion

In conclusion, in collaboration with the research group of Prof. Tamm, it was possible to solve a longstanding challenge in direct labelling of phenylacetic acid derivatives. While former methods have utilised non-catalytic reaction pathways or large excess of isotope source, the first efficient catalytic protocol for *ortho*-selective hydrogen isotope exchange of

pharmacologically important phenylacetic acid esters and amides with gaseous D_2/T_2 under very mild reaction conditions was developed.

By direct tritium labelling of Benalaxyl **10** and Camylofine **5,** it was proven that the method was fully adaptable to the specific requirements of tritium chemistry mentioned in the objectives of this thesis (Part I). DFT calculations and kinetic studies performed in collaboration with Braunschweig, indicated why the Tamm catalyst **F** is so successful for phenylacetic acid derivatives via a six-membered ring metallacycle transition-state. Therefore, one of the longstanding challenges in iridium-catalyzed C–H functionalization and HIE has been solved, and we believe that our findings will stimulate further applications of **F** and related catalysts in this field. Nevertheless, modifications in the catalyst structure needs to be performed to overcome the steric constraints identified in benzylic substituted phenylacetic acid derivative drugs **54-60** which have not been successful so far.

1 A. Y. L. Shu, W. Chen, J. R. Heys, *J. Organomet. Chem.* **1996**, *524*, 87–93.

2 a) H. Sajiki, N. Ito, H. Esaki, T. Maesawa, T. Maegawa, K. Hirota, *Tetrahedron Lett*. **2005**, *46*, 6995-6998; b) Y. Sawama, Y. Monguchi, H. Sajiki, *Synlett* **2012**, 959–972.

3 R. Voges, J. R. Heys, T. Moenius, *Preparation of Compounds Labeled with Tritium and Carbon-14*, Wiley **2009**, Chichester, UK

4 S. Ma, G. Villa, P. S. Thuy-Boun, A. Homs, J.-Q. Yu, *Angew. Chem. Int. Ed.* **2014**, *53*, 734–737.

5 H. Yang, P. G. Dormer, N. R. Rivera, A. J. Hoover, *Angew. Chem. Int. Ed.* **2018**, *57*, 1883–1887.

6 J. A. Brown, A. R. Cochrane, S. Irvine, W. J. Kerr, B. Mondal, J. A. Parkinson, L. C. Paterson, M. Reid, T. Tuttle, S. Andersson, G. N. Nilsson, *Adv. Synth. Catal.* **2014**, *356*, 3551–3562.

7 a) K. Jess, V. Derdau, R. Weck, J. Atzrodt, M. Freytag, P. G. Jones, M. Tamm*, Adv. Synth. Catal*. **2017**, *359*, 629–638; b) M. Valero, A. Burhop, K. Jess, R. Weck, M. Tamm, J. Atzrodt, V. Derdau, *J. Label. Comp. Radiopharm.* **2018**, *16*, 380–385.

8 a) P. K. S. Siegl, A. I. Goldberg, M. R. Goldberg, P. I. Chang, US 5817658; b) Y.-J. Shi, K. M. Wells, P. J. Pye, W.-B. Choi, H. R. O. Churchill, J. E. Lynch, A. Maliakal, J. W. Sager, K. Rossen, R. P.Volante, P. J. Reider, *Tetrahedron* **1999**, *55*, 909–918.

9 W. J. Kerr, M. Reid, T. Tuttle, *ACS Catal.* **2015**, *5*, 402−410.

10 D. G. Gusev, H. Berke, *Chem. Ber.* **1996**,*129*, 1143−1155.

11 a) E. M. Simmons, J. F. Hartwig, *Angew. Chem. Int. Ed.* **2012**, *51*, 3066–3072; b) N. J. Christensen, P. Fristrup, *Synlett* **2015**, *26*, 508–513.

12 M. Valero, D. Becker, K. Jess, R. Weck, J. Atzrodt, T. Bannenberg, V. Derdau and M. Tamm, *Chem. Eur. J.*, **2019**, *25*(26), 6517-6522.

Supporting information Part II – Chapter 2

Materials and General deuteration procedure: see Annex 1

HIE reactions on phenylacetic acid esters 11, 12, 21-37

Methyl phenylacetate (**12**)

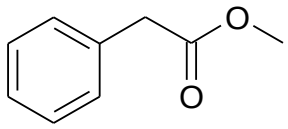

Molecular Weight =150.1789
Molecular Formula =C9H10O2

12

^{1}H NMR (300 MHz, $CDCl_3$): δ 7.33 (br s, 5H, CH phenyl), 3.72 (s, 3H, OCH_3), 3.66 (s, 2H, C*H*$_2$ benzylic) ppm. Incorporation expected at δ 7.33 (red arrow). Determined against integral at δ 3.69 (blue arrow).

General method: 10.0 mg (67.0 µmol) **12**; 10.2 mg (6.7 µmol) catalyst **F**, 2h.

Yield: a) 8.7 mg, 58.0 µmol, 87%; 90% D for δ 7.33.
b) 7.9 mg, 53.0 µmol, 79%; 84% D for δ 7.33.

Average: y=83%, 87% D

^{1}H-NMR Reference **12**

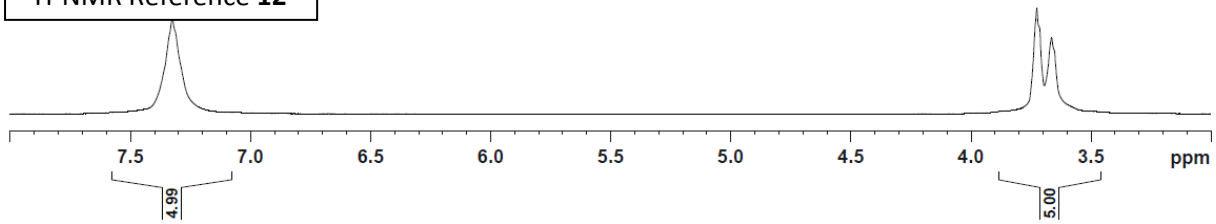

^{1}H-NMR HIE reaction **12**

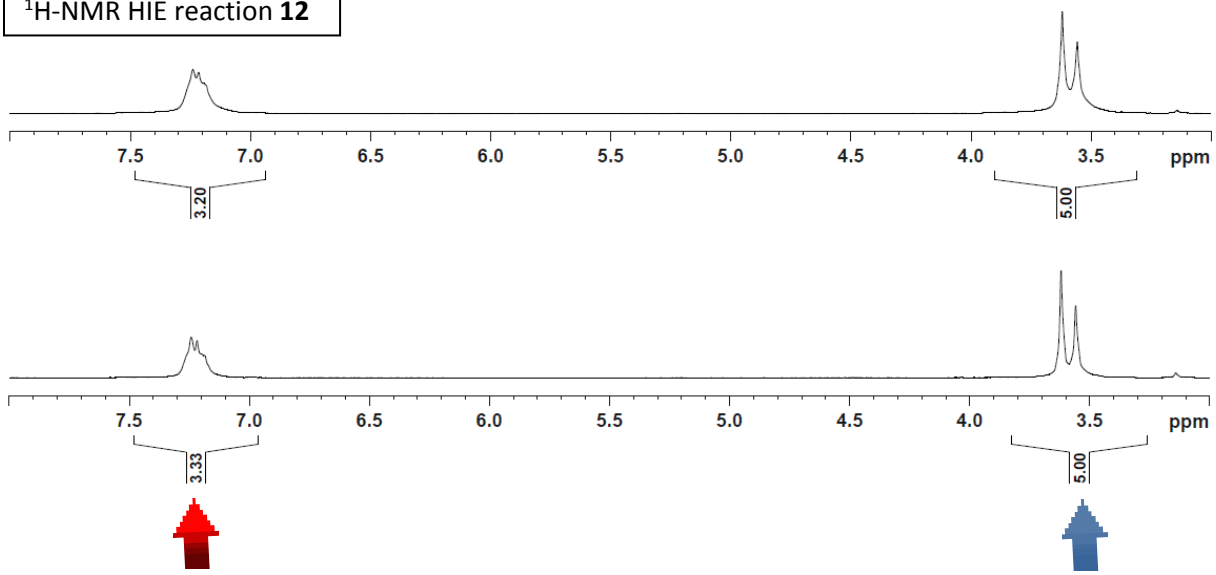

Ethyl phenylacetate (**11**)

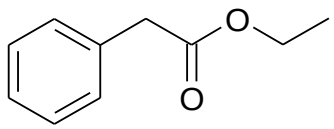

Molecular Weight =164.2059
Molecular Formula =C10H12O2

11

^{1}H NMR (300 MHz, $CDCl_3$): 7.32 (m, 5H, CH phenyl), 4.18 (q, ^3J = 7.0 Hz, 2H, CH_2 ethyl), 3.63 (s, 2H, CH_2 benzylic), 1.27 (t, ^3J = 7.0 Hz, 3H, CH_3 ethyl) ppm. Incorporation expected at δ 7.32 (red arrow). Determined against integral at δ 4.18 (blue arrow).

General method: 9.8 mg (60.0 µmol) **11**; 9.2 mg (6.0 µmol) catalyst **F**, 2h.

Yield: a) 7.5 mg, 45.0 µmol, 76%; 66% D for δ 7.32.
c) 7.9 mg, 48.0 µmol, 80%; 70% D for δ 7.32.

Average: y=78%, 68% D

^{1}H-NMR Reference **11**

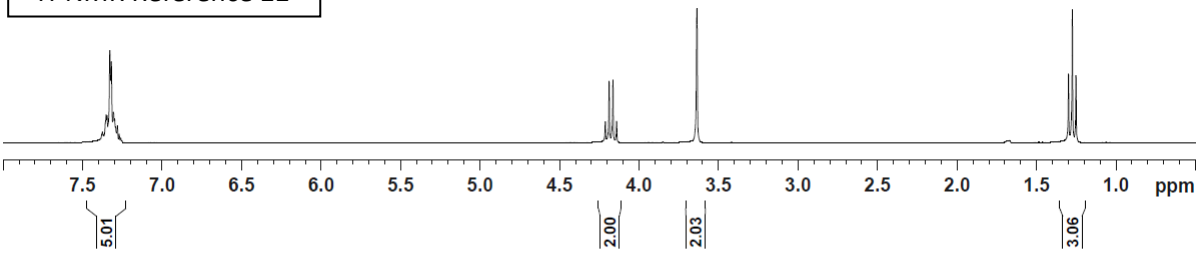

^{1}H-NMR HIE reaction **11**

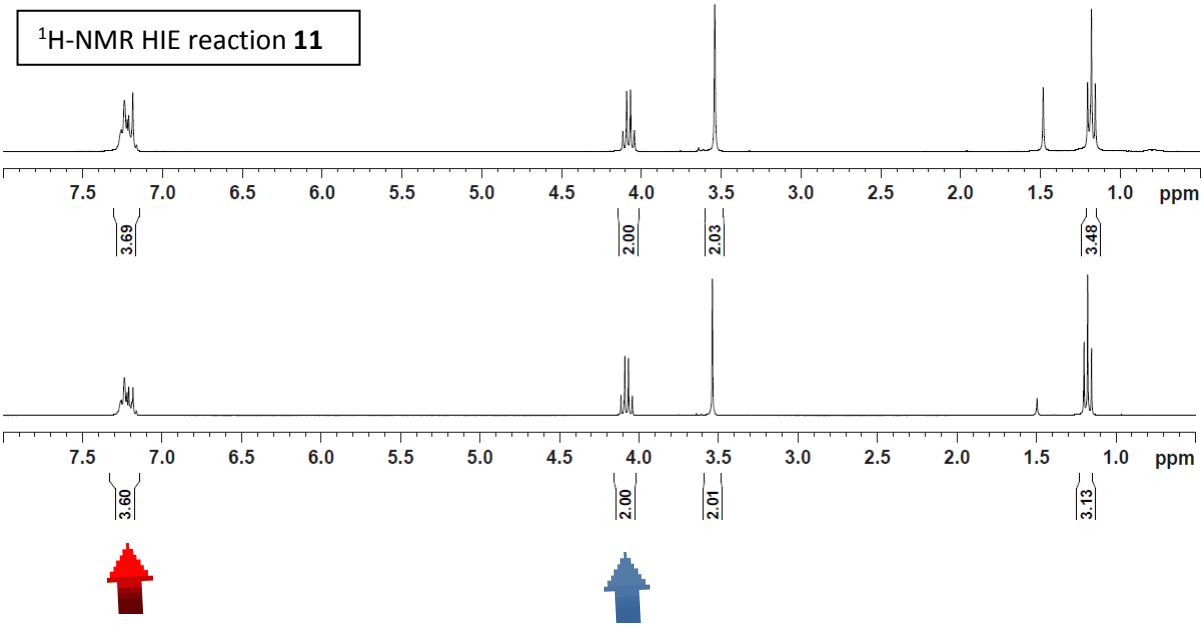

Isopropyl phenylacetate (**21**)

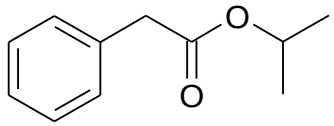

Molecular Weight =178.2330
Molecular Formula =C11H14O2

21

^{1}H NMR (300 MHz, $CDCl_3$): 7.33 (m, 5H, CH phenyl), 5.06 (m,1H, CH isopropyl), 3.63 (s, 2H, CH_2 benzylic), 1.25 (m, 6H, $2CH_3$ isopropyl) ppm. Incorporation expected at δ 7.33 (red arrow). Determined against integral at δ 1.25 (blue arrow).

General method: 10.0 mg (56.0 µmol) **21**; 8.5 mg (5.6 µmol) catalyst **F**, 2h.

Yield: a) 8.8 mg, 49.0 µmol, 88%; 54% D for δ 7.33.
b) 7.4 mg, 42.0 µmol, 74%; 44% D for δ 7.33.

Average: y=81%, 49% D

^{1}H-NMR Reference **21**

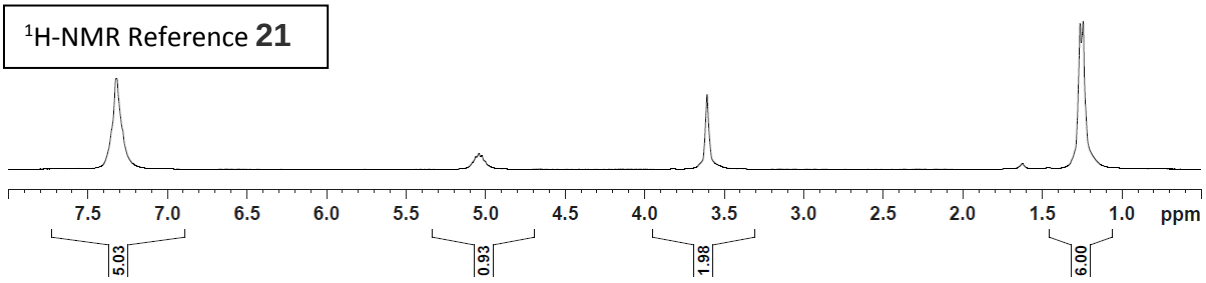

^{1}H-NMR HIE reaction **21**

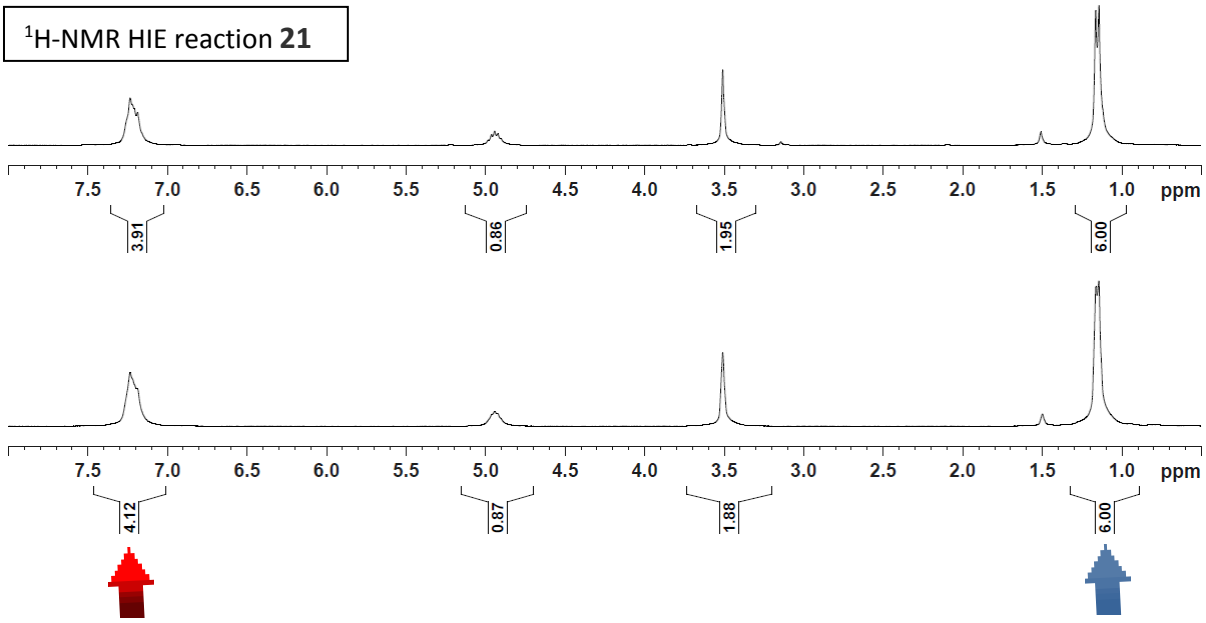

Methyl 4-methylphenylacetate (**22**)

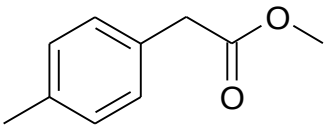

Molecular Weight =164.2059
Molecular Formula =C10H12O2

22

^{1}H NMR (300 MHz, $CDCl_3$): δ 7.19 (d, ^3J=8.5 Hz, 2H, CH_2 *meta*-phenyl), 7.14 (d, ^3J=8.5 Hz, 2H, CH_2 *ortho*-phenyl), 3.70 (s, 3H, OCH_3), 3.60 (s, 2H, CH_2 benzylic), 2.34 (s, 3H, CH_3 *para*-phenyl) ppm. Incorporation expected at δ 7.14 (red arrow). Determined against integral at δ 3.70 (blue arrow).

General method: 10.0 mg (61.0 µmol) **22**; 9.3 mg (6.1 µmol) catalyst **F**, 2h.

Yield: a) 8.1 mg, 49.0 µmol, 81%; 79%D for δ 1.91-1.85.
c) 9.2 mg, 56.0 µmol, 92%; 91% D for δ 91-1.85.

Average: y=87%, 85% D

^{1}H-NMR Reference **22**

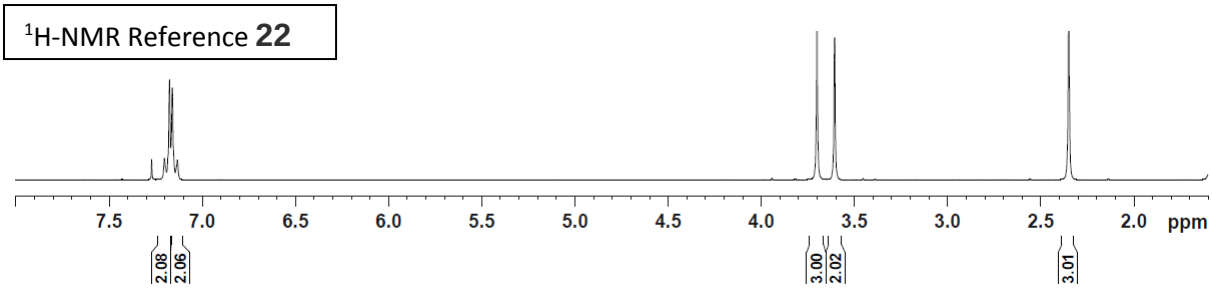

^{1}H-NMR HIE reaction **22**

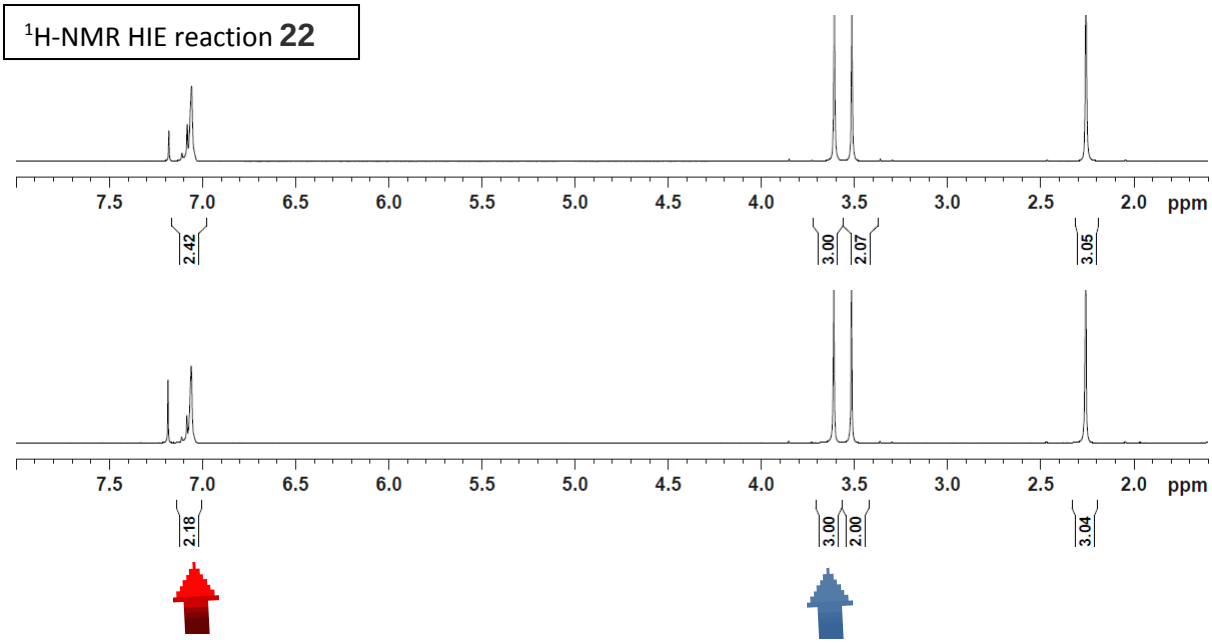

Methyl 3-methylphenylacetate (**23**)

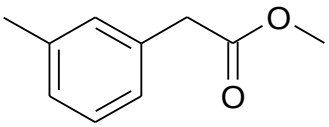

Molecular Weight =164.2059
Molecular Formula =C10H12O2

23

^{1}H NMR (300 MHz, $CDCl_3$): δ 7.23 (m, 1H, CH_2 *meta*-phenyl), 7.11 (s, 1H, *Me-C-CH-C-R*), 7.09 (m, 2H, *ortho/para*-CH), 3.72 (s, 3H, OCH_3), 3.61 (s, 2H, CH_2 benzylic), 2.37 (s, 3H, CH_3 *meta*-phenyl) ppm. Incorporation expected at δ 7.11 and δ 7.09 (red arrow). Determined against integral at δ 3.72 (blue arrow).

General method: 9.9 mg (60.0 µmol) **23**; 9.0 mg (6.0 µmol) catalyst **F**, 2h.

Yield: a) 8.7 mg, 53.0 µmol, 88%; 53%D for δ 7.09 and 40%D for δ 7.11.
b) 9.2 mg, 56.0 µmol, 93%; 57% D for δ 7.09 and 51%D for δ 7.11.

Average:
y=91%
55%D δ 7.09
45%D δ 7.11

^{1}H-NMR Reference **23**

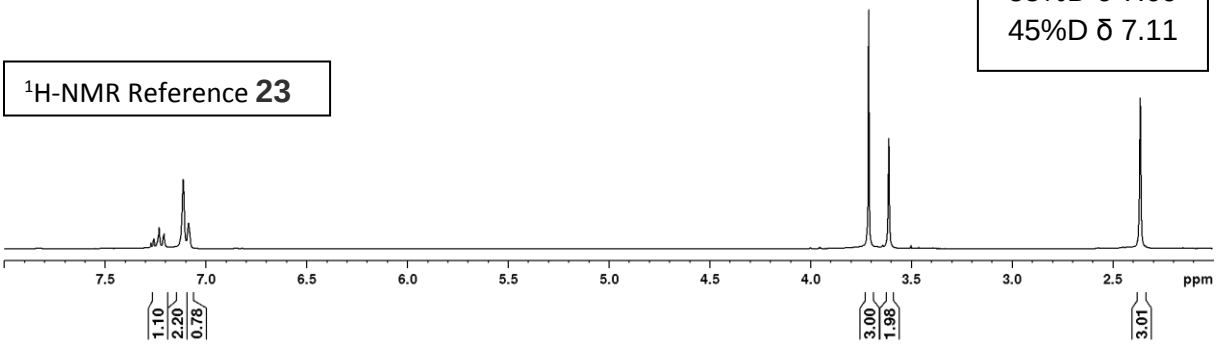

^{1}H-NMR HIE reaction **23**

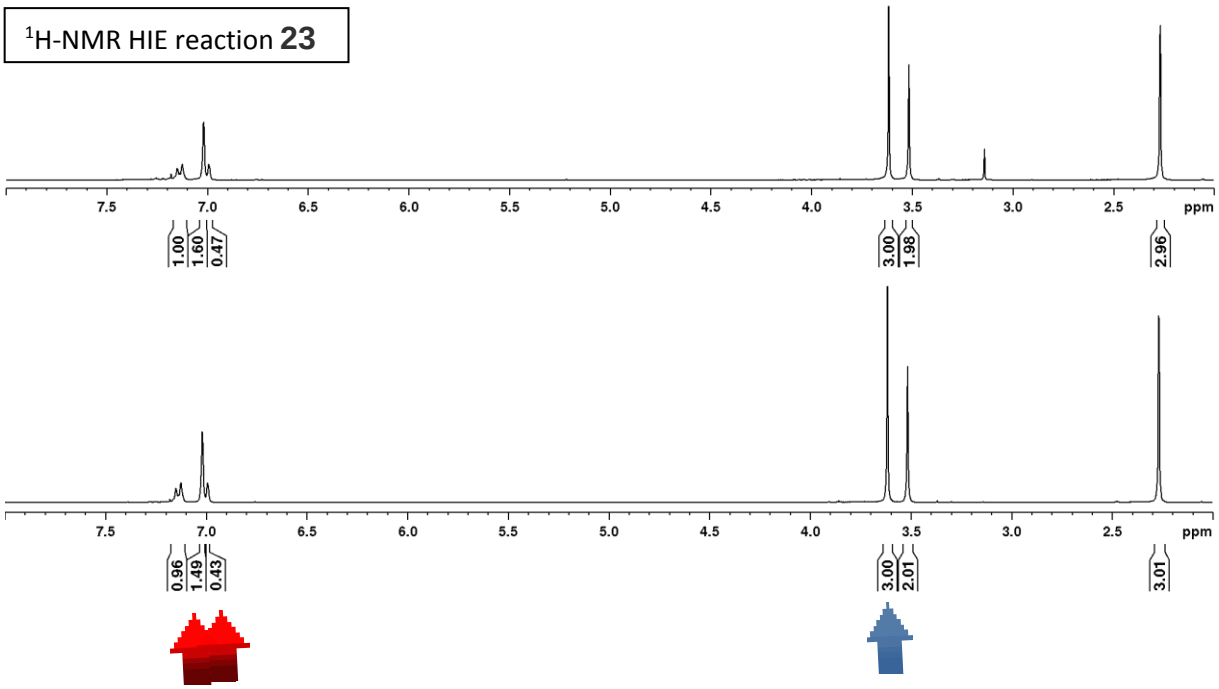

Methyl 2-methylphenylacetate (**24**)

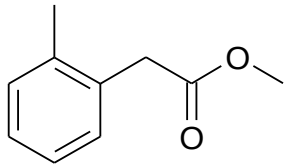

Molecular Weight =164.2059
Molecular Formula =C10H12O2

24

^{1}H NMR (300 MHz, $CDCl_3$): δ 7.20 (m, 4H, aromatic), 3.70 (s, 3H, OC*H*$_3$), 3.67 (s, 2H, CH_2 benzylic), 2.32 (s, 3H, CH_3 *ortho*-phenyl) ppm. Incorporation expected at δ 7.20 (red arrow). Determined against integral at δ 3.70 (blue arrow).

General method: 9.9 mg (60.0 µmol) **24**; 9.0 mg (6.0 µmol) catalyst **F**, 2h.

Yield: a) 7.7 mg, 47.0 µmol, 78%; 95% D for δ 7.10.
b) 8.4 mg, 51.0 µmol, 85%; 93% D for δ 7.10.

Average: y=82%, 94% D

^{1}H-NMR Reference **24**

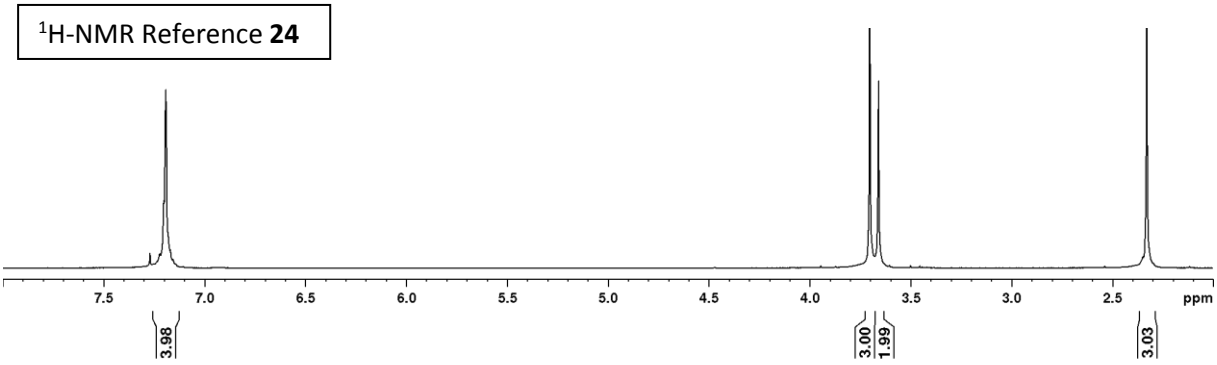

^{1}H-NMR HIE reaction **24**

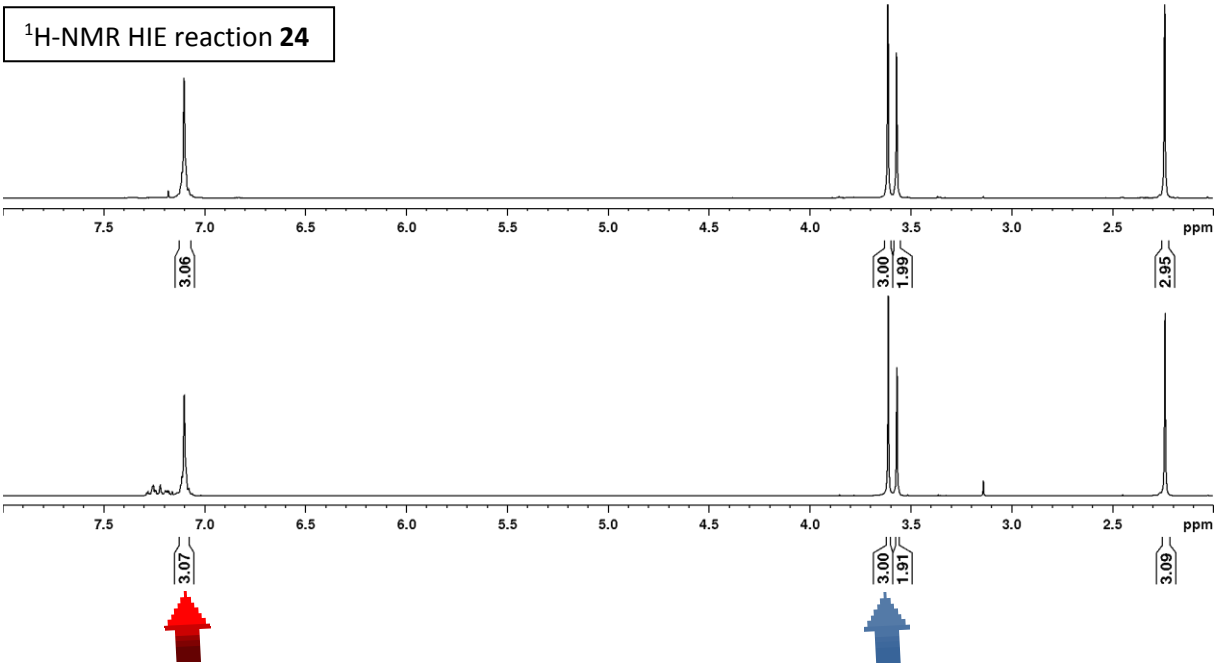

Methyl 4-hydroxyphenylacetate (**25**)

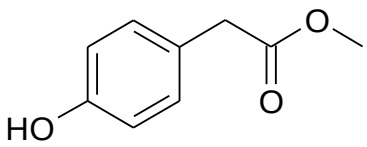

Molecular Weight =166.1782
Molecular Formula =C9H10O3

25

^{1}H NMR (300 MHz, $CDCl_3$): δ 7.14 (d, ^3J=8.5 Hz, 2H, CH_2 *ortho*-phenyl), 6.77 (d, ^3J=8.5 Hz, 2H, CH_2 *meta*-phenyl), 5.15 (s, 1H, OH), 3.71 (s, 3H, OCH_3), 3.56 (s, 2H, CH_2 benzylic) ppm. Incorporation expected at δ 7.14 (red arrow). Determined against integral at δ 3.71 (blue arrow).

General method: 10.0 mg (60.0 µmol) **25**; 9.2 mg (6.0 µmol) catalyst **F**, 2h.

Yield: a) 7.8 mg, 47.0 µmol, 78%; 87% D for δ 7.14.
b) 10.8 mg, 65.0 µmol, 100%; 77% D for δ 7.14.

Average: y=89%, 82%

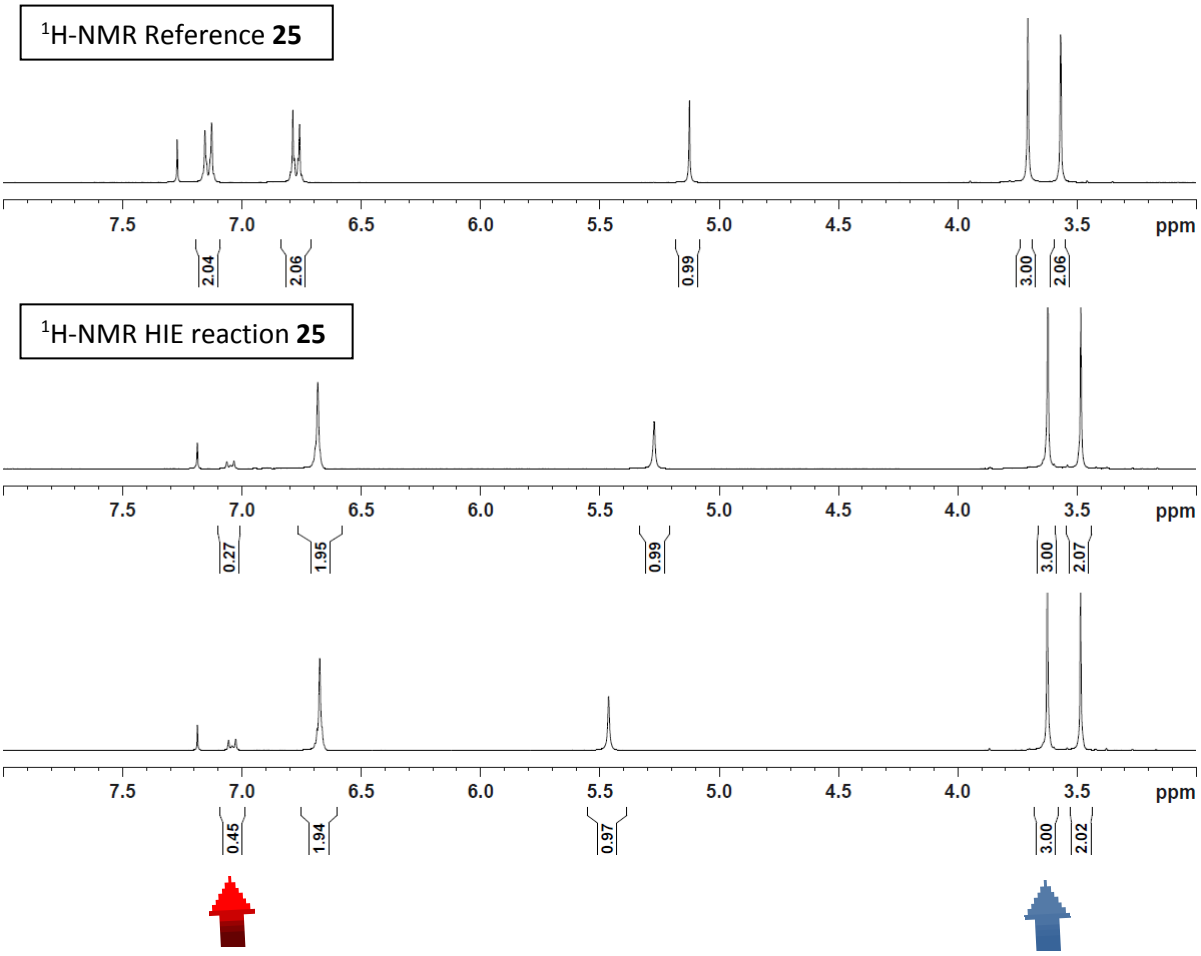

Methyl 3-hydroxyphenylacetate (**26**)

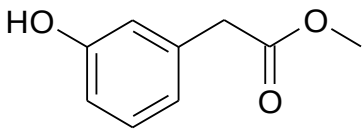

Molecular Weight =166.1782
Molecular Formula =C9H10O3

26

^{1}H NMR (300 MHz, $CDCl_3$): δ 7.17 (m, 1H, CH *meta*-phenyl), 6.82 (m, 1H, CH *ortho*-phenyl), 6.77 (s, 1H, CH *ortho*-phenyl), 6.75 (m, 1H, CH *para*-phenyl), 3.72 (s, 3H, CH_3), 3.59 (s, 2H, CH_2 benzylic) ppm. Incorporation expected at δ 6.82 and 6.77 (red arrow). Determined against integral at δ 3.72 (blue arrow).

General method: 10.1 mg (61.0 µmol) **26**; 9.3 mg (6.1 µmol) catalyst **F**, 2h.

Yield: a) 8.9 mg, 54.0 µmol, 88%; 77% D for δ 6.82 and 96% D for δ 6.77.
b) 9.5 mg, 57.0 µmol, 94%; 75% D for δ 6.82 and 93% D for δ 6.77.

Average: y=91%
76% D δ 6.82
95% D δ 6.77

^{1}H-NMR Reference **26**

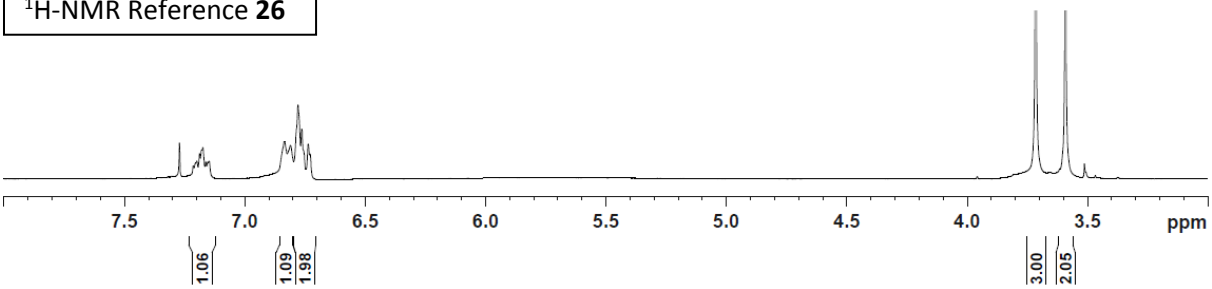

^{1}H-NMR HIE reaction **26**

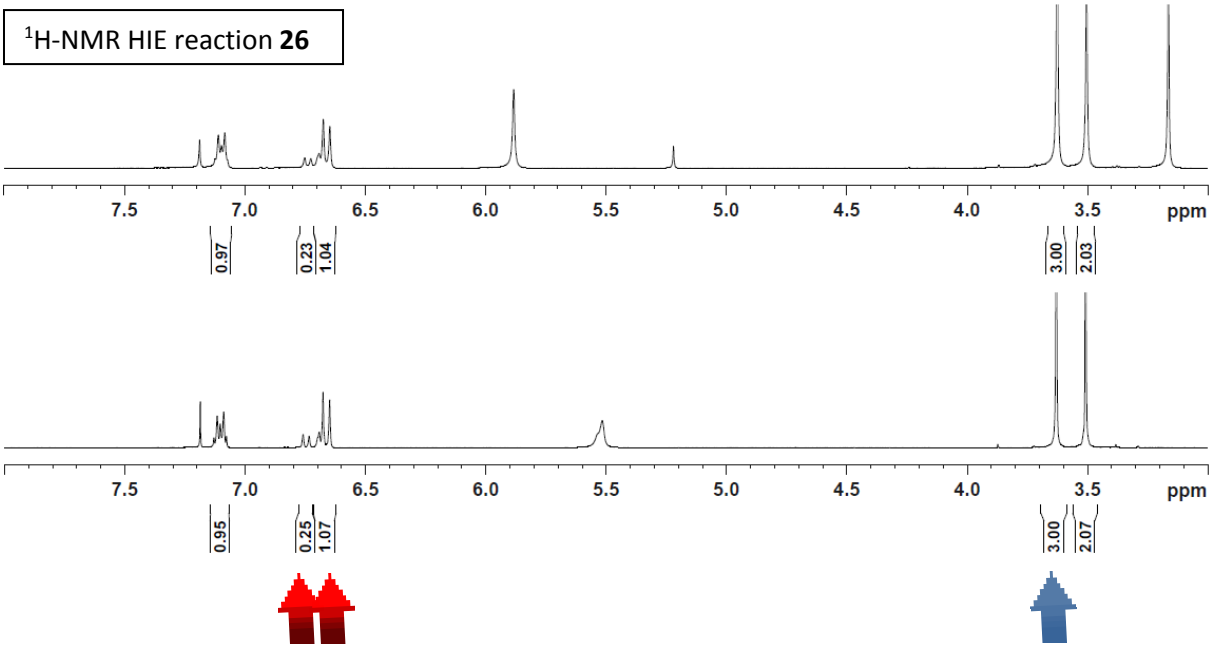

Methyl 2-hydroxyphenylacetate (**27**)

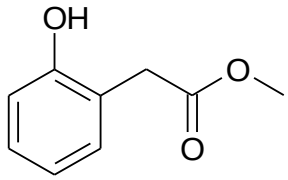

Molecular Weight =166.1782
Molecular Formula =C9H10O3

27

^{1}H NMR (300 MHz, $CDCl_3$): δ 7.23 (s, 1H, OH), 7.12 (m, 1H, CH *para*-phenyl), 7.02 (s, 1H, CH *ortho*-phenyl), 6.83 (m, 2H, CH *meta*-phenyl), 3.67 (s, 3H, CH_3), 3.61 (s, 2H, CH_2 benzylic) ppm. Incorporation expected at δ 7.02 and 6.83 (red arrow). Determined against integral at δ 3.67 (blue arrow).

General method: 10.0 mg (60.0 µmol) **27**; 9.2 mg (6.0 µmol) catalyst **F**, 2h.

Yield: a) 9.4 mg, 57.0 µmol, 94%; 48%D for δ 7.02 and 20% D for δ 6.83.
b) 8.8 mg, 53.0 µmol, 88%; 56%D for δ 7.02 and 33% D for δ 6.83.

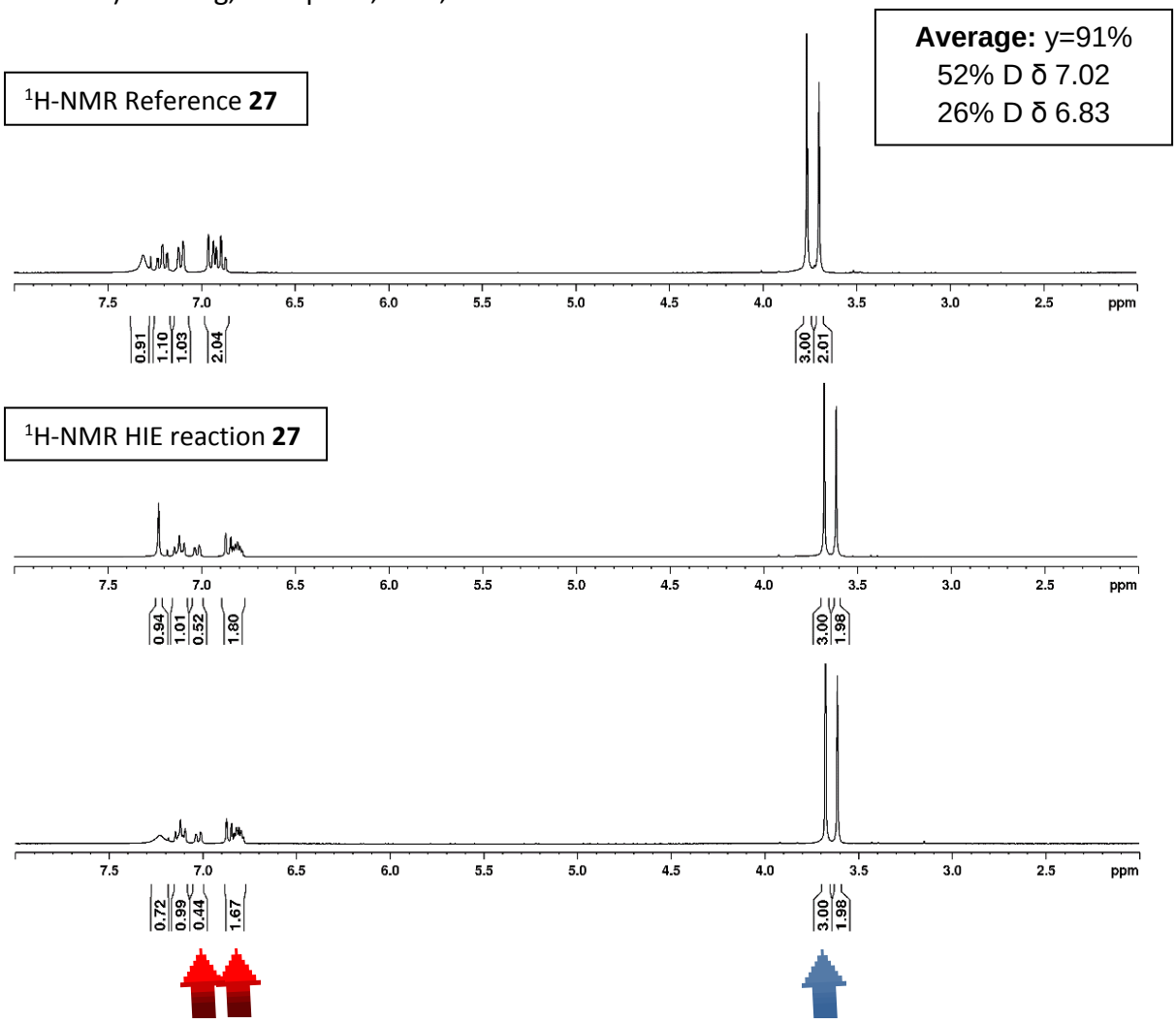

Methyl 4-fluorophenylacetate (**28a**)

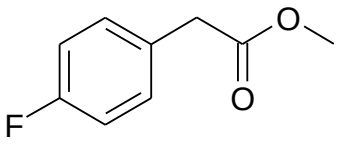

Molecular Weight =168.1693
Molecular Formula =C9H9FO2

28a

^{1}H NMR (300 MHz, $CDCl_3$): δ 7.25 (d, ^3J=8.5 Hz, 2H, CH_2 *ortho*-phenyl), 7.02 (d, ^3J=8.5 Hz, 2H, CH_2 *meta*-phenyl), 3,70 (s, 3H, CH_3), 3.60 (s, 2H, CH_2 benzylic) ppm. Incorporation expected at δ 7.25 (red arrow). Determined against integral at δ 3.70 (blue arrow).

General method: 10,2 mg (61.0 µmol) **28a**; 9.3 mg (6.1 µmol) catalyst **F**, 2h.

Yield: a) 3.4 mg, 20.2 µmol, 33%; 82% D for δ 7.25 and 14% D for δ 7.02.
b) 3.0 mg, 18.0 µmol, 29%; 91% D for δ 7.25 and 5% D for δ 7.02.

Average: y=32%
87% D δ 7.25
9% D δ 7.02

^{1}H-NMR Reference **28a**

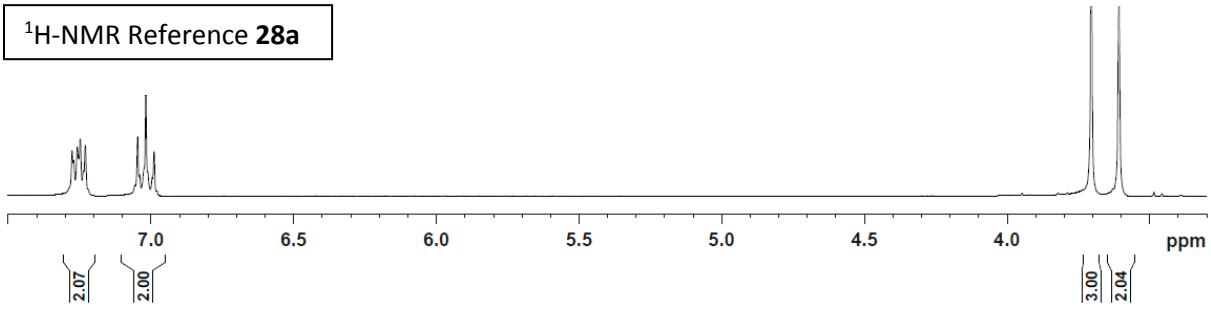

^{1}H-NMR HIE reaction **28a**

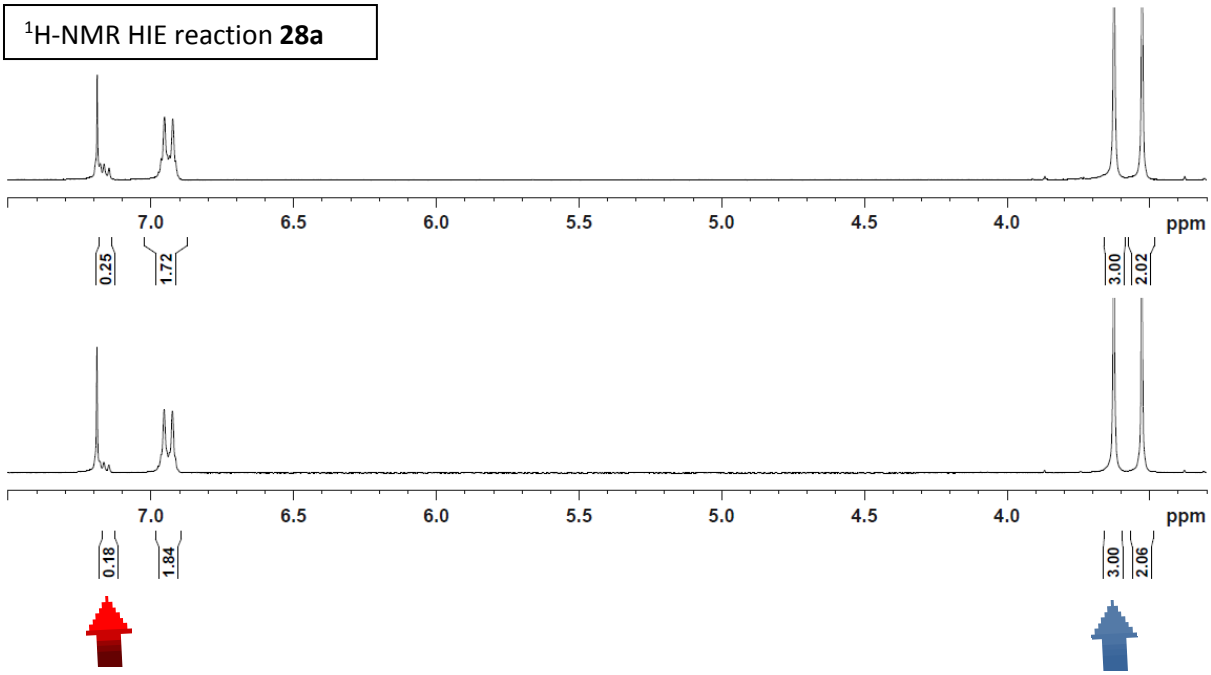

Methyl 4-chlorophenylacetate (**28b**)

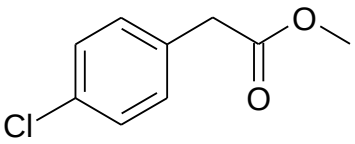

Molecular Weight =184.6239
Molecular Formula =C9H9ClO2

28b

^{1}H NMR (300 MHz, $CDCl_3$): δ 7.31 (d, ^3J=8.3 Hz, 2H, CH_2 *meta*-phenyl), 7.22 (d, ^3J=8.3 Hz, 2H, CH_2 *ortho*-phenyl), 3,71 (s, 3H, CH_3), 3.61 (s, 2H, CH_2 benzylic) ppm. Incorporation expected at δ 7.22 and δ 7.31 (red arrow). Determined against integral at δ 3.71 (blue arrow).

General method: 11.1 mg (60.0 µmol) **28b**; 9.0 mg (6.0 µmol) catalyst **F**, 2h.

Yield: a) 9.7 mg, 53.0 µmol, 87%; 77% D for δ 7.22 and 16% for δ 7.31.
b) 10.2 mg, 55.0 µmol, 92%; 77% D for δ 7.22 and 16% for δ 7.31.

Average: y=90%
77% D for δ 7.22
16% D for δ 7.31

^{1}H-NMR Reference **28b**

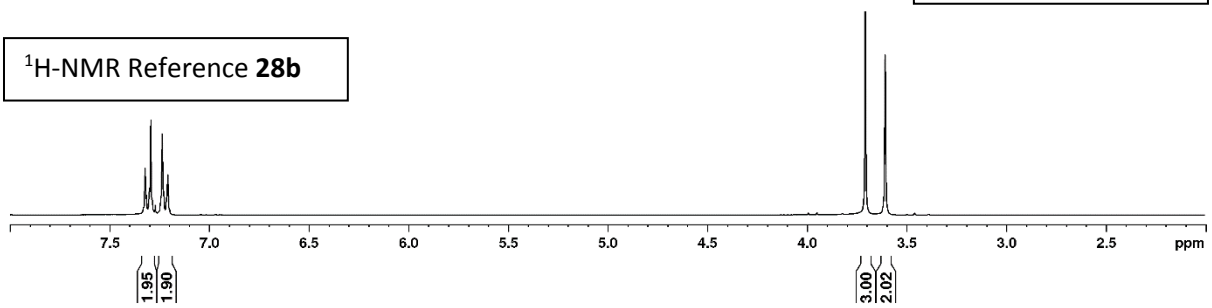

^{1}H-NMR HIE reaction **28b**

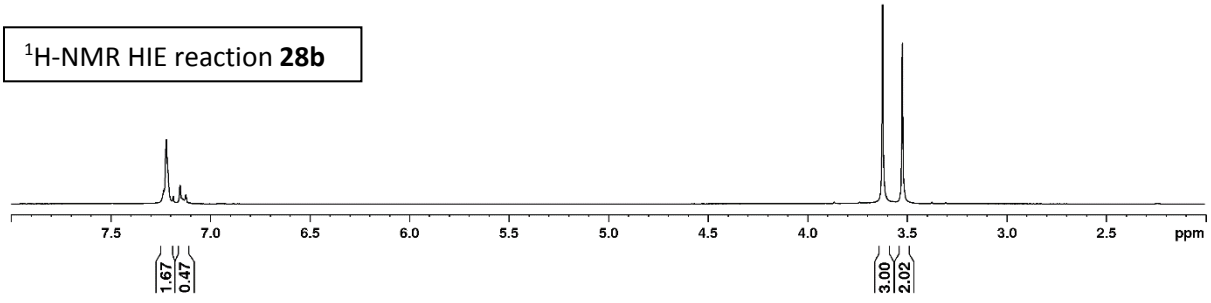

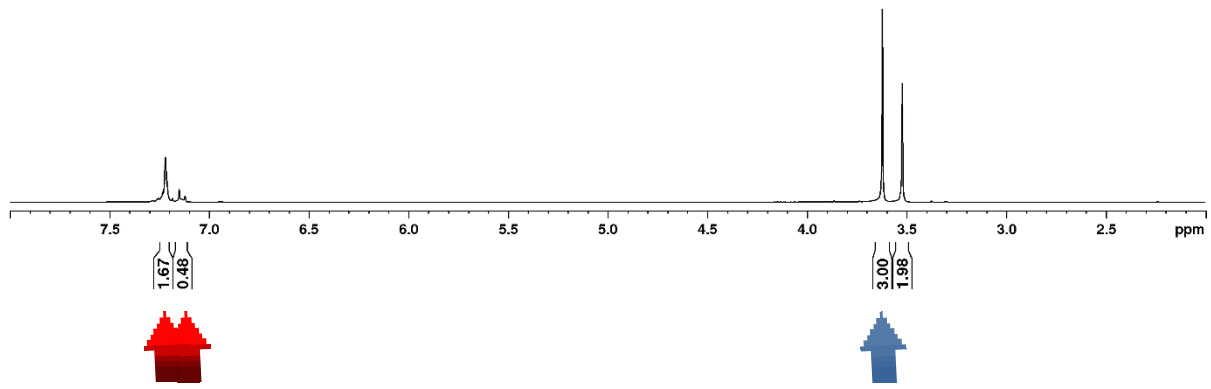

Methyl 4-bromophenylacetate (**28c**)

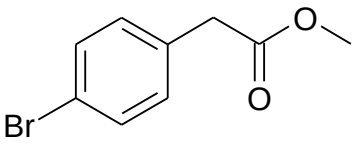

Molecular Weight =229.0749
Molecular Formula =C9H9BrO2

28c

^{1}H NMR (300 MHz, $CDCl_3$): δ 7.37 (d, ^3J=8.0 Hz, 2H, CH_2 *meta*-phenyl), 7.08 (d, ^3J=8.0 Hz, 2H, CH_2 *ortho*-phenyl), 3.62 (s, 3H, OCH_3), 3.50 (s, 2H, CH_2 benzylic) ppm. Incorporation expected at δ 7.08 (red arrow). Determined against integral at δ 3.62 (blue arrow).

General method: 13.70 mg (60.0 µmol) **28c**; 9.20 mg (6.0 µmol) catalyst **F**, 2h.

Yield: a) 12.5 mg, 55.0 µmol, 91%; 14% D for δ 7.37 and 84% D for δ 7.08.
c) 11.7 mg, 51.0 µmol, 85%; 15% D for δ 7.37 and 86% D for δ 7.08.

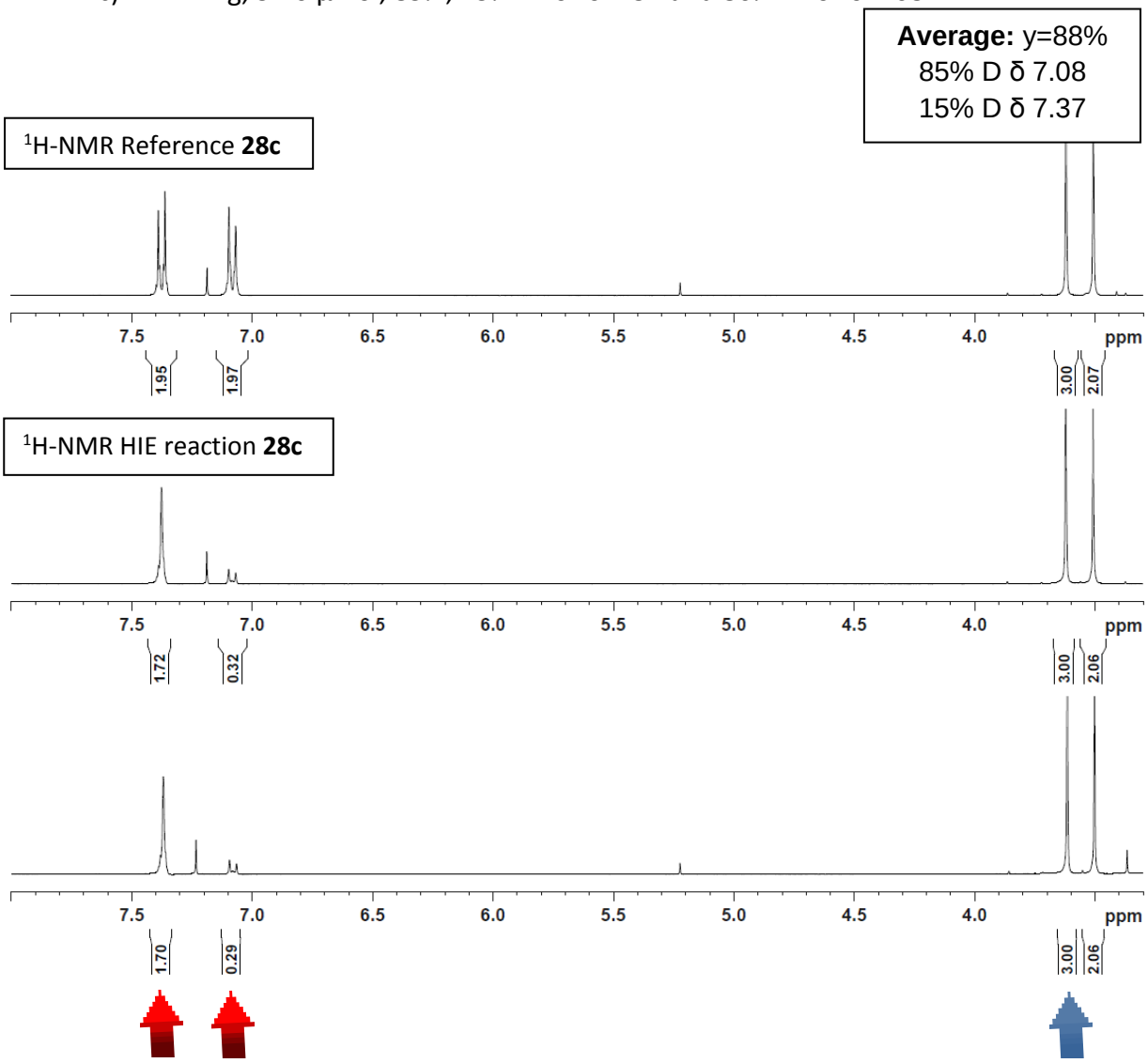

Methyl 3-fluorophenylacetate (**29a**)

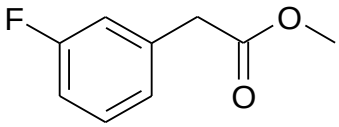

Molecular Weight =168.1693
Molecular Formula =C9H9FO2

29a

^{1}H NMR (300 MHz, $CDCl_3$): δ 7.29 (m, 1H, arom. CH), 7.05 (m, 1H, arom. CH), 7.01 (m, 1H, arom. CH), 6.98 (m, 1H, arom. CH), 3.72 (s, 3H, CH_3), 3.63 (s, 2H, CH_2 benzylic) ppm. Incorporation expected at δ 7.05 and 7.01 (red arrow). Determined against integral at δ 3.72 (blue arrow).

General method: 10.2 mg (61.0 µmol) **29a**; 9.3 mg (6.1 µmol) catalyst **F**, 2h.

Yield: a) 8.0 mg, 48.0 µmol, 78%; 88% D for δ 7.01 and 53% D for δ 7.05.
d) 7.3 mg, 43.0 µmol, 72%; 83% D for δ 7.01 and 53% D for δ 7.05.

Average: y=75%
86% D δ 7.01
53% D δ 7.05

^{1}H-NMR Reference **29a**

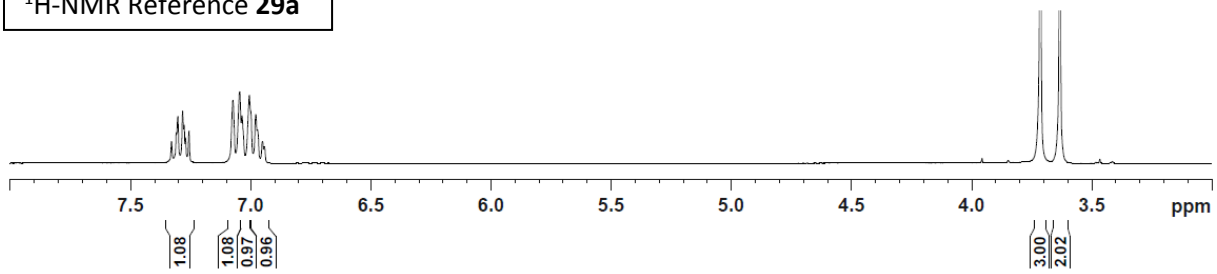

^{1}H-NMR HIE reaction **29a**

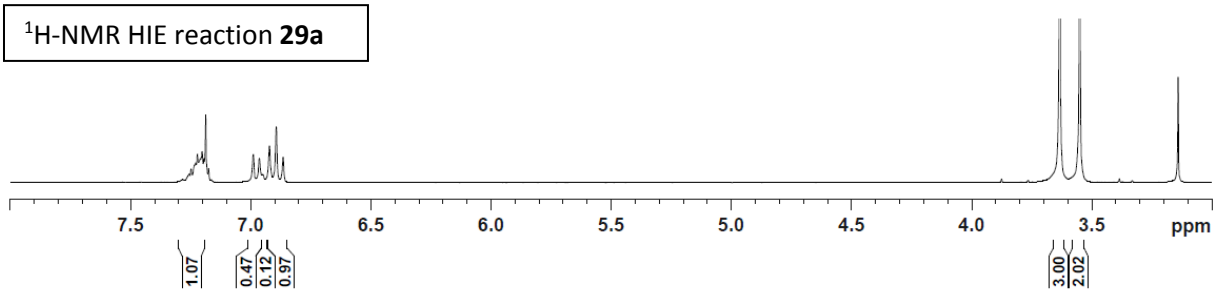

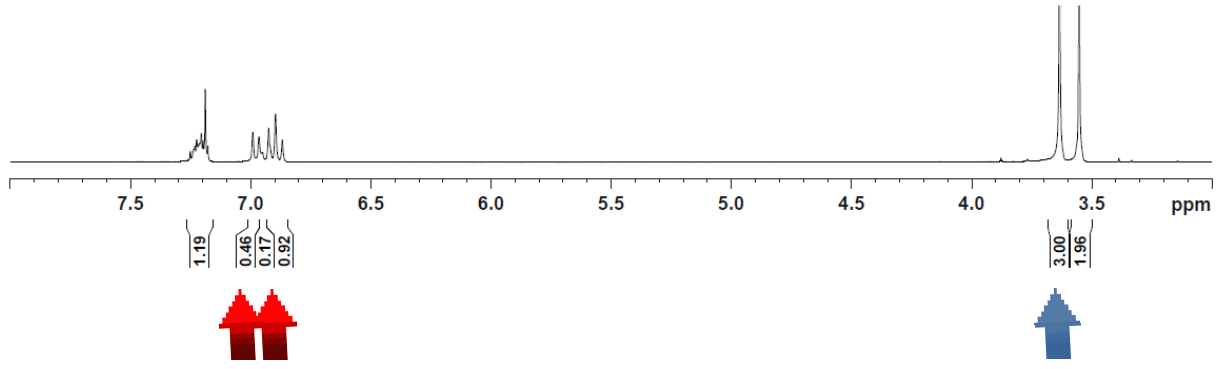

Methyl 3-chlorophenylacetate (**29b**)

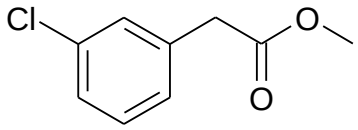

Molecular Weight =184.6239
Molecular Formula =C9H9ClO2

29b

^{1}H NMR (300 MHz, $CDCl_3$): δ 7.29 (s, 1H, CH *ortho*), 7.26 (m, 2H, CH *meta* and *para*), 7.17 (m, 1H, CH *ortho*), 3.71 (s, 3H, CH_3), 3.61 (s, 2H, CH_2 benzylic) ppm. Incorporation expected at δ 7.29 and 7.17 (red arrow). Determined against integral at δ 3.71 (blue arrow).

General method: 11.2 mg (61.0 µmol) **29b**; 9.3 mg (6.1 µmol) catalyst **F**, 2h.

Yield: a) 10.1 mg, 55.0 µmol, 90%; 37% D for δ 7.29 and 73% D for δ 7.17.
b) 9.8 mg, 53.0 µmol, 88%; 44% D for δ 7.29 and 72% D for δ 7.17.

Average: y=89%
40% D δ 7.29
73% D δ 7.17

^{1}H-NMR Reference **29b**

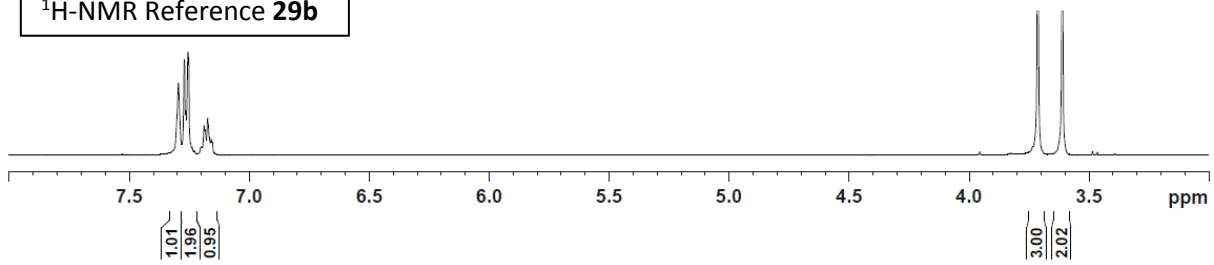

^{1}H-NMR HIE reaction **29b**

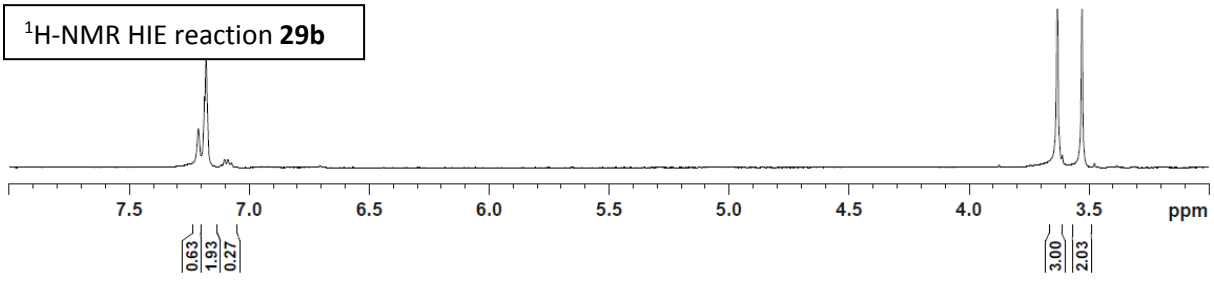

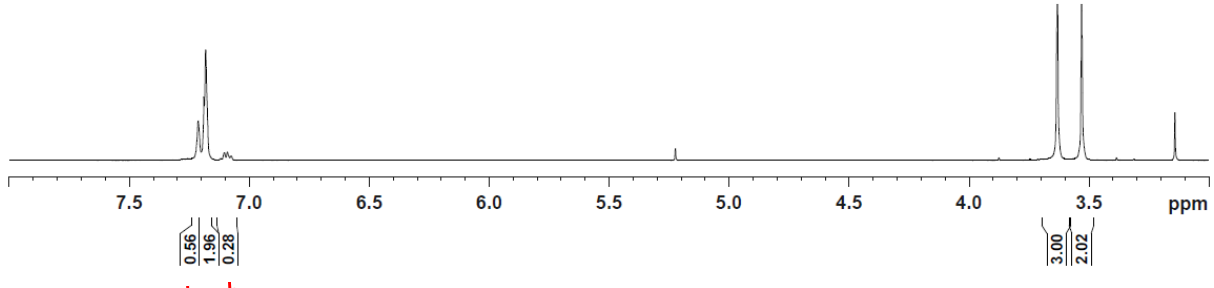

Methyl 3-bromophenylacetate (**29c**)

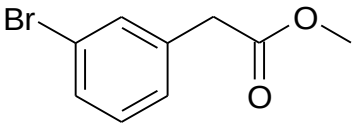

Molecular Weight =229.0749
Molecular Formula =C9H9BrO2

29c

^{1}H NMR (300 MHz, $CDCl_3$): δ 7.43 (m, 2H, CH *ortho-Br*), 7.21 (m, 2H, CH *meta*/*para-Br*), 3.72 (s, 3H, CH_3), 3.61 (s, 2H, CH_2 benzylic) ppm. Incorporation expected at δ 7.43 and 7.21 (red arrow). Determined against integral at δ 3.72 (blue arrow).

General method: 13.8 mg (60.0 µmol) **29c**; 9.0 mg (6.0 µmol) catalyst **F**, 2h.

Yield: a) 12.6 mg, 55.0 µmol, 91%; 21% D for δ 7.43 and 68% D for δ 7.21.
b) 13.7 mg, 60.0 µmol, 99%; 24%D for δ 7.43 and 75% D for δ 7.21.

Average: y=95%
22% D δ 7.43
72% D δ 7.21

^{1}H-NMR Reference **29c**

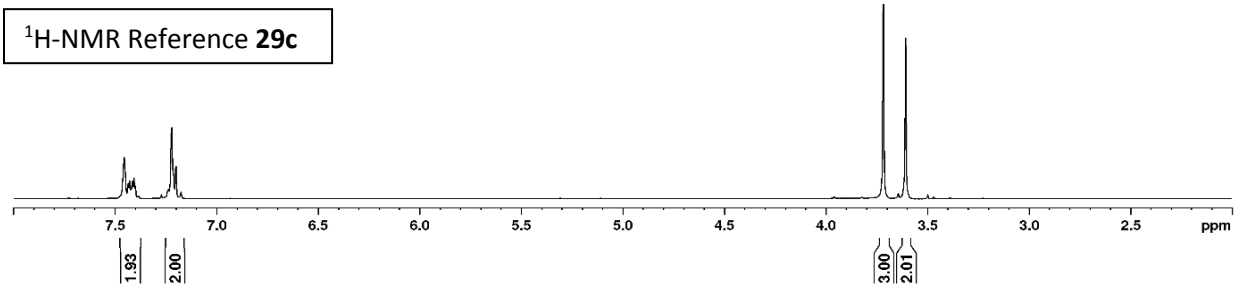

^{1}H-NMR HIE reaction **29c**

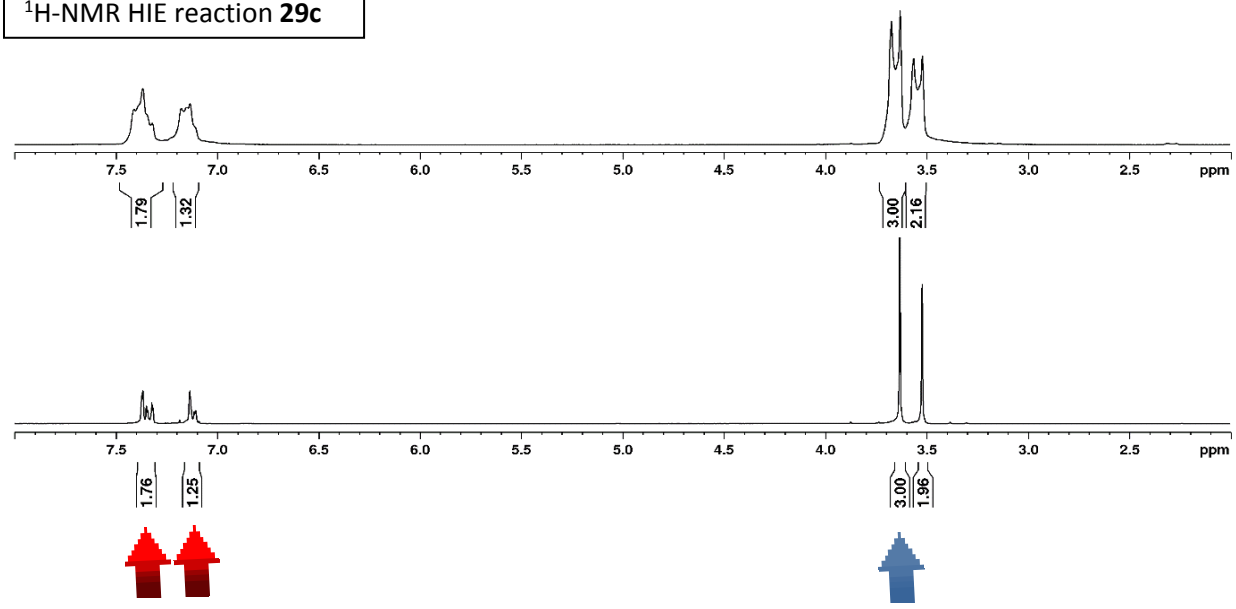

Methyl 4-*N*,*N*-dimethylaminophenylacetate (**30**)

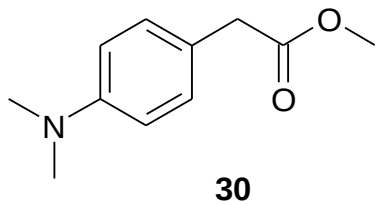

30

Molecular Weight =193.2477
Molecular Formula =C11H15NO2

^{1}H NMR (300 MHz, $CDCl_3$): δ 7.16 (d, ^3J = 8.7 Hz, 2H, CH *ortho*), 6.72 (d, ^3J = 8.7 Hz, 2H, CH *meta*), 3.69 (s, 3H, CH_3), 3.55 (s, 2H, CH_2 benzylic), 2.94 (s, 6H, $N(CH_3)_2$) ppm. Incorporation expected at δ 7.16 (red arrow). Determined against integral at δ 3.69 (blue arrow).

General method: 11.7 mg (61.0 µmol) **30**; 9.3 mg (6.1 µmol) catalyst **F**, 2h.

Yield: a) 9.7 mg, 50.0 µmol, 83%; 73% D for δ 7.16.
b) 9.5 mg, 49.0 µmol, 81%; 79% D for δ 7.16.

Average: y=82%, 76% D δ 7.16

^{1}H-NMR Reference **30**

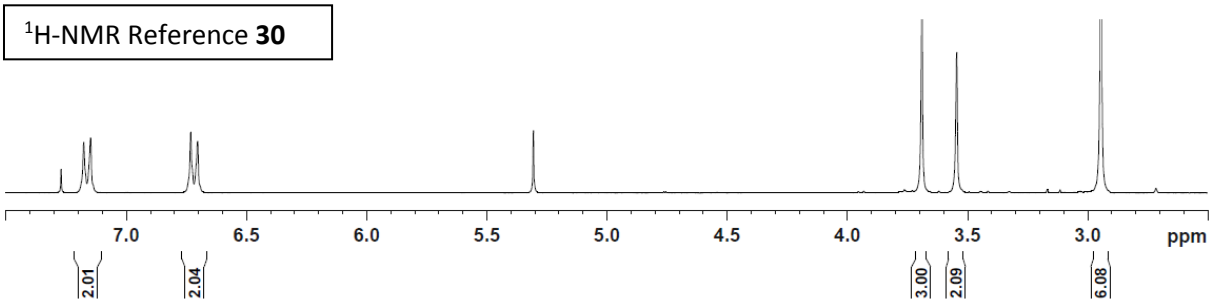

^{1}H-NMR HIE reaction **30**

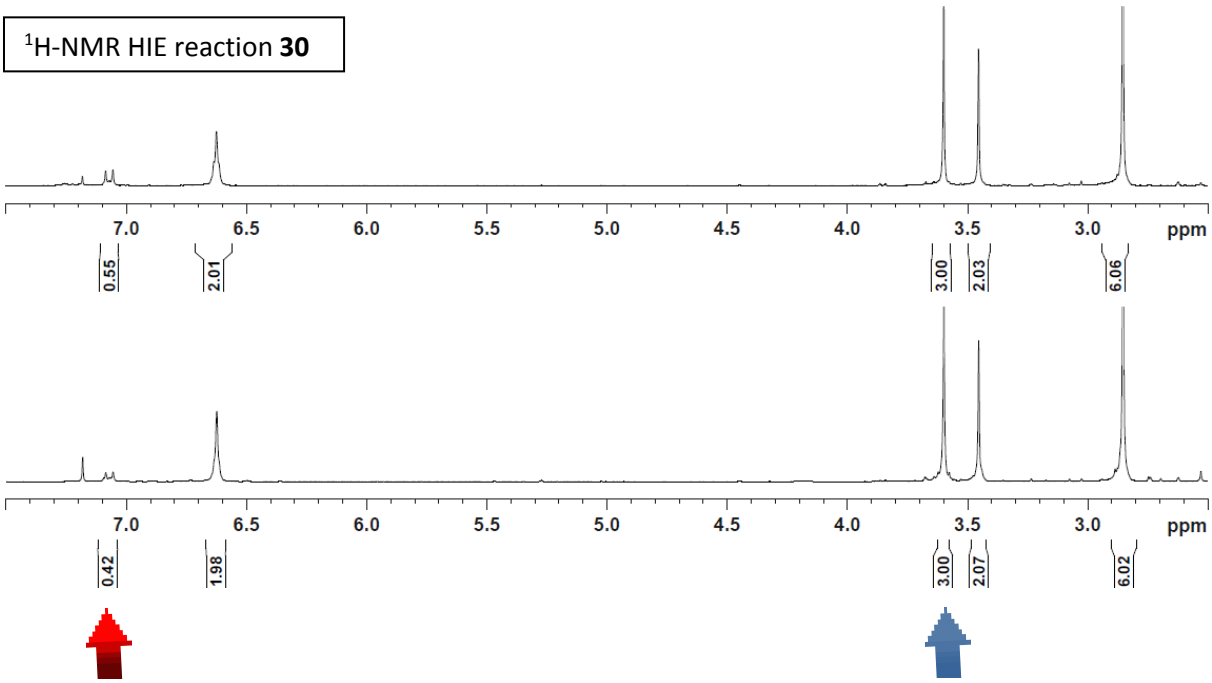

N-Methylbenzeneacetamide (**38**)

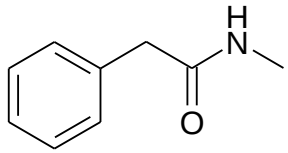

Molecular Weight =149.1941
Molecular Formula =C9H11NO

38

^{1}H NMR (300 MHz, $CDCl_3$): δ 7.23 (m, 5H, phenyl), 5.39 (br s, 1H, N*H*), 3.50 (s, 2H, CH_2 benzylic), 2.68 (d, ^3J = 5.0 Hz, 3H, NCH_3) ppm. Incorporation expected at δ 7.23 (red arrow). Determined against integral at δ 3.50 (blue arrow).

General method: 9.7 mg (65.0 µmol) **38**; 10.0 mg (6.5 µmol) catalyst **F**, 2h.

Yield: a) 8.8 mg, 59.0 µmol, 91%; 100% D for δ 7.23 and 33% D for δ 2.68.
b) 8.1 mg, 54.0 µmol, 84%; 96% D for δ 7.23 and 33% D for δ 2.68.

Average: y=88%
98% D δ 7.23
33% D δ 2.68

^{1}H-NMR Reference **38**

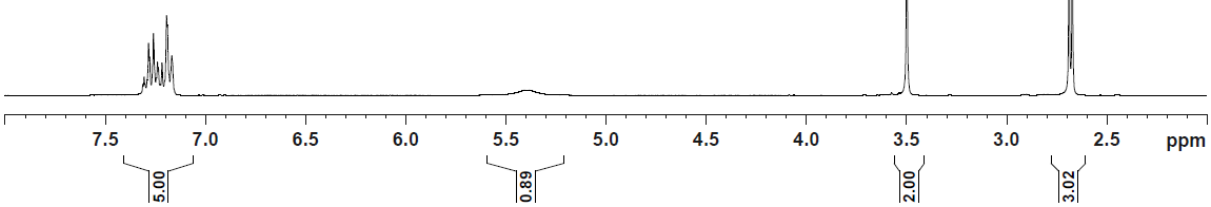

^{1}H-NMR HIE reaction **38**

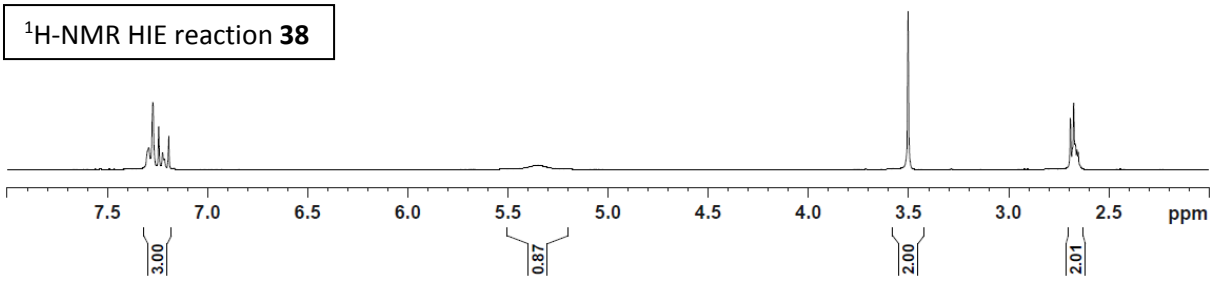

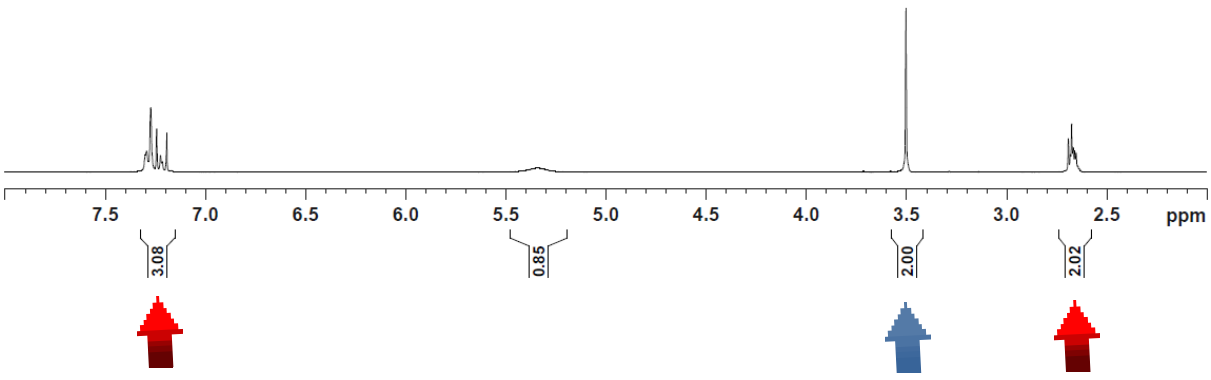

N,N-Dimethylbenzeneacetamide (**39**)

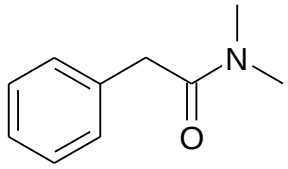

Molecular Weight =163.2212
Molecular Formula =C10H13NO

39

^{1}H NMR (300 MHz, $CDCl_3$): δ 7.22 (m, 5H, phenyl), 3.65 (s, 2H, CH_2 benzylic), 2.91 (ds, ^3J = 8.0 Hz, 6H, $N(CH_3)_2$) ppm. Incorporation expected at δ 7.22 (red arrow). Determined against integral at δ 3.65 (blue arrow).

General method: 10.1 mg (62.0 µmol) **39**; 9.5 mg (6.2 µmol) catalyst **F**, 2h.

Yield: a) 10.1 mg, 62.0 µmol, 100%; 97% D for δ 7.22 and 66% D for δ 2.91.
b) 9.5 mg, 58.0 µmol, 94%; 99% D for δ 7.22 and 61% D for δ 2.91.

Average: y=97%
98% D δ 7.22
63% D δ 2.91

^{1}H-NMR Reference **39**

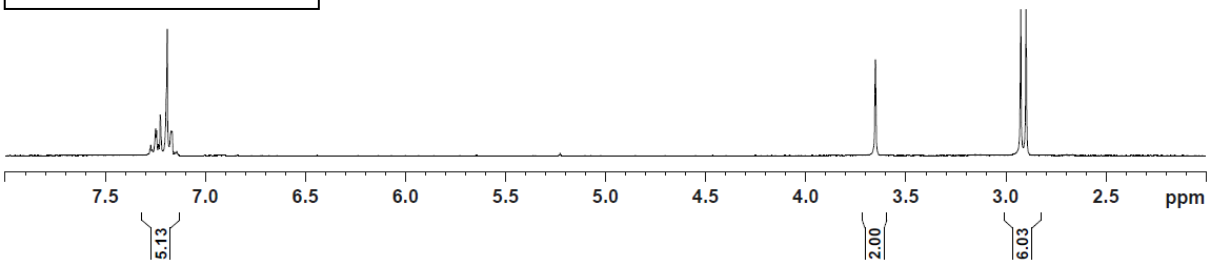

^{1}H-NMR HIE reaction **39**

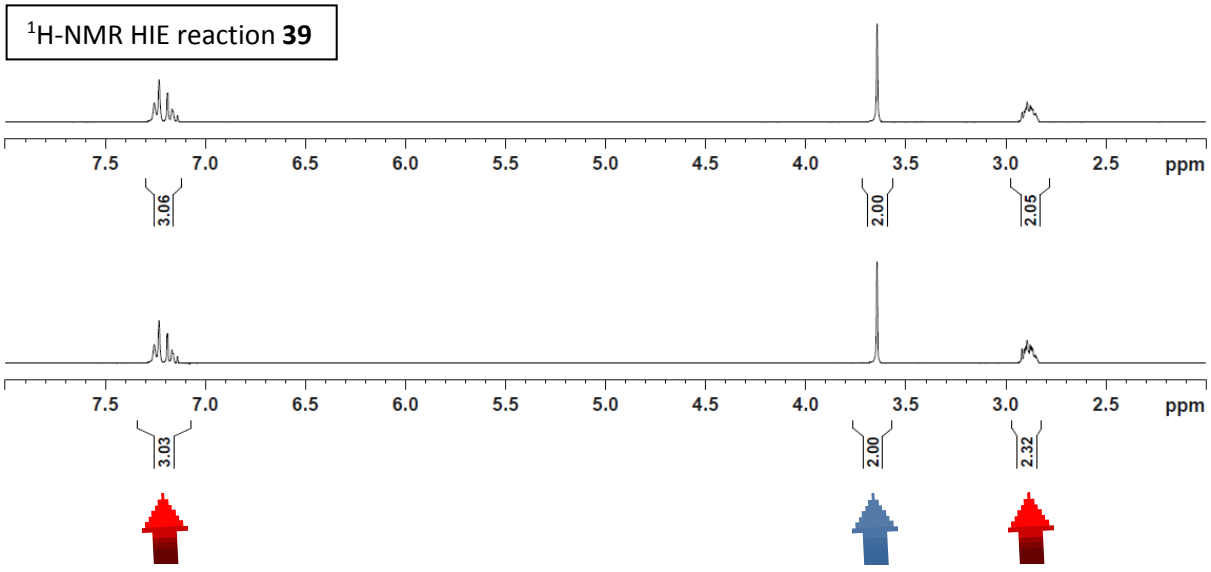

N,N-diethylbenzeneacetamide (**40**)

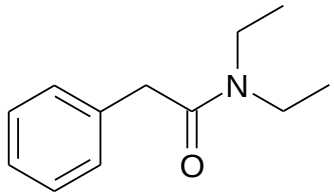

Molecular Weight =191.2754
Molecular Formula =C12H17NO

40

^{1}H NMR (300 MHz, $CDCl_3$): δ 7.20 (m, 5H, phenyl), 3.62 (s, 2H, CH_2 benzylic), 3.32 (q, ^3J = 7.0 Hz, 2H, CH_2 ethyl), 3.23 (q, ^3J = 7.0 Hz, 2H, CH_2 ethyl), 1.05 (t, ^3J = 7.0 Hz, 3H, CH_3 ethyl), 1.01 (t, ^3J = 7.0 Hz, 3H, CH_3 ethyl) ppm. Incorporation expected at δ 7.20 (red arrow). Determined against integral at δ 3.62 (blue arrow).

General method: 11.8 mg (62.0 µmol) **40**; 9.50mg (6.2 µmol) catalyst **F**, 2h.

Yield: a) 11.6 mg, 61.0 µmol, 98%; 100% D for δ 7.20.
b) 11.3 mg, 59.0 µmol, 96%; 98% D for δ 7.20.

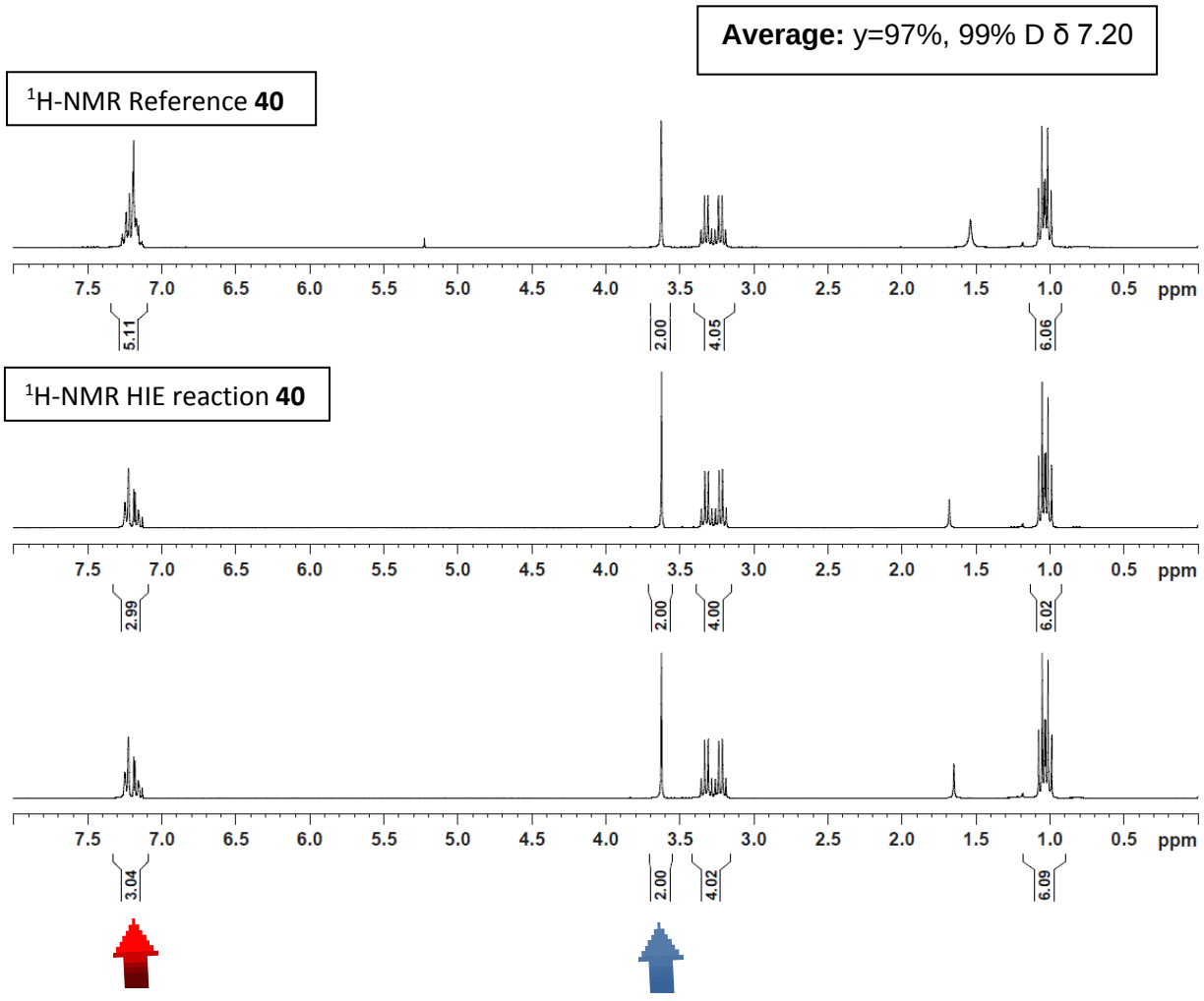

N-Methyl-4-methoxybenzeneacetamide (**41**)

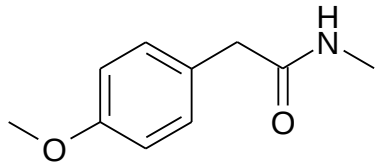

Molecular Weight =179.2206
Molecular Formula =C10H13NO2

41

^{1}H NMR (300 MHz, $CDCl_3$): δ 7.09 (d, ^3J = 8.5 Hz, 2H, CH_2 *ortho*-phenyl), 6.81 (d, ^3J = 8.5 Hz, 2H, CH_2 *meta*-phenyl), 5.32 (br s, 1H, N*H*), 3.73 (s, 3H, OCH_3), 3.44 (s, 2H, CH_2 benzylic), 2.68 (d, ^3J = 5.0 Hz, 3H, NCH_3) ppm. Incorporation expected at δ 7.09 (red arrow). Determined against integral at δ 3.73 (blue arrow).

General method: 11.6 mg (65.0 µmol) **41**; 10.0 mg (6.5 µmol) catalyst **F**, 2h.

Yield: a) 8.4 mg, 47.0 µmol, 72%; 93% D for δ 7.09 and 23% D for δ 2.68.
b) 6.9 mg, 39.0 µmol, 60%; 90% D for δ 7.09 and 21% D for δ 2.68.

Average: y=66%
92% D δ 7.09
22% D δ 2.68

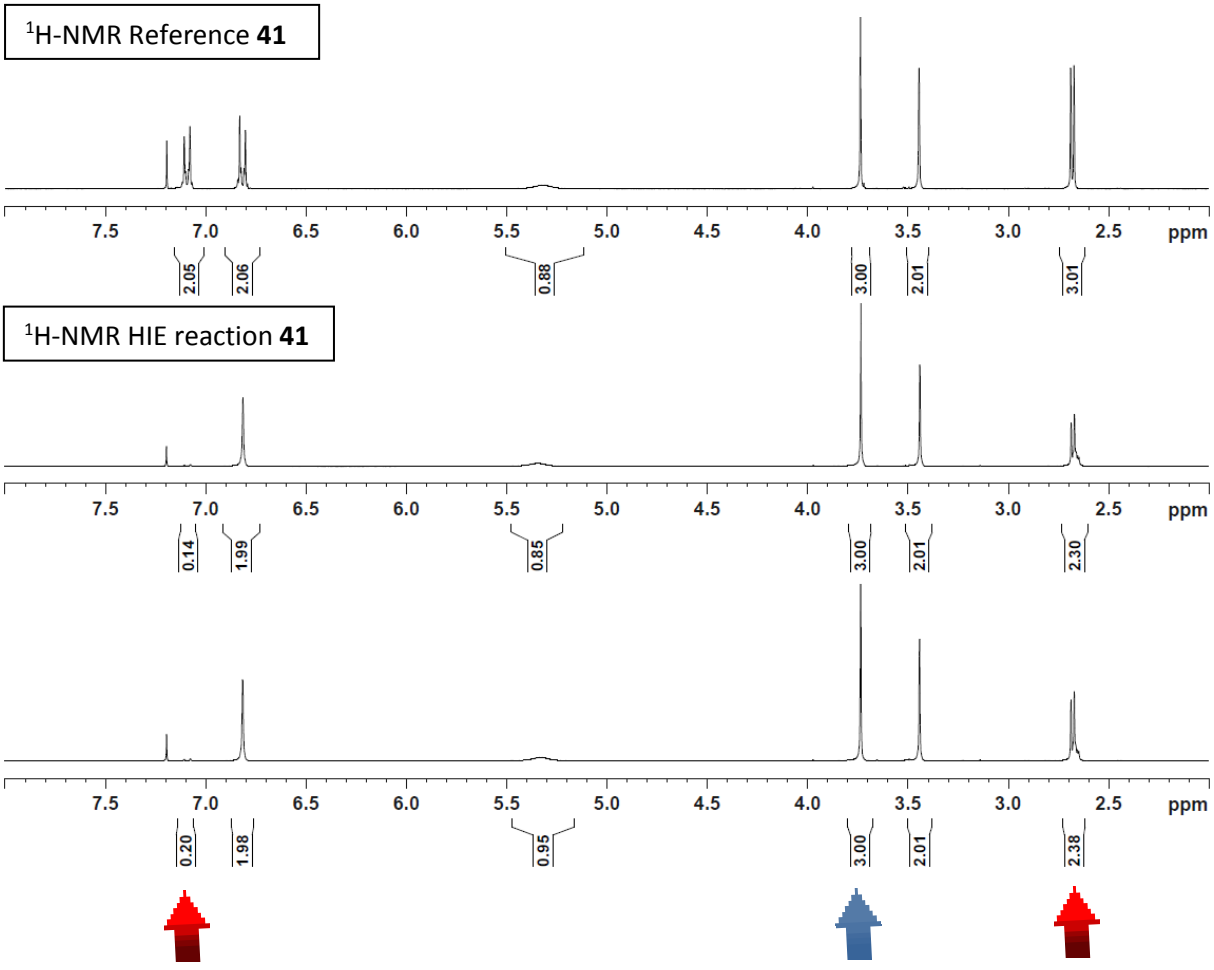

N,N-Dimethyl-4-methoxybenzeneacetamide (**42**)

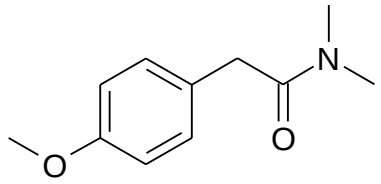

42

Molecular Weight =193.2477
Molecular Formula =C11H15NO2

^{1}H NMR (300 MHz, $CDCl_3$): δ 7.10 (d, ^3J = 8.5 Hz, 2H, CH_2 *ortho*-phenyl), 6.78 (d, ^3J = 8.5 Hz, 2H, CH_2 *meta*-phenyl), 3.72 (s, 3H, OCH_3), 3.58 (s, 2H, CH_2 benzylic), 2.90 (ds, 6H, $N(CH_3)_2$) ppm. Incorporation expected at δ 7.10 (red arrow). Determined against integral at δ 3.72 (blue arrow).

General method: 12.0 mg (62.0 µmol) **42**; 9.50 mg (6.2 µmol) catalyst **F**, 2h.

Yield: a) 11.1 mg, 58.0 µmol, 92%; 80% D for δ 7.10.
b) 11.7 mg, 61.0 µmol, 98%; 78% D for δ 7.10.

Average: y=95%, 79% D δ 7.10

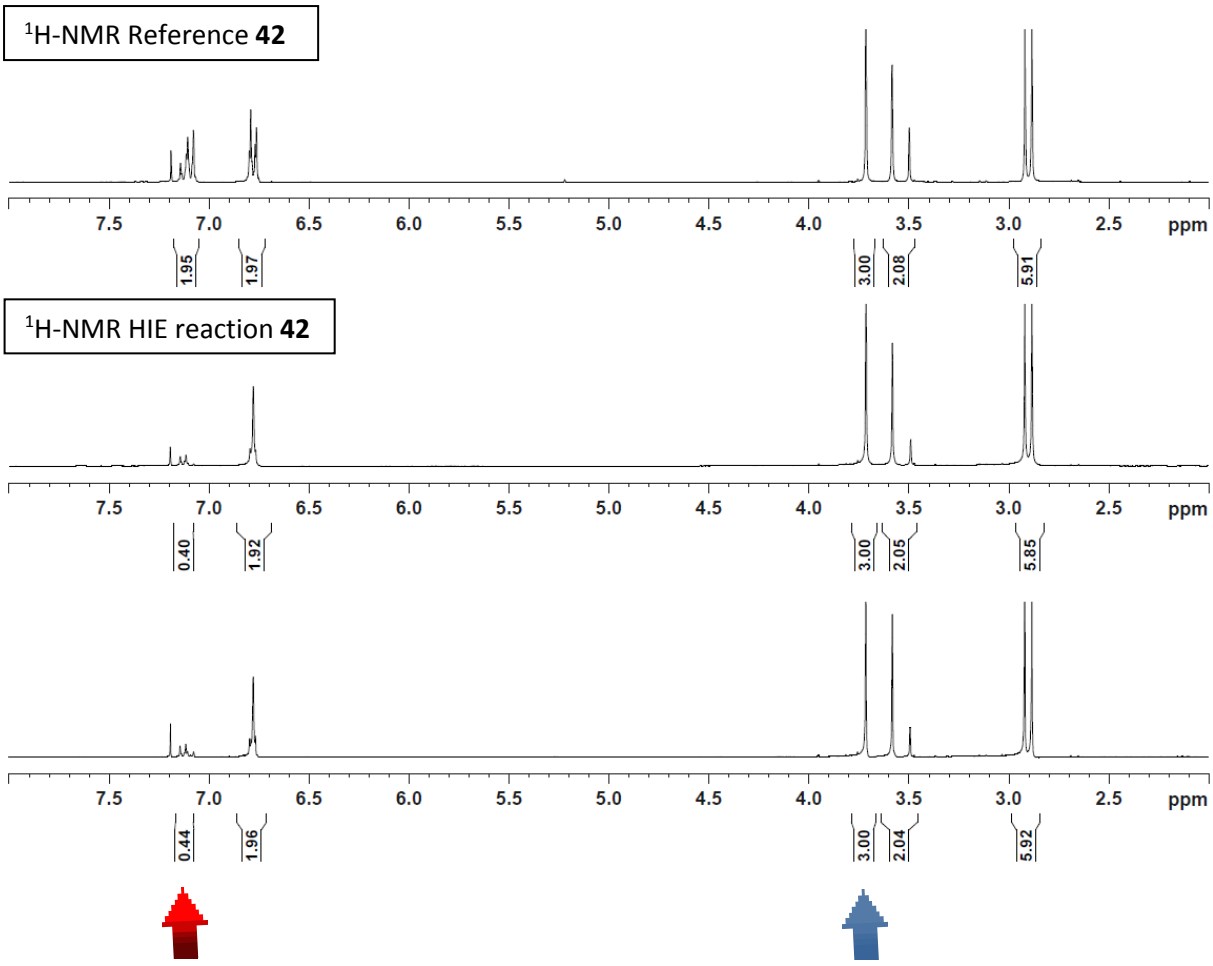

N,N-Diethyl-4-methoxybenzeneacetamide (**43**)

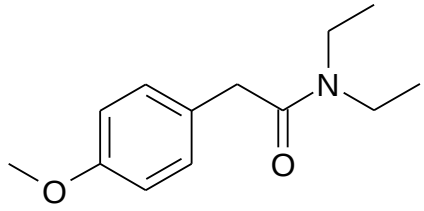

43

Molecular Weight =221.3019
Molecular Formula =C13H19NO2

^{1}H NMR (300 MHz, $CDCl_3$): δ 7.09 (d, ^3J = 8.7 Hz, 2H, CH_2 *ortho*-phenyl), 6.77 (d, ^3J = 8.7Hz, 2H, CH_2 *meta*-phenyl), 3.71 (s, 3H, OCH_3), 3.55 (s, 2H, CH_2 benzylic), 3.31 (q, ^3J = 7.0 Hz, 2H, CH_2 ethyl), 3.22 (q, ^3J = 7.0 Hz, 2H, CH_2 ethyl), 1.04 (t, ^3J = 7.0 Hz, 3H, CH_3 ethyl), 1.02 (t, ^3J = 7.0 Hz, 3H, CH_3 ethyl) ppm. Incorporation expected at δ 7.09 (red arrow). Determined against integral at δ 3.71 (blue arrow).

General method: 13.7 mg (62.0 µmol) **43**; 9.5 mg (6.2 µmol) catalyst **F**, 2h.

Yield: a) 13.0 mg, 59.0 µmol, 95%; 96% D for δ 7.09.
b) 13.2 mg, 60.0 µmol, 96%; 96% D for δ 7.09.

Average: y=96%, 96% D δ 7.09

^{1}H-NMR Reference **43**

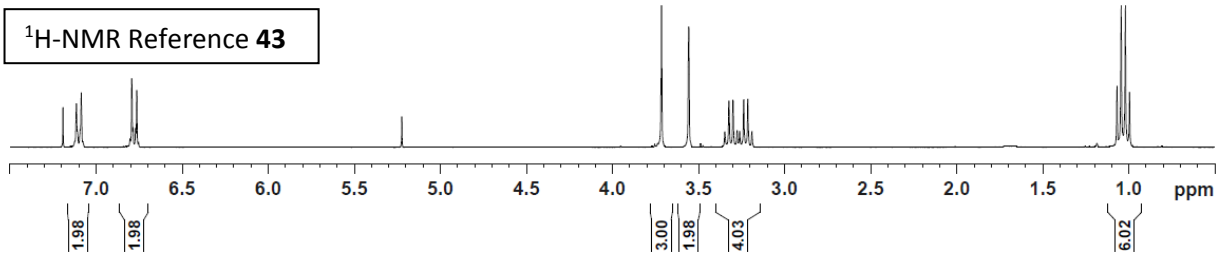

^{1}H-NMR HIE reaction **43**

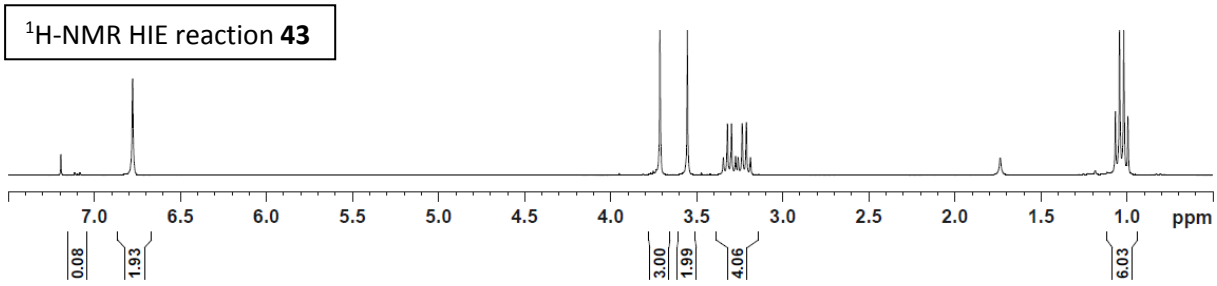

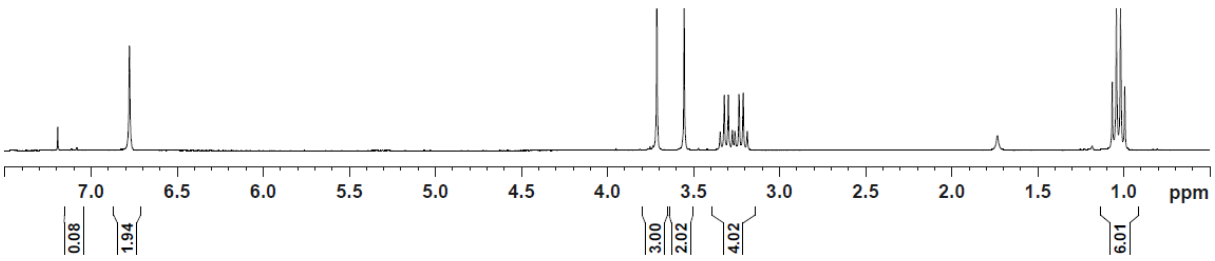

N-Methyl-4-*N,N*-dimethylaminobenzeneacetamide (**44**)

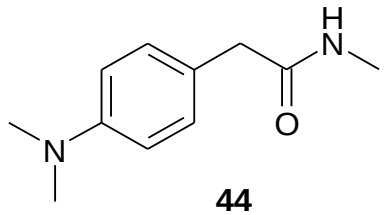

44

Molecular Weight =192.2630
Molecular Formula =C11H16N2O

^{1}H NMR (300 MHz, $CDCl_3$): δ 7.03 (d, ^3J = 8.7 Hz, 2H, CH_2 *ortho*-phenyl), 6.64 (d, ^3J = 8.7 Hz, 2H, CH_2 *meta*-phenyl), 5.32 (br s, 1H, N*H*), 3.42 (s, 2H, CH_2 benzylic), 2.89 (s, 6H, $N(CH_3)_2$), 2.66 (d, ^3J = 5.0 Hz, 3H, NCH_3) ppm. Incorporation expected at δ 7.03 (red arrow). Determined against integral at δ 2.89 (blue arrow).

General method: 12.5 mg (65.0 µmol) **44**; 10.00 mg (6.5 µmol) catalyst **F**, 2h.

Yield: a) 7.9 mg, 41.0 µmol, 63%; 95% D for δ 7.03 and 11% D for δ 2.66.
b) 7.3 mg, 38.0 µmol, 58%; 95% D for δ 7.03 and 16% D for δ 2.66.

Average: y=61%
95% D δ 7.03
13% D δ 2.66

^{1}H-NMR Reference **44**

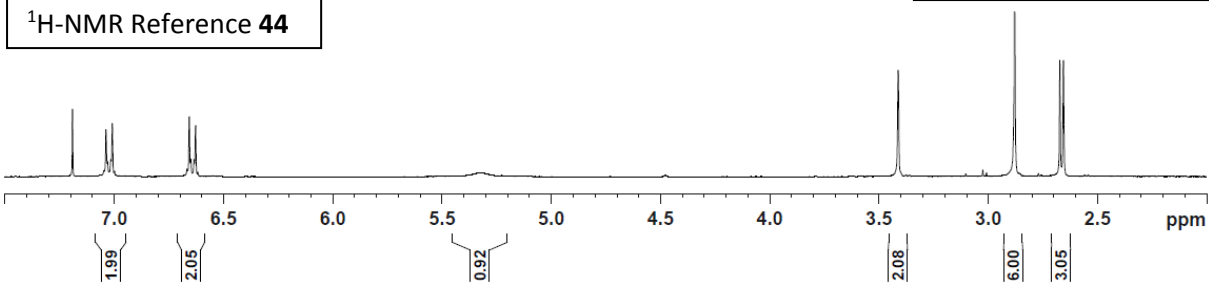

^{1}H-NMR HIE reaction **44**

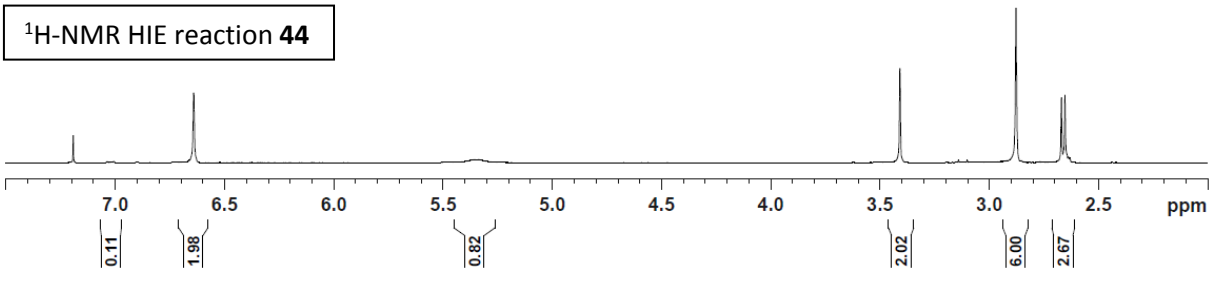

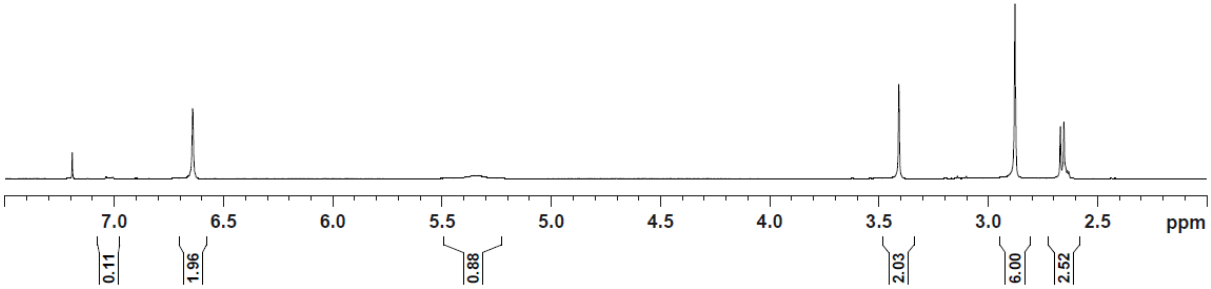

N,N-Dimethyl-4-*N',N'*-dimethylaminobenzeneacetamide (**45**)

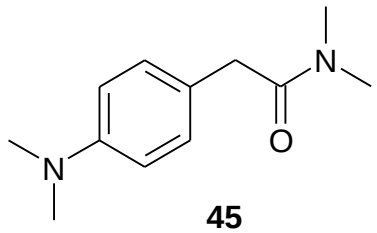

45

Molecular Weight =206,29
Molecular Formula =C12H18N2O

^{1}H NMR (300 MHz, $CDCl_3$): δ 7.05 (d, ^3J = 8.5 Hz, 2H, CH_2 *ortho*-phenyl), 6.62 (d, ^3J = 8.5 Hz, 2H, CH_2 *meta*-phenyl), 3.54 (s, 2H, CH_2 benzylic), 2.89 (ds, 6H, $N(CH_3)_2$), 2.84 (s, 6H, $N(CH_3)_2$) ppm. Incorporation expected at δ 7.05 (red arrow). Determined against integral at δ 3.54 (blue arrow).

General method: 8.2 mg (40.0 µmol) **45**; 6.1 mg (4.0 µmol) catalyst **F**, 2h.

Yield: a) 5.9 mg, 29.0 µmol, 72%; 97% D for δ 7.05 and 34% D for δ 2.89.
b) 5.1 mg, 25.0 µmol, 62%; 98% D for δ 7.05 and 25% D for δ 2.89.

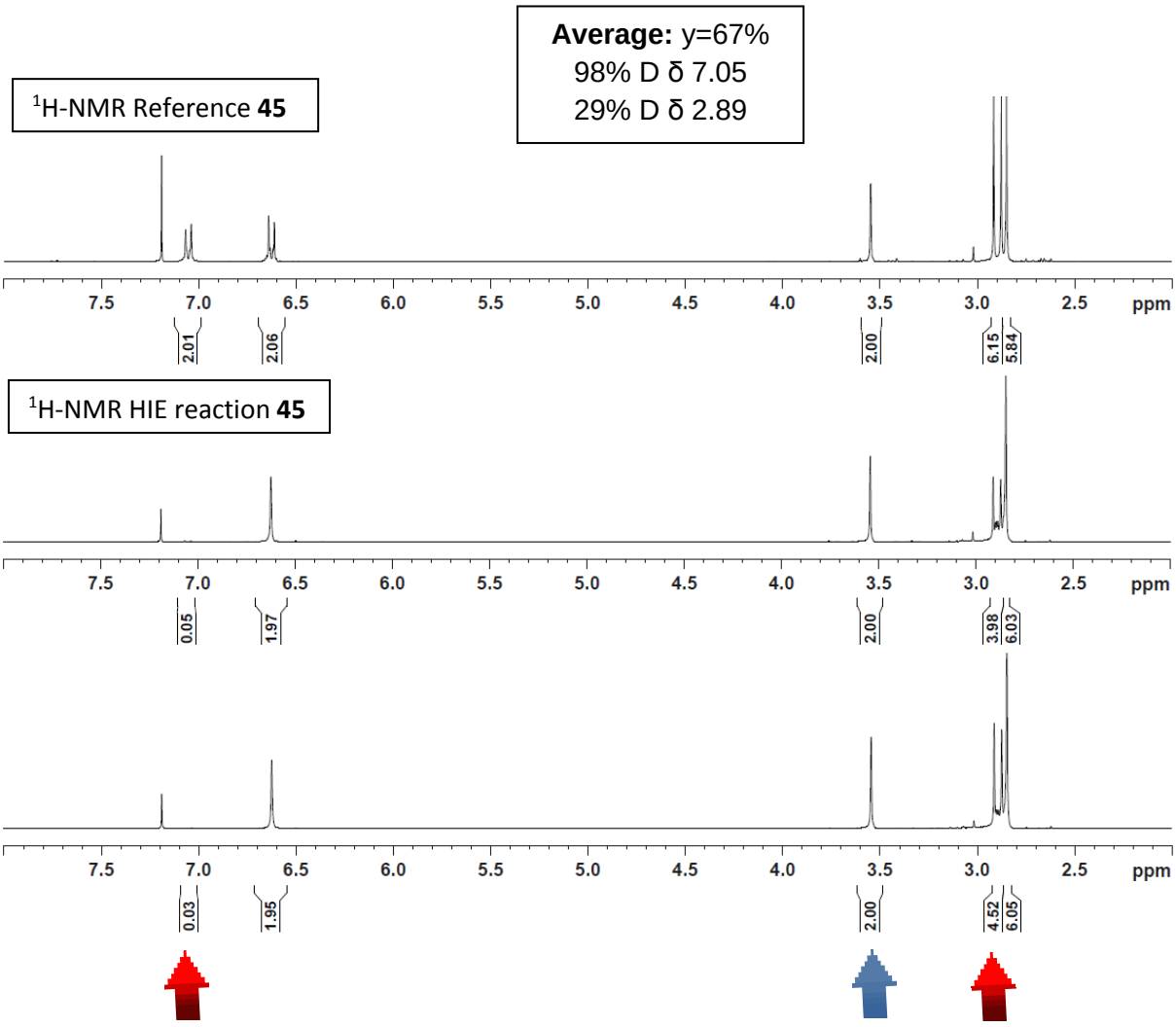

N-(1-Methylcyclohexyl)-4-methoxybenzeneacetamide (**46**)

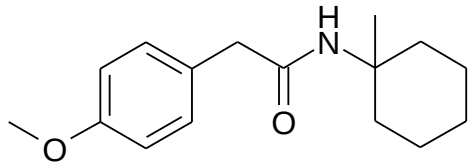

Molecular Weight =261.3672
Molecular Formula =C16H23NO2

46

^{1}H NMR (300 MHz, $CDCl_3$): δ 7.17 (d, ^3J = 8.5 Hz, 2H, CH_2 *ortho*-phenyl), 6.89 (d, ^3J = 8.5 Hz, 2H, CH_2 *meta*-phenyl), 5.05 (br s, 1H, NH), 3.81 (s, 3H, OCH_3), 3.46 (s, 2H, CH_2 benzylic), 1.89 (m, 2H, cyclohexyl), 1.42 (m, 3H, cyclohexyl), 1.32 (s, 3H, CH_3), 1.20 (m, 5H, cyclohexyl) ppm. Incorporation expected at δ 7.17 (red arrow). Determined against integral at δ 3.81.

General method: 10.4 mg (40.0 µmol) **46**; 6.1 mg (4.0 µmol) catalyst **F**, 2h.

Yield: a) 10.9 mg, 42.0 µmol, 100%; 75% D for δ 7.17.
b) 9.9 mg, 38.0 µmol, 95%; 75% D for δ 7.17.

Average: y=98%, 75% D δ 7.17

^{1}H-NMR Reference **46**

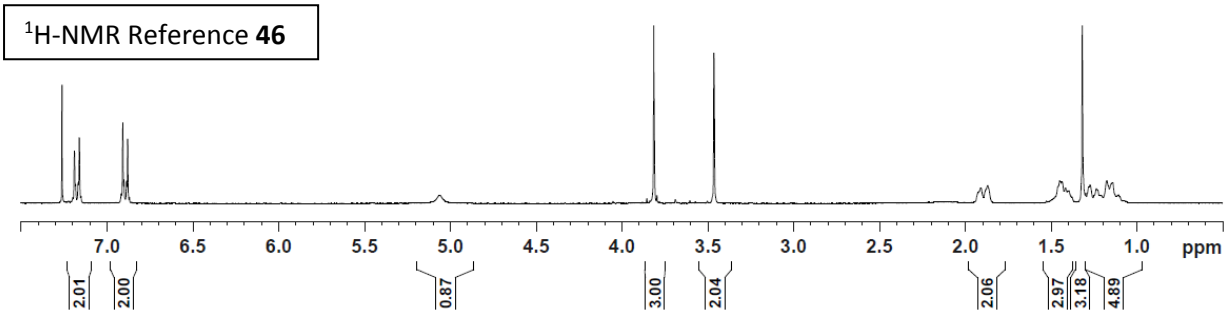

^{1}H-NMR HIE reaction **46**

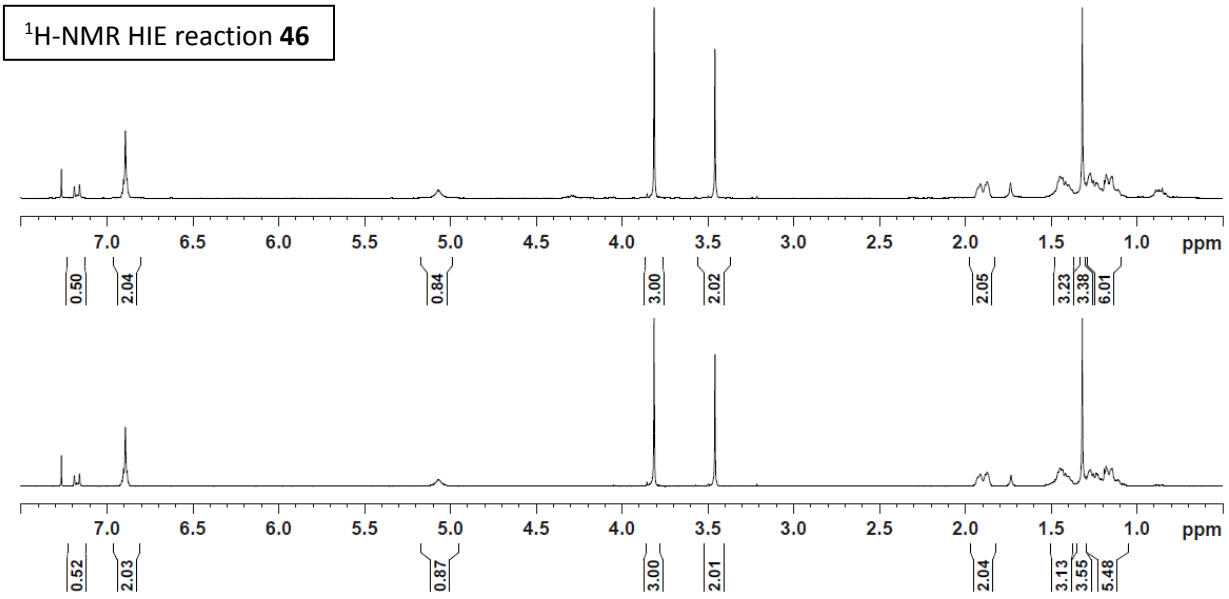

N-[(4-Chlorophenyl)acetyl]glycine ethyl ester (**47**)

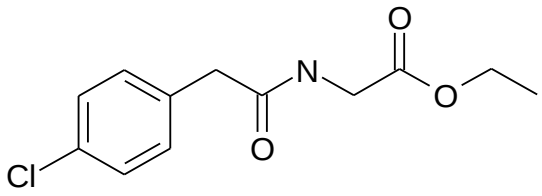

Molecular Weight =255.7033
Molecular Formula =C12H14ClNO3

47

^{1}H NMR (300 MHz, $CDCl_3$): δ 7.32 (d, ^3J = 8.5 Hz, 2H, CH_2 *meta*-phenyl), 7.22 (d, ^3J = 8.5 Hz, 2H, CH_2 *ortho*-phenyl), 5.96 (br s, 1H, NH), 4.18 (q, ^3J = 7.2 Hz, 2H, CH_2 ethyl), 4.00 (d, ^3J = 5.2 Hz, 2H, CH_2 glycine), 3.57 (s, 2H, CH_2 benzylic), 1.26 (s, 3H, CH_3 ethyl) ppm. Incorporation expected at δ 7.22 (red arrow). Determined against integral at δ 3.57 (blue arrow).

General method: 10.2 mg (40.0 µmol) **47**; 6.10 mg (4.0 µmol) catalyst **F**, 2h.

Yield: a) 11.0 mg, 43.0 µmol, 100%; 99% D for δ 7.22.
b) 8.9 mg, 35.0 µmol, 87%; 99% D for δ 7.22.

Average: y=94%, 99% D δ 7.22

^{1}H-NMR Reference **47**

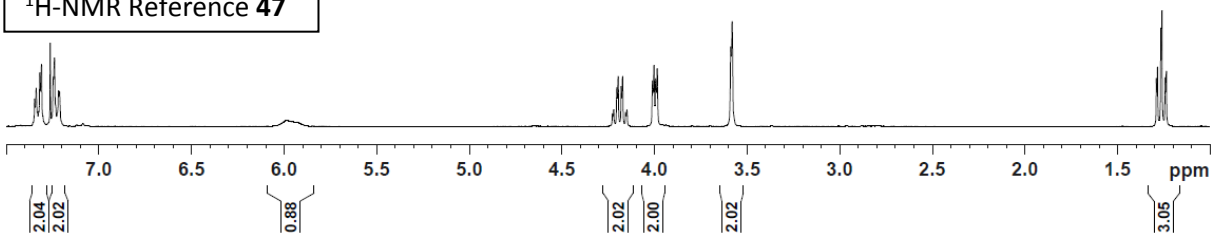

^{1}H-NMR HIE reaction **47**

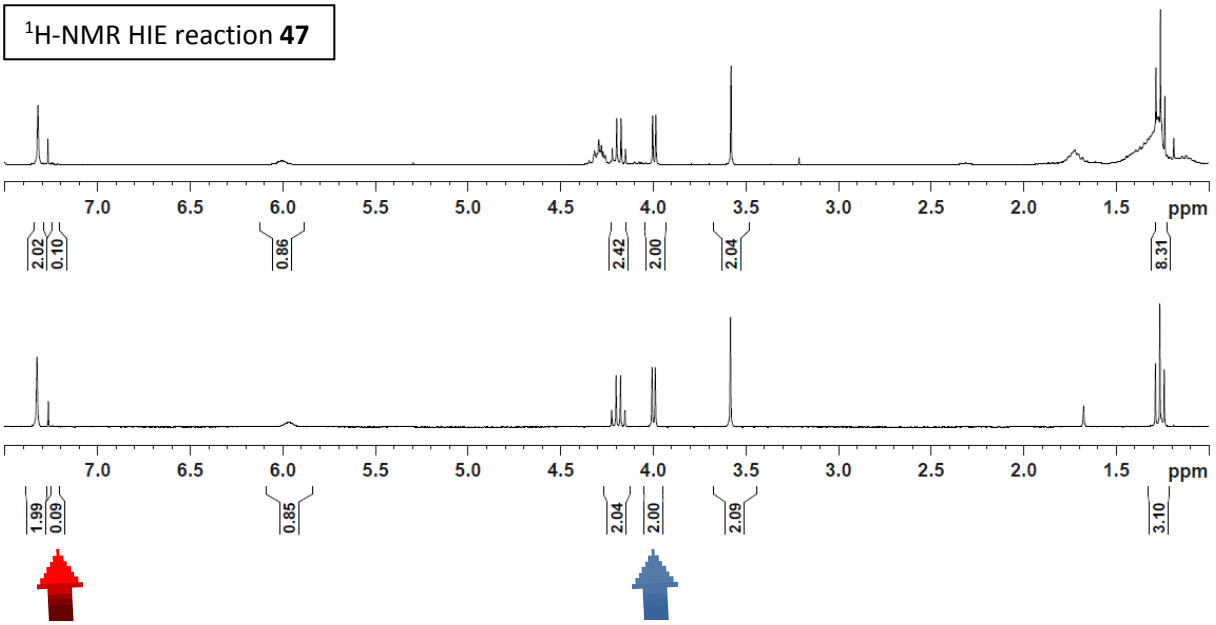

HIE reactions on drugs 5, 10, 50-53

a) Ibuprofen amide **50a**

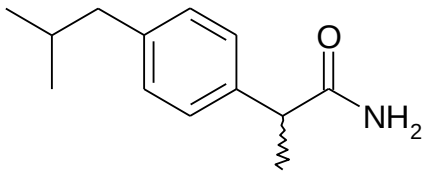

Molecular Weight =205.3025
Molecular Formula =C13H19NO

50a

^{1}H NMR (300 MHz, $CDCl_3$): δ 7.21 (d, ^3J = 8.5 Hz, 2H, CH_2 *ortho*-phenyl), 7.09 (d, ^3J = 8.5 Hz, 2H, CH_2 *meta*-phenyl), 3.69 (q, ^3J = 7.0 Hz, 1H, CH benzylic), 2.43 (d, ^3J = 7.0 Hz, 2H, CH_2 *i*Pr), 1.84 (sept, ^3J = 7.0 Hz, 1H, CH *i*Pr), 1.49 (d, ^3J = 7.0 Hz, 3H, CH_3), 0.89 (d, ^3J = 7.0 Hz, 6H, CH_3 *i*Pr) ppm. Incorporation expected at δ 7.21 (red arrow). Determined against integral at δ 2.43.

General method: 10.3 mg (50.0 µmol) **50a**; 7.6 mg (5.0 µmol) catalyst **F**, 2h.

Yield: a) 10.0 mg, 49.0 µmol, 97%; 0% D for δ 7.21.

^{1}H-NMR Reference **50a**

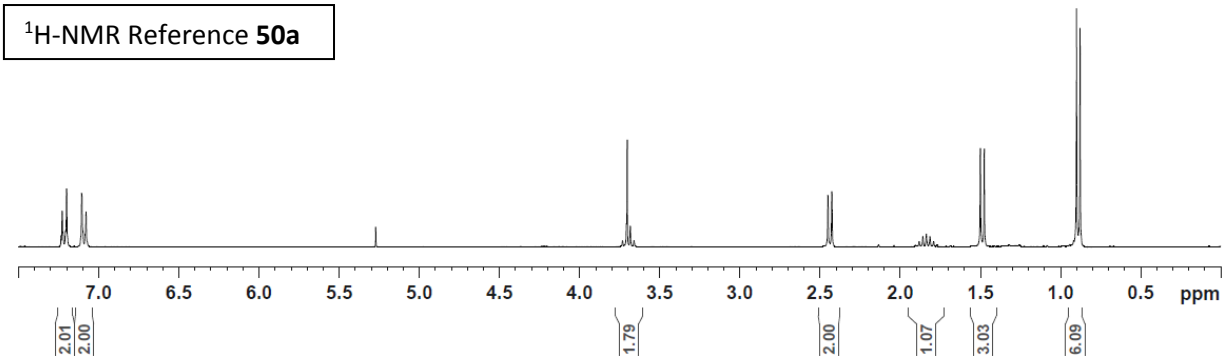

^{1}H-NMR HIE reaction **50a**

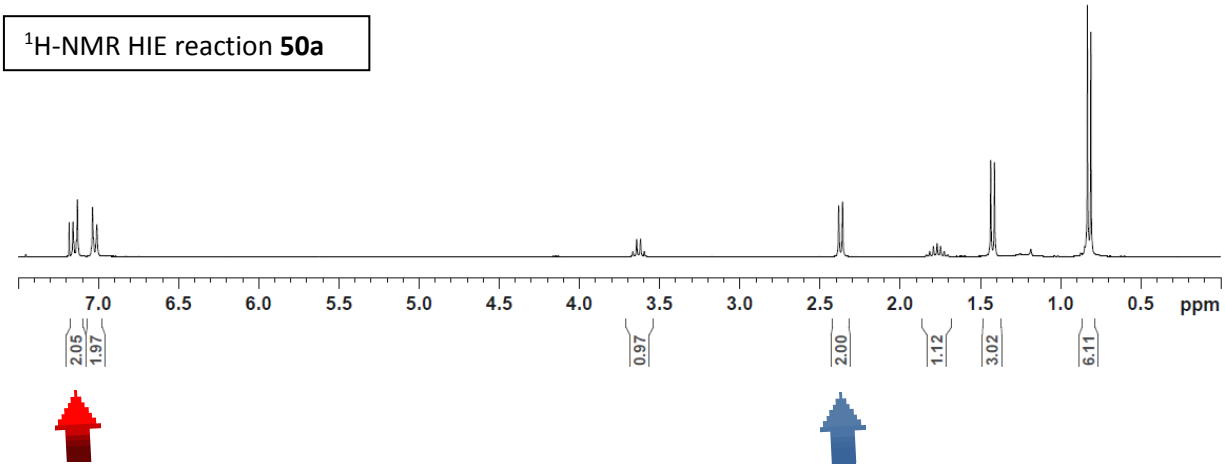

b) Ibuprofen propylamide **50b**

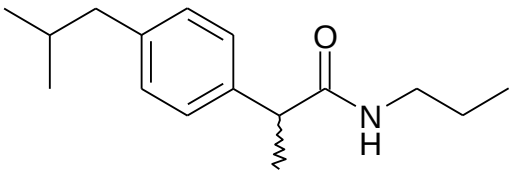

Molecular Weight =247.3838
Molecular Formula =C16H25NO

50b

^{1}H NMR (300 MHz, $CDCl_3$): δ 7.19 (d, ^3J = 8.0 Hz, 2H, CH_2 *ortho*-phenyl), 7.11 (d, ^3J = 8.0 Hz, 2H, CH_2 *meta*-phenyl), 5.43 (bs, 1H, NH), 3.53 (q, ^3J = 7.0 Hz, 1H, CH benzylic), 3.14 (m, 2H, CH_2 propyl), 2.45 (d, ^3J = 6.9 Hz, 2H, CH_2 *i*Pr), 1.85 (sept, ^3J = 6.9 Hz, 1H, CH *i*Pr), 1.51 (d, ^3J = 7.0 Hz, 3H, CH_3), 1.41 (sext, ^3J = 7.5 Hz, 2H, CH_2 propyl), 0.89 (d, ^3J = 6.9 Hz, 6H, CH_3 *i*Pr), 0.80 (t, ^3J = 7.5 Hz, 3H, CH_3 propyl) ppm. Incorporation expected at δ 7.19 (red arrow). Determined against integral at δ 2.45.

General method: 11.1 mg (45.0 µmol) **50b**; 6.9 mg (4.5 µmol) catalyst **F**, 2h.

Yield: a) 10.5 mg, 43.0 µmol, 95%; 80% D for δ 7.19.
b) 11.9 mg, 48.0 µmol, 100%; 82% D for δ 7.19.

Average: y=98%, 81% D δ 7.19

^{1}H-NMR Reference **50b**

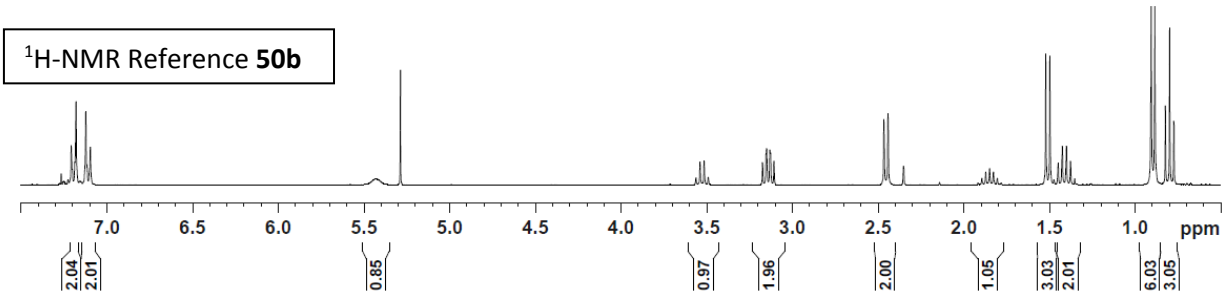

^{1}H-NMR HIE reaction **50b**

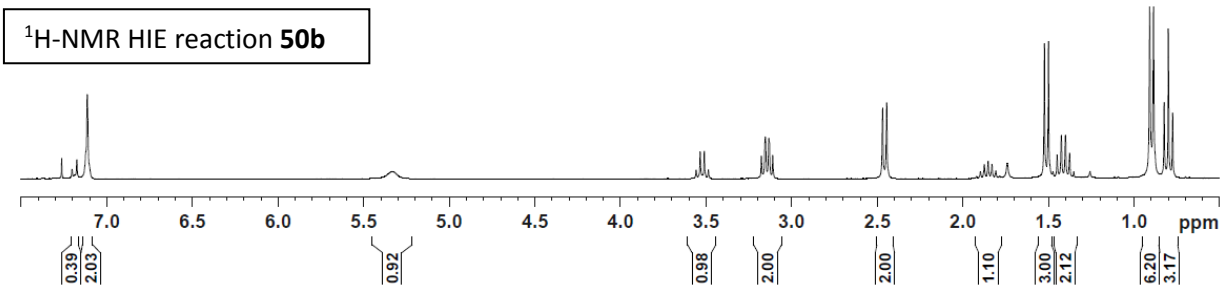

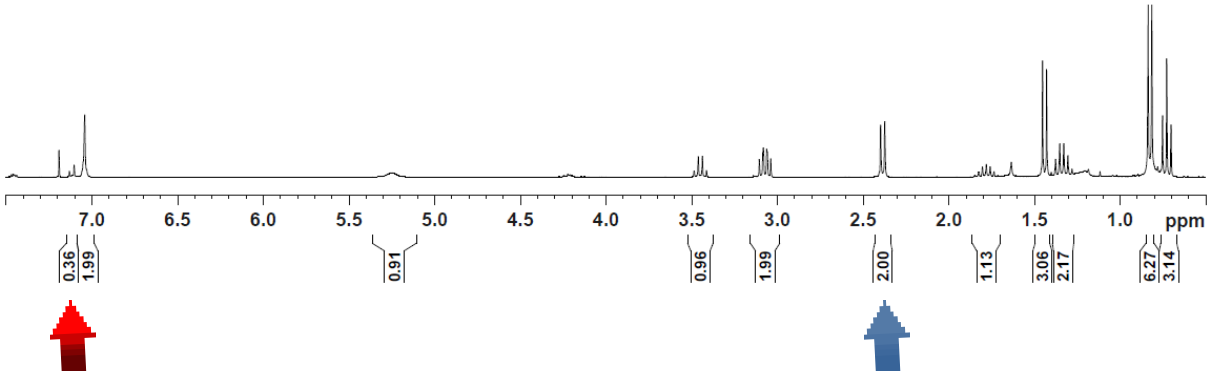

c) Ibuprofen diethylamide **50c**

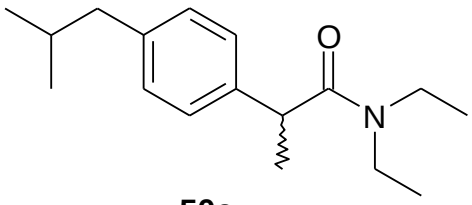

50c

Molecular Weight =261.4108
Molecular Formula =C17H27NO

^{1}H NMR (300 MHz, $CDCl_3$): δ 7.16 (d, ^3J = 8.0 Hz, 2H, CH_2 *ortho*-phenyl), 7.06 (d, ^3J = 8.0 Hz, 2H, CH_2 *meta*-phenyl), 3.79 (q, ^3J = 7.0 Hz, 1H, CH benzylic), 3.28 (m, 4H, CH_2 ethyl), 2.43 (d, ^3J = 7.0 Hz, 2H, CH_2 *i*Pr), 1.83 (sept, ^3J = 7.0 Hz, 1H, CH *i*Pr), 1.42 (d, ^3J = 7.0 Hz, 3H, CH_3), 1.09 (t, ^3J = 7.0 Hz, 3H, CH_3 ethyl), 0.94 (t, ^3J = 7.0 Hz, 3H, CH_3 ethyl), 0.88 (d, ^3J = 7.0 Hz, 6H, CH_3 *i*Pr) ppm. Incorporation expected at δ 7.16 (red arrow). Determined against integral at δ 2.43.

General method: 11.7 mg (45.0 µmol) **50c**; 6.9 mg (4.5 µmol) catalyst **F**, 2h.

Yield: a) 11.7 mg, 45.0 µmol, 100%; 96% D for δ 7.16.
b) 12.5 mg, 48.0 µmol, 100%; 96% D for δ 7.16.

Average: y=100%, 96% D δ 7.16

^{1}H-NMR Reference **50c**

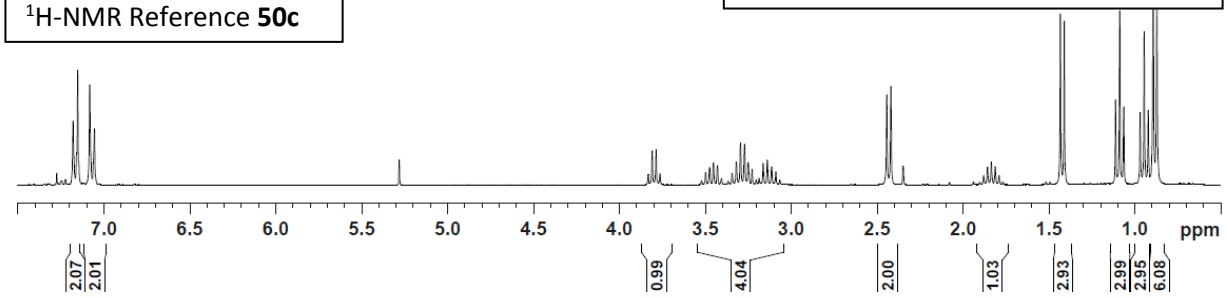

^{1}H-NMR HIE reaction **50c**

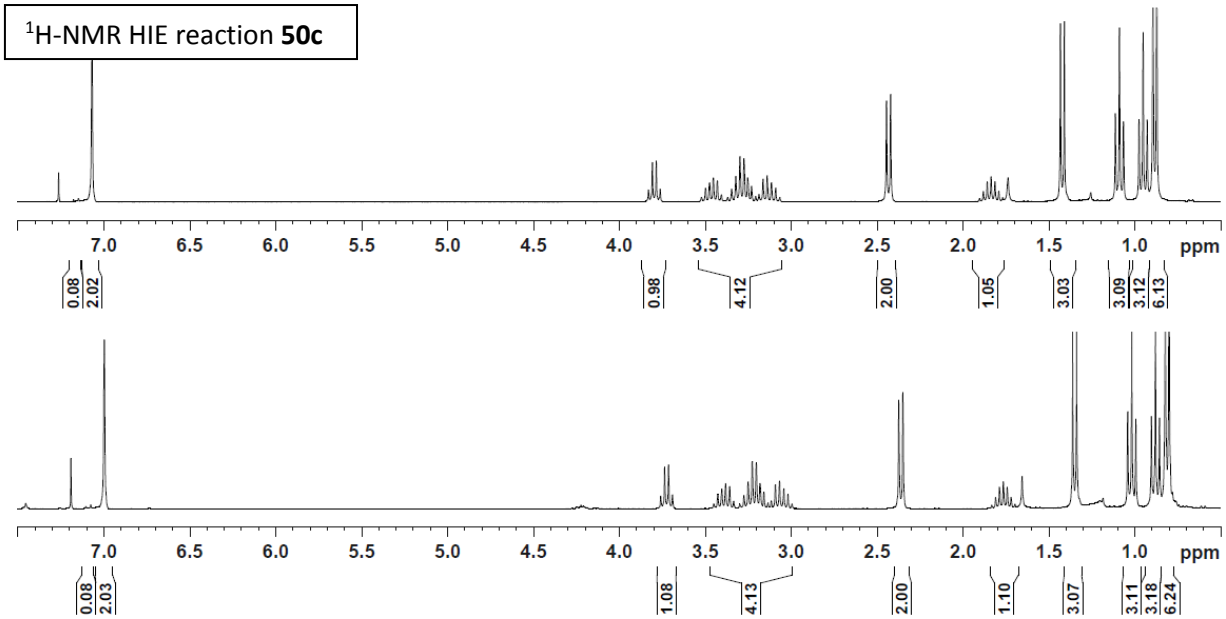

d) Ibuprofen diisobutylamide **50d**

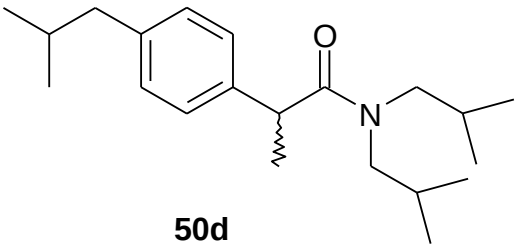

50d

Molecular Weight =317.5192
Molecular Formula =C21H35NO

^{1}H NMR (300 MHz, $CDCl_3$): δ 7.18 (d, ^3J = 8.0 Hz, 2H, CH_2 *ortho*-phenyl), 7.06 (d, ^3J = 8.0 Hz, 2H, CH_2 *meta*-phenyl), 3.87 (q, ^3J = 7.0 Hz, 1H, CH benzylic), 3.58 (m, 1H, CH_2 *t*Bu), 3.26 (m, 1H, CH_2 *t*Bu), 2.79 (m, 2H, CH_2 *t*Bu), 2.43 (d, ^3J = 7.0 Hz, 2H, CH_2 *i*Pr), 1.98 (m, 2H, CH *t*Bu), 1.85 (m, 1H, CH *i*Pr), 1.42 (d, ^3J = 7.0 Hz, 3H, CH_3), 0.85 (m, 12H, CH_3 *t*Bu), 0.76 (m, 6H, CH_3 *i*Pr) ppm. Incorporation expected at δ 7.18 (red arrow). Determined against integral at δ 2.43.

General method: 14.3 mg (45.0 µmol) **50d**; 6.9 mg (4.5 µmol) catalyst **F**, 2h.

Yield: a) 13.4 mg, 42.0 µmol, 94%; 87% D for δ 7.18.
b) 13.6 mg, 43.0 µmol, 95%; 90% D for δ 7.18.

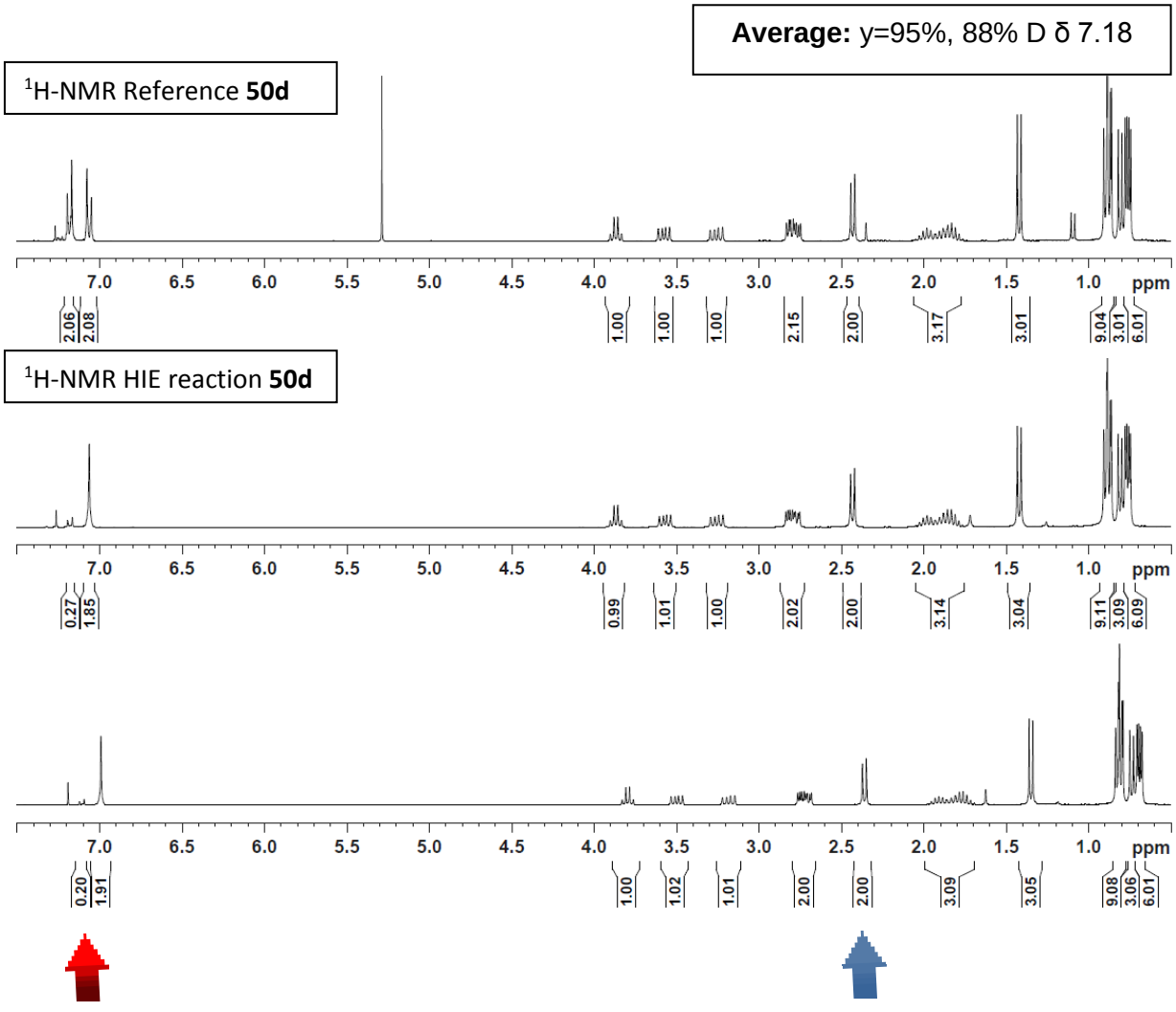

e) Ibuprofen methyl ester **50e**

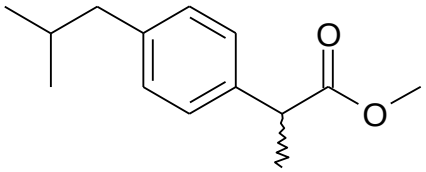

50e

Molecular Weight =220.3143
Molecular Formula =C14H20O2

^{1}H NMR (300 MHz, $CDCl_3$): δ 7.19 (d, ^3J = 8.0 Hz, 2H, CH_2 *ortho*-phenyl), 7.08 (d, ^3J = 8.0 Hz, 2H, CH_2 *meta*-phenyl), 3.69 (q, ^3J = 7.2 Hz, 1H, CH benzylic), 3.64 (s, 3H, OCH_3), 2.43 (d, ^3J = 6.8 Hz, 2H, CH_2 *i*Pr), 1.84 (sept, ^3J = 6.8 Hz, 1H, CH *i*Pr), 1.48 (d, ^3J = 7.2 Hz, 3H, CH_3), 0.89 (d, ^3J = 6.8 Hz, 6H, CH_3 *i*Pr) ppm. Incorporation expected at δ 7.19 (red arrow). Determined against integral at δ 2.43.

General method: 11.0 mg (50.0 µmol) **50e**; 7.6 mg (5.0 µmol) catalyst **F**, 2h.

Yield: a) 10.9 mg, 49.0 µmol, 99%; 33% D for δ 7.19.
b) 10.5 mg, 48.0 µmol, 95%; 30% D for δ 7.19.

Average: y=97%, 32% D δ 7.19

^{1}H-NMR Reference **50e**

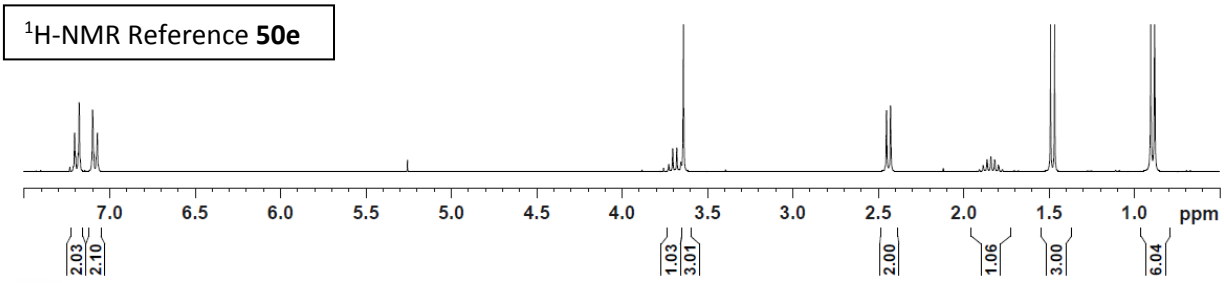

^{1}H-NMR HIE reaction **50e**

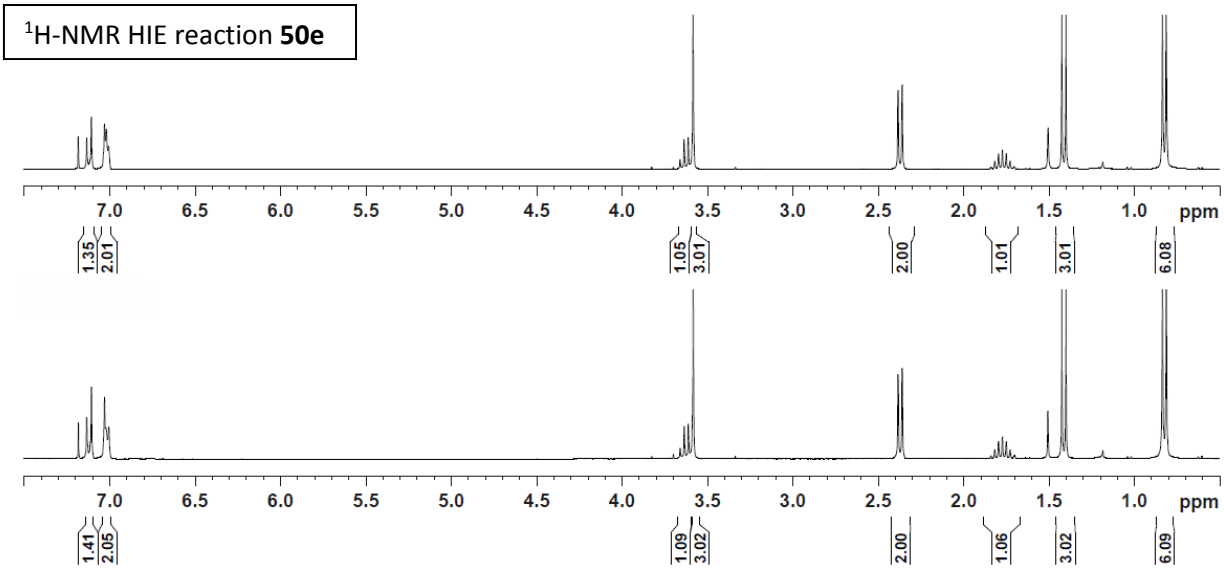

2-[2,4-Bis(trifluoromethyl)phenyl]-*N*-[(R)-2-oxo-5-phenyl-1-(2,2,2-trifluoro-ethyl)-2,3-dihydro-1H-1,4-benzodiazepin-3-yl]-acetamide (**51**)

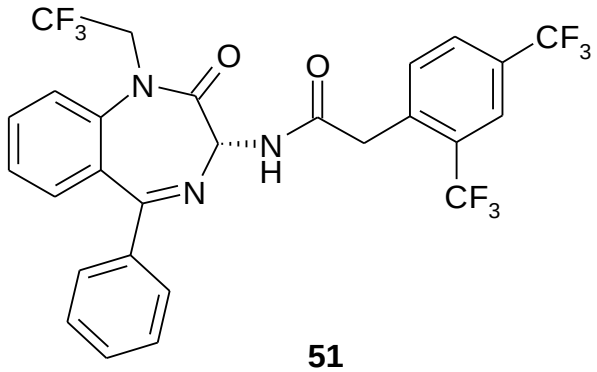

Molecular Weight =425.5351
Molecular Formula =C27H27N3O2

51

^{1}H NMR (300 MHz, $CDCl_3$): δ 7.93 (s, 1H, CH aromatic), 7.80 (d, ^3J = 8.0 Hz, 1H, CH *meta*-phenylacetamide), 7.71 (d, ^3J = 8.0 Hz, 1H, CH *ortho*-phenylacetamide), 7.61 (m, 1H, CH aromatic), 7.55 (m, 1H, CH aromatic), 7.53 (m, 1H, CH aromatic), 7.48 (m, 1H, CH aromatic), 7.42 (m, 1H, CH aromatic), 7.39 (m, 2H, CH_2 aromatic), 7.32 (m, 2H, CH_2 aromatic), 5.60 (d, ^3J = 8.0 Hz, 1H, C*H*-NH), 5.20 (sext, ^3J = 8.0 Hz, 1H, CH_2-CF_3), 4.16 (sext, ^3J = 8.0 Hz, 1H, CH_2-CF_3), 3.96 (s, 2H, CH_2 benzylic). Incorporation expected at δ 7.71 (red arrow). Determined against integral at δ 3.96.

General method: 11.7 mg (20.0 µmol) **51**; 3.1 mg (2.0 µmol) catalyst **F**, 2h.

Yield: a) 8.7 mg, 15.0 µmol, 74%; 95% D for δ 7.71.
b) 12.8 mg, 22.0 µmol, 100%; 81% D for δ 7.71.

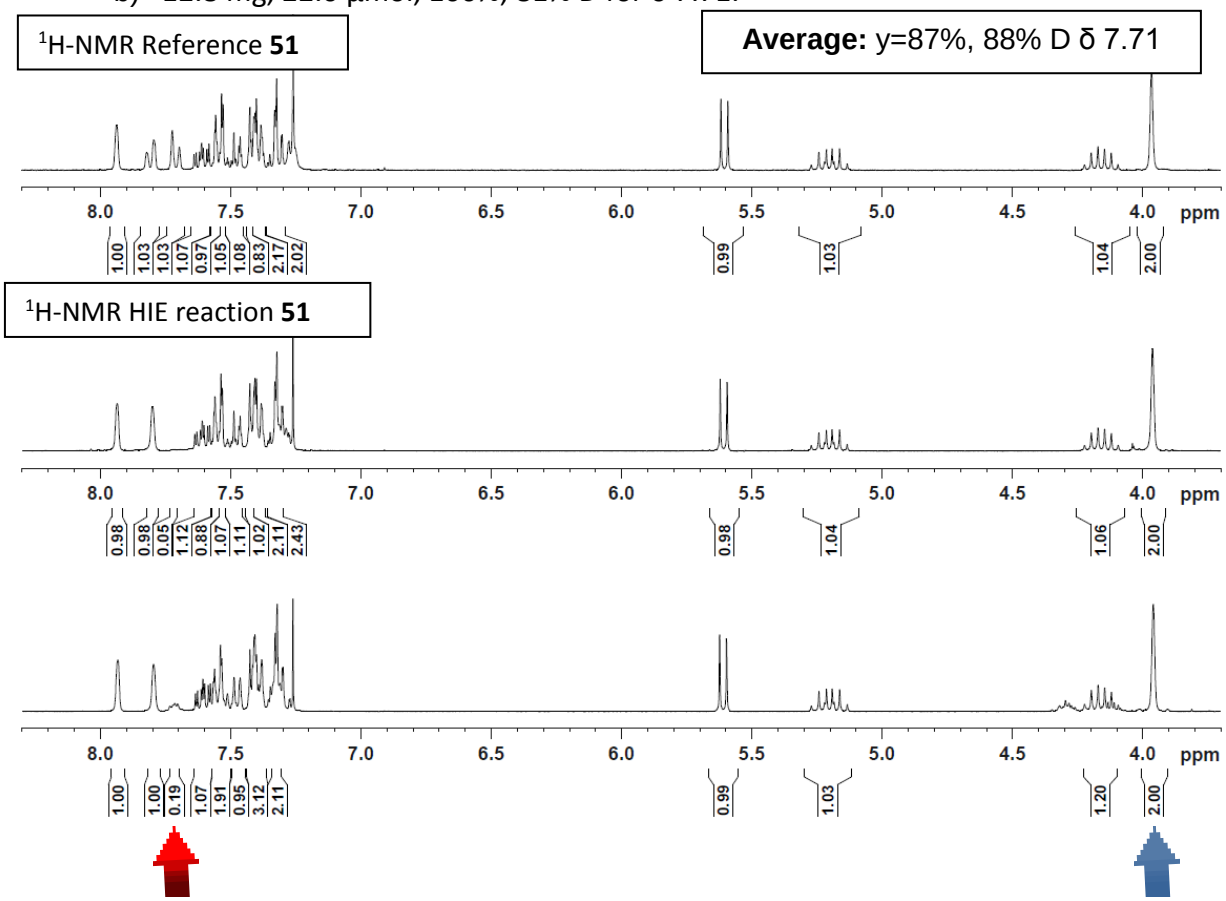

Naproxen methyl ester **52a**

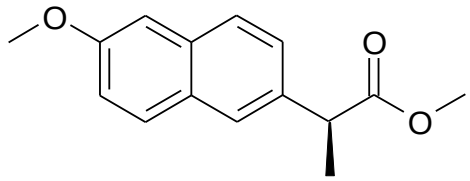

52a

Molecular Weight =244.2930
Molecular Formula =C15H16O3

^{1}H NMR (300 MHz, $CDCl_3$): δ 7.69 (m, 3H, CH aromatic), 7.40 (m, 1H, CH aromatic), 7.13 (m, 2H, CH aromatic), 3.91 (s, 3H, OCH_3), 3.86 (q, ^3J = 7.2 Hz, 1H, CH benzylic), 3.67 (s, 3H, CH_3 ester), 1.58 (d, ^3J = 7.3 Hz, 3H, CH_3 benzylic) ppm. Incorporation expected at δ 7.40 (red arrow). Determined against integral at δ 3.68 (blue arrow).

General method: 10.0 mg (39.0 µmol) **52a**; 6.0 mg (3.9 µmol) catalyst **F**, 2h.

Yield: a) 7.6 mg, 29.6 µmol, 76%; 76% D for δ 7.40.
b) 8.1 mg, 31.6 µmol, 81%; 74% D for δ 7.40.

Average: y=79%, 75% D δ 7.40

^{1}H-NMR Reference **52a**

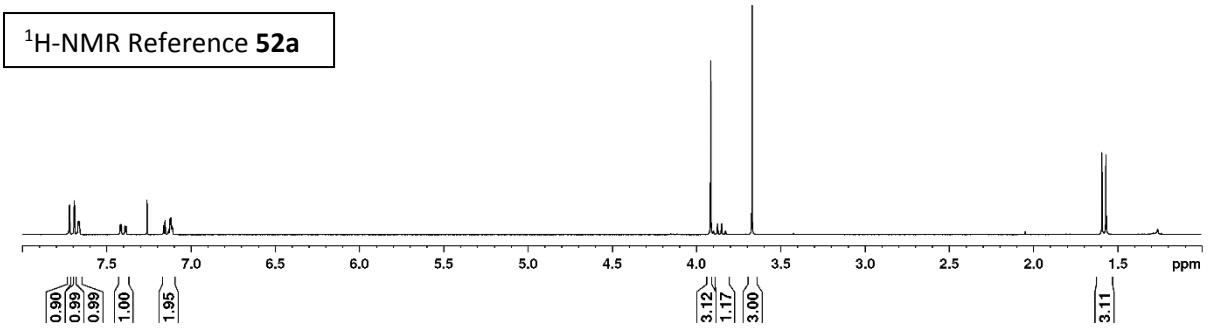

^{1}H-NMR HIE reaction **52a**

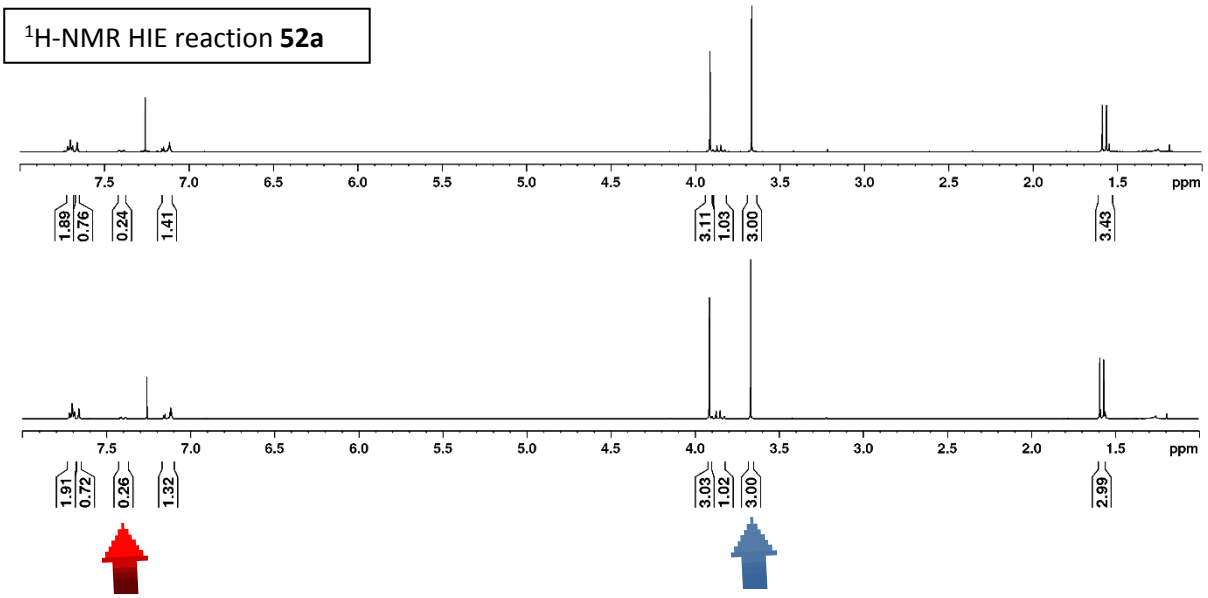

Naproxen ethyl ester **52b**

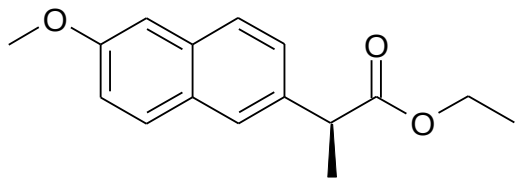

52b

Molecular Weight =258.3201
Molecular Formula =C16H18O3

^{1}H NMR (300 MHz, $CDCl_3$): δ 7.70 (m, 3H, CH aromatic), 7.42 (m, 1H, CH aromatic), 7.14 (m, 2H, CH aromatic), 4.14 (m, 2H, CH_2 ethyl), 3.92 (s, 3H, OCH_3), 3.84 (q, ^3J = 7.2 Hz, 1H, CH benzylic), 1.57 (d, ^3J = 7.2 Hz, 3H, CH_3), 1.21 (t, ^3J = 7.0 Hz, 3H, CH_3 ethyl) ppm. Incorporation expected at δ 7.42 (red arrow). Determined against integral at δ 4.14.

General method: 10.0 mg (39.0 µmol) **52b**; 6.0 mg (3.9 µmol) catalyst **F**, 2h.

Yield: a) 10.3 mg, 40.0 µmol, 100%; 77% D for δ 7.42.
b) 10.6 mg, 41.0 µmol, 100%; 74% D for δ 7.42.

Average: y=100%, 76% D δ 7.42

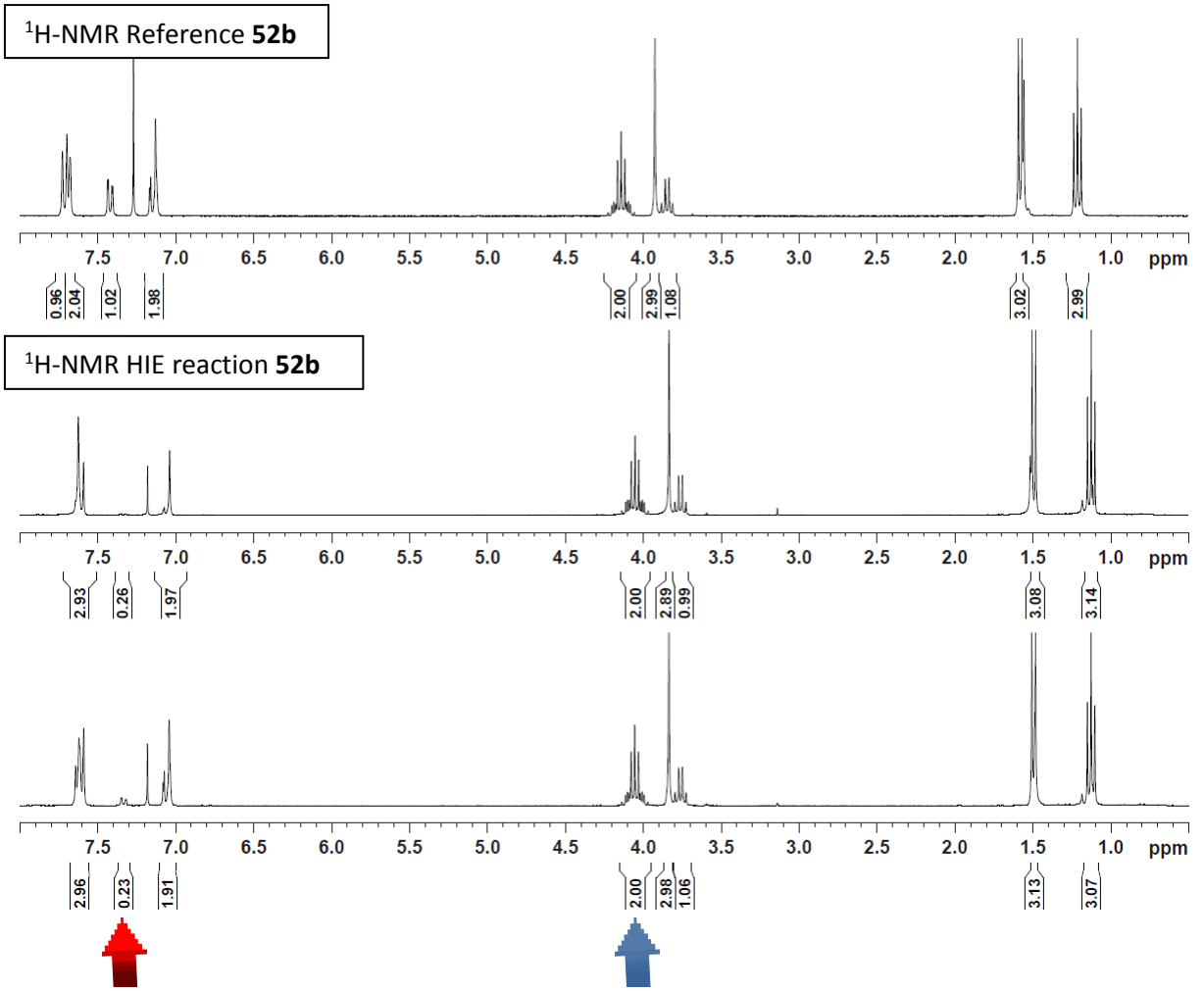

Saponification of deuterated naproxen ethyl ester **52b**

The deuterated naproxen ethyl ester **52b** (5.0 mg, 19 µmol, 1 eq.) was dissolved in 2 mL of ethanol. A solution of 20 mol% KOH was added (200 µL, 0.1 eq.) and the reaction was heated at 80°C for 2 h in the microwave.

An aliquote was analyzed by LC-MS showing quantitative conversion to the corresponding acid.

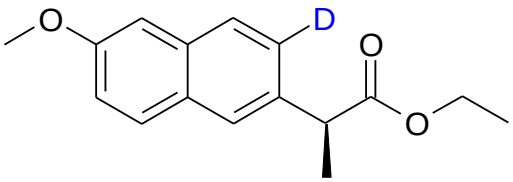

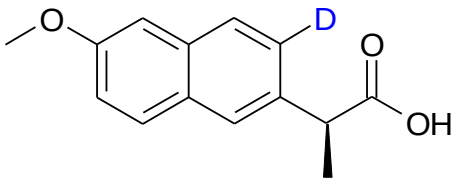

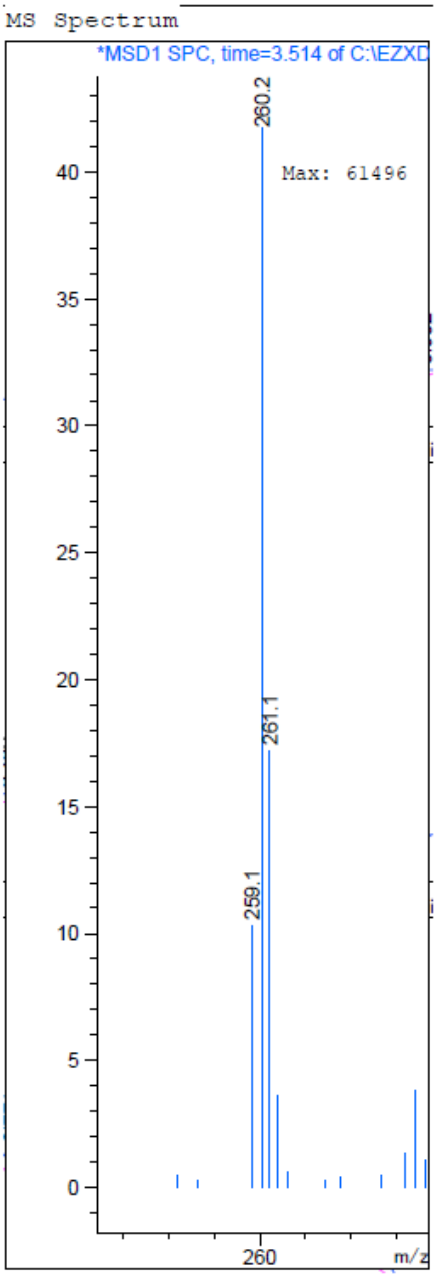

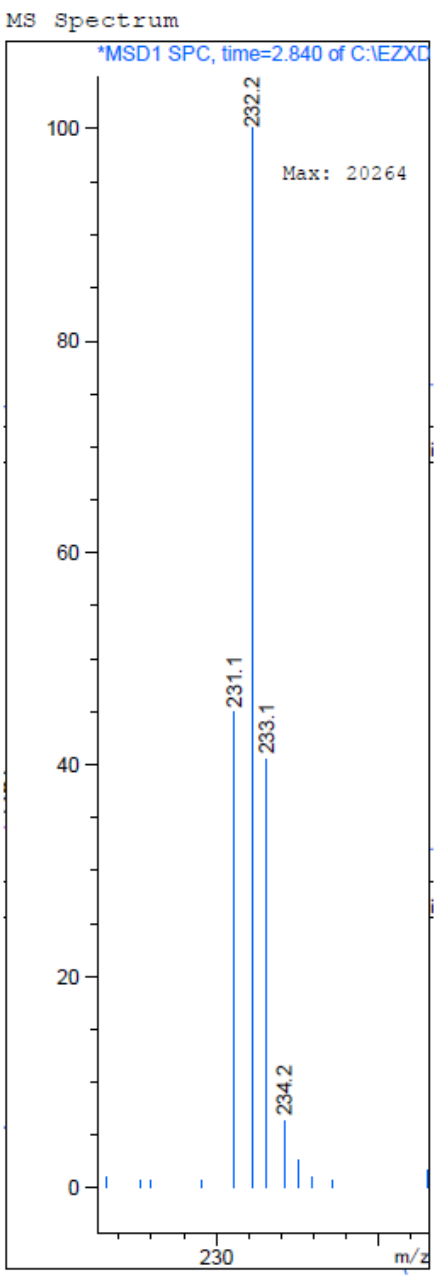

Camylofine (**5**)

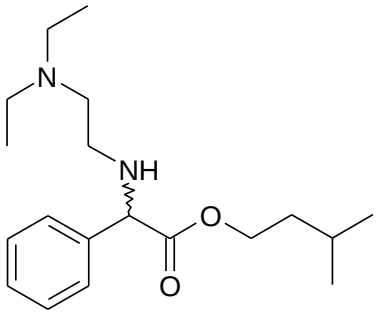

Molecular Weight =320.4791
Molecular Formula =C19H32N2O2

5

^{1}H NMR (300 MHz, CD_2Cl_2): δ 7.25 (m, 5H, CH aromatic), 4.27 (s, 1H, CH benzylic), 3.91 (m, 2H, $CO(=O)CH_2$), 2.38 (m, 9H, 4 x N-CH_2; NH), 1.37 (m, 3H, CH_2-CH aliphatic), 0.83 (br m, 12H, 4x CH_3). Incorporation expected at δ 7.25 and δ 4.27 (red arrow). Determined against integral at δ 0.83 (blue arrow).

General method: 10.0 mg (31.0 µmol) **5**; 4.7 mg (3.1 µmol) catalyst **F**, 2h.

Yield: a) 8.7 mg, 26.9 µmol, 87%; 71% D for δ 7.25 and 63% D for δ 4.27.
b) 8.2 mg, 25.4 µmol, 82%; 72% D for δ 7.25 and 64% D for δ 4.27.

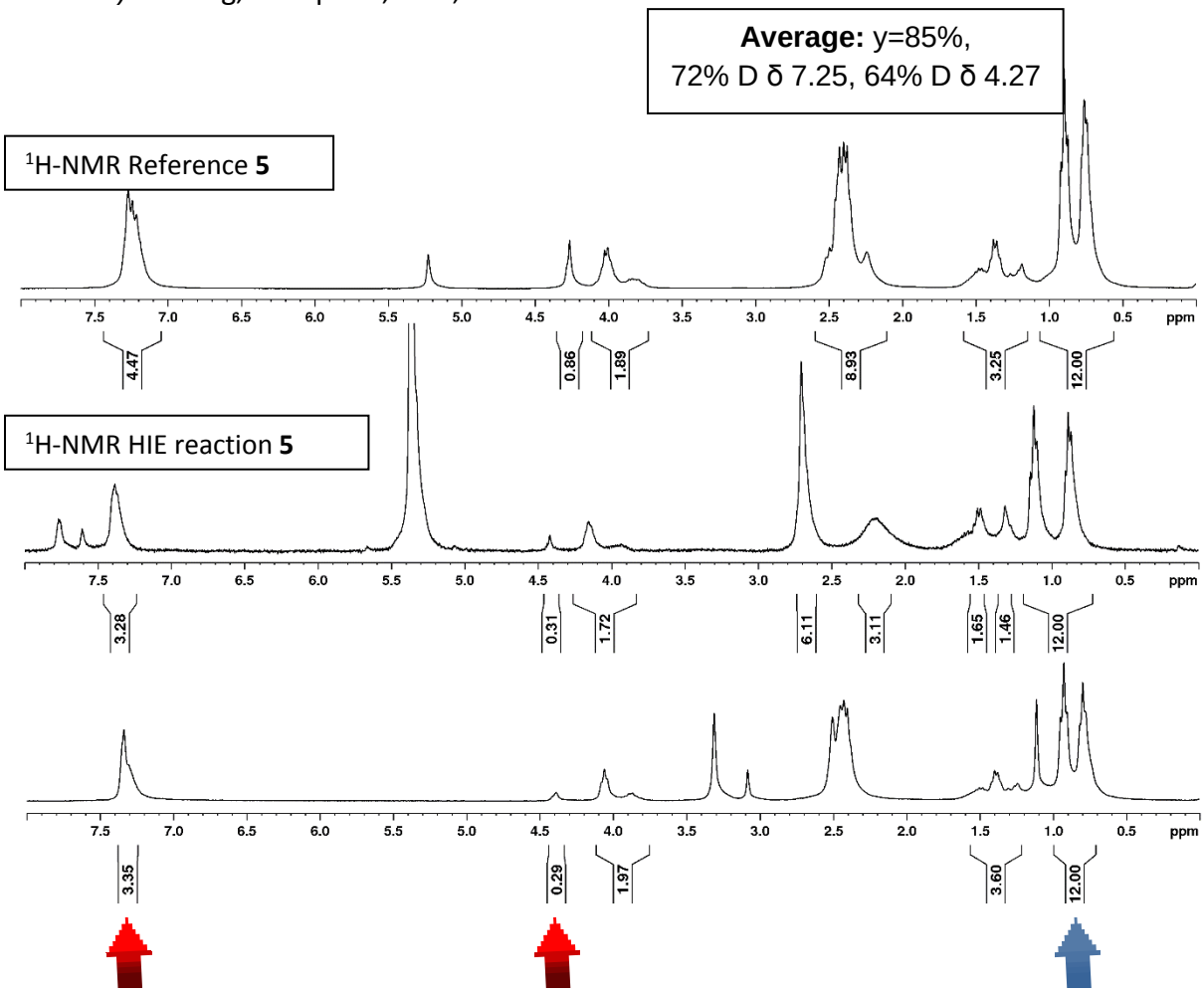

N-Methylcamylofine (**53**)

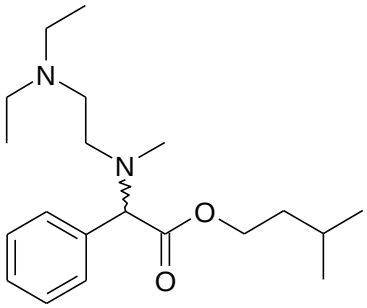

53

Molecular Weight =334.5062
Molecular Formula =C20H34N2O2

^{1}H NMR (300 MHz, $CDCl_3$): δ 7.32 (m, 5H, CH aromatic), 4.24 (s, 1H, CH benzylic), 4.02 (m, 2H, $CO(=O)CH_2$), 2.62 (m, 8H, $N\text{-}CH_2$), 2.30 (s, 3H, $N\text{-}CH_3$), 1.51 (m, 3H, CH_2-CH aliphatic), 1.06 (t ^3J = 7.1 Hz, 6H, CH_3 ethyl), 0.82 (m, 6H, CH_3-C-CH_3). Incorporation expected at δ 7.32 (red arrow). Determined against integral at δ 2.30 (blue arrow).

General method: 10.0 mg (29.9 µmol) **53**; 4.40 mg (2.9 µmol) catalyst **F**, 2h.

Yield: a) 7.6 mg, 22.7 µmol, 76%; 31% D for δ 7.32.
b) 8.1 mg, 24.2 µmol, 81%; 30% D for δ 7.32.

Average: y=79%
31%D δ 7.32

^{1}H-NMR Reference **53**

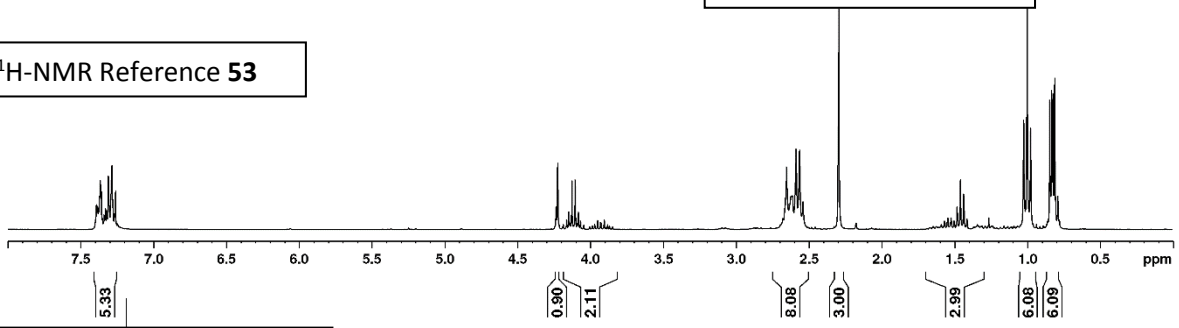

^{1}H-NMR HIE reaction **53**

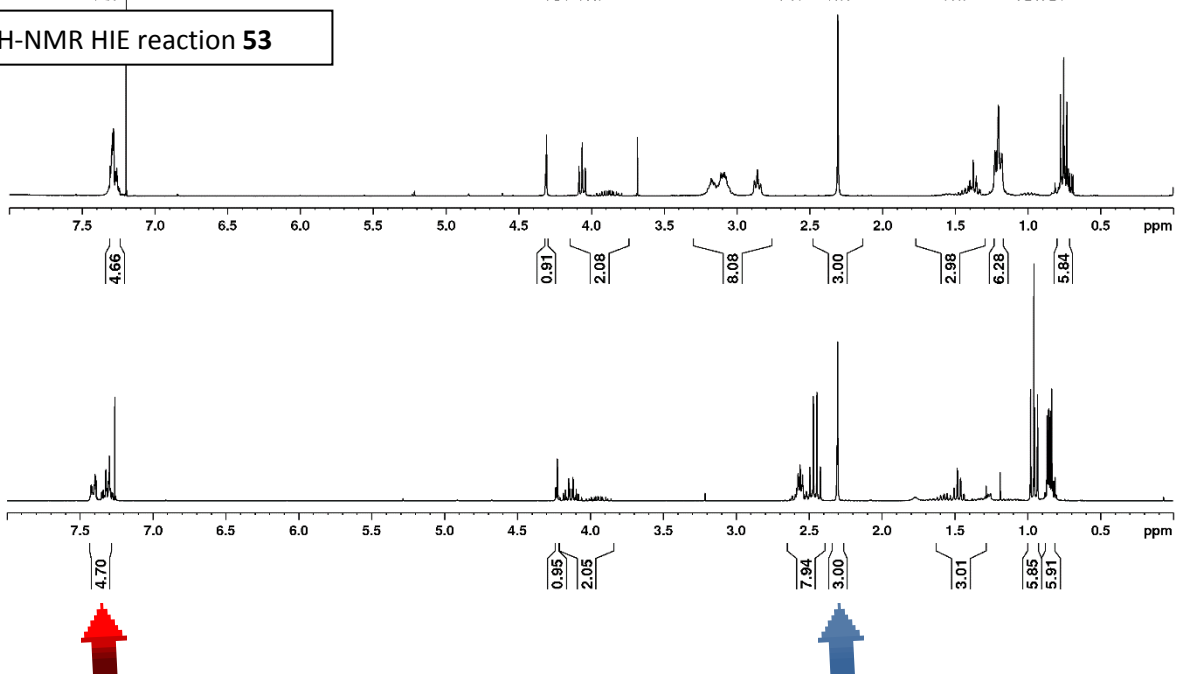

^{3}H-Camylofine (**5**)

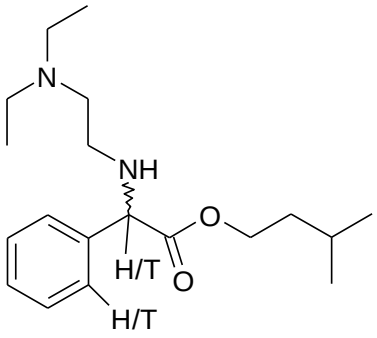

Molecular Weight =320.4791
Molecular Formula =C19H32N2O2

5

The tritiation of Camylofine **5** was carried out using a standard Tritec® tritium manifold. 3.2 mg (9980 µmol) of Camylofine was dissolved in 0.35 mL dry chlorobenzene followed by addition of a solution of 1.5 mg Tamm-catalyst **F** in 0.35 mL dry chlorobenzene. The 1 mL reaction flask was adapted to a tritium manifold and the solution was frozen in liquid nitrogen. The flask was evacuated, charged with tritium (2.5 Ci, 49.9 mmol, 5. eq). The reaction mixture was then allowed to warm to room temperature before stirring at rt for 2 hours. After removal of solvent in vacuo the labile tritium was exchanged and removed by addition of methanol and a freeze-drying process (three times repeated). The solid residue was dissolved in 3 mL methanol. Purification and isolation *via* HPLC (Phenomenex Gemini NX C18 10x150 mm, 5 mm, 5 mL/min flow, ACN/water gradient program) gave **5** (1,5 mg, 5513 MBq, 5,9 % RCY, 1184 GBq/mmol (32 Ci/mmol) in>98% purity (HPLC, UV/RD).

HRMS (positive ESI): m/z 321.3 $[M+H]^+$, 323.3 $[M(T)+H]^+$; 325.3 $[M(T2)+H]^+$

^{1}H NMR (300 MHz, CD_2Cl_2): δ 7.25 (m, 5H, CH aromatic), 4.27 (s, 1H, CH benzylic), 3.91 (m, 2H, $CO(=O)CH_2$), 2.38 (m, 9H, 4 x N-CH_2; NH), 1.37 (m, 3H, CH_2-CH aliphatic), 0.83 (br m, 12H, 4x CH_3).

533 MHz 3H/T Camylofine-3H FF-URA384 ; DMSO-d
zg3H

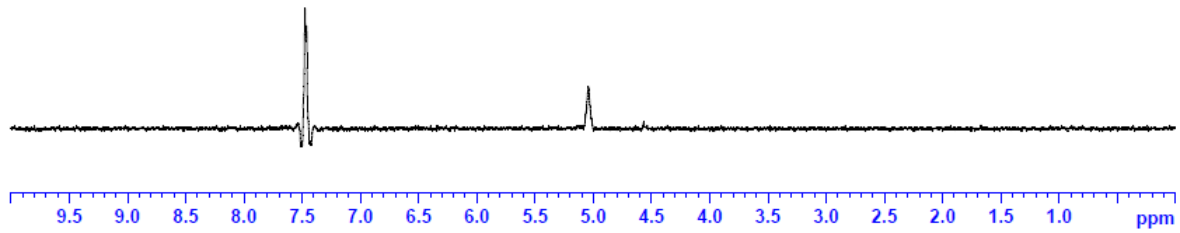

500MHz 1H Camylofine-VG, no batch no. given ; 4m g in DMSO-d
zg30

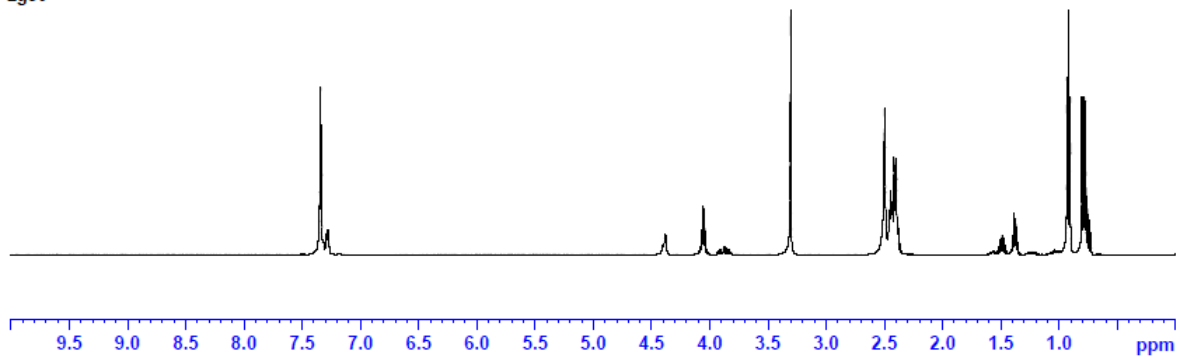

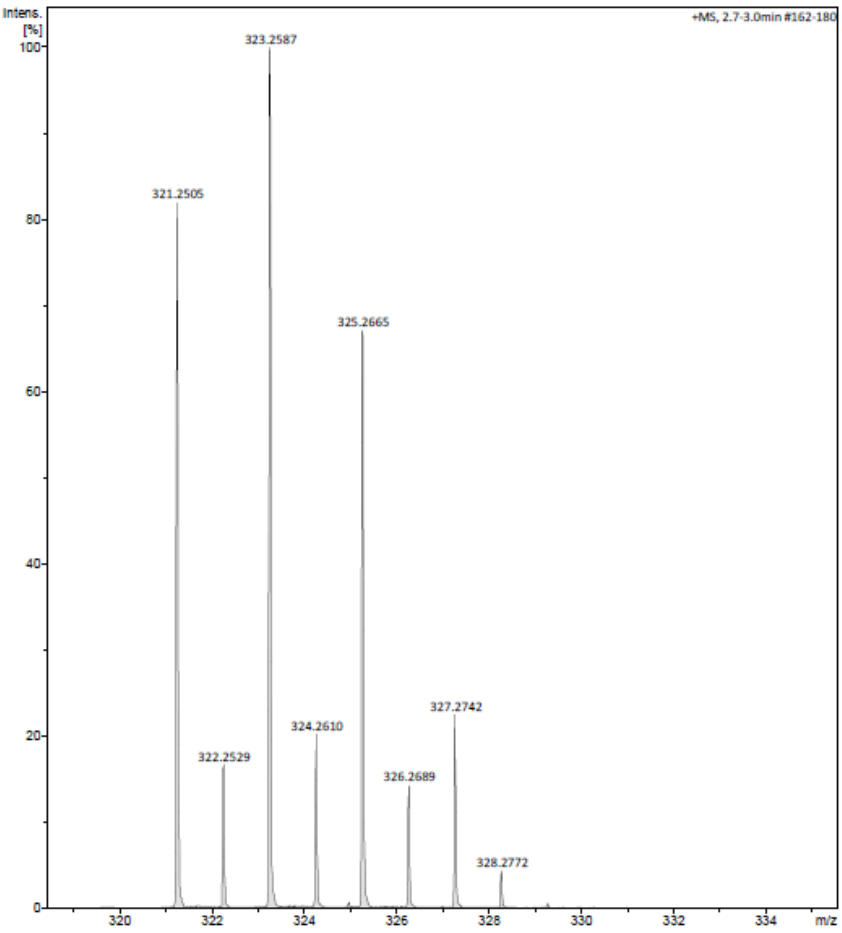

Benalaxyl (**10**)

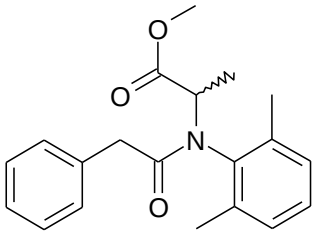

Molecular Weight =325.4112
Molecular Formula =C20H23NO3

10

^{1}H NMR (300 MHz, $CDCl_3$): δ 7.20 (m, 5H, 2CH *meta*-phenyl, 2CH' *meta*-aniline, CH *para*-phenyl), 7.05 (d, ^3J = 7.0 Hz, 1H, CH *para*-aniline), 6.95 (m, 2H, CH *ortho*-phenyl), 4.45 (q, ^3J = 7.5 Hz, 1H, CH), 3.79 (s, 3H, OCH_3), 3.36 (d, ^3J = 14.5 Hz, 1H, CH benzylic), 3.22 (d, ^3J = 14.5 Hz, 1H, CH benzylic), 2.41 (s, 3H, CH_3 *ortho*-aniline), 1.89 (s, 3H, CH_3 *ortho*-aniline),1.01 (d, ^3J = 7.5 Hz, 3H, CH_3) ppm. Incorporation expected at δ 6.95 (red arrow). Determined against integral at δ 3.79.

General method: 12.7 mg (39.0 µmol) **10**; 6.0 mg (3.9 µmol) catalyst **F**, 2h.

Yield: a) 11.6 mg, 36.0 µmol, 91%; 96% D for δ 6.95.
b) 11.3 mg, 35.0 µmol, 89%; 96% D for δ 6.95.

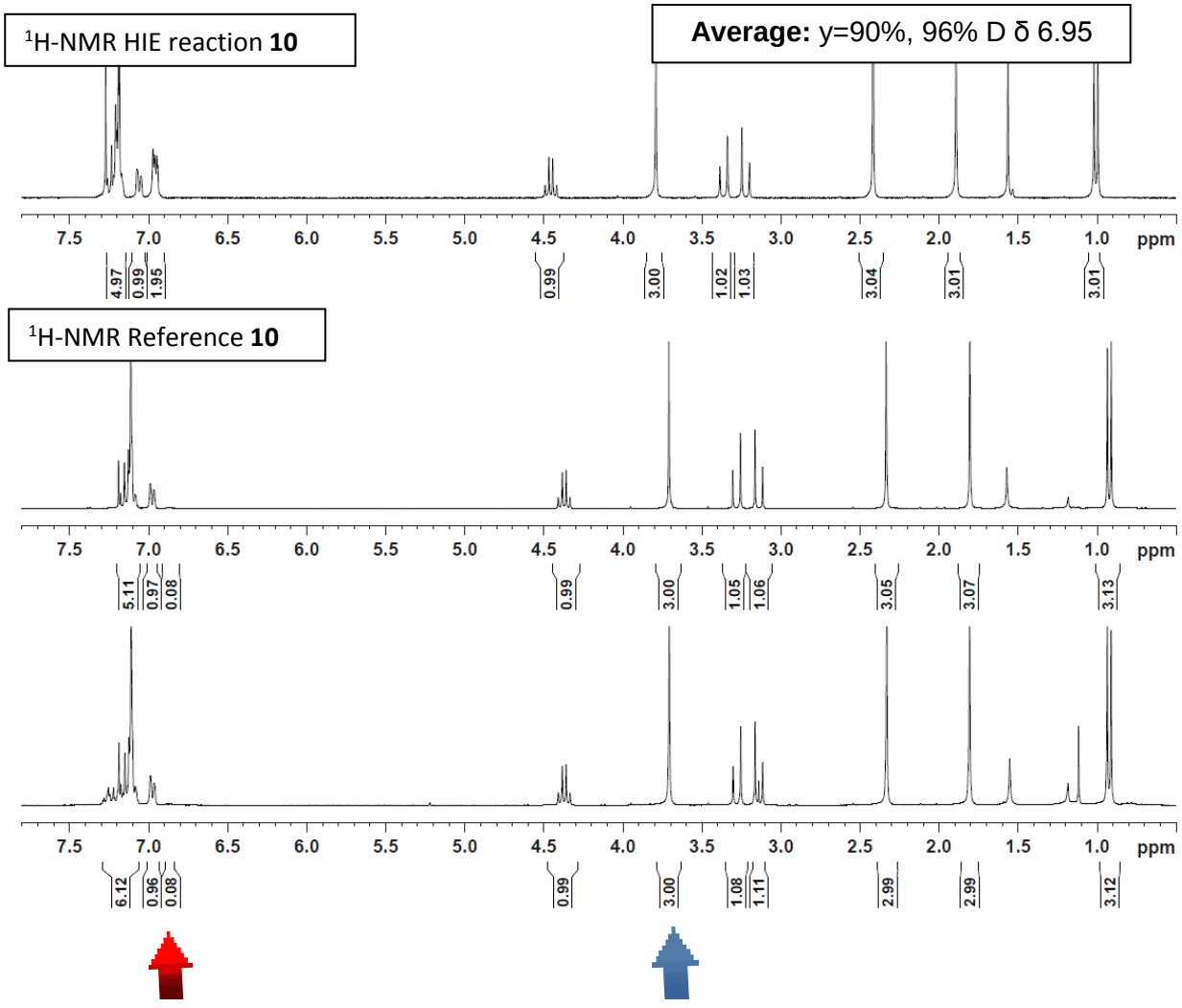

^{3}H-Benalaxyl (**10**)

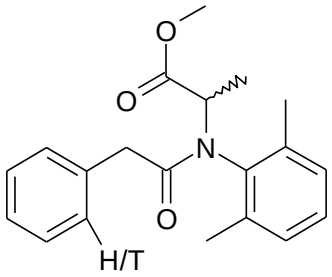

Molecular Weight =325.4112
Molecular Formula =C20H23NO3

10

The tritiation of Benalaxyl **10** was carried out using a standard Tritec® tritium manifold. 2.50 mg (7680 µmol) Benalaxyl was dissolved in 0.35 mL dry chlorobenzene followed by addition of a solution of 1.2 mg Tamm-catalyst **F** in 0.35 mL dry chlorobenzene. The 1 mL reaction flask was adapted to a tritium manifold and the solution was frozen in liquid nitrogen. The flask was evacuated, charged with tritium (2.5 Ci, 42.2 mmol, 5.5 eq). The reaction mixture was then allowed to warm to room temperature before stirring at rt for 2.3 hours. After removal of solvent in vacuo the labile tritium was exchanged and removed by addition of methanol and a freeze-drying process (three times repeated). The solid residue was dissolved in 3 mL methanol. Purification and isolation *via* HPLC (Phenomenex Gemini NX C18 10x150 mm, 5 mm, 5 mL/min flow, ACN/water gradient program) gave **10** (2 mg, 3188 MBq, 3,5 % RCY, 518GBq/mmol (14 Ci/mmol) in 98% purity (HPLC, UV and RD).

HRMS (positive ESI): m/z 326.2 $[M+H]^+$, 328.2 $[M(T)+H]^+$; 330.2 $[M(T2)+H]^+$

^{1}H NMR (500 MHz, $CDCl_3$): δ 7.20 (m, 5H, 2CH *meta*-phenyl, 2CH' *meta*-aniline, CH *para*-phenyl), 7.05 (d, ^{3}J = 7.0 Hz, 1H, CH *para*-aniline), 6.95 (m, 2H, CH *ortho*-phenyl), 4.45 (q, ^{3}J = 7.5 Hz, 1H, CH), 3.79 (s, 3H, OCH_3), 3.36 (d, ^{3}J = 14.5 Hz, 1H, CH benzylic), 3.22 (d, ^{3}J = 14.5 Hz, 1H, CH benzylic), 2.41 (s, 3H, CH_3 *ortho*-aniline), 1.89 (s, 3H, CH_3 *ortho*-aniline),1.01 (d, ^{3}J = 7.5 Hz, 3H, CH_3) ppm. Incorporation expected at δ 6.95 (red arrow).

533 MHz 3H/T BENALAXYL-3H FF-URA329; DMSO-d
zg3H

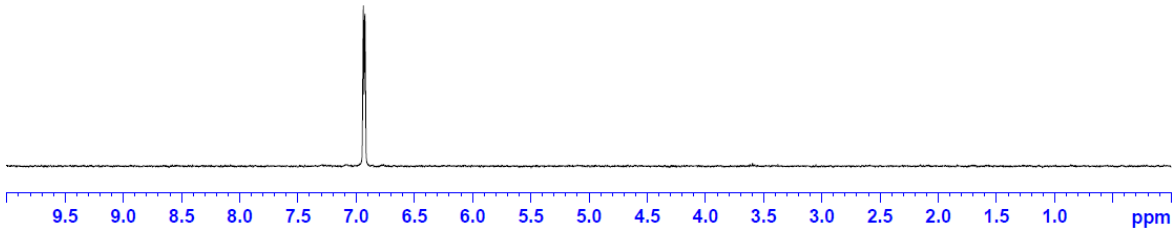

500MHz 1H BENALAXYL-3H FF-URA329 ; DMSO-d
zg30

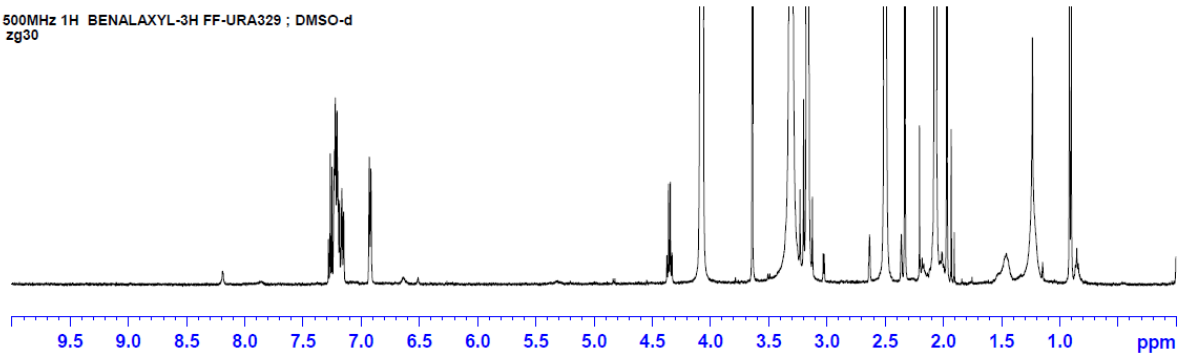

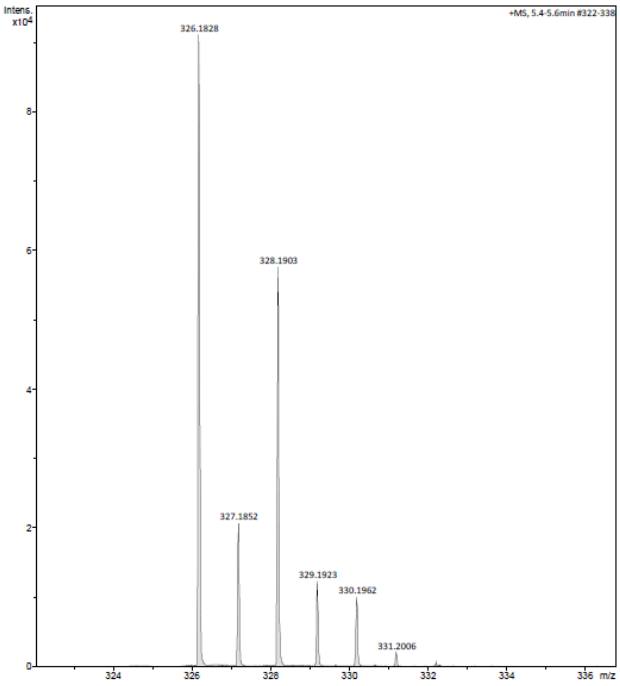

The following part of this supporting information was done by Daniel Becker, PhD student in the group of Prof. Matthias Tamm in Braunschweig, due to our collaboration.

Synthesis of iridium dihydride dimer (**61**)

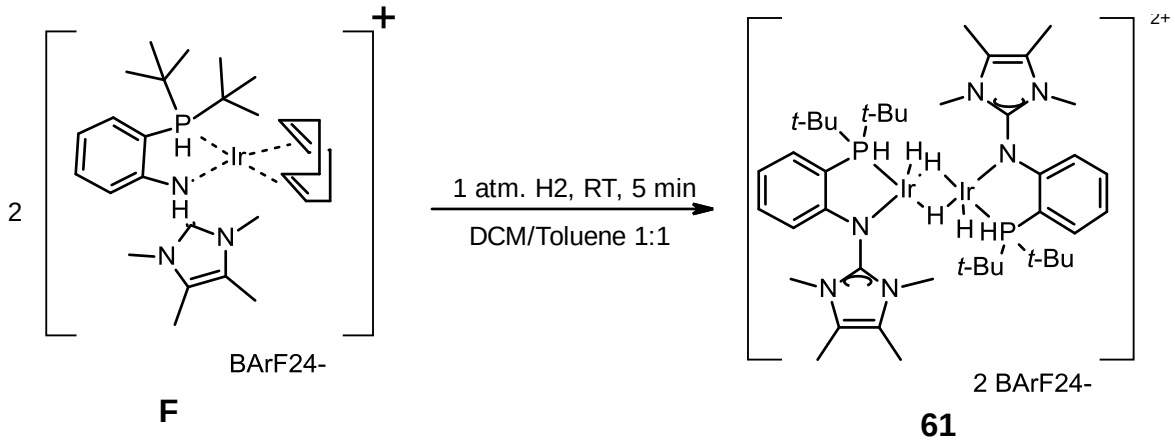

F **61**

Scheme 1. Synthesis of **61**

F (76.2 mg, 0.05 mmol) was dissolved in 5 mL of a 1:1 mixture of dichloromethane and toluene. The flask was evacuated and filled with hydrogen gas three times. The mixture was then stirred over night until the color changed to a dark blue. The solvent was removed under vacuum and the blue precipitate was washed two times with 0.5 mL toluene each and three times with 0.5 mL hexane each. The product **61** was isolated as a dark blue solid.

Crystals for X-Ray diffraction analysis were generated by slow diffusion of hexane into a saturated solution of **61** in dichloromethane.

Yield: 63.0 mg, 0.022 mmol, 88 %.

^{1}H NMR (500 MHz, CD_2Cl_2): δ 7.71 (m, 16H, *ortho* CH BAr^{F}_{24}), 7.63 (m, 2H, CH aromatic), 7.55 (m, 8H, *para* CH BAr^{F}_{24}), 7.23 (m, 2H, CH aromatic), 6.88 (m, 2H, CH aromatic), 6.07 (m, 2H, CH aromatic), 3.28 (s, 12H, N-CH_3), 2.18 (s, 12H, C-CH_3), 1.28 (d $^{3}J_{HP}$ = 14.9 Hz, 36H, *tert*-butyl), -28.14 (m, 4H, Ir-H).

^{13}C NMR (125 MHz, CD_2Cl_2): δ 161.9 (d, $^{2}J_{C,P}$ = 15 Hz, C-1), 162.1 (q, $^{1}J_{C,B}$ = 49 Hz, BArF-i-C), 147.2 (NCN), 135.2 (br s, BArF-o-CH), 134.2 (d, $^{4}J_{C,P}$ = 2 Hz, C-5), 134.1 (C-3), 125.0 (q, $^{1}J_{C,F}$ = 272 Hz,BArF-CF_3), 121.7 (CCH_3), 123.9 (d, $^{1}J_{C,P}$ = 25 Hz, C-2), 120.7 (d, $^{3}J_{C,P}$ = 7 Hz, C-4), 117.9(m, BArF-p-CH), 114.1 (d, $^{3}J_{C,P}$ = 10 Hz, C-6), 38.6 (d, $^{1}J_{C,P}$ = 30 Hz, **C**(CH_3)$_3$), 31.1 (NCH_3) 29.8 (d, $^{2}J_{C,P}$ = 3 Hz, C(**C**H_3)$_3$), 8.9 (CCH3).

^{31}P NMR (202 MHz, CD_2Cl_2): δ 67.8 (br m, 2P)

Elemental Analysis Calcd. for $C_{106}H_{96}B_2F_{48}Ir_2N_6P_2$: C 44.93, H 3.41, N 2.97. **Found:** C 44.62, H 3.18, N 2.86 (average of three measurements).

IR (CH_2Cl_2): $\nu_{Ir\text{-}H}$ = 2307 cm^{-1}.

^{1}H NMR spectrum of **61** in CD_2Cl_2 at 296 K.

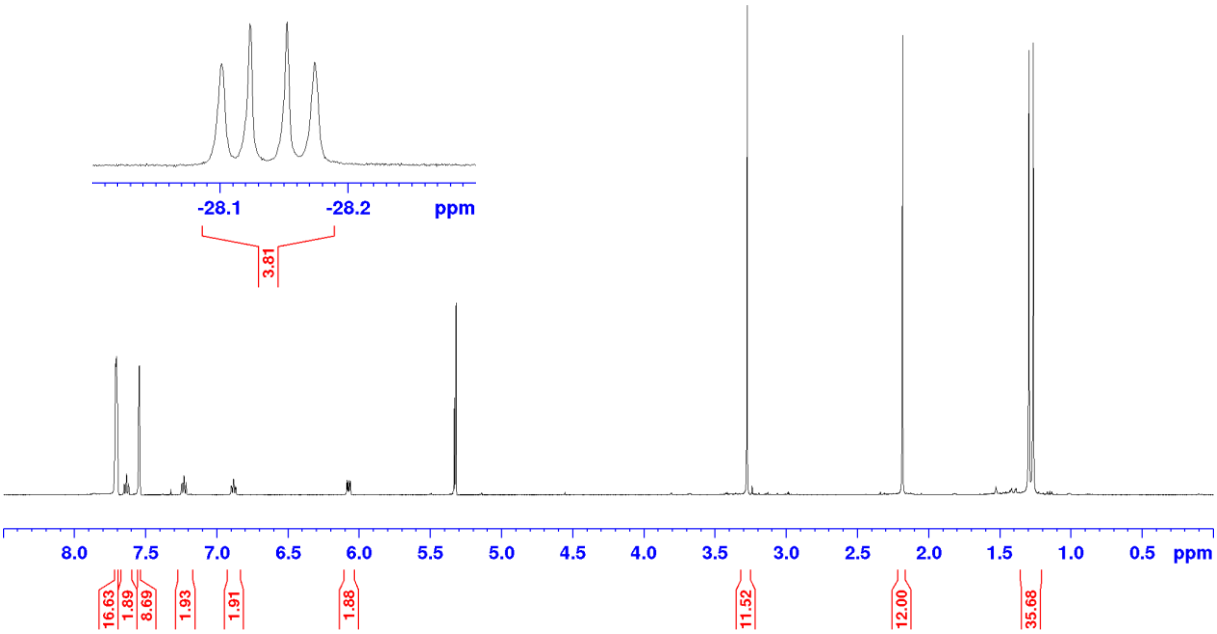

^{1}H{^{31}P} NMR spectrum of **61** in CD_2Cl_2 at 296 K.

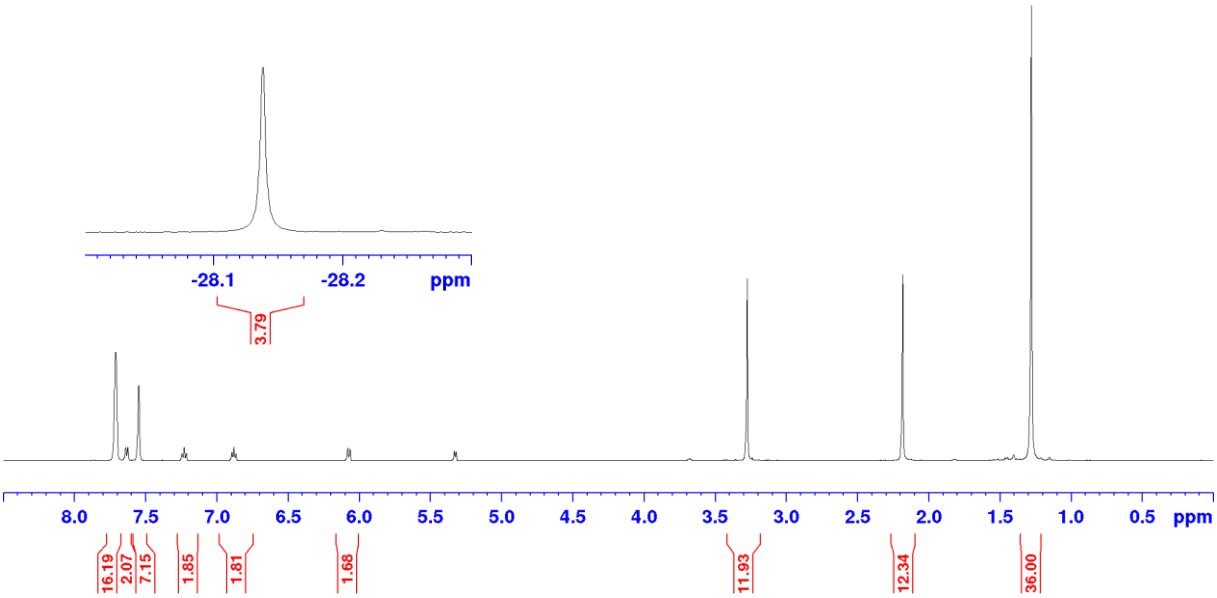

^{31}P NMR spectrum of **61** in CD_2Cl_2 at 296 K.

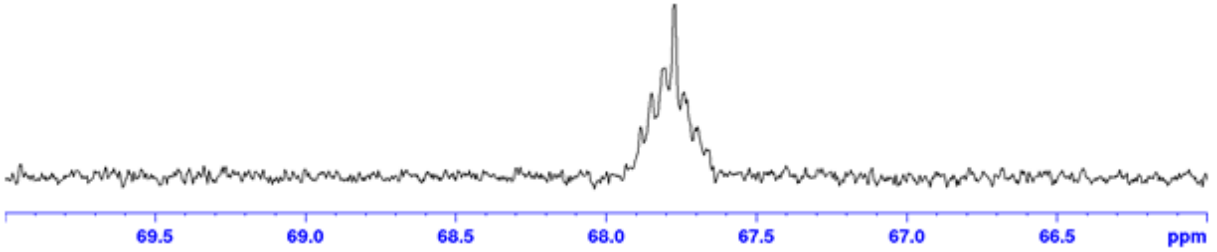

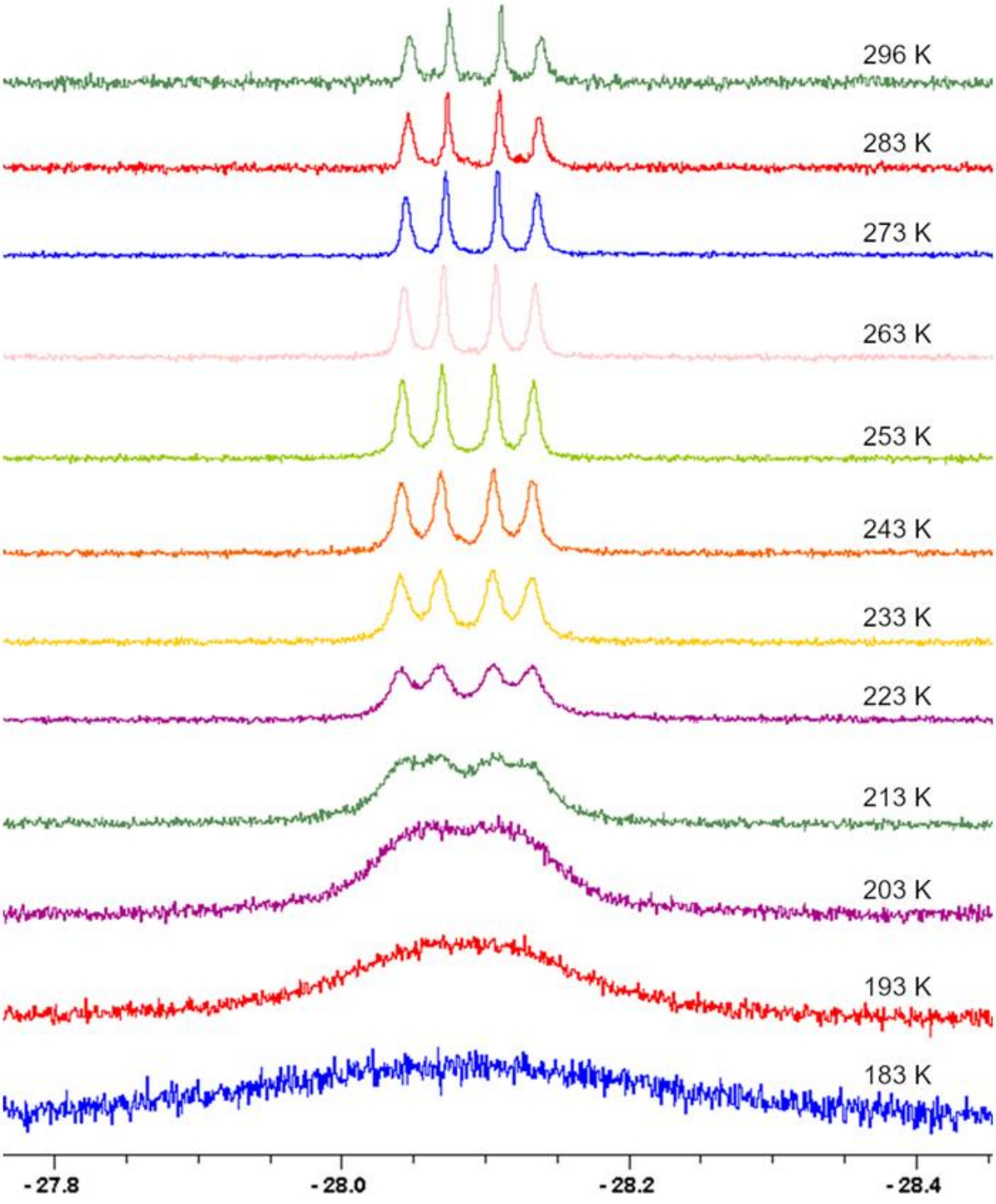

Figure 2. ^{1}H NMR spectrum of **61** at various temperatures from 296 K to 183 K.

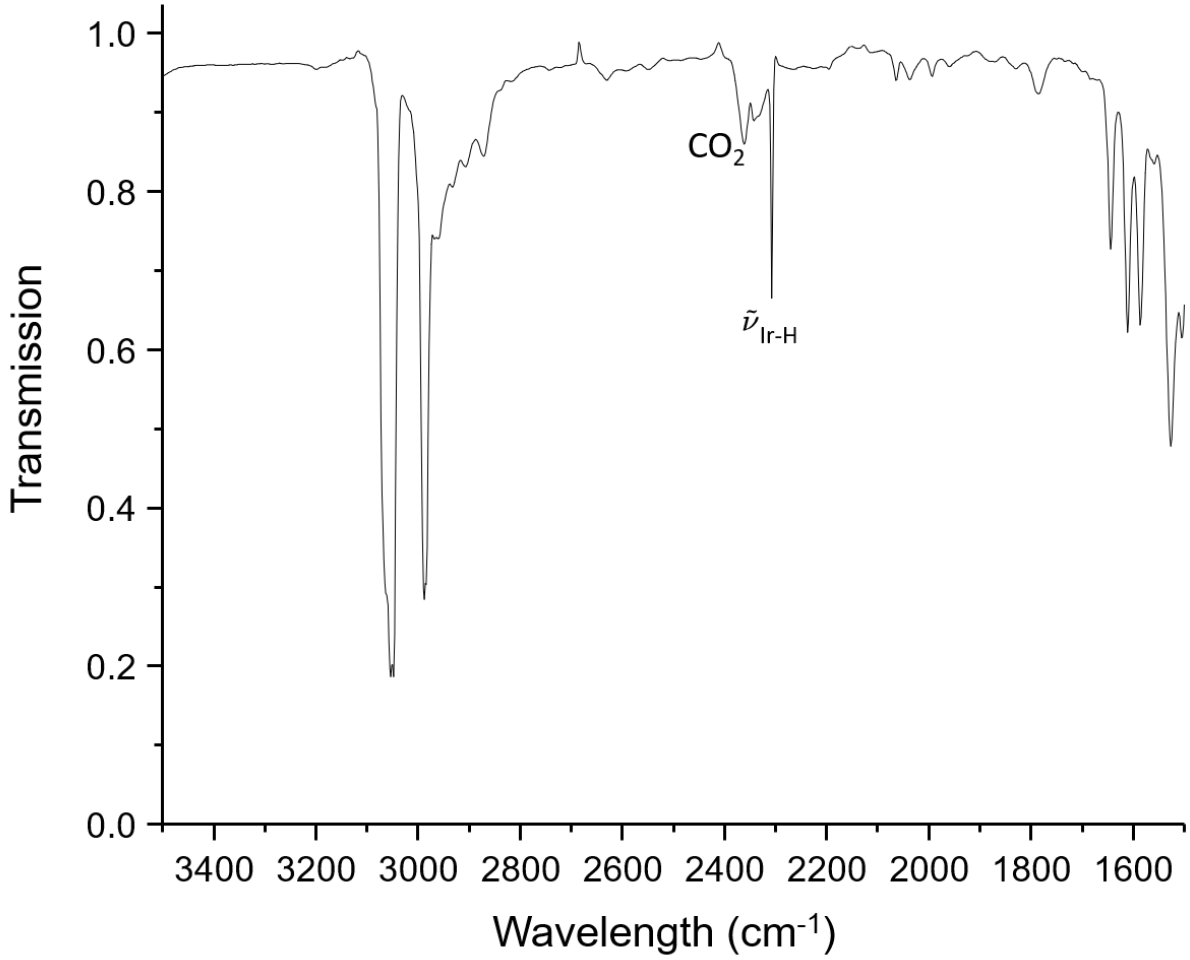

Figure 3. IR-Spectra of **61** in CH_2Cl_2.

Crystallographic details

Crystal data and refinement parameters for **61** are shown in Table 5. Suitable single crystals were mounted on MiTeGen mounts in per-fluorinated inert oil. Intensity measurements were performed at 100K using Rigaku Oxford Diffraction XtaLAB Synergy S diffractometers and HyPix-6000HE Hybrid Photon Counting (HPC) detector with mirror-focussed Mo$K\alpha$ radiation. The diffractometer software CrysAlisPRO was employed.[1] Absorption correction was based on multi-scans in combination with face indexation and gaussian absorption correction. The structure was refined anisotropically on F^2 using the program SHELXL-2018.[2] The compound was crystallized from a partially deuterated sample. Because of a deuteration grade of approximately only 30 %, all H atoms were treated as protium atoms rather than deuterium atoms. One hydrogen atom on each iridium atom could not be found and refined freely and was therefore omitted. The sum formula and all derived parameters are based on the refined structure without this second set of hydrogen atoms. The bridging hydrogen atom H1 was refined freely. All other H atoms were placed in idealised positions and refined using a riding model, with a common U restrained to be 1.2 (1.5 for methyl groups) times the equivalent isotropic displacement parameter of the parent atom. Ordered methyl groups were treated as rigid bodies and allowed to rotate around the E-CH3 bond.

Crystallographic data for **61** have been deposited with the Cambridge Crystallographic Data Centre, CCDC, 12 Union Road, Cambridge CB21EZ, UK. Copies of the data can be obtained free of charge on quoting the depository number CCDC-1886537 (Fax: +44-1223-336-033; E-Mail: deposit@ccdc.cam.ac.uk, http://www.ccdc.cam.ac.uk).

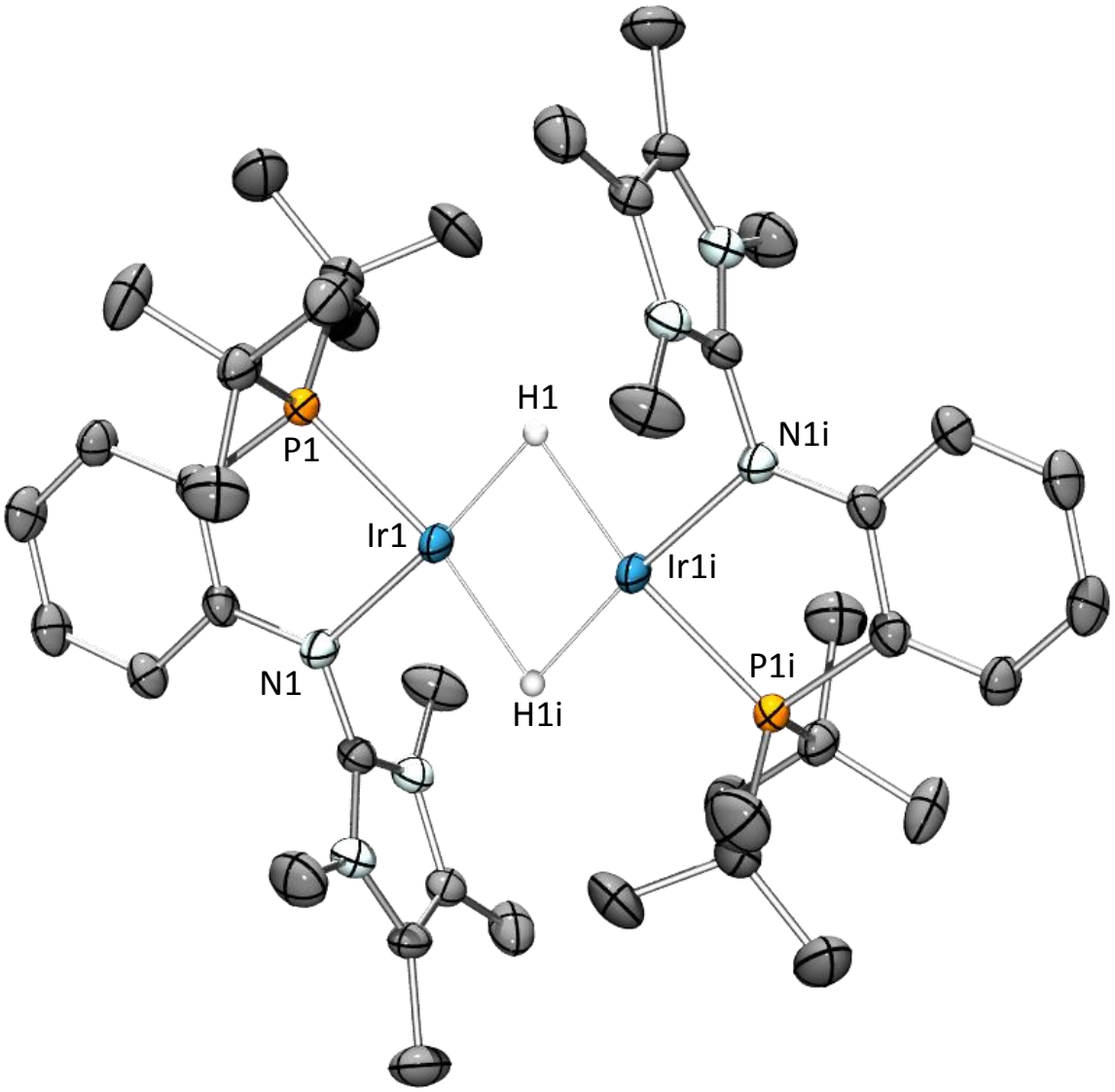

Figure 4. ORTEP plot of the molecular structure of the dication of **61** with thermal ellipsoids set at 50% probability level. Two $BArF_{24}$ counteranions and all hydrogens, except the bridging ones, are omitted for clarity. Ir1i, H1i and the corresponding ligand moiety is generated via a crystallographic centre of inversion situated between the two iridium atoms.

Table 5. Crystallographic data

Compound	**61**
CCDC	1886537
Empirical formula	$C_{107}H_{96}B_2Cl_2F_{48}Ir_2N_6P_2$
Formula weight	2916.75
Temperature	100(2) K
Wavelength	0.71073 Å
Instrument (scan mode)	XtaLAB Synergy S, HyPix (ω scan)
Crystal system	Triclinic
Space group	*P*1
Unit cell dimensions	a = 12.0377(2) Å α= 100.0440(10)°
	b = 14.8035(2) Å. β= 101.6020(10)°
	c = 16.8587(3) Å. γ = 96.9800(10)°
Volume	2859.29(8) $Å^3$
Z	1
Density (calculated)	1.694 Mg/m^3
Absorption coefficient	2.528 mm^{-1}
F(000)	1440
Crystal habitus	plate (violet)
Crystal size	0.311 x 0.177 x 0.147 mm^3
θ range for data collection	2.475 to 38.602°
Index ranges	$-21 \leq h \leq 20$, $-25 \leq k \leq 25$, $-29 \leq l \leq 28$
Reflections collected	327737
Independent reflections	30311 [R(int) = 0.0652]
Completeness to θ = 25.242°	99.9 %
Absorption correction	Gaussian
Max. and min. transmission	1.000 and 0.317
Refinement method	Full-matrix least-squares on F^2
Data / restraints / parameters	30311 / 52 / 802
Goodness-of-fit on F^2	1.092
Final R indices [I>2σ(I)]	R1 = 0.0476, wR2 = 0.1329
R indices (all data)	R1 = 0.0608, wR2 = 0.1383
Largest diff. peak and hole	5.580 and -2.623 $e·Å^{-3}$

Investigation of the Kinetic Isotope Effect

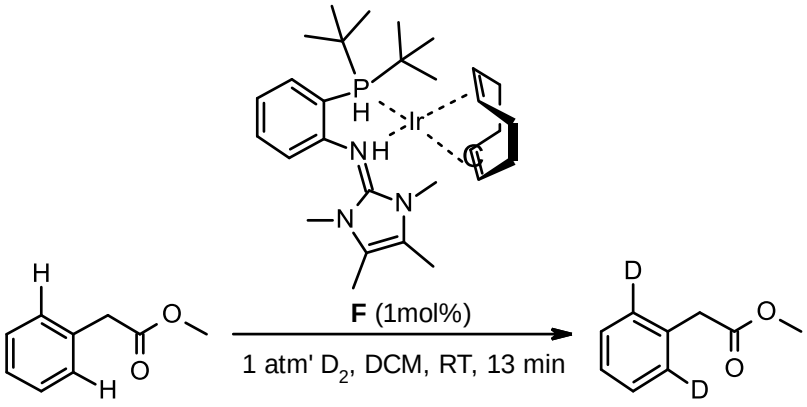

12

Scheme 2: Forward reaction (deuteration).

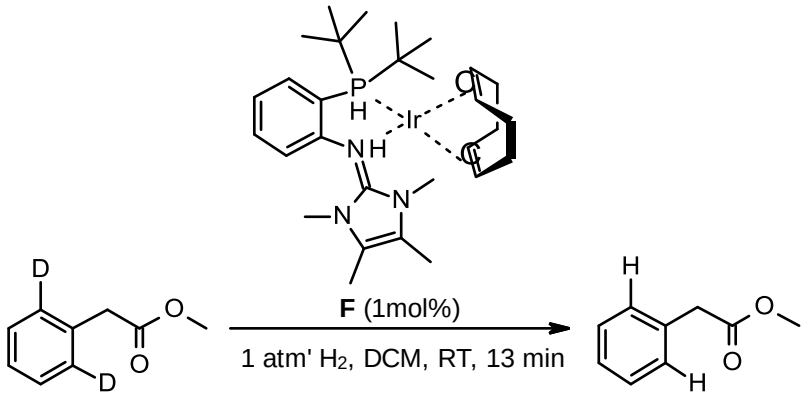

12-D 2 (98%)

Scheme 3: Backward reaction (hydrogenation).

A 100 mL 3-neck round bottomed flask, equipped with a stopcock valve and a suba seal was charged with the substrate (0.533 mmol; Phenylacetic acid methyl ester for the forward reaction or phenylacetic acid methyl ester-d_2 for the backwards reaction), catalyst **F** (8 mg, 1 mol%) and DCM (15 mL). The flask was sealed with open connection to the gas inlet and then evacuated until slight bubbling of the solution and then refilled with deuterium (or hydrogen) gas from a balloon for three times. The mixture was then stirred vigorously at room temperature. 0.3 mL aliquots were taken from the reaction mixture after 5 min, 7 min, 9 min, 11 min and 13 min via syringe. The samples were purified as described in the general procedure for HIE.

To determine the kinetic isotope, effect the reaction progress was plotted over time (Figure 5). Dividing the rate of the forward reaction (k_D) by the rate of the backward reaction (k_H) leads to the kinetic isotope effect $\frac{k_D}{k_H}$.

$$KIE = \frac{k_D}{k_H} = \frac{1.5065}{0.4345} = 3.47 \pm 0.29$$

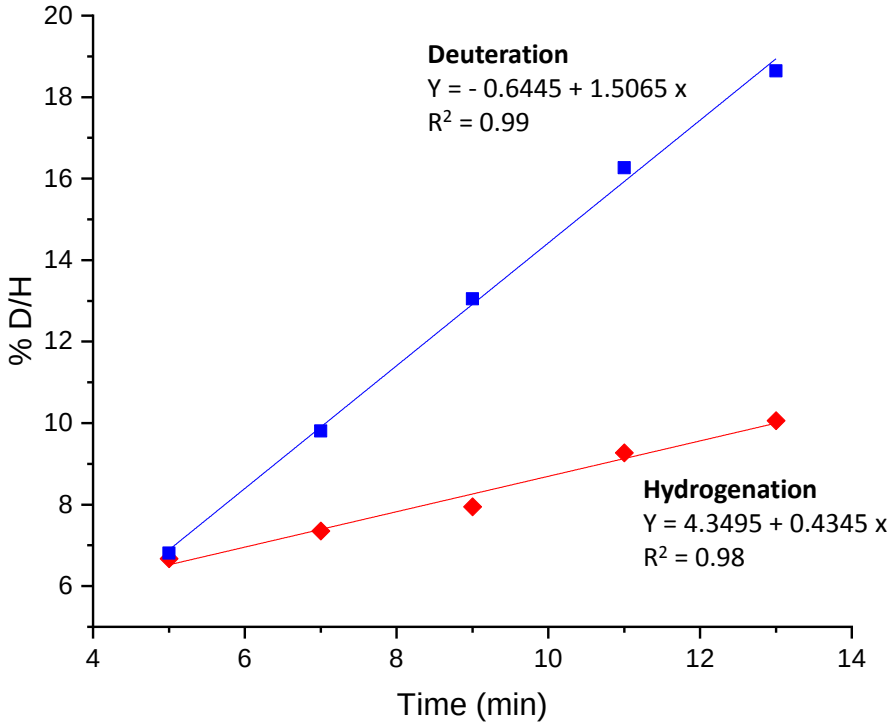

Figure 5. Reaction progress plotted over reaction time of forward reaction (deuteration, blue) and backward reaction (hydrogenation, red).

Computational Details

All computations to calculate the gas-phase electronic structures and energies for all species involved in H/D exchange reactions were performed using the density functional method M06[3] as implemented in the Gaussian09 program.[4] For all main group elements (C, H, D, N, P, and O) the all-electron triple-ζ basis set 6-311G(d,p)[5] was used and a Stuttgart RSC[6,7] effective core potential basis set for the 5d transition metal iridium. The participating transition states (TS) are located at the same level of theory. Harmonic vibrational frequencies are calculated to characterize respective minima (reactants, intermediates, and products with no imaginary frequency) and first order saddle points (transition states with one imaginary frequency).

Table 6. Energies for all optimized structures

	Compound	$E_{0K}{}^{a}$ / [Ha]	$E_{298K}{}^{b}$ / [Ha]	$H_{298K}{}^{b}$ / [Ha]	$G_{298K}{}^{b}$ / [Ha]
catalytic H/D exchange of methyl phenylacetate (**2**)	starting point (ed.)	-1929.776523	-1929.735103	-1929.734159	-1929.846725
	TS1	-1929.762204	-1929.721008	-1929.720064	-1929.831777
	IN1	-1929.767073	-1929.725775	-1929.724831	-1929.836191
	TS2	-1929.766763	-1929.725852	-1929.724908	-1929.835384
	IN2	-1929.767039	-1929.725754	-1929.724809	-1929.836144
	TS3	-1929.761817	-1929.720726	-1929.719781	-1929.831344
	terminal point (prod.)	-1929.777271	-1929.735940	-1929.734996	-1929.847414
Kinetic Isotope Effect (KIE) of (**2**)	starting point (ed.)	-1929.777961	-1929.736691	-1929.735747	-1929.848108
	TS1	-1929.762458	-1929.721415	-1929.720471	-1929.831985
	IN1	-1929.767656	-1929.726419	-1929.725475	-1929.836756
HIE of N-phenyl	starting point (ed.)	-1870.642419	-1870.602203	-1870.601258	-1870.711315
	TS1	-1870.636885	-1870.596656	-1870.595712	-1870.704967
	IN1	-1870.643128	-1870.603023	-1870.602079	-1870.710680
HIE of phenyl	starting point (ed.)	-1890.522761	-1890.481916	-1890.480972	-1890.592887
	TS1	-1890.511071	-1890.470753	-1890.469809	-1890.580556

	IN1	-1890.517163	-1890.477118	-1890.476173	-1890.585022
HIE of phenyl acetone	starting point (ed.)	-1854.572270	-1854.531451	-1854.530507	-1854.641918
	TS1	-1854.554900	-1854.513893	-1854.512948	-1854.624576
	IN1	-1854.560326	-1854.519657	-1854.518712	-1854.628742

[a] DFT energy incl. ZPE.

[b] standard conditions T = 298.15 K and p = 1 atm.

Calculation of theoretical Kinetic Isotope Effect (KIE)

Having calculated the thermal properties of the CH activation process for the deuterium incorporation, similar calculations were carried out started from the analogous aryl 2,6-di-deuterated product and working in reverse. The relative enthalpy (Δ*H*) values for the forward and backward reactions are shown on Figure S6. Subsequently, the theoretical KIE value can be obtained from Equation 1:

$$\frac{k_D}{k_H} = e^{\frac{(\Delta H_H^{\ddagger} - \Delta H_D^{\ddagger})}{RT}} \qquad \textbf{(Equation 1)}$$

k_D = rate of forward reaction – "deuteration"
k_H = rate of backward reaction – "hydration"
$\Delta H_D^{\ddagger}$ = transition state enthalpy of forward reaction (*J* mol^{-1})
$\Delta H_H^{\ddagger}$ = transition state enthalpy of backward reaction (*J* mol^{-1})
R = gas constant (8.314 *J* mol^{-1} K^{-1})
T = temperature (298.15 K)

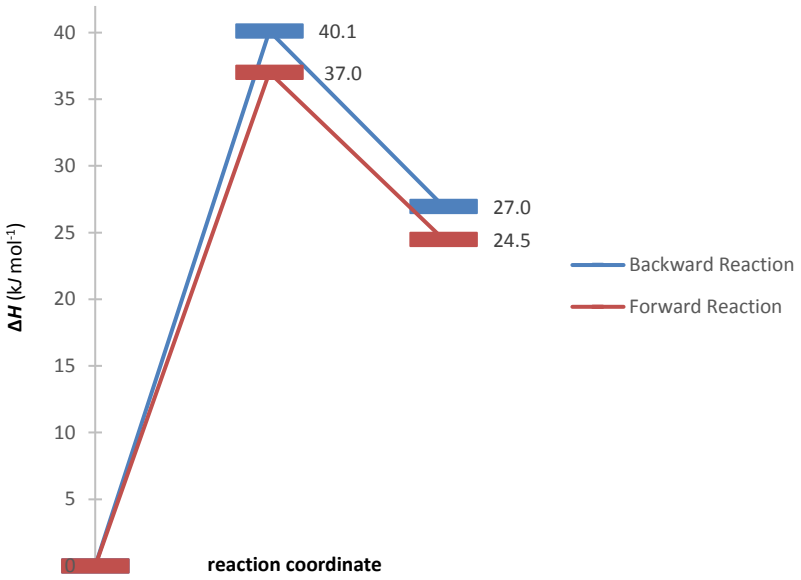

Figure 6. Relative enthalpy values for forward and backward CH activation processes.

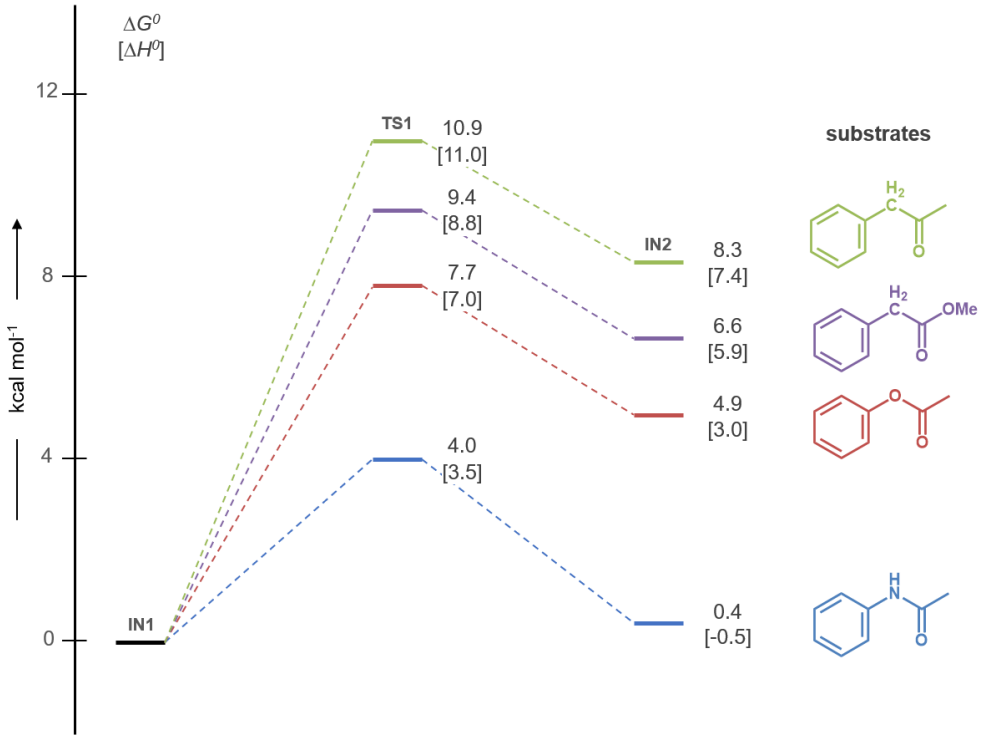

Figure 7. Potential energy profile for *ortho*-deuteration of N-phenyl acetanilide (PhNH-C(O)Me), phenyl acetate (PhOC(O)Me), methyl phenylacetate (**[H]-12**) and phenylacetone ($PhCH_2(O)Me$) with iridium catalyst **F**, scaled to Gibbs free energy (ΔG^0).

Literature

[1] Rigaku Oxford Diffraction, **2018**, CrysAlisPro Software system, version 1.171.40.26a, Rigaku Corporation, Oxford, UK.

[2] G. M. Sheldrick, *Acta Crystallogr., Sect. A* **2008**, *64*, 112–122.

[3] Y. Zhao, D. G. Truhlar, *Theor. Chem. Acc.* **2008**, *120*, 215.

[4] Gaussian 09, Revision D.01, M. J. Frisch, G. W. Trucks, H. B. Schlegel, G. E. Scuseria, M. A. Robb, J. R. Cheeseman, G. Scalmani, V. Barone, G. A. Petersson, H. NakatsuJi, X. Li, M. Caricato, A. Marenich, J. Bloino, B. G. Janesko, R. Gomperts, B. Mennucci, H. P. Hratchian, J. V. Ortiz, A. F. Izmaylov, J. L. Sonnenberg, D. Williams-Young, F. Ding, F. Lipparini, F. Egidi, J. Goings, B. Peng, A. Petrone, T. Henderson, D. Ranasinghe, V. G. Zakrzewski, J. Gao, N. Rega, G. Zheng, W. Liang, M. Hada, M. Ehara, K. Toyota, R. Fukuda, J. Hasegawa, M. Ishida, T. NakaJima, Y. Honda, O. Kitao, H. Nakai, T. Vreven, K. Throssell, J. A. Montgomery, Jr., J. E. Peralta, F. Ogliaro, M. Bearpark, J. J. Heyd, E. Brothers, K. N. Kudin, V. N. Staroverov, T. Keith, R. Kobayashi, J. Normand, K. Raghavachari, A. Rendell, J. C. Burant, S. S. Iyengar, J. Tomasi, M. Cossi, J. M. Millam, M. Klene, C. Adamo, R. Cammi, J. W. Ochterski, R. L. Martin, K. Morokuma, O. Farkas, J. B. Foresman, and D. J. Fox, Gaussian, Inc., Wallingford CT, **2016**.

[5] X. Cao, M. Dolg, *J. Chem. Phys.* **2001**, *115*, 7348.

[6] D. Andrae, U. Haussermann, M. Dolg, H. Stoll, H. Preuss, *Theor. Chim. Acta* **1990**, *77*, 123.

[7] Stuttgart RSC 1997 ECP Basis set (for Ir) was obtained from the Extensible Computational Chemistry Environment Basis Set Database, Version 1.2.2 [https://bse.pnl.gov/bse/portal]. a) The Role of Databases in Support of Computational Chemistry Calculations, D. Feller, *J. Comp. Chem.* **1996**, *17*, 1571; b) Basis Set Exchange: A Community Database for Computational Sciences, K. L. Schuchardt, B. T. Didier, T. Elsethagen, L. Sun, V. Gurumoorthi, J. Chase, J. Li and T. L. Windus, *J. Chem. Inf. Model.* **2007**, *47*, 1045.

Part III

Insights in the parameters driving selectivity and reactivity of the Hydrogen Isotope Exchange reactions with complex structures

Chapter 1: Temperature mediated Iridium(I) catalyzed Hydrogen Isotope Exchange reactions

III.1.1. Introduction

As mentioned in Part I, an introduction of a radioactive label in a metabolically stable position is essential for the application of tritiated compounds for *in-vivo* experiments. This implies that chemists have access to a complete toolbox of catalysts and HIE reactions in order to specifically and selectively label particular positions into drug molecules. For this purpose, it is necessary to understand the influence of the different directing groups (e.g. DG1 versus DG2, *scheme III.1.1*) on HIE in complex molecules. One parameter which is known to influence reactivity and selectivity in HIE reactions is the reaction temperature. Even though many details on the optimisation of reactions conditions in iridium-catalysed HIE are already reported,[1] there is still a lack of head to head comparison. For this reason, we have concluded that a general comparison study with the most commonly applied catalysts **A-G** could help to use the optimized approach, for either high selectivity or maximum deuterium incorporation.

Scheme III.1. 1: *Modulation of the reactivity and selectivity in directed HIE reactions by change of temperature*

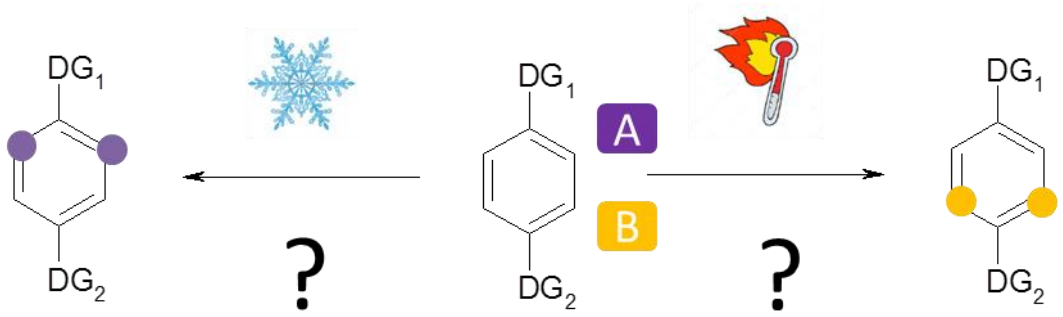

III.1.2. Comparison study of the catalysts A-G in the HIE of 8

We began our investigations with the model substrate 4-acetamido-acetophenone **8** (see t*able III.1.1)*. In plus of being visible in LC-UV-MS, easily analysed by NMR and commercially available, model substrate **8** have been chosen because acetamido- and ketone DGs are known to facilitate HIE reactions with iridium catalysts.[2] Moreover, these two DGs are common in drugs, e.g acetanilide moiety is present in Leflunomide **1**, Flutamide **2**, Imatinib **3** or Otamixaban **4**. Keton moieties are present e.g. in Dyclonine **5**, Raloxifene **6** and Dronedarone **7** (*scheme III.1.2*).

Scheme III.1. 2: *Structure of drugs* ***1-7***

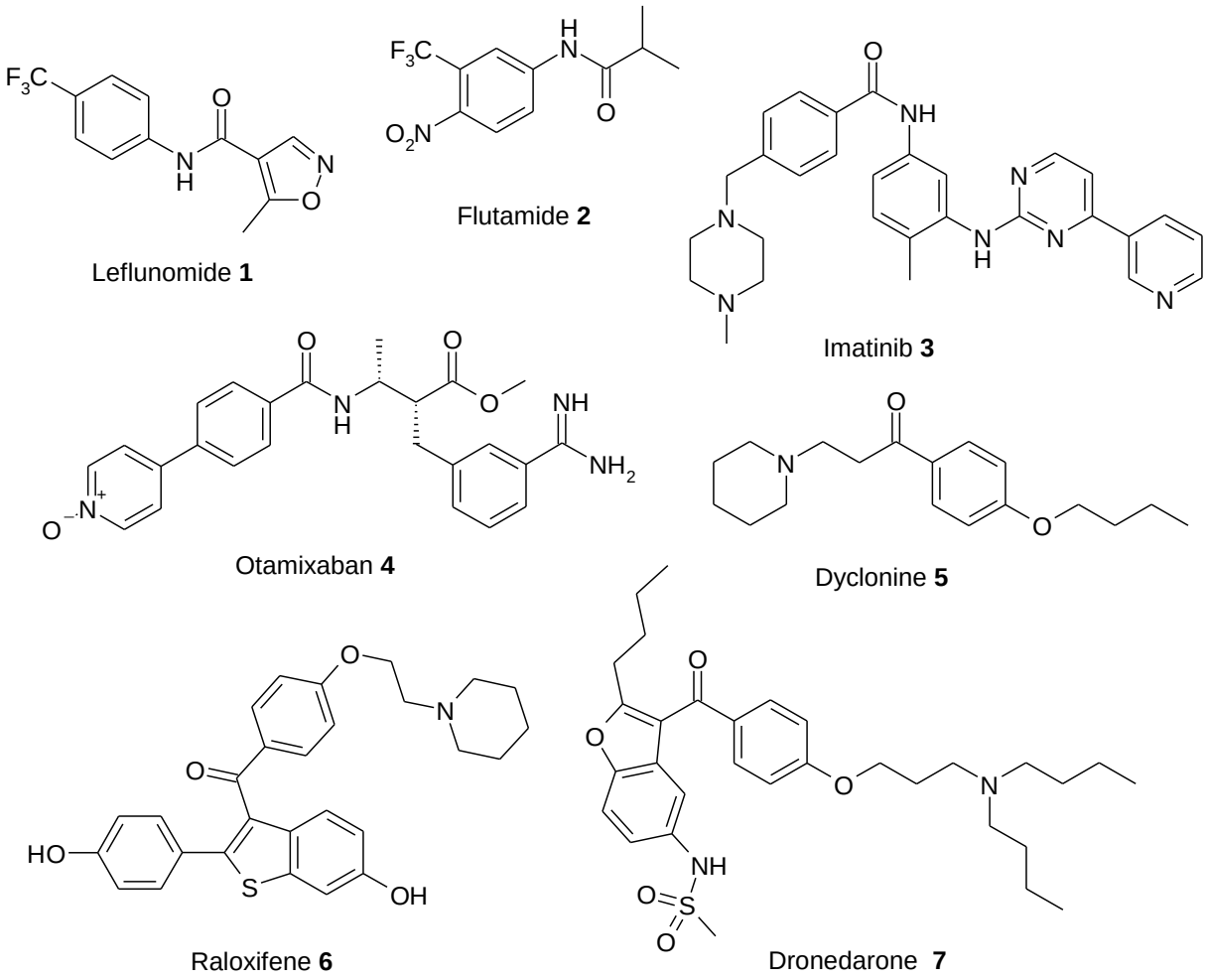

III.1.2.1. Comparison study at low temperatures

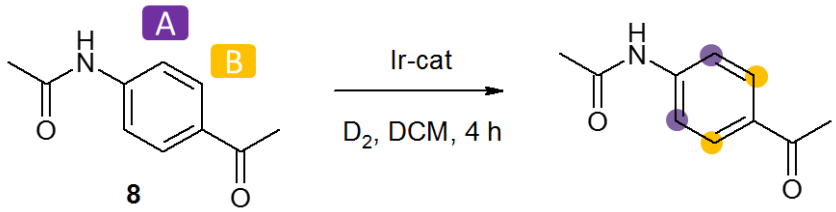

At first, 4-acetamido-acetophenone **8** has been run in HIE reactions with catalysts **A-G** in dichloromethane at various low temperatures. Beside general deuterium introduction, assessment of the change in selectivity in the HIE reaction between position A and B has been done (*Table III.1.1*). Interestingly, depending on the used catalyst, we observed strong differences in reactivities and selectivities of the HIE reaction leading to the deuterated equivalents of compound **8**.

Table III.1. 2: *Evaluations of iridium(I) catalysts **A**-**G** in a HIE reaction of 4-acetamido-acetophenone **8** at temperatures from –80°C to 25°C in dichloromethane*

Entry	catalyst	T (°C)	8_A (D%) [a]	8_B (D%)[a]	D_{total} [b]
1	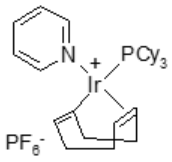 **A** (Crabtree)	25	93	94	3.7
2		0	91	94	3.7
3		-15	54	87	2.8
4		-30	50	74	2.5
5		-60	33	40	1.5
6		-80	14	34	1
7	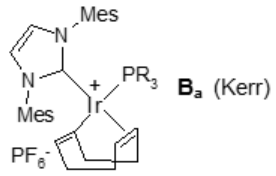 **B_a** (Kerr)	25	92	99	3.8
8		0	30	87	2.3
9		-15	10	70	1.6
10		-30	0	38	0.8
11		-60	0	34	0.7
12	**D** (Pfaltz) 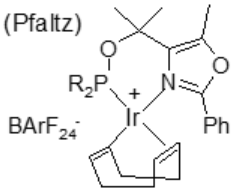	25	0	46	1
13		0	0	20	0.4
14		-15	0	10	0.2
15		-30	0	0	-
16		-60	0	0	-
17	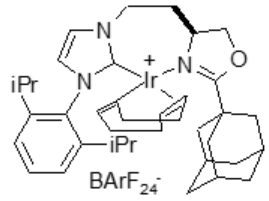 **E** (Burgess)	25	67	93	3.2
18		0	51	93	2.9
19		-15	20	90	2.2
20		-30	0	50	1
21		-60	0	32	0.6
22	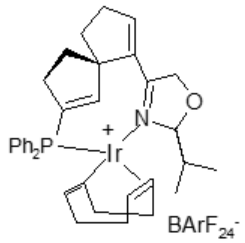 **G** (Ding), Spinphox	25	24	82	2.1
23		0	18	81	2
24		-15	24	75	2
25		-30	0	50	1
26		-60	0	11	0.2
27	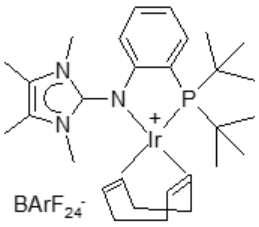 **F** (Tamm)	25	65	94	3.2
28		0	86	91	3.6
29		-15	70	92	3.3
30		-30	21	79	2
31		-60	0	48	1
32		-80	0	13	0.3

a)Conditions: substrate **8** (1 eq.), catalyst (5 mol%), D_2 (1 atm), dichloromethane (3 mL), 4 h. b)Determined by ^{1}H-NMR, [b] determined by LC-MS.

At -80°C only catalysts **A** (entry 6) showed reasonable reactivity (> 25%D incorporation), however with only low selectivity in favour of position B (ketone directing group). At lower temperatures, the other catalysts had increasing reactivity in the order of **F** > **B_a** = **E** > **G** > **D**. For catalysts **B_a** (entry 10), **E** (entry 20) and **G** (entry 25), a complete selectivity in favour of position B was observed at -30°C. It is further noted that for catalysts **A, E, G** and **F** there are no big differences in the outcome of the HIE reaction of 25 or 0°C. These reactions clearly indicate that HIE reactions at lower temperature have a chance to change the reactions outcome and should be studied more intensively in the future.

Kerr *et al*. reported the different free energy profiles for HIE reactions of aromatic compounds in the gas phase with catalyst **B_a**. A ΔH activation energy in the transition state (**9**) of 18.13 kcal/mol (298 K) was calculated for acetophenone whereas a value of 23.04 kcal/mol (**10**) was reported for acetanilide (*scheme III.1.3*).[2c] This difference of 4.91 kcal/mol makes acetanilide DG more energetically demanding to proceed the HIE reaction, which is in line with the observed selectivities of all used catalysts in table III.1.1 and III.1.2. Indeed, the deuterium incorporation in *ortho*-position of the ketone is higher or at least equal to the one related to the acetanilide. This might suggest that all catalysts **A-G** could either go through a five- or six-membered-ring transition-state as both positions were exchanged by deuterium in the products.

Scheme III.1. 3: *Simplified transition states in the HIE reaction of acetophenone and acetanilide with a iridium catalyst. DFT calculation values of catalyst* ***B_a***.[2c]

ketone coordination
5-membered transition state

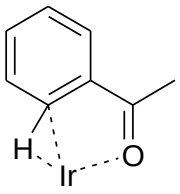

9

ΔH =18.13 kcal/mol

anilide coordination
6-membered transition state

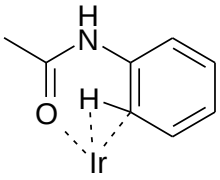

10

ΔH =23.04 kcal/mol

III.1.2.2. Comparison study at high temperatures

Next, the HIE reaction of the model compound **8** has been studied at elevated temperatures up to 130°C (*table III.1.2*). Therefore, the solvent had to be changed to chlorobenzene (bp: 131°C) due to the low boiling point of dichloromethane (bp: 40°C). Interestingly, catalysts **A, B_a, E, G** showed their highest deuterium incorporation at 75-100°C with nearly full deuteration of the aromatic positions (entry 3, 8, 19, 24).

Table III.1. 3: *Evaluations of iridium(I) catalysts* ***A-G*** *in a HIE reaction of 4-acetamido-acetophenone* ***8*** *at temperatures from 25 to 130°C in chlorobenzene*

Entry	catalyst	T (°C)	8_A (D%) [a]	8_B (D%)[a]	D_{total} [b]
1	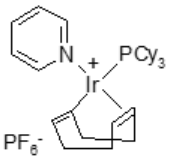 **A** (Crabtree)	25	87	94	3.6
2		50	84	99	3.7
3		75	99	99	4
4		100	15	68	1.8
5		130	13	64	1.6
6	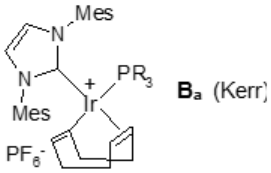 **B_a** (Kerr)	25	94	92	3.8
7		50	90	99	3.8
8		75	98	99	4
9		100	52	81	2.7
10		130	0	47	1
11	**D** (Pfaltz) 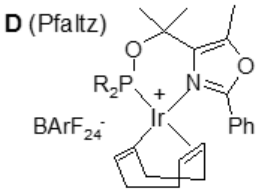	25	0	45	0.9
12		50	0	48	1
13		75	0	35	0.7
14		100	0	0	0.1
15		130	0	0	0
16	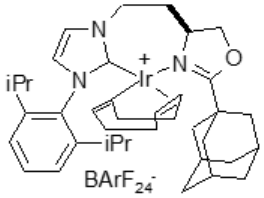 **E** (Burgess)	25	63	97	3
17		50	58	99	3.2
18		75	62	99	3.3
19		100	98	99	4
20		130	49	84	2.9
21	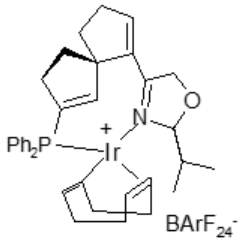 **G** (Ding), Spinphox	25	35	85	2.4
22		50	79	99	3.6
23		75	79	99	3.6
24		100	96	98	3.9
25		130	8	93	1.8
26	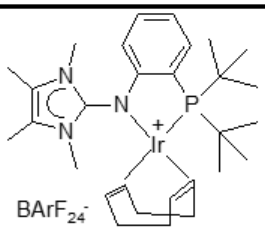 **F** (Tamm)	25	56	87	3
27		50	23	63	1.7
28		75	30	35	1.4
29		100	8	26	0.8
30		130	0	0	0

a)Conditions: substrate **8** (1 eq.), catalyst (5 mol%), D_2 (1 atm), C_6D_5Cl (3 mL), 4 h b) Determined by ^1H NMR, [b] determined by LC-MS.

Remarkably, no H/D exchange at the C(sp^3)-positions was observed, neither on the ketone or acetanilide methyl-groups. Catalysts **D** showed generally a moderate activity in the HIE reaction of compound **8**. Catalyst **F** was the most sensitive one in relation to heat. Above 50°C the deuterium introduction decreased significantly, indicating that the HIE activity with these catalysts decreased due to their deactivation. To prove this, the active catalyst of **F** was formed with D_2 (without substrate), and then the mixture was heated to 50°C for one hour. After, substrate **8** was added via syringe and the HIE reaction was continued at 50°C for an additional hour. LC-MS analysis of the reaction mixture showed only compound **8** without any deuterium incorporation indicating that the catalyst activity was completely lost while heating in the first hour.

Figure III.1. 1: *Graphical overview in which temperature window the catalysts* ***A-G*** *are efficiently working (threshold 25%D) for HIE reactions with compound* ***8****.*[a]

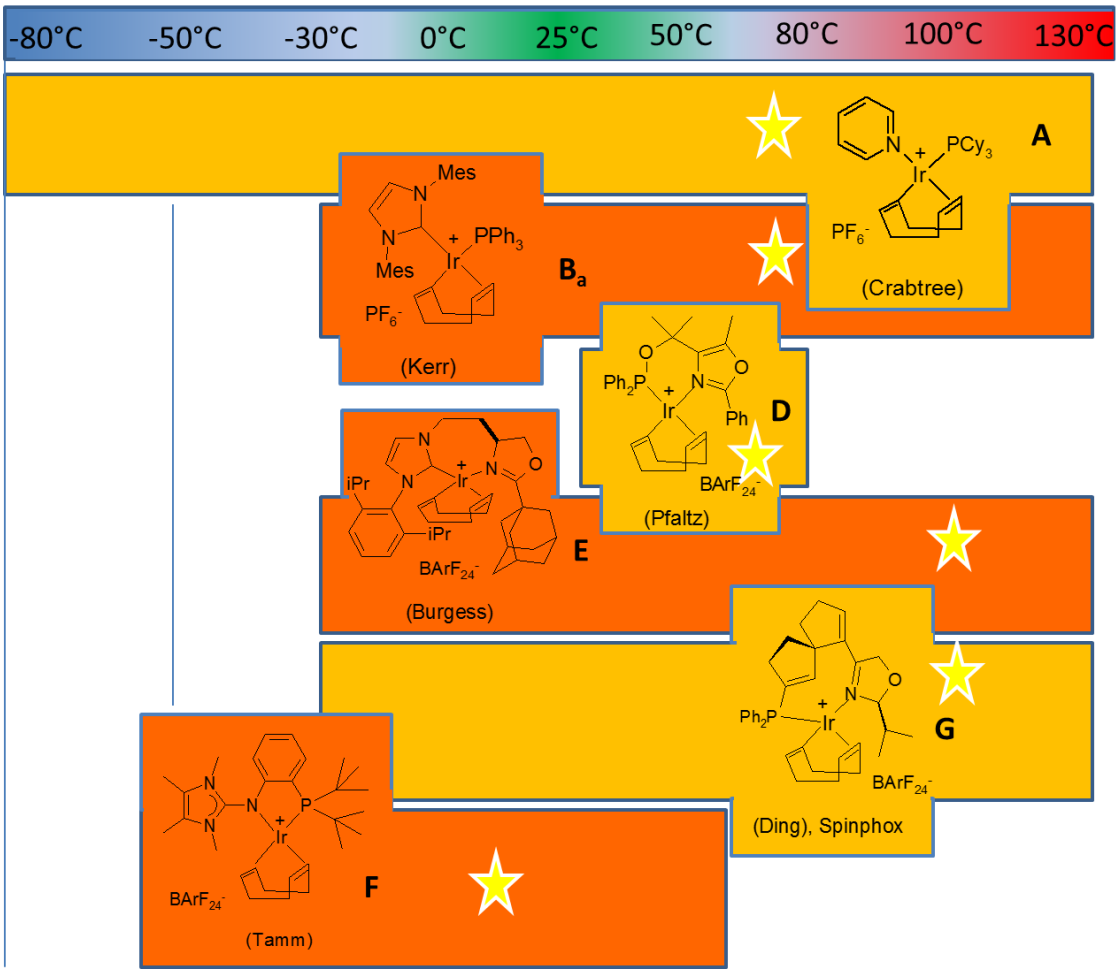

[a]Position of the yellow star shows the highest deuterium incorporation

Even though we know that a full picture on the efficiency and reactivity of the different catalysts **A-G** cannot be given by a HIE reaction of just a single substrate, we believe that together with a lot of different literature examples[2,3,4] a general statement can be made.
Our graphical overview (*figure III.1.1*) should only be seen as a principal direction in which kind of temperature window the catalysts are reactive, and without significant deactivation.

As a prove of concept, we were interested to demonstrate how this knowledge of the labelling specificity and selectivity can be applied to industry and influence the efficient isotope chemistry planning. Indeed, any labelling request is expected to be delivered as soon as possible. Therefore, speed is the crucial parameter in industry and academic research. The time and difficulty for labelling a drug candidate strongly depends on knowledge of the catalysts and their reactivities. Improved prediction of potential HIE outcomes, or in other words to pick the best catalyst and reactions conditions, is increasing the probability of success for a fast delivery of the target compound. Therefore, we selected five more complex molecules in order to validate our strategy.

III.1.3. Application on complex drug-like compounds

One interesting example for the different reactivity of iridium catalysts is described in *scheme III.1.4.* With catalyst **F** at 25°C, we have obtained selectively deuterium incorporation in the aromatic position A of phenylacetic amide **11**.[5] Interestingly, with catalyst $\mathbf{B_a}$ we observed no deuterium introduction at all at 25°C. However, when we increased the temperature to 80°C, the deuteration in both positions A and B was obtained, indicating that by increasing the temperature both activation energies ΔH for the transitions states of the pathways for either C(sp^2)- or C(sp^3)-carbons are sufficient. The labelling of glycine C(sp^3)-positions with catalyst $\mathbf{B_a}$ has been demonstrated by us already (see Part IV).[6] With catalyst **F**, we obtained only traces of deuterated product, probably due to the prior described inactivation of the catalyst at elevated temperatures (80°C). Unfortunately, we haven't found a catalyst and/or conditions to selectively introduce deuterium at the C(sp^3)-position (B) only until now.

Scheme III.1. 4: *HIE reaction of phenylacetic glycine amide derivative **11** with two iridium catalysts (5 mol%). No deuterated product with catalyst $\mathbf{B_a}$ at 25°C and catalyst **F** at 80°C*

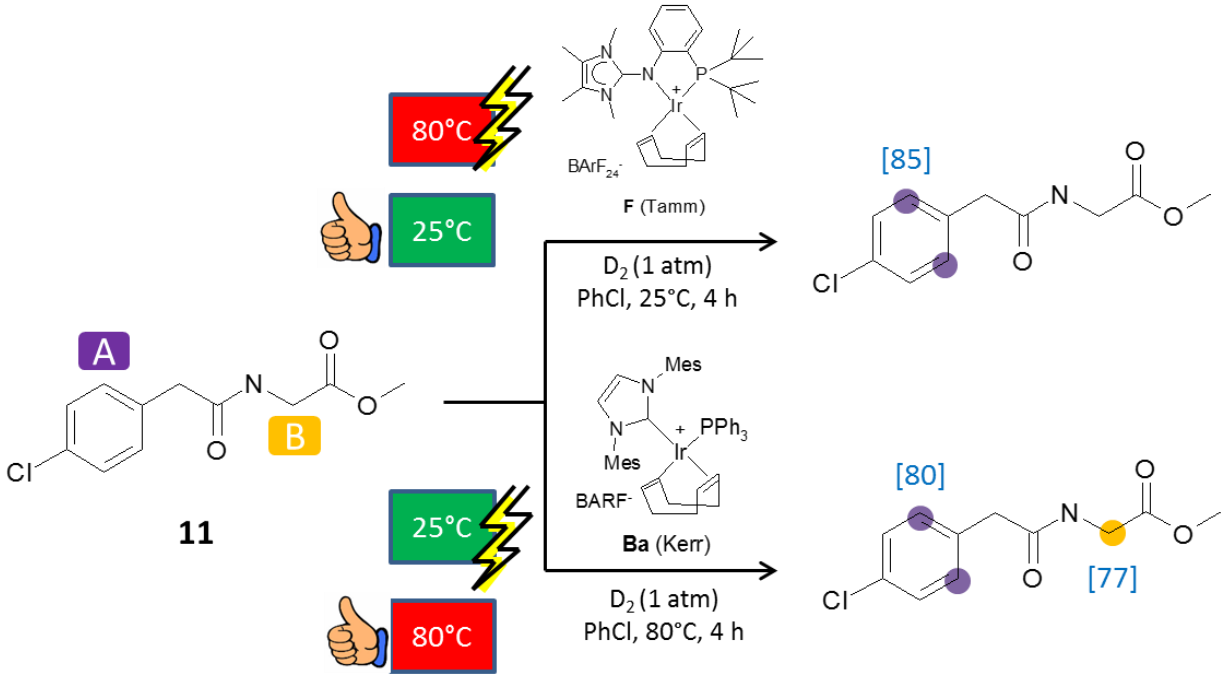

In this context, we tried the HIE reaction of diclofenac methylester **12**, a nonsteroidal anti-inflammatory drug (NSAID), used to treat pain and inflammatory diseases such as gout or arthritis. Drug **12** was only deuterated by using catalyst **G** at 100°C (*scheme III.1.5*). No deuteration was observed at 80°C and below with catalyst **G**, as with all other tested catalysts **A-F** at in the 25-100°C range. As it was discussed in Part II Chapter 2, we were not able to do a successful HIE reaction with diclofenac before. Therefore, it is remarkable to have identified a further alternative for HIE reactions with this compound class with catalyst **G**.[6]

Scheme III.1. 5: *HIE reaction of diclofenac **12** with five different iridium catalysts; no reactivity at <=80°C with catalysts **A-G.***

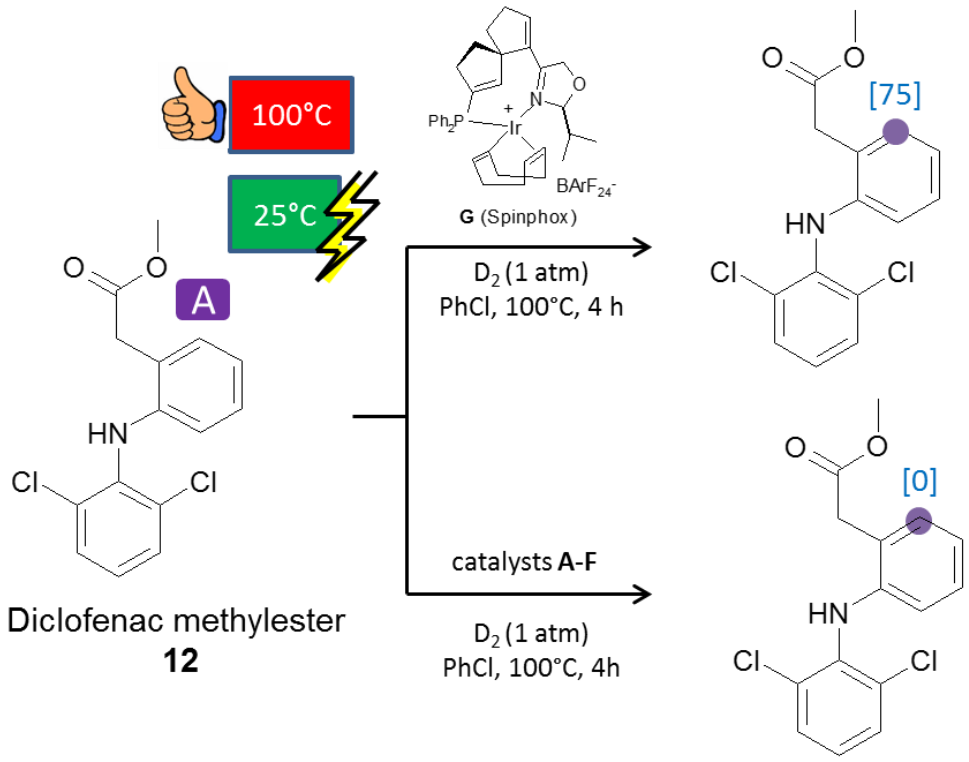

In a third example we have studied the deuteration of celecoxib **13** (*scheme III.1.6*), a COX-2 selective NSAID to treat arthritis. With catalyst **F** at 0°C, we observed only an exchange in the *B*-position (62%D) directed by the sulfonamide group, while with catalyst **A** we found the product labelled at the *A*-position (78%D) only. At 80°C, the selectivity of catalyst **A** was reduced to 3:1 (60%D for position *A* and 20%D for *B*). Interestingly, using catalyst **E** at 100°C both C(sp^2)-positions, *A* and *B*, were exchanged almost completely (92%D) confirming that an appropriate and proactive choice of catalyst and temperature can modulate the HIE reaction outcome.

Scheme III.1. 6: *HIE reaction of celecoxib* ***13*** *with three different iridium catalysts and temperatures*

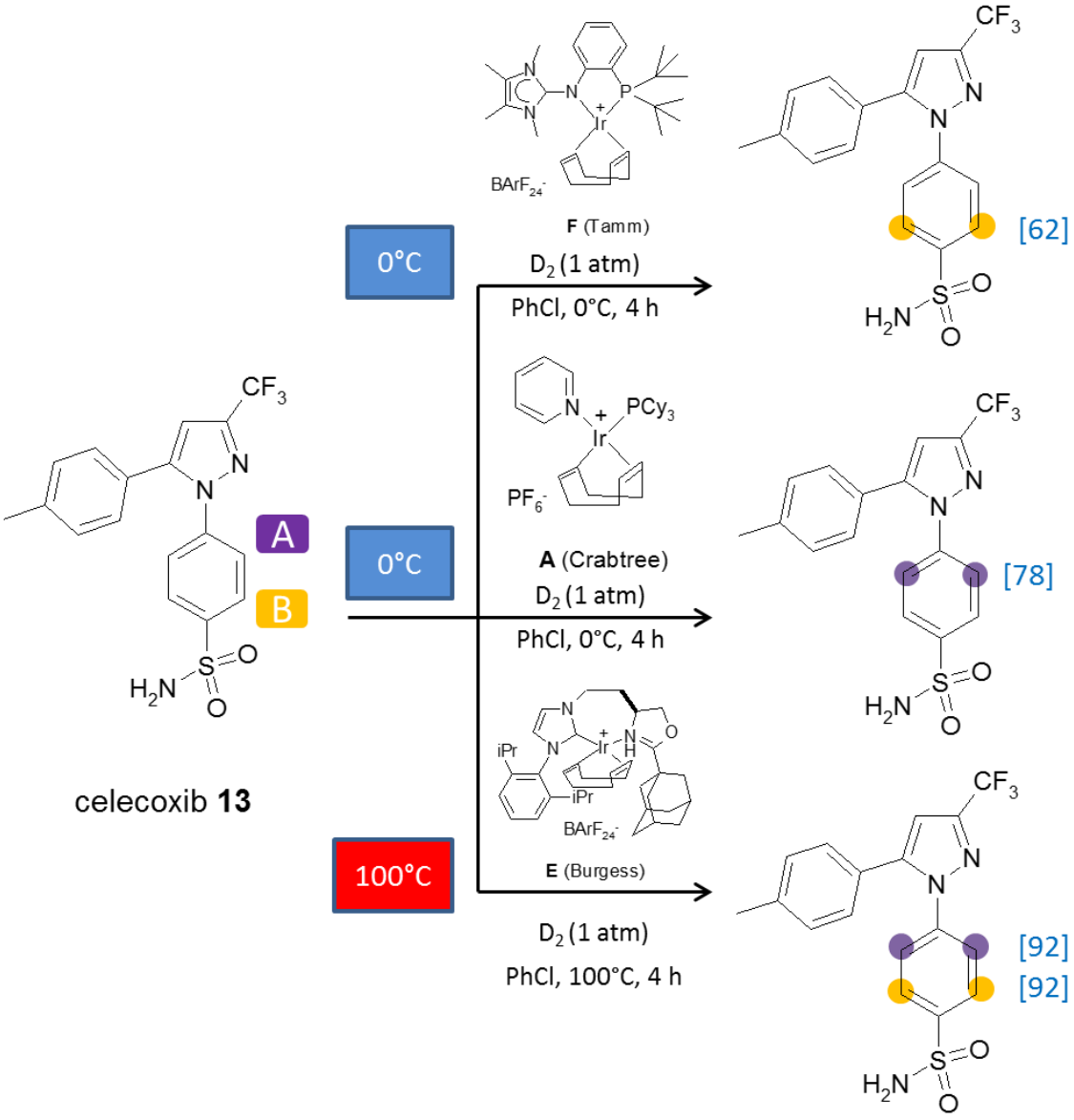

Next, we performed HIE reactions with glibenclamide **14** (*scheme III.1.7*), an inhibitor of the ATP-sensitive potassium channels (K_{ATP}). With catalyst **G** at 100°C selectively only position A was deuterated, while with catalyst **E,** as reported before,[7a] both positions A and B (59%D and 83%D) with favoring of deuterated position B was obtained. Both catalysts (**E, G**) showed no reactivity in reactions at 25°C.

Scheme III.1. 7: *HIE of glibenclamide **14** with two different iridium catalysts **E,G** at 25-120°C.*

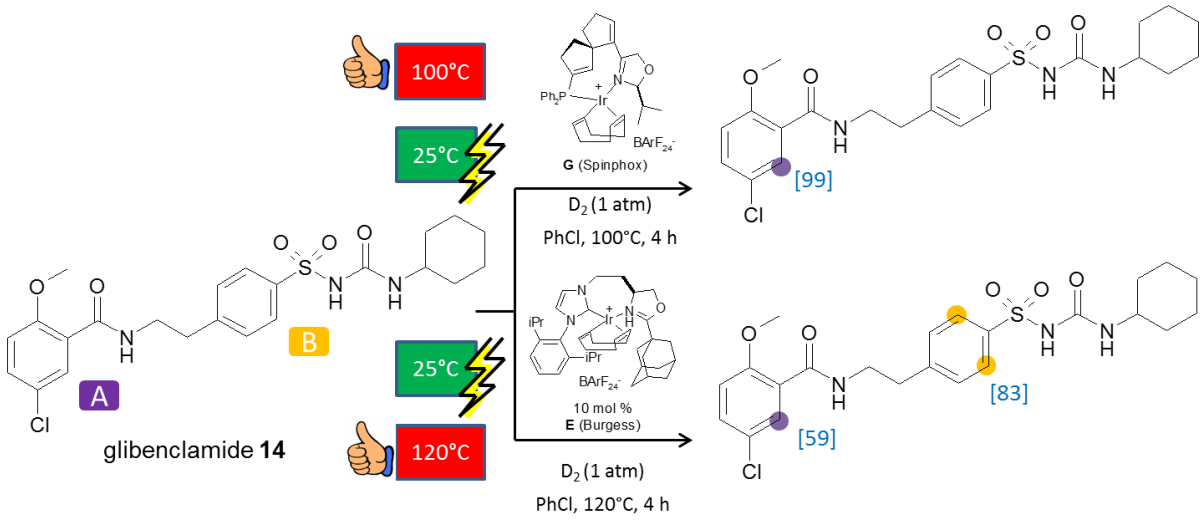

We studied the HIE reaction of apixaban **15** (*scheme III.1.8*), a reversible direct inhibitor of factor Xa to prevent stroke, with two different iridium catalysts at the same temperature (100°C). Interestingly, with catalyst **G** only deuteration of position C was observed, with a total of one deuterium introduced into the molecule. In comparison the HIE reaction with catalyst E generated a highly deuterated product with overall four deuterium atoms, however all three possible positions A, B and C were deuterated.

Scheme III.1. 8: *HIE of apixaban **15** with two different iridium catalysts **E,G** at 25-100°C*

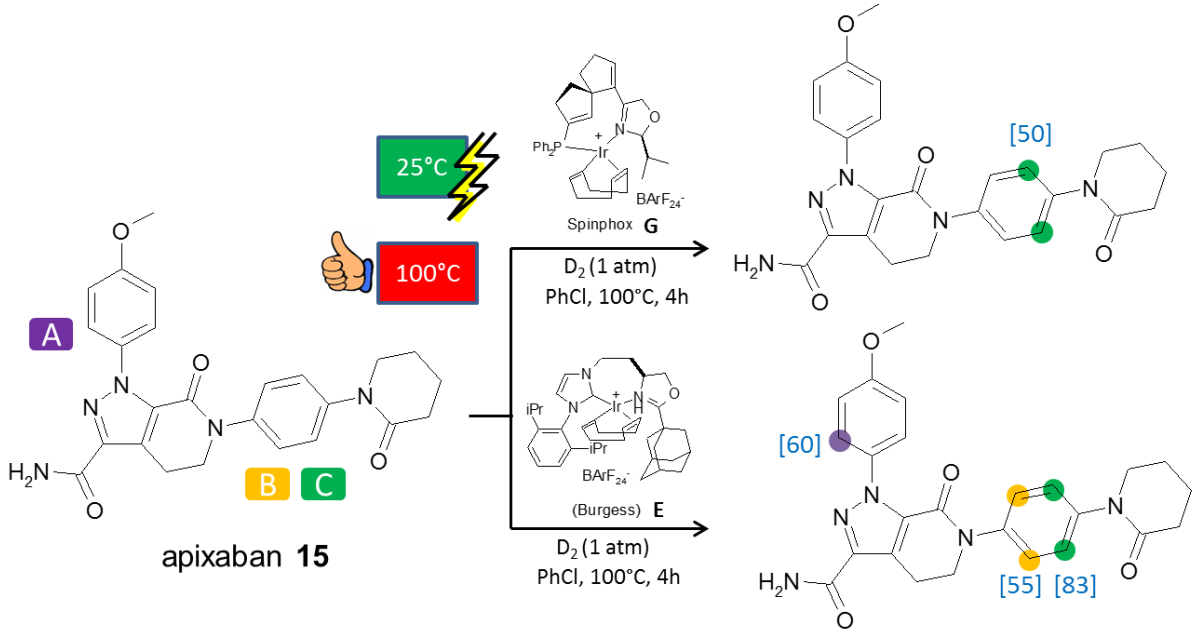

In an internal Sanofi research project, a HIE reaction with compound **16** in the presence of an alkyne moiety was tried. Unfortunately, no reaction conditions could be found to perform a successful HIE exchange without reduction of the triple bond. Triple bonds are generally easily reduced by platinum, palladium and nickel. Considering the lower reactivity of iridium in hydrogenation processes, it was anticipated that iridium catalyst could be inactive enough towards the unwanted hydrogenation side-reaction. However, in first experiments at room temperature, we obtained the deuterated product with up to 8-10 additional mass units indicating that the triple bond was mainly reduced by deuterium. Therefore, we intended to overcome this hydrogenation side reaction by performing the HIE reaction at low temperatures (0 to -30°C, *scheme III.1.9*). Unfortunately, even though we tested all catalyst **A-G**, we couldn't circumvent the triple bond reduction. As the triple bond was crucial to proceed with the research project, the decision was taken to stop. The idea to find a more suitable application for HIE reactions with catalysts **A-F** at low temperatures (<0°C) was not further followed due to other priorities.

Scheme III.1. 9: *HIE reaction of building block **16** with iridium catalysts **A-G** at low temperatures*

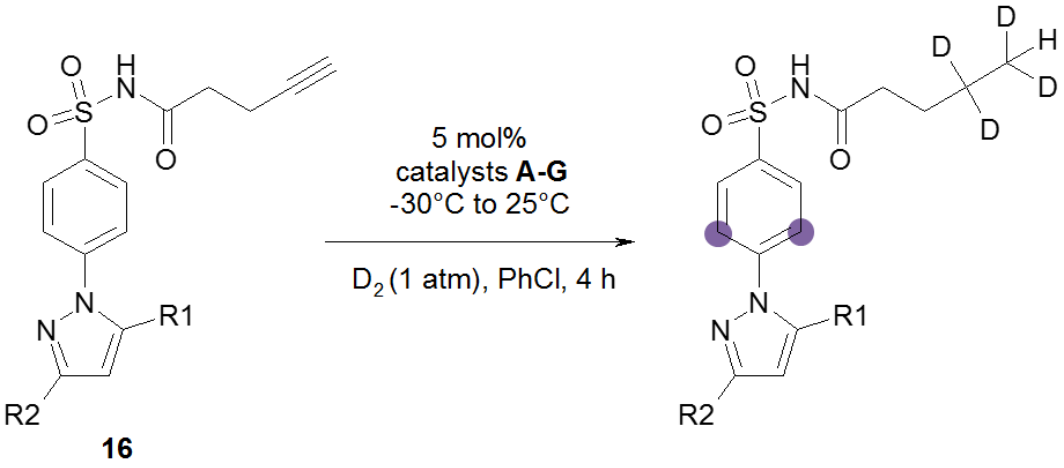

III.1.4. Conclusions

We have demonstrated that, by using the optimized combination of iridium catalysts **A-G** and varying reaction temperatures (-60 to 130°C), different HIE reaction outcomes can be achieved in terms of efficiency, specificity and selectivity. Notably the temperature window for HIE reactions with most studied iridium catalysts **A-G** was surprisingly broad. To use the right catalyst with the ideal reaction conditions, is the trigger to increase the selectivity or the deuterium incorporation. Rising the reaction temperature to a maximum prior facing catalyst deactivation is the key for maximum deuterium incorporation into the target molecule. On the other hand, decreasing the temperature can circumvent unwanted side-reactions (hydrogenation) or substrate decomposition. Therefore, it should be possible to

tune either regioselectivity and catalyst HIE activity. However, more studies in this context need to be done in the future. Even though these iridium complex catalysts seem to be remarkably efficient to perform HIE reactions at higher temperatures methodological studies at elevated temperature are still few in number.[6,7,8] Furthermore to our knowledge there is only one study on HIE reactions at -20°C.[9] Based on our results, we suggest to start the HIE optimization experiments with catalysts $\mathbf{B_a}$, **E** and **G** at room temperature and at 80°C in parallel.

[1] a) RH. Crabtree, EM. Holt, M. Lavin, SM. Morehouse. *Inorg. Chem*. **1985**; 24: 1986-1992. (b) JR. Heys, AYL. Shu, SG. Senderoff, NM. Phillips. *J. Labelled Compd. Radiopharm*. **1993**; *33*: 431-438. (c) AYL. Shu, W. Chen, JR. Heys. *J. Organomet. Chem.* **1996;** *524*: 87-93. (d) JG. Ellames, SJ. Gibson, JM. Herbert, WJ. Kerr, AH. McNeill. *Tetrahedron Lett*. **2001**; *42*: 6413-6416. (e) PWC. Cross, JG. Ellames, JS. Gibson, JM. Herbert, WJ. Kerr, AH. McNeill, TW. Mathers. *Tetrahedron.* **2003**; *59*: 3349-3358. (f) JG. Ellames, JS. Gibson, JM. Herbert, WJ. Kerr, AH. McNeill. *J. Labelled Compd. Radiopharm*. **2004**; *47*: 1-10. (g) MB. Skaddan, CM. Yung, RG. Bergman. *Org. Lett*. **2004**; *6*: 11-13. (h) CM. Yung, MB. Skaddan, RG. Bergman. *J. Am. Chem. Soc*. **2004**; *126*: 13033-13043. (i) RN. Garman, MJ. Hickey, LP. Kingston, B. McAuley, JR. Jones, WJS. Lockley, AN. Mather, DJ. Wilkinson. *J. Labelled Compd. Radiopharm.* **2005**; *48*: 75-84. (j) J. Krueger, B. Manmontri, G. Fels. Eur. *J. Org. Chem*. **2005**; 1402-1408. (k) MB. Skaddan, RG. Bergman. *J. Labelled Compd. Radiopharm*. **2006;** *49*, 623-634. (l) GJ. Ellames, JS. Gibson, JM. Herbert, AH. McNeill. *Tetrahedron.* **2001**; *57*: 9487.

[2] a) JA. Brown, S. Irvine, AR. Kennedy, WJ. Kerr, S. Andersson, GN. Nilsson. *Chem. Commun.* **2008**; 1115-1117. b) AR. Cochrane, C. Idziak, WJ. Kerr, B. Mondal, LC. Paterson, T. Tuttle, S. Andersson, GN. Nilsson. *Org. Biomol. Chem.* **2014**; *12*: 3598-3603. c) JA. Brown, AR. Cochrane, S. Irvine, WJ. Kerr, B. Mondal, JA. Parkinson, LC. Paterson, M. Reid, T. Tuttle, S. Andersson, GN. Nilsson. *Adv. Synth. Catal.* **2014**; *356*: 3551-3562. d) AR. Kennedy, WJ. Kerr, R. Moir, M. Reid. *Org. Biomol. Chem.* **2014**; *12*: 7927-7931. e). WJ. Kerr, RJ. Mudd, LC. Paterson, JA. Brown. *Chem. Eur. J.* **2014**; *20*: 14604-14607. f) J. Atzrodt, V. Derdau, WJ. Kerr, M. Reid, P. Rojahn, R. Weck. *Tetrahedron* **2015**; *71*: 1924-1929. g) WJ. Kerr, DM. Lindsay, M. Reid, J. Atzrodt, V. Derdau, P. Rojahn, R. Weck. *Chem. Commun.* **2016**; *52*: 6669-6672. h) WJ. Kerr, RJ. Mudd, PK. Owens, M. Reid, JA. Brown, S. Campos. *J. Label. Compd. Radiopharm.* **2016**; *59*: 601-603. i) WJ. Kerr, DM. Lindsay, PK. Owens, M. Reid, T. Tuttle, S. Campos. *ACS Catal.* **2017**; *7*: 7182-7186.

[3] M. Parmentier, Hartung, AT. Pfaltz, D. Muri. *Chem. Eur. J.* **2014**; *20*: 11496-11504.

[4] JM. Herbert. J. *Label. Compd. Radiopharm*. **2007**; *50*: 73–78.

[5] M. Valero, D. Becker, K. Jess, R. Weck, T. Bannenberg, J. Atzrodt, V. Derdau, M. Tamm. *Chem Eur. J*. **2019**; *25*: 6517-6522.

[6] M. Valero, R. Weck, S. Güssregen, J. Atzrodt, V. Derdau. *Angew. Chem. Int. Ed*. 2018; *57*: 8159–8163.

[7] a) A. Burhop, R. Weck, J. Atzrodt, V. Derdau. *Eur. J. Org. Chem.* **2017**; *11*: 1418–1424. b) A. Burhop, R. Prohaska, R. Weck, J. Atzrodt, V. Derdau. *J. Label. Compd. Radiopharm.* **2017**; *60*: 343-348.

[8] CA. Lukey, MA. Long, JL. Garnett. *Aust. J. Chem*. **1995**; *48*: 79-91.

[9] JM. Herbert. J. *Label. Compd. Radiopharm*. **2007**; *50*: 73–78.

Supporting information Part III – Chapter 1

Materials: see Annex 1

General deuteration procedure (Annex 1):

- **Method A (*table III.1.1*):** substrate **8** (1 eq.), catalyst **A-G** (5 mol%, 0.05 eq), DCM (3 mL), D_2 (1 atm), 4 h, indicated temperature from -60 °C to 25 °C. After four hours the reaction was stopped by evacuation of the flask and evaporation of DCM. The products were analyzed by LC-MS and ^{1}H-NMR without purification needed.
- **Method B (*table III.1.2*):** substrate **8** (1 eq.), catalyst **A-G** (5 mol%, 0.05 eq), chlorobenzene-D_5 (3 mL), D_2 (1 atm), 4 h, indicated temperature from 25 °C to 130 °C. After four hours the reactions were stopped by evacuation of the flask and the products were analysed directly by ^{1}H-NMR and LC-MS.
-

Deuteration results (tables):

See Annex 1 for the details about the deuterium incorporation calculations showed in the tables III.1.1 and III.1.2. To give an overview of the HIE reactions described in table III.1.2 (applicable to table III.1.1), we have shown two NMR results from the crude reaction in deuterated chlorobenzene at 25°C and 130°C. In all these reactions we have not observed any decomposition of substrate **8** under the reaction conditions.

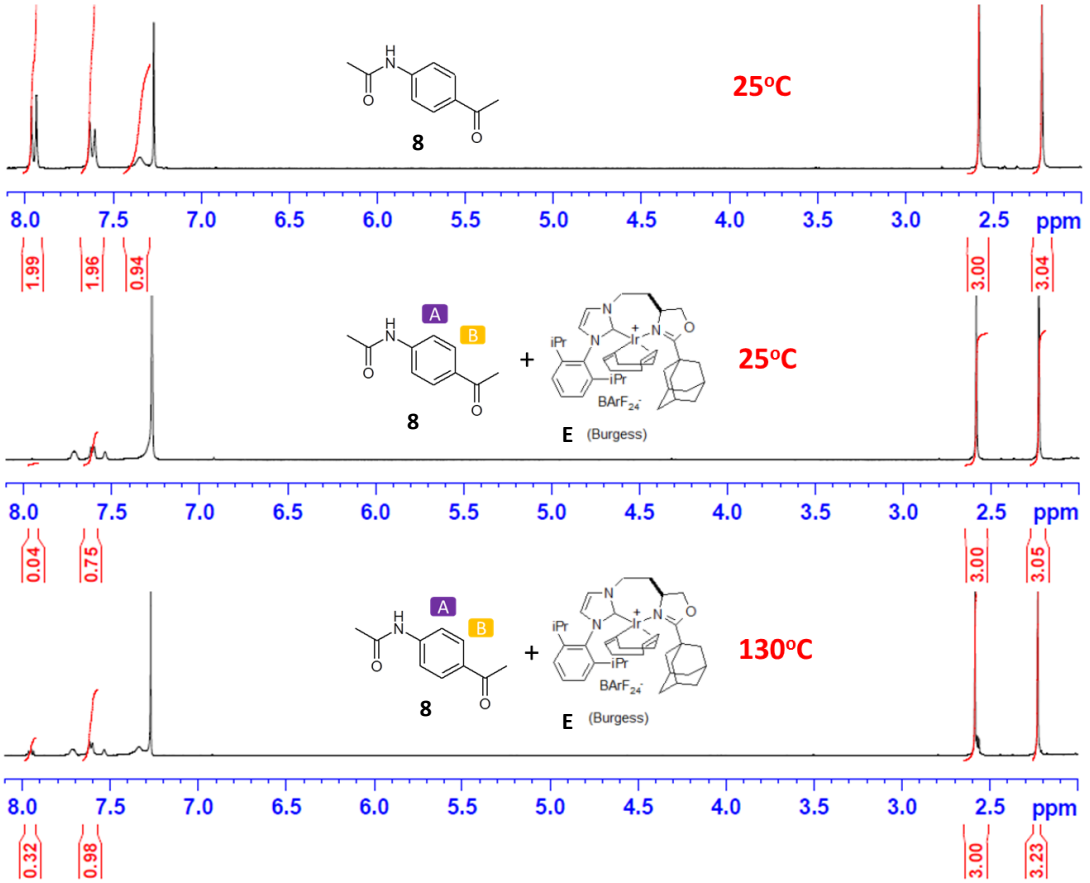

Complex molecules

Glycine, *N*-[2-(4-chlorophenyl)acetyl] ethylester **11**

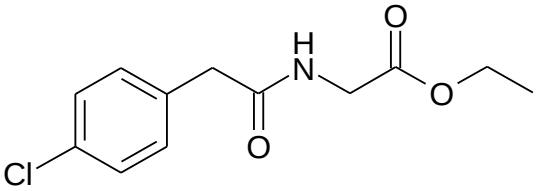

Molecular Weight =255.7033
Molecular Formula =C12H14ClNO3

11

^{1}H NMR (300 MHz, $CDCl_3$): δ 7.35 (d, ^3J = 8.5 Hz, 2H, CH_2 *ortho*-chloro), 7.27 (d, ^3J = 8.5 Hz, 2H, CH_2 *ortho*-phenyl), 4.06 (q, ^3J = 7.1 Hz, 2H, CH_2 ethyl), 3.81 (d, ^3J = 5.9 Hz, 2H, CH_2 glycine), 3.48 (s, 2H, CH_2 benzylic), 1.15 (t, ^3J = 7.1 Hz, 3H, CH_3 ethyl) ppm. Deuterium incorporation notified by the coloured dots. Determined against integral at δ 3.48 (blue arrow).

Conditions: 10.2 mg (40.0 µmol) **11**, 5 mol% cat., PhCl (3 mL), 4h.

a) 3.1 mg (2.0 µmol) catalyst **F**, RT.
b) 3.5 mg (2.0 µmol) catalyst $\mathbf{B_b}$, 80°C.

LC-MS (positive ESI): no interpretation because of the natural isotopes of the Cl.

Yields: a) 10.2 mg, 40.0 µmol, 100%; 85% D for δ 7.27.
b) 10.0 mg, 39.0 µmol, 98%; 80% D for δ 7.27 and 77% D for δ 3.81.

^{1}H-NMR Reference **11**

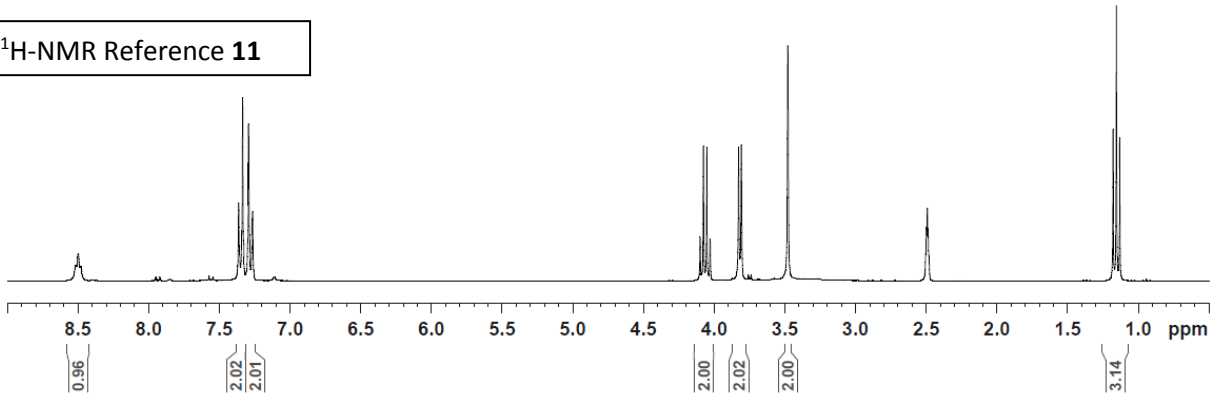

^{1}H-NMR reaction with catalyst **F**

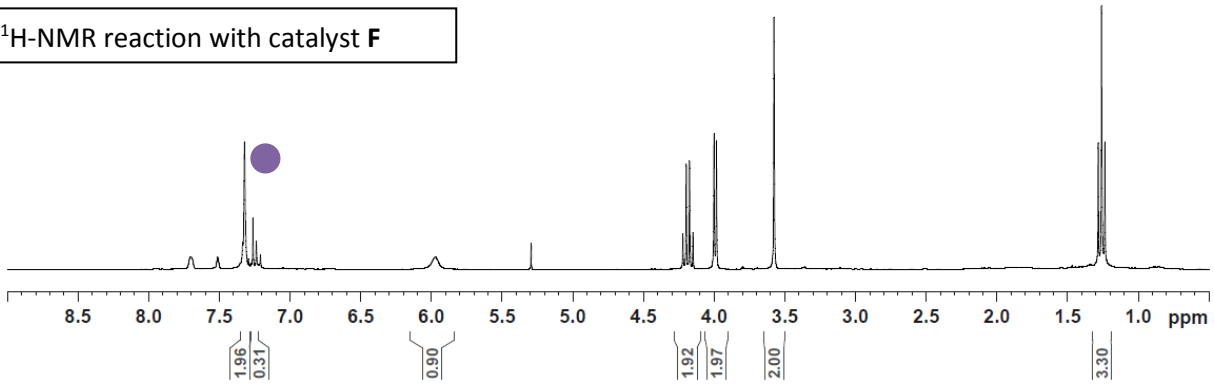

^{1}H-NMR reaction with catalyst $\mathbf{B_b}$

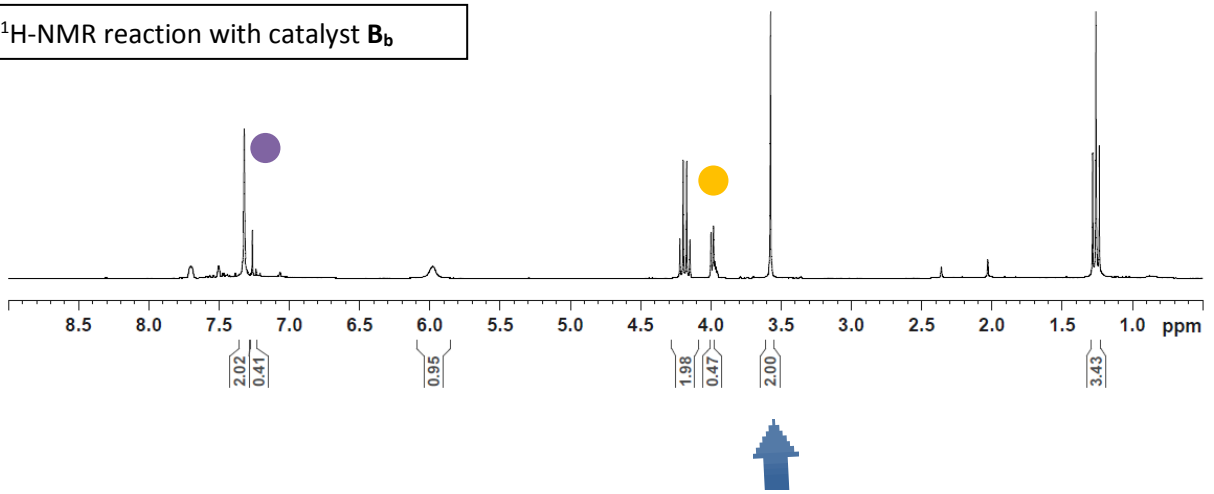

Diclofenac methylester **12**

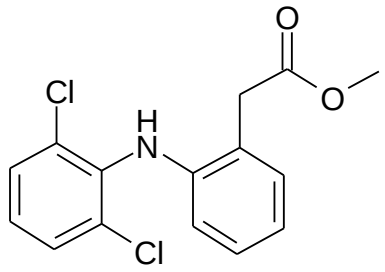

Molecular Weight =310.1824
Molecular Formula =C15H13Cl2NO2

12

^{1}H NMR (300 MHz, $CDCl_3$): δ 7.35 (s, 1H, CH aromatic *ortho* Cl), 7.32 (s, 1H, CH aromatic *ortho* Cl), 7.22 (dd, ^3J = 7.6 Hz and 1.5 Hz, 1H, CH aromatic *ortho*-phenylester), 7.12 (dd, ^3J = 7.8 Hz and 1.8 Hz, 1H, CH_2 aromatic *ortho*-nitrogen), 6.96 (m, 3H, CH aromatic), 6.54 (m, 1H, NH), 3.81 (s, 2H, CH_2 benzyl), 3.75 (s, 3H, CH_3 methyl ester) ppm. Deuterium incorporation notified by the coloured dots. Determined against integral at δ 3.75 (blue arrow).

Conditions: 7.4 mg (24.0 µmol) **12**, 5 mol% cat., PhCl (3 mL), 4h.

a) 1.9 mg (1.2 µmol) catalyst **G**, 100°C.

LC-MS (positive ESI): no interpretation because of the natural isotopes of the Cl.

Yields: a) 6.8 mg, 22 µmol, 92%, 75% D for δ 7.22.

^{1}H-NMR Reference **12**

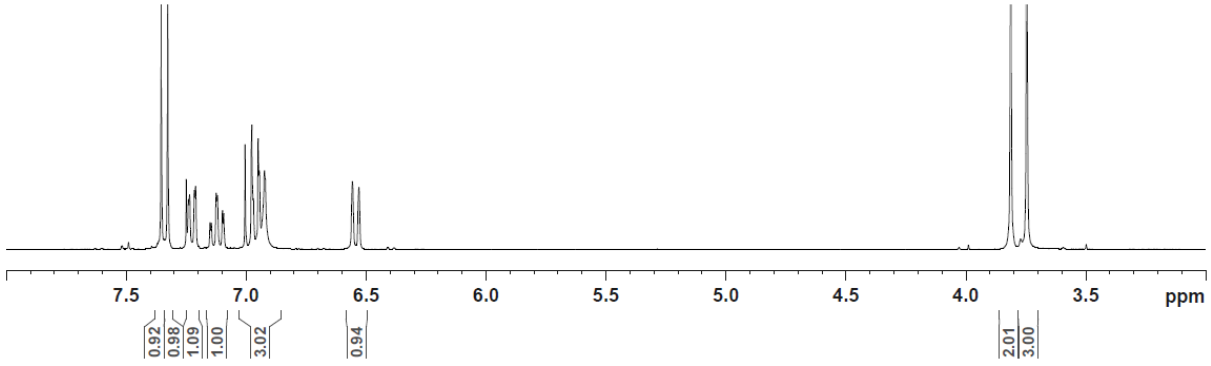

^{1}H-NMR reaction with catalyst **G**

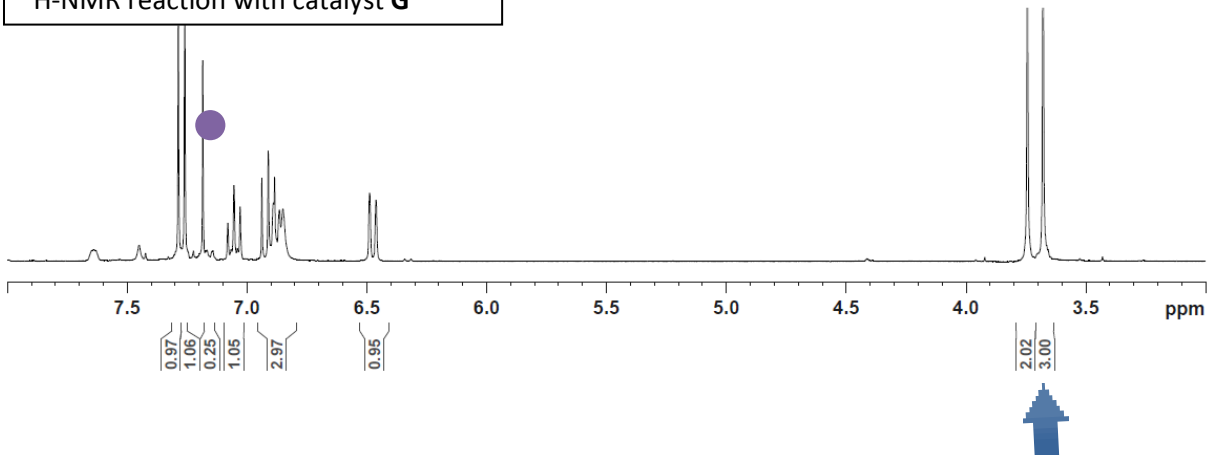

Celecoxib **13**

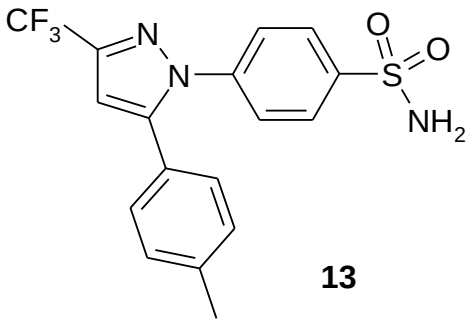

13

Molecular Weight =327.4079
Molecular Formula =C17H17N3O2S

^{1}H NMR (300 MHz, $CDCl_3$): δ 7.90 (d, ^3J = 8.3 Hz, 2H, CH_2 aromatic *ortho* S), 7.47 (d, ^3J = 8.3 Hz, 2H, CH_2 aromatic *ortho* N), 7.18 (d, ^3J = 8.0 Hz, 2H, CH_2 aromatic), 7.11 (d, ^3J = 8.0 Hz, 2H, CH_2 aromatic), 6.74 (s, 1H, CH pyrazole), 4.97 (s, 2H, NH_2), 2.39 (s, 3H, CH_3) ppm. Deuterium incorporation notified by the coloured dots. Determined against integral at δ 2.39 (blue arrow).

Conditions: 9.1 mg (24.0 µmol) **13**, 5 mol% cat., PhCl (3 mL), 4h.

a) 1.9 mg (1.2 µmol) catalyst **E**, 100°C.
b) 1.0 mg (1.2 µmol) catalyst **A**, 0°C.
c) 1.8 mg (1.2 µmol) catalyst **F**, 0°C.

LC-MS (positive ESI): a) m/z 330.4 $[M(2D)+H]^+$ (5%), 331.3 $[M(3D)+H]^+$ (25%), 332.3 $[M(4D)+H]^+$ (60%), 333.1 $[M(5D)+H]^+$ (10%).
b) m/z 329.4 $[M(1D)+H]^+$ (40%), 330.4 $[M(2D)+H]^+$ (55%), 331.3 $[M(3D)+H]^+$ (5%).
c) m/z 328.4 $[M+H]^+$ (5%), 329.4 $[M(1D)+H]^+$ (67%), 330.4 $[M(2D)+H]^+$ (28%).

Yields:

a) 9.2 mg, 24 µmol, 100%, 91% D for δ 7.90 and 92% D for δ 7.47.
b) 10.6 mg, 28 µmol, 100%, 78% D for δ 7.47.
c) 10.4 mg, 27 µmol, 100%, 62% D for δ 7.90

^{1}H-NMR Reference **13**

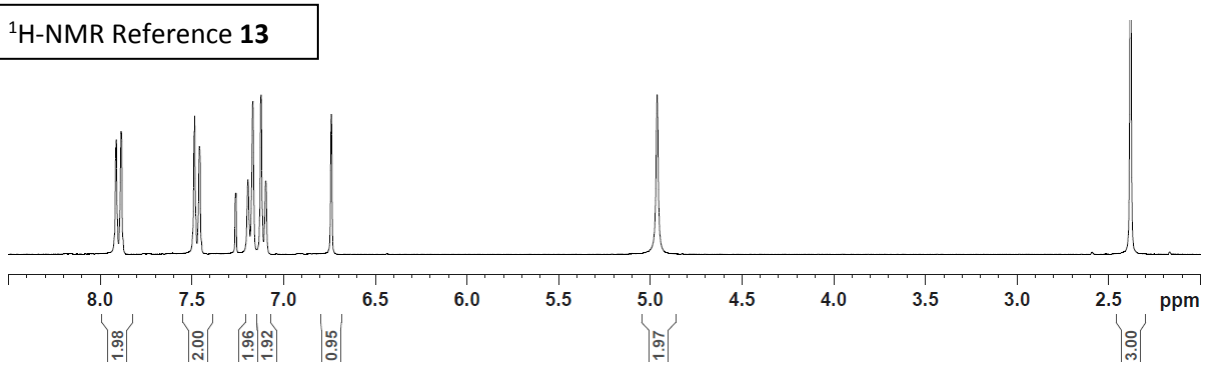

^{1}H-NMR reaction with catalyst **E**

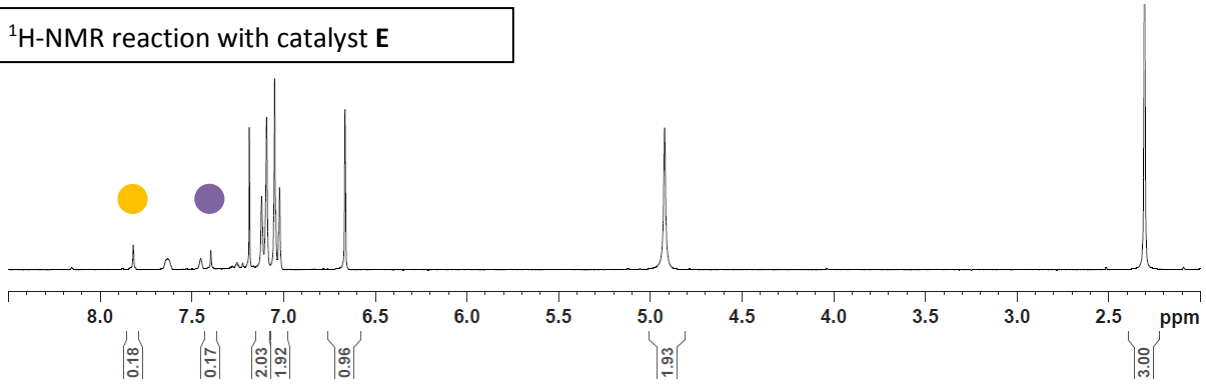

^{1}H-NMR reaction with catalyst **A**

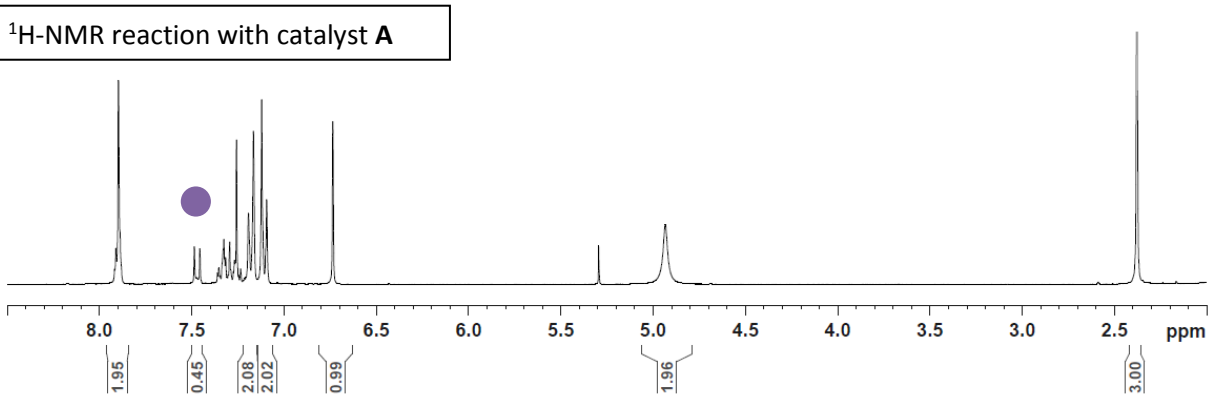

^{1}H-NMR reaction with catalyst **F**

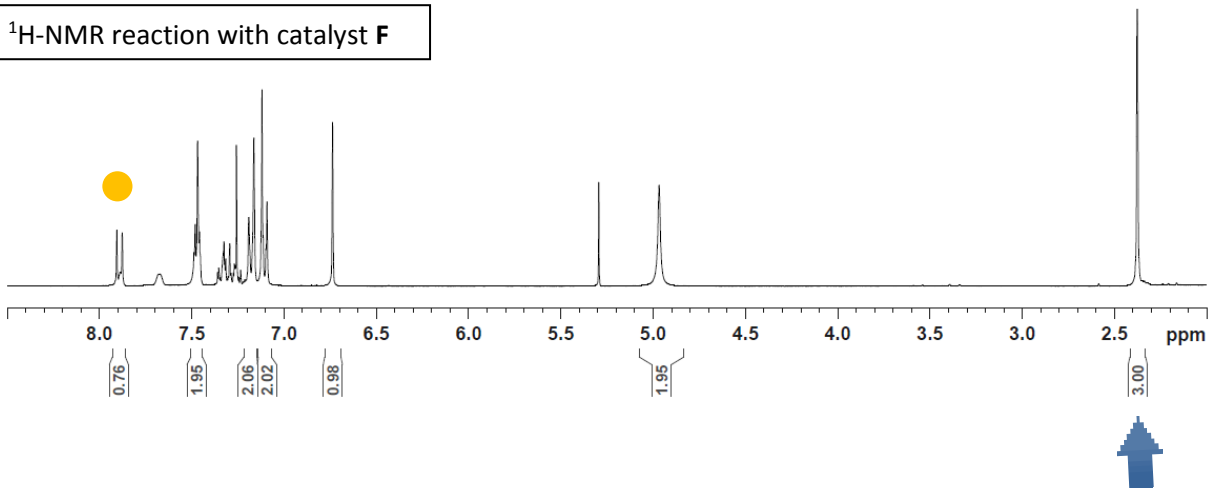

Glibenclamide **14**

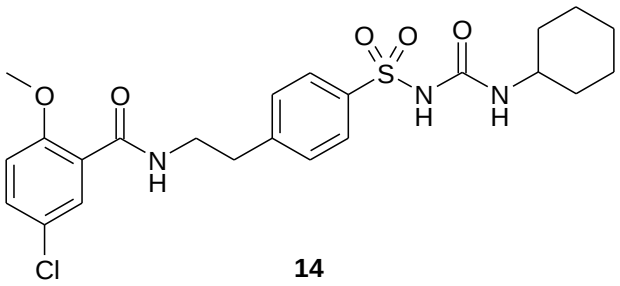

14

Molecular Weight =494.0137
Molecular Formula =C23H28ClN3O5S

^{1}H NMR (300 MHz, $CDCl_3$): δ 8.16 (d, ^3J = 2.8 Hz, 1H, CH aromatic *ortho*-amide), 7.84 (d, ^3J = 8.4 Hz, 1H, CH aromatic *ortho*-sulphonamide), 7.81 (broad s, 1H, NH), 7.42 (d, ^3J = 8.4 Hz, 1H, CH aromatic *ortho*-ethyl), 7.38 (dd, ^3J = 8.8 Hz and ^3J = 2.8 Hz, 1H, CH aromatic *ortho*-chloro), 6.87 (d, ^3J = 8.8 Hz, 1H, CH aromatic *ortho*-methoxy), 6.45 (broad s, 1H, NH), 3.78 (s, 3H, OCH_3), 3.75 (q, ^3J = 6.5 Hz, 2H, $N\underline{CH_2}CH_2$), 3.59 (broad s, 1H, CH cyclohexyl), 3.03 (t, ^3J = 6.5 Hz, 2H, $NCH_2\underline{CH_2}$), 1.83 (m, 2H, CH_2 cyclohexyl), 1.67 (m, 2H, CH_2 cyclohexyl), 1.56 (m, 2H, CH_2 cyclohexyl), 1.25 (m, 4H, $2CH_2$ cyclohexyl) ppm. Deuterium incorporation notified by the coloured dots. Determined against integral at δ 3.03 (blue arrow).

Conditions : 11.8 mg (24.0 µmol) **14**, 5 mol% cat., PhCl (3 mL), 4h.
a) 1.9 mg (1.2 µmol) catalyst **G**, 100°C.

LC-MS (positive ESI): no interpretation because of the natural isotopes of the Cl.

Yield: a) 10.6 mg, 21.0 µmol, 90%, 99% D for δ 8.16.

^{1}H-NMR Reference **14**

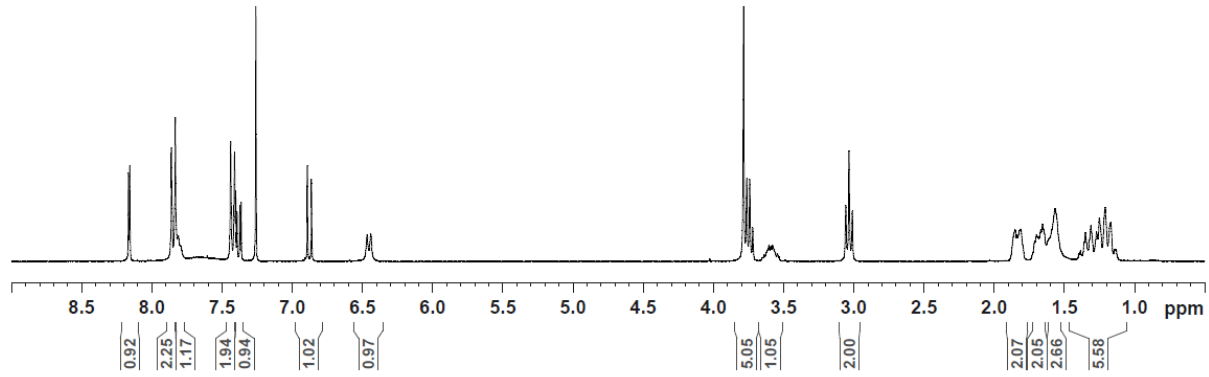

^{1}H-NMR: reaction with catalyst **G**

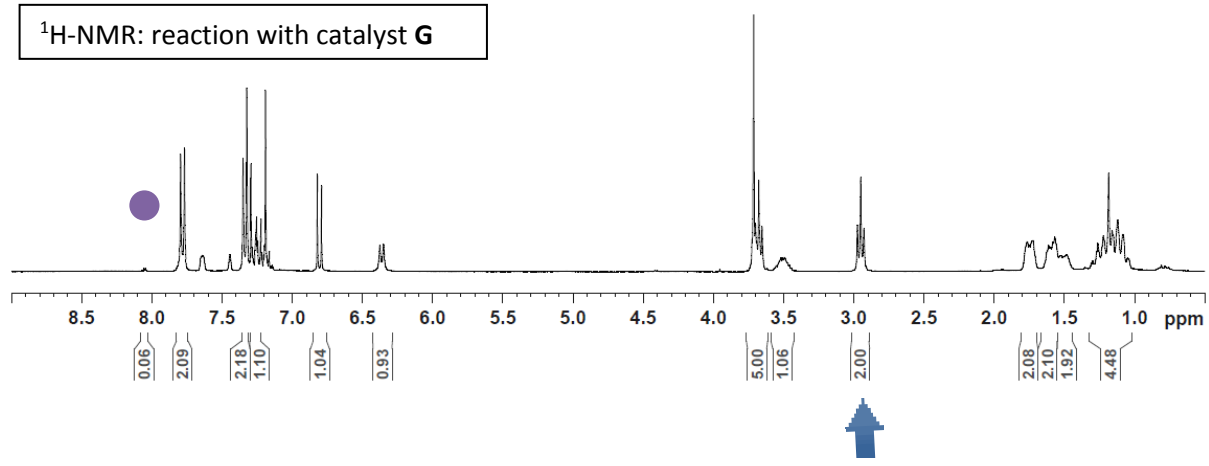

Apixaban **15**

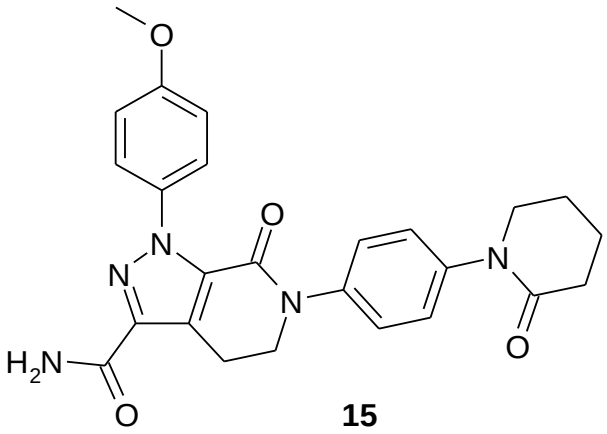

15

Molecular Weight =459.5091
Molecular Formula =C25H25N5O4

^{1}H NMR (300 MHz, MeOD): δ 7.51 (d, ^3J = 9.0 Hz, 2H, CH_2 aromatic *meta*-methoxy), 7.42 (d, ^3J = 8.5 Hz, 2H, CH_2 aromatic *ortho*-amide), 7.32 (d, ^3J = 8.5 Hz, 2H, CH_2 aromatic *ortho*-cyclohxylamide), 7.00 (d, ^3J = 9.0 Hz, 2H, CH_2 aromatic *ortho*-methoxy), 4.14 (m, 2H, CH_2 *ortho*-Nitrogen amide), 3.85 (s, 3H, CH_3 methoxy), 3.68 (m, 2H, CH_2 *ortho*-Nitrogen amide cyclohexyl), 3.34 (m, 2H, CH_2 *ortho*-pyrazole cycle), 2.52 (m, 2H, CH_2 cyclohexyl), 1.97 (m, 4H, $2CH_2$ cyclohexyl) ppm. Deuterium incorporation notified by the coloured dots. Determined against integral at δ 3.85 (blue arrow).

Conditions: 11.00 mg (24.0 µmol) **15**, 5 mol% cat., PhCl (3 mL), 4h.

a) 1.9 mg (1.2 µmol) catalyst **E**, 100°C.
b) 1.9 mg (1.2 µmol) catalyst **G**, 100°C.

LC-MS (positive ESI): a) m/z 462.4 $[M(2D)+H]^+$ (5%), 463.3 $[M(3D)+H]^+$ (10%), 464.3 $[M(4D)+H]^+$ (55%), 465.3 $[M(5D)+H]^+$ (30%).
b) m/z 460.5 $[M+H]^+$ (5%), 461.4 $[M(1D)+H]^+$ (80%), 462.4 $[M(2D)+H]^+$ (15%).

Yields:

a) 9.1 mg, 20 µmol, 83%, 60% D for δ 7.51, 55% D for δ 7.42, 83% D for δ 7.32.
b) 11.5 mg, 25 µmol, 100%, 50% D for δ 7.32.

^{1}H-NMR Reference **15**

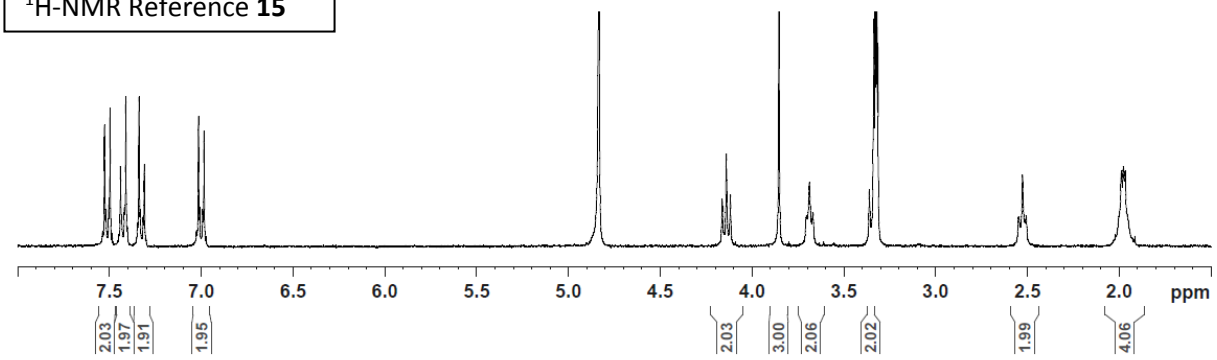

^{1}H-NMR catalyst **E**

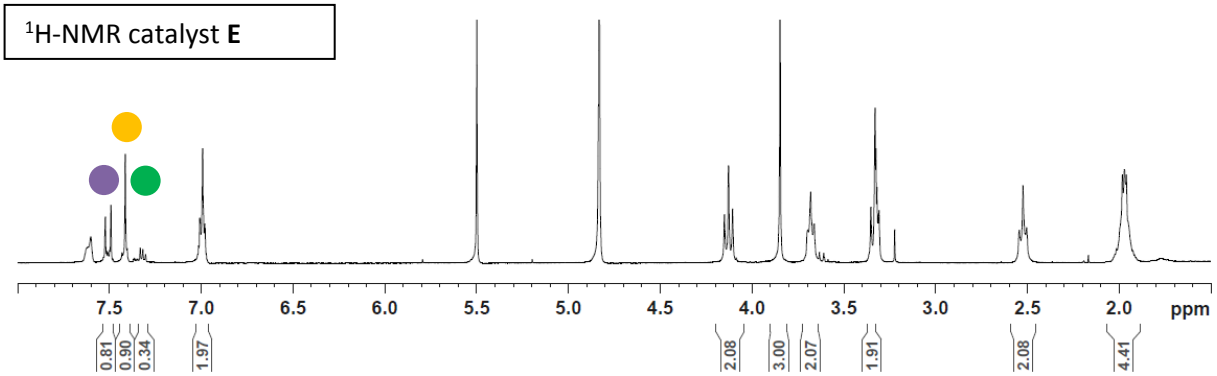

^{1}H-NMR catalyst **G**

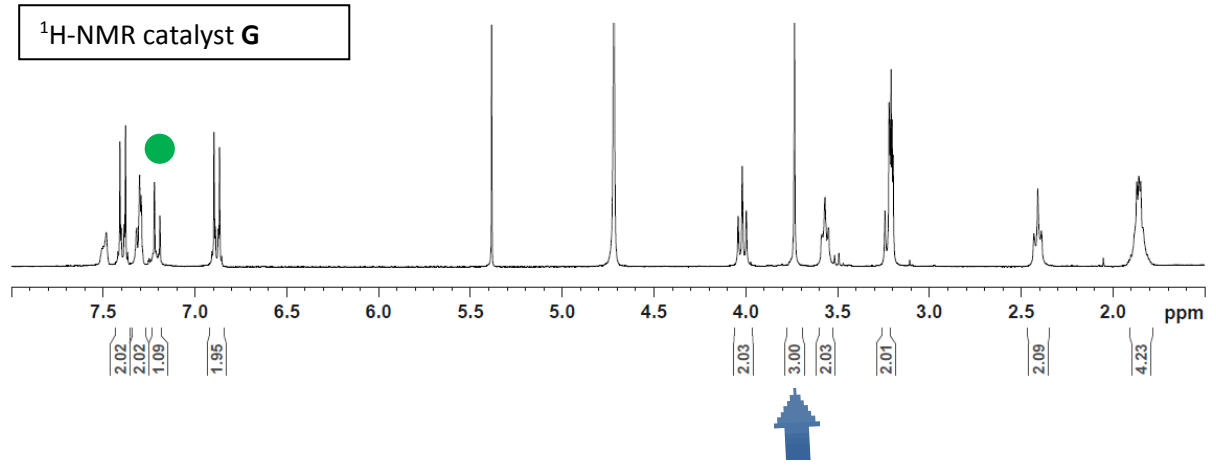

Chapter 2: Prediction of selectivity in iridium(I) catalyzed hydrogen isotope exchange competition reactions

III.2.1. Introduction

As previously described in Part I-II, numerous HIE protocols utilizing homogeneous (or heterogeneous) catalysts have already been described.[1,2] Even though a new generation of bidentate iridium catalyst systems such as those from Pfaltz **D**,[3] Burgess **E**,[4] and Tamm **F**,[5] have extended the scope of the aromatic *ortho*-directing HIE reactions, the commercially available Crabtree's **A**[6] and Kerr's catalyst $\mathbf{B_a}$[7,8] stay the most regularly applied iridium catalysts in radiochemistry laboratories today. Nevertheless, while there are numerous publications on the use of different directing groups such as ketones, esters, amides, carboxylic acids, nitro groups, sulfones, sulfonamides etc., there is still a lack of understanding and prediction for how the different directing groups enable HIE if more than one directing group is present in the molecule (*scheme III.2.1*). This is especially important as the introduction of a radioactive label in a metabolically stable position is essential for the application of tritiated compounds for *in vivo* experiments.[9] In comparison to ^{14}C-labelling, where a loss of the radioactive marker is less frequent, the loss of tritium can occur by simple metabolic enzymatic hydroxylations (see Part I).[9] Therefore, it would be useful for synthetic chemists to be able to predict the labelling position in complex molecules, instead of performing multiple try and error experiments.

Scheme III.2. 1: *Concept of prediction about iridium-catalyzed ortho-directed aromatic HIE reactions*

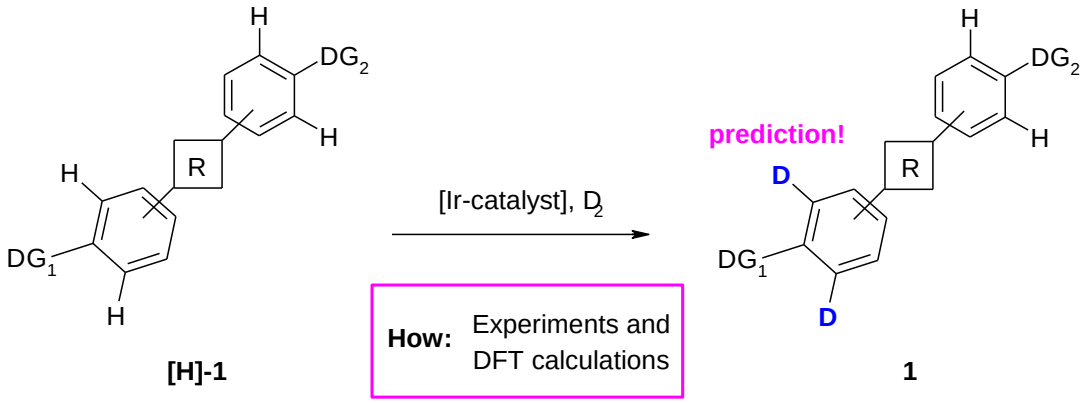

To evaluate the potential scope of such a prediction, we were motivated to perform a comprehensive analysis of the most commonly occurring directing groups in the top 200 most prescribed drugs in 2016, in particular those containing aromatic rings as reported by Njardarson *et al.* (*figure III.2.1*).[10] We have identified several functional groups, for example, imidazole (N-heterocycle), ketones, esters, amides, carbamates, acids, nitro groups, sulfones, sulfonamides, phenols, etc. repeatedly being present in aromatic drug molecules.

Based on these outcomes, we have studied the influence of the previously mentioned functional groups as a directing group in a standard HIE reaction with deuterium gas as the isotope source.[11]

Figure III.2. 1: *Analysis of 68 aromatic drugs and their different aromatic directing groups (analysed from 200 drugs rated by number of prescriptions, 2016, united states)*[10]

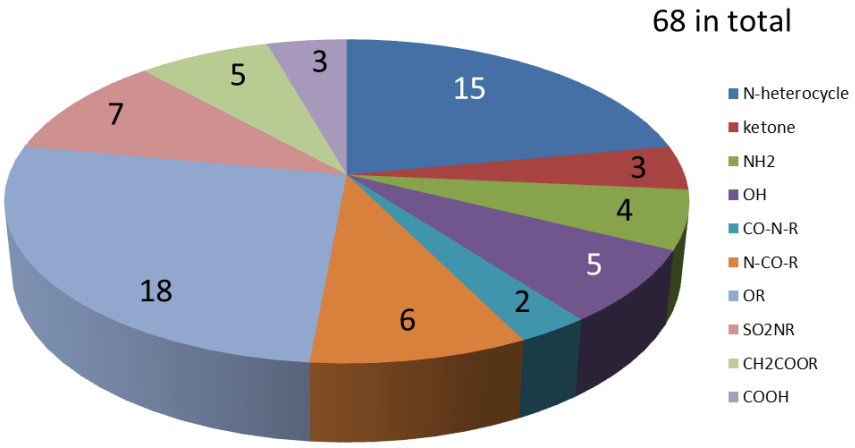

III.2.2. Competition HIE reactions study

To achieve our aim, initial experiments have been run under standard HIE conditions applying the commercial Kerr catalyst **B_a** (1 atm D_2, rt, dichloromethane, 2h) to make our results as comparable as possible with literature results.[12] We conducted a series of competition experiments,[13] employing two simple mono-substituted aromatic substrates in one reaction flask, along with catalyst **B_a**, to examine which of the two directing groups is giving a better result in deuteration in the HIE reaction (*scheme III.2.2*). Applying this methodology to aromatic compounds **2–10**, we have obtained the results presented in table III.2.1.

Scheme III.2. 2: *Competition HIE experiment of aromatic compounds with catalysts* ***B_a***[a]

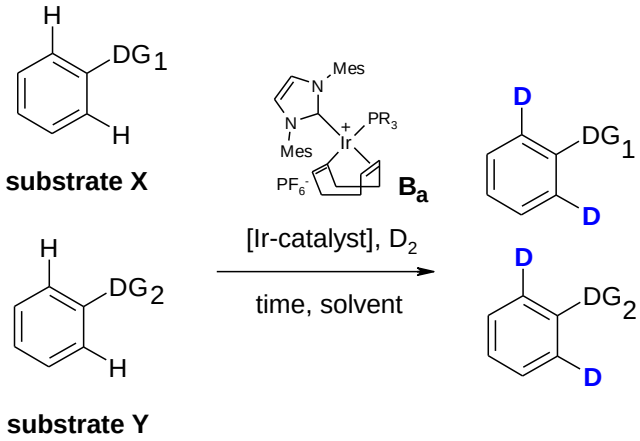

a) Conditions: substrate X, Y (1 eq.), catalyst **B_a** (5 mol%, 0.05 eq.), DCM (6 mL), D_2 (1 atm), rt, 2h.

Scheme III.2. 3: *Experimentally found order of different aryl-DGs in competition HIE experiments*

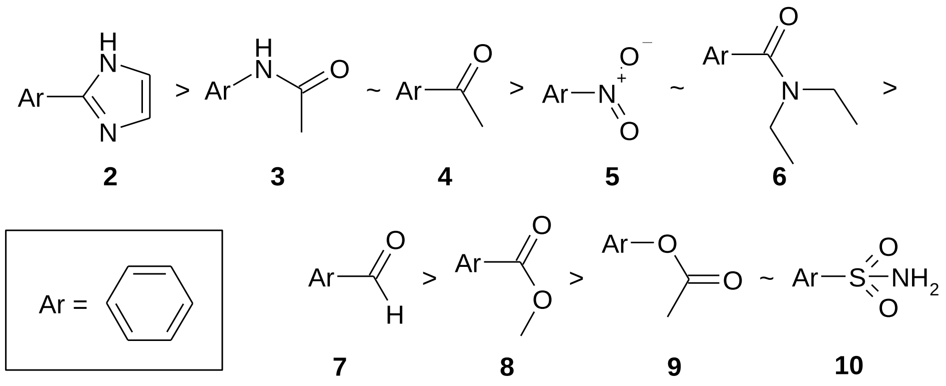

Table III.2. 1: *Deuterium incorporation results of the competition HIE experiments with catalyst* $\boldsymbol{B_a}$ [a,b]

Substrate	3	4	5	6	7	8	9	10
2	0%D / 82%D	0%D / 89%D	0%D / 89%D	0%D / 82%D	0%D / 80%D	5%D / 85%D	0%D / 78%D	2%D / 85%D
3		89%D / 87%D	21%D / 73%D	22%D / 78%D	15%D / 86%D	10%D / 66%D	8%D / 81%D	11%D / 89%D
4			69%D / 82%D	56%D / 87%D	50%D / 77%D	12%D / 91%D	25%D / 91%D	7%D / 91%D
5				69%D / 62%D	25%D / 31%D	21%D / 44%D	9%D / 88%D	9%D / 92%D
6					28%D / 44%D	16%D / 77%D	6%D / 77%D	2%D / 78%D
7						10%D / 34%D	3%D / 33%D	13%D / 20%D
8							11%D / 39%D	12%D / 59%D
9								10%D / 8%D

a) Conditions: substrate X,Y (1 eq.), catalyst $\boldsymbol{B_a}$ (5 mol%, 0.05 eq.), DCM (6 mL), D_2 (1 atm), rt, 2h. b) The analysis was done either by mass spectrometry (if substrate ionizable and no overlapping between the two substrates) or by ^{1}H-NMR.

The competition HIE experiment between substrates **4** and **10** for example, showed 91%D incorporated in substrate **4** and only 7%D incorporated in substrate **10**. As a conclusion, the DG of **4** is predominant compared to **10** regards to its reactivity in HIE reaction with catalyst $\boldsymbol{B_a}$. The difference of deuterium incorporation in substrates **5** and **6**, 62%D and 69%D respectively, is very small so these two DGs can be considered as equal in their capacity to direct HIE with catalyst $\boldsymbol{B_a}$.

The interpretation of the data provided in table III.2.1, have enabled us to determine experimentally the general relative directing group strength in the following order: imidazole **2** (heterocycle[14]) > acetylanilide **3** ~ ketone **4** > nitro **5** > tertiary amide **6** > aldehyde **7** > ester **8** > carbamate **9** > primary sulfonamide **10** (*scheme III.2.3*). In an earlier contribution, Derdau and Atzrodt *et al.* have studied the relative directing group strength of different heterocyclic directing groups such as imidazole **2** in HIE reactions using similar competition experiments.[14] These results add to the proposed reactivity order in the HIE reactions.

III.2.3. DFT calculations and energy profiles for insights into the competition study

The interpretation of the previous results can allow an estimation on the prediction of the labelling positions with catalyst $\mathbf{B_a}$, in more complex molecules containing these directing groups. However, to understand the theoretical background of our proposal, density functional theory (DFT) calculations,[15] have been done by Dr. Stefan Güssregen from the Computational Drug Design group in Sanofi. These calculations were following the approach applied by Kerr *et al*.[16,17,18] based on the mechanism suggested by Heys.[19]

It is important to remember that the Gibbs free energy ΔG is defined by the following relation: $\Delta G=\Delta H-T\Delta S$ (H=enthalpy and S=entropy). The more the ΔG value is negative, the easier the reaction is. The enthalpy ΔH represents the activation energy needed to form the transition state **11b** from the coordination complex **11a** (see figure III.2.2). Based on the Gibbs free energy equation, we can see that the temperature T is also playing an important role and this will be discussed below. The calculated ΔG values are given in table III.2.2 and sorted by their ΔG_{rel} energy values for their formation of coordination complex **11a** (*table III.2.2*). For comparison, we also added the activation energy $\Delta\Delta H$ for the CH-activation step (**11a**=>**11b**), showing that there are significant differences between these two parameters.

Based on the data from table III.2.2, the free energy profiles have been constructed (with catalyst $\mathbf{B_a}$), and shown in figure III.2.2, for the first leg step of the HIE reaction. The activation energy ΔH (**11a** => **11b**) is known to be the main parameter for explaining formation of the deuterated products.[18] The theoretical ΔG values given in table III.2.2 are in adequacy with the experimental order found in scheme III.2.3, except for the DG nitro **9** interestingly. In these competition experiments, which take place at room temperature, the relative populations of the coordination complex **11a** (ΔG) is strongly influencing the outcome of the overall reaction. Once the coordination complex **11a** has been formed, the reaction will proceed to completion, via transition-state **11b** (ΔH) and insertion product **11c**. This is reflected in the order of the calculated relative energies of the coordination complex **11a**, which matches very well the order experimentally observed. For those similar coordinating directing groups where the coordination complexes are populated almost

equally, relative energies of the transition-states become dominating again. This can be seen nicely for compound pairs **4** vs **6**, **7** vs **8** and **9** vs **10**. This is a significant contribution to the understanding of CH activation mechanism processes with complex substrates. In competition cases it is not the activation barrier[20,17,18] between the coordination complex **11a** and transition state **11b** responsible for the HIE reaction outcome, but the lower energy of the initially formed coordination complex **11a.** Overall, table III.2.2 summarizes most of the common directing groups in Drug Discovery and therefore should be very helpful for synthesis planning.

Figure III.2. 2: *Calculated potential energy surfaces (PES) for the HIE reaction of substrates* ***2-10*** *with catalyst* B_a [a]

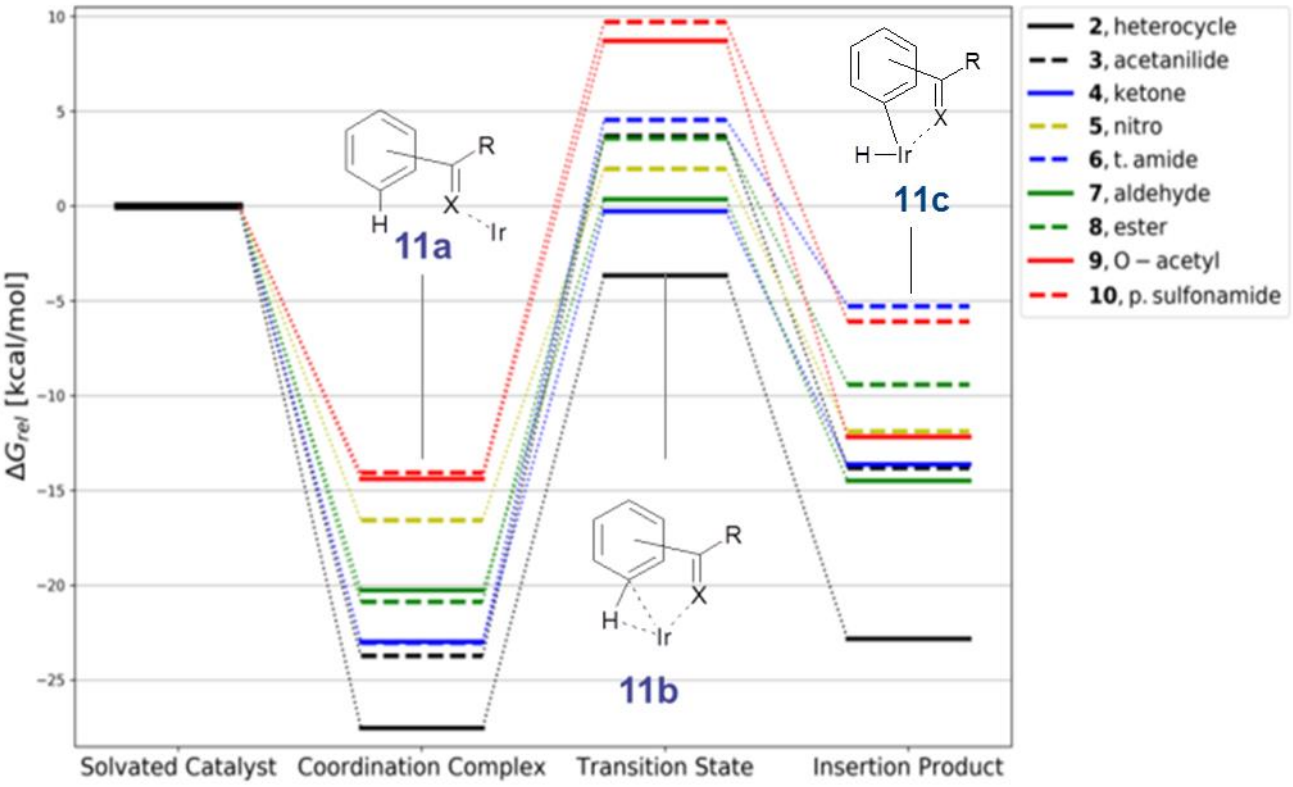

a) Energies calculated in dichloromethane at 298K, shown for the first leg of the reaction.

Table III.2. 2: *Calculated values of different DGs to form coordination complex* ***11a*** *(sorted by ΔG_{rel}) and the activation energy $\Delta\Delta H$ to generate* ***11c*** *via transition state* ***11b***

	DG	ΔG_{rel} complex **11a**	$\Delta\Delta H$ (**11a**=>**11b**)
Ar	-N-imidazole **2**	-27.5	23.9
	-N-CO-Me **3**	-23.7	27.4
	-CO-Me **4**	-23.0	22.7
	-CO-NEt_2 **6**	-23.0	27.6
	-COOMe **8**	-20.9	24.4
	-CO-H **7**	-20.3	20.6
	-NO_2 **5**	-16.6	18.5
	-OCOMe **9**	-14.3	23.0
	-SO_2NH_2 **10**	-14.0	23.8

III.2.4. Prediction and experimental prove in HIE reactions of disubstituted molecules

After the success of the competition experiments, we sought to obtain more insight into the role of competing directing groups in the same molecule. We studied aromatic compounds **12-22** with at least two different substituents. Due to the higher complexity of ^{1}H-NMR analysis in 1,2- or 1,3-disubstituted benzenes, we focused on 1,4-disubstituted ones (*scheme III.2.4*). Furthermore, the $\Delta\Delta$H values of each of the two directing groups have been calculated. These $\Delta\Delta$H values are shown below the respective substrates in scheme III.2.4. The higher the difference in $\Delta\Delta$H energy between each of the two directing groups is, the higher the difference on deuterium incorporation is expected to be. It is highlighted by a yellow star in the scheme which of the two directing groups to be the predominant one. This is calculated by subtraction of the coordination complex **11a** energies $\Delta\Delta$H of both DGs. By comparing the experimental results with the predicted energy difference in the coordination complex, we were hoping to obtain a rational correlation.

All predicted results of the deuteration of **12-22** support the reported order obtained in the competition experiments (*table III.2.1* and *scheme III.2.3*). However, by this method we are able to predict the main product but not the final deuteration result in %D. Indeed, if we look at compound **18**, the $\Delta\Delta$H value (6.2 kcal/mmol^{-1}) is high, therefore we expected a high difference between the deuterium incorporation of both DG, with a higher incorporation in *ortho*-position of the aldehyde. This is true as more deuterium has been incorporated in this

position (52%D against 19%D in ortho-position of the sulfonamide). Nevertheless, the deuteration ratio between the two positions is not dramatically high. For comparison, compound **19** with a lower ΔΔH value (2.2 kcal/mmol^{-1}) than for compound **18** (6.2 kcal/mmol^{-1}), shows a higher ratio (97:22) in deuterium incorporation between the two *ortho*-positions.

Compounds **14** and **15** have been run at 0°C to see if the prediction would correlate better with the experiment. Interestingly, it has shown than by lowering the reaction temperature to 0°C, the selectivity of deuteration was shifted in favor of the ketone as the main directing group. This strongly suggests that differences in regioselectivities in the HIE reactions play a much bigger role at temperatures below 0°C.

Scheme III.2. 4: *HIE experiment of disubstituted aromatic substrates* ***12-22*** [a,b,c]

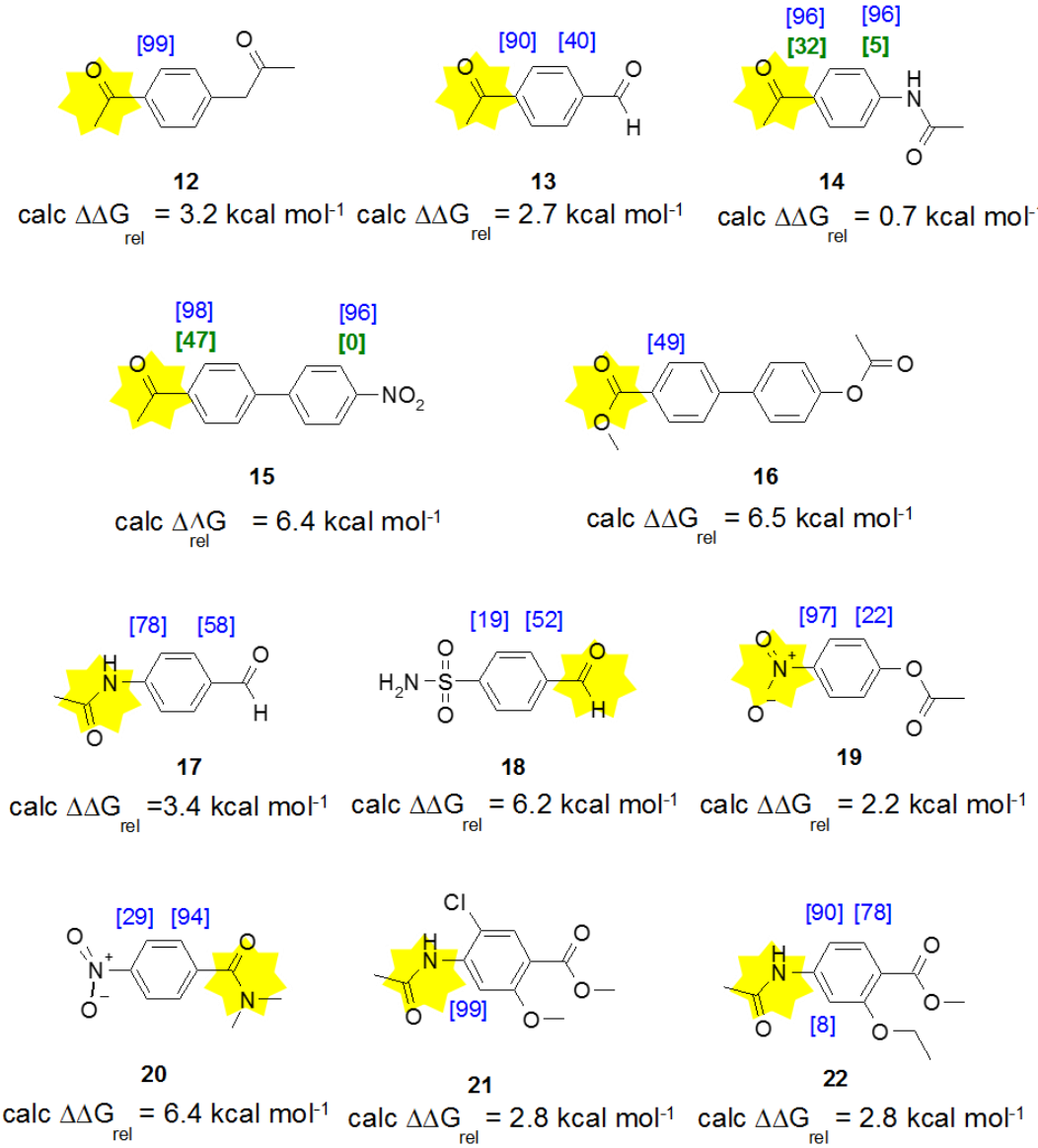

a)Conditions: substrate (1 eq.), catalyst **B$_a$** (5 mol%, 0.05 eq.), D_2 (1 atm), DCM (3 mL), rt, 2 h. b) [Blue values]: %D at 25°C; [green values]: %D at 0°C. c) Yellow star is the predicted less demanding DG.

III.2.5. Prediction and experimental prove in HIE reactions of complex molecules and drugs

Finally, we have performed HIE reactions catalyst $\mathbf{B_a}$ on complex molecules **23-31** where at least two different directing groups were present (*scheme III.2.5*). The red arrow is showing the predicted main deuteration position based on our order from table III.2.1 and scheme III.2.3. The deuterium incorporation in blue is the experimental result. In all cases shown, we were able to predict the correct labelling position. However, as this is a thermodynamic model there are many other factors such as solubility, salts and impurities can which can influence the HIE outcome.

Scheme III.2. 5: *HIE experiment of drugs* ***23-31*** *catalysts* $\mathbf{B_a}$ [a]

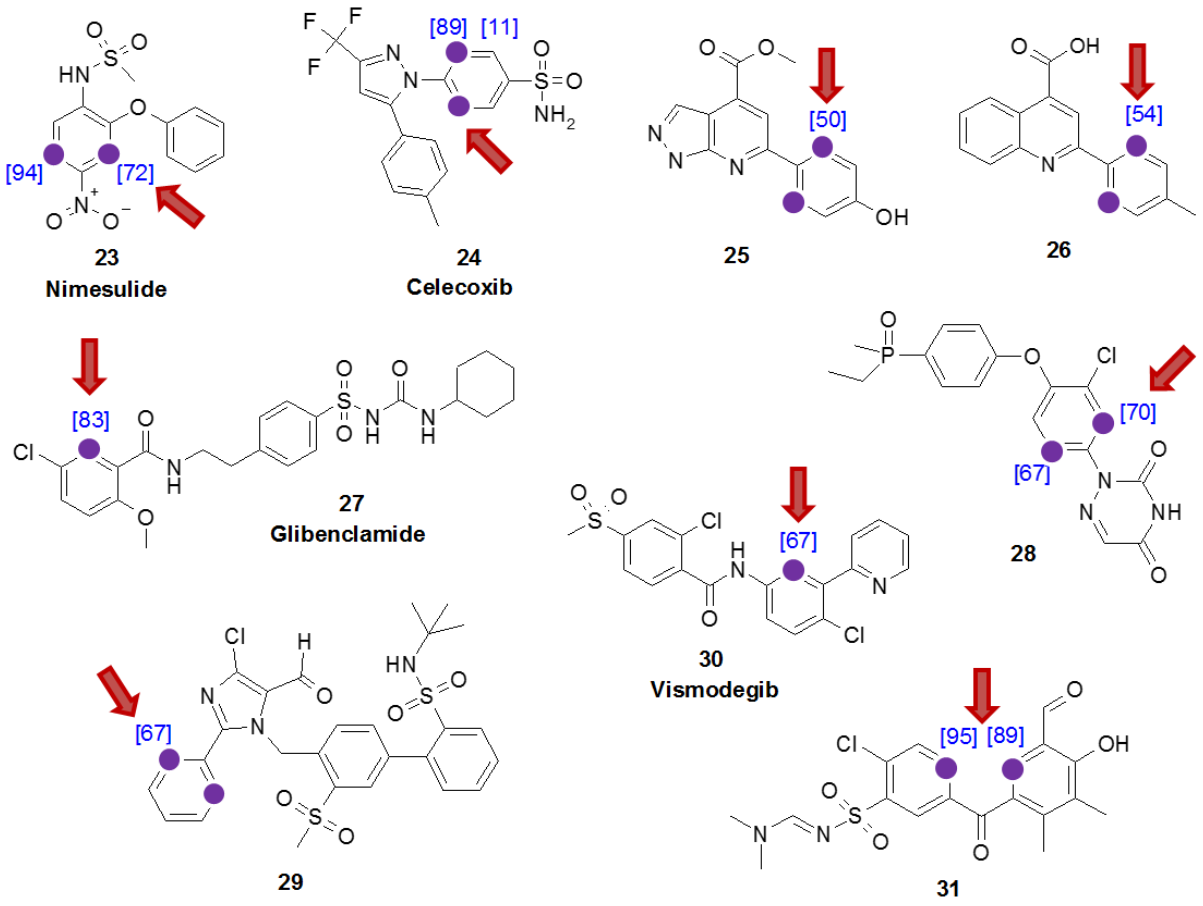

a) Conditions: substrate (1 eq.), catalyst $\mathbf{B_a}$ (5 mol%, 0.05 eq.), D_2 (1 atm), DCM (3 mL), rt, 2 h.

III.2.6. Conclusion

The work presented in this chapter have enabled us to elaborate a clear order of directing group influence on HIE reactions with catalyst **B_a**. With DFT calculations, we have identified the iridium-substrate coordination complex to be the main trigger for reactivity and selectivity, in the competition situation with two and more directing groups. Only if the energies of two competing coordination complexes are very similar, the formation of the CH activation transition-state became the most demanding parameter.

These results are not only allowing predictions in regioselective HIE reactions of complex molecules, but also give an outreach to develop the concept of directing group-induced late-stage functionalization in general. Understanding the influence of the directing groups could allow a much better planning and successful prediction of late-stage functionalization pathways. Such a prediction methodology could save time and resources in drug discovery research or could even broaden the applications of tritiated molecules to new fields of the life sciences. Most generally this would make iridium catalysed HIE reactions a significantly improved tool in isotope chemistry.

In summary, this finding could be a general principle to understand competition situations of different directing groups in one molecule and can be probably transferred to further transition metal catalyzed CH functionalization reactions. Other research groups have found empirically similar regioselectivities in directed CH functionalization competition reactions for C-C or C-X bond formations in complex molecules,[21] either applying catalysts like iridium,[22] rhodium,[23] palladium,[24] cobalt,[25] or ruthenium[26] metals. There is furthermore a standing interest to establish convenient prediction models.[27]

[1] a) J. Atzrodt, V. Derdau, W.J. Kerr, M. Reid, *Angew. Chem. Int. Ed.* **2018**, *57*, 3022 – 3047*; b)* J. Atzrodt, V. Derdau, T. Fey, J. Zimmermann, *Angew. Chem. Int. Ed.* **2007**, *46*, 7744-7765; c) T. Junk, W.J. Catallo *Chem. Soc. Rev.* **1997**; *26*, 401−406; d) A. Di Giuseppe, R. Castarlenas, L.A. Oro *Comptes Rendus Chimie.* **2015**; *18*: 713-741; e) R. Voges, J. R. Heys, T. Moenius Preparation of Compounds Labeled with Tritium and Carbon-14. New York: John Wiley and Sons; **2009**; f) M. Valero, V. Derdau, *J. Label. Compd. Radiopharm*. **2019**, doi.org/10.1002/jlcr.3783.

[2] For selected reviews, see: a) J.R. Heys, *J. Label. Compd. Radiopharm.* **2007**, *50*, 770-778; b) G.N. Nilsson, W.J. Kerr, *J. Label. Compd. Radiopharm.* **2010**, *53*, 662-667; c) R. Salter, J. *Label. Compd. Radiopharm.* **2010**, 53, 645-657; d) P.H. Allen, M.J. Hickey, L.P. Kingston, D.J. Wilkinson, *J. Label. Compd. Radiopharm.* **2010**, *53*, 731-738; e) W.J.S. Lockley, A. McEwen, R. Cooke, *J. Label. Compd. Radiopharm.* **2012**, *55*, 235-257; f) J. Atzrodt, V. Derdau, *J. Label. Compd. Radiopharm.* **2010**, *53*, 674-685.

[3] M. Parmentier, T. Hartung, A. Pfaltz, D. Muri, *Chem. Eur. J.* **2014**, *20*, 11496-11504.

[4] a) A. Burhop, R. Weck, J. Atzrodt, V. Derdau, *Eur. J. Org. Chem.* **2017**, *11*, 1418**–**1424; b) A. Burhop, R. Prohaska, R. Weck, J. Atzrodt, V. Derdau, *J. Label. Compd. Radiopharm.* **2017**, *60*, 343-348; c) M. Valero, A. Mishra, J. Blass, R. Weck, V. Derdau, ChemistryOpen **2019**, https://doi.org/10.1002/open.201900204

[5] a) K. Jess, V. Derdau, R. Weck, J. Atzrodt, M. Freytag, P.G. Jones, M. Tamm*, Adv. Synth. Catal*. **2017**, *359*, 629-638; b) M. Valero, A. Burhop, K. Jess, R. Weck, M. Tamm, J. Atzrodt, V. Derdau, *J. Label. Comp. Radiopharm.* **2018**, DOI: 10.1002/jlcr.3595. c) M. Valero, D. Becker, K. Jess, R. Weck, T. Bannenberg, J. Atzrodt, V. Derdau, M. Tamm, *Chem Eur. J.* **2019**, *25*, 6517-6522.

[6] R. Crabtree, *Acc. Chem. Res.* **1979**, *12*, 331-337.

[7] a) J.A. Brown, S. Irvine, A.R. Kennedy, W.J. Kerr, S. Andersson and G.N. Nilsson, *Chem. Commun.* **2008**, 1115-1117.

[8] a) W.J. Kerr, D.M. Lindsay, M. Reid, J. Atzrodt, V. Derdau, P. Rojahn, R. Weck, *Chem. Commun.* **2016**, *52*, 6669-6672; b) J. A. Brown, A. R. Cochrane, S. Irvine, W. J. Kerr, B. Mondal, J. A. Parkinson, L.C. Paterson, M. Reid, T. Tuttle, S. Andersson, G.N. Nilson, *Adv. Synth. Catal.* **2014**, *356*, 3551-3562; c) A.R. Cochrane, C. Idziak, W.J. Kerr, B. Mondal, L.C. Paterson, T. Tuttle, S. Andersson, G.N. Nilsson, *Org. Biomol. Chem.* **2014**, *12*, 3598-3603.

[9] a)J. Atzrodt, V. Derdau, W.J. Kerr, M. Reid, *Angew. Chem. Int. Ed.* **2018**, *57*, 1758-1784. b) J. Atzrodt, V. Derdau, W.J. Kerr, M. Reid*, Angew.Chem.* **2018**, *130*, 1774 -1802.

[10] https://njardarson.lab.arizona.edu/content/top-pharmaceuticals-poster; David T. Smith, Michael D. Delost, Haziq Qureshi, Jón T. Njarðarson *J. Chem. Ed.* **2010**, *87*, 1348; Poster information gathered by the Njardarson group with data from DrugTopics & Pharmacompass.

[11] Please note that there is no standard protocol to apply phenols, anilins or carboxylic acids in iridium catalyzed HIE reactions. Therefore these directing groups have been left out.

[12] a) Kennedy AR, Kerr WJ, Moir R, Reid M. *Org. Biomol. Chem.* **2014**; *12*: 7927-7931. b). Kerr WJ, Mudd RJ, Paterson LC, Brown JA. *Chem. Eur. J.* **2014**; *20*: 14604-14607. c) Kerr WJ, Mudd RJ, Owens PK, Reid M, Brown JA, Campos S. *J. Label. Compd. Radiopharm.* **2016**; *59*: 601-603. d) Kerr WJ, Lindsay DM, Owens PK, Reid M, Tuttle T, Campos S. *ACS Catal.* **2017**; *7*: 7182-7186.

[13] For an account on the synthetic relevance of competition experiments, see: K. D. Collins and F. Glorius, *Nature Chem*., **2013**, 5, 597.

[14] J. Atzrodt, V. Derdau, W. J. Kerr, M. Reid, P. Rojahn and R. Weck, *Tetrahedron* **2015**, *71*, 1924-1924.

[15] DFT calculation have been done by Dr. Stefan Güssregen. Details of the calculation method along with further calculation results can be found in the Supporting Information.

[16] A.R. Cochrane, C. Idziak, W.J. Kerr, B. Mondal, L.C. Paterson, T. Tuttle, S. Andersson, G.N. Nilsson, *Org. Biomol. Chem.* **2014**, *12*, 3598-3603.

[17] W.J. Kerr, M. Reid, T. Tuttle, *Angew. Chem. Int. Ed.* **2017**, *56*, 7808-7812.

[18] W.J. Kerr, M. Reid, T. Tuttle, *ACS Catal.* **2015**, *5*, 402-410.

[19] A.Y.L. Shu, W. Chen, J.R. Heys, *J. Organomet. Chem.* **1996**, *524*, 87-93.

[20] J. A. Brown, A. R. Cochrane, S. Irvine, W. J. Kerr, B. Mondal, J. A. Parkinson, L.C. Paterson, M. Reid, T. Tuttle, S. Andersson, G.N. Nilson, *Adv. Synth. Catal.* **2014**, *356*, 3551-3562.

[21] D. J. Abrams, P. A. Provencher, E. J. Sorensen, *Chem. Soc. Rev*. **2018**, *47*, 8925-8967.

[22] G. Wu, W. Ouyang, Q. Chen, Y. Huo, X. Li, *Org. Chem. Front*. **2019**, *6*, 284-289.

[23] J. He, L. G. Hamann, H. M. L. Davies, R. E. J. Beckwith, *Nat. Communications* **2015**, *6*, 5943

[24] a) B. R. Rosen, L. R. Simke, P. S. Thuy-Boun, D. D. Dixon, J. Q. Yu and P. S. Baran, *Angew. Chem., Int. Ed.* **2013**, *52*, 7317–7320; b) Y. Oh, Y. J. Jang, M. Jeon, H. S. Kim, J. H. Kwak, K. H. Chung, S. Pyo, Y. H. Jung and I. S. Kim, *J. Org. Chem*. **2017**, *82*, 11566–11572; c) K. Orito, A. Horibata, T. Nakamura, H. Ushito, H. Nagasaki, M. Yuguchi, S. Yamashita and M. Tokuda, *J. Am. Chem. Soc.* **2004**, *126*, 14342–14343.

[25] S. Qu, C.J. Cramer *J. Org Chem.* **2017**, *82*, 1195-1204.

[26] a) P. Shi, S. Li, L.-M. Hu, C. Wang, T.-P. Loh, X.-H. Hu *Chem. Commun.* **2019**, ***55***, 11115-11118; b) J. A. Leitch, C, G. Frost, *Chem. Soc. Rev.* **2017**, *46*, 7145-7153; c) R. Mei, C. Zhu, L. Ackermann *Chem. Commun.* **2016**, ***52***, 13171-13174.

[27] a) T.J. Struble, C.W. Coley, K.F. Jensen: Multitask Prediction of Site Selectivity in Aromatic C-H Functionalization Reactions. ChemRxiv. **2019** Preprint; b) K.A. Margrey, J.B. McManus, S. Bonazzi, F. Zecri, D. A. Nicewicz *J. Am. Chem. Soc.* **2017**,*139*, 32, 11288-11299.

Supporting information Part III – Chapter 2

Materials: see Annex 1

General deuteration procedure (Annex 1):

- **Method A (*table III.2.1*):** two competing substrates (0.2 mmol each, 1 eq.), catalyst $\mathbf{B_a}$ (10.0 µmol, 5 mol%, 0.05 eq.), DCM (6 mL), D_2 (1 atm), rt, 2 h. After 2 h the reaction was stopped, and the DCM was evaporated in vacuo. For substrates with overlapping ^{1}H-NMR spectra, the products were separated on a silica flash column with a gradient of pentane and MTBE. The products were analyzed by ^{1}H-NMR or LC/MS. Each competition reactions were run twice and are noted as 1) and 2).
- **Method B (*scheme III.2.4*):** substrate (10.0 mg, 1 eq.), catalyst $\mathbf{B_a}$ (5 mol%, 0.05 eq), DCM (3 mL), D_2 (1 atm), rt unless otherwise specified, 2 h. After 2 h the reaction was stopped, and the DCM was evaporated in vacuo. The products were analyzed by ^{1}H-NMR.

^{1}H-NMR spectra of the commercially available substrates used for the competition reactions

2-Phenylimidazole **2**

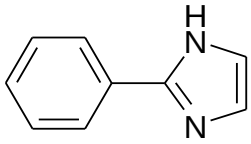

2

Molecular Weight =144,18
Molecular Formula =C9H8N2

^{1}H NMR (300 MHz, DMSO-d_6): δ 12.50 (s, 1H, N*H*), 7.92 (d, ^{3}J= 8.0 Hz, 2H, C*H*C($C_3N_2H_3$)C*H*), 7.43 (t, ^{3}J= 7.5 Hz, 2H, C*H*CHC*H*), 7.32 (t, ^{3}J= 7.5 Hz, 1H, CHC*H*CH), 7.12 (s, 2H, NHC*H*C*H*) ppm.

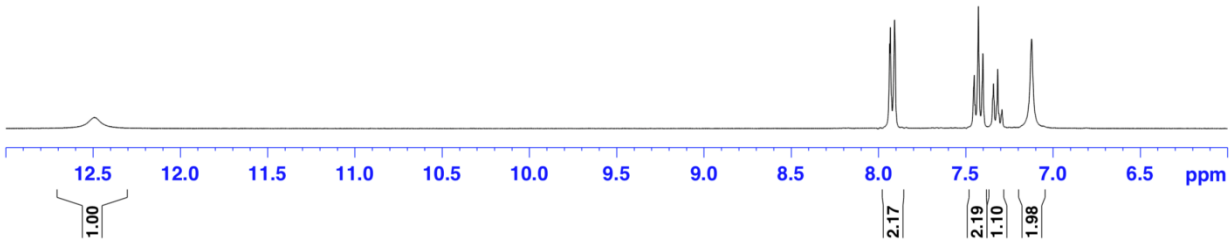

Acetanilide **3**

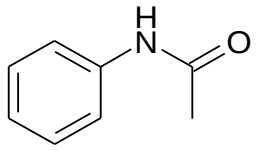

Molecular Weight =135,17
Molecular Formula =C8H9NO

3

^{1}H NMR (300 MHz, DMSO-d_6): δ 9.91(s, 1H, N*H*), 7.56 (d, ^{3}J= 8.3 Hz, 2H, C*H*C(NHCOCH$_3$)C*H*), 7.27 (t, ^{3}J= 7.8 Hz, 2H, C*H*CHC*H*), 7.01 (t, ^{3}J= 7.4 Hz, 1H, CHC*H*CH), 2.03 (s, 3H, C*H*$_3$) ppm.

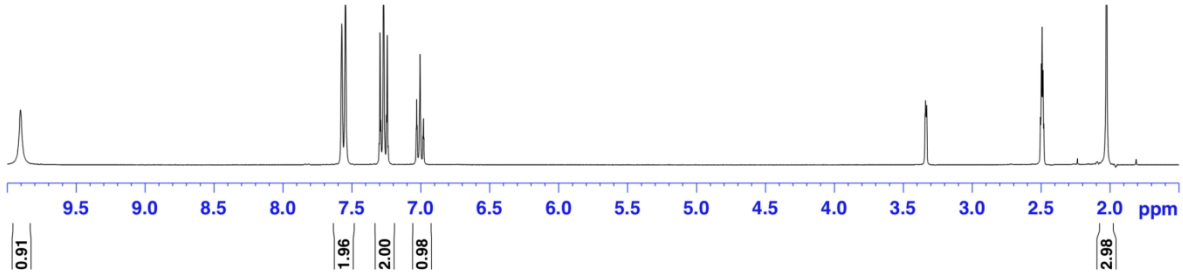

4-Acetylbiphenyl **4**

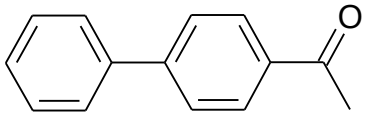

Molecular Weight =196,25
Molecular Formula =C14H12O

4

^{1}H NMR (300 MHz, DMSO-d_6): δ 8.05 (d, ^{3}J= 8.5 Hz, 2H, C*H*C(COCH$_3$)C*H*), 7.83 (d, ^{3}J= 8.5 Hz, 2H, C*H*C(C$_6$H$_5$)C*H*), 7.75 (d, ^{3}J= 8.5 Hz, 2H, C*H*C$_3$H$_3$C*H*), 7,48 (sex, ^{3}J= 7.5 Hz, 3H, CHC$_3$*H*$_3$CH), 2.63 (s, 1H, C*H*$_3$) ppm.

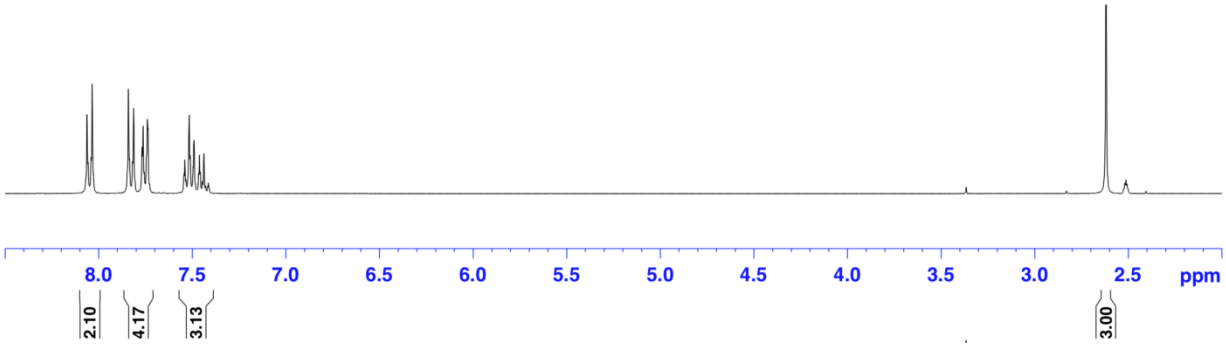

Nitrobenzene **5**

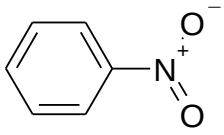

5

Molecular Weight =123,11
Molecular Formula =C6H5NO2

^{1}H NMR (300 MHz, DMSO-d_6): δ 8.21 (d, ^{3}J= 8.0 Hz, 2H, C*H*C(NO_2)C*H*), 7.83 (t, ^{3}J= 7.5 Hz, 1H, C_2H_2C*H*C_2H_2), 7,66 (t, ^{3}J= 7.5 Hz, 2H, C*H*CHC*H*) ppm.

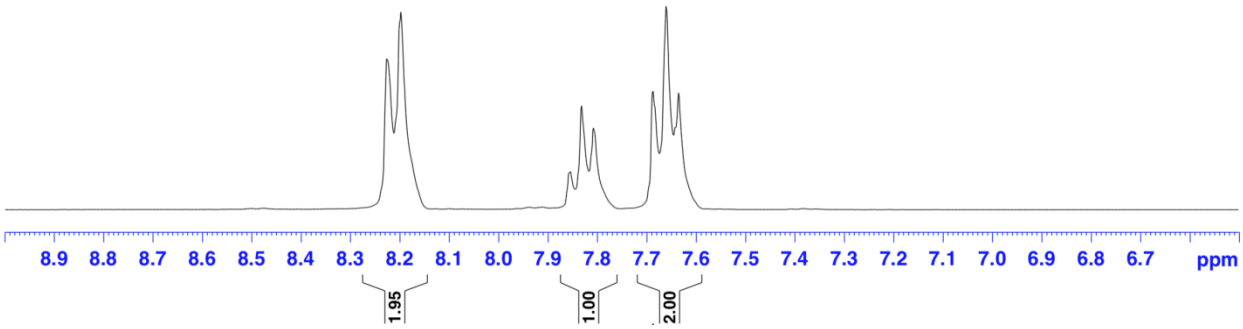

N,N-diethyl benzamide **6**

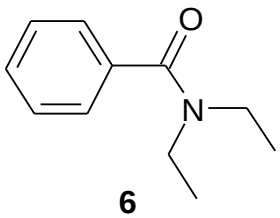

6

Molecular Weight =177,25
Molecular Formula =C11H15NO

^{1}H NMR (300 MHz, DMSO-d_6): δ 7.45-7.39 (m, 3H, CHC_3*H*$_3$CH), 7.35-.7.29 (m, 2H, C*H*C_3H_3C*H*), 3.51-3.02 (br d, ^{3}J= 75 Hz, 4H, N(C*H*$_2$$CH_3$)$_2$), 1.21-0.96 (br d, ^{3}J= 21.5 Hz, 6H, N(CH_2C*H*$_3$)$_2$) ppm.

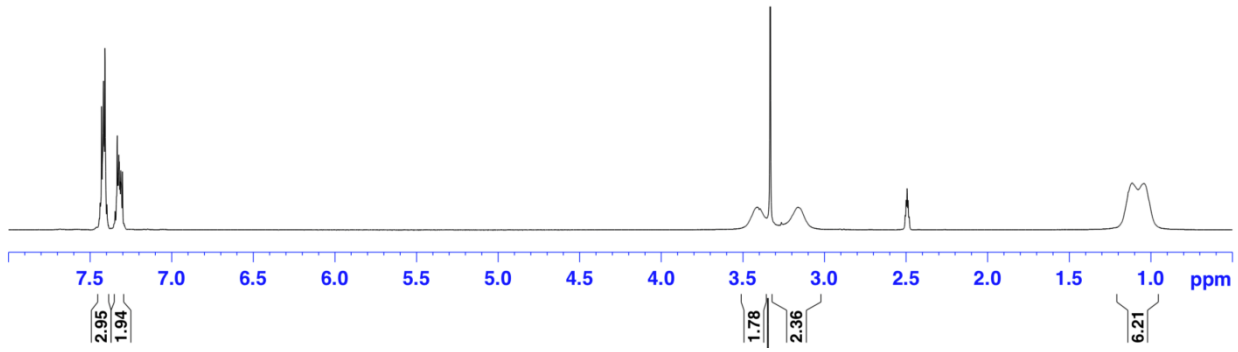

Benzaldehyde **7**

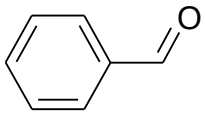

7

Molecular Weight =106,13
Molecular Formula =C7H6O

^{1}H NMR (300 MHz, DMSO-d_6): δ 10.01 (s, 1H, C*H*O), 7.91 (d, ^{3}J= 7.5 Hz, 2H, C*H*C(CHO)C*H*), 7.71 (t, ^{3}J= 7.5 Hz, 1H, $C_2H_2CHC_2H_2$), 7.60 (t, ^{3}J= 7.5 Hz, 2H, CHC*H*CHC*H*CH) ppm.

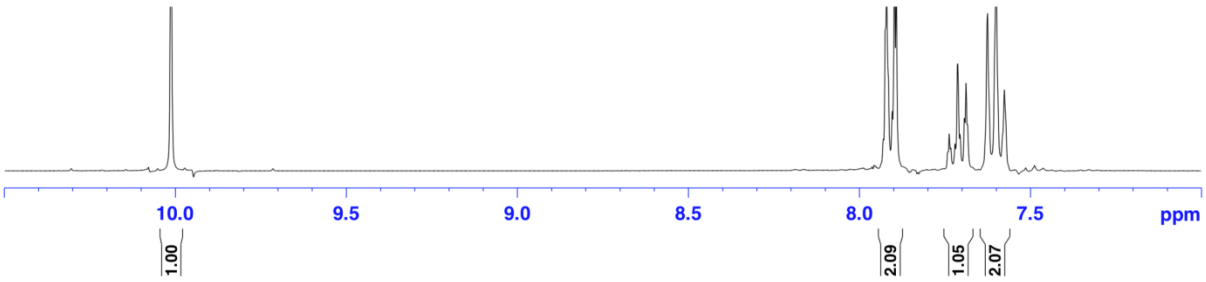

Methyl-Benzoate **8**

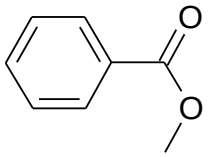

8

Molecular Weight =136,15
Molecular Formula =C8H8O2

^{1}H NMR (300 MHz, DMSO-d_6): δ 7.96 (d, ^{3}J= 8.0 Hz, 2H, C*H*C($C_2O_2H_3$)C*H*), 7.66 (t, ^{3}J= 7.5 Hz, 1H, $C_2H_2CHC_2H_2$), 7.52 (t, ^{3}J= 7.5 Hz, 2H, CHC*H*CHC*H*CH), 3.82 (s, 3H, CH_3) ppm.

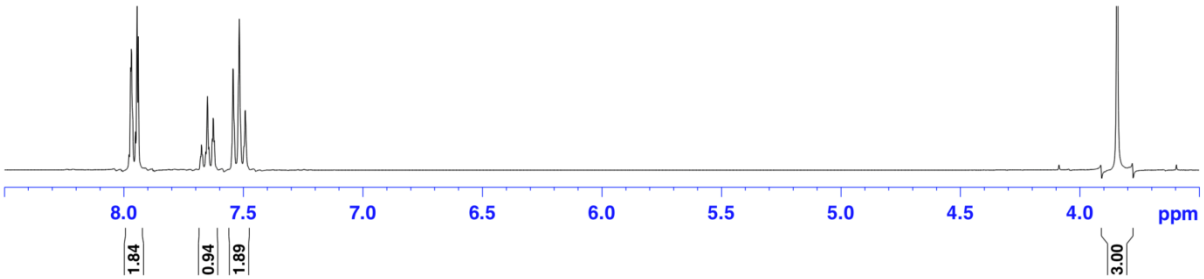

Phenyl-Acetate **9**

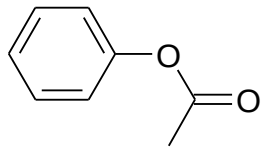

9

Molecular Weight =136,15
Molecular Formula =C8H8O2

^{1}H NMR (300 MHz, DMSO-d_6): δ 7.41 (t, ^{3}J= 8.0 Hz, 2H, CHC*H*CHC*H*CH), 7.25 (t, ^{3}J= 7.5 Hz, 1H, $C_2H_2CHC_2H_2$), 7.12 (d, ^{3}J= 8.5 Hz, 2H, C*H*C($C_2O_2H_3$)C*H*), 2.26 (s, 3H, CH_3) ppm.

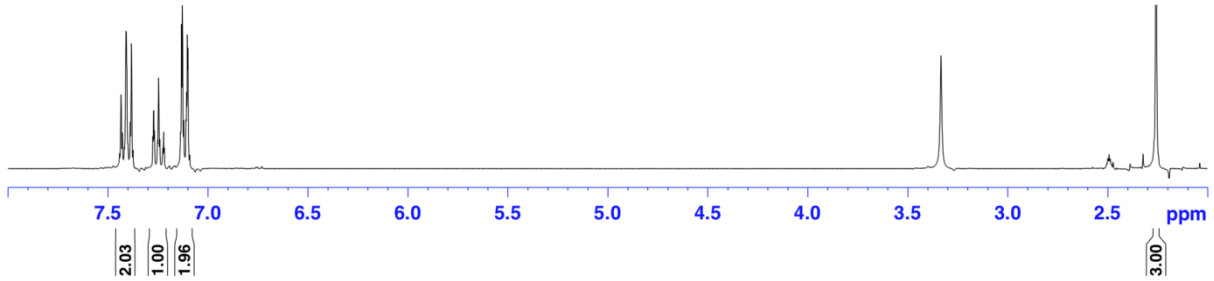

p-Toluenesulfonamide **10**

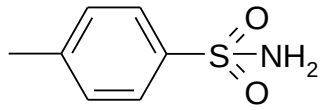

10

Molecular Weight =171,22
Molecular Formula =C7H9NO2S

^{1}H NMR (300 MHz, DMSO-d_6): δ 7.72 (d, ^{3}J= 8.2 Hz, 2H), 7.36 (d, ^{3}J= 8.2 Hz, 2H), 7.28 (s, 2H), 2.36 (s, 3H) ppm.

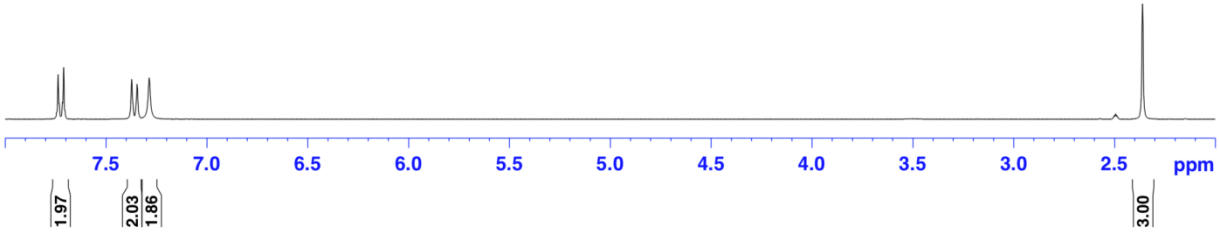

Competition reactions (*table III.2.1*)

Compounds **2**+**6**:

Method A: 29 mg, 200 µmol **2**, 36 mg, 200 µmol **8**, 10.1 mg, 10 µmol catalyst $\mathbf{B_a}$.

2: Incorporation expected at δ 7.92 ppm (red arrow). Determined against reference-integral at δ 12.50 ppm (blue arrow).

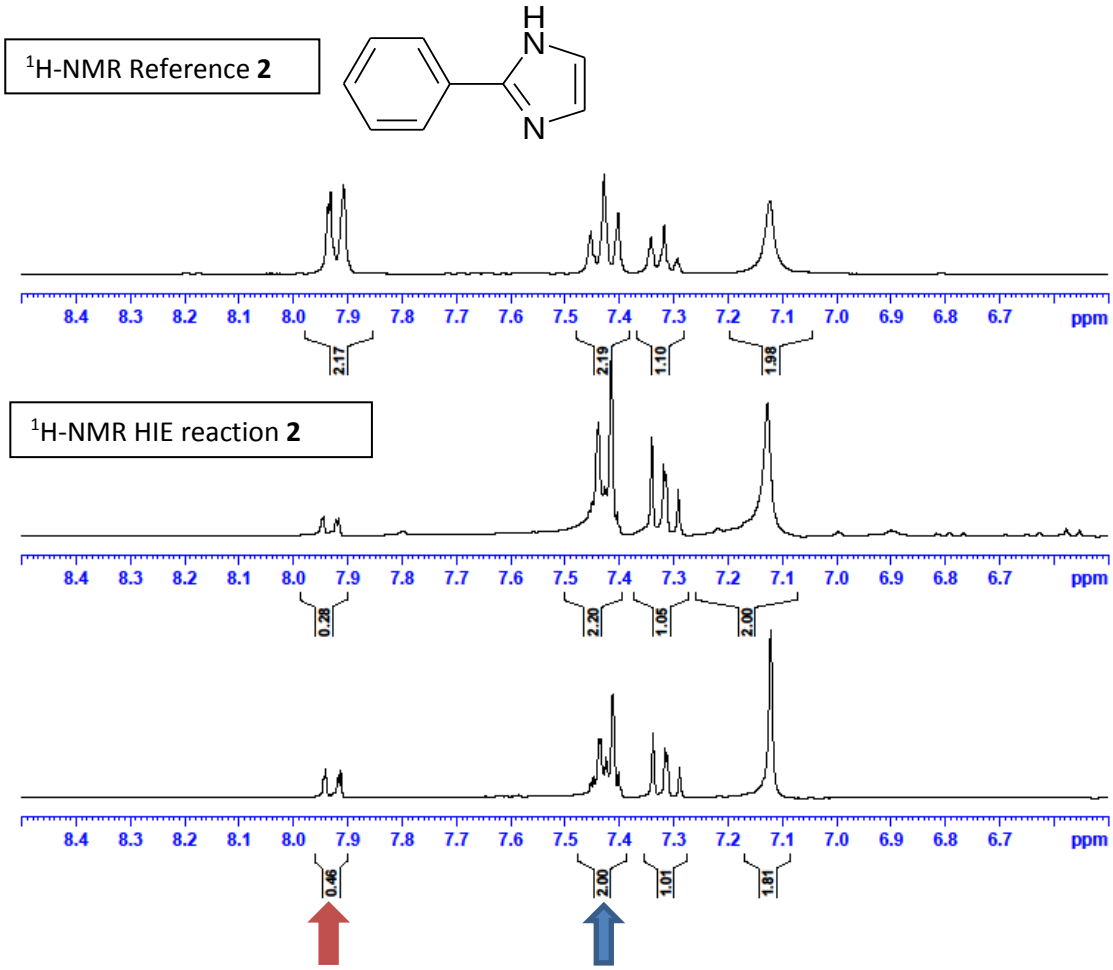

6: Incorporation expected at δ 7.45-7.39 ppm (red arrow). Determined against reference-integral at δ 7.35-7.29 ppm (blue arrow).

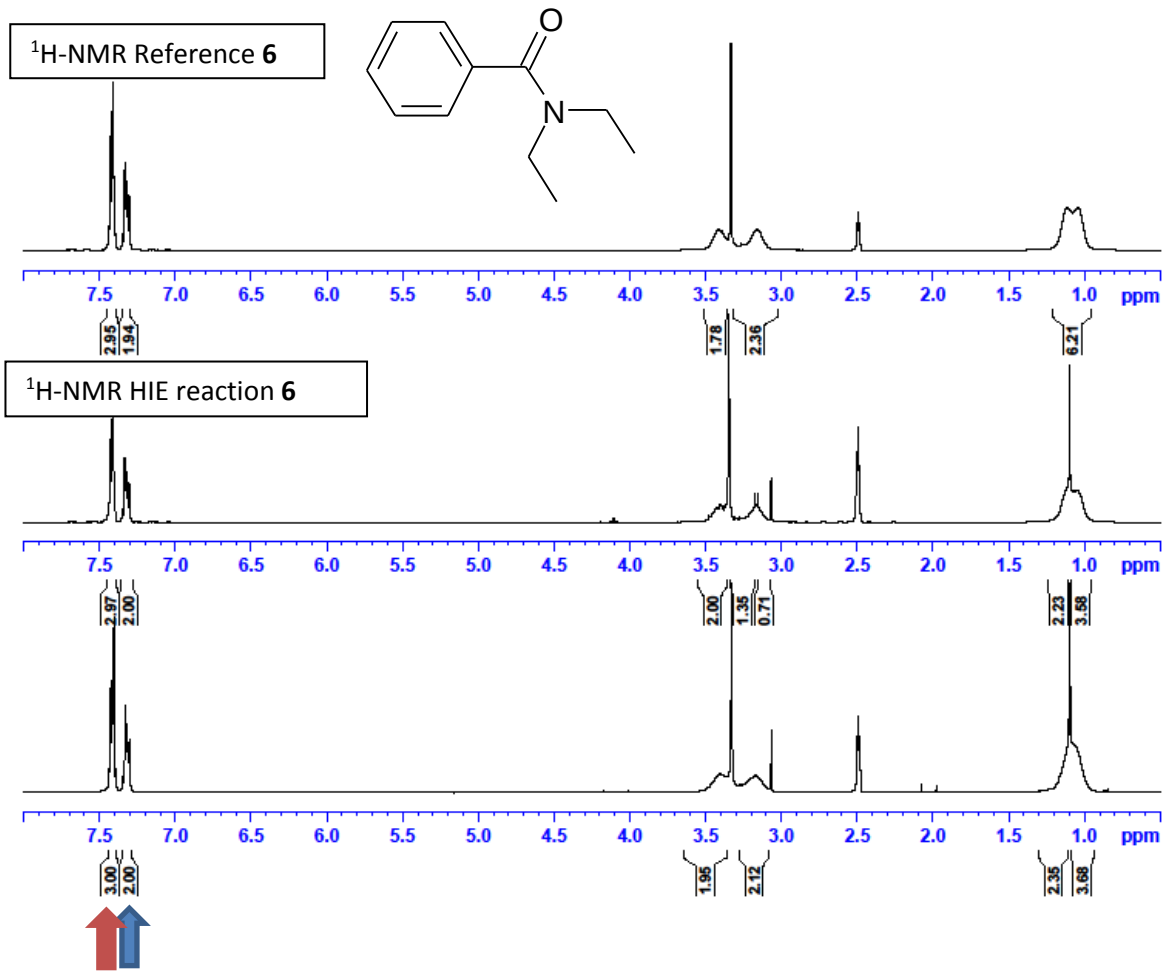

Result: 1) 86% D for compound **2**, 1% D for compound **6**.
2) 78% D for compound **2**, 0% D for compound **6**.

Average: 82% D for **2**, 0% D for **6**.

Compounds **2**+**8**:

Method A: 29 mg, 200 µmol **2**, 27 mg, 200 µmol **8**, 10.1 mg, 10 µmol catalyst $\mathbf{B_a}$

2: Incorporation expected at δ 7.92 ppm (red arrow). Determined against reference-integral at δ 12.50 ppm (blue arrow).

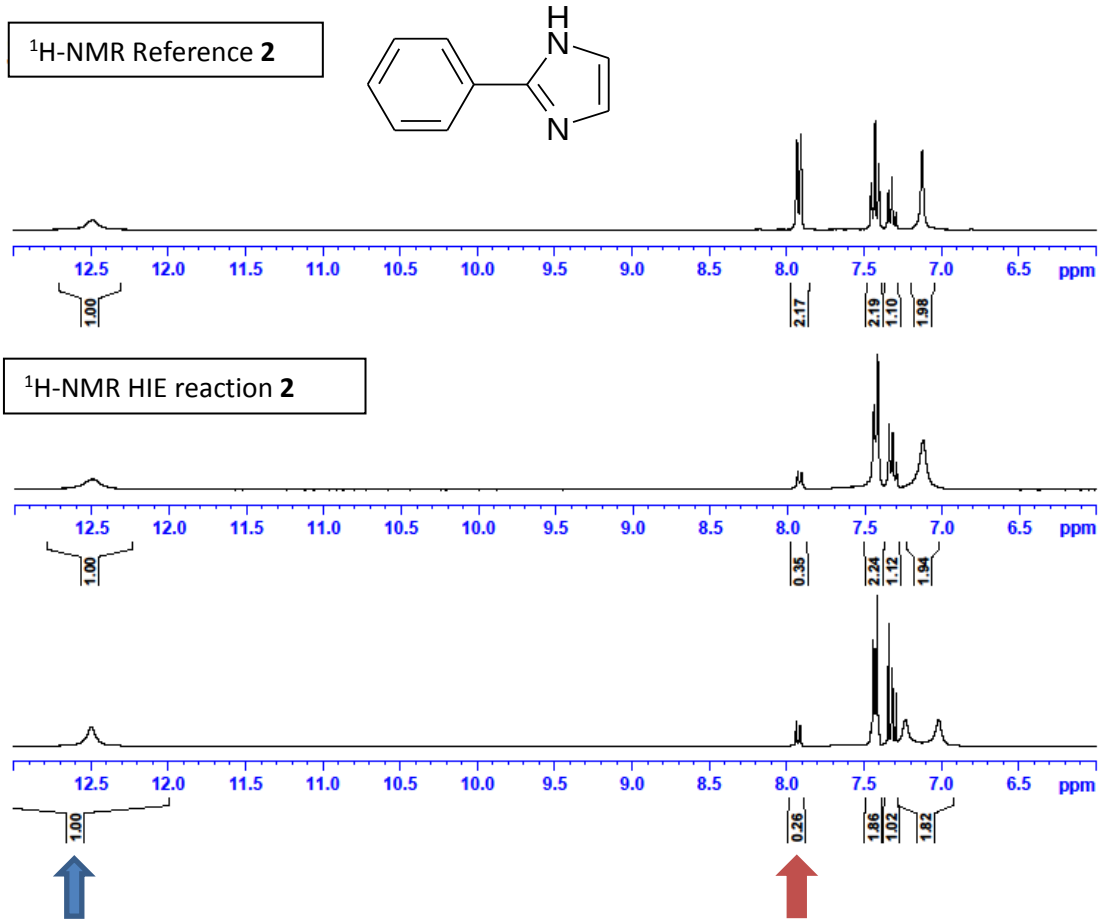

8: Incorporation expected at δ 7.96 ppm (red arrow). Determined against reference-integral at δ 3.82 ppm (blue arrow).

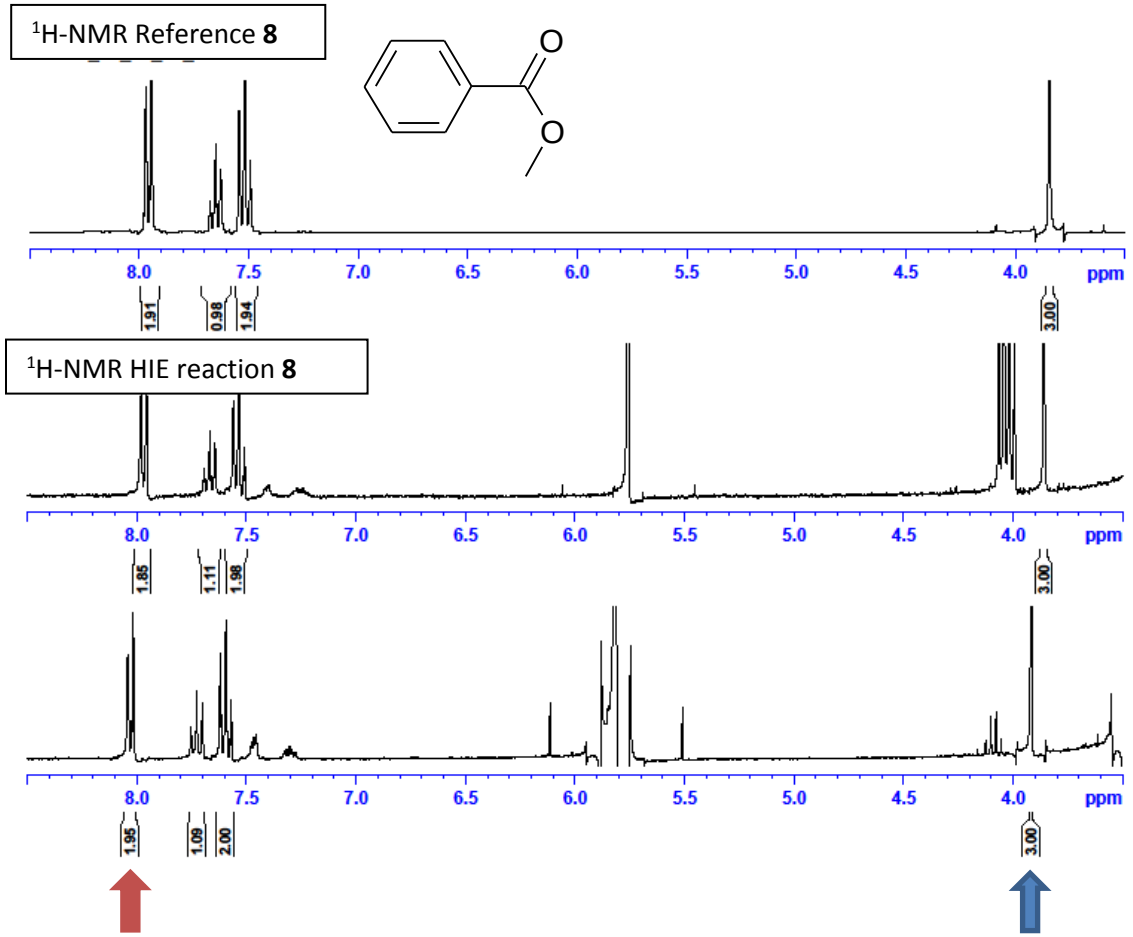

Result: 1) 83% D for compound **2**, 8% D for compound **8**.
2) 87% D for compound **2**, 3% D for compound **8**.

Average: 85% D for **2**, 5% D for **8**.

Compounds **4**+**3**

Method A: 39 mg, 200 µmol **4**, 27 mg, 200 µmol **3**, 10.1 mg, 10 µmol catalyst $\mathbf{B_a}$.

4:

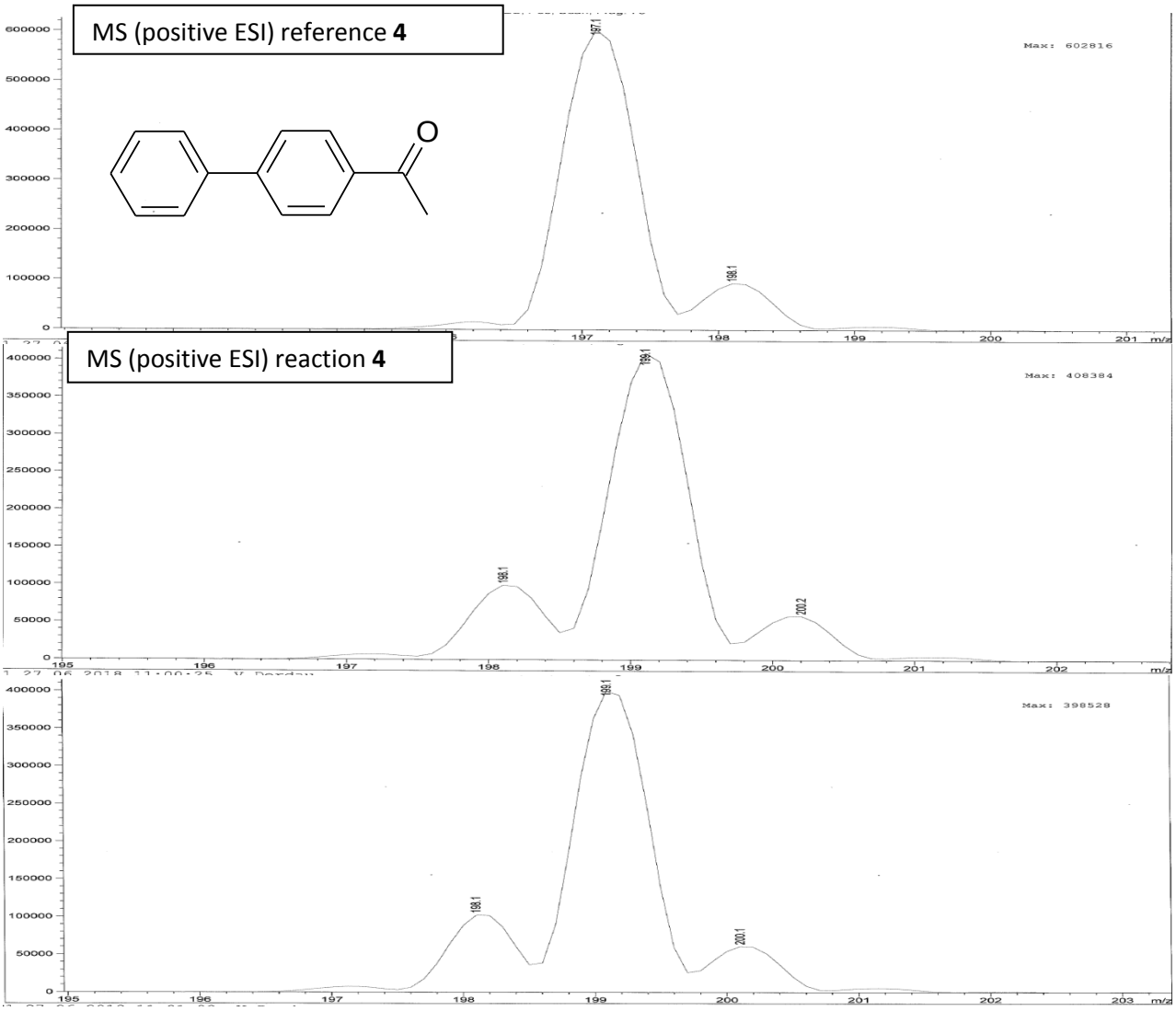

MS (positive ESI): Reference: m/z = 197.1 ($M+H^+$) (127), 198.1 ($M+H^+$+1 Natural isotope). (20). 14% natural isotope M+1.

Result: 1) 197.1 ($M+H^+$) (2), 198.1 ($M+H^+$+D_1) (32), 199.1 ($M+H^+$+D_2) (130), 200.1 ($M+H^+$+D_3) (19). Calculated & normalized: 89% D
2) 197.1 ($M+H^+$) (2), 198.1 ($M+H^+$+D_1) (33), 199.1 ($M+H^+$+D_2) (127), 200.1 ($M+H^+$+D_3) (19). Calculated & normalized: 89% D

3:

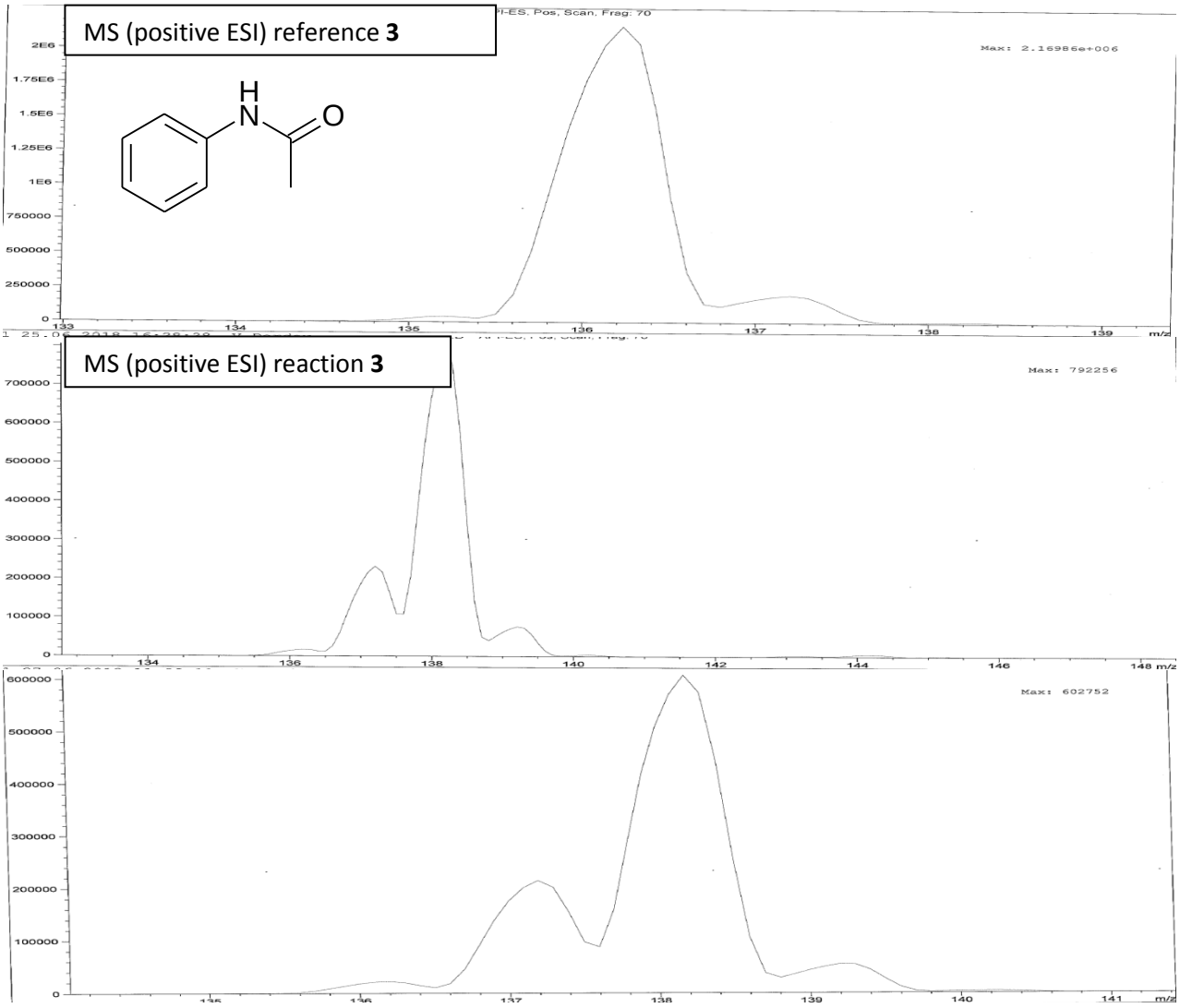

MS (positive ESI): Reference: m/z = 136.2 ($M+H^+$) (129), 137.2 ($M+H^+$+1 Natural isotope). (12). 9% natural isotope M+1.

Result: 1) 136.2 ($M+H^+$) (3), 137.2 ($M+H^+$+D_1) (38), 138.2 ($M+H^+$+D_2) (130), 139.2 ($M+H^+$+D_3) (13). Calculated & normalized: 88% D
2) 136.2 ($M+H^+$) (5), 137.2 ($M+H^+$+D_1) (46), 138.2 ($M+H^+$+D_2) (128), 139.2 ($M+H^+$+D_3) (12). Calculated & normalized: 87% D

Average:
89% D for **4**,
87% D for **3**.

Compounds **4**+**3**

Method A (0 °C): 39 mg, 200 µmol **4**, 27 mg, 200 µmol **3**, 10.1 mg, 10 µmol catalyst $\mathbf{B_a}$.

4:

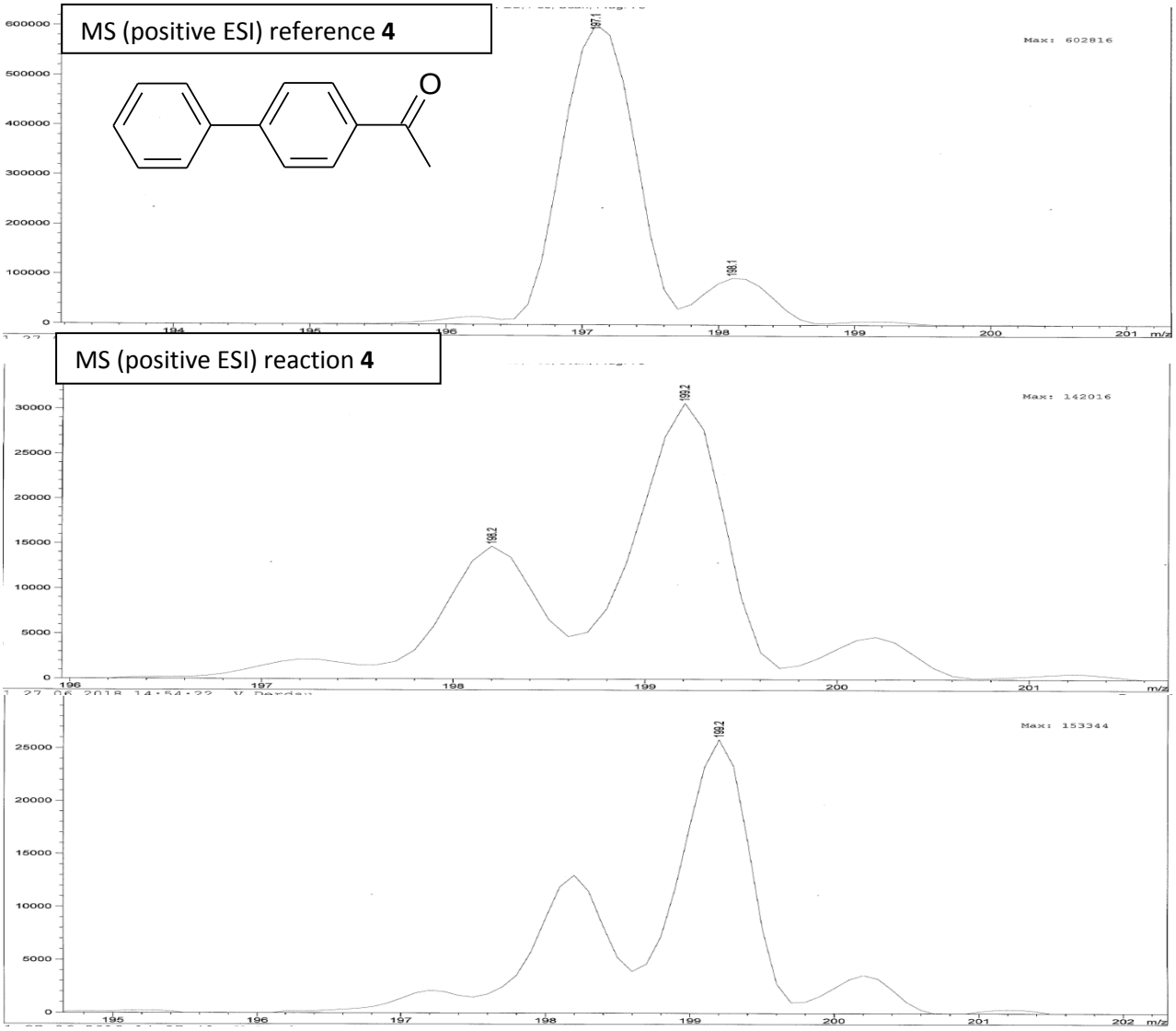

MS (positive ESI): Reference: m/z = 197.1 ($M+H^+$) (127), 198.1 ($M+H^+$+1 Natural isotope). (20). 14% natural isotope M+1.

Result: 1) 197.1 ($M+H^+$) (8), 198.1 ($M+H^+$+D_1) (56), 199.1 ($M+H^+$+D_2) (117), 200.1 ($M+H^+$+D_3) (18). Calculated & normalized: 79% D
2) 197.1 ($M+H^+$) (9), 198.1 ($M+H^+$+D_1) (58), 199.1 ($M+H^+$+D_2) (115), 200.1 ($M+H^+$+D_3) (16). Calculated & normalized: 79% D

3:

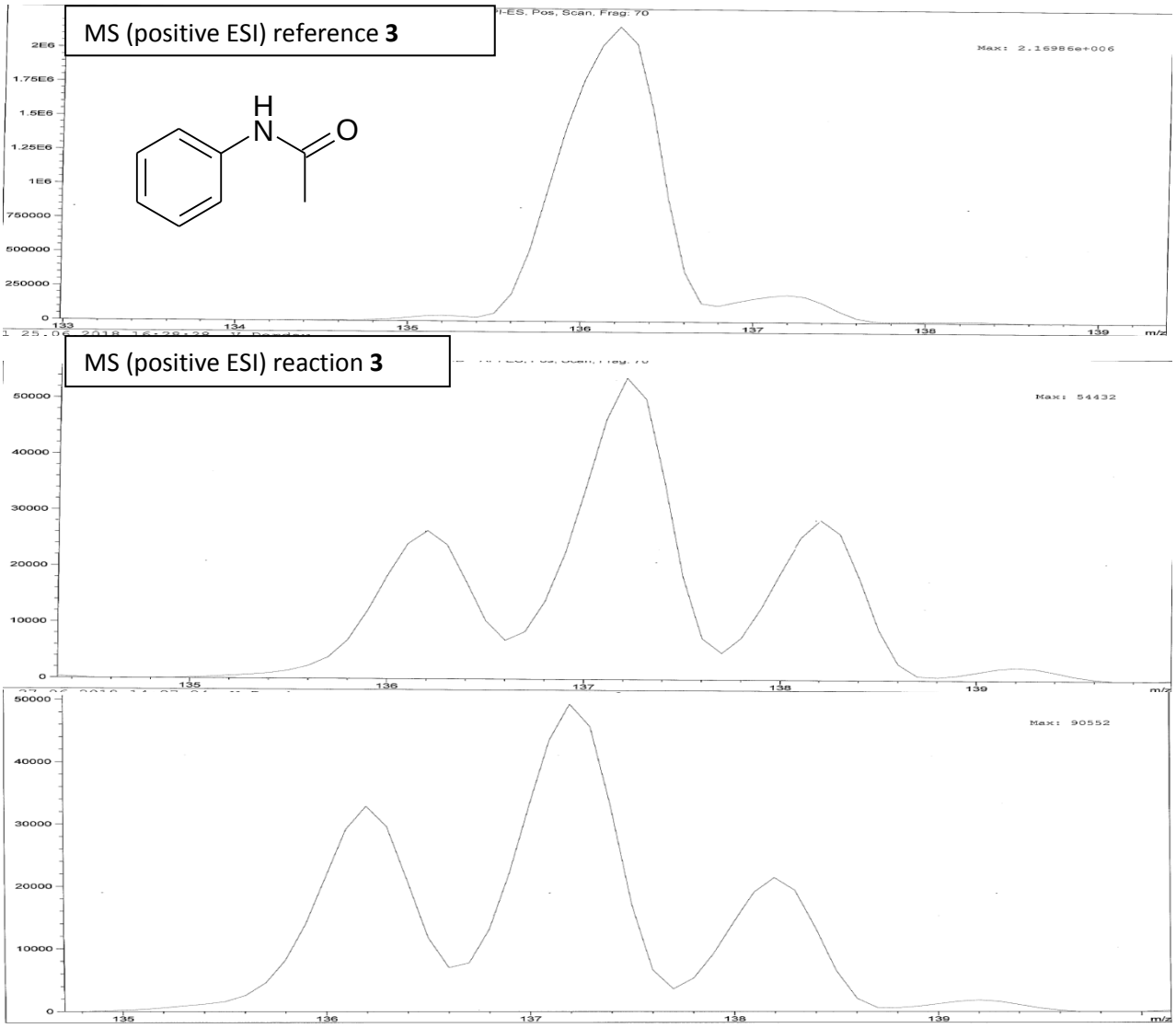

MS (positive ESI): Reference: m/z = 136.2 ($M+H^+$) (129), 137.2 ($M+H^+$+1 Natural isotope). (12). 9% natural isotope M+1.

Result: 1) 136.2 ($M+H^+$) (62), 137.2 ($M+H^+$+D_1) (127), 138.2 ($M+H^+$+D_2) (67), 139.2 ($M+H^+$+D_3) (5). Calculated & normalized: 63% D
2) 136.2 ($M+H^+$) (86), 137.2 ($M+H^+$+D_1) (129), 138.2 ($M+H^+$+D_2) (56), 139.2 ($M+H^+$+D_3) (5). Calculated & normalized: 58% D

Average:
79% D for **4**,
60% D for **3**.

Compounds **4**+**10**:

Method A: 39 mg, 200 µmol **4**, 34 mg, 200 µmol **10**, 10.1 mg, 10 µmol catalyst $\mathbf{B_a}$.

4: Incorporation expected at δ 8.05 ppm (red arrow). Determined against reference-integral at δ 2.63 ppm (blue arrow).

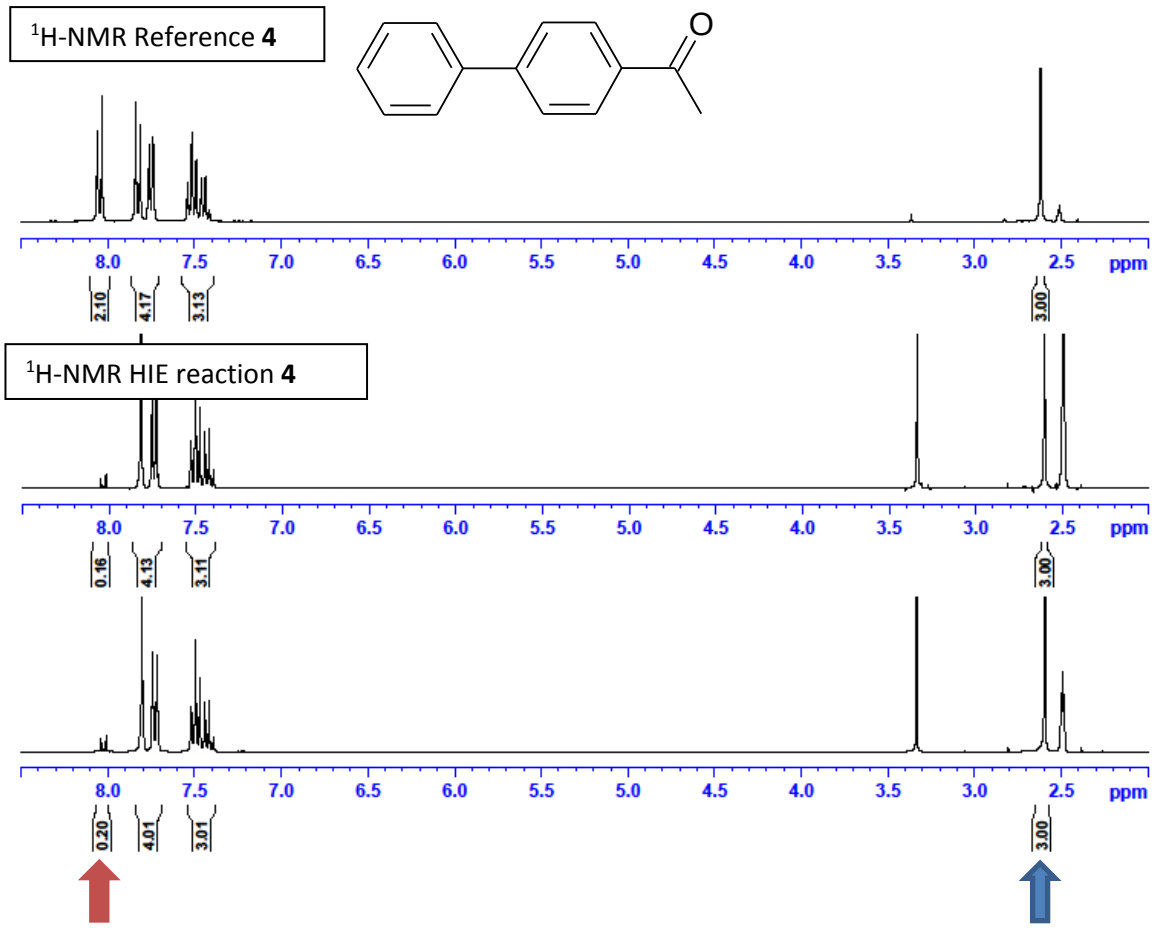

10: Incorporation expected at δ 7.72 ppm (red arrow). Determined against reference-integral at δ 2.36 ppm (blue arrow).

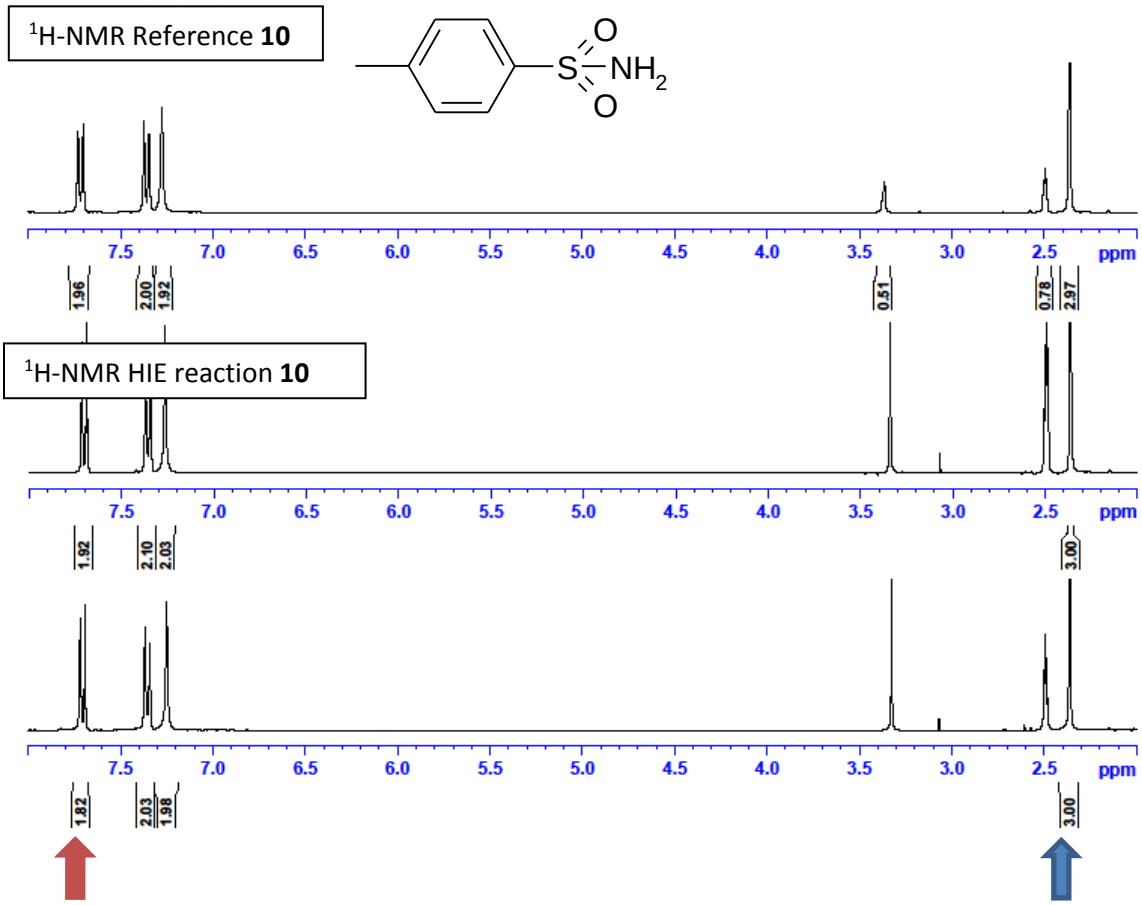

Result: 1) 92% D for compound **4**, 4% D for compound **10**.
2) 90% D for compound **4**, 9% D for compound **10**.

Average:
91% D for **4**,
7% D for **10**.

Compounds **3**+**5**:

Method A: 27 mg, 200 µmol **3**, 25 mg, 200 µmol **5**, 10.1 mg, 10 µmol catalyst $\mathbf{B_a}$. N.B.: These reactions were not separated before NMR analysis, since the respective spectra of the compounds do not overlap.

3: Incorporation expected at δ 7.56 ppm (red arrow). Determined against reference-integral at δ 2.03 ppm (blue arrow).

.

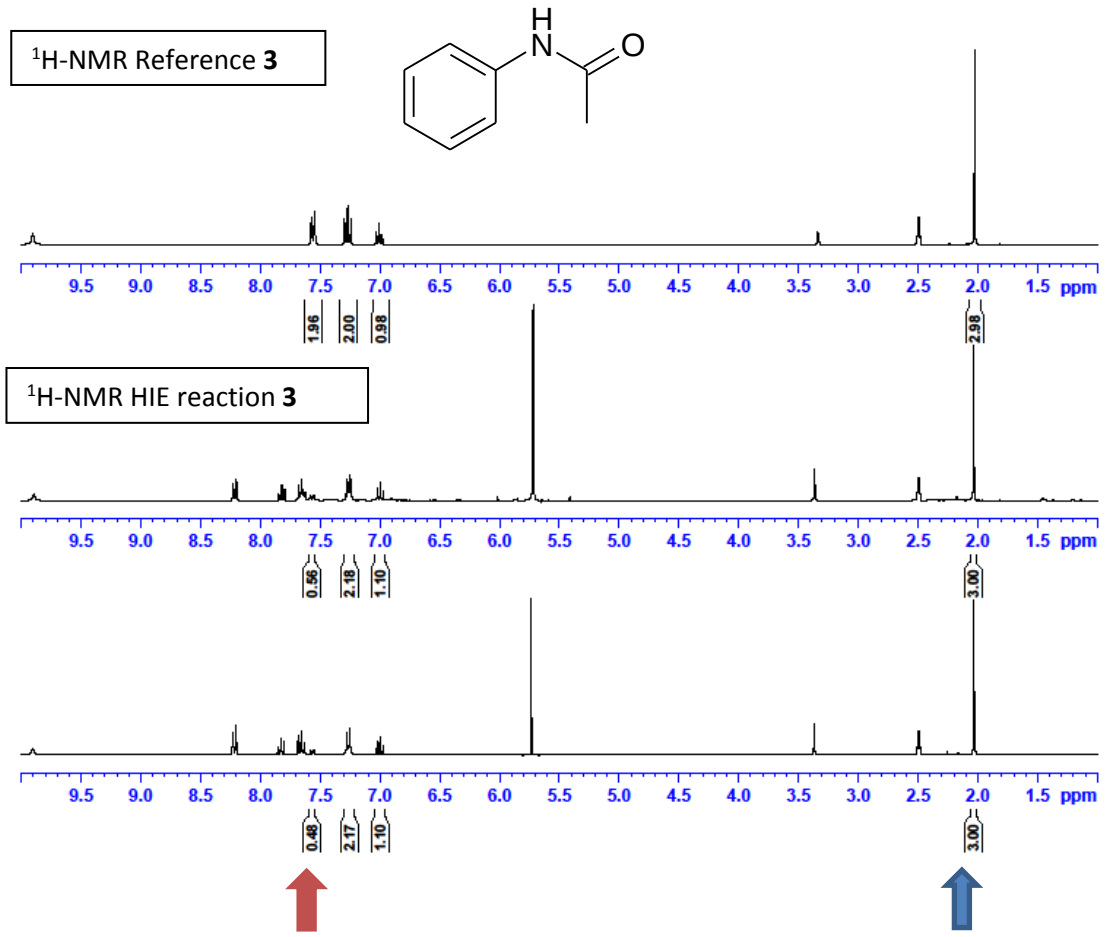

5: Incorporation expected at δ 8.21 ppm (red arrow). Determined against reference-integral at δ 7.66 ppm (blue arrow).

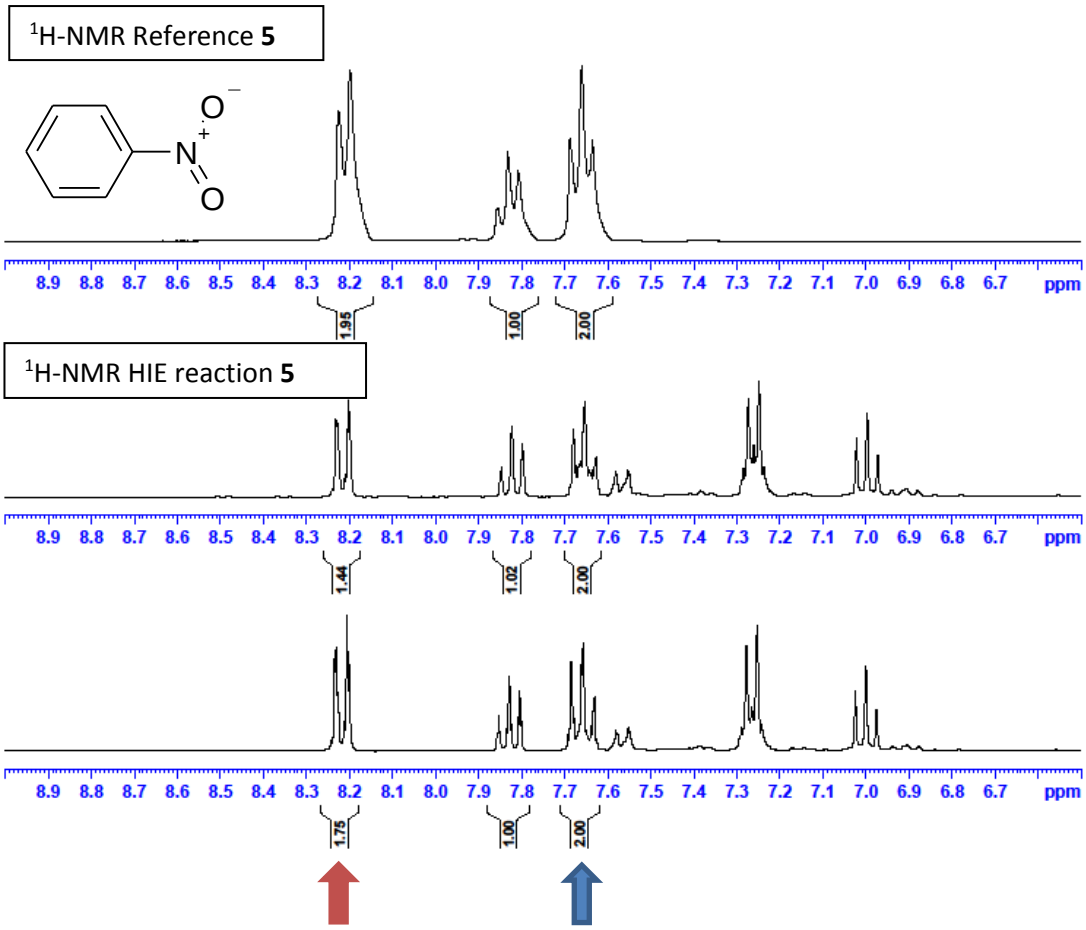

Result: 1) 72% D for compound **3**, 28% D for compound **5**.
2) 76% D for compound **3**, 13% D for compound **5**

Average:
73% D for **3**,
21% D for **5**.

Compounds **4**+**6**:

Method A: 27 mg, 200 µmol **3**, 36 mg, 200 µmol **6**, 10.1 mg, 10 µmol catalyst $\mathbf{B_a}$.

3:

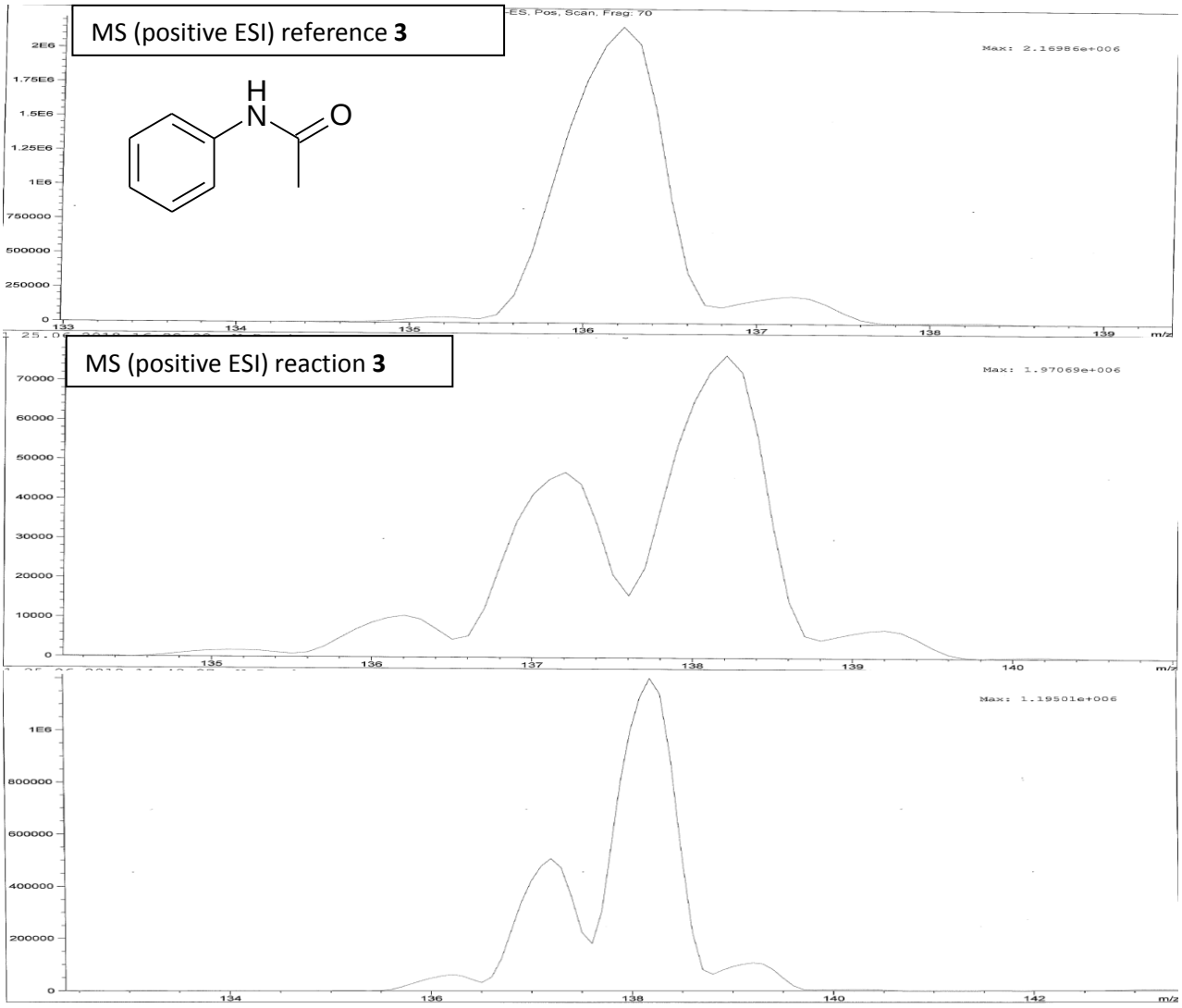

MS (positive ESI): Reference: m/z = 136.2 ($M+H^+$) (129), 137.2 ($M+H^+$+1 Natural isotope). (12). 9% natural isotope M+1.

Result: 1) 136.2 ($M+H^+$) (17), 137.2 ($M+H^+$+D_1) (77), 138.2 ($M+H^+$+D_2) (126), 139.2 ($M+H^+$+D_3) (12). Calculated & normalized: 73% D
2) 136.2 ($M+H^+$) (7), 137.2 ($M+H^+$+D_1) (55), 138.2 ($M+H^+$+D_2) (130), 139.2 ($M+H^+$+D_3) (12). Calculated & normalized: 82% D

6:

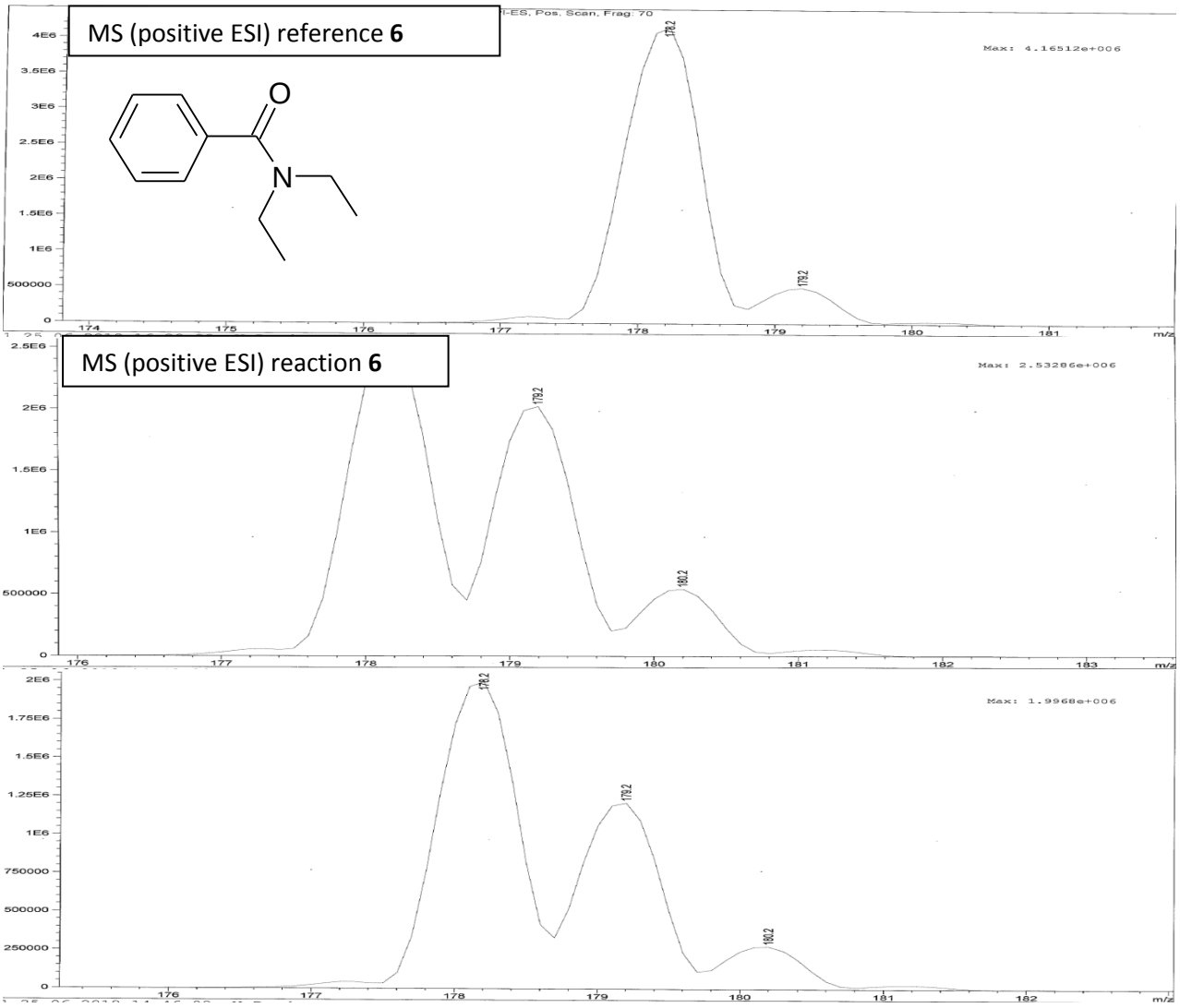

MS (positive ESI): Reference: m/z = 178.2 ($M+H^+$) (129), 179.2 ($M+H^+$+1 Natural isotope). (15). 10% natural isotope M+1.

Result: 1) 178.2 ($M+H^+$) (130), 179.2 ($M+H^+$+D_1) (104), 180.2 ($M+H^+$+D_2) (28).
Calculated & normalized: 26% D
2) 178.2 ($M+H^+$) (128), 179.2 ($M+H^+$+D_1) (78), 180.2 ($M+H^+$+D_2) (18).
Calculated & normalized: 21% D

Average:
78% D for **3**,
24% D for **6**.

Compounds **3**+**9**:

Method A: 27 mg, 200 µmol **3**, 27 mg, 200 µmol **9**, 10.1 mg, 10 µmol catalyst $\mathbf{B_a}$.

3: Incorporation expected at δ 7.56 ppm (red arrow). Determined against reference-integral at δ 2.03 ppm (blue arrow).

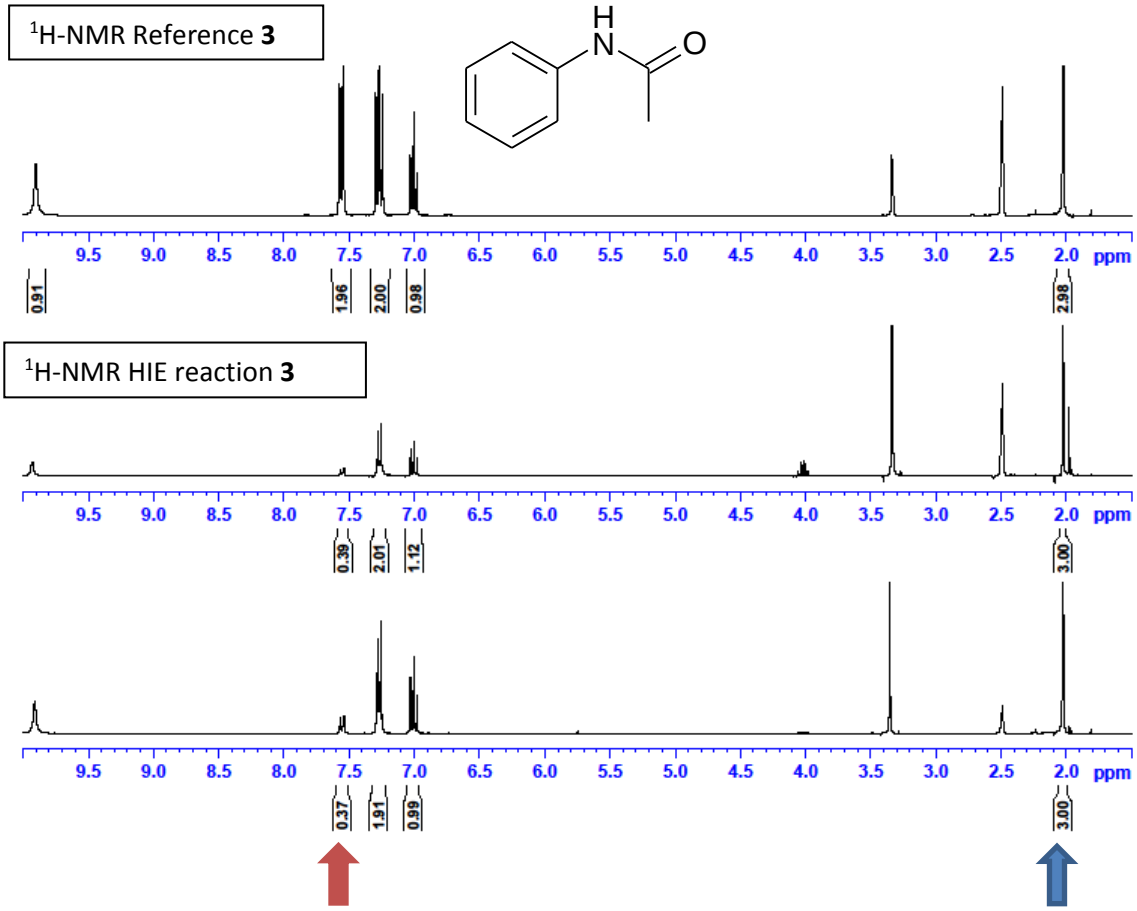

9: Incorporation expected at δ 7.12 ppm (red arrow). Determined against reference-integral at δ 2.26 ppm (blue arrow).

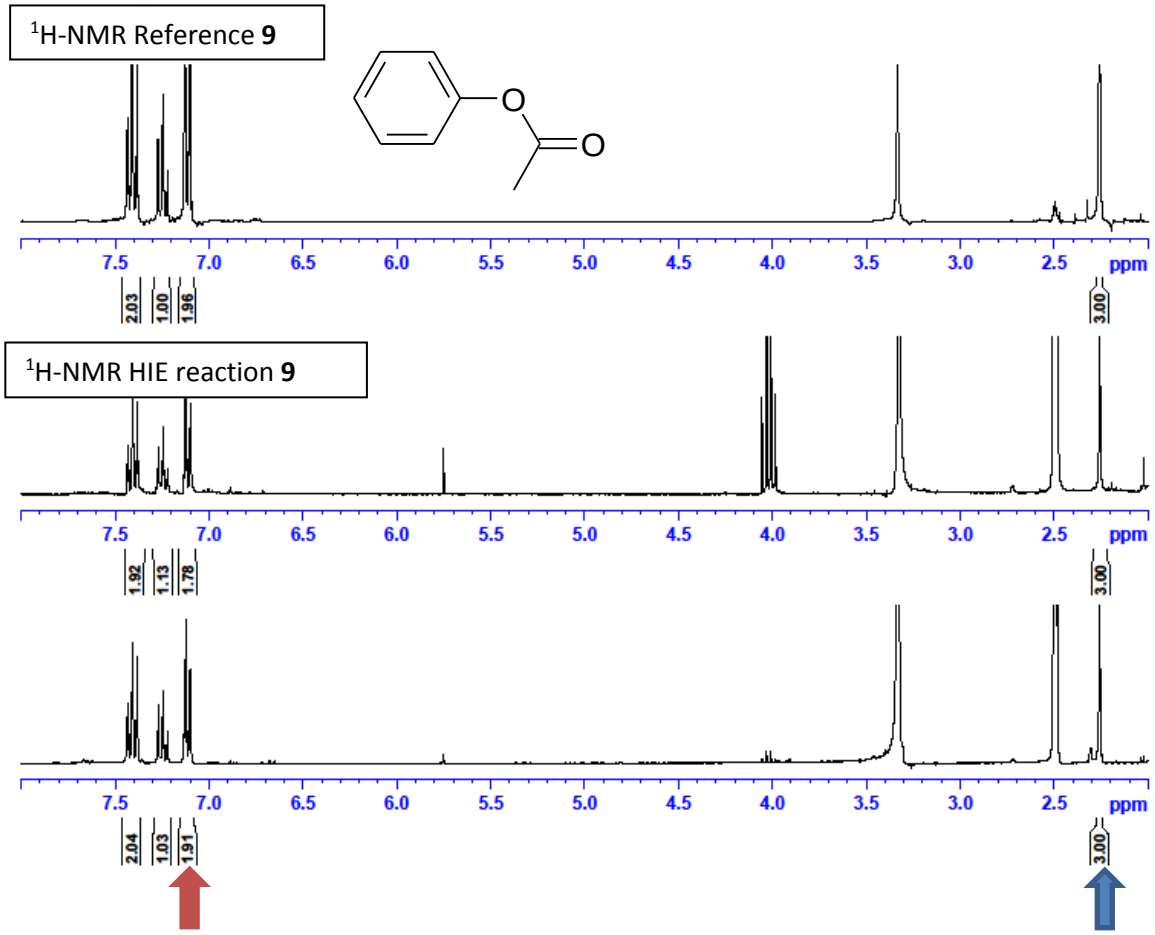

Result: 1) 81% D for compound **3**, 11% D for compound **9**.
2) 82% D for compound **3**, 5% D for compound **9**.

Average:
81% D for **3**,
8% D for **9**.

Compounds **3**+**10**:

Method A: 27 mg, 200 µmol **3**,34 mg, 200 µmol **10**, 10.1 mg, 10 µmol catalyst $\mathbf{B_a}$.

3: Incorporation expected at δ 7.56 ppm (red arrow). Determined against reference-integral at δ 2.03 ppm (blue arrow).

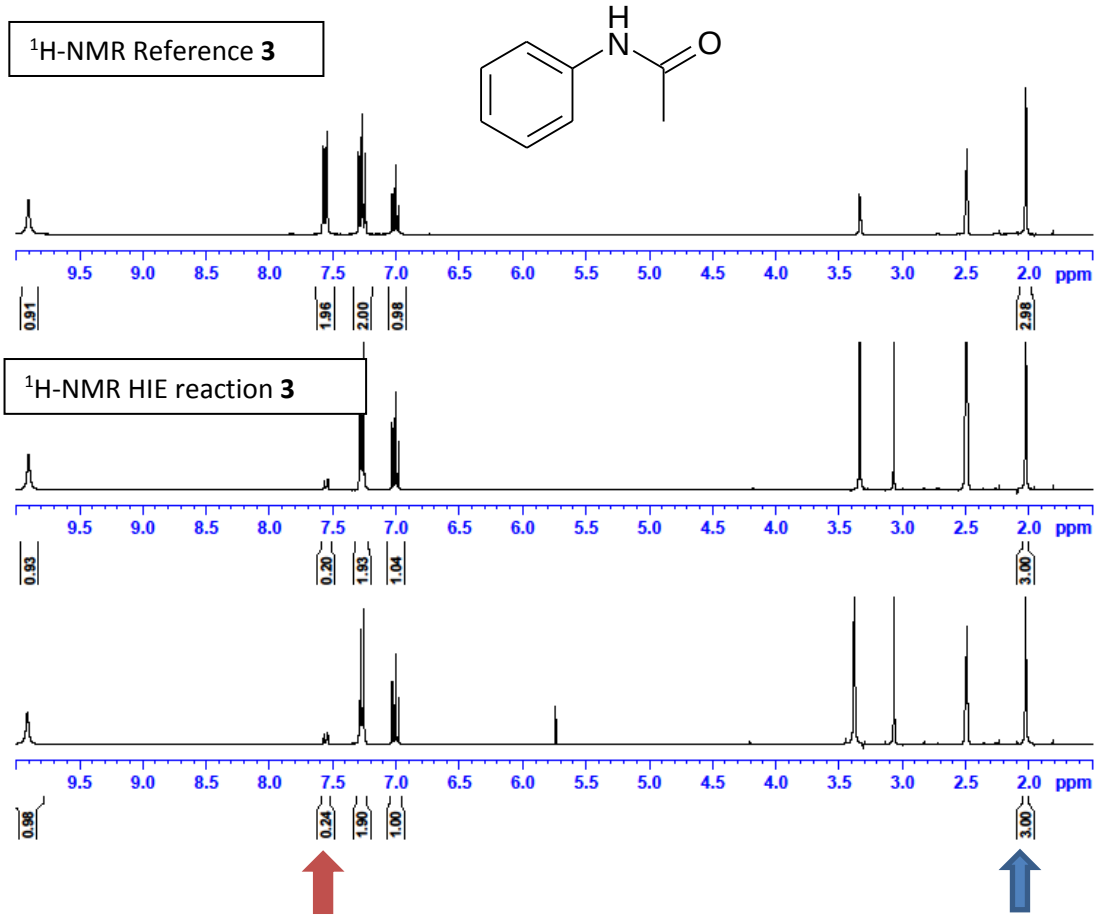

10: Incorporation expected at δ 7.72 ppm (red arrow). Determined against reference-integral at δ 2.36 ppm (blue arrow).

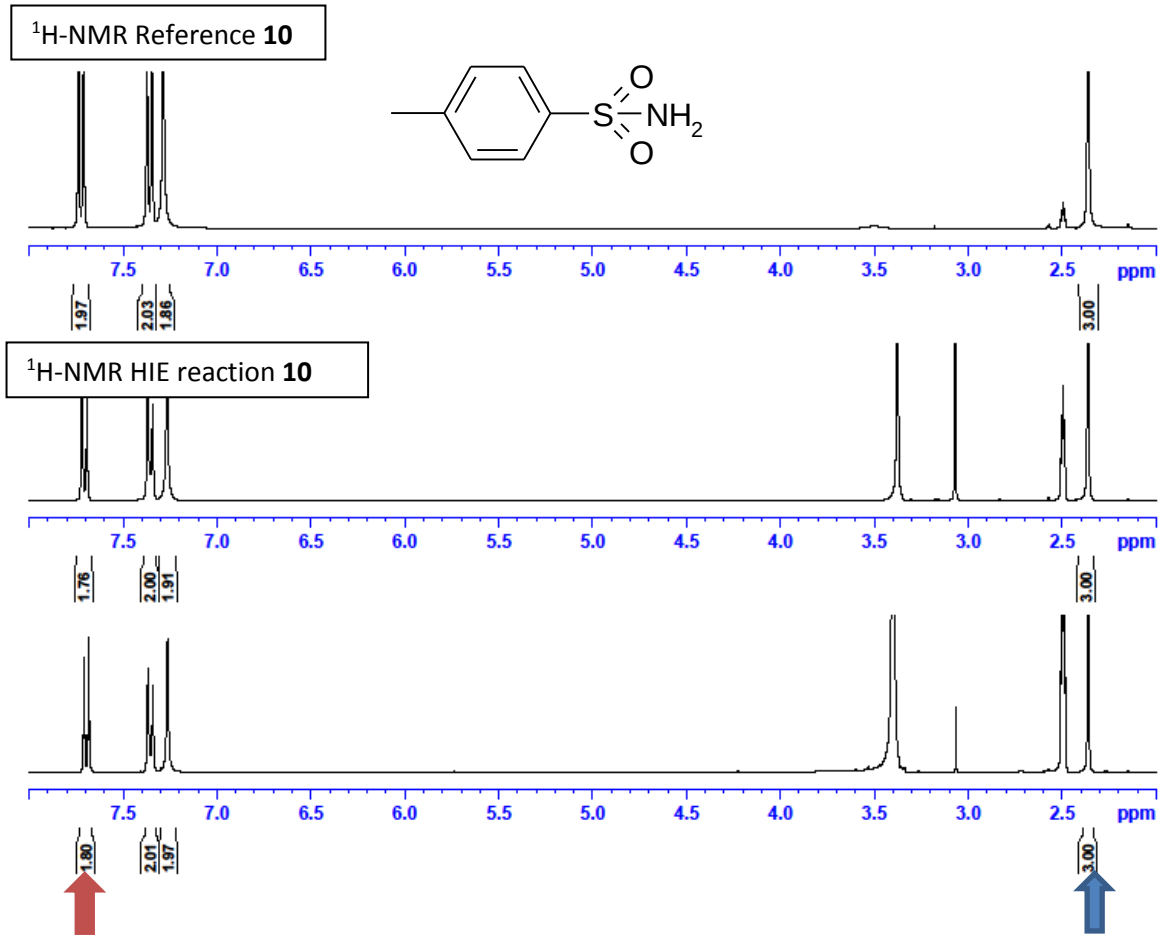

Result: 1) 90% D for compound **3**, 11% D for compound **10**.
2) 88% D for compound **3**, 2% D for compound **10**.

Average:
89% D for **3**,
7% D for **10**.

Compounds **5**+**7**:

Method A: 25 mg, 200 µmol **5**, 21 mg, 200 µmol **7**, 10.1 mg, 10 µmol catalyst $\mathbf{B_a}$.

5: Incorporation expected at δ 8.21. ppm (red arrow). Determined against reference-integral at δ 7.66 ppm (blue arrow).

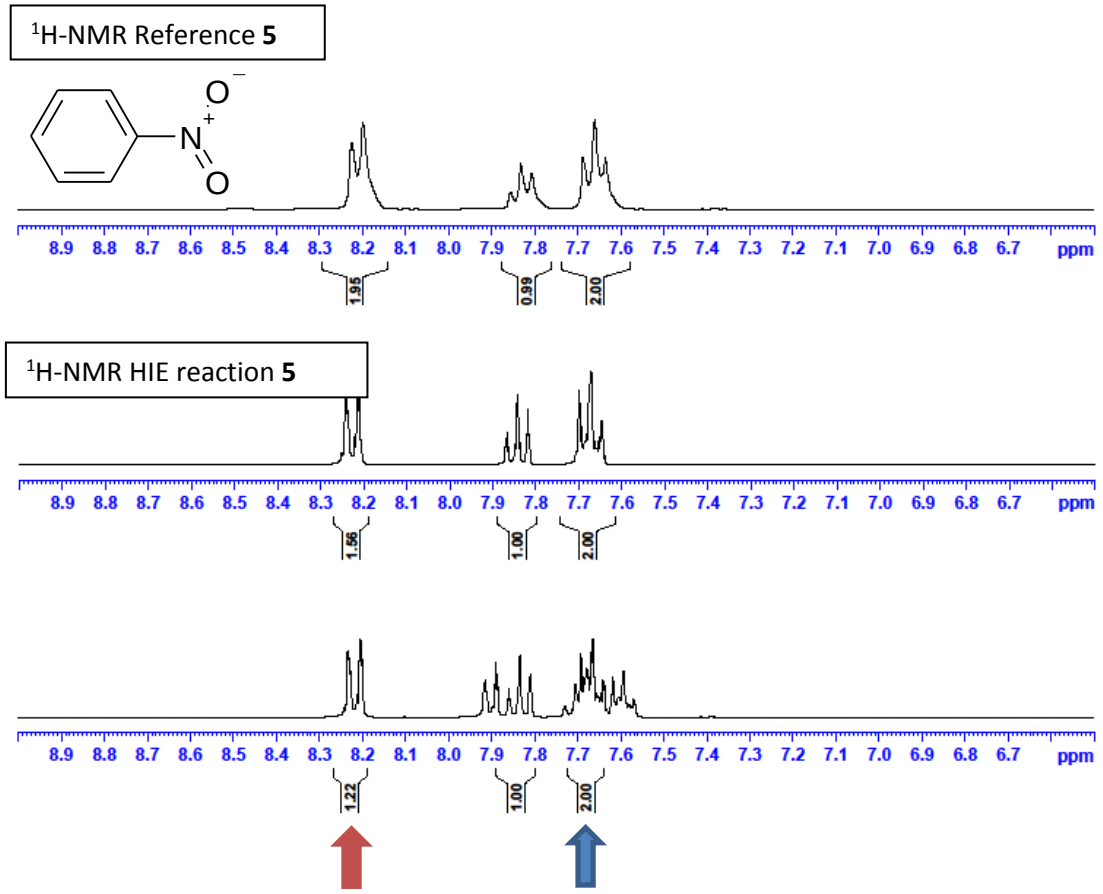

7: Incorporation expected at δ 7.91 ppm (red arrow). Determined against reference-integral at δ 7.60 ppm (blue arrow).

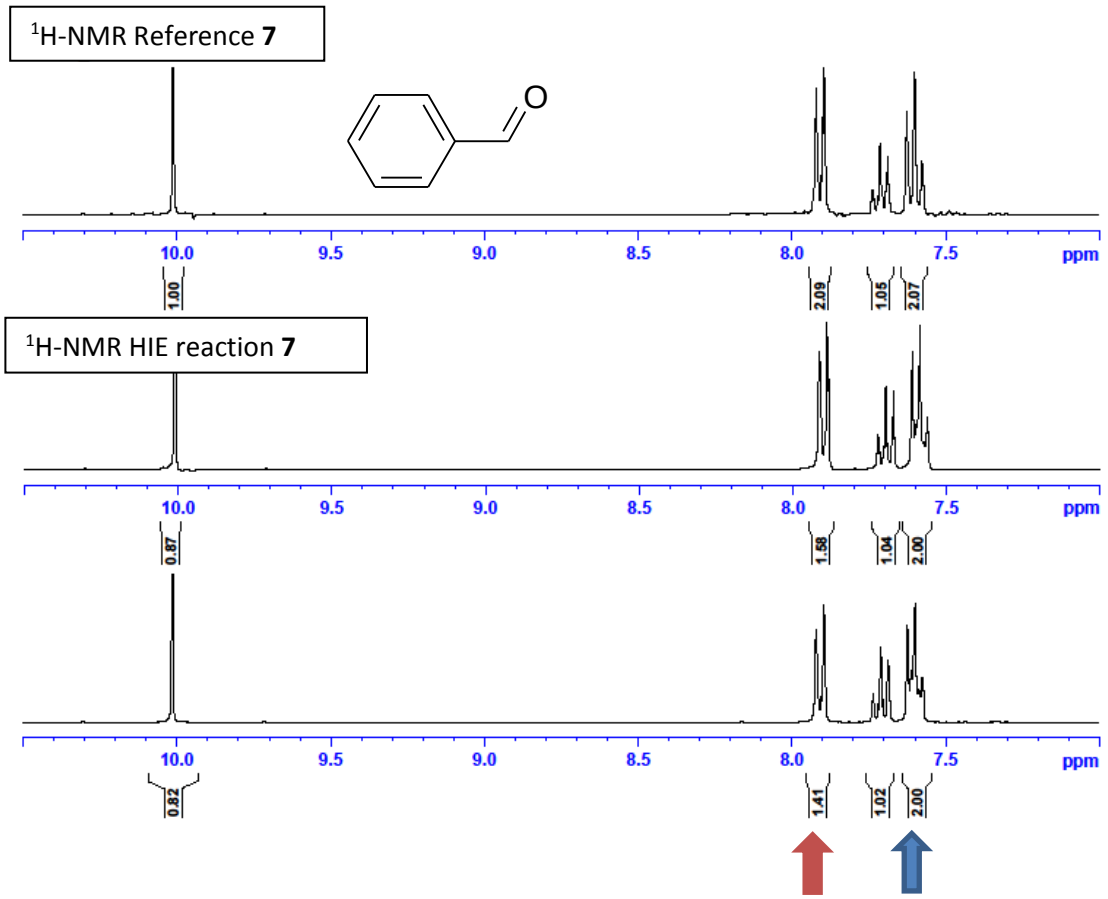

Result: 1) 22% D for compound **5**, 21% D for compound **7**.
2) 39% D for compound **5**, 30% D for compound **7.**

Average:
31% D for **5**,
25% D for **7**.

Compounds **4**+**5**:

Method A: 39 mg, 200 µmol **4**, 25 mg, 200 µmol **5**, 10.1 mg, 10 µmol catalyst $\mathbf{B_a}$. N.B.: Two separate reactions were done but were pooled before purification.

4: Incorporation expected at δ 8.05 ppm (red arrow). Determined against reference-integral at δ 2.63 ppm (blue arrow).

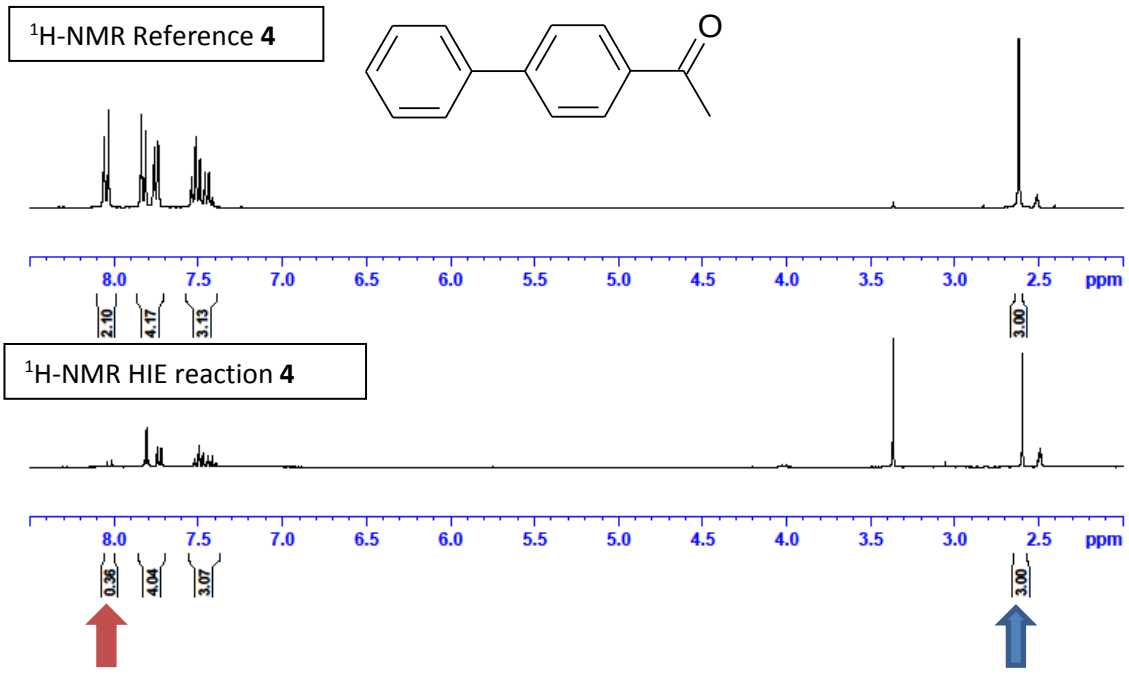

5: Incorporation expected at δ 8.05 ppm (red arrow). Determined against reference-integral at δ 2.63 ppm (blue arrow).

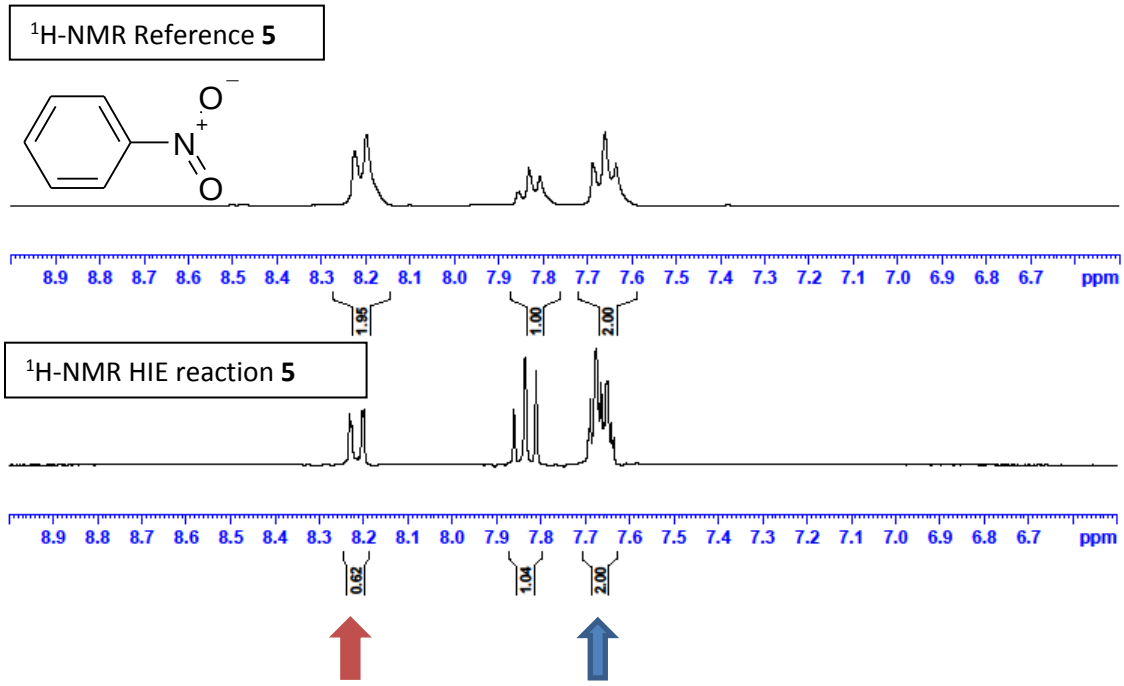

Result: 1) 82% D for compound **4**, 69% D for compound **5**.

Average:
82% D for **4**,
69% D for **5**.

Compounds **6**+**8**:

Method A: 36 mg, 200 µmol **6**, 27 mg, 200 µmol **8**, 10.1 mg, 10 µmol catalyst $\mathbf{B_a}$.

6: Incorporation expected at δ 7.35-7.29 ppm (red arrow). Determined against reference-integral at δ 7.45-7.39 ppm (blue arrow).

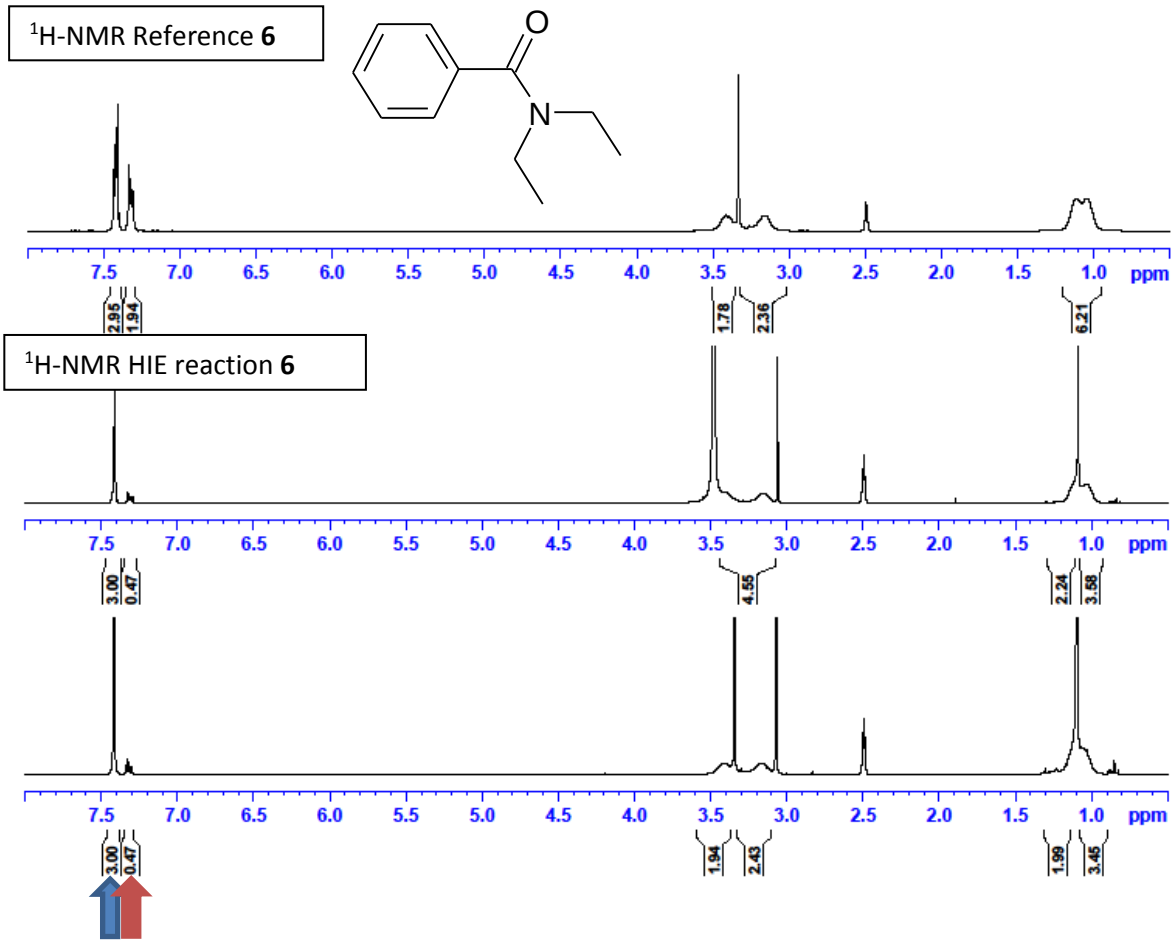

8: Incorporation expected at δ 7.96 ppm (red arrow). Determined against reference-integral at δ 3.82 ppm (blue arrow).

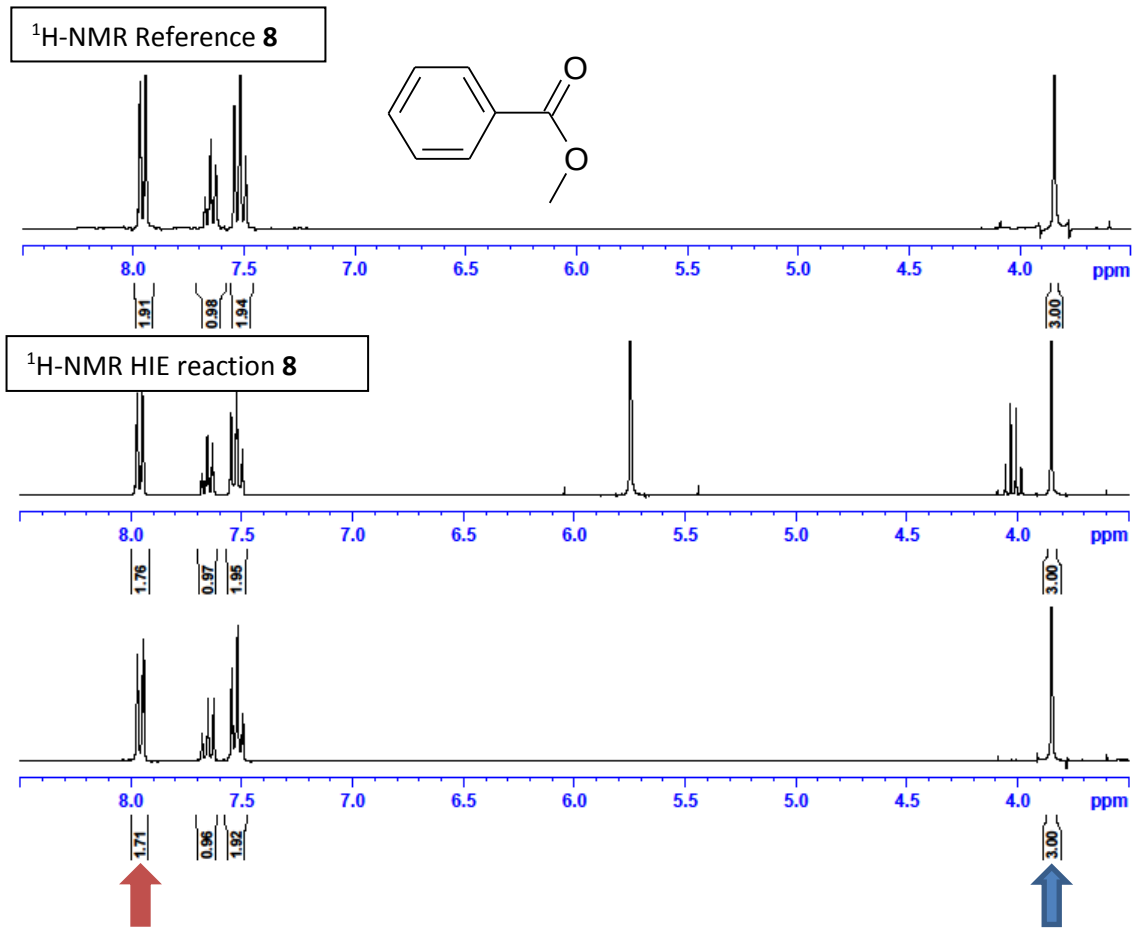

Result: 1) 77% D for compound **6**, 11% D for compound **8**.
2) 77% D for compound **6**, 14% D for compound **8.**

Average:
77% D for **6**,
16% D for **8**.

Compounds **6**+**9**:

Method A: 36 mg, 200 µmol **6**, 27 mg, 200 µmol **9**, 10.1 mg, 10 µmol catalyst $\mathbf{B_a}$.

6: Incorporation expected at δ 7.35-7.29 ppm (red arrow). Determined against reference-integral at δ 7.45-7.39 ppm (blue arrow).

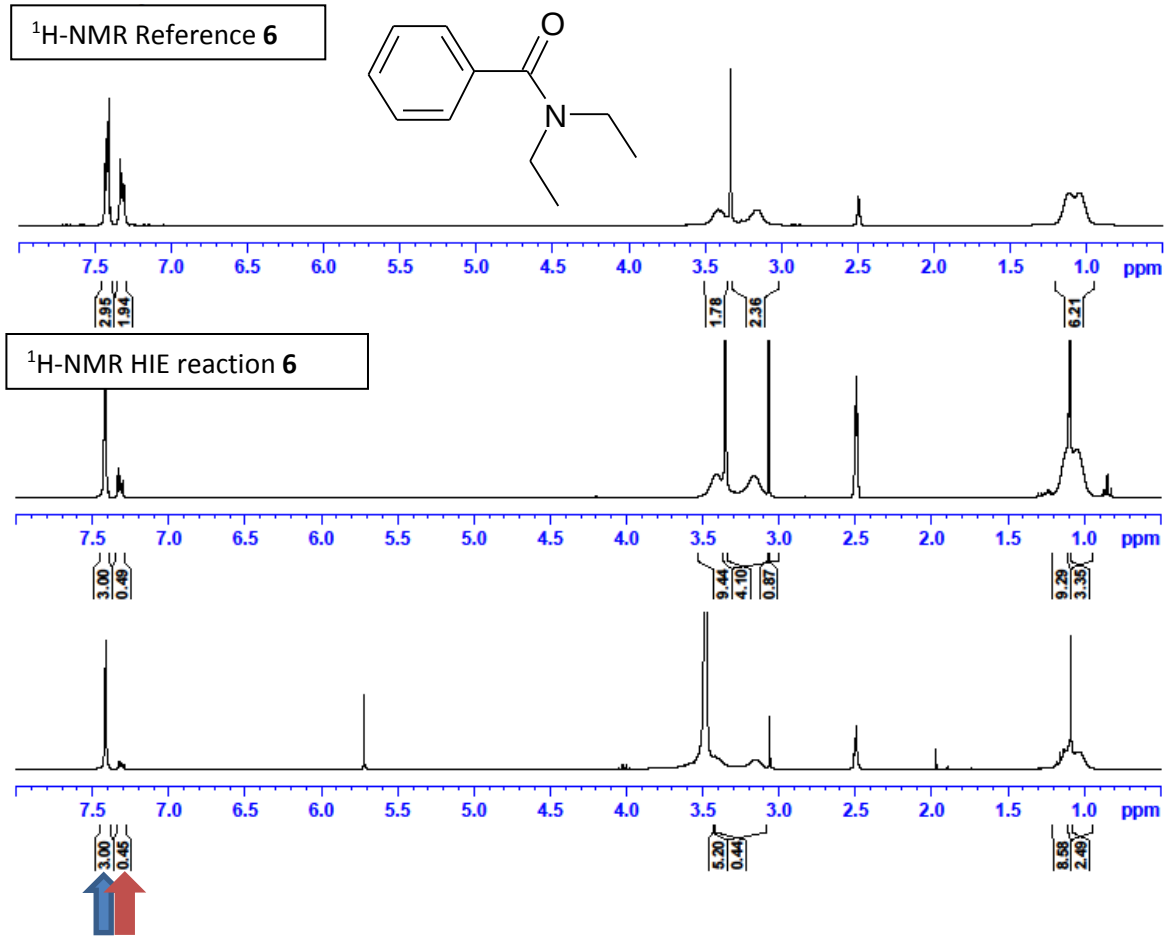

9: Incorporation expected at δ 7.12 ppm (red arrow). Determined against reference-integral at δ 2.26 ppm (blue arrow).

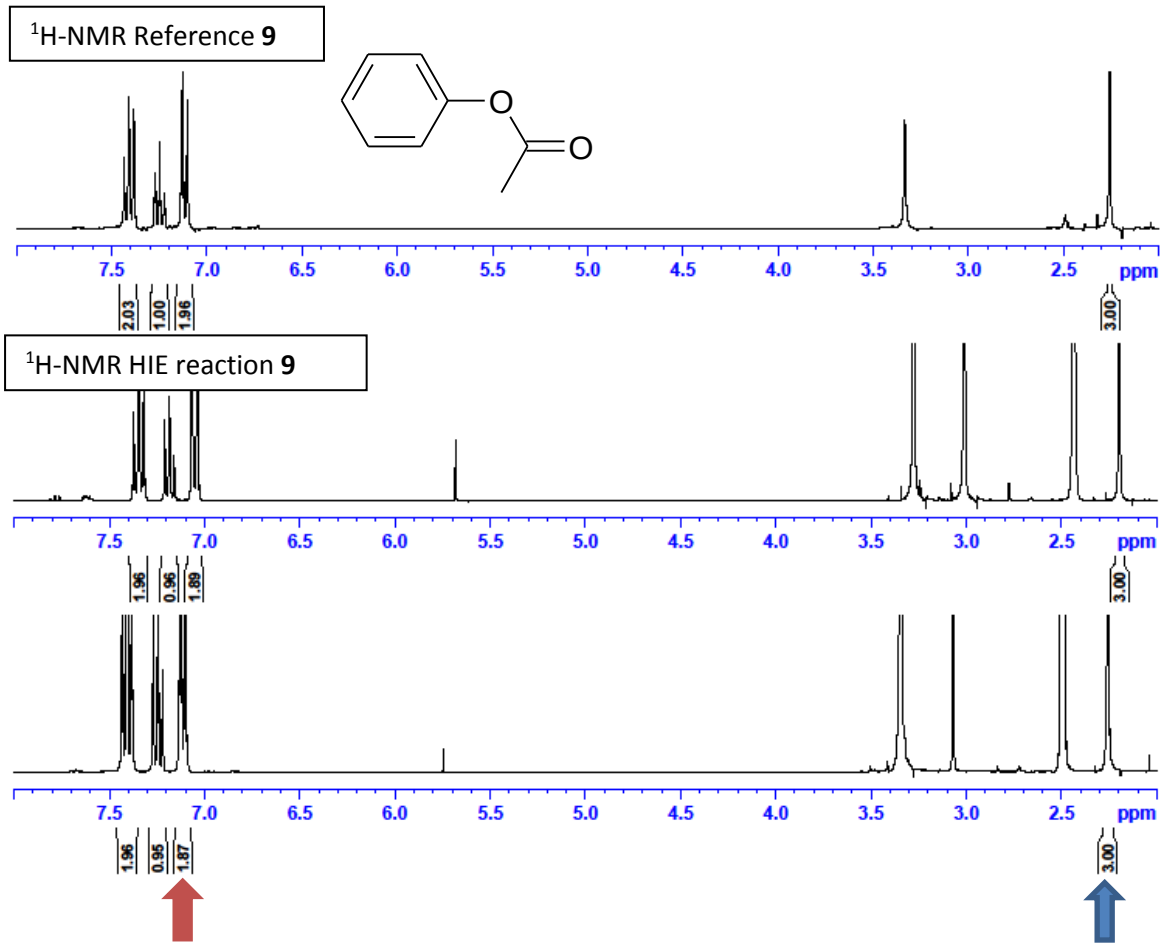

Result: 1) 76% D for compound **6**, 6% D for compound **9**.
2) 78% D for compound **6**, 7% D for compound **9**.

Average:
77% D for **6**,
6% D for **9**.

Compounds **6**+**10**:

Method A: 36 mg, 200 µmol **6**, 34 mg, 200 µmol **10**, 10.1 mg, 10 µmol catalyst $\mathbf{B_a}$.

6: Incorporation expected at δ 7.35-7.29 ppm (red arrow). Determined against reference-integral at δ 7.45-7.39 ppm (blue arrow).

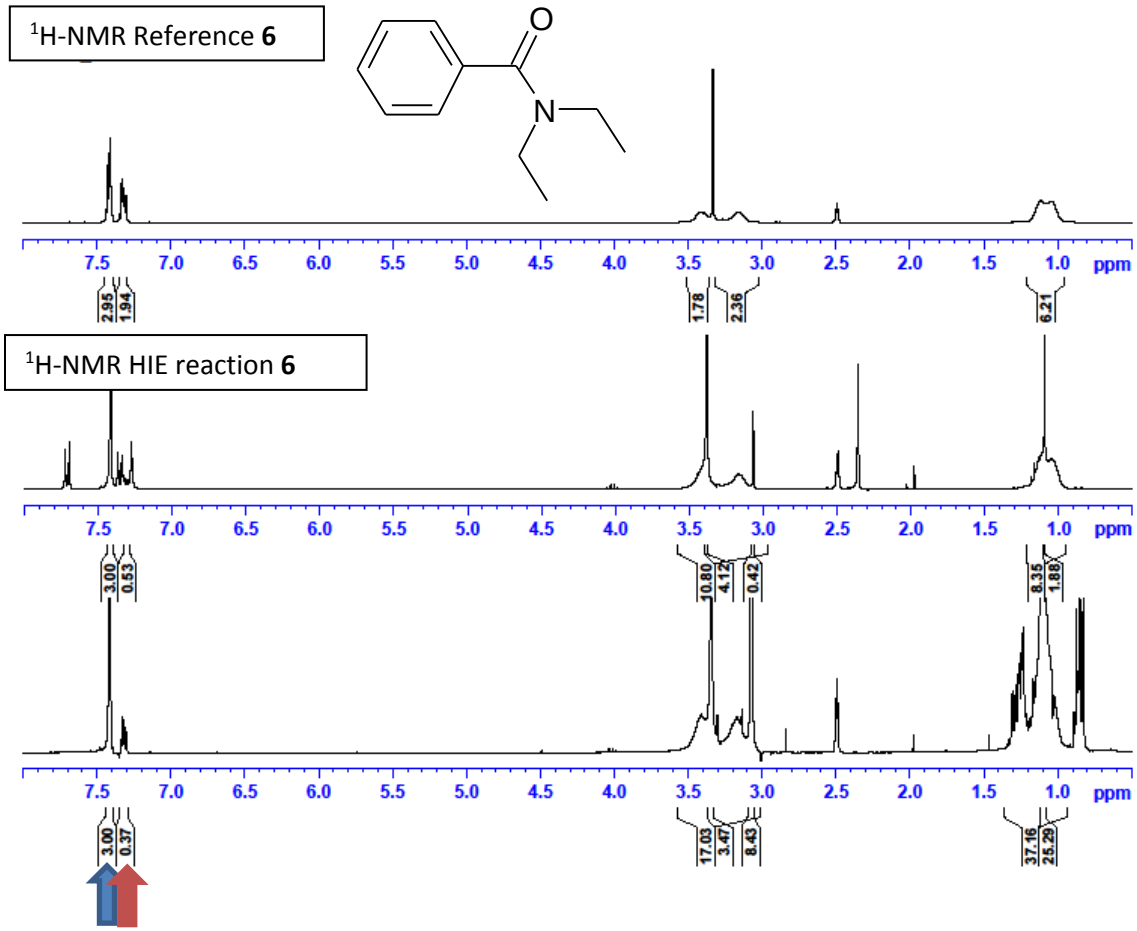

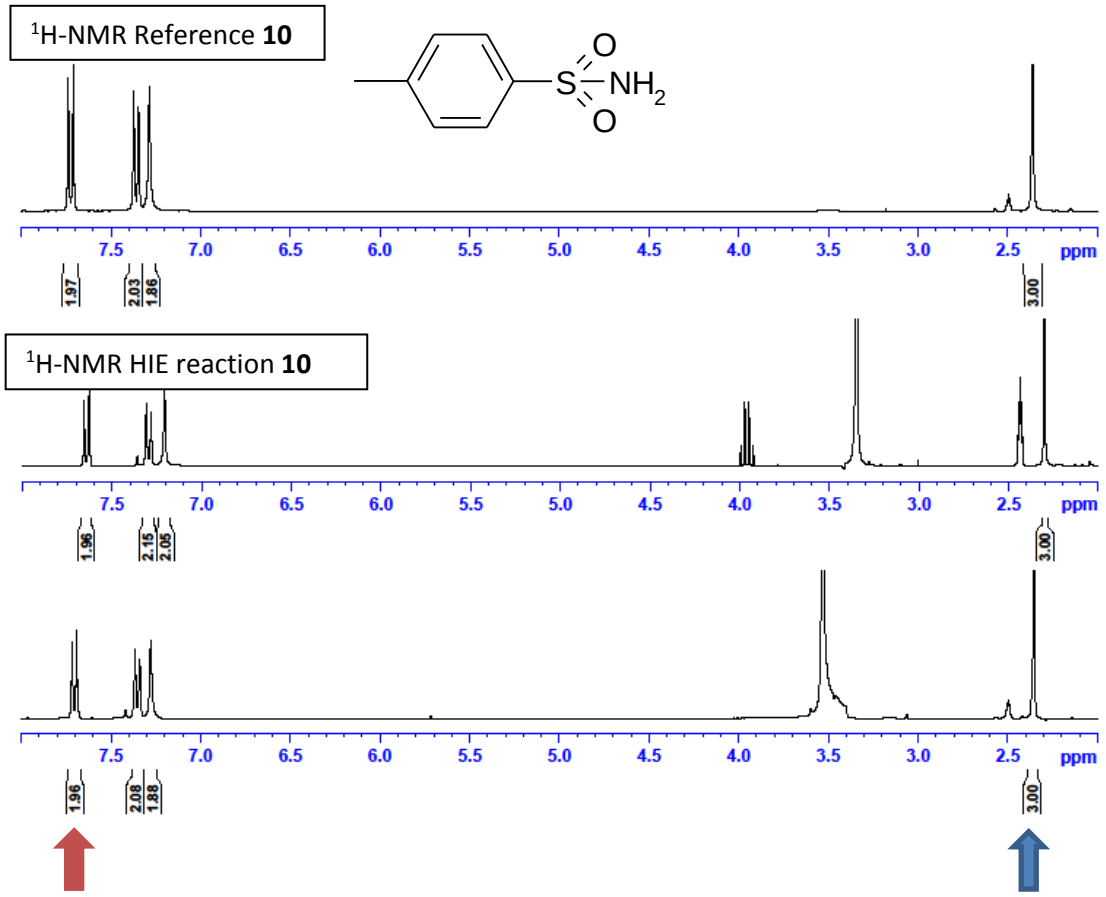

Result: 1) 74% D for compound **6**, 2% D for compound **10**.
2) 82% D for compound **6**, 2% D for compound **10**.

Average:
78% D for **6**,
2% D for **10**.

Compounds **7**+**8**:

Method A: 21 mg, 200 µmol **7**, 27 mg, 200 µmol **8**, 10.1 mg, 10 µmol catalyst $\mathbf{B_a}$.
N.B.: Two separate reactions were done but were pooled before purification.

7: Incorporation expected at δ 7.60 ppm (red arrow). Determined against reference-integral at δ 7.91 ppm (blue arrow).

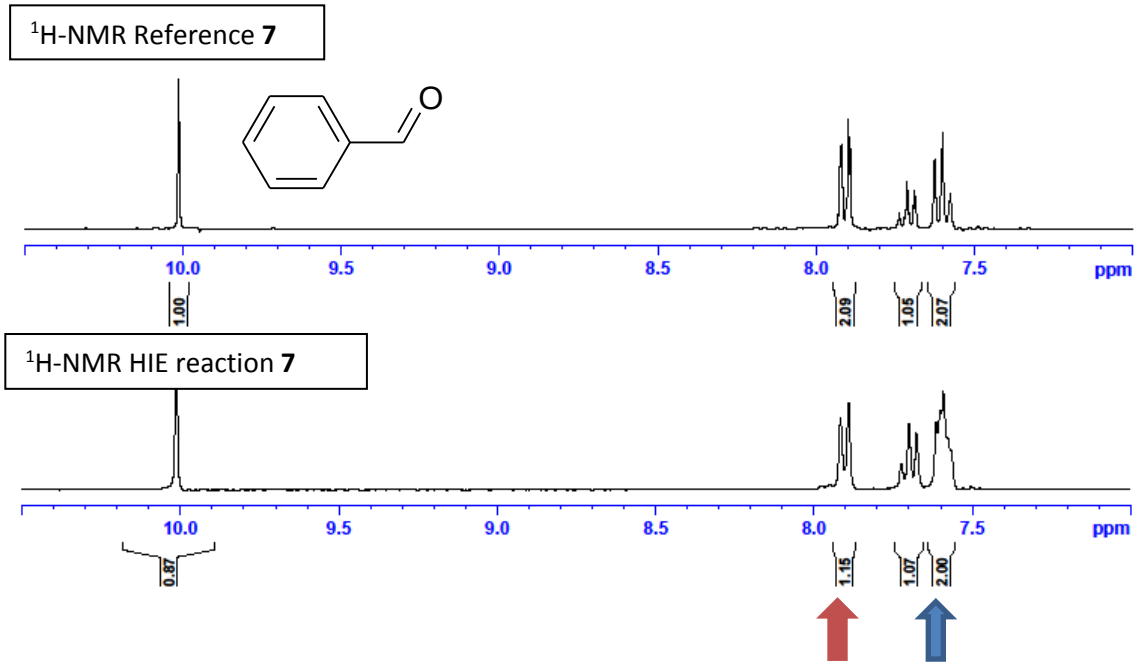

8: Incorporation expected at δ 7.96 ppm (red arrow). Determined against reference-integral at δ 3.82 ppm (blue arrow).

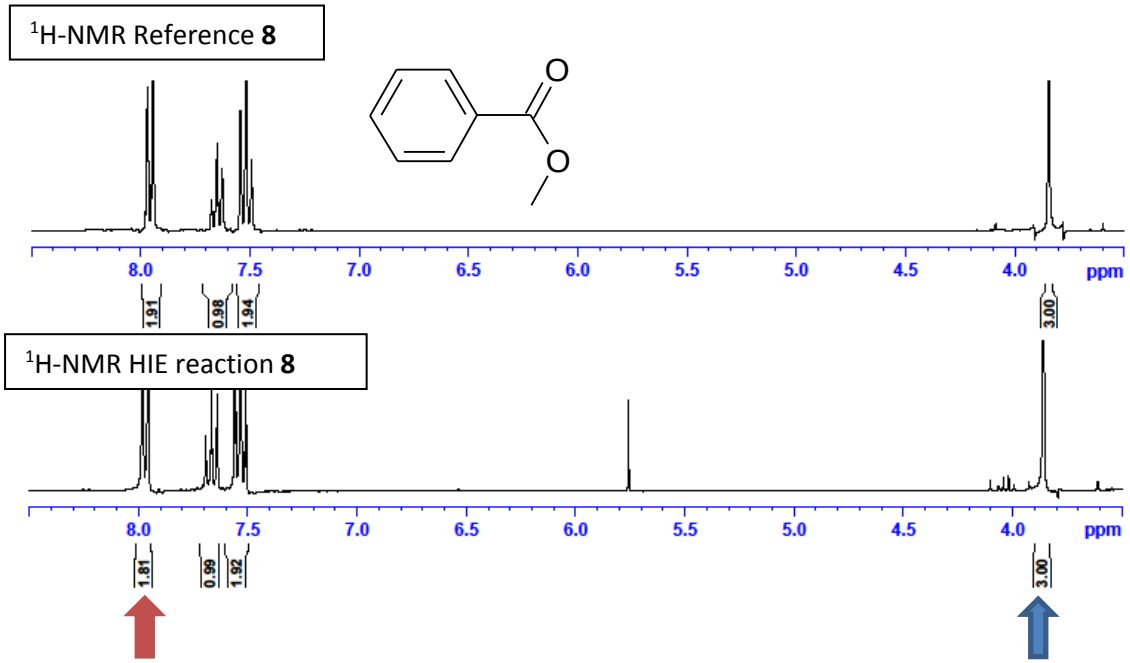

Result: 1) 43% D for compound **7**, 10% D for compound **8**.

Average:
43% D for **7**,
10% D for **8**.

HIE experiment of disubstituted aromatic substrates 12-22 (*scheme III.2.4*)

1-(4-acetylphenyl)-propan-2-one **12**

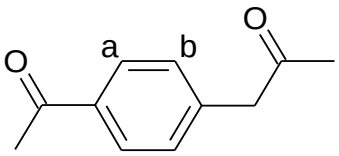

Molecular Weight =176,22
Molecular Formula =C11H12O

12

^{1}H NMR (300 MHz, DMSO-d_6): δ 7.89 (d, ^{3}J= 8.5 Hz, 2H, H_b), 7.32 (d, ^{3}J= 8.5 Hz, 2H, H_a), 3.87 (s, 2H), 2.55 (s, 3H), 2.15 (s, 3H) ppm. Incorporation expected at δ 7.89 and/or δ 7.32 ppm (red arrow). Determined against reference-integral at δ 2.15 ppm (blue arrow).

Method B: 10 mg, 57 µmol **12**, 2.9 mg, 2.8 µmol catalyst **B_a**.

LC-MS (positive ESI): m/z 178.1 $[M(1D)+H]^+$ (5%), 179.1 $[M(2D)+H]^+$ (80%), 180.1 $[M(3D)+H]^+$ (15%).

Yield: 1) 9.9 mg, 56 µmol, 99%; 99% D for δ 7.89.
2) 7.1 mg, 40 µmol, 71%%; 99% D for δ 7.89.

Average: y=85%,
99% D at position b.

^{1}H-NMR Reference **12**

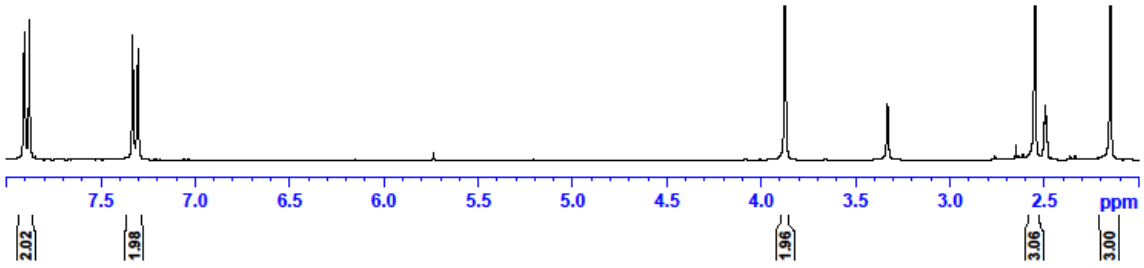

^{1}H-NMR HIE reaction **12**

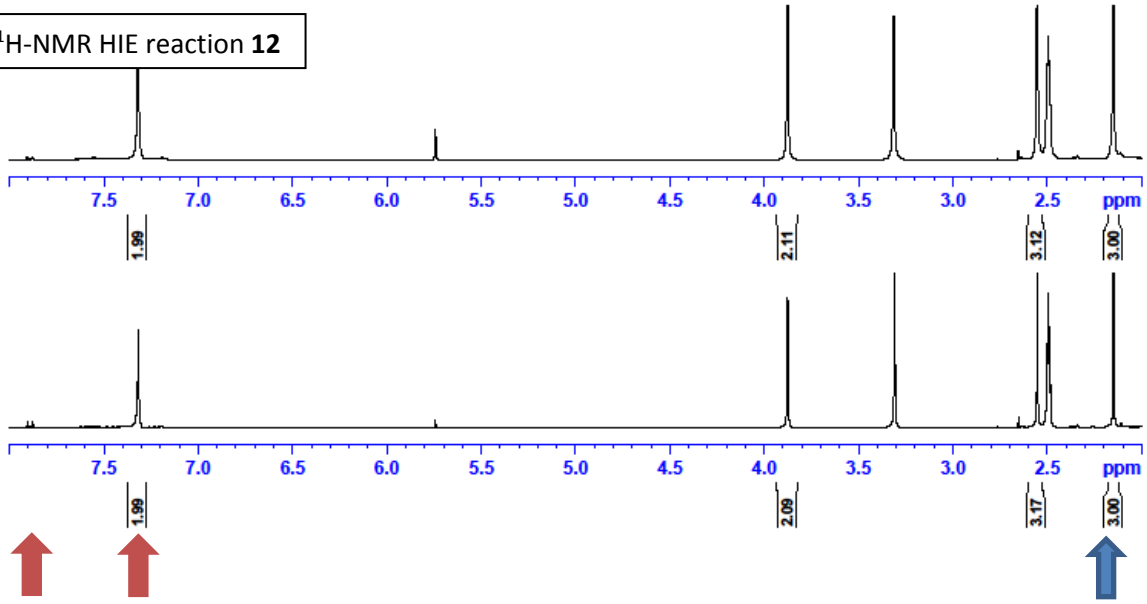

4-Acetylbenzaldehyde **13**

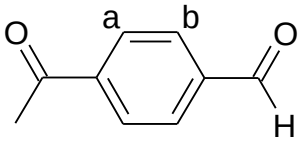

Molecular Weight =148,16
Molecular Formula =C9H8O2

13

^{1}H NMR (300 MHz, DMSO-d$_6$): δ 10.11 (s, 1H), 8.13 (d, ^{3}J= 8.2 Hz, 2H, *H$_a$*), 8.03 (d, ^{3}J=8.2 Hz, 2H, *H$_b$*), 2.64 (s, 3H) ppm. Incorporation expected at δ 8.13 and/or δ 8.03 ppm (red arrow). Determined against reference-integral at δ 2.64 ppm (blue arrow).

Method B: 10 mg, 67 µmol **13**, 3.4 mg, 3.4 µmol catalyst **B$_a$**.

LC-MS (positive ESI): m/z 151.1 $[M(2D)+H]^+$ (33%), 152.1 $[M(3D)+H]^+$ (62%), 153.1 $[M(3D)+H]^+$ (5%).

Yield: 1) 8.6 mg, 58 µmol, 86%; 90% D for δ 8.13, 40% D for δ 8.03.
2) 9.3 mg, 63 µmol, 93%; 91% D for δ 8.13, 40% D for δ 8.03.

Average: y=90%,
90% D at position a,
40% D at position b.

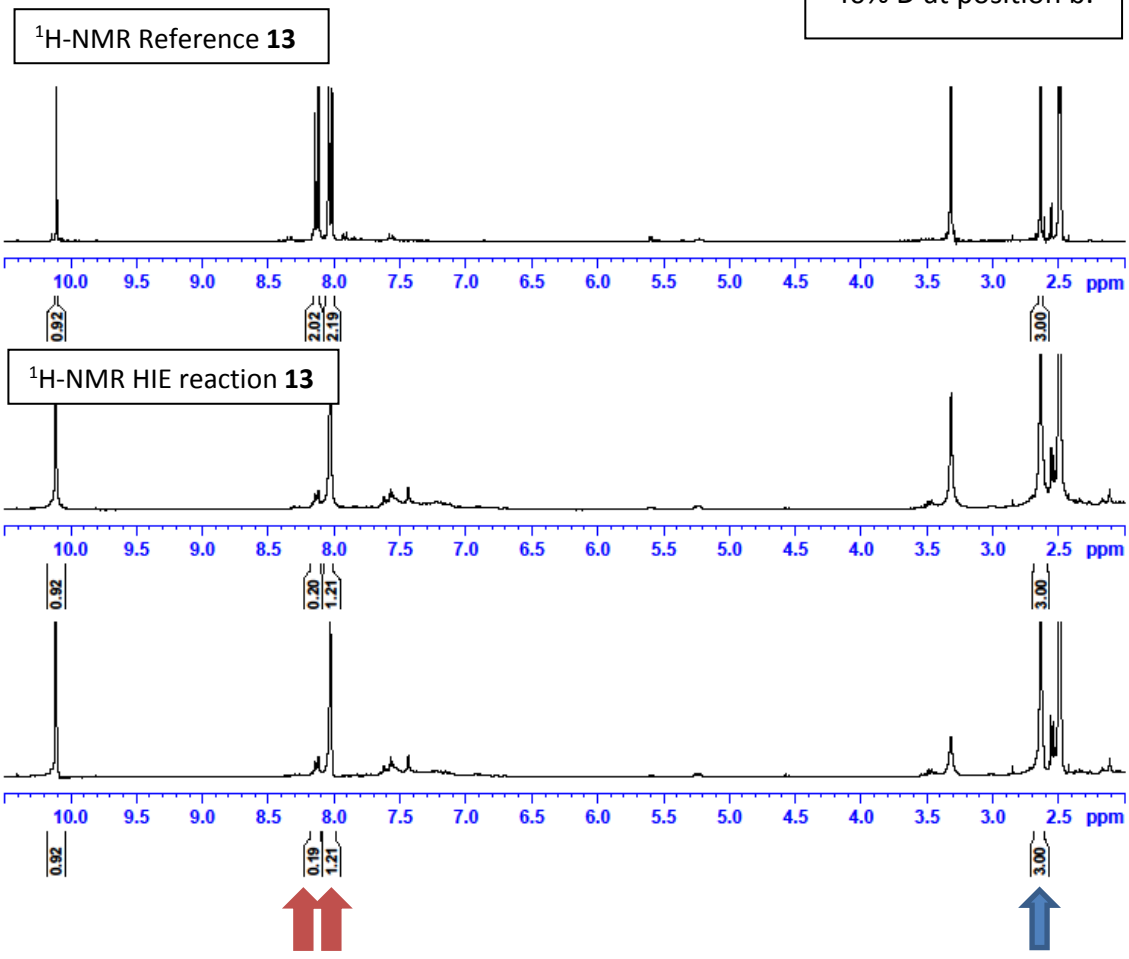

N-(4-acetylphenyl)-acetamide **14**

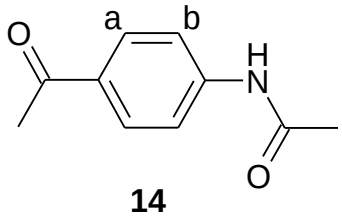

14

Molecular Weight =177,20
Molecular Formula =C10H11NO2

^{1}H NMR (300 MHz, DMSO-d_6): δ 10.24 (s, 1H, NH), 7.90 (d, ^{3}J= 8.75 Hz, 2H, H_a), 7.69 (d, ^{3}J= 8.75 Hz, 2H, H_b), 2.50 (s, 3H), 2.07 (s, 3H) ppm. Incorporation expected at δ 7.90 and/or δ 7.69 ppm (red arrow). Determined against reference-integral at δ 2.07 ppm.

Method B: 10 mg, 56 µmol **14**, 2.9 mg, 2.8 µmol catalyst **B_a**.

LC-MS (positive ESI): m/z 180.2 $[M(2D)+H]^+$ (5%), 182.2 $[M(3D)+H]^+$ (12%), 183.1 $[M(4D)+H]^+$ (78%), 184.1 $[M(5D)+H]^+$ (5%).

Yield: 1) 9.8 mg, 55 µmol, 98%; 96% D for δ 7.90, 96% D for δ 7.69.
2) 9.6 mg, 54 µmol, 96%; 96% D for δ 7.90, 96% D for δ 7.69.

Average: y=97%,
96% D at position a,
96% D at position b.

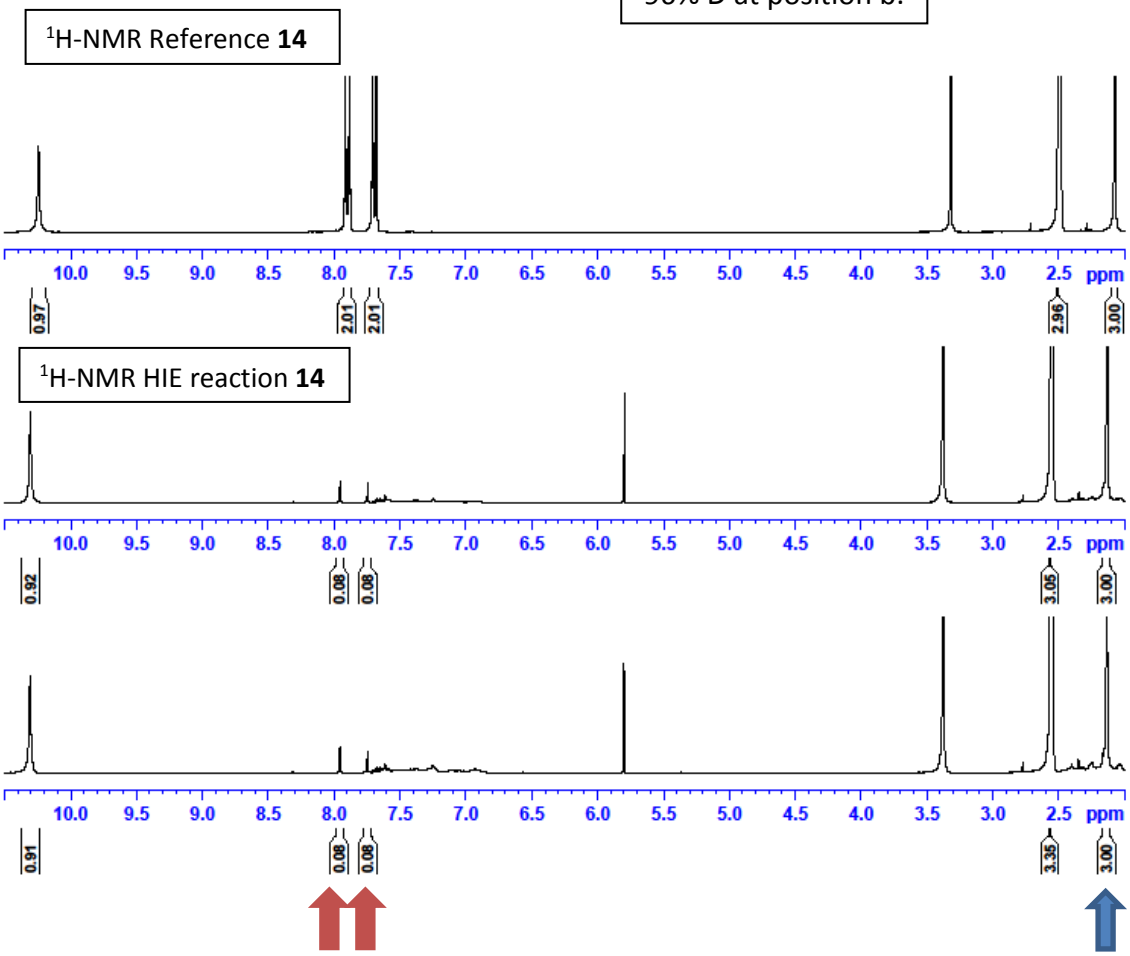

Method B (-15 °C): 10 mg, 56 µmol **14**, 2.9 mg, 2.8 µmol catalyst $\mathbf{B_a}$.

LC-MS (positive ESI): m/z 178.2 $[M+H]^+$ (31%), 179.2 $[M(1D)+H]^+$ (58%), 180.1 $[M(2D)+H]^+$ (11%).

Yield: 1) 9.9 mg, 56 µmol, 99%; 27% D for δ 7.90, 2% D for δ 7.69.
2) 9.1 mg, 51 µmol, 91%; 37% D for δ 7.90, 9% D for δ 7.69.

Average: y=95%,
32% D at position a,
5% D at position b.

^{1}H-NMR Reference **14**

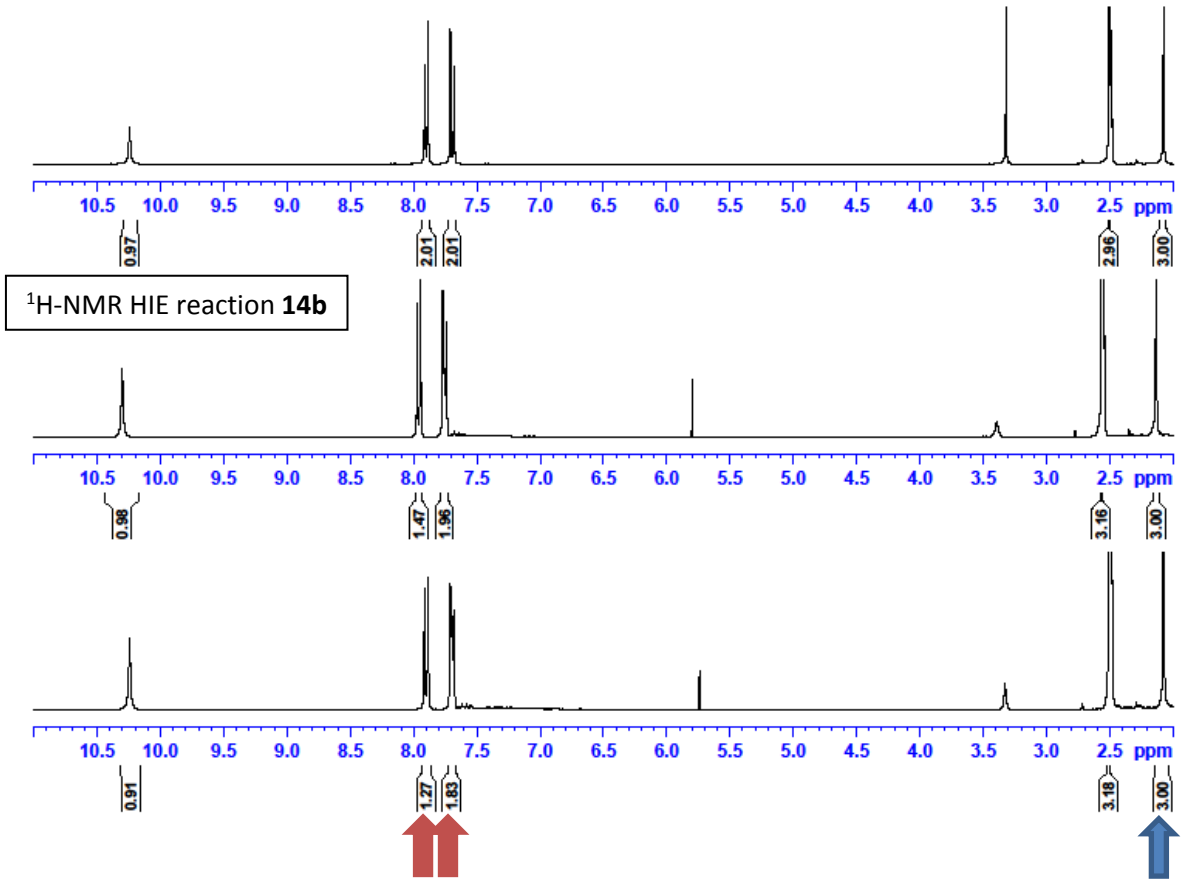

^{1}H-NMR HIE reaction **14b**

4-Acetyl-4'-nitrobiphenyl **15**

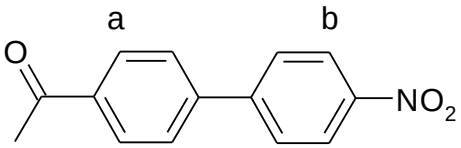

Molecular Weight =241,25
Molecular Formula =C14H11NO3

15

^{1}H NMR (300 MHz, DMSO-d$_6$): δ 8.33 (d, ^{3}J= 9.0 Hz, 2H, *H$_b$*), 8.09 (d, ^{3}J= 8.5 Hz, 2H, *H$_a$*), 8.04 (d, ^{3}J= 9.0 Hz, 2H), 7.94 (d, ^{3}J= 8.5 Hz, 2H), 2.63 (s, 3H) ppm. Incorporation expected at δ 8.33 and/or δ 8.09 ppm (red arrow). Determined against reference-integral at δ 2.63 ppm (blue arrow).

Method B: 10 mg, 41 µmol **15**, 2.1 mg, 2.1 µmol catalyst **B$_a$**.

LC-MS (positive ESI): m/z 244.2 $[M(2D)+H]^+$ (4%), 245.2 $[M(3D)+H]^+$ (13%), 246.1 $[M(4D)+H]^+$ (77%), 247.1 $[M(5D)+H]^+$ (6%).

Yield: 1) 9.3 mg, 38 µmol, 93%; 96% D for δ 8.33, 98% D for δ 8.09.
2) 8.9 mg, 37 µmol, 89%; 96% D for δ 8.33, 98% D for δ 8.09.

Average: y=91%,
98% D at position a,
96% D at position b.

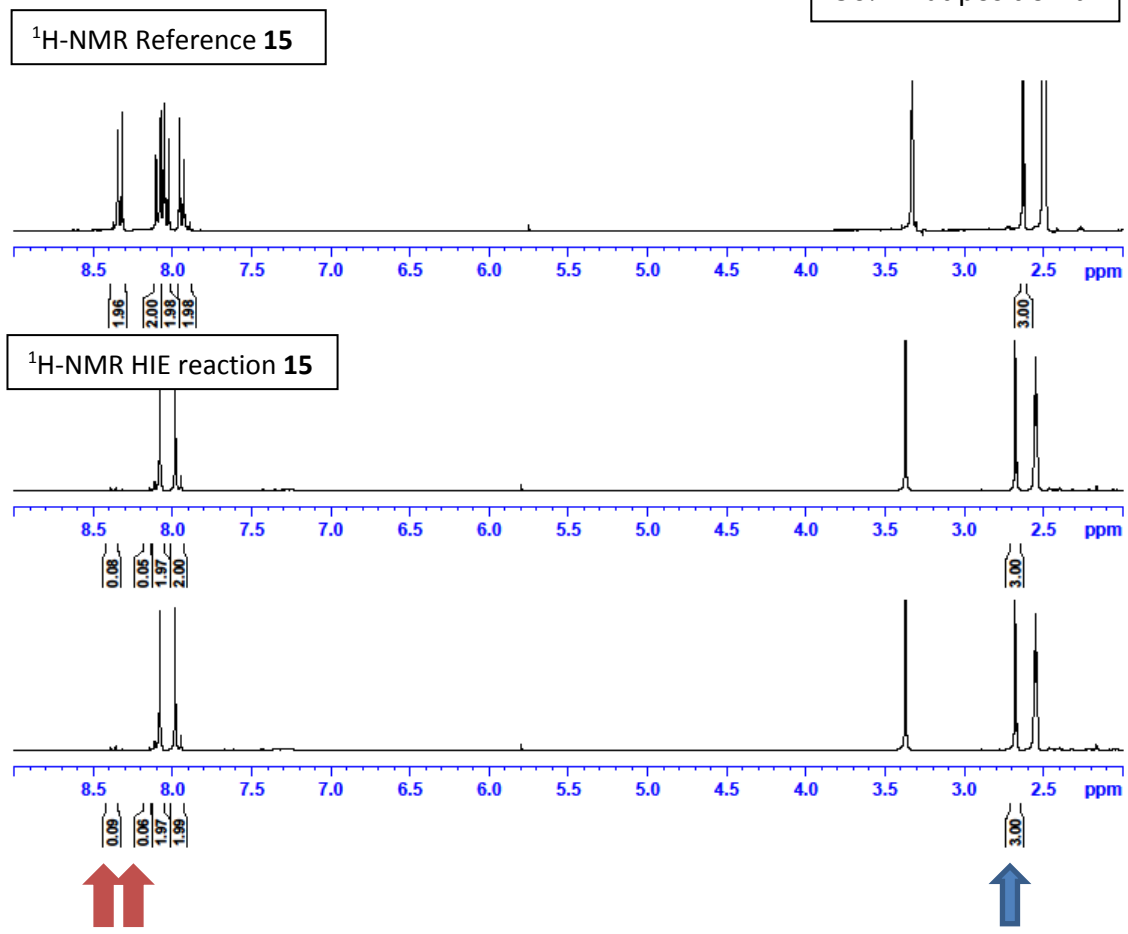

Method B (-15°C): 10 mg, 41 µmol **15**, 2.1 mg, 2.1 µmol catalyst $\mathbf{B_a}$.

LC-MS (positive ESI): m/z 242.2 $[M+H]^+$ (52%), 243.2 $[M(1D)+H]^+$ (40%), 244.1 $[M(2D)+H]^+$ (8%).

Yield: 1) 8.7 mg, 36 µmol, 87%; 0% D for δ 8.33, 40% D for δ 8.09.
2) 8.2 mg, 34 µmol, 82%; 4% D for δ 8.33, 55% D for δ 8.09.

Average: y=85%, 47% D at position a, 2% D at position b.

^{1}H-NMR Reference **15**

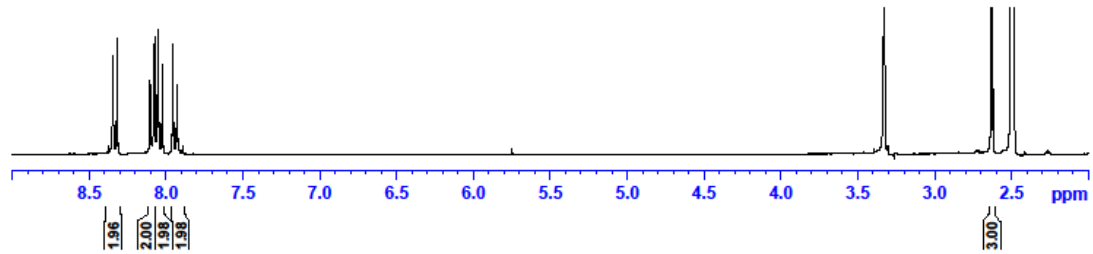

^{1}H-NMR HIE reaction **15b**

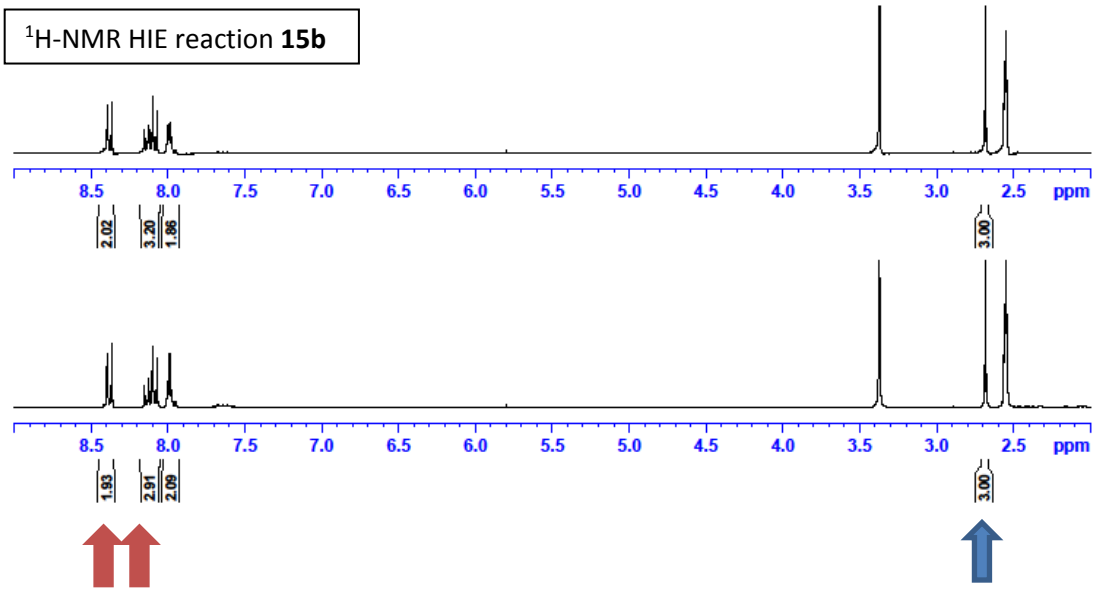

Methyl 4-acetoxy-4'-biphenylcarboxylate **16**

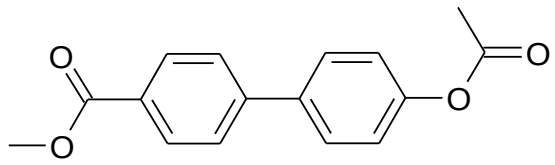

Molecular Weight =270.2876
Molecular Formula =C16H14O4

16

^{1}H NMR (300 MHz, DMSO-d$_6$: δ 8.08 (d, ^{3}J= 8.3 Hz, 2H, *H$_a$*), 7.86 (d, ^{3}J= 8.3 Hz, 2H), 7.80 (d, ^{3}J= 8.7 Hz, 2H), 7.30 (d, ^{3}J= 8.7 Hz, 2H, *H$_b$*), 3.92 (s, 3H), 2.34 (s, 3H) ppm. Incorporation expected at δ 8.08 and/or δ 7.30 ppm (red arrow). Determined against reference-integral at δ 2.34 ppm (blue arrow).

Method B: 10 mg, 37 µmol **16**, 1.9 mg, 1.8 µmol catalyst **B$_a$**.

LC-MS (positive ESI): m/z 271.3 $[M+H]^+$ (53%), 272.2 $[M(1D)+H]^+$ (38%), 273.1 $[M(2D)+H]^+$ (9%).

Yield: 1) 10 mg, 37 µmol, 100%; 55% D for δ 8.08.
2) 8.3 mg, 31 µmol, 83%; 42% D for δ 8.08.

Average: y=92%,
49% D at position a.

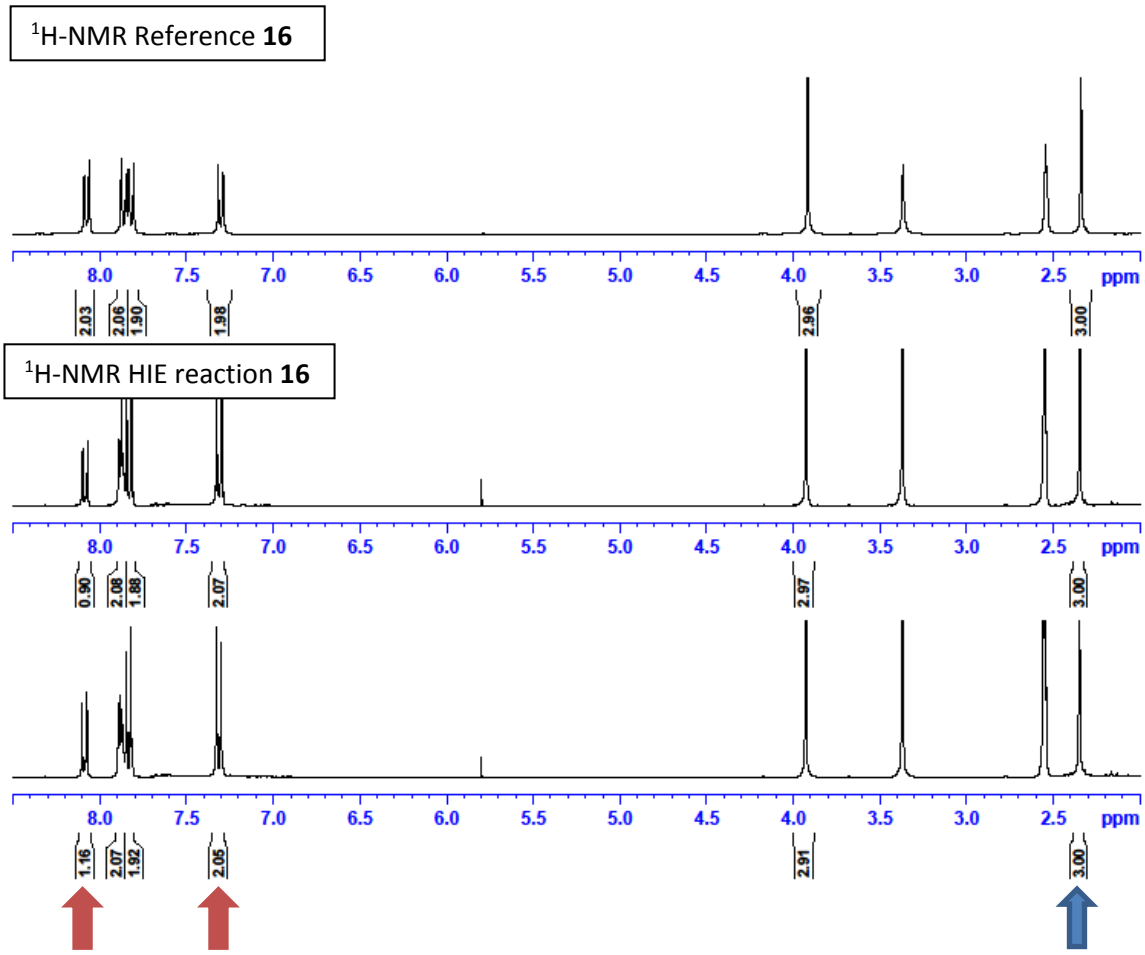

4-Acetamidobenzaldehyde **17**

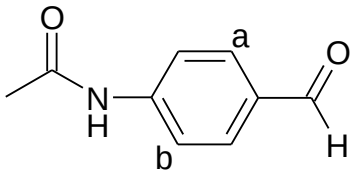

Molecular Weight =163,18
Molecular Formula =C9H9NO2

17

^{1}H NMR (300 MHz, DMSO-d_6): δ 10.33 (s,1H), 9.85 (s,1H), 7.84 (d, ^{3}J= 8.7 Hz, 2H, H_a), 7.78 (d, ^{3}J= 8.7 Hz, 2H, H_b), 2.09 (s, 3H) ppm. Incorporation expected at δ 7.84 and/or δ 7.78 ppm (red arrow). Determined against reference-integral at δ 2.09 ppm (blue arrow).

Method B: 10 mg, 61 µmol **17**, 3.1 mg, 3.1 µmol catalyst **B_a**.

LC-MS (positive ESI): m/z 165.1 $[M(1D)+H]^+$ (7%), 166.1 $[M(2D)+H]^+$ (15%), 167.1 $[M(3D)+H]^+$ (75%), 168.1 $[M(4D)+H]^+$ (3%).

Yield: 1) 9.8 mg, 60 µmol, 98%; 58% D for δ 7.84, 78% for δ 7.78.
2) 9.9 mg, 60 µmol, 99%; 59% D for δ 7.84, 79% for δ 7.78.

Average: y=99%,
58% D at position a,
78% D at position b.

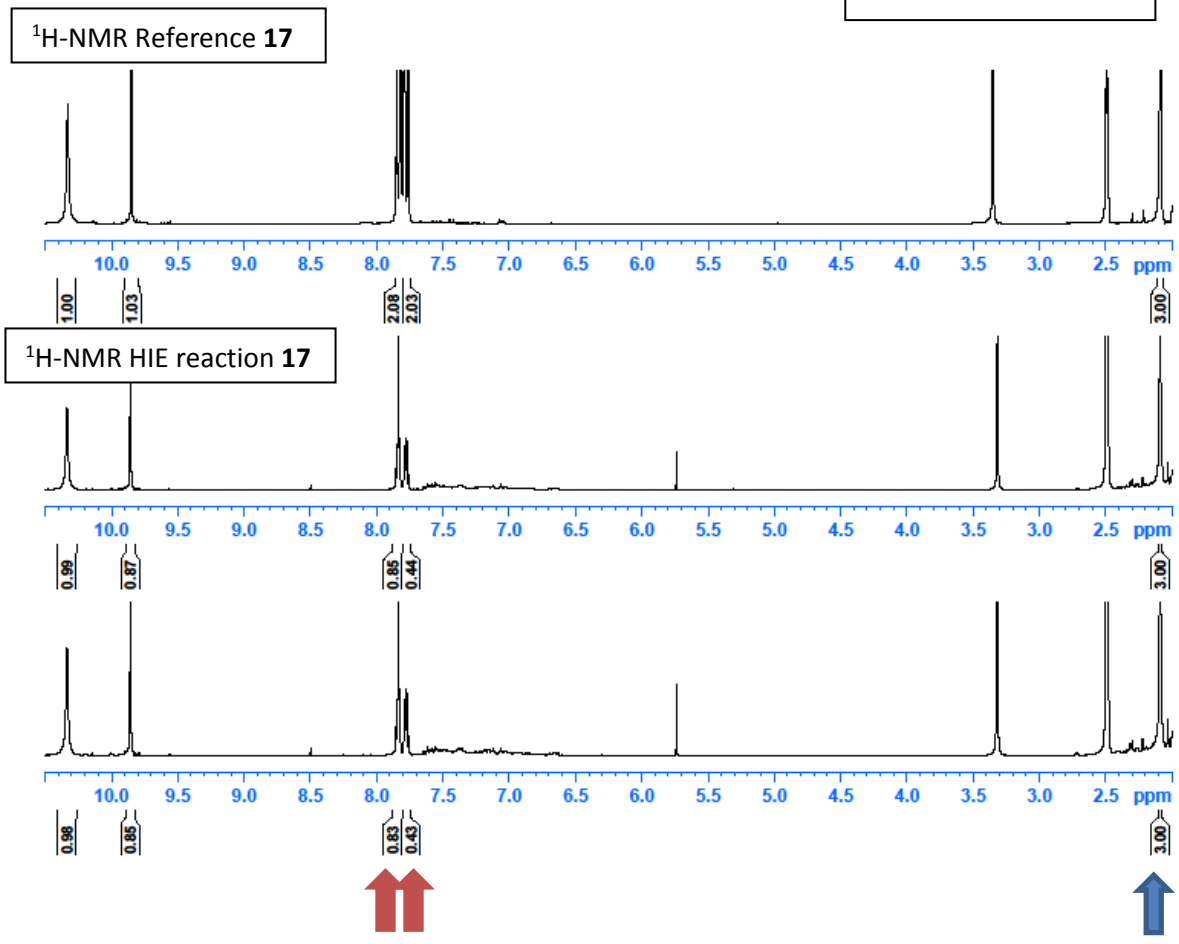

4-Formylbenzenesulfonamide **18**

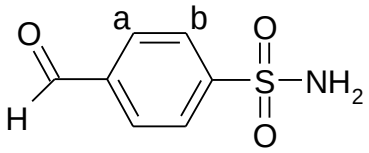

Molecular Weight =185,20
Molecular Formula =C7H7NO3S

18

^{1}H NMR (300 MHz, DMSO-d$_6$): δ 10.08 (s, 1H), 8.09 (d, ^{3}J= 8.4 Hz, 2H, *H$_a$*), 8.01 (d, ^{3}J= 8.4 Hz, 2H, *H$_b$*), 7.58 (s, 2H) ppm. Incorporation expected at δ 8.09 and/or δ 8.01 ppm (red arrow). Determined against reference-integral at δ 7.58 ppm (blue arrow).

Method B: 10 mg, 54 µmol **18**, 2.7 mg, 2.7 µmol catalyst **B$_a$**.

LC-MS (positive ESI): m/z 186.2 $[M+H]^+$ (5%), 187.2 $[M(1D)+H]^+$ (52%), 188.1 $[M(2D)+H]^+$ (39%), 189.1 $[M(3D)+H]^+$ (4%).

Yield: 1) 9.2 mg, 40 µmol, 92%; 50% D for δ 8.09, 24% D for δ 8.01.
2) 8.6 mg, 36 µmol, 86%; 53% D for δ 8.09, 15% D for δ 8.01.

Average: y=89%,
52% D at position a,
19% D at position b.

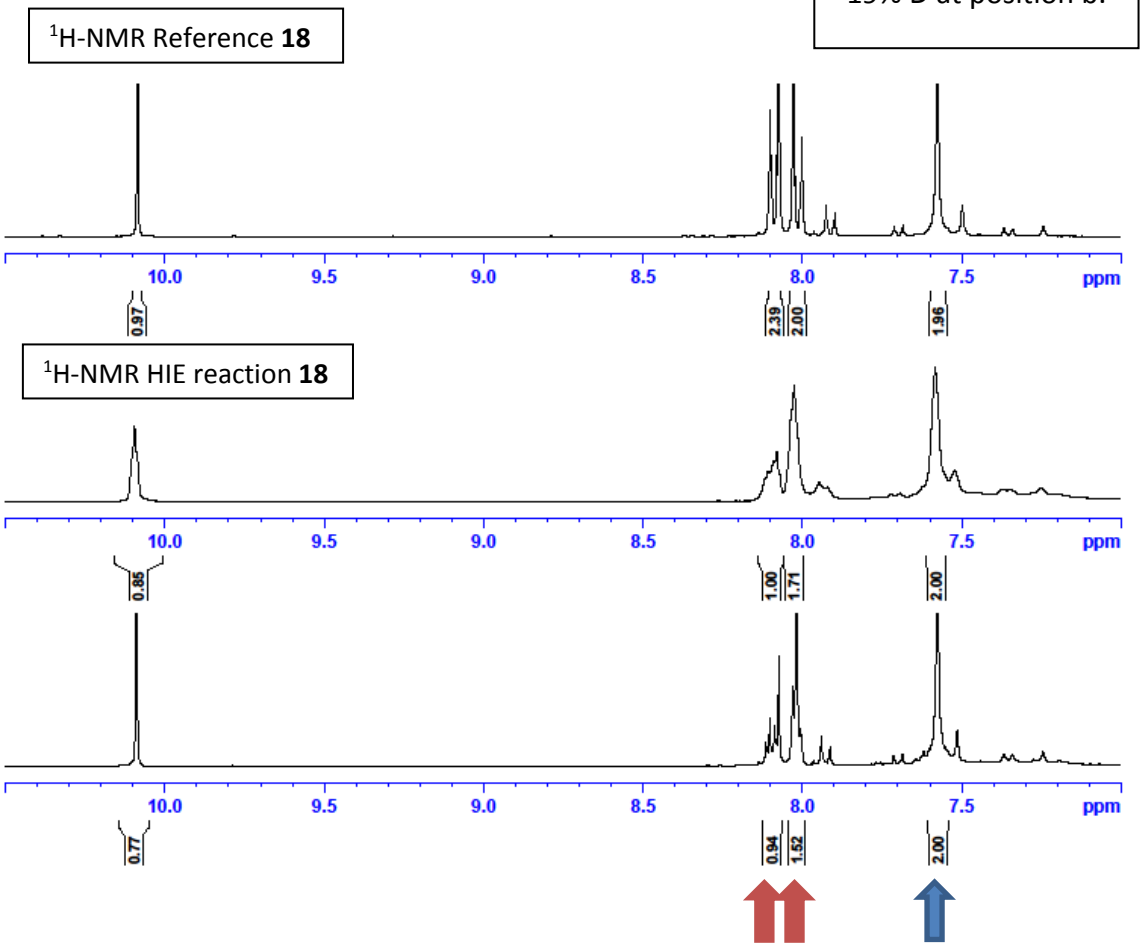

Nitrophenyl-acetate **19**

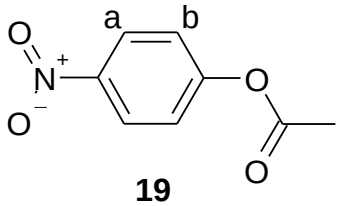

19

Molecular Weight =181,15
Molecular Formula =C8H7NO4

^{1}H NMR (300 MHz, DMSO-d$_6$): δ 8.28 (d, ^{3}J= 9.3 Hz, 2H, *H$_a$*), 7.43 (d, ^{3}J= 9.3 Hz, 2H, *H$_b$*), 2.32 (s, 3H) ppm. Incorporation expected at δ 8.28 and/or δ 7.43 (red arrow). Determined against reference-integral at δ 2.32 ppm (blue arrow).

Method B: 10 mg, 55 µmol **19**, 2.8 mg, 2.8 µmol catalyst **B$_a$**.

LC-MS (positive ESI): m/z 183.1 $[M(1D)+H]^+$ (4%), 184.1 $[M(2D)+H]^+$ (44%), 185.1 $[M(3D)+H]^+$ (48%), 186.1 $[M(4D)+H]^+$ (4%).

Yield: 1) 9.3 mg, 51 µmol, 93%; 97% D for δ 8.28, 22% D for 7.43.
2) 8.2 mg, 45 µmol, 82%; 97% D for δ 8.28, 21% D for 7.43.

Average: y=88%,
97% D at position a,
22% D at position b.

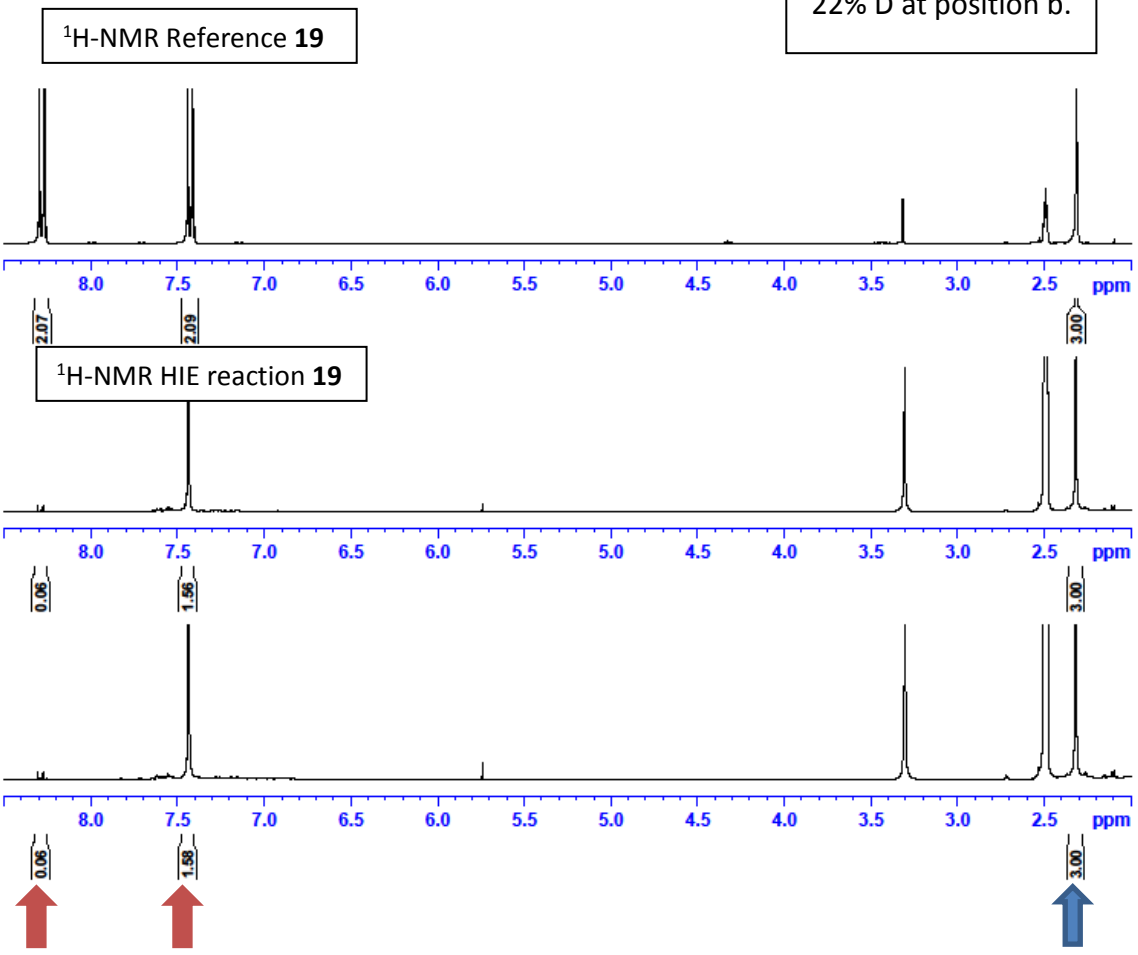

20

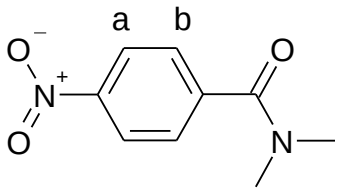

Molecular Weight =194.1917
Molecular Formula =C9H10N2O3

20

^{1}H NMR (300 MHz, DMSO-d_6): δ 8.29 (d, ^{3}J= 8.6 Hz, 2H, *H_a*), 7.59 (d, ^{3}J= 8.6 Hz, 2H, *H_b*), 3.15 (s, 3H, NMe), 2.97 (s, 3H, NMe) ppm. Incorporation expected at δ 8.29 and/or δ 7.59 (red arrow). Determined against reference-integral at δ 3.15 ppm (blue arrow).

Method B: 7.7 mg, 40 µmol **20**, 2.0 mg, 2.0 µmol catalyst **B_a**.

LC-MS (positive ESI): m/z 196.1 $[M(1D)+H]^+$ (5%), 197.1 $[M(2D)+H]^+$ (46%), 198.1 $[M(3D)+H]^+$ (49%).

Yield: 1) 7.5 mg, 39 µmol, 97%; 27% D for δ 8.29, 93% D for 7.59.
2) 7.1 mg, 36 µmol, 92%; 31% D for δ 8.29, 94% D for 7.59.

Average: y=95%, 29% D at position a, 94% D at position b.

^{1}H-NMR Reference **20**

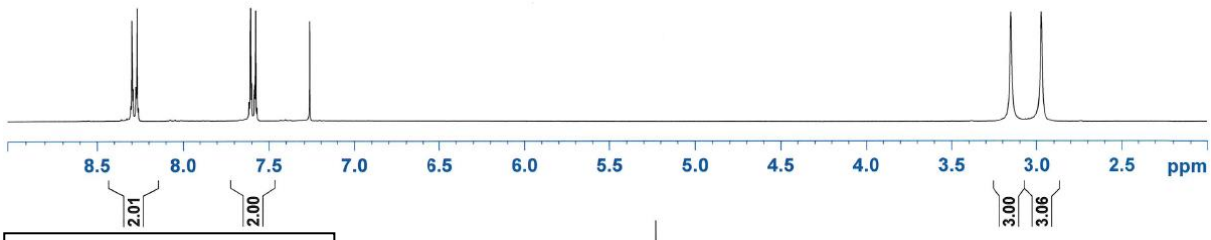

^{1}H-NMR HIE reaction **20**

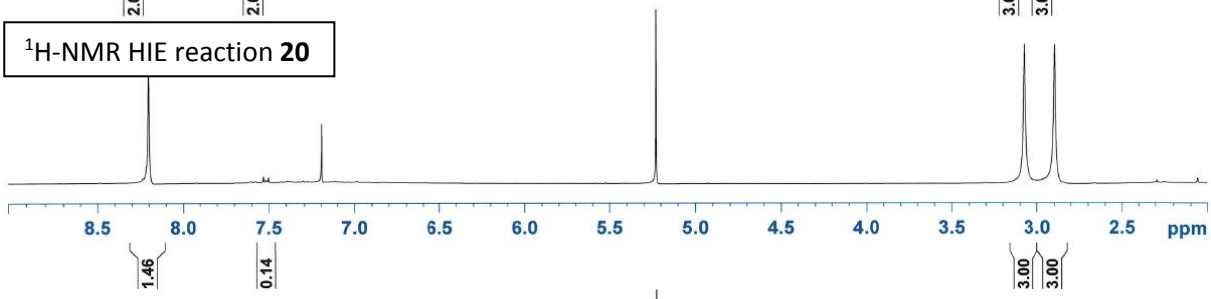

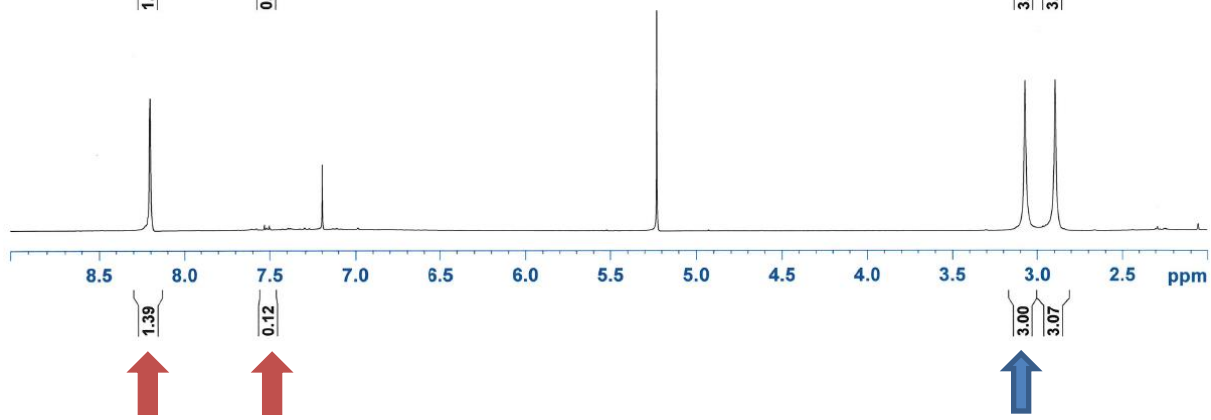

Methyl 4-acetamido-5-chloro-2-methoxybenzoate **21**

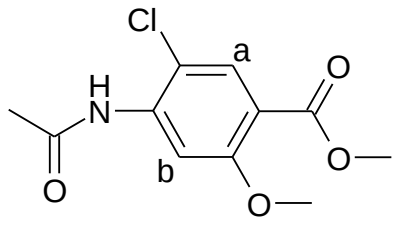

21

Molecular Weight =257.6756
Molecular Formula =C11H12ClNO4

^{1}H NMR (300 MHz, DMSO-d$_6$): δ 9.56 (s, 1H), 7.81 (s, 1H, *H_a*), 7.73 (s, 1H, *H_b*), 3.78 (s, 3H), 3.76 (s, 3H), 2.16 (s, 3H) ppm. Incorporation expected at δ 7.81 and/or δ 7.73 ppm (red arrow). Determined against reference-integral at δ 2.16 ppm (blue arrow).

Method B: 10 mg, 39 µmol **21**, 2.0 mg, 1.9 µmol catalyst **B$_a$**.

LC-MS (positive ESI): no interpretation because of the natural isotopes of the Cl.

Yield: 1) 9.1 mg, 35 µmol, 91%; 99% D for δ 7.73.
2) 9.2 mg, 36 µmol, 92%; 99% D for δ 7.73.

Average: y=92%,
99% D at position b.

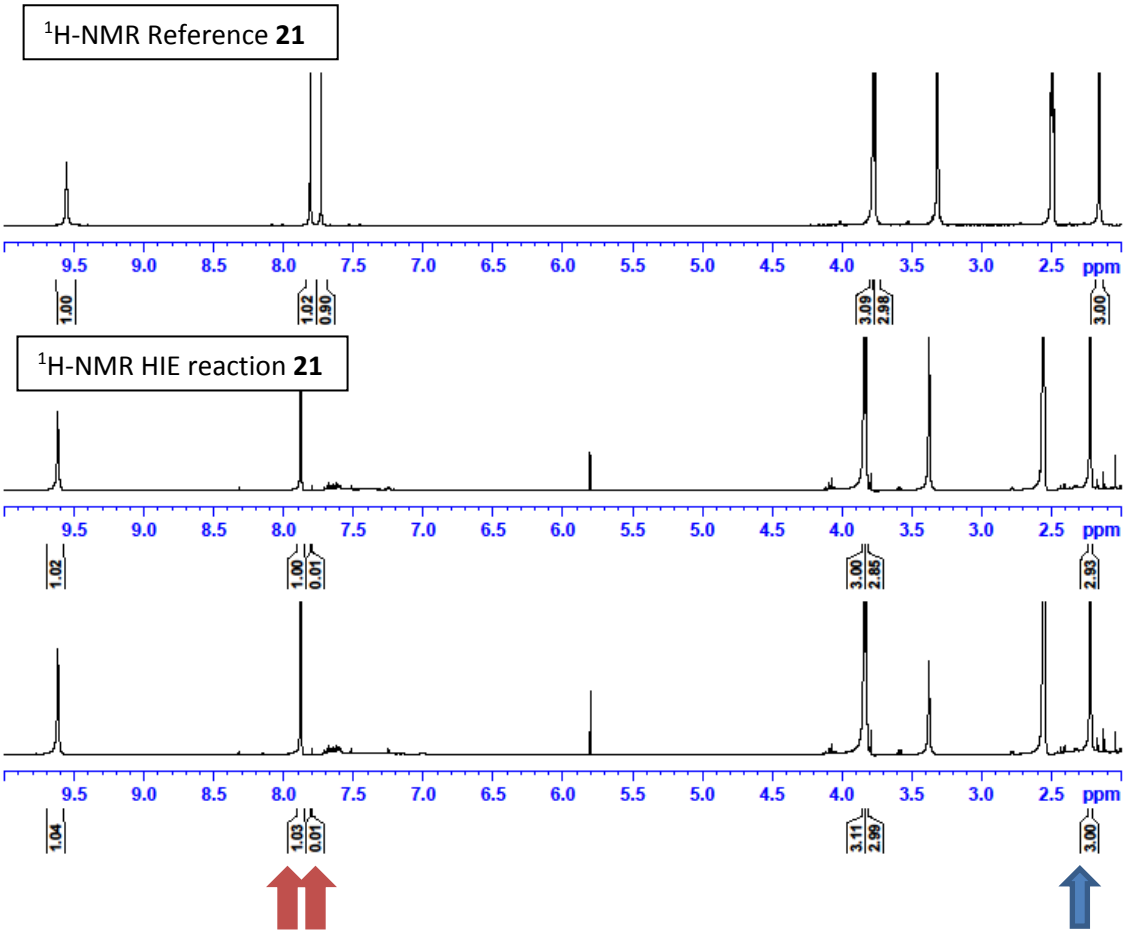

Methyl-4-acetamido-2-ethoxybenzoate **22**

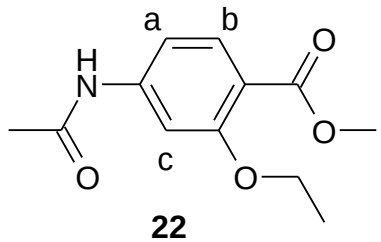

22

Molecular Weight =237,26
Molecular Formula =C12H15NO4

^{1}H NMR (300 MHz, DMSO-d$_6$): δ 10.16 (s, 1H), 7.64 (d, ^{3}J= 8.5 Hz, 1H, *H$_b$*), 7.46 (s, 1H, *H$_c$*), 7.16 (d, ^{3}J= 8.5 Hz, 1H, *H$_a$*), 4.02 (q, ^{3}J= 7 Hz, 2H), 3.73 (s, 3H), 2.06 (s, 3H), 1.33 (t, ^{3}J= 7 Hz, 3H) ppm. Incorporation expected at δ 7.64 and/or δ 7.46 and/or δ 7.16 ppm (red arrow). Determined against reference-integral at δ 1.33 ppm.

Method B: 10 mg, 42 µmol **22**, 2.1 mg, 2.1 µmol catalyst **B$_a$**.

LC-MS (positive ESI): m/z 239.2 $[M(1D)+H]^+$ (10%), 240.1 $[M(2D)+H]^+$ (80%), 241.1 $[M(3D)+H]^+$ (10%).

Yield: 1) 9.5 mg, 40 µmol, 95%; 75% D for δ 7.64, 6% D for δ 7.64, 89% D for δ 7.16.
2) 8.5 mg, 36 µmol, 85%; 81% D for δ 7.64, 9% D for δ 7.64, 90% D for δ 7.16.

Average: y= 90%, 90% D at position a, 78% D at position b, 8% D at position c.

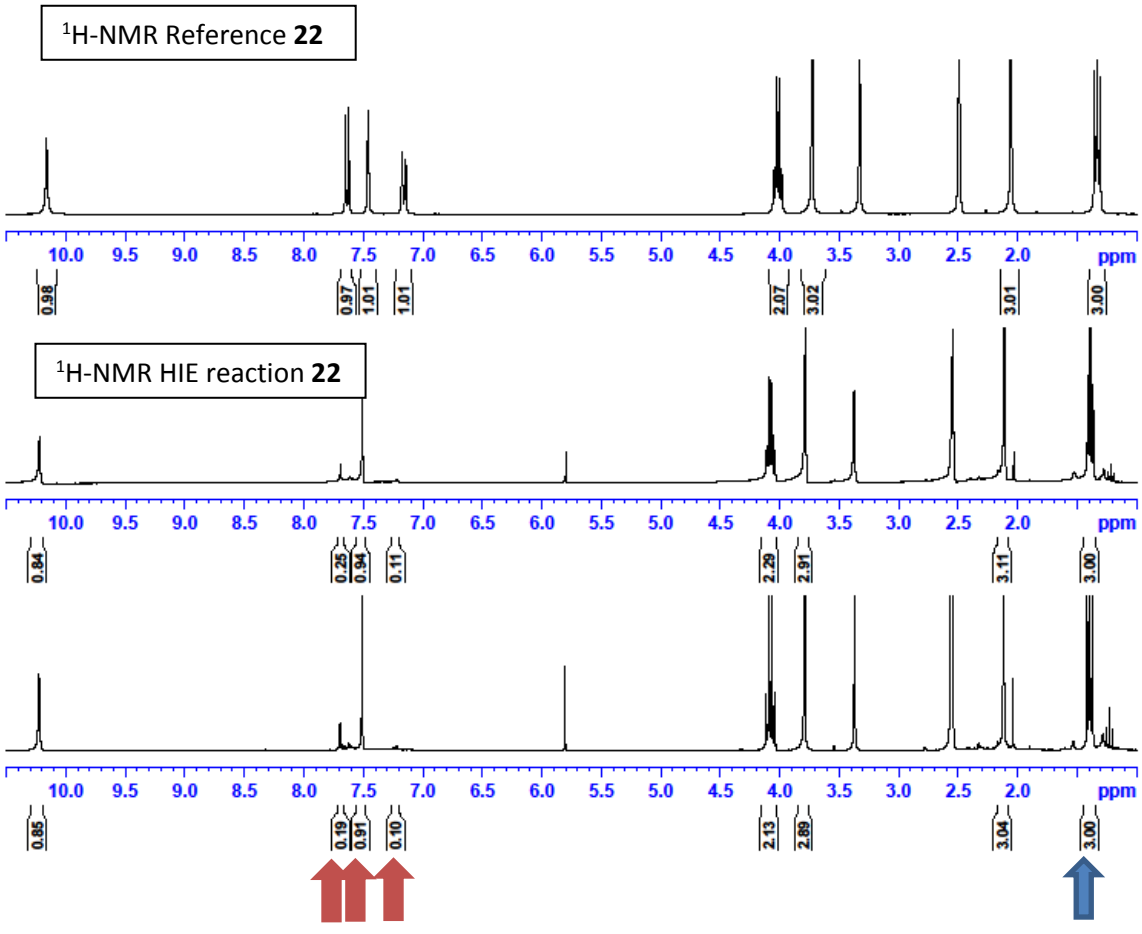

Method B (0 °C): 10 mg, 42 µmol **22**, 2.1 mg, 2.1 µmol catalyst $\mathbf{B_a}$.

Yield: 1) 9.5 mg, 40 µmol, 95%; 37% D for δ 7.64, 0% D for δ 7.64, 60% D for δ 7.16.
2) 8.9 mg, 38 µmol, 89%; 37% D for δ 7.64, 0% D for δ 7.64, 56% D for δ 7.16.

Average: y= 92%, 58% D at position a, 37% D at position b, 0% D at position c.

^{1}H-NMR Reference **22**

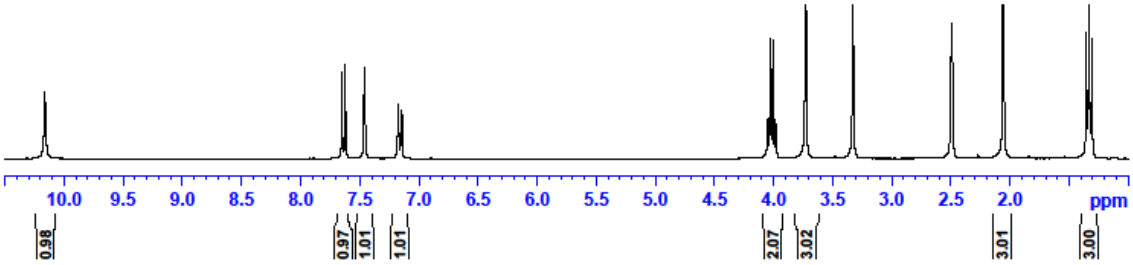

^{1}H-NMR HIE reaction **22**

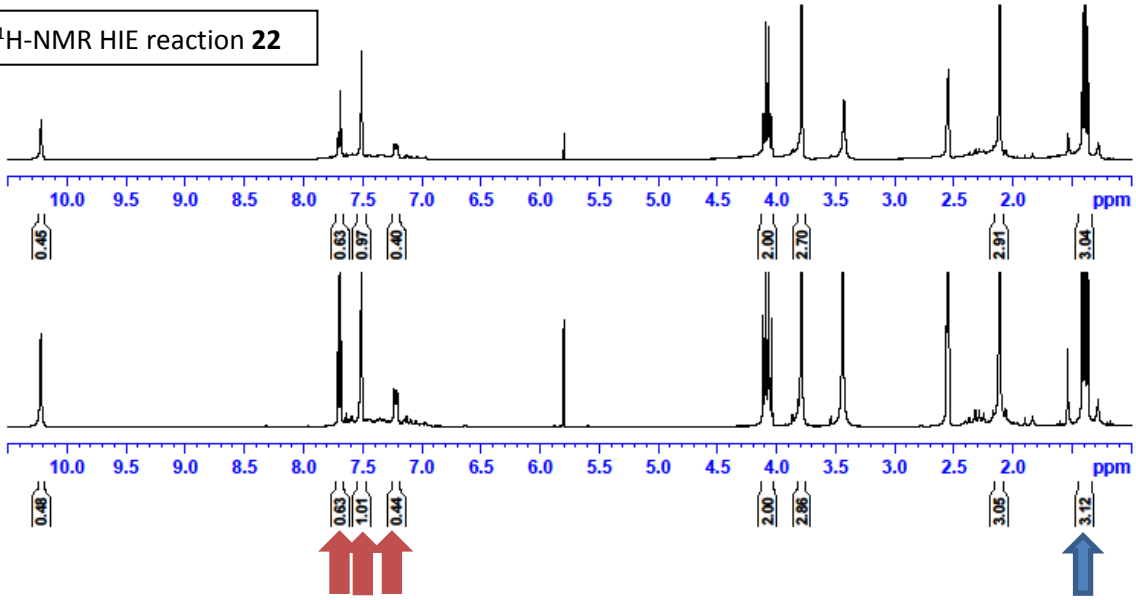

HIE experiments on drugs 23-31 (*scheme III.2.5*)

Nimesulide **23**

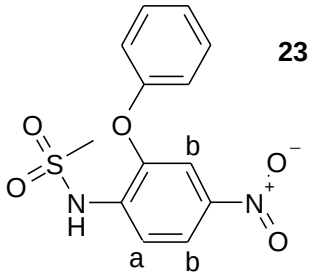

Molecular Weight =308,31
Molecular Formula =C13H12N2O5S

^{1}H NMR (300 MHz, DMSO-d$_6$: δ 10.13 (s, 1H), 8.02 (dd, ^{3}J= 9.0 Hz, ^{4}J= 2.6 Hz, 1H, *H$_b$*), 7.73 (d, ^{3}J= 9.0 Hz, 1H, *H$_a$*), 7.53 (d, ^{4}J= 2.6 Hz, 1H, *H$_b$*), 7.48 (t, ^{3}J= 8.1 Hz, 2H), 7.27 (t, ^{3}J= 7.4 Hz, 1H), 7.16 (d, ^{3}J= 7.6 Hz, 2H), 3.19 (s, 3H) ppm. Incorporation expected at δ 8.02 and δ 7.53 and/or 7.73 ppm (red arrow). Determined against reference-integral at δ 3.19 ppm (blue arrow).

Method B: 10 mg, 32 µmol **23**, 1.6 mg, 1.6 µmol catalyst **B$_a$**.

LC-MS (positive ESI): m/z, 309.2 [M+H]$^+$ (3%), 310.2 [M(1D)+H]$^+$ (20%), 311.2 [M(2D)+H]$^+$ (63%), 312.2 [M(3D)+H]$^+$ (14%).

Yield: 1) 9.6 mg, 31 µmol, 96%; 92%D for δ 8.02 and 64%D for δ 7.53 ppm.
2) 9.3 mg, 30 µmol, 93%; 95%D for δ 8.02 and 80%D for δ 7.53 ppm.

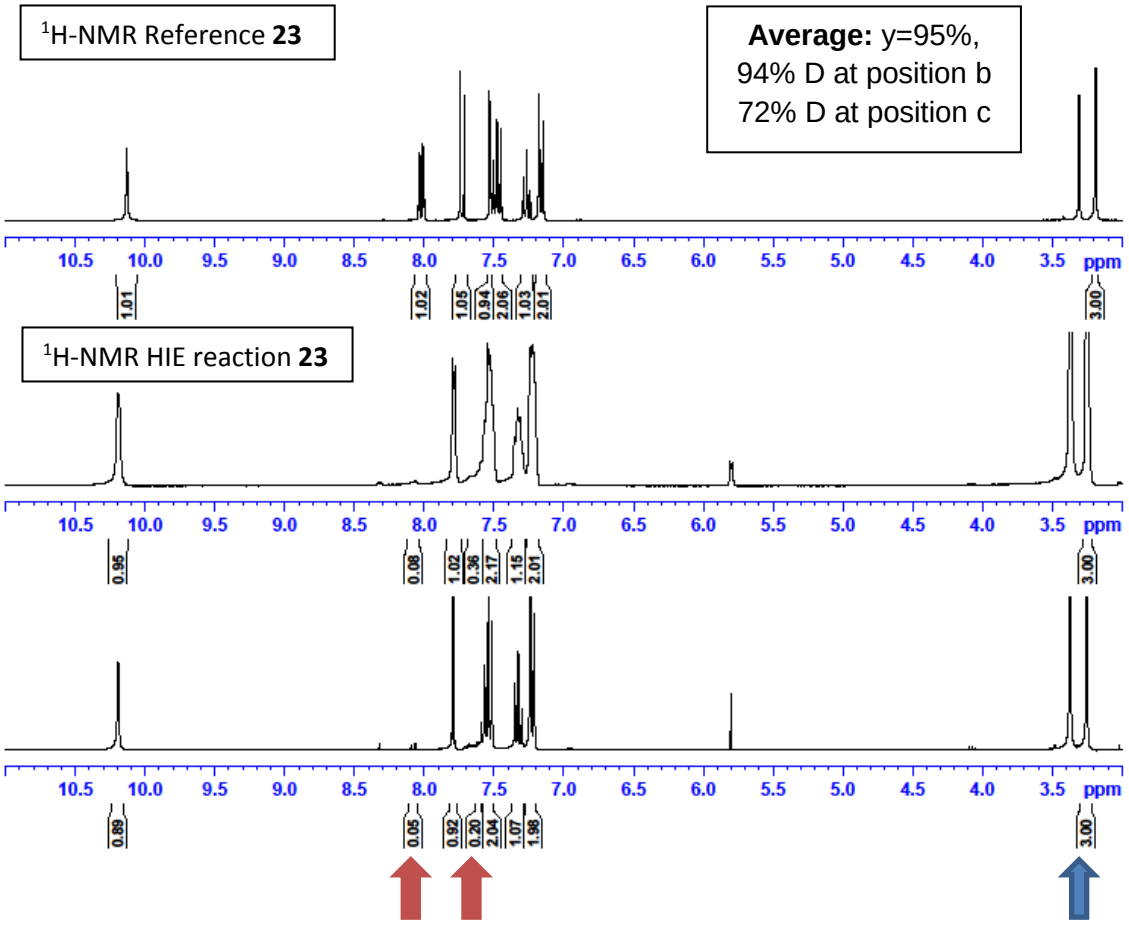

Celecoxib **24**

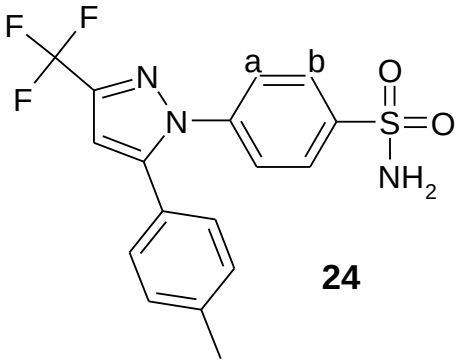

24

Molecular Weight =381,38
Molecular Formula =C17H14F3N3O2S

^{1}H NMR (300 MHz, DMSO-d$_6$: δ 7.86 (d, ^{3}J= 8.7 Hz, 2H, *H$_b$*), 7.53 (d, ^{3}J= 8.7 Hz, 2H, *H$_a$*), 7.51 (s, 2H), 7.25-7.15 (m, 5H), 2.31 (s, 3H) ppm. Incorporation expected at δ 7.86 and/or δ 7.53 ppm (red arrow). Determined against reference-integral at δ 2.31 ppm (blue arrow).

Method B: 10 mg, 26 µmol **24**, 1.3 mg, 1.3 µmol catalyst **B$_a$**.

LC-MS (positive ESI): m/z, 382.3 $[M+H]^+$ (3%), 383.2 $[M(1D)+H]^+$ (10%), 384.2 $[M(2D)+H]^+$ (63%), 312.2 $[M(3D)+H]^+$ (24%).

Yield: 1) 9.9 mg, 26 µmol, 99%; 13% D for δ 7.86, 86% D for δ 7.53.
2) 9.6 mg, 25 µmol, 96%; 10% D for δ 7.86, 91% D for δ 7.53.

Average: y=98%, 89% D at position a, 11% D at position b.

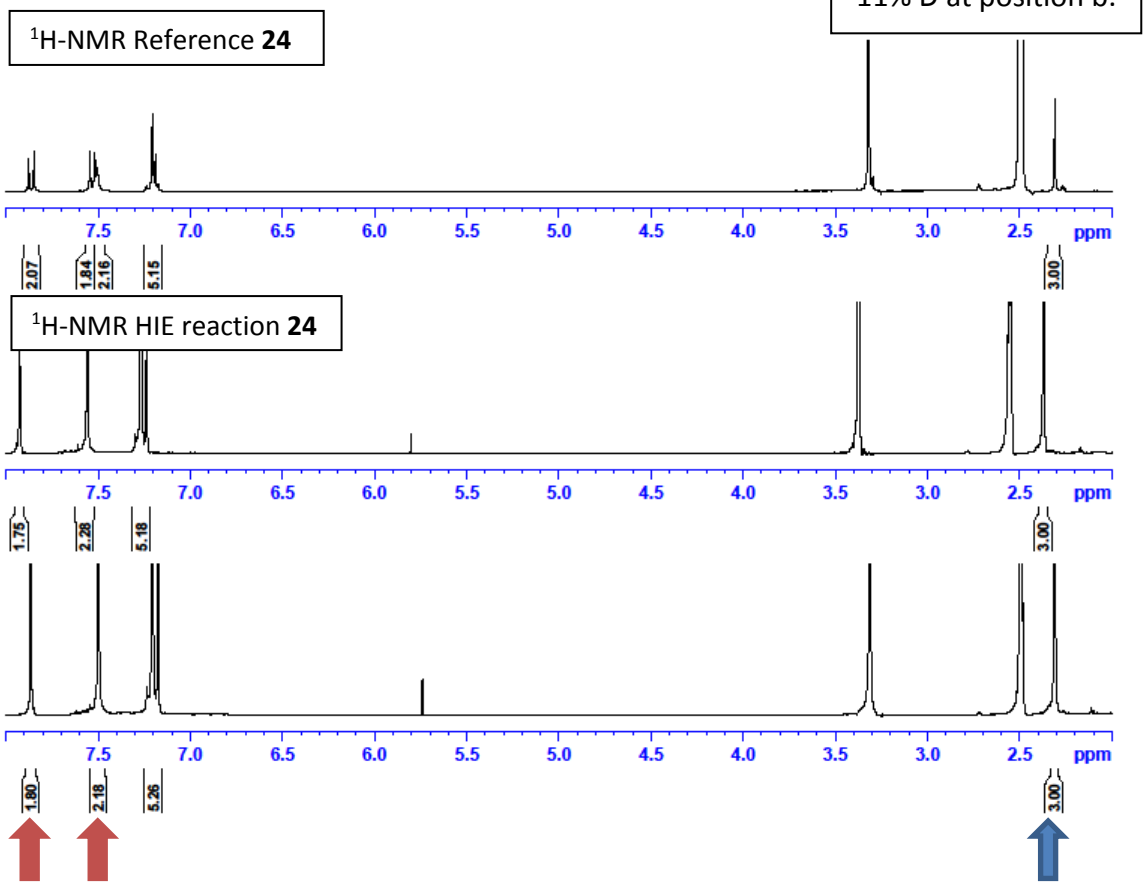

25

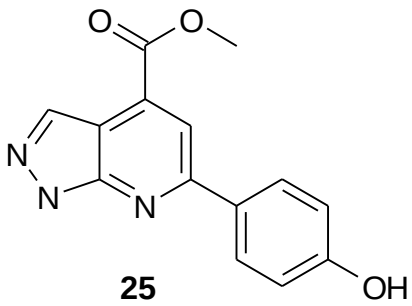

25

Molecular Weight =269.2621
Molecular Formula =C14H11N3O3

^{1}H NMR (300 MHz, MeOD): δ 8.03 (m, 3H, $CH_{(a)}$ and 2 $CH_{(b)}$), 6.92 (d, ^3J= 8.7 Hz, 2H, 2 $CH_{(c)}$), 4.04 (s, 3H, CH_3), 2.67 (s, 3H, CH_3) ppm. Incorporation expected at δ 8.03 ppm (red arrow). Determined against reference-integral at δ 4.04 ppm (blue arrow).

Method B (80°C): 5.7 mg, 20 µmol **25**, 1.0 mg, 1.0 µmol catalyst **B_a**.

LC-MS (positive ESI): m/z, 270.2 $[M+H]^+$ (9%), 271.2 $[M(1D)+H]^+$ (79%), 272.1 $[M(2D)+H]^+$ (12%).

Yield: 1) 5.2 mg, 18 µmol, 91%; 50%D for δ 8.03.

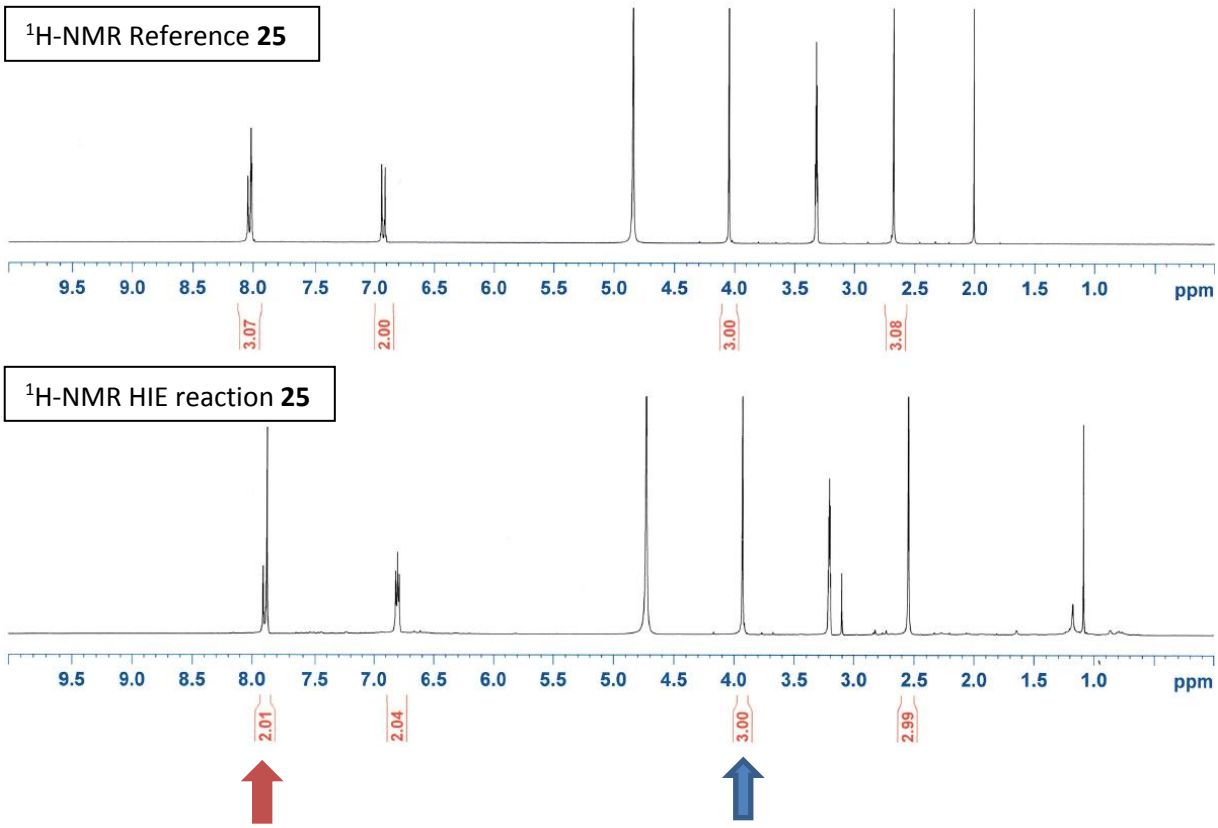

26

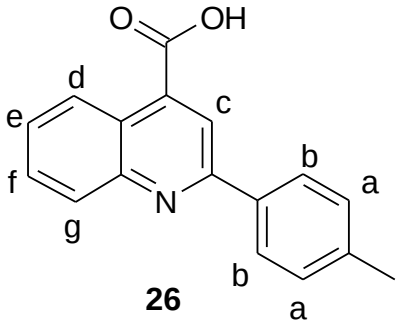

26

Molecular Weight =263.2987
Molecular Formula =C17H13NO2

^{1}H NMR (300 MHz, MeOD): δ 8.78 (d, ^3J= 8.6, 1H, $CH_{(d)}$ or $CH_{(g)}$), 8.44 (s, 1H, $CH_{(c)}$), 8.19 (d, ^3J= 8.6 Hz, 1H, $CH_{(d)}$ or $CH_{(g)}$), 8.09 (d, ^3J= 8.5, 2H, 2 $CH_{(b)}$), 7.84 (m, 1H, $CH_{(e)}$ or $CH_{(f)}$), 7.67 (m, 1H, $CH_{(e)}$ or $CH_{(f)}$), 7.40 (d, ^3J= 8.5, 2H, 2 $CH_{(a)}$), 2.45 (s, 3H, CH_3) ppm. Incorporation expected at δ 8.09 ppm (red arrow). Determined against reference-integral at δ 2.45 ppm (blue arrow).

Method B (80°C): 5.3 mg, 20 µmol **26**, 1.0 mg, 1.0 µmol catalyst **B_a**.

LC-MS (positive ESI): m/z, 264.2 $[M+H]^+$ (5%), 265.1 $[M(1D)+H]^+$ (85%), 266.1 $[M(2D)+H]^+$ (10%).

Yield: 1) 4.7 mg, 18 µmol, 89%; 54%D for δ 8.09.

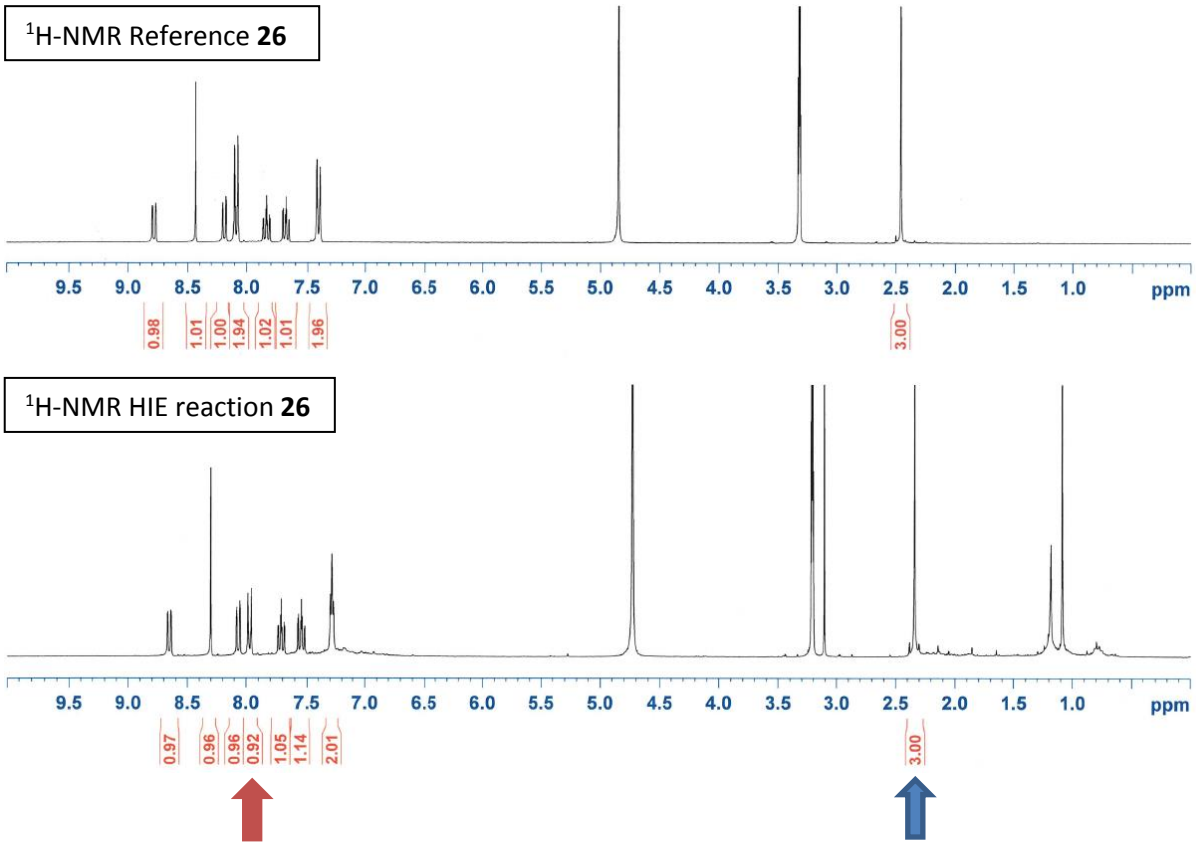

Glybenclamide **27**

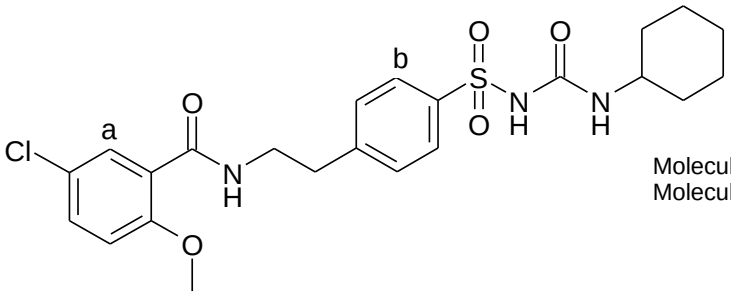

Molecular Weight =494,01
Molecular Formula =C23H28ClN3O5S

^{1}H NMR (300 MHz, DMSO-d$_6$: δ 10.30 (s, 1H), 8.26 (t, ^{3}J= 5.6 Hz, 1H), 7.83 (d, ^{3}J= 8.3 Hz, 2H, *H$_b$*), 7.63 (d, ^{4}J= 2.9 Hz, 1H, *H$_a$*), 7.53-7.44 (m, 3H), 7.14 (d, ^{3}J= 9.0 Hz, 1H), 6.32 (d, ^{3}J= 7.8 Hz, 1H), 3.79 (s, 3H), 3.54 (q, ^{3}J= 6.7 Hz, 2H), 2.92 (t, ^{3}J= 7.0 Hz, 2H), 1.70-1.41 (m, 5H), 1.14 (sep, ^{3}J= 9.7 Hz, 6H) ppm. Incorporation expected at δ 7.83 and/or δ 7.63 ppm (red arrow). Determined against reference-integral at δ 3.79 ppm (blue arrow).

Method B: 10 mg, 20 µmol **25**, 1.0 mg, 1.0 µmol catalyst **B$_a$**.

LC-MS (positive ESI): no interpretation because of the natural isotopes of the Cl.

Yield: 1) 10.0 mg, 20 µmol, 100%; 82% for δ 7.63.
2) 9.5 mg, 19 µmol, 95%; 83% for δ 7.63.

Average: y=98%,
83% D at position a.

^{1}H-NMR Reference **25**

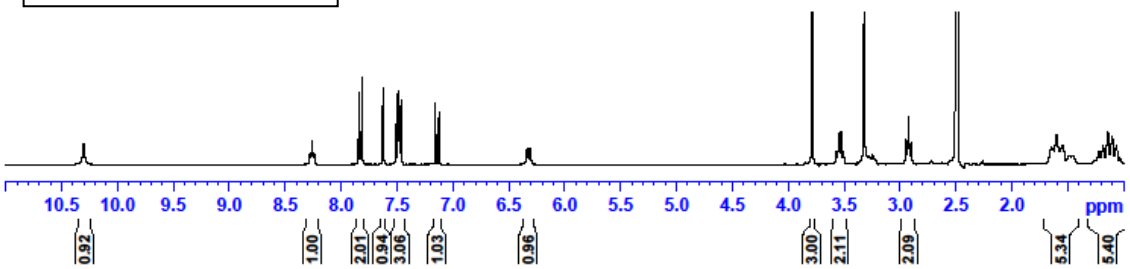

^{1}H-NMR HIE reaction **25**

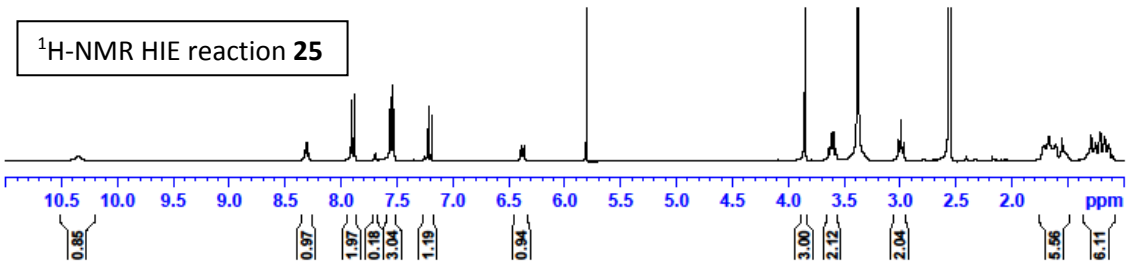

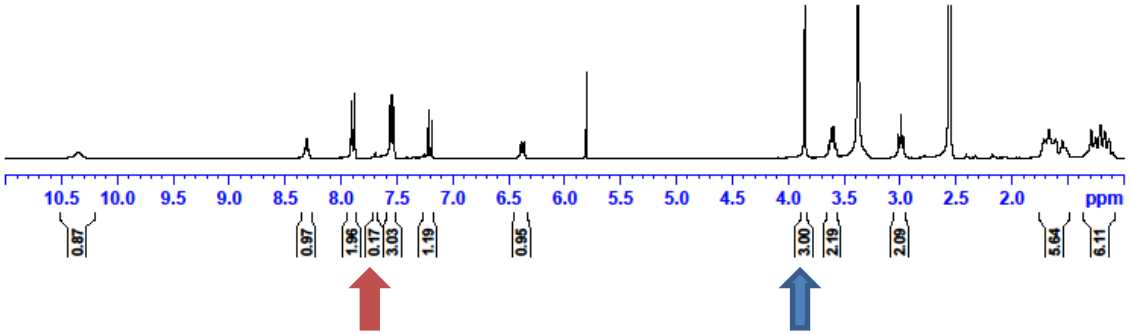

28

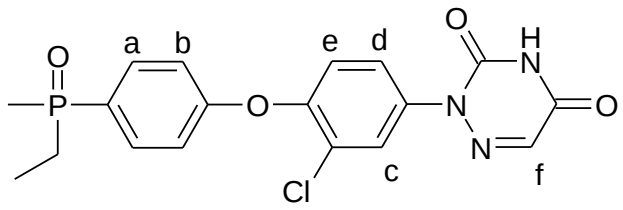

Molecular Weight =405.78
Molecular Formula =C18H17ClN3O4P

28

^{1}H NMR (300 MHz, DMSO-d$_6$: δ 12.42 (s, 1H, NH), 7.81 (d, ^{3}J= 2.5 Hz, 1H, CH$_c$), 7.77 (d, ^{3}J= 8.8 Hz, 2H, 2 CH$_a$), 7.68 (s, 1H, CH$_f$), 7.56 (dd, ^{3}J= 8.8 Hz and ^{4}J= 2.5 Hz, 1H, CH$_d$), 7.34 (d, ^{3}J= 8.8 Hz, 1H, CH$_e$), 7.11 (d, ^{3}J= 8.8 Hz, 2H, 2 CH$_a$), 1.88 (m, 2H, CH$_2$), 1.62 (m, 3H, CH$_3$), 0.97 (m, 3H, CH$_3$) ppm. Incorporation expected at δ 7.81 and/or δ 7.56 ppm (red arrow). Determined against reference-integral at δ 1.62 ppm (blue arrow).

Method B: 5.0 mg, 12.3 µmol **28**, 1.2 mg, 1.2 µmol catalyst **B$_a$**.

LC-MS (positive ESI): no interpretation because of the natural isotopes of the Cl.

Yield: 1) 4.9 mg, 12.0 µmol, 98%; 70%D for δ 7.81 and 67%D for δ 7.56.

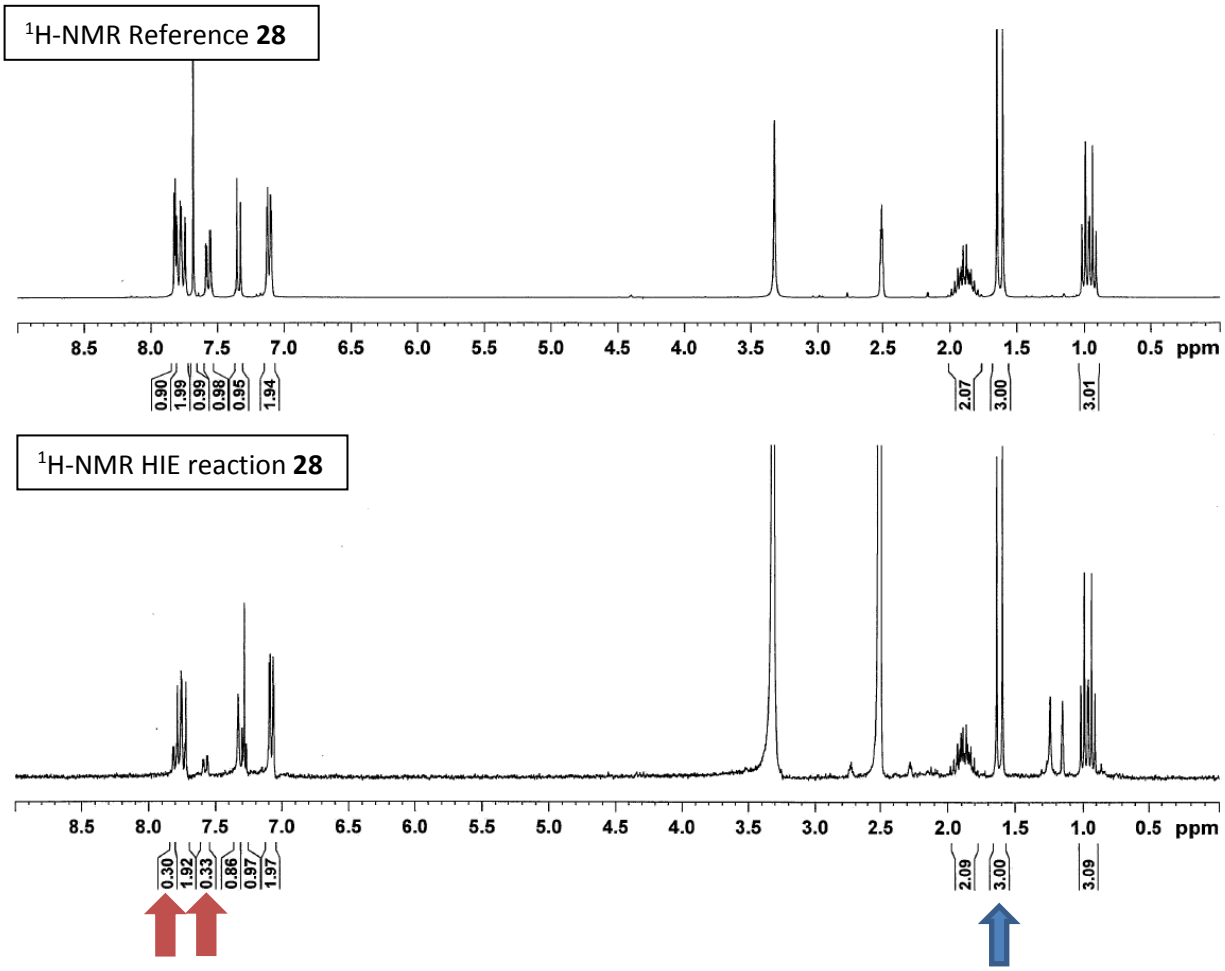

29

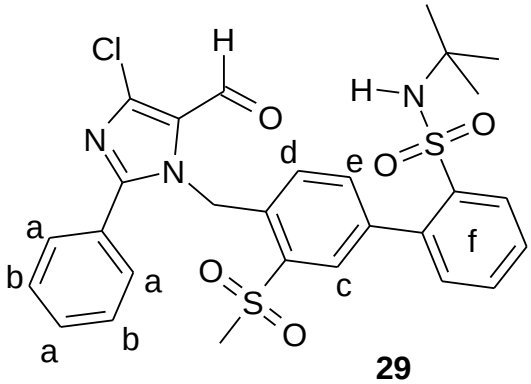

29

Molecular Weight =586.13
Molecular Formula =C28H28ClN3O5S2

^{1}H NMR (300 MHz, DMSO-d$_6$: δ 9.76 (s, 1H, CHO), 8.08 (dd, ^{3}J= 7.7 Hz and ^{4}J= 1.5 Hz, 1H, CH ring f), 8.02 (d, ^{3}J= 1.89 Hz, 1H, CH_c), 7.67 (m, 3H, CH_e, CH ring f), 7.58 (m, 3H, 3 CH_a), 7.52 (m, 2H, 2 CH_b), 7.39 (m, 1H, CH ring f), 6.93 (m, 1H, CH ring f), 5.93 (s, 2H, CH_2), 3.34 (s, 2H, CH_2), 0.97 (s, 9H, tBu) ppm. Incorporation expected at δ 7.58 and/or δ [ring f] ppm (red arrow). Determined against reference-integral at δ 0.97 ppm (blue arrow).

Method B: 5.0 mg, 8.5 µmol **29**, 0.9 mg, 0.9 µmol catalyst **B$_a$**.

LC-MS (positive ESI): no interpretation because of the natural isotopes of the Cl.

Yield: 1) 5.2 mg, 8.8 µmol **29**, quant.; 67%D for δ 7.58 ppm.

^{1}H-NMR Reference **29**

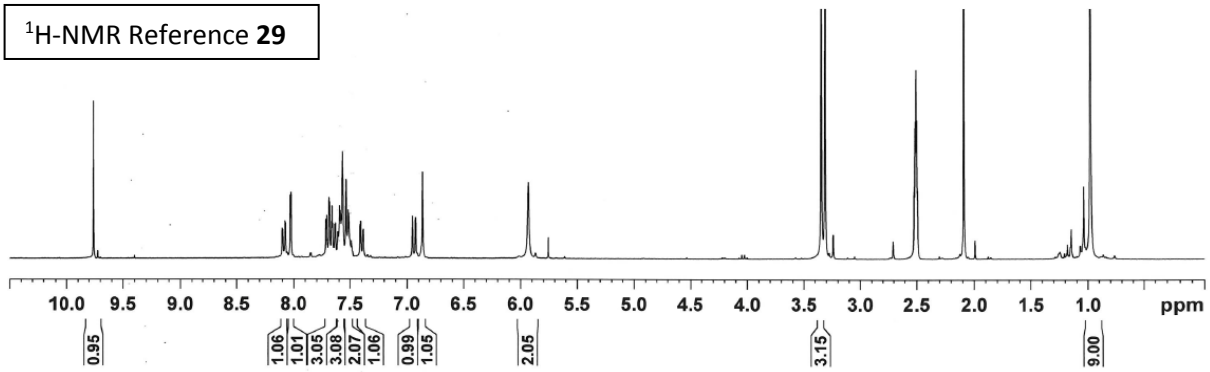

^{1}H-NMR HIE reaction **29**

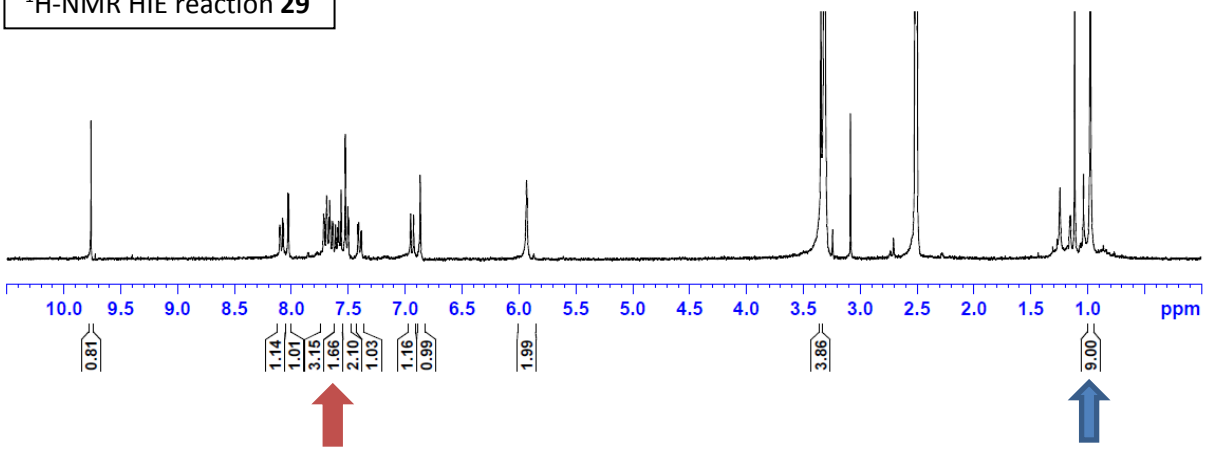

Vismodegib **30**

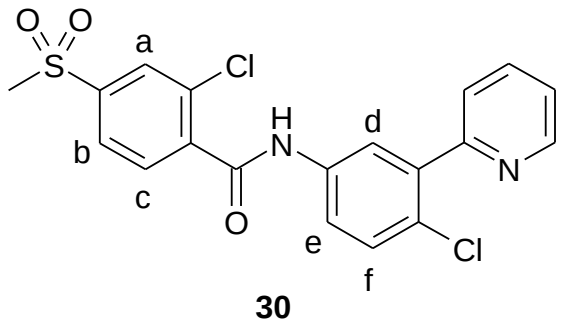

30

Molecular Weight =421.3050
Molecular Formula =C19H14Cl2N2O3S

^{1}H NMR (300 MHz, $CDCl_3$): δ 9.56 (s, 1H, NH), 8.42 (m, 1H, CH pyridine), 8.04 (dd, ^{3}J= 8.6 Hz and 2.6 Hz, 1H, CH_e), 7.89 (d, ^{4}J= 1.6 Hz, 1H, CH_a), 7.72 (m, 4H, 1 CH pyridine, CH_b, CH_c, CH_d), 7.60 (d, ^{3}J= 8.0 Hz, 1H, CH pyridine), 7.50 (d, ^{3}J= 8.6 Hz, 1H, CH_f), 7.21 (m, 1H, CH pyridine), 3.02 (s, 3H, CH_3) ppm. Incorporation expected at δ 7.72 ppm (red arrow). Determined against reference-integral at δ 3.02 ppm (blue arrow).

Method B: 10.5 mg, 25 µmol **30**, 1.3 mg, 1.3 µmol catalyst **B_a**.

LC-MS (positive ESI): no interpretation because of the natural isotopes of the Cl.

Yield: 1) 8.6 mg, 20 µmol, 82%; 62%D for δ 7.72.
2) 9.9 mg, 23 µmol, 94%; 72%D for δ 7.72.

Average: y=88%,
67% D at position d

^{1}H-NMR Reference **30**

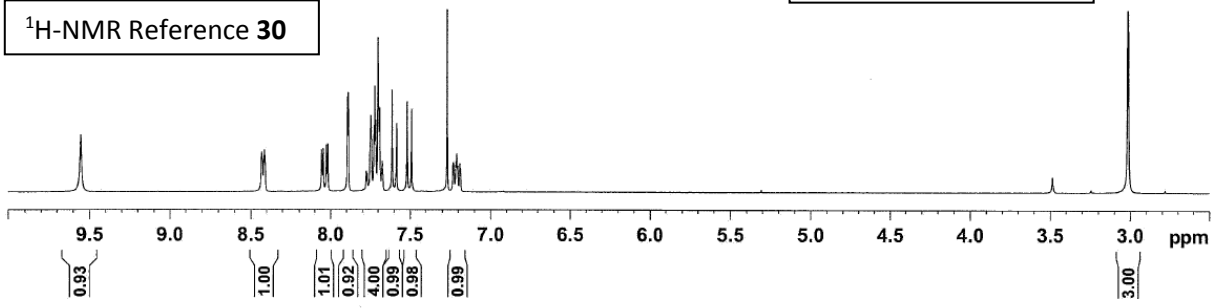

^{1}H-NMR HIE reaction **30**

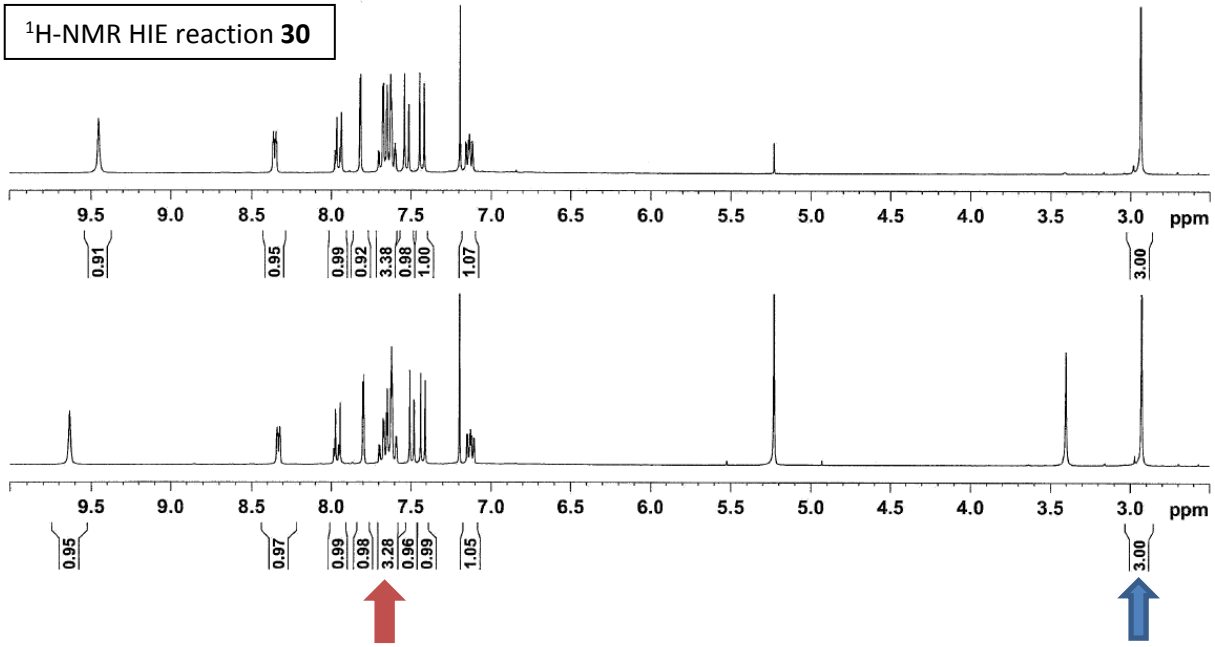

31

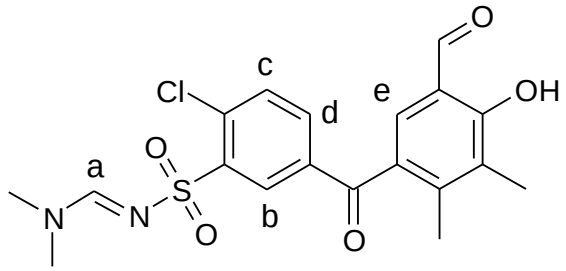

Molecular Weight =422.89
Molecular Formula =C19H19ClN2O5S

31

^{1}H NMR (300 MHz, DMSO-d$_6$: δ 11.52 (s, 1H, CHO), 9.98 (s, 1H, OH), 8.35 (d, ^{3}J= 2.2 Hz, 1H,), 8.29 (s, 1H,), 7.87 (dd, ^{3}J= 8.2 Hz, ^{4}J= 2.0 Hz, 1H,), 7.77 (d, ^{3}J= 8.4 Hz, 1H,), 7.73 (s, 1H,), 3.20 (s, 3H, CH3), 2.93 (s, 3H, CH3), 2.28 (s, 3H, CH3), 2.21 (s, 3H, CH3) ppm. Incorporation expected at δ and δ ppm (red arrow). Determined against reference-integral at δ 2.21 ppm (blue arrow).

Method B: 5.0 mg, 12.3 µmol **31**, 1.2 mg, 1.2 µmol catalyst **B$_a$**.

LC-MS (positive ESI): no interpretation because of the natural isotopes of the Cl.

Yield: 1) 5.3 mg, 12.6 µmol, quant.; 95% D for δ 7.87 and 89% D for δ 7.73 ppm.

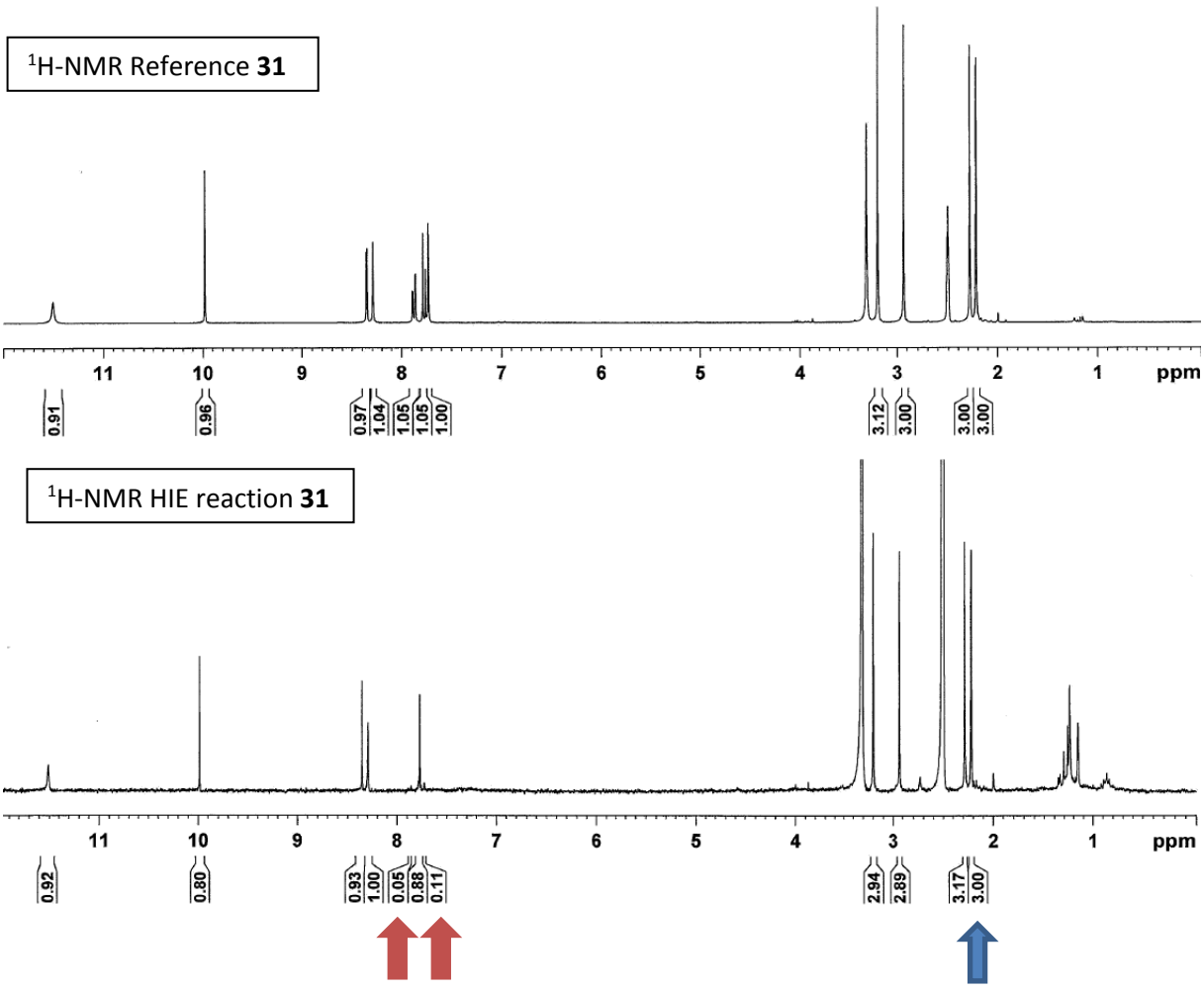

Computational Studies

Density functional theory calculations were done by Dr. Stefan Güssregen from the Computational Drug Design group in Sanofi.

Details of Computational Methods

Density functional theory (DFT)[1,2] has been employed to calculate gas-phase electronic structures and energies for all species in this paper. We followed the approach validated by Kerr *et al*.[3] and used the hybrid meta-GGA exchange correlation functional M06[4] in combination with the 6-31G(d)[5] basis set for non-metal atoms and the Stuttgart RSC[6] effective core potential for Iridium to optimize all structures. Transition states were located at the same level of theory. Harmonic vibrational frequencies have been calculated at the same level of theory to characterize the respective minima (i.e.) and first order saddle points (TS). Thermal energies have been calculated at 298.15K corresponding to experimental conditions. Atomic coordinates for Iridium, Deuterium and the Triphenylphosphine and NHC ligands were taken from Kerr *et al.*[3] as starting point of the calculations. All calculations have been performed using the Gaussian 09[7] quantum chemistry program package. All coordinates provided are listed in Cartesian format, with charge and multiplicity of each system given at the top of the coordinate list (i.e. 0 1 = neutral singlet; 1 1 = 1+ charged singlet).

Calculation of stationary points

Following the approach published by Kerr *et al*.[3] a catalytic complex was calculated assuming that two molecules of dichloromethane (DCM) are coordinated to the iridium center. The relative free energies (ΔG_{rel}) of the stationary points (SP) on the potential energy surface (PES) for coordination complexes **11a**, transition states **11b** and insertion products **11c** were calculated based on the sums of the free and electronic energies for the respective reaction partners using the following calculation scheme:

$$\Delta Grel(\text{SP}) = [\ E(\text{SP}) + 2{*}E(\text{DCM})\ ] - [\ E(\text{Catalytic Complex}) + E(\text{Substrate})\ ]$$

If directing groups bear more than one atom that is suitable for coordination, all possible reactions routes were investigated, in order to identify the one with the lowest energy profile. All results are summarized in Table S1.

Table S1. Relative free energy values (ΔG_{rel}) for different directing groups to form the coordination complex (CC), insertion product (IP) and transition state (TS) in the HIE reaction.

Directing Group	Coord. Atom	ΔG_{rel}(CC,11a) [kcal mol^{-1}]	ΔG_{rel}(IP,11c) [kcal mol^{-1}]	ΔG_{rel}(TS,11b) [kcal mol^{-1}]	$\Delta\Delta G_{rel}$(11a→11b) [kcal mol^{-1}]
-2-imidazole 2	N	-27.5	-22.8	-3.7	23.9
-N-CO-Me 3	O	-23.7	-13.8	3.7	27.4
	N	-2.5	12.8	24.5	27.0
-CO-Me 4	O	-23.0	-13.6	-0.3	22.7
-NO_2 5	O	-16.6	-11.9	2.0	18.5
-CO-NEt_2 6	O	-23.0	-5.3	4.6	27.6
-CO-H 7	O	-20.3	-14.5	0.4	20.6
-COOMe 8	O	-20.9	-9.4	3.6	24.4
-OCOMe 9	O	-14.3	-12.2	8.7	23.0
-SO_2-NH_2 10	O1	-18.7	-14.2	3.0	21.7
	O2	-17.5	-11.7	6.7	24.2
	N	-21.5	-16.3	-0.4	21.1

References

(1) Kohn, W.; Sham, L., J., Phys. Rev. 1965, 140, 1133 - 1138.

(2) Parr, R. G.; Yang, W. T., Density Functional Theory of Atoms and Molecules, Oxford University Press, New York, 1989.

(3) a) A.R. Cochrane, C. Idziak, W.J. Kerr, B. Mondal, L.C. Paterson, T. Tuttle, S. Andersson, G.N. Nilsson, *Org. Biomol. Chem.* **2014**, *12*, 3598-3603. b) W.J. Kerr, M. Reid, T. Tuttle, *Angew. Chem. Int. Ed.* **2017**, *56*, 7808-7812. c) W.J. Kerr, M. Reid, T. Tuttle, *ACS Catal.* **2015**, *5*, 402-410.

(4) Zhao, Y.; Truhlar, D. G., Theor. Chem. Acc. 2008, 120, 215 - 241.

(5) a) Frisch, M. J.; Pople, J. A.; Binkley, J. S., J. Chem. Phys., 1984, 80, 3265 – 3269. b) Ditchfield, R.; Hehre, W. J.; Pople, J. A., J. Chem. Phys. 1971, 54, 724 - 728.

(6) Andrae, D.; Haussermann, U.; Dolg, M.; Stoll, H.; Preuss, H., Theor. Chim. Acta 1990, 77, 123 - 141.

(7) Gaussian 09, Revision E.01, M. J. Frisch, G. W. Trucks, H. B. Schlegel, G. E. Scuseria, M. A. Robb, J. R. Cheeseman, G. Scalmani, V. Barone, B. Mennucci, G. A. Petersson, H. Nakatsuji, M. Caricato, X. Li, H. P. Hratchian, A. F. Izmaylov, J. Bloino, G. Zheng, J. L. Sonnenberg, M. Hada, M. Ehara, K. Toyota, R. Fukuda, J. Hasegawa, M. Ishida, T. Nakajima, Y. Honda, O. Kitao, H. Nakai, T. Vreven, J. A. Montgomery, Jr., J. E. Peralta, F. Ogliaro, M. Bearpark, J. J. Heyd, E. Brothers, K. N. Kudin, V. N. Staroverov, T. Keith, R. Kobayashi, J. Normand, K. Raghavachari, A. Rendell, J. C. Burant, S. S. Iyengar, J. Tomasi, M. Cossi, N. Rega, J. M. Millam, M. Klene, J. E. Knox, J. B. Cross, V. Bakken, C. Adamo, J. Jaramillo, R. Gomperts, R. E. Stratmann, O. Yazyev, A. J. Austin, R. Cammi, C. Pomelli, J. W. Ochterski, R. L. Martin, K. Morokuma, V. G. Zakrzewski, G. A. Voth, P. Salvador, J. J. Dannenberg, S. Dapprich, A. D. Daniels, O. Farkas, J. B. Foresman, J. V. Ortiz, J. Cioslowski, and D. J. Fox, Gaussian, Inc., Wallingford CT, 2013.

Part IV
Homogeneous iridium catalysis on C(sp^3)-H centers

IV.1. Isotopic labeling of the drug payload of antibody-drug conjugates used for cancer treatment

As shown in the previous Part II-III, we were able to develop new efficient, fast and simple methods of HIE on C(sp2)-H carbon centers using iridium catalysis. Interestingly the hydrogen isotope labelling methods on C(sp3)-H carbons is in comparison to aromatic C(sp2)-H carbons still rarely described.[1] Within a Sanofi research project there was a specific request for labelling a maytansinoid DM4 **1a** involved in a serie of antibody drug conjugates (ADCs) (*figure IV.1*).

Figure IV. 1: *Structure of DM4* ***1a-c*** *and DM1* ***2****.*

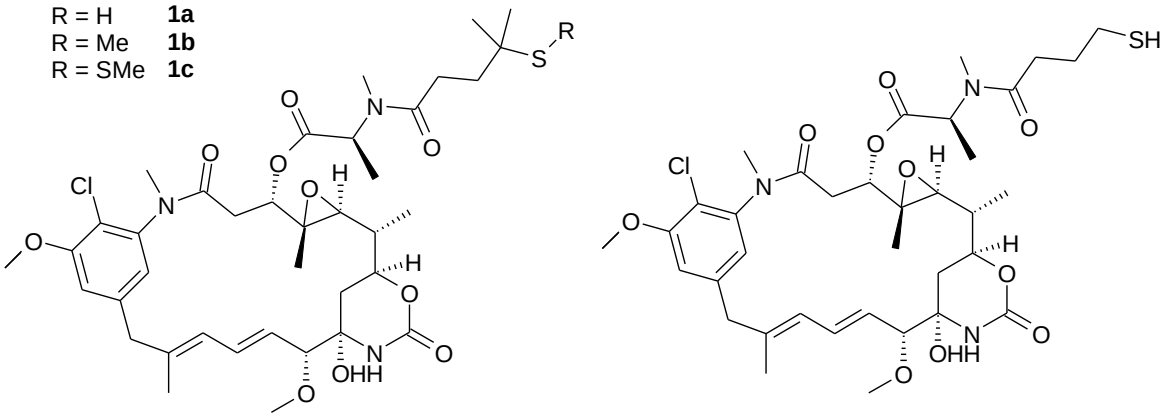

IV.1.1. Application of ADC for treatment in oncology

Antibody-drug conjugates have become promising anticancer treatment agents that combine the selectivity of targeted treatment with the cytotoxic potency of chemotherapy drugs.[2,3] They are composed of a monoclonal antibody linked to a biologically active cytotoxic drug. The monoclonal antibody targets the antigen present in high quantity at the surface of the tumor cells whereas its expression is limited on healthy cells. The linker is stable in blood circulation and able to release the active drug into the tumor cells due to an internalization process (endocytosis). The drug with a highly potent cytotoxic activity is able to trigger the apoptosis process of the cell (*figure IV.2, left*). By combination of the unique targeting capabilities of monoclonal antibodies with the cancer-killing ability of cytotoxic drugs, ADCs allow unlike standard chemotherapy, the sensitive discrimination between healthy and cancer tissue. This huge advantage compare to unselective treatments, which are damaging healthy cells around, allows the injection of a higher dose of the complex which gives a larger window of action (*figure IV.2, right*).

Figure IV. 2: *Structure of an ADC (left) and comparison of unselective and selective toxic agent (right).*

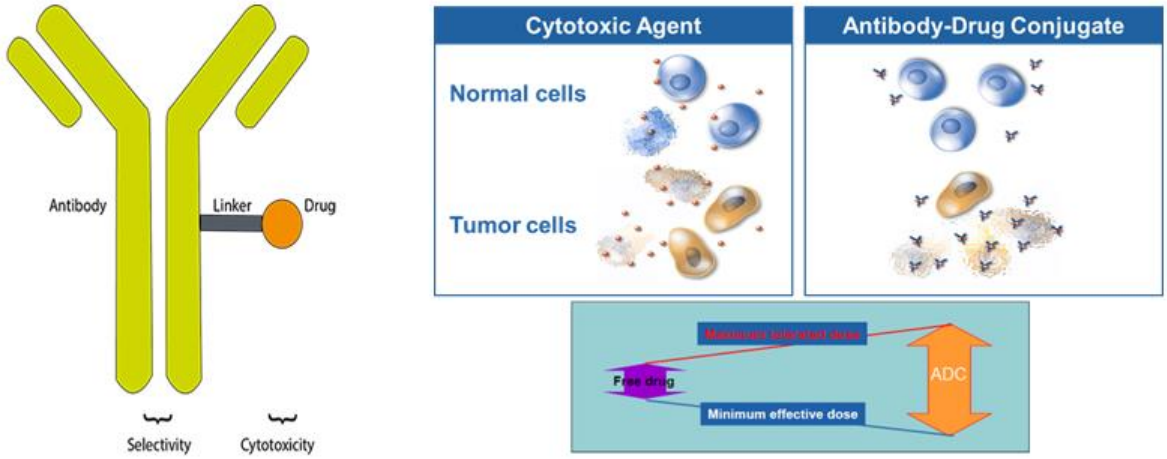

After injection of the ADC in the blood circulation (*figure IV.3, step 1*), the antigen binding site of the antibody will bind specifically the antigen present on the tumor cell (*step 2*). The endocytosis will allow the ADC to be internalized in the cell via the endosome pathway (*step 3*), which will maturate as a lysosome during the trafficking of the vesicle (*step 4*). The acidic media present in the lysosome will enable to release the cytotoxic drug in the cytoplasm (*step 5*) and trigger the apoptosis of the cancer cell (*step 6*).

Figure IV. 3: *Mode of action of the antibody drug conjugate*

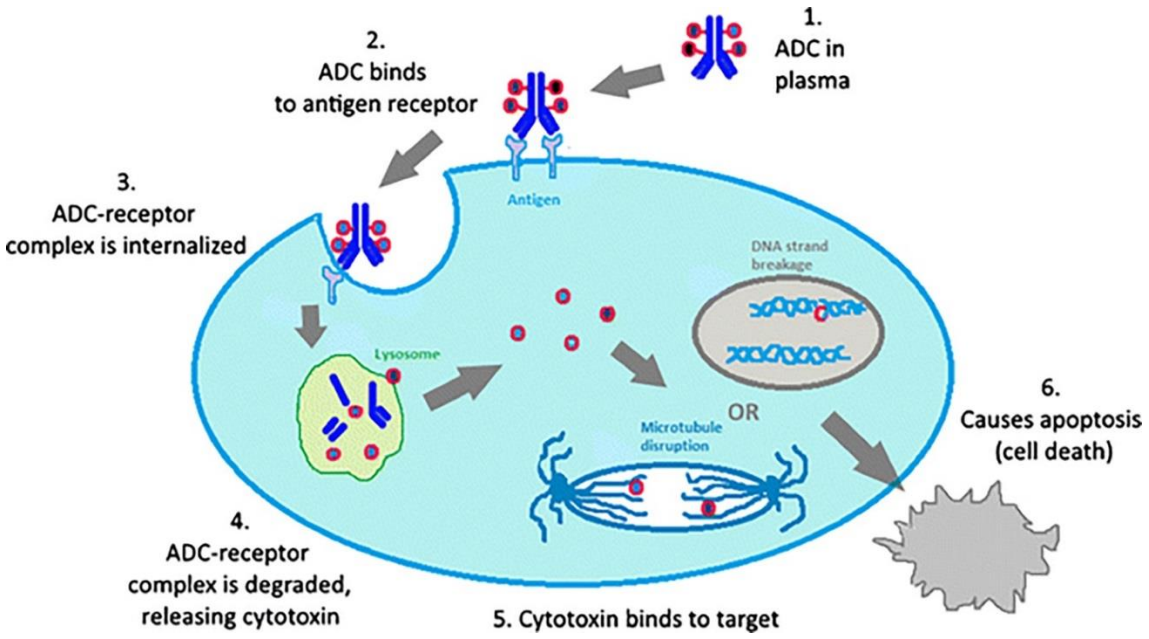

IV.1.2. The Maytansine derivatives as ADCs

Maytansine, originally isolated from the bark of the Ethiopian shrub *Maytenus ovatus*,[4] displayed highly potent cytotoxic activity with IC50 values in the picomolar range resulting from its ability to disrupt microtubule polymerization.[5] Maytansine was extensively evaluated in human clinical trials, but failed to demonstrate a therapeutic benefit at tolerable doses.[6] However, maytansine analogues (maytansinoides) modified by ImmunoGen Inc. for conjugation with antibodies through disulfide-containing linkers enabled the development of antibody-maytansinoid conjugates.[7] Besides DM1 **2** utilized for example in Trastuzumab emtansine (T-DM1), DM4 **1a** is another frequently applied synthetic maytansinoid payload. In DM4 **1a**, next to the C-S bond, two germinal dimethyl groups have been installed to increase sterical hindrance for improved chemical stability (*figure IV.1*).[8]

Examples of DM4-conjugated antibodies in clinical development include oltuximab ravtansine (SAR3419)[9] targeting CD19 to treat acute lymphoblastic leukemia (ALL), mirvetuximab soravtansine (IMGN853),[10] a FRα-targeting ADC for the treatment of FRα-positive, platinum-resistant ovarian cancer and lorvotuzumab mertansine (IMGN901), a CD56-targeting ADC for treatment of small-cell lung cancer (SCLC) (*figure IV.4*).[11]

Figure IV. 4: *Maytansinoid-conjugated antibodies examples*[9,10,13]

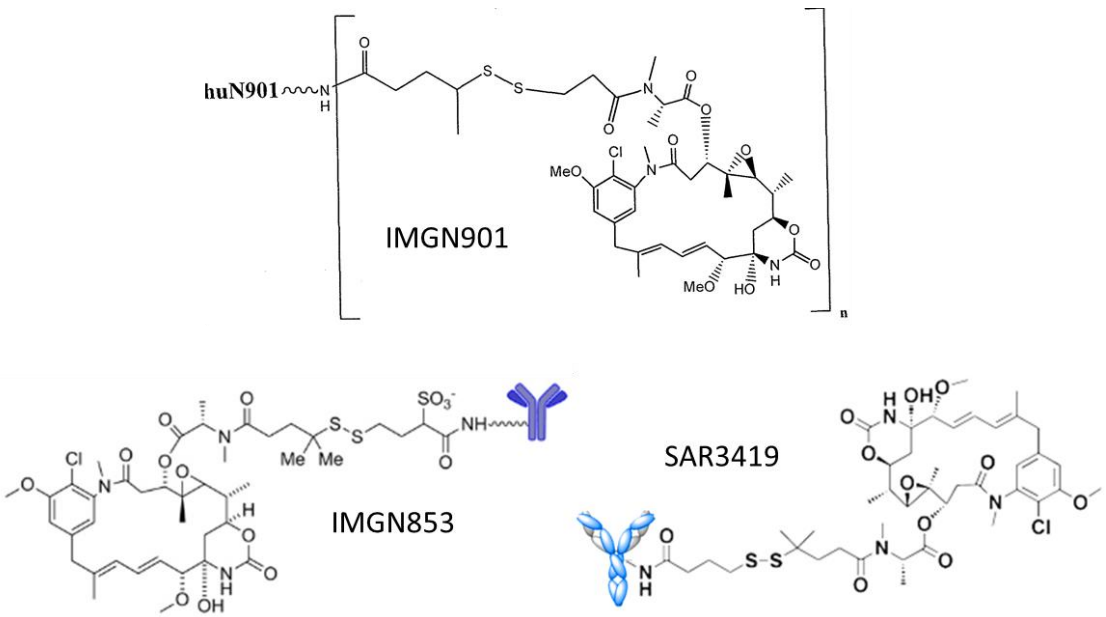

IV.1.3. Former approach for the synthesis of ^{3}H-DM4

With regards to the isotope labelling of DM1 **2,** DM4 **1a** and the subsequent antibody conjugation, tritium is the label of choice because of the approx. 500 times higher specific activity (28.8 Ci/mmol) achievable as compared to a single carbon-14 label (62.4 mCi/mmol).[12] Thus, several reported studies utilized tritium tracer with a tritium label at the C-20 methoxy group of the maytansinoid, which proved to be a metabolically stable position.[13] However, the synthesis of [methoxy-^{3}H]DM1 or [methoxy-^{3}H]DM4 is quite tedious, comprising at least 5 partly low yielding radioactive steps as well as a fermentative demethylation. Although utilized and referenced several times, no detailed procedures have been described in literature to date.[12] Consequently, we became interested in developing an alternative synthesis approach for the preparation of ^{3}H labelled DM4 **1** for decreasing precursor costs and synthetic efforts.

Typically, the preparation of maytansinoid analogues labelled with tritium at the C-20 position starts from ansamytocin P-3 **3** produced by fermentation of the bacterial actinomycetes strain *Actinosynnema pretiosum* (*scheme IV.1*).[14] First the methyl ether of the methoxy group in ansamytocin P-3 **3** was removed in 30% yield applying *Streptomyces platensis*, another actinobacteria strain followed by extensive preparative HPLC purification. The resulting phenol moiety of PDM-3 **4** is then re-alkylated with ^{3}H-methylnosylate (specific activity >80 Ci/mmol) to obtain ^{3}H-ansamitocin P3 **5** in 71% yield. Depending on study requirements, at this stage the specific activity can be adjusted (e.g. to <1 Ci/mmol) by dilution with unlabeled ansamitocin P3 to increase the scale for subsequent reaction steps following previously described pathways for DM1 **2** and/or DM4 **1a** synthesis.[15] Hydrolysis of the C3 isobutyrate ester is achieved under reductive conditions using DIBALH to obtain ^{3}H-maytansiol **6** in 92% yield.

A significantly improved diastereoselectivity for the acylation of maytansinol **6** is achieved by applying a two-step procedure for the installation of the side chain. Firstly ^{3}H-maytansinol **6** is acylated with the N-carboxyanhydride (NCA, **7**), generated from Boc-NMe-Ala-OH with PCl_3, followed by coupling with an activated ester of 4-methyl-4-(methyldithio) pentanoic acid **9**. However, the acylation of the maytansinol **6** with N-carboxy anhydride (NCA, **7**) of N-methylalanine proved to be crucial due to moisture sensitivity and sometimes incomplete conversion. The small amount of the undesired diasteromer formed in this step was separated by preparative HPLC to obtain pure L-DM4-SMe **1c** in 35% yield. Finally, cleavage of the disulfide with Cleland's reagent[16] (dithiothreitol, DTT) in phosphate buffer at pH 7.5 and subsequent preparative HPLC purification afforded ^{3}H-DM4 **1a** with an overall yield of 7% in five radioactive steps. Depending on the anticipated DAR values (drug antibody ratio) the specific activity may have to be further adjusted prior to conjugation to the respective antibody.

Scheme IV. 1: *Conventional Synthesis of ^{3}H-DM4* ***1a***

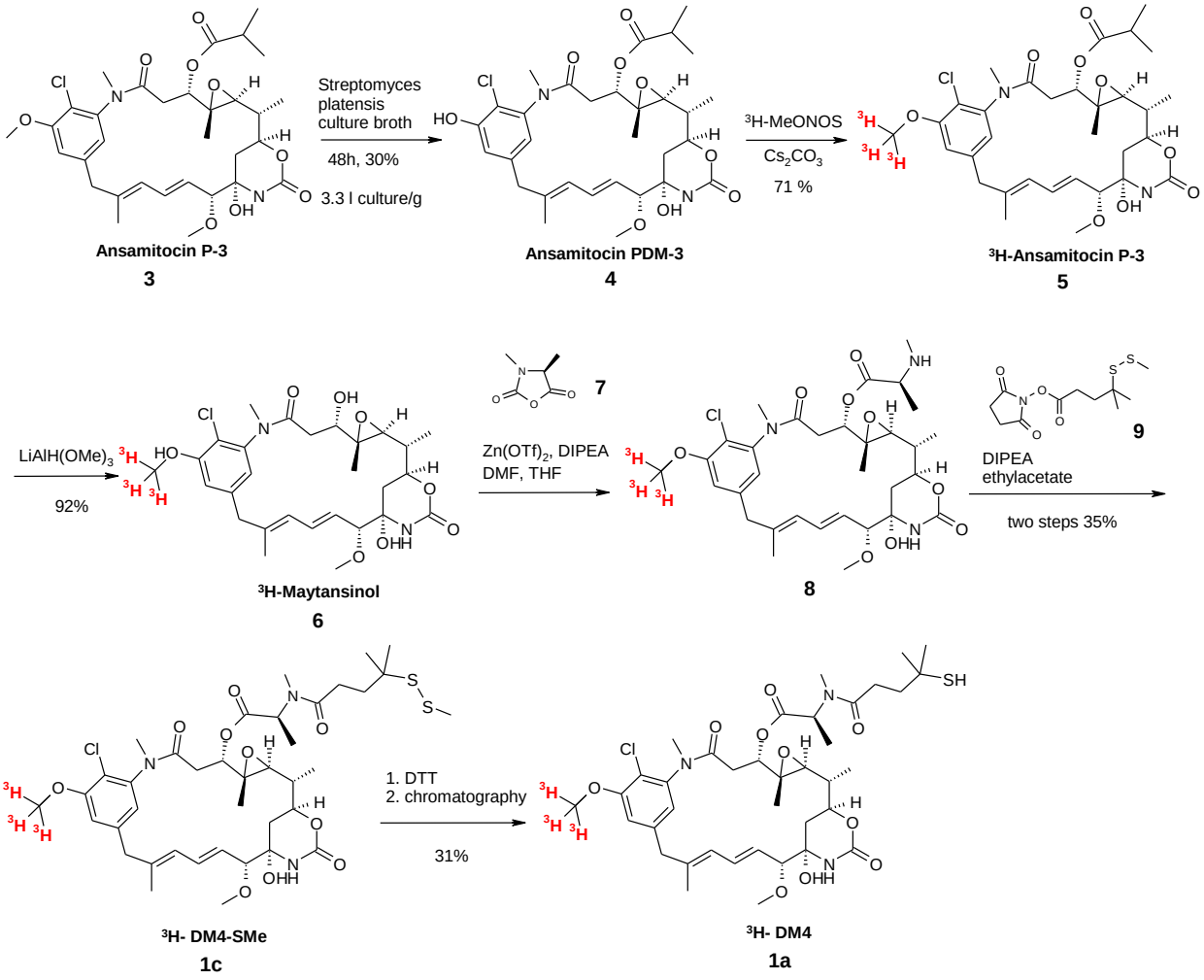

According to the approach described above, the Sanofi team had prepared several ^{3}H-DM4-conjugated ADCs for *in-vivo* metabolism studies. Throughout these ADME studies, it appeared that the stability of ^{3}H-DM4 **1a,** particularly at higher specific activity, was quite limited and that the compound completely decomposed after three months. Thus, a resynthesis was needed from time to time. However, revisiting the lengthy and costly synthesis of ^{3}H-DM4 **1a**, we evaluated potential alternative options such as hydrogen isotope exchange.[17]

IV.2. Iridium-catalyzed hydrogen isotope exchange on L-DM4

During this project we have worked mainly with the derivative DM4 (-SMe) **1c** which was chemically more stable than DM4 (-H) **1a** and was neither prompt to uncontrolled oxidation nor side-reaction with the catalyst through metal chelation by the thiol moieties. We have also worked with DM4 (-Me) **1b** which is chemically more stable but as the following step

after isotope labelling is the conjugation, the disulfide bond S-S has to be deprotected easily to provide the free S-H.

To investigate conditions for direct HIE on DM4 **1c**, a catalyst screening had been done previously,[18] using commonly available iridium catalysts known to show success in HIE (*table IV.1*).

***Table IV. 1:** Condition screening on DM4 **1c** in HIE reaction [a,b. 28]*

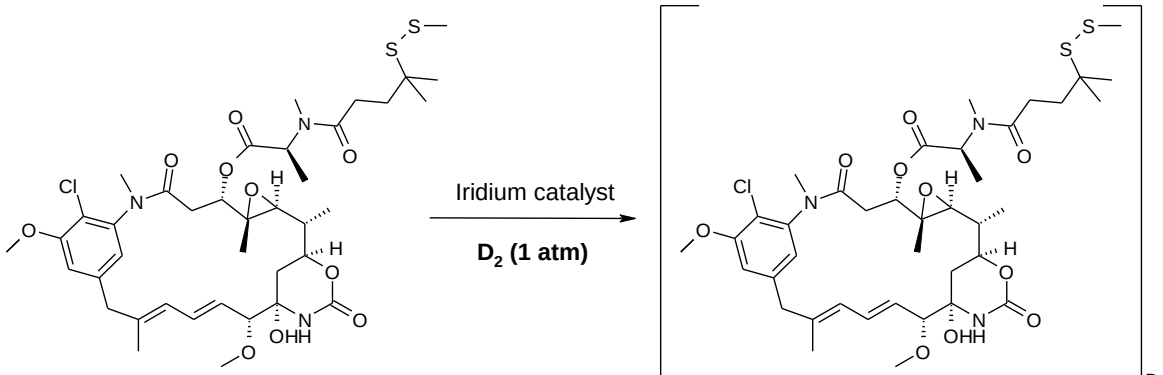

1c
LDM4-SMe

D_x-1c
D_x-LDM4-SMe

Entry	Catalyst	Solvent	Temp.	Time	D/molecule
1	Tamm **F**	MTBE	rt	3 h	0
2	Crabtree **A**	MTBE	rt	3 h	0
3	Pfaltz **D**	MTBE	rt	3 h	0
4	Burgess **E**	MTBE	rt	3 h	0
5	Kerr PF_6 **B_a**	MTBE	rt	3 h	0
6	Kerr Barf **B_b**	MTBE	rt	3 h	0.05
7	Kerr Barf **B_b**	THF	rt	3 h	0
8	Kerr Barf **B_b**	Chlorobenzene	rt	3 h	0
9	Kerr Barf **B_b**	Isopropyl acetate	rt	3 h	0.2
10	Kerr Barf **B_b**	Isopropyl acetate	50 °C	3 h	2
11	Kerr Barf **B_b**	Isopropyl acetate	rt	20 h	1.9

a) Conditions: substrate **1c** (1 eq.), catalyst (50 mol%, 0.5 eq.), solvent (1 mL), D_2 (1 atm). b) Number of incorporated deuterium atoms determined by LC-MS.

From the catalyst screening, no success was achieved (*table IV.1, entry 1-5*) except with catalyst Kerr Barf $\mathbf{B_b}$ where a slight reactivity started to be observed (*entry 6*). Keeping the catalyst $\mathbf{B_b}$, the solvent has been changed and whereas THF (*entry 7*) and chlorobenzene (*entry 8*) gave no deuterium incorporation at all, isopropyl acetate allowed a very moderate incorporation up to 0.2 D/molecule (*entry 9*). When heating up the reaction to 50 °C, a remarkable deuterium incorporation reaching 2.0 D/molecule has been found (*entry 10*). A similar incorporation was obtained by running the reaction at room temperature but for 20 h (*entry 11*). The very high catalyst loading chosen for the initial experiment reflects the urgent need in labelled LMD4 for the implementation of a Sanofi project.

With regards to the functionalities present in DM4 **1c**, the labelling was expected to occur on the aromatic ring in *ortho*-position of the acetanilide, even though the nitrogen was methylated. Surprisingly, after deuteration, the aromatic proton signals in the ^{1}H-NMR spectrum of **1c** appeared unchanged. However, a clear assignment of the labelling position was not possible, because of a highly complex aliphatic region in the ^{1}H-NMR spectrum of **1c**. Therefore, to run a tritium experiment under the same reaction conditions to enable ^{3}H-NMR for determination of the labelling position was decided (*figure IV.5*).

Figure IV. 5: *^{3}H-NMR of ^{3}H-DM4-SMe* ***1c*** *[a]*

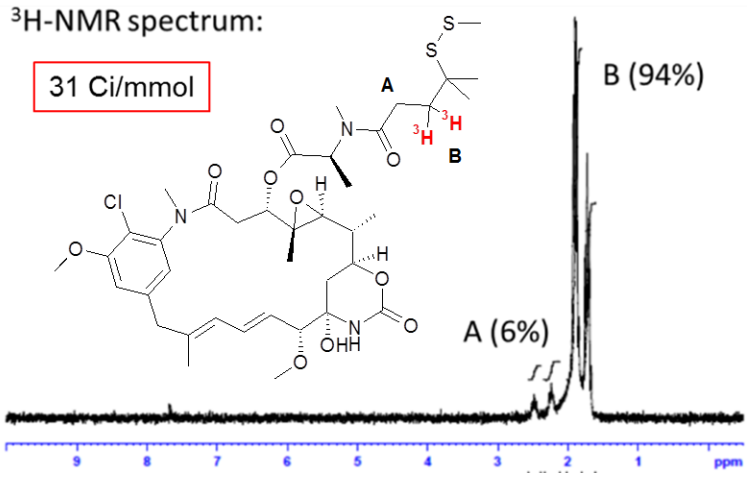

a) Conditions: catalyst $\mathbf{B_b}$ (50 mol%), T_2 (74 mBar = 12eq), isopropyl acetate (1 mL), 50°C, 3h.

Interestingly, a very selective tritium incorporation was found into the side chain of **1c** with a 94 to 6 ratio in favor of the β-carbonyl position. This is particularly interesting because iridium catalysed HIE usually results in highly *ortho*-selective exchange of aromatic positions. H/T exchange of sp^{3}-centers has been observed only occasionally, often with low selectivity or specific activity.[19] In our case, a specific activity of 31 Ci/mmol was obtained which was more than sufficient for the planned *in-vivo* studies with ^{3}H-DM4 and corresponding ^{3}H-ADCs.

The identification of the labelling position through analysis of the tritium experiment prompted us to apply the optimum conditions described above on the three DM4 **1a-c** derivatives. The HIE reaction with deuterium ran on these three compounds have given very good results in LC-MS up to 2.0 D/molecule (*figure IV.6*).

Figure IV. 6:** HIE reaction with catalyst **B_b** on **1a-c

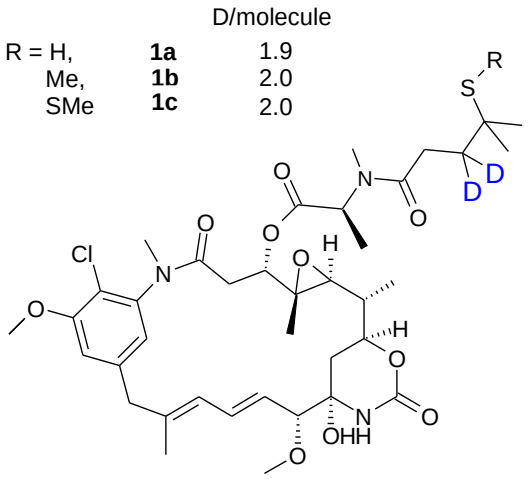

Motivated by these exciting initial results and impressed by the high regioselectivity, we became interested whether we could develop a real methodology of hydrogen isotope labelling on C(sp3)-H centers.

IV.3. Methodology development of Hydrogen isotope Exchange on sp^3-carbon centers

IV.3.1. Methodology development on the sulfur side chain

We started our investigation using model substrate **[H]-10** containing the sulfur side-chain and a benzyl group which was making the compound UV-visible. Moreover, ionization on the nitrogen renders possible the LC-MS monitoring of **[H]-10** with regards to the deuterium incorporation.

The conditions developed previously have shown to be the best for the labelling of DM4 **1a**. Nevertheless, we still evaluated these conditions in a more general way on model substrate **[H]-10**.

IV.3.1.a) Conditions screening of [H]-10 in HIE reaction

The conditions screening started by evaluation of the iridium catalysts activity towards the HIE of **[H]-10** (*table IV.2*). We observed no deuterium incorporation at all with catalysts **F** (*entry 5*) and **G** (*entry 6*), and between 0.5 and 0.8 D/molecule with catalysts **A** (*entry 1*), **B_a** (*entry 2*) and **E** (*entry 4*). The best result was obtained with catalyst **B_b** (10 mol%) which enabled deuterium incorporation up to 1.9 D/molecule at 50 °C (*entry 3*) and up to 2.0

D/molecule at 80°C (entry 7). Keeping a temperature of 80 °C, the reaction run with 5 mol% of catalyst **B_b** gave only 0.6 D/molecule as maximum deuterium exchange (*entry 8*).

Table IV. 2: *Catalyst screening of* ***[H]-10*** *in HIE* [a]

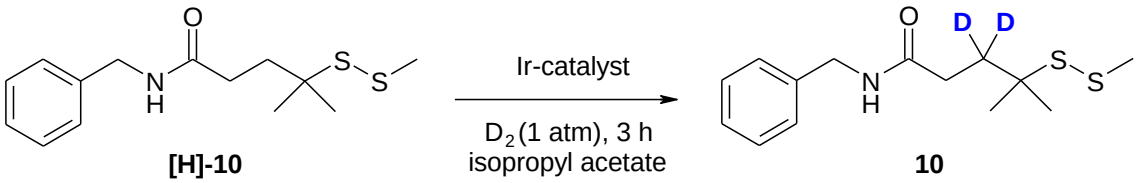

Entry	Catalyst	Loading (mol%)	Temp.	D/molecule 10
1	Crabtree **A**	10	50	0.5
2	Kerr PF_6 **B_a**	10	50	0.6
3	Kerr Barf **B_b**	10	50	1.9
4	Burgess **E**	10	50	0.8
5	Tamm **F**	10	50	0
6	Ding **G**	10	50	0
7	Kerr Barf **B_b**	10	80	2
8	Kerr Barf **B_b**	5	80	0.6

a)Conditions: substrate **[H]-10** (1 eq.), isopropylacetate (1 mL), D_2 (1 atm), 3 h. b) Position determined by ^{1}H NMR and percentage of deuterium incorporation analysed by LC-MS.

Table IV. 3: *Solvent screening in HIE reaction of* ***[H]-10*** *with catalyst* ***B_b***

Entry	Solvent	D/molecule
1	chloroform	1.1
2	MTBE	0.5
3	ethanol	1.2
4	MeTHF	0.5
5	Isopropyl acetate	1.9
6	chlorobenzene	1.8

[a]Conditions: substrate **[H]-10** (1 eq.), catalyst **B_b** (10 mol%), solvent (1 mL), D_2 (1atm), 50°C, 3 h. [b]Position determined by ^{1}H NMR and percentage of deuterium incorporation analysed by LC-MS.

We studied the influence of the solvent (*table IV.3*) through a comparison between chloroform (*entry 1*), MTBE (*entry 2*), ethanol (*entry 3*), MeTHF (*entry 4*), and chlorobenzene (*entry 6*). Finally, isopropyl acetate (entry 5) provided the highest deuterium incorporation in **10**.

After identification of the optimum conditions (10 mol% of catalyst $\mathbf{B_b}$ reaction at 80 °C in isopropyl acetate), we have applied them to diverse DM4 side chain precursors.

IV.3.1.b) Application of the developed methodology on DM4 side chain precursors

Our optimized conditions have been applied first to side chain precursors **11** and **12** (*scheme IV.2*). We obtained complete deuterium incorporation of 95-99% for these simple amide derivatives. The reaction is very selective for the β-amide carbon with no deuterium incorporation into the aromatic or benzyl-position in **10**.

Scheme IV. 2:** HIE reaction ofDM4 side chain precursor **10-12** with catalyst **B_b [a]

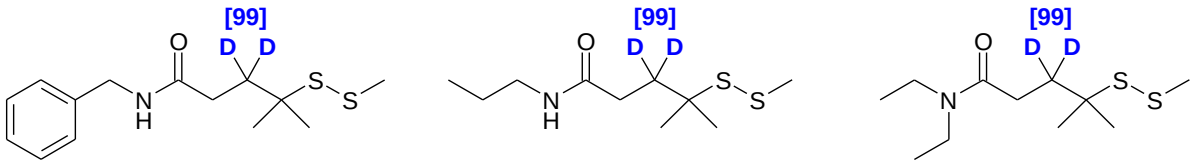

10 **11** **12**

a) Conditions: substrate (1 eq.), catalyst $\mathbf{B_b}$ (10 mol%), D_2 (1 atm), isopropylacetate (1 mL), 80°C, 3h.

We were interested to apply our conditions to the Ir-catalyzed HIE on a precursor which looks even more like the original DM4 **1c** containing and amino acyl moiety. Three precursors have been tested: the alanine derivative **13**, the serine derivative **14** and the glycine derivative **15** (*scheme IV.3*). During the screening of these DM4 side-chain model substrates, an interesting observation attracted our attention. The very high β-selectivity still observed for **13** and **14** (99 %D and 95%D respectively) was lost in the glycine containing substrate **15**. In this specific case, two positions were reactive with a clear preference for the α-glycine protons (84%D) in comparison to the β-amide position (36%D).

By going further with our investigation, steric and electronically modified derivatives **16** and **17** have been tested (*scheme IV.3*). A complete change in selectivity in favor of the α-amino acid protons was observed in the glycine conjugates **16** and **17**. In both cases excellent deuterium incorporation in the glycine position was observed while the β-amide position was not labelled at all. Obviously even small steric changes in the substrates may have a strong effect on the selectivity and outcome of the HIE which triggered us to investigate this reaction on amino acid derivatives in more detail.

Scheme IV. 3: *HIE reaction of DM4 side chain precursors* ***13-17*** *with catalyst* $\mathbf{B_b}$ [a]

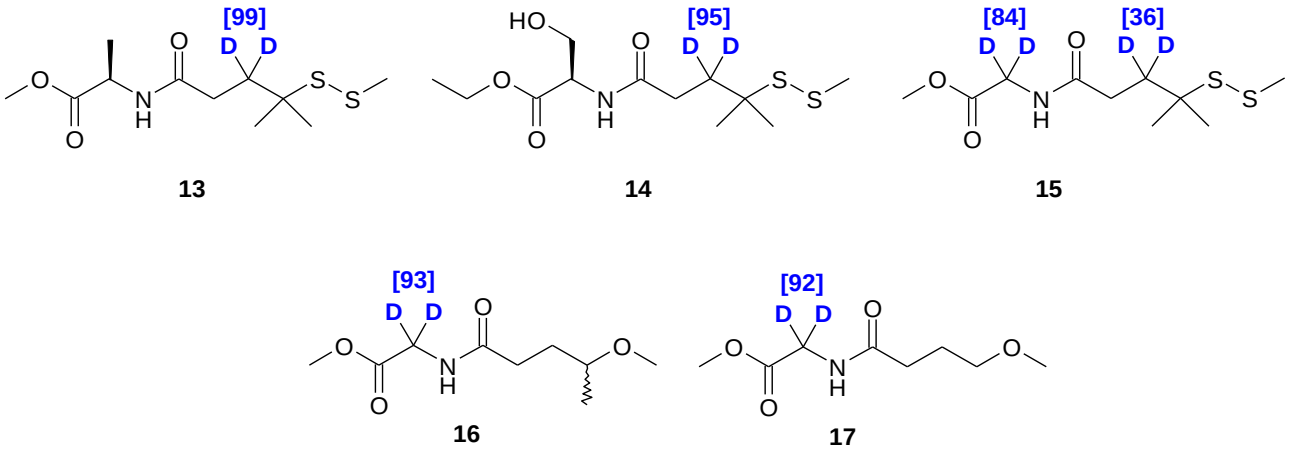

13 **14** **15** **16** **17**

a) Conditions: substrate (1 eq.), catalyst $\mathbf{B_b}$ (10 mol%), D_2 (1 atm), isopropylacetate (1 mL), 80°C, 3h.

IV.3.2. Investigation of the small amino acids reactivity in HIE

IV.3.2.a) Influence of the *N*-terminal protecting group

The influence of the protecting group in glycine methyl ester **18** has been investigated (*table IV.4*). Unfortunately, high deuterium incorporation was observed only for acetyl (**18a**), while more synthetically versatile protecting groups such as Cbz **18b** or Fmoc **18c** resulted only in moderate deuteration. For Boc **18d** or Bn **18e** no deuterium incorporation was observed under these conditions. More insights are given from the DFT calculations (see section *IV.3.4*).

Table IV. 4: *Influence of the N-protecting group on the deuterium incorporation in HIE of* ***18*** *with catalyst* $\mathbf{B_b}$ [a]

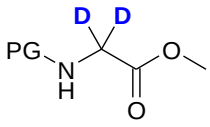

18a-e

18	PG	%D	%Yield
a	Ac	93	99
b	Cbz	50	98
c	FMoc	30	72
d	Boc	0	n.d.
e	Bn	0	n.d.

a) Conditions: substrate (1 eq.), catalyst $\mathbf{B_b}$ (10 mol%), D_2 (1 atm), isopropylacetate (1 mL), 80°C, 3h.

IV.3.2.b) Analysis of the stereocontrol in HIE reaction of alanine

As the stereo information in amino acids is crucial and must be conserved during the reaction, we tested our HIE method on the protected L-alanine **19a** and D-alanine **19b**. On top of analyzing the deuterium incorporation, we have looked by enantioselective HPLC-separation if the original stereo information was kept in both cases.

Figure IV. 7: *Enantioselective HPLC-Separation of L-Ac-Ala-OMe* ***19a*** *and D-Ac-Ala-OMe* ***19b***

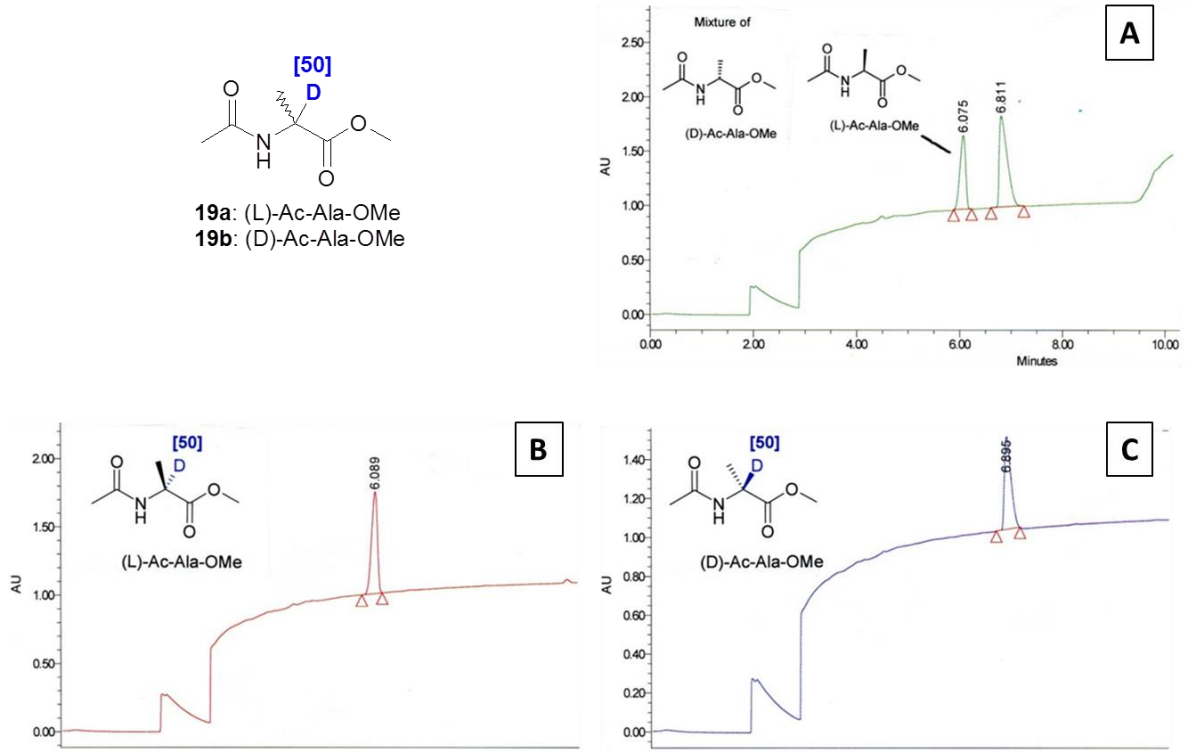

As expected, the HIE reactions on alanine **19a** and **19b** (*figure IV.7*) resulted in a lower deuterium intake (50%D) as compared to the glycine **18a** previously showed (99%D). As expected, the value of incorporated deuterium was independent of whether the D- or L-alanine was used. For both compounds **19a** and **19b**, complete retention of stereo information was observed, as proven by chiral HPLC analysis (*figure IV.7, A-C*). Indeed, the analysis of the non-deuterated protected L- and D-alanine (*figure IV.7,* A) showed retention times at 6.075 min for the L-Ac-Ala-OMe and 6.811 min for the D-Ac-Ala-OMe. The deuterated product **19a** and **19b** have been run in the same chiral HPLC conditions, and in both cases the resulting retention times demonstrated that no isomerization of the stereocenter have occurred throughout the HIE reaction (*figure IV.7,* B-C).

IV.3.2.c) Application of the HIE method on sterically more demanding amino acids

Sterically more demanding amino acids such as Ac-Leu-OMe **20** or Ac-Phe-OMe **21** displayed no deuteration at all (*scheme IV.4*). In contrast Ac-βGly-OMe **22** gave a high deuterium incorporation (91%D) similar to what was observed on glycine **18a**.

Scheme IV. 4: *HIE reaction with amino acids* ***20-22*** [a]

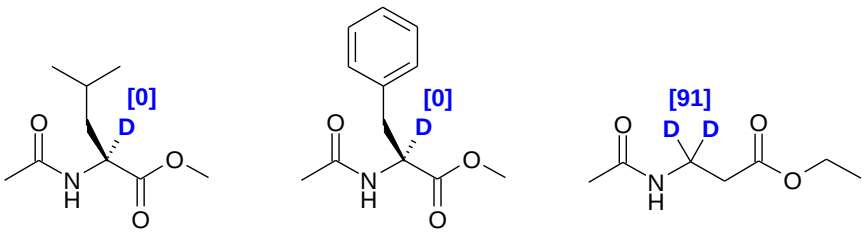

20 Ac-leu-OMe

21 Ac-Phe-OMe

22 Ac-Beta-Gly-OEt

a) Conditions: substrate (1 eq.), catalyst $\mathbf{B_b}$ (10 mol%), D_2 (1 atm), isopropylacetate (1 mL), 80°C, 3h.

We have noticed from these results that our method was working mainly on the glycine moiety. This prompted us to investigate larger glycine-containing peptides.

IV.3.3. Application of the optimized method in larger peptides

We started by applying our conditions on dipeptides with N-terminal glycine moiety (*scheme IV.5*). The dipeptide (L)-Ac-Gly-Phe-OMe **23** was selectively labelled at the glycine position with 55%D. We looked at the HIE on the dipeptides (L)-Gly-Phe methyl ester, as N-Cbz (**24**), N-Fmoc (25) and N-Boc (**25**) protected. In accordance to what we have observed already on the Ac-Gly-OMe **18a-e** (table IV.4), the deuterium incorporation dropped to 14%D in **24** (N-Cbz) and there was no deuteration at all for **25** (N-Fmoc) and **26** (N-Boc). By using the acetyl protection group, which had demonstrated to be the best one for deuterium incorporation, we have obtained up to 93%D in (L)-Ac-Gly-Tyr(OtBu)-OtBu **27**. From these examples, we have noticed that the steric demand of the C-terminal amino acid does not influence strongly the deuterium incorporation. The high selectivity for glycine brought us to test the deuteration of the Ac-Gly-Gly-OMe dipeptide **28** and in this case the deuterium was incorporated on both glycine with 56%D (N-Terminal) and 37%D (C-Terminal).

Considering this result, we thought to make one of the method limitations a strength. Indeed, we have seen that the Boc protecting group was inhibiting the deuterium labelling on the N-terminal glycine (**18d** and **26**), and with the result on **28**, compound **29** has been

investigated. Successfully, **29** has been labelled with up to 52%D selectively at the C-terminal glycine.

The results obtained in the different dipeptides **23-29** showed that the regioselectivity of the deuterium labelling can be tuned by the choice of protecting group. We became interested to look at more dipeptides containing a C-terminal glycine.

Scheme IV. 5: *HIE reaction on dipeptides with N-terminal glycine* ***23-29*** [a]

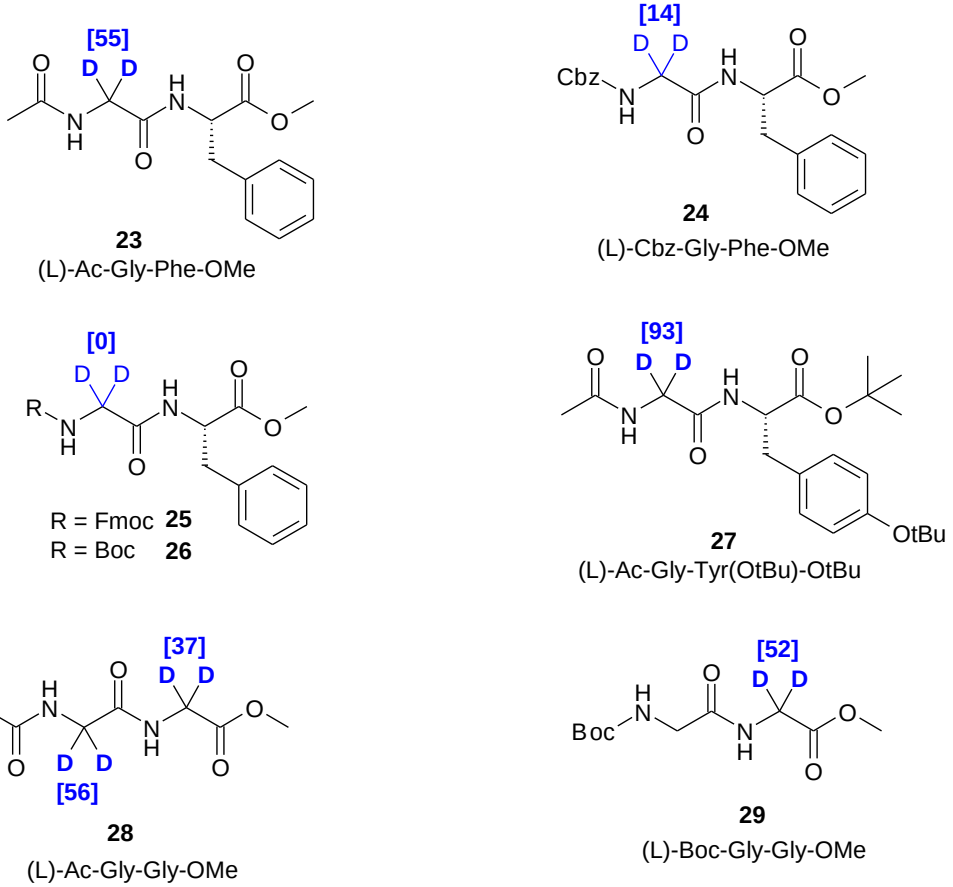

a)Conditions: substrate (1 eq.), catalyst $\mathbf{B_b}$ (10 mol%), isopropylacetate (1mL), 80°C, 8h.

As expected, the selectivity of the HIE reaction for the C-terminal glycine was confirmed on dipeptides **30-34** when applying our reaction conditions (*scheme IV.6*). This effect is even more pronounced for more sterically demanding N-terminal amino acids, resulting in a good deuterium incorporation for Boc-Ala-Gly-OMe **30** (60%D) to very good deuterium incorporations for Boc-Leu-Gly-OMe **31** (74%D) and Boc-Phe-Gly-OMe **32** (92%D). In line with previous findings (**22**), protons in both the α–glycine and β-amide positions of Boc-Gln(NEt)-Gly-OMe **33** were exchanged. Interestingly in Boc-Pro-Gly-OMe **34**, the deuterium labelling happened at the n+1 amino acid position relative to glycine (93%D) and to proline

(36%D). Even though the N-terminal proline was Boc-protected, the deuterium labelling in the n+1 position occurred. It is known that the proline is giving a different 3-Dimensional geometry to a peptide chain. We postulate that the proline geometry and the connected amide or carbamate bonds cis:trans effect (20:80; higher cis amide bond isomer compared to other amino acids where it is 5:95) enables the α–carbon of the proline to be in closer interaction with the iridium catalyst, and by allowing deuterium incorporation in this position.[20]

Scheme IV. 6: *HIE reaction on dipeptides with C-terminal glycine* ***30-34*** [a]

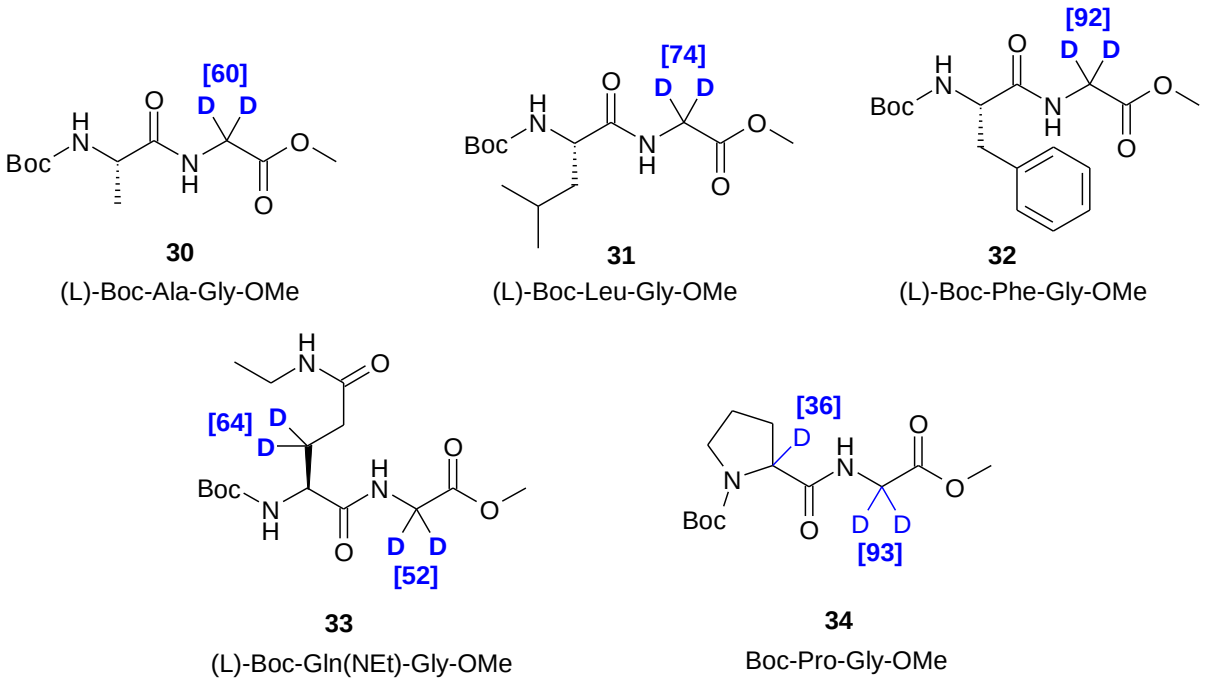

a)Conditions: substrate (1 eq.), catalyst $\mathbf{B_b}$ (10 mol%), isopropylacetate (1mL), 80°C, 8h.

To our great delight, the method can be extended to longer peptides as demonstrated by the excellent D incorporation obtained for tripeptide Cbz-Tyr(OtBu)-Gly-Leu-OtBu **35** (94%D) and tetrapeptide Boc-Trp-Gly-Ala-Phe-OMe **36** (95%D) (*scheme IV.7*). Like for **33**, the β-amide protons in **36** also exchanged well. A slight deuterium incorporation was observed in dipeptide **37** (23%D) which is aligned with the values obtained in table IV.4 on the Fmoc protected glycine **18c**.

Unexpectedly, selective HIE reaction have occurred in the α–carbon of the methionine in dipeptide **38** (95%D). Unfortunately, we observed no deuterium incorporation in the α–carbon of the serine or the tyrosine in dipeptides **39** and **40**, respectively.

Scheme IV. 7: *HIE reaction on peptides* ***35-40*** [a]

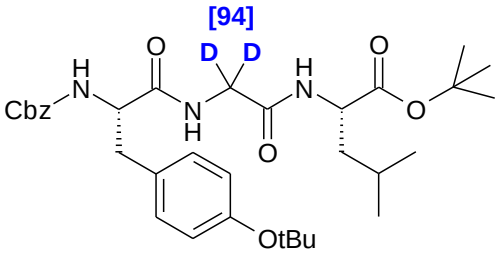

35
(L)-Cbz-Tyr(OtBu)-Gly-Leu-OtBu

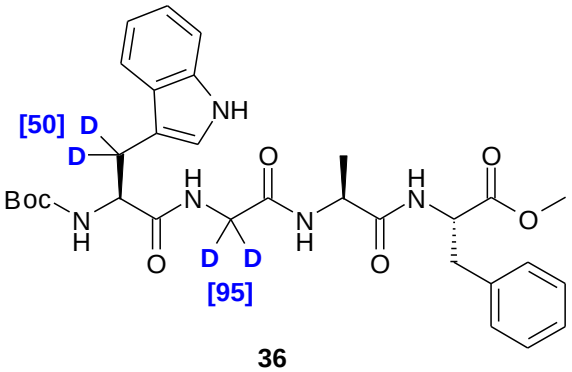

36
(L)-Boc-Trp-Gly-Ala-Phe-OMe

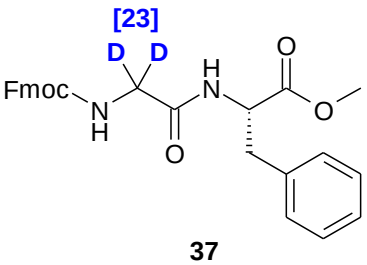

37
(L)-Fmoc-Gly-Phe-OMe

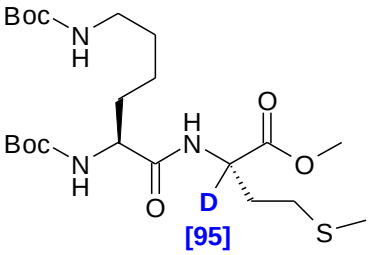

38
(L)-Boc-Lys(boc)-Met-OMe

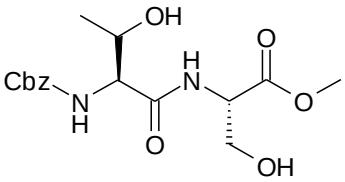

39 [0]
(L)-Cbz-Thr-Ser-OMe

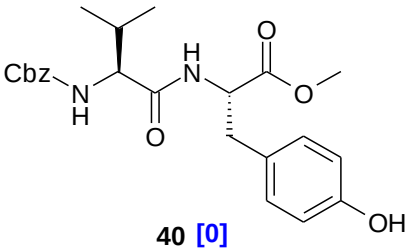

40 [0]
(L)-Cbz-Val-Tyr-OMe

a)Conditions: substrate (1 eq.), catalyst $\mathbf{B_b}$ (10 mol%), isopropylacetate (1mL), 80°C, 8h.

IV.3.4. Insights in the mechanism

DFT calculations (M06 functional) have been done by Dr. Stefan Güssregen from the Computational Drug Design group in Sanofi, following the approach successfully applied by Kerr et al.[21] based on the mechanism suggested by Heys.[22] Our purpose was to better understand the pronounced glycine selectivity of the HIE reaction.[23] The constructed free energy profile with catalyst $\mathbf{B_b}$ and compound **18a** is shown in figure IV.8. After initial iridium coordination (**40**), the insertion product **42a** is reached via transition-state **41**. The equilibrium between **42a** and **42b** is going through a low barrier transition-state. The deuterated iridium adduct **44** is formed via the reductive elimination transition-state **43**. We

found that the relative energies of the transition-states for the oxidative addition step **41** (+23.8 kcal mol^{-1}) and the reductive elimination step **43** (+24.1 kcal mol^{-1}) are significantly higher than those calculated for HIE reactions with catalyst $\mathbf{B_b}$ at aromatic C(sp^2)-carbons like benzaldehydes (+18.6 kcal mol^{-1}).[21a] This difference in energy might explain why elevated temperatures are needed (in our cases).

Figure IV. 8: *Calculated free energy profile for selective deuteration of Ac-Gly-OMe* ***18a*** *with catalyst* $\mathbf{B_b}$ *(ligands not drawn)*

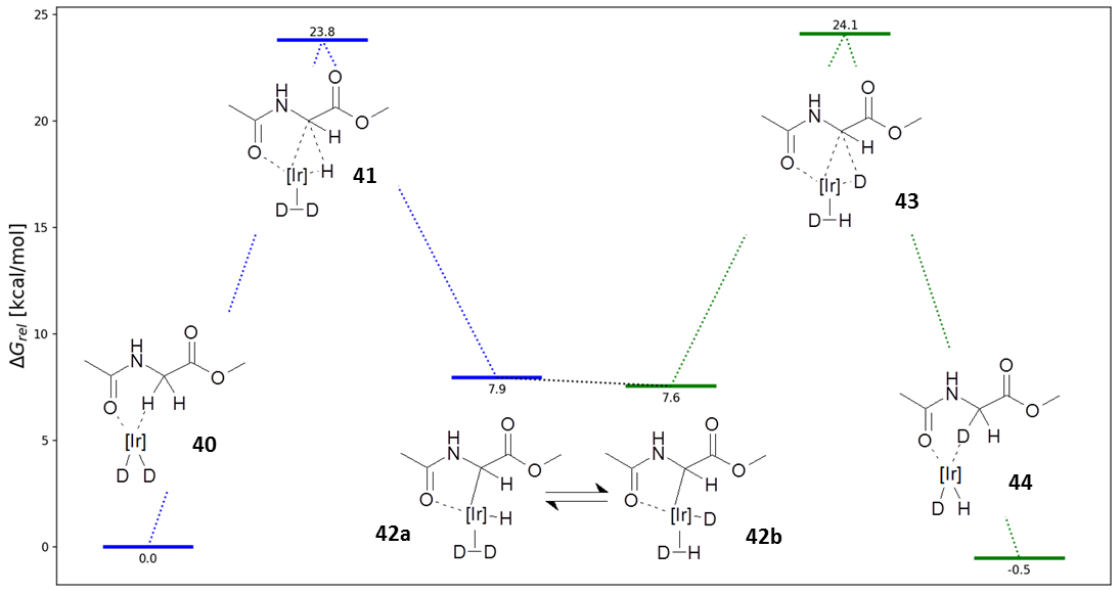

As we have seen in section IV.3.2.a), the Boc protecting group totally inhibits the HIE on glycine **18d**, in comparison to the acetyl protecting group in glycine **18a**. A comparison of the relative transition-state energies ($\Delta\Delta G_{trans}$) for the reaction with catalyst $\mathbf{B_b}$ revealed +7.3 kcal mol^{-1} for Boc-Gly-OMe **18d** compared to Ac-Gly-OMe **18a** (*figure IV.9*). Also, a comparison of the relative transition-state energies ($\Delta\Delta G_{trans}$) has been done for Ac-Ala-OMe **19a** and revealed a +4.3 kcal mol^{-1}compared to Ac-Gly-OMe **18a**. These results are fully consistent with the experimental findings and explain the different deuterium incorporation for **18a** (93%D), **18d** (0%D) and **19a** (50%D).

Furthermore, sterically more demanding amino acids increase the $\Delta\Delta G_{trans}$ values in the -tates in the following order: Gly (**18a**) < Ala (**19**) < Phe (**21**). Finally, we found that the proposed mechanism is well in line with the experimental observations. Our results show that the observed energetic differences of C(sp^3)- and C(sp^2)-labelling can be attributed to increased steric demands of the substrate.[24]

Figure IV. 9: *5-membered transition state of catalyst* $\mathbf{B_b}$ *and Ac-Gly-OMe* ***18a*** *(left) and of Boc-Gly-OMe* ***18d*** *(right)*

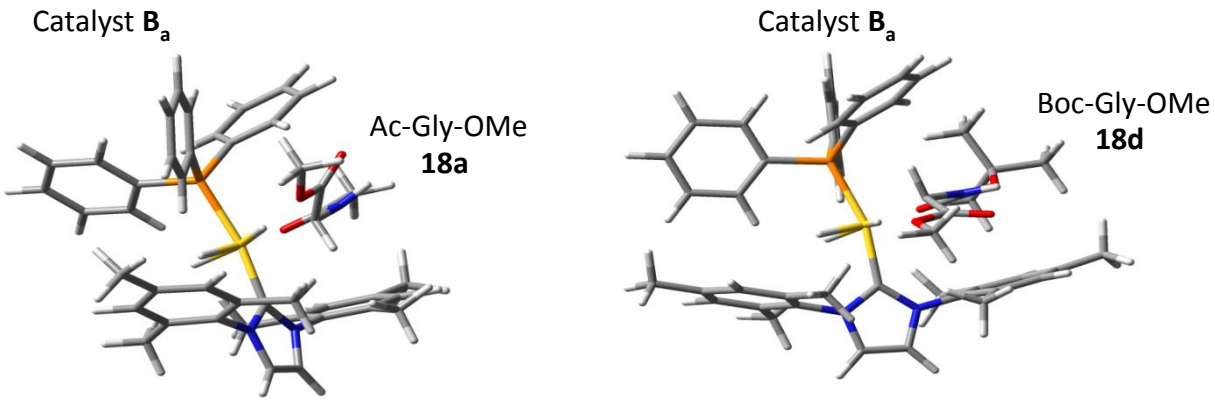

IV.4. Conclusion

A new method for highly selective hydrogen isotope exchange of C(sp^3)-centers in aliphatic amides has been developed. Starting from commercially available Kerr-catalyst $\mathbf{B_b}$, the HIE reaction on a series of common linker side chains of antibody-drug-conjugates proceeded with high chemical yields, high regioselectivity and with deuterium incorporations up to 99%D. The scope of the method was further extended to alpha amino acids, especially successful for glycine and alanine (up to 93%D). In di- and tripeptides, a very interesting protecting group-dependent selectivity was observed. This suggest new options for selective labelling approaches by varying the N-protecting group. While with N-acetyl-protecting groups the labelling at the α-carbon was observed, this could be completely circumvented by using Boc or Fmoc protecting groups. Furthermore, DFT calculations gave insights into the mechanism and steric requirements of the HIE reaction with glycine (**18**) and alanine (**19**) derivatives, and explained the observed selectivity and the influence of the amino acid N-protecting groups. The method is fully translatable to the specific requirements of tritium chemistry discussed in the objectives of the thesis. This latter point was demonstrated through tritium labelling of the maytansine DM4 drug, suggesting that the developed method is a suitable and highly valuable new tool in isotope research.

[1] For recent selected reviews: a) J. Atzrodt, V. Derdau, WJ. Kerr, M. Reid. *Angew. Chem. Int. Ed.* **2018**; *57*: 3022-3047. b) M.Valero, V. Derdau, *JLCR*, **2019**, https://doi.org/10.1002/jlcr.3783. c)D. Hesk, *JLCR*, **2019**, https://doi.org/10.1002/jlcr.3801.

[2] For selected recent books, see: a) Antibody-Drug Conjugates: The 21st Century Magic Bullets for Cancer, Ed. J. Wang, W.-C. Shen, J. L. Zaro, Springer **2015**, Cham, Heidelberg, New York; b) Antibody-Drug Conjugates: Fundamentals, Drug Development, and Clinical outcomes to target Cancer, Ed. K. J. Olivier Jr., S. A. Hurvitz, Wiley **2017**, Hoboken, New Jersey; c) E. I. Graziani, L. N. Tumey, Recent advances in antibody–drug conjugates. In Biotherapeutics: Recent Developments using Chemical and Molecular Biology, Ed. L. Jones, A. J. McKnight, **2013.**

[3] For selected recent reviews, see: a) B. ECG de Goeij, J. M. Lambert, *Curr. Opin. Immunol.* **2016**, *40*, 14–23; b) P. Polakis, *Pharmacol. Rev.* **2016**, *68*, 3–19; c) N. Diamantis, U. Banerji, *Brit. J. Canc.* **2016**, *114*, 362-367; d) R. Bakhtiar, *Biotechnol. Lett.* **2016**, *38*(10), 1655-1664; d) K. Tsuchikama, Z. An, *Protein Cell.* **2017**, DOI 10.1007/s13238-016-0323-0; e) E.G. Kim, K. M. Kim, *Biomol. Ther.* **2015**, *23*(6), 493–509; d) R. V. J. Chari, M. L. Miller, W. C. Widdison, *Angew. Chem. Int. Ed.* **2014**, *53*, 3796- 3827; e) R. J. Y. Ho, J. Chien, *J. Pharm. Sci.* **2014**, *103*(1), 71- 77.

[4] a) S. M. Kupchan, Y. Komoda, W. A. Court, *J. Am. Chem Soc.* **1972**, *94*, 1354–1356; b) S. M. Kupchan, Y. Komoda, A. R. Branfman, *J. Org. Chem.* **1977**, *42*, 2349–2357.

[5] S. Remillard, L. I. Rebhun, G. A. Howie, S. M. Kupchan, *Science.* **1975**, *189*, 1002–1005

[6] J. M. Cassady, K. K. Chan, H. G. Floss, E. Leistner, *Chem Pharm. Bull. (Tokyo)* **2004**, *52*, 1–26.

[7] a) M. Lopus, E. Oroudjev, L. Wilson, S. Wilhelm, W. Widdison, R. Chari, M. A. Jordan, *Mol. Cancer Ther.* **2010**, *9*(10), 2689-2699; b) H. K. Erickson, P.U. Park, W.C. Widdison, *Cancer Res.* **2006**, *66*, 4426–4433.

[8] B. A. Kellogg, L. Garrett, Y. Kovtun, K. C. Lai, B. Leece, M. Miller, G. Payne, R. Steeves, K. R. Whiteman, W. Widdison, H.G Xie, R. Singh, R. V. J. Chari, J. M. Lambert, R. J. Lutz, *Bioconjug. Chem.* **2011**, *22*, 717–727.

[9] a) V. Blanc, A. Bousseau, A. Caron, C. Carrez, R. J. Lutz, J. M. Lambert, *Clin Cancer Res* **2011**, *17*(20); 6448–6458; b) A. Raufi, A. S. Ebrahim, A. Al-Katib, *Cancer Manag. Res.* **2013**, *5*, 225-233; c) H. Carol, B. Szymanska, K. Evans, I. Boehm, P. J. Houghton, M. A. Smith, R. B. Lock, *Clin. Cancer Res.* **2013**; *19*(7), 1795–1805.

[10] a) J. F. Ponte, O. Ab, L. Lanieri, J. Lee, J. Coccia, L. M. Bartle, M. Themeles, Y. Zhou, J. Pinkas, R. Ruiz-Soto, *Neoplasia* **2016**, *18*, 775–784; b) K. N. Moore, L. P. Martin, D. M. O'Malley, U. A. Matulonis, J. A. Konner, R. P. Perez, T. M. Bauer, R. Ruiz-Soto, Mi. J. Birrer, *J. Clin. Oncol.* **2017** DOI: 10.1200/JCO.2016.69.9538.

[11] a) M. A. Socinski, F. J. Kaye, D. R. Spigel, F. J. Kudrik, S. Ponce, P. M. Ellis, M. Majem, P. Lorigan, L. Gandhi, M. E. Gutierrez, D. Nepert, J. Corral, L. P. Ares, *Clin. Lung Cancer*, **2017**, *18*(1), 68-76.

[12] T. Sawada, Y. Kato, H. Kobayashi, Y. Hashimoto, T. Watanabe, Y. Sugiyama, S. Iwasaki, *Bioconjugate Chem.* **1993**, *4*, 284-289.

[13] B. Q. Shen, D. Bumbaca, O. Saad, Q. Yue, C.V. Pastuskovas, S.C. Khojasteh, J. Tibbitts, S. Kaur, B. Wang, Y. W. Chu, P. M. Lorusso, S. Girish, *Curr. Drug Metab.* **2012**, *13*(10), 901-910.

[14] a) E. Higashide, M. Asai, K. Ootsu, S. Tanida, Y. Kozai, T. Hasegawa, T. Kishi, Y. Sugino, M. Yoneda, *Nature* **1977**, *29*, 721-722; M. Asai, E. Mizuta, M. Izawa, K. Haibaba, T.Kishi, *Tetrahedron* **1978**, *35*, 1079-1085.

[15] W. C. Widdison, S. D. Wilhelm, E. E. Cavanagh, K. R. Whiteman, B. A. Leece , Y. Kovtun, V. S. Goldmacher, H. Xie , R. M. Steeves , R. J. Lutz , R. Zhao , L. Wang , W. A. Blättler , R. V. J. Chari, *J. Med. Chem.* **2006**, *49*, 4392-4408.

[16] W. W. Cleland, *Biochemistry* **1964**, *3*, 480–482.

[17] For selected reviews, see: a) J. Atzrodt, V. Derdau, T. Fey, J. Zimmermann, *Angew Chem. Int. Ed.* **2007**, *46*, 7744-7765; b) N. Modutlwa, T. Maegawa, Y. Monguchi, H. Sajiki, *J. Label. Compd.*

Radiopharm. **2010**, *53*, 686-692; c) J. Atzrodt, V. Derdau, *J. Label. Compd. Radiopharm.* **2010**, *53*, 674-685; d) J. R. Heys, *Label. Compd. Radiopharm.* **2010**, *53*, 716-721; e) W. J. S. Lockley, J. R. Heys *J. Label. Compd. Radiopharm.* **2010**, *53*, 635-644; f) W. J. S. Lockley, D. Hesk, *J. Label. Compd. Radiopharm.* **2010**, *53*, 704-715; g) Y. Sawama, Y. Monguchi, H. Sajiki, *Synlett* **2012**, *23*, 959-972; h) A. Di Guiseppe, R. Castarlenas, L. a. Oro, *C. R. Chim.* **2015**, *18*, 713-741.

[18] These data are collected from Remo Weck, a co-worker in our Isotope Chemistry group at Sanofi.

[19] For recent selected examples of sp^3-labelling with tritium see: a) D. Hesk, C. F. Lavey, P. McNamara, *J. Label Compd. Radiopharm.* **2010**, *53*, 722-730; b) P. H. Allen, M. J. Hickey, L. P. Kingston, D. J. Wilkinson, *J. Label Compd. Radiopharm*. **2010**, *53*, 731-738; c) J. R. Heys, *J. Label Compd. Radiopharm.* **2010**, *53*, 716-721; d) V. P. Shevchenko, I. Y. Nagaev, N. F. Myasoedov, *J. Label Compd. Radiopharm*. **2010**, *53*, 693-703; e) R. Voges, R. Heys, T. Moenius, *Preparation of Compounds labeled with Tritium and Carbon-14*, Wiley **2009**, Chichester, UK.

[20] For a review see: Dugave C., Demange L. *Chem. Rev.* **2003**, *103*, 2475-2532.

[21] a) A.R. Cochrane, C. Idziak, W.J. Kerr, B. Mondal, L.C. Paterson, T. Tuttle, S. Andersson, G.N. Nilsson, *Org. Biomol. Chem.* **2014**, *12*, 3598-3603.b) W.J. Kerr, M. Reid, T. Tuttle, *Angew. Chem. Int. Ed.* **2017**, *56*, 7808-7812. c) W.J. Kerr, M. Reid, T. Tuttle, *ACS Catal.* **2015**, *5*, 402-410.

[22] A.Y.L. Shu, W. Chen, J.R. Heys, *J. Organomet. Chem.* **1996**, *524*, 87-93.

[23] Details of the calculation method along with further calculation results can be found in the Supporting Information available online: https://doi.org/10.1002/anie.201804010.

[24] M. Valero, R. Weck, S. Güssregen, J. Atzrodt, V. Derdau, *Angew. Chem. Int. Ed.* **2018**, *57*(*27*), 8159-8163.

Supporting information Part IV

Materials and General deuteration procedure: Annex 1**.**

Deuteration of DM4 derivatives 1a-c

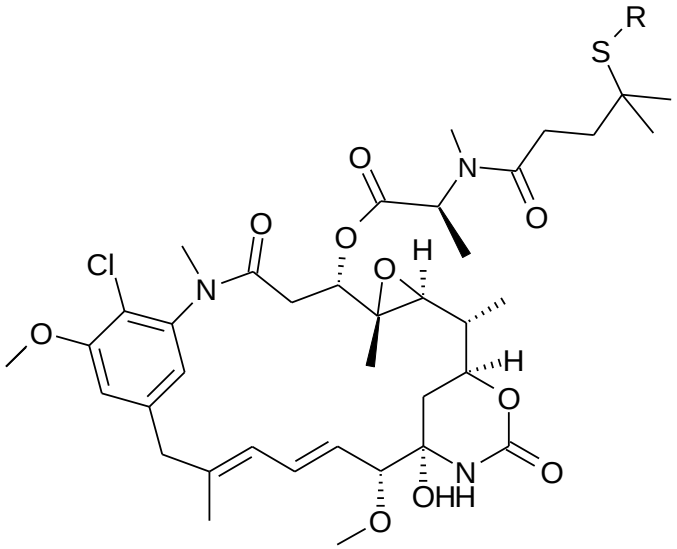

R = H, **1a**
Me, **1b**
SMe **1c**

Deuteration of DM4-H 1a

Conditions: 2.0 mg (2.5 µmol) **1a**; 0.5 mg (0.25 µmol) catalyst $\mathbf{B_b}$, 50°C, 3h

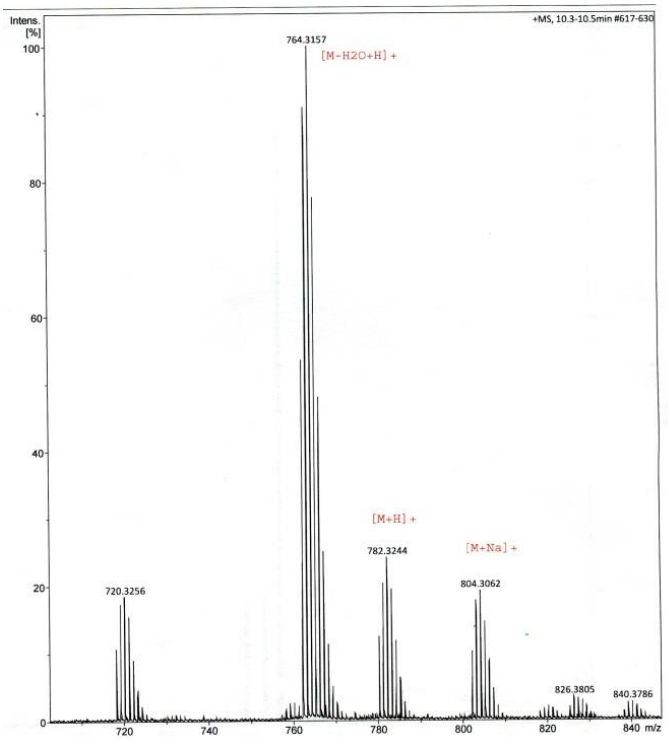

MS (positive ESI): m/z = 762.3 $(M\text{-}H_2O+H)^+$ (13); 763.3 $(M\text{-}H_2O+D_1+H)^+$ (22), 764.3 $(M\text{-}H_2O+D_2+H)^+$ (24), 765.3 $(M\text{-}H_2O+D_3+H)^+$ (19), 766.3 $(M\text{-}H_2O+D_4+H)^+$ (12), 767.3 $(M\text{-}H_2O+D_5+H)^+$ (6).

Calculated D-content/molecule: 2.0.

Yield: 1.3 mg (1.6 µmol) **1a**, 65%.

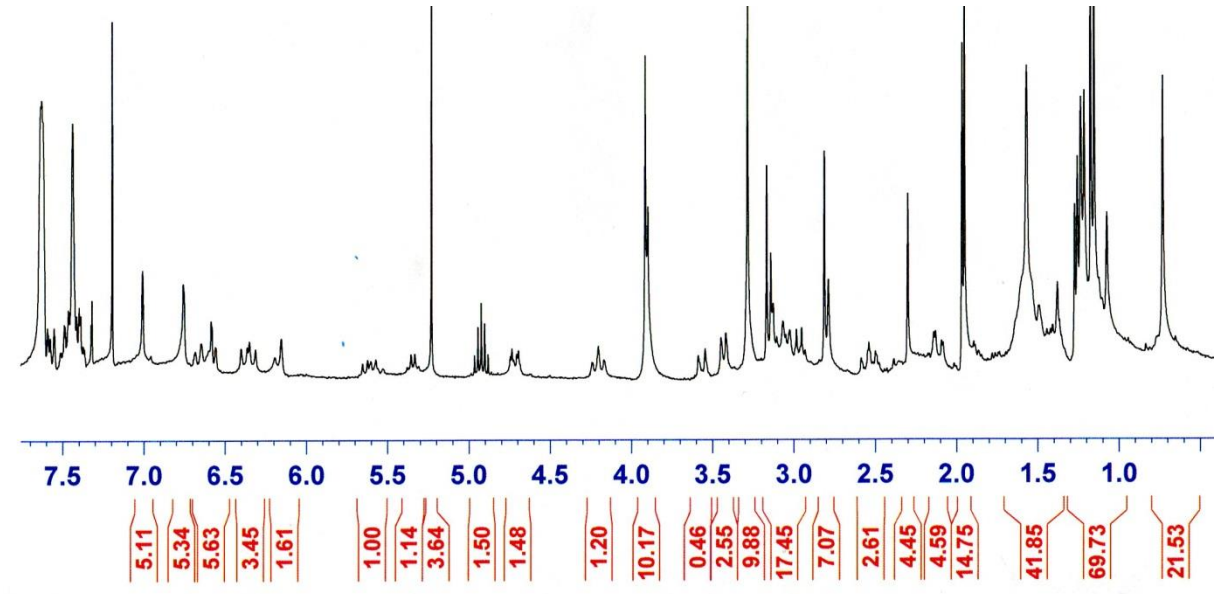

No determination of labelling position with ^{1}H-NMR possible.

Deuteration of DM4-Me 1b

Conditions: 2.0 mg (2.5 µmol) **1b**; 0.5 mg (0.25 µmol) catalyst $\mathbf{B_b}$, 50°C, 3h.

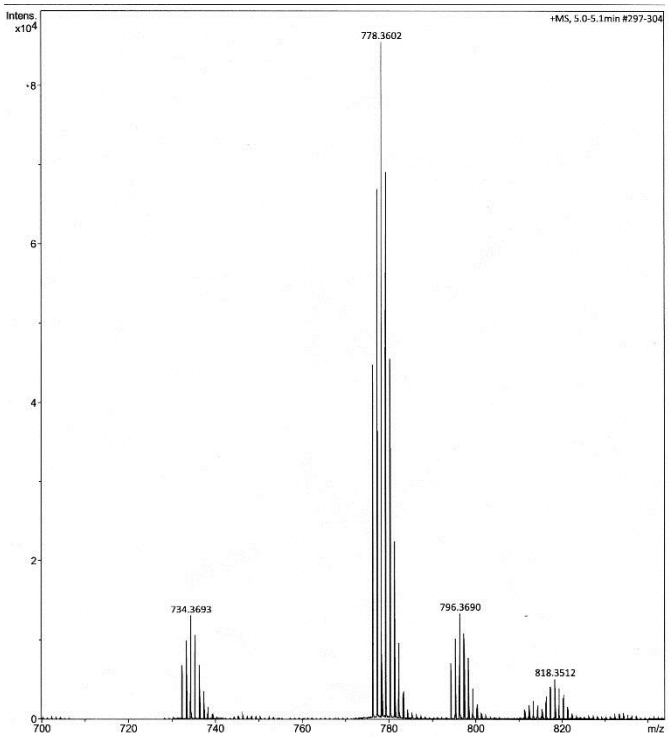

MS (positive ESI): m/z = 776.3 $(M\text{-}H_2O+H)^+$ (14); 777.3 $(M\text{-}H_2O+D_1+H)^+$ (21), 778.3 $(M\text{-}H_2O+D_2+H)^+$ (27), 779.3 $(M\text{-}H_2O+D_3+H)^+$ (22), 780.3 $(M\text{-}H_2O+D_4+H)^+$ (15).

Calculated D-content/molecule: 2.0.

Yield: 1.6 mg (2.0 µmol) **1b**, 80%.

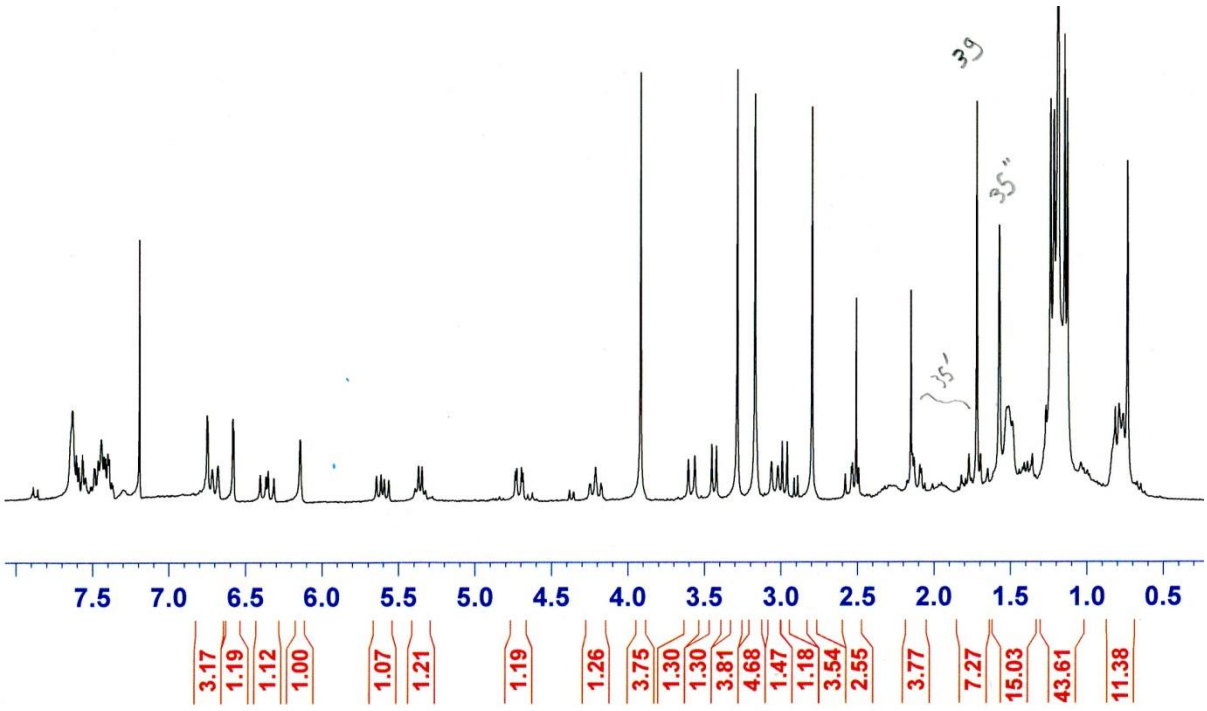

No determination of labelling position with ^{1}H-NMR possible.

Deuteration of DM4-Me 1c

Conditions: 2.0 mg (2.5 µmol) **8c**; 0.5 mg (0.25 µmol) catalyst $\mathbf{B_b}$, 50°C, 3h.

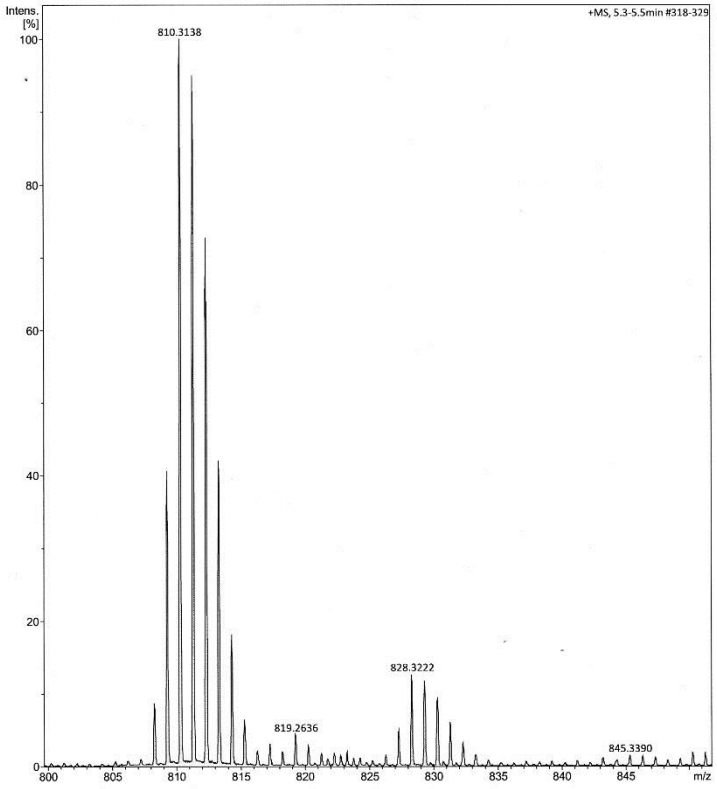

MS (positive ESI): m/z = 808.3 $(M\text{-}H_2O+H)^+$ (4); 809.3 $(M\text{-}H_2O+D_1+H)^+$ (22), 810.3 $(M\text{-}H_2O+D_2+H)^+$ (47), 811.3 $(M\text{-}H_2O+D_3+H)^+$ (20), 812.3 $(M\text{-}H_2O+D_4+H)^+$ (3).

Calculated D-content/molecule: 1.9.

Yield: 1.6 mg (2.0 µmol) **1c**, 80%.

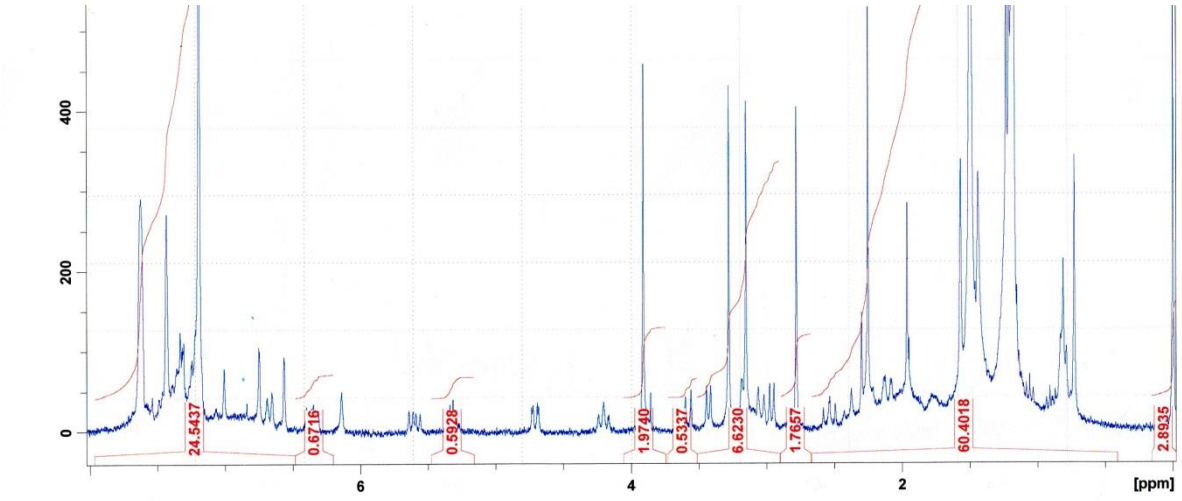

No determination of labelling position with ^{1}H-NMR possible.

Tritiation of DM4-SMe 1c (reaction 1; 7 eq tritium)

The tritiation of DM4-SMe **1c** was carried out using a standard Tritec® tritium manifold. DM4-SMe (4.0 mg, 4.8 µmol) **1c**, and catalyst $\mathbf{B_b}$ (2.1 mg, 1.2 µmol, 25 mol%) were dissolved in isopropyl acetate (0.7 mL) in a 1.0 mL reaction flask before being connected to the manifold. The solution was frozen in liquid nitrogen and the flask was evacuated, then charged with tritium (1.9 Ci, 61 mbar, 7eq.). The reaction mixture was then allowed to warm to room temperature over 15 min before stirring at r.t. for a further 30 min (168mbar pressure). The reaction mixture was then heated to 50 °C (245 mbar pressure) and stirred for 180 min before cooling again to r.t. The solvents were evaporated; methanol added and the solvent evaporated into a waste ampule. This procedure was repeated three times in total. The residue was dissolved in methanol and filtered. Purification and isolation *via* HPLC gave the tritiated product (3.1 mg, 3.7 µmol **1c**, 96.4% radiochemical purity, 1374 MBq, 0.37 TBq/mmol = 10 Ci/mmol).

MS (positive ESI): m/z 808.3 $[M\text{-}H_2O+H]^+$, 810.3 $[M(T)\text{-}H_2O+H]^+$; 848.3 $[M+Na]^+$; 826.3 $[M+H]^+$

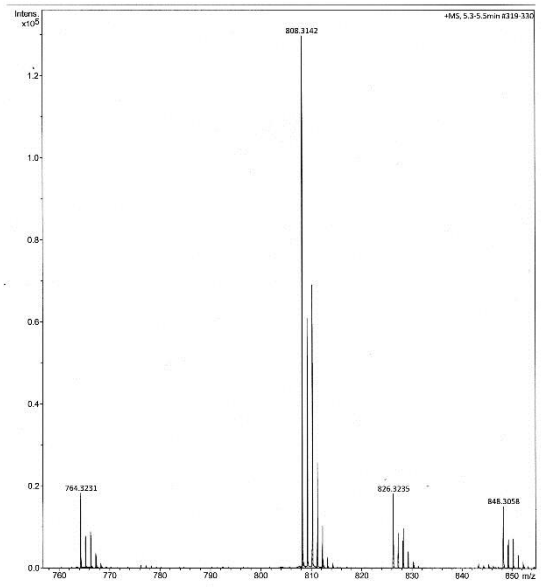

MS (DM4-SMe **1c**, unlabelled)

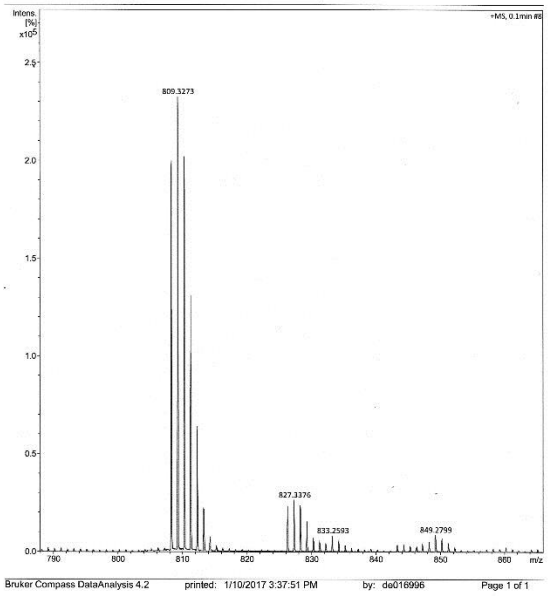

MS (DM4-SMe **1c**, ^{3}H-labelled)

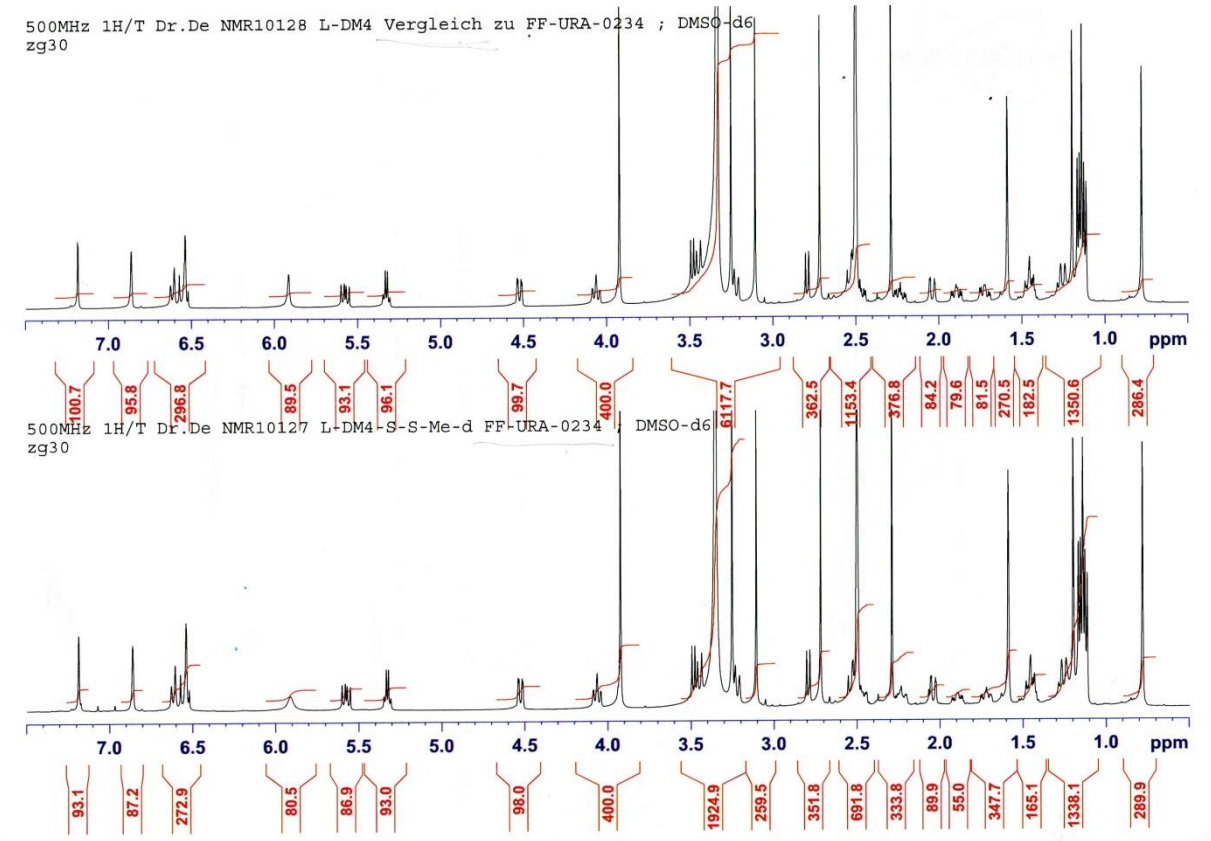

^{1}H-NMR: DM4-SMe **1c** unlabeled comparison (upper spectra); ^{3}H-DM4-SMe **1c** (below)

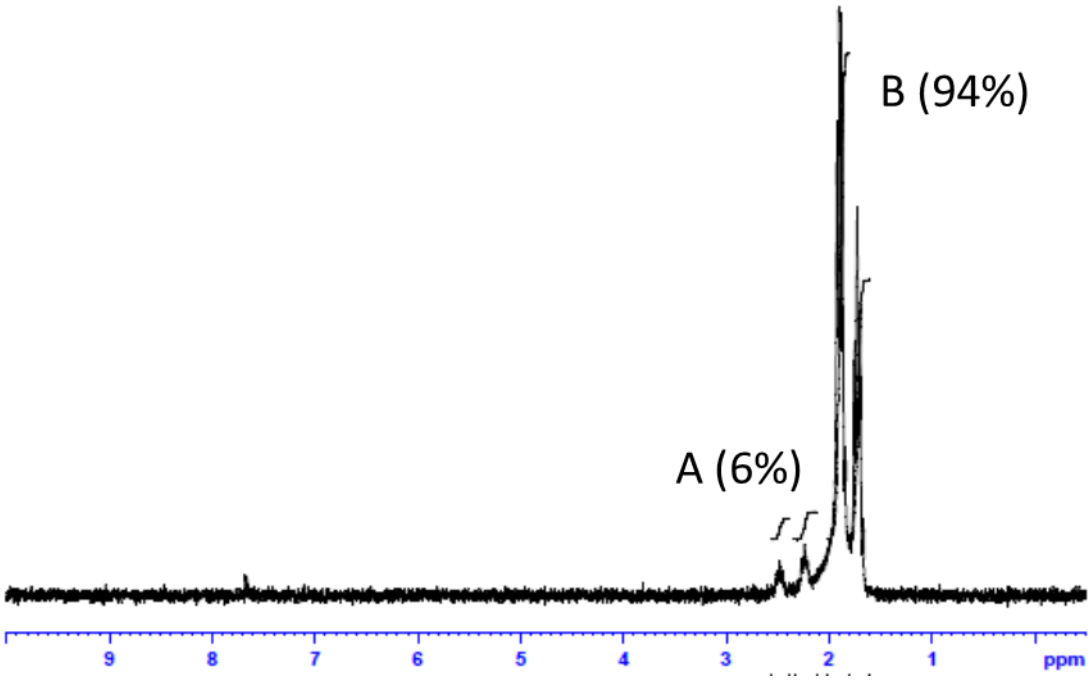

^{3}H-NMR (533 MHz): ^{3}H-DM4-SMe **1c**

^{3}H NMR 1c (533 MHz, DMSO-d$_6$): δ 2.52-2.43, 2.25-2.16 (m, 2H, 6%); 1.98-1.66 (m, 2H, 94%) ppm.

Tritiation of DM4-SMe 1c (reaction 2; 12 eq tritium)

The tritiation of DM4-SMe **8c** was carried out using a standard Tritec® tritium manifold. DM4-SMe (3.0 mg, 3.3 µmol) **1c**, and catalyst $\mathbf{B_a}$ (3.0 mg, 1.7 µmol, 51 mol%) were dissolved in isopropyl acetate (0.7 mL) in a 1.0 mL reaction flask before being connected to the manifold. The solution was frozen in liquid nitrogen and the flask was evacuated, then charged with tritium (2.5 Ci, 74 mbar, 12eq.). The reaction mixture was then allowed to warm to room temperature over 15 min before stirring at r.t. for a further 30 min (186 mbar pressure). The reaction mixture was then heated to 50 °C (270 mbar pressure) and stirred for 180 min before cooling again to r.t. The solvents was evaporated; methanol added and the solvent evaporated into a waste ampulle. This procedure was repeated three times in total. The residue was dissolved in methanol and filtered. Purification and isolation *via* HPLC gave the tritiated product (1.7 mg, 1.9 µmol **1c**, 96.7% radiochemical purity, 2787 MBq; 1.15 TBq/mmol = 31 Ci/mmol).

MS (positive ESI): m/z 808.3 $[M\text{-}H_2O+H]^+$, 810.3 $[M(T)\text{-}H_2O+H]^+$; 848.3 $[M+Na]^+$; 826.3 $[M+H]^+$

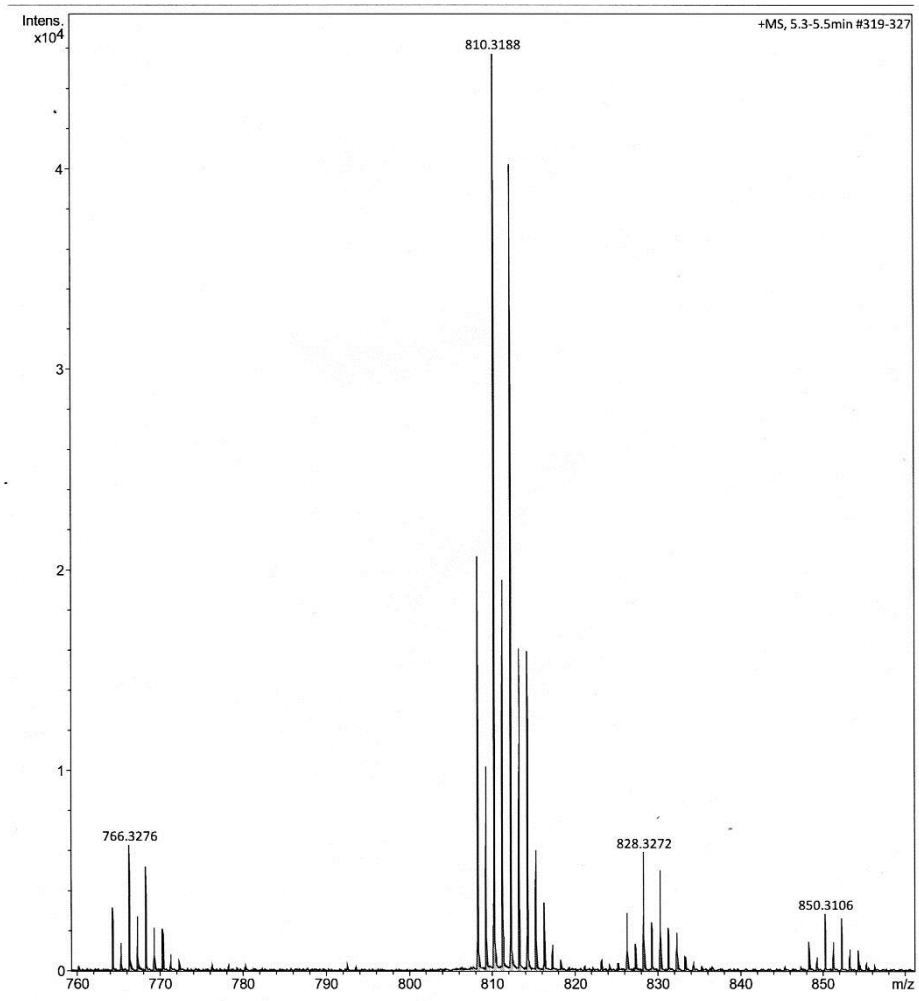

Conditions screening (table IV.2 and IV.3)

For the screening of different solvents, catalysts, catalysts loading, temperature and time, the following conditions have been applied on model substrate **[H]-10**. 4-[(4-methyl)dithio]-4-methyl-*N*-(benzyl)-pentanamide **[H]-10** (14 µmol, 500 µL, 1 eq.) and the catalyst of choice (5 to 10 mol%) were dissolved in 1 mL of the solvent of choice. All reactions were performed according to the general HIE protocol at the temperature and time of choice.

The data presented in the tables have been determined by ^{1}H-NMR for the labelling position and by LC-MS for the percentage of deuterium incorporation.

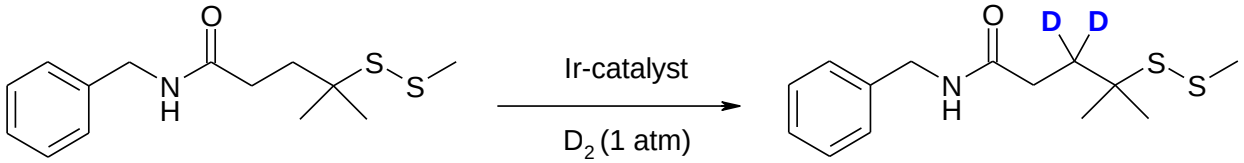

[H]-10 **10**

All spectra about the HIE experiments are available from the following page.

4-[(4-methyl)dithio]-4-methyl-*N*-(benzyl)-pentanamide **10**

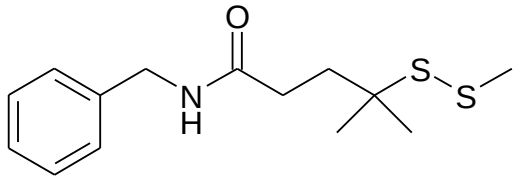

Molecular Weight =283,4576
Molecular Formula =C14H21NOS2

10

^{1}H NMR (300 MHz, $CDCl_3$): δ 7.28-7.16 (m, 5H), 5.90 (br s, 1H, N*H*), 4.36 (d, ^{3}J=6.9 Hz, 2H, CH_2Ph), 2.32 (s, 3H, SCH_3), 2.22-2.16 (m, 2H), 1.90-1.85 (m, 2H), 1.22 (s, 6H, CH_3) ppm. Incorporation expected at δ 1.90-1.85 (red arrow). Determined against integral at δ 4.36 (blue arrow).

HRMS (positive ESI): m/z calculated for $C_{14}H_{21}NOS_2$ $[M+H]^+$: 284.1137; found: 284.1151.

Conditions: 3.5 mg (12.0 µmol) **10**; 2.1 mg (1.2 µmol) catalyst **B_b**, 3h.

Yield: 3.2 mg, 11.0 µmol, 91%; 99%D for δ 1.90-1.85.

^{1}H-NMR Reference **10**

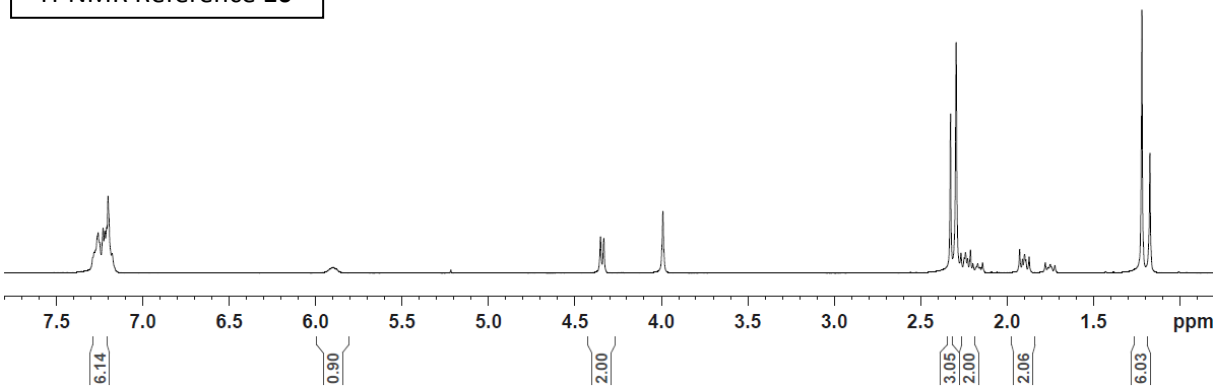

^{1}H-NMR HIE reaction **10**

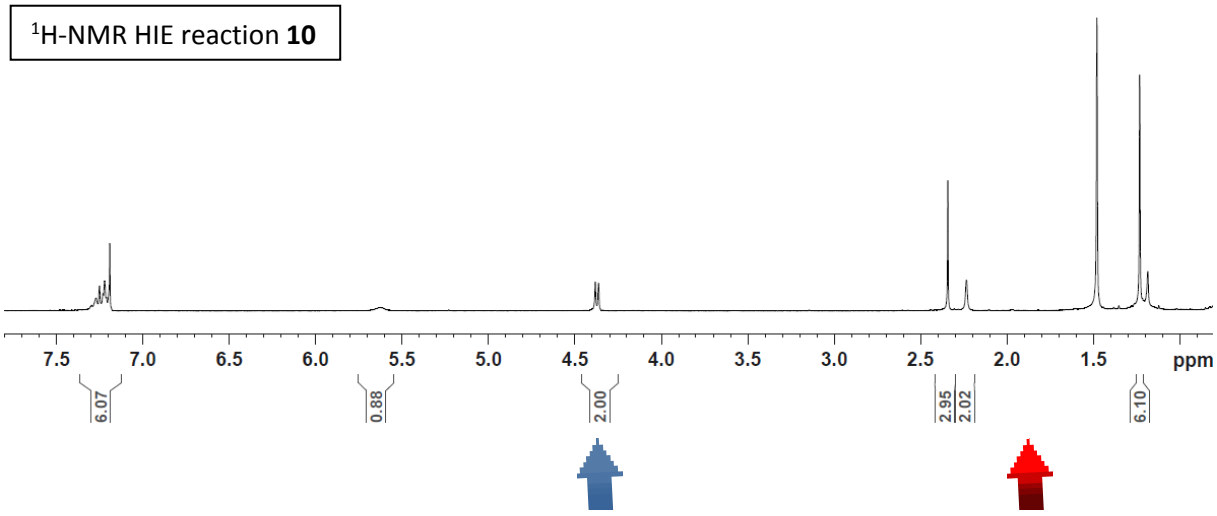

4-[(4-methyl)dithio]-4-methyl-*N*-(propyl)-pentanamide **11**

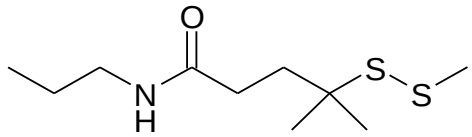

Molecular Weight =235,4130
Molecular Formula =C10H21NOS2

11

^{1}H NMR (300 MHz, $CDCl_3$): δ 5.56 (br s, 1H, N*H*), 3.17 (dd, ^{3}J= 6.9 Hz, ^{3}J= 6.9 Hz, 2H), 2.35 (s, 3H, SCH_3), 2.23-2.18 (m, 2H), 1.91-1.86 (m, 2H), 1.51 (dt, ^{3}J= 6.9 Hz, ^{3}J= 7.5 Hz, 2H), 1.23 (s, 6H, CH_3), 0.88 (t, ^{3}J= 7.5 Hz, 3H) ppm. Incorporation expected at δ 1.91-1.86 (red arrow). Determined against integral at δ 2.35 (blue arrow).

HRMS (positive ESI): m/z calculated for $C_{10}H_{21}NOS_2$ $[M+H]^+$: 236.1137; found: 236.1139.

Conditions: 3.0 mg (13.0 µmol) **11**; 2.3 mg (1.3 µmol) catalyst **B_b**, 3h.

Yield: 2.6 mg, 11.0 µmol, 88%; 99%D for δ 1.91-1.86.

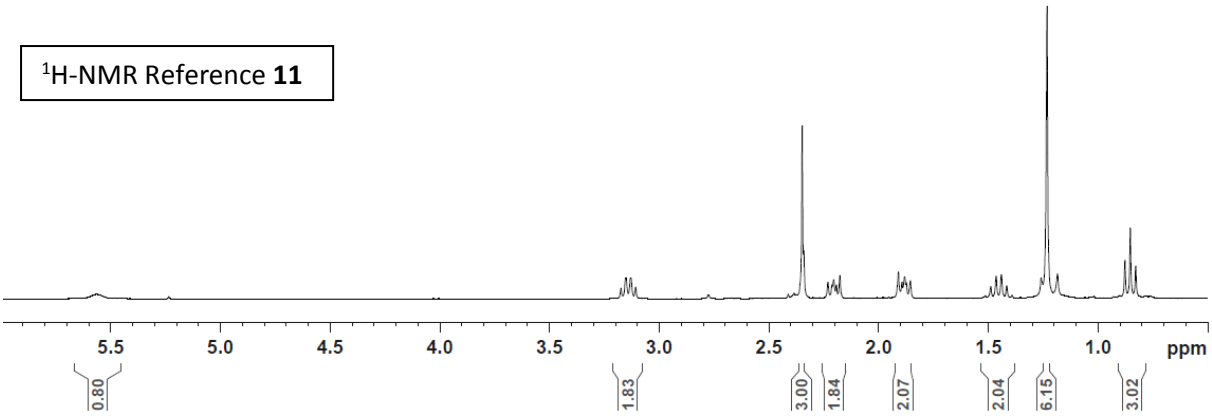

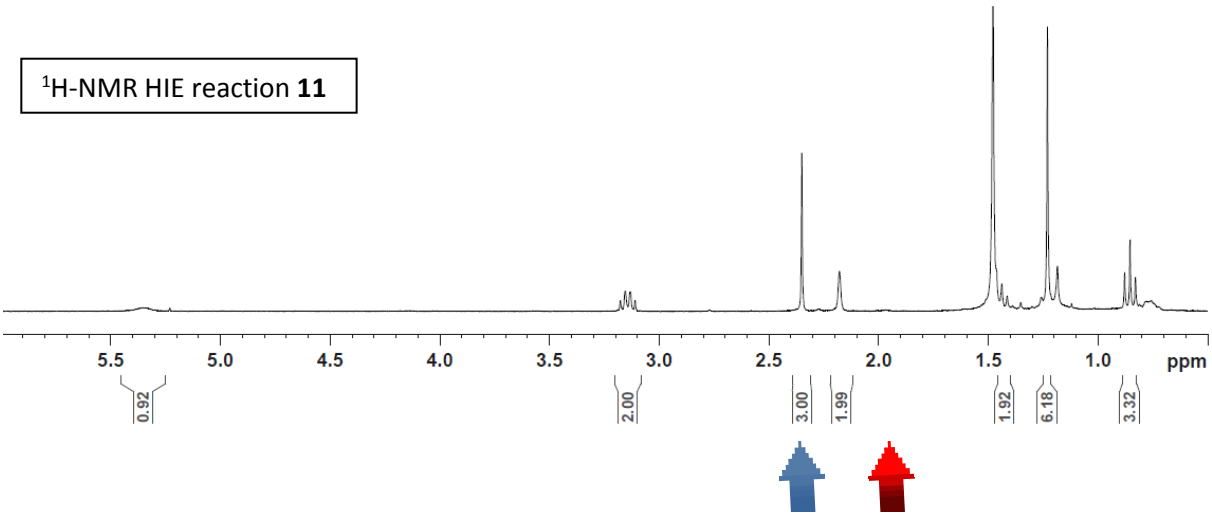

4-[(4-methyl)dithio]-4-methyl-*N*-(diethyl)-pentanamide **12**

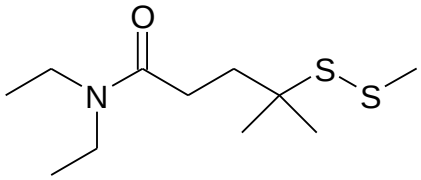

12

Molecular Weight =249,4401
Molecular Formula =C11H23NOS2

^{1}H NMR (300 MHz, $CDCl_3$): 3.33-3.22 (m, 4H), 2.34 (s, 3H, SCH_3), 2.27-2.24 (m, 2H), 1.87-1.80 (m, 2H) 1.25 (s, 6H), 1.15 (t, ^{3}J = 7.2 Hz, 3H), 1.06 (t,^{3}J = 7.2 Hz, 3H) ppm. Incorporation expected at δ 1.87-1.80 (red arrow). Determined against integral at δ 3.33-3.22 (blue arrow).

HRMS (positive ESI): m/z calculated for $C_{11}H_{23}NOS_2$ $[M+H]^+$: 250.1293; found: 250.1300.

Conditions: 3.0 mg (12.0 µmol) **12**; 2.1 mg (1.2 µmol) catalyst **B_b**, 3h.

Yield: 2.8 mg, 11.0 µmol, 93%; 99%D for δ 1.87-1.80

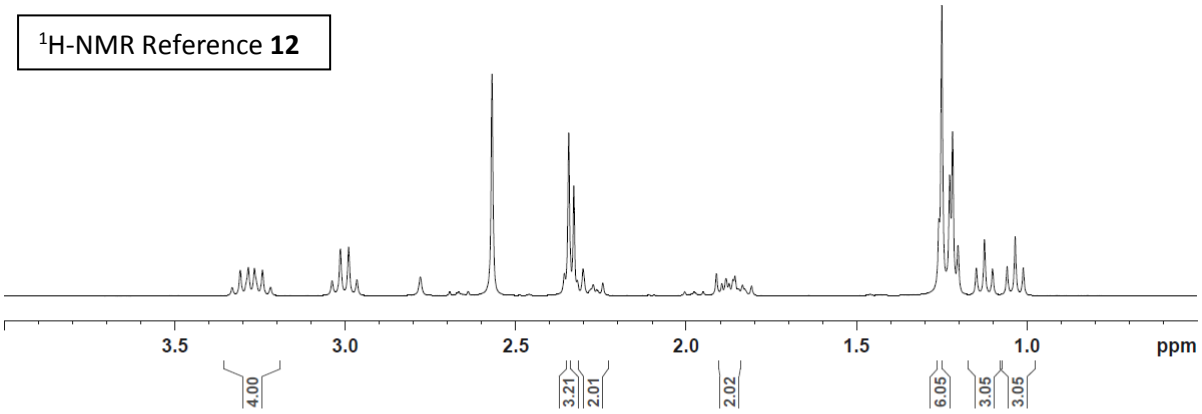

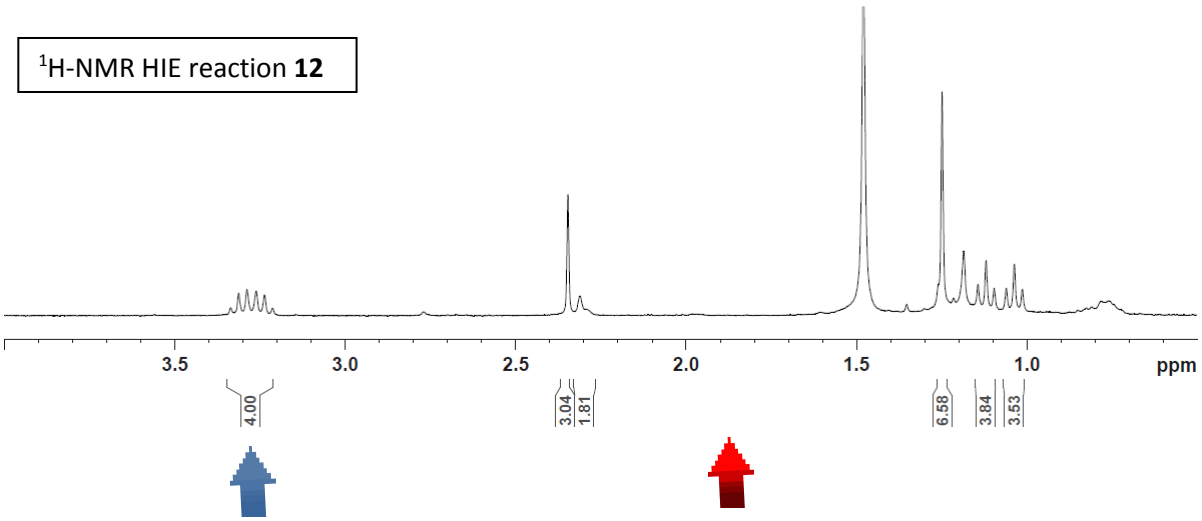

L-Alanine, *N*-[4-methyl-4-(methyldithio)-1-oxopentyl]-methyl ester **13**

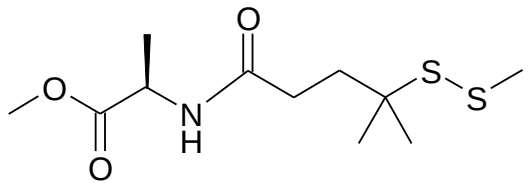

Molecular Weight =281,4350
Molecular Formula =C11H19NO3S2

13

^{1}H NMR (300 MHz, $CDCl_3$): δ 6.13 (br s, 1H, N*H*), 4.57 (dt, ^{3}J=6.9 Hz, ^{3}J=7.5 Hz, 1H), 3.69 (s, 3H, COOCH_3), 2.35 (s, 3H, SCH_3), 2.29-2.23 (m, 2H), 1.91-1.85 (m, 2H), 1.35 (d, ^{3}J=7.5 Hz, 3H), 1.23 (s, 6H, CH_3) ppm. Incorporation expected at δ 1.91-1.85 (red arrow). Determined against integral at δ 2.35 (blue arrow).

HRMS (positive ESI): m/z calculated for $C_{11}H_{19}NO_3S_2$ $[M+H]^+$: 280.1035; found: 280.1045.

Conditions: 5.0 mg (19.0 µmol) **13**; 3.3 mg (1.9 µmol) catalyst **B_b**, 3h.

Yield: a) 4.4 mg, 15.0 µmol, 87%; 99%D for δ 1.91-1.85.
b) 4.5 mg, 16.0 µmol, 91%; 99% D for δ 91-1.85.

Average: y=89%, 99% D

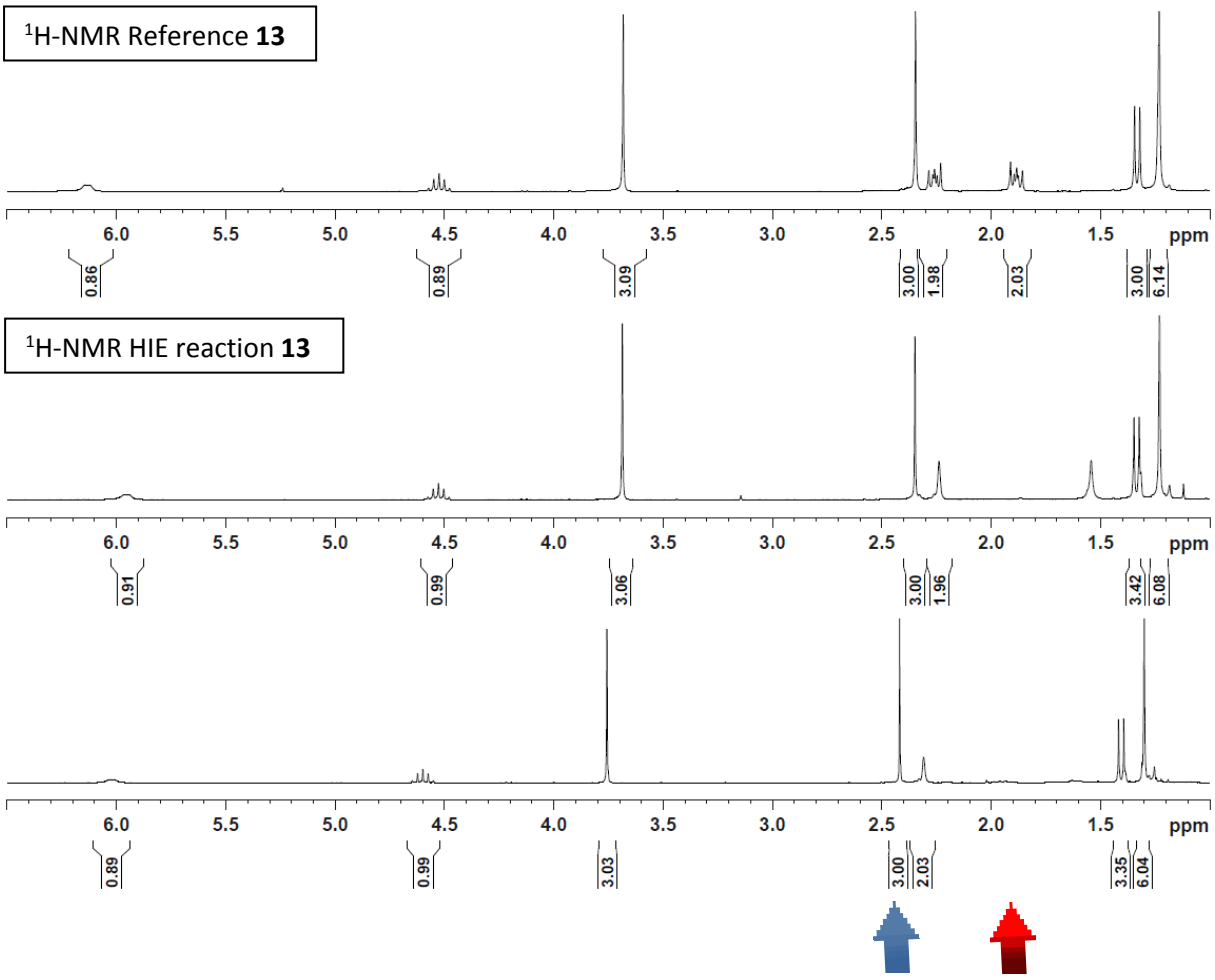

L-Serine, *N*-[4-methyl-4-(methyldithio)-1-oxopentyl]-ethyl ester **14**

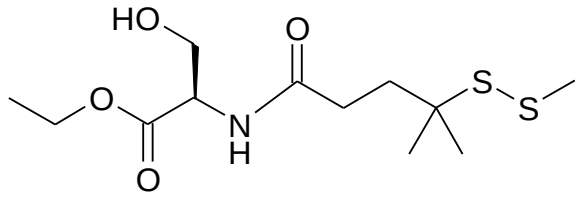

14

Molecular Weight =309,4494
Molecular Formula =C12H23NO4S2

^{1}H NMR (300 MHz, $CDCl_3$): δ 6.73 (br s, 1H, N*H*), 4.65-4.58 (m, 1H), 4.25 (q, ^{3}J=7.5 Hz, 2H, OCH_2CH$_3$), 3.96 (dd, ^{3}J=9.6 Hz, ^{3}J=3.9 Hz, 2H, CH_2OH), 2.39 (s, 3H, SCH_3), 2.37-2.33 (m, 2H), 1.96-1.90 (m, 2H), 1.29-1.25 (m, 9H) ppm. Incorporation expected at δ 1.96-1.90 (red arrow). Determined against integral at δ 4.25 (blue arrow).

HRMS (positive ESI): m/z calculated for $C_{12}H_{23}NO_4S_2^+$ $[M+H]^+$: 310.1141; found: 310.1144.

Conditions: 5.0 mg (16.0 µmol) **14**; 2.8 mg (1.6 µmol) catalyst **B_b**, 3h.

Yield: a) 4.5 mg, 15.0 µmol, 90%; 98% D for δ 1.96-1.90.
b) 4.9 mg, 16.0 µmol, 98%; 91% D for δ 1.96-1.90.

Average: y=94%, 95% D

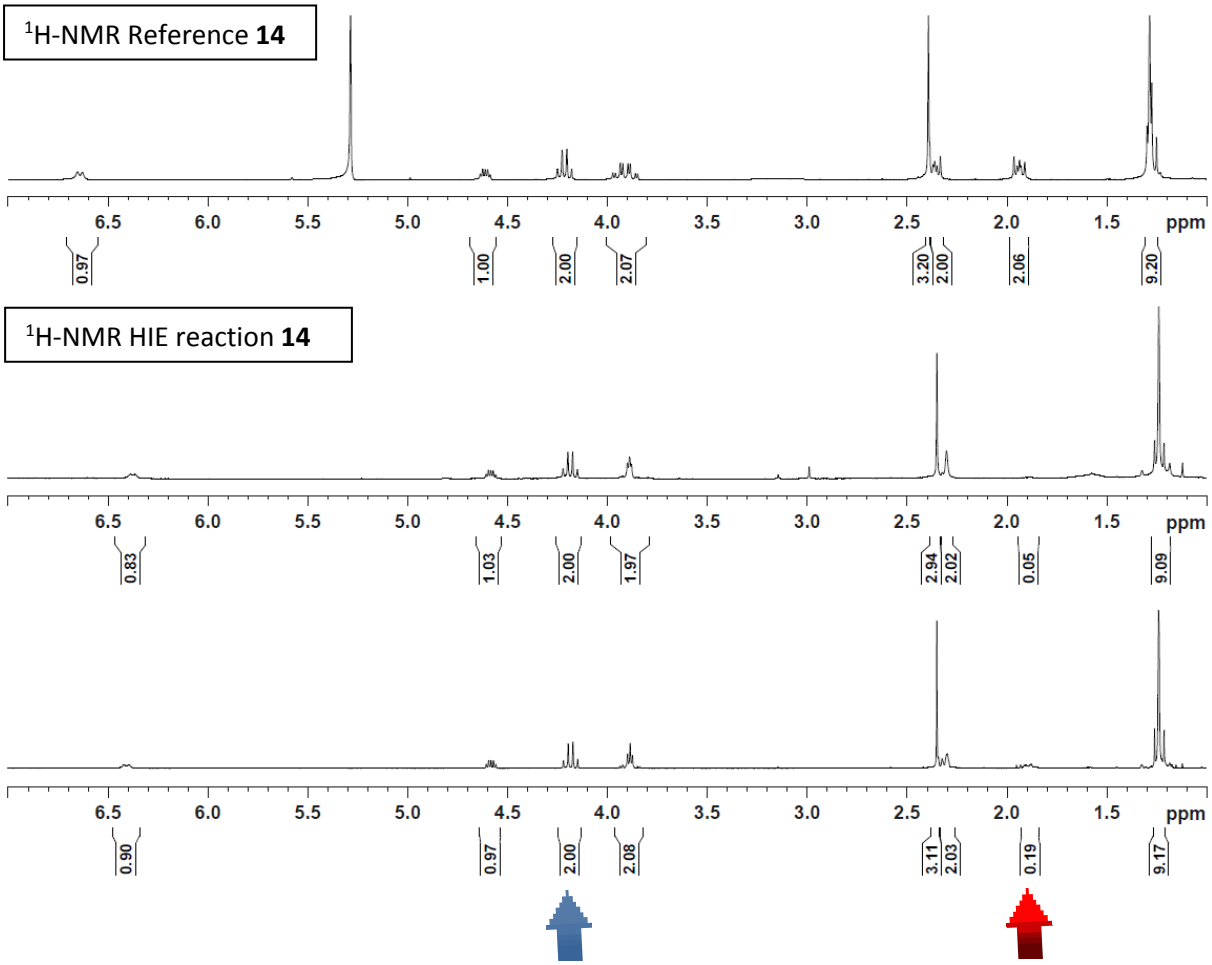

Glycine, *N*-[4-methyl-4-(methyldithio)-1-oxopentyl]-ethyl ester **15**

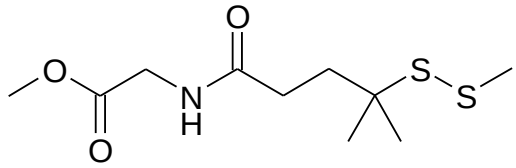

Molecular Weight =265,3958
Molecular Formula =C10H19NO3S2

15

^{1}H NMR (300 MHz, $CDCl_3$): δ 6.11 (br s, 1H, N*H*), 3.99 (d, ^{3}J=5.4 Hz, 2H, CH_2NH), 3.70 (s, 3H, COOCH_3), 2.35 (s, 3H, SCH_3), 2.29-2.23 (m, 2H), 1.89-1.84 (m, 2H), 1.24 (s, 6H, CH_3) ppm. Incorporation expected at δ 1.89-1.84 and 3.99 (red arrows). Determined against integral at δ 3.70 (blue arrow).

HRMS (positive ESI): m/z calculated for $C_{10}H_{19}NO_3S_2^+$ $[M+H]^+$: 266.0879; found: 266.0888.

Conditions: 5.0 mg (19.0 µmol) **15**; 3.3 mg (1.9 µmol) catalyst **B_b**, 3h.

Yield: a) 4.3 mg, 16.0 µmol, 85%; 42% D for δ 1.89-1.84 and 88% D for δ 3.99.
b) 4.9 mg, 18.0 µmol, 98%; 30% D for δ 1.89-1.84 and 80% D for δ 3.99.

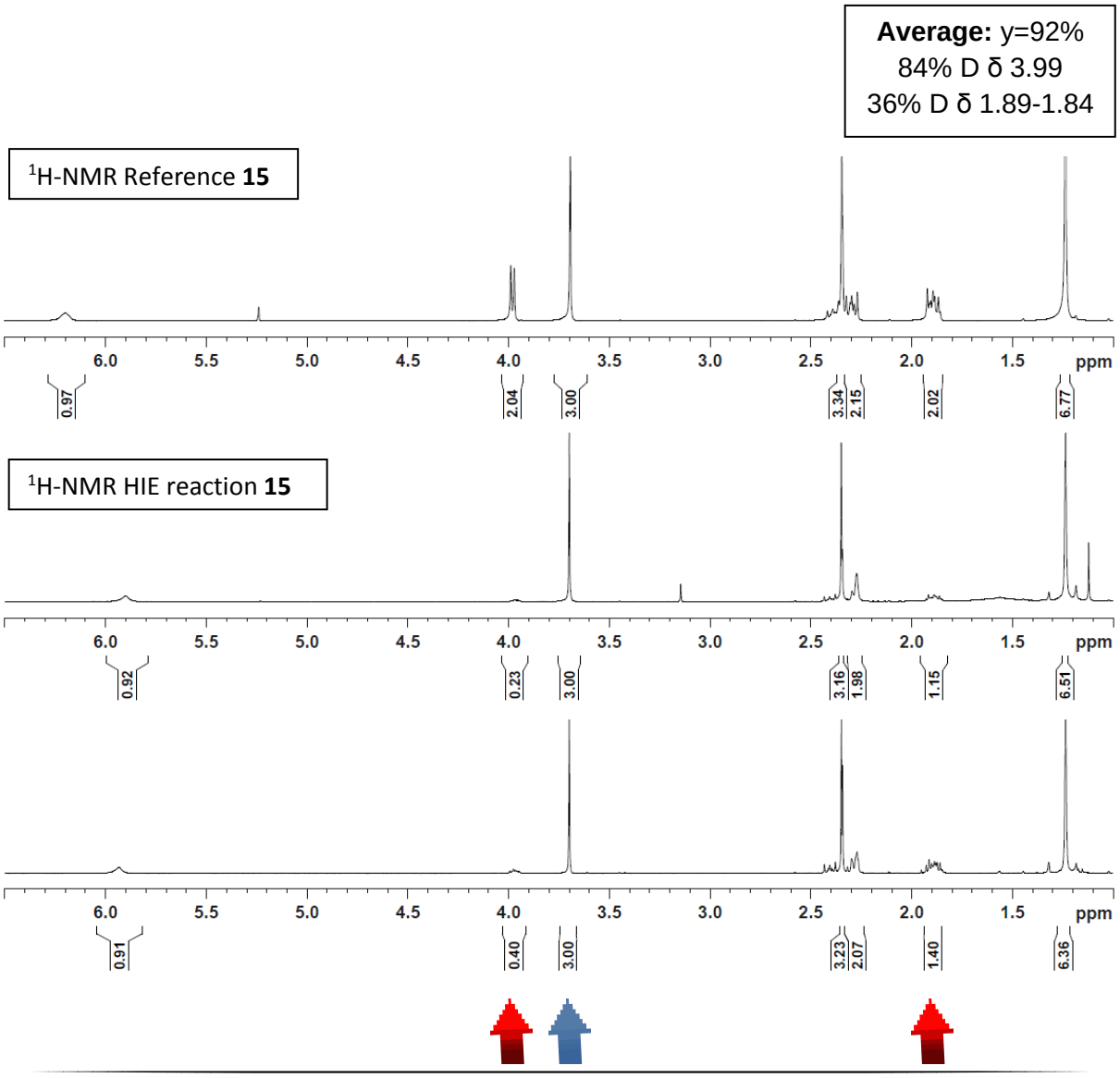

Glycine, *N*-[4-methyl-4-methoxy-1-oxopentyl]-methyl ester **16**

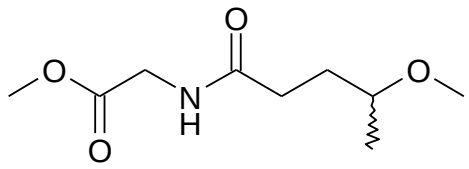

Molecular Weight =203,2401
Molecular Formula =C9H17NO4

16

^{1}H NMR (300 MHz, $CDCl_3$): δ 6.21 (br s, 1H, N*H*), 3.99 (dd, ^{3}J=9.6 Hz, ^{3}J=7.5 Hz, 2H, CH_2NH), 3.69 (s, 3H, COOCH_3), 3.33-3.29 (m, 1H), 3.26 (s, 3H, OCH_3), 2.31 (t, ^{3}J=7.5 Hz, 2H), 1.81-1.65 (m, 2H), 1.09 (d, ^{3}J=6.6 Hz, 3H) ppm. Incorporation expected at δ 3.99 (red arrow). Determined against integral at δ 3.69 (blue arrow).

HRMS (positive ESI): m/z calculated for $C_9H1_7NO_4^+$ [M+H]$^+$: 204.1230; found: 204.1234.

Conditions: 7.0 mg (35.0 µmol) **16**; 6.1 mg (3.5 µmol) catalyst **B_b**, 3h.

Yield: 5.3 mg, 26.0 µmol, 76%; 93%D for δ 3.99.

^{1}H-NMR Reference **16**

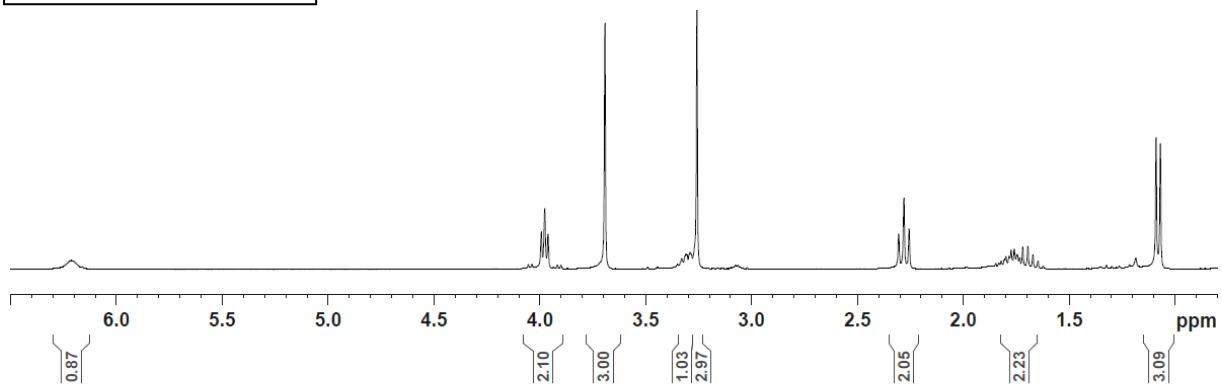

^{1}H-NMR HIE reaction **16**

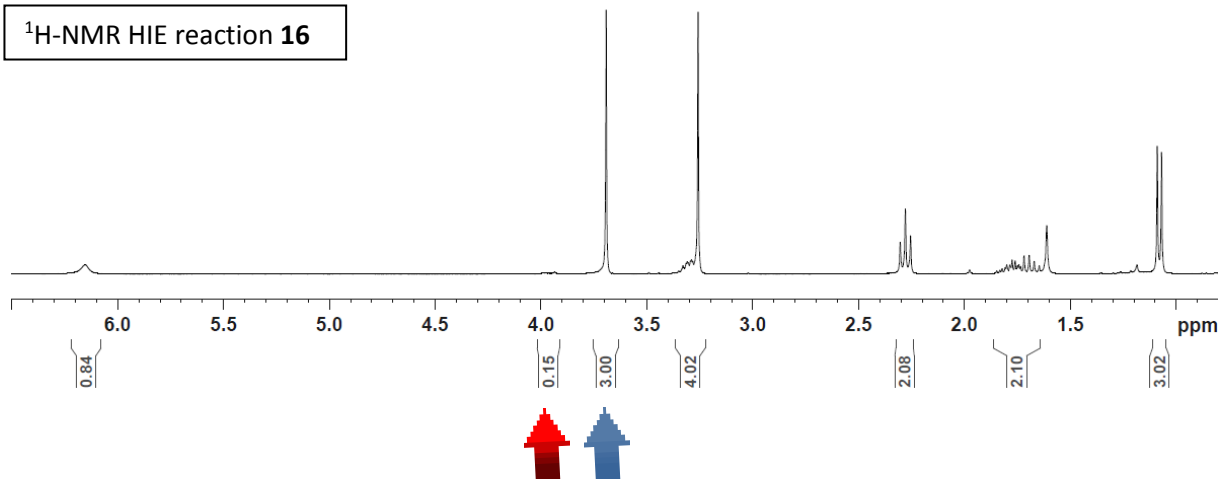

Glycine, *N*-[4-methoxy-1-oxopentyl]-methyl ester **17**

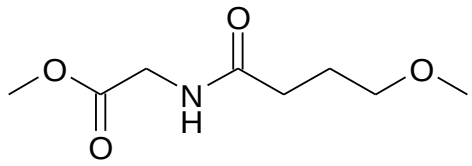

Molecular Weight =189,2131
Molecular Formula =C8H15NO4

17

^{1}H NMR (300 MHz, $CDCl_3$): δ 6.43 (br s, 1H, N*H*), 3.98 (d, ^{3}J=8.1 Hz, 2H, CH_2NH), 3.69 (s, 3H, COOCH_3), 3.38 (t, ^{3}J=12.0 Hz, 2H), 3.27 (s, 3H, OCH_3), 2.31 (t, ^{3}J=7.2 Hz, 2H), 1.89-1.80 (m, 2H) ppm. Incorporation expected at δ 3.99 (red arrow). Determined against integral at δ 3.69 (blue arrow).

HRMS (positive ESI): m/z calculated for $C_8H_{15}NO_4^+$ [M+H]$^+$: 190.1074; found: 190.1074.

Conditions: 9.5 mg (50.0 µmol) **17**; 8.7 mg (5.0 µmol) catalyst **B_b**, 3h.

Yield: 6.8 mg, 36.0 µmol, 72%; 92%D for δ 3.99.

^{1}H-NMR Reference **17**

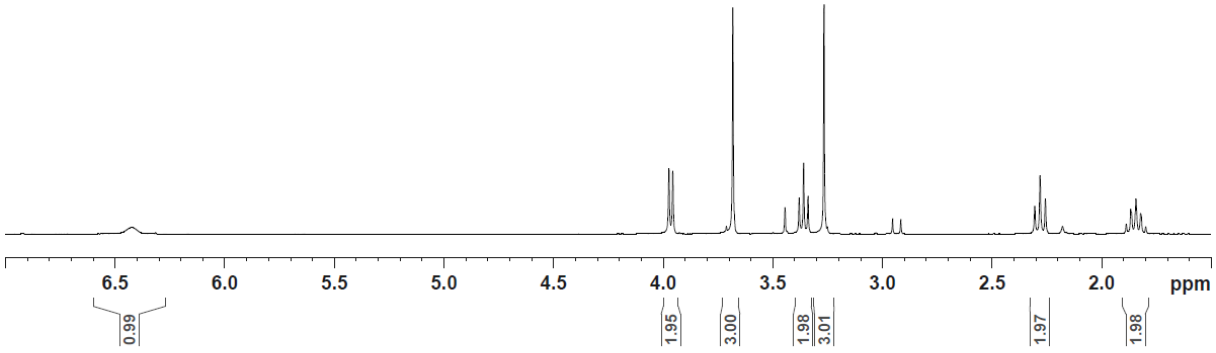

^{1}H-NMR HIE reaction **17**

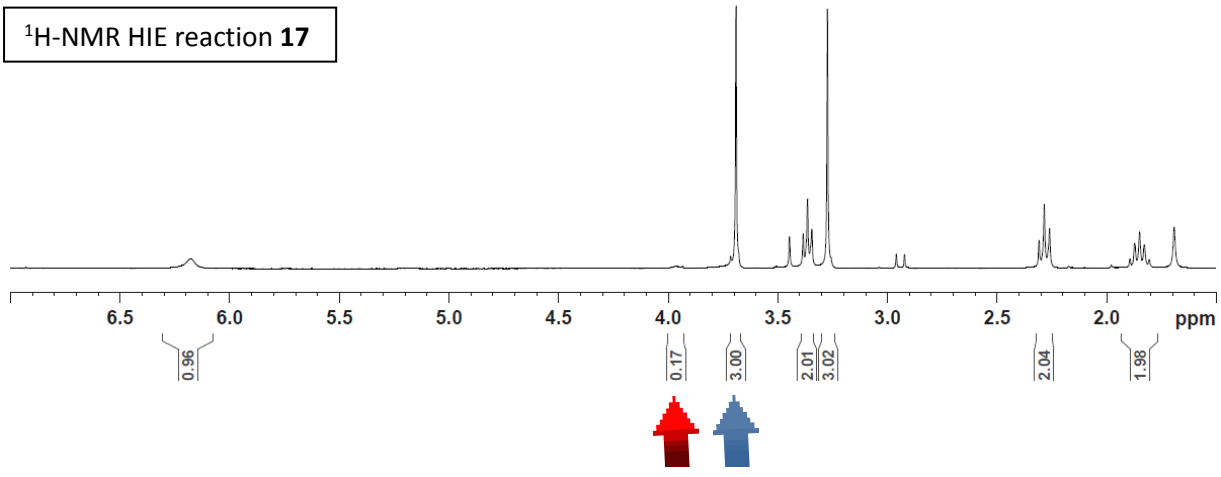

Protected glycine methyl ester 18 a-e

Conditions: 10.0 mg (76.0 µmol) **18a**; 13.0 mg (7.6 µmol) catalyst $\mathbf{B_b}$, 8h.
10.0 mg (45.0 µmol) **18b**; 7.8 mg (4.5 µmol) catalyst $\mathbf{B_b}$, 8h.
10.0 mg (32.0 µmol) **18c**; 5.5 mg (3.2 µmol) catalyst $\mathbf{B_b}$, 8h.
10.0 mg (53.0 µmol) **18d**; 9.2 mg (5.3 µmol) catalyst $\mathbf{B_b}$, 8h.
10.0 mg (56.0 µmol) **18e**; 9.7 mg (5.6 µmol) catalyst $\mathbf{B_b}$, 8h.

Yields **18a:** 9.0 mg, 75.0 µmol, 99%; 93%D for δ 3.89.
18b: 9.8 mg, 43.0 µmol, 98%; 50%D for δ 3.99.
18c: 7.20 mg, 23.0 µmol, 72%; 30%D for δ 3.95.
18d: 0%D for δ 3.65.
18e: 0%D for δ 3.82.

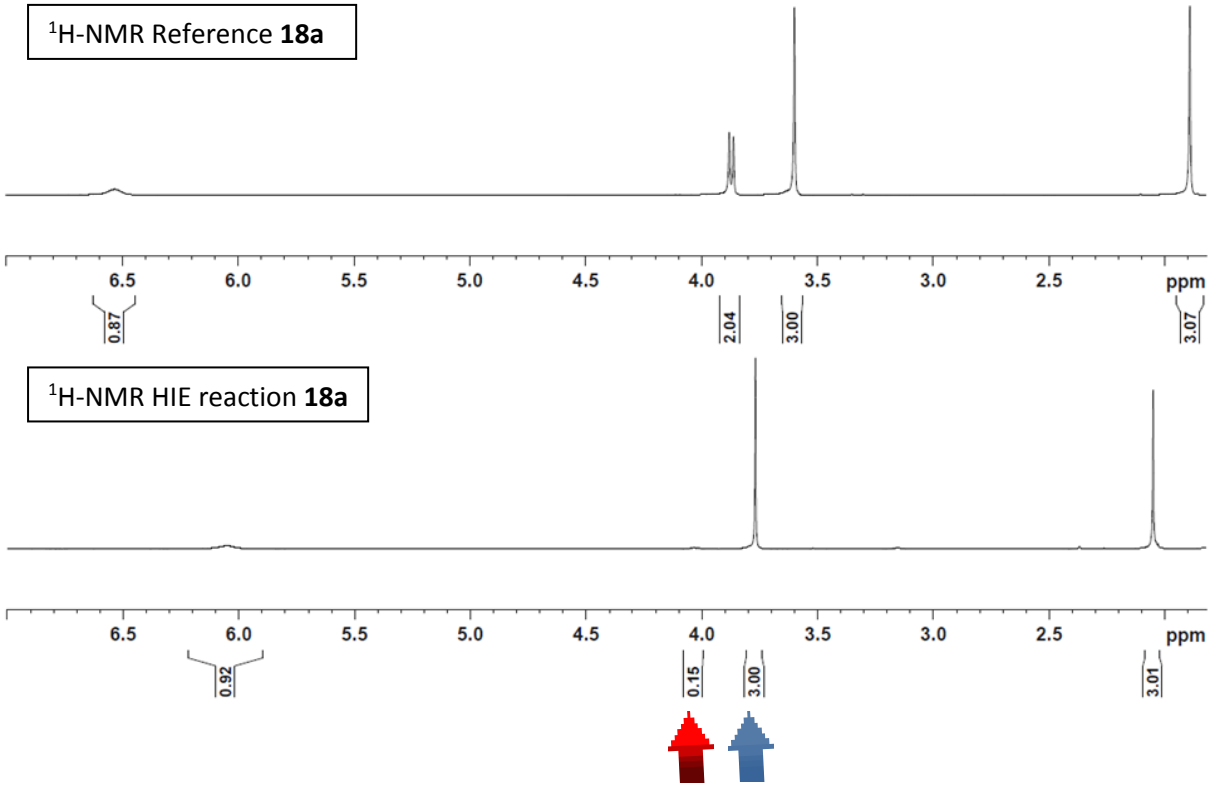

^{1}H-NMR Reference **18b**

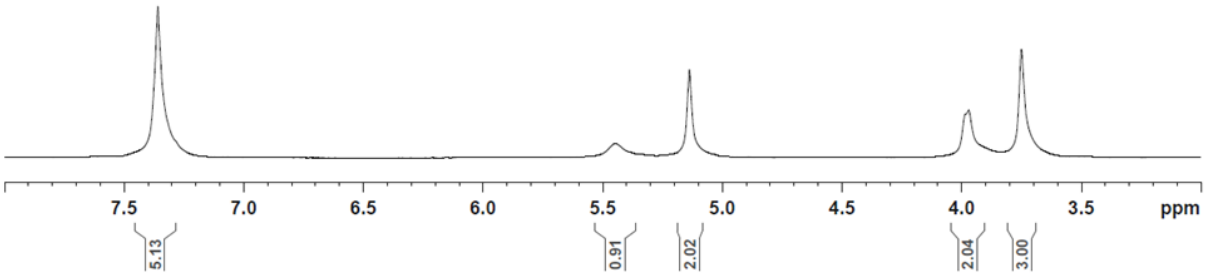

^{1}H-NMR HIE reaction 18**b**

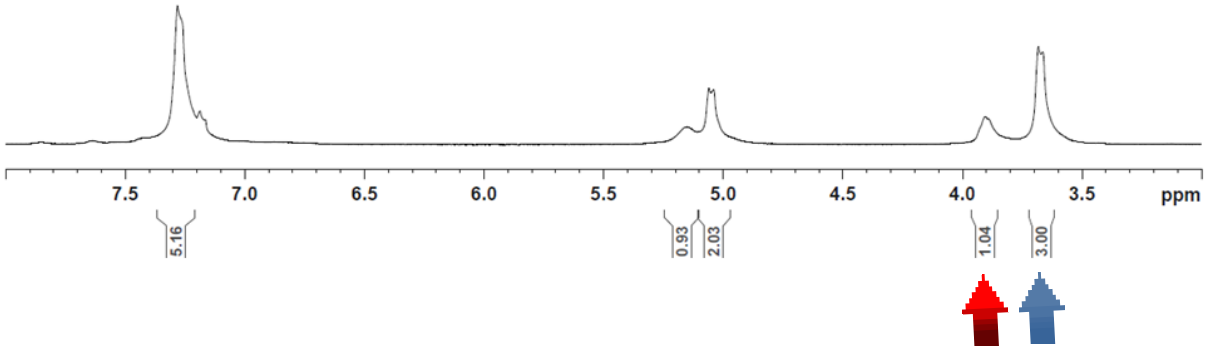

^{1}H-NMR Reference **18c**

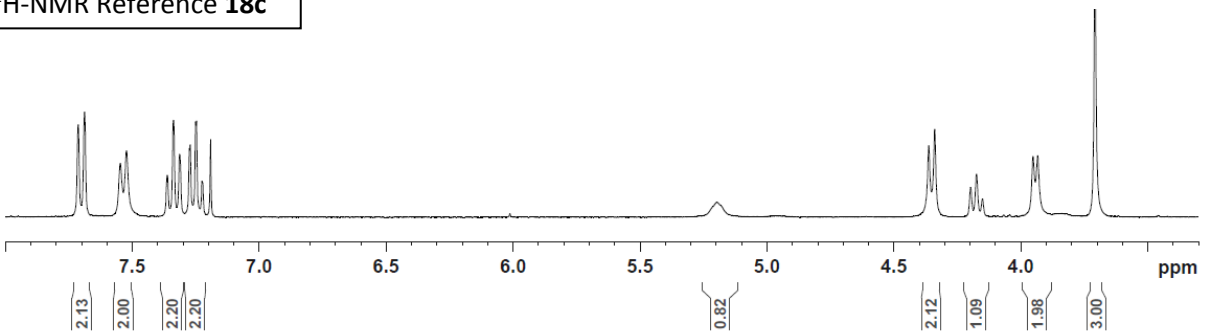

^{1}H-NMR HIE reaction **18c**

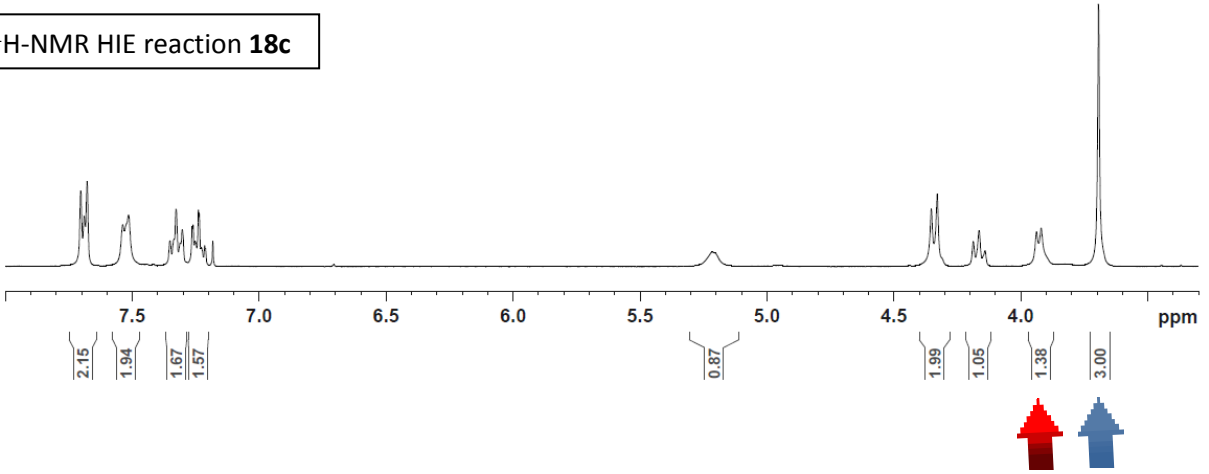

L-Ac-Ala-OMe **19a**

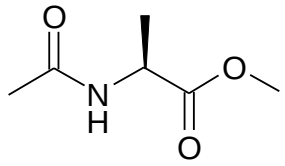

Molecular Weight =145,1595
Molecular Formula =C6H11NO3

19a

^{1}H NMR (300 MHz, $CDCl_3$): δ 6.36 (br s, 1H, N*H*), 4.51-4.42 (m, 1H), 3.61 (s, 3H, COOCH_3), 1.89 (s, 3H, COCH_3), 1.28 (d, 3J= 9.0 Hz, 3H) ppm. Incorporation expected at δ 4.51-4.42 (red arrow). Determined against integral at δ 3.61 (blue arrow).

Conditions: 10.0 mg (69.0 µmol) **19a**; 12 mg (6.9 µmol) catalyst $\mathbf{B_b}$, 8h.

Yield: 6.5 mg, 45.0 µmol, 65%; 50%D for δ 4.51-4.42

^{1}H-NMR Reference **19a**

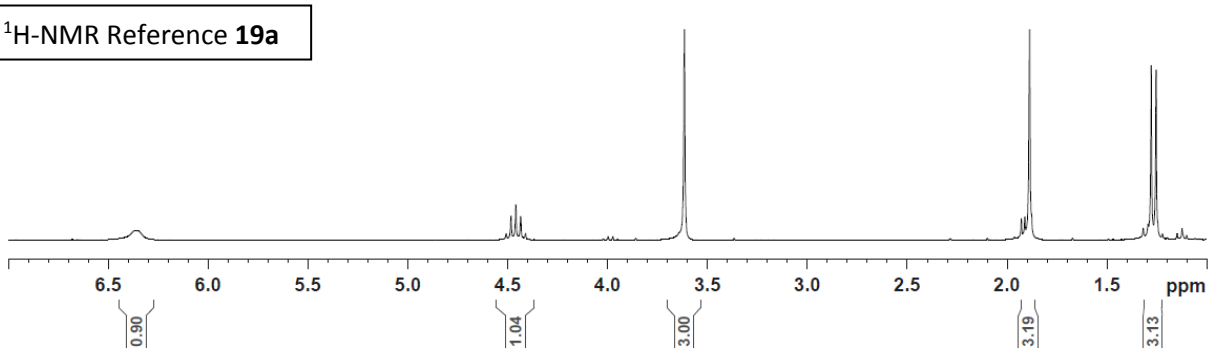

^{1}H-NMR HIE reaction **19a**

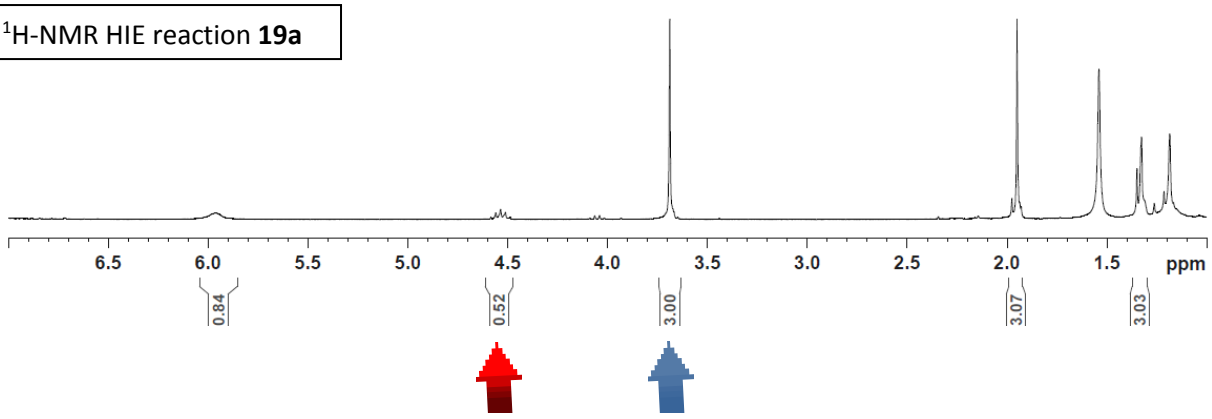

D-Ac-Ala-OMe **19b**

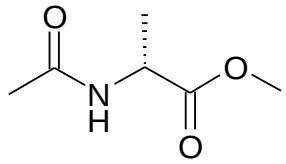

Molecular Weight =145,1595
Molecular Formula =C6H11NO3

19b

^{1}H NMR (300 MHz, $CDCl_3$): δ 6.75 (br s, 1H, N*H*), 4.55-4.45 (m, 1H), 3.67 (s, 3H, COOCH_3), 1.94 (s, 3H, COCH_3), 1.33 (d, 3J= 9.0 Hz, 3H) ppm. Incorporation expected at δ 4.51-4.42 (red arrow). Determined against integral at δ 3.61 (blue arrow).

Conditions: 10.0 mg (69.0 µmol) **19b**; 12 mg (6.9 µmol) catalyst **B_b**, 8h.

Yield: 7.8 mg, 54.0 µmol, 78%; 50%D for 4.51-4.42.

^{1}H-NMR Reference **19b**

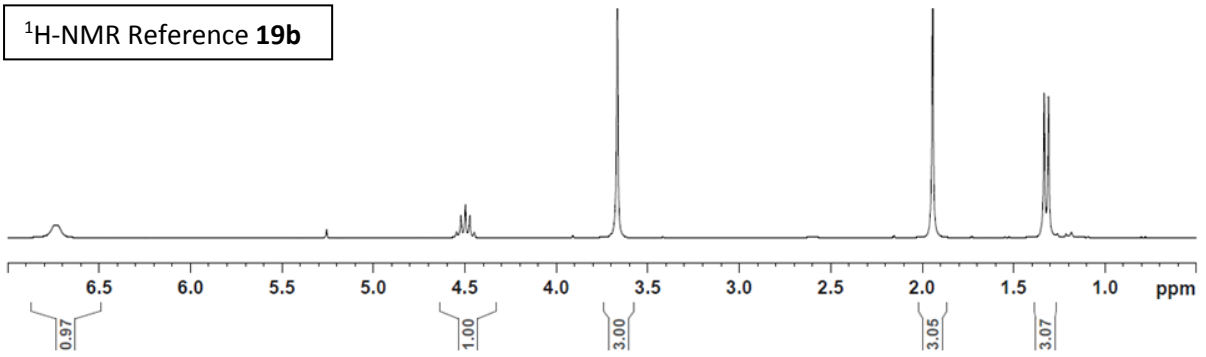

^{1}H-NMR HIE reaction **19b**

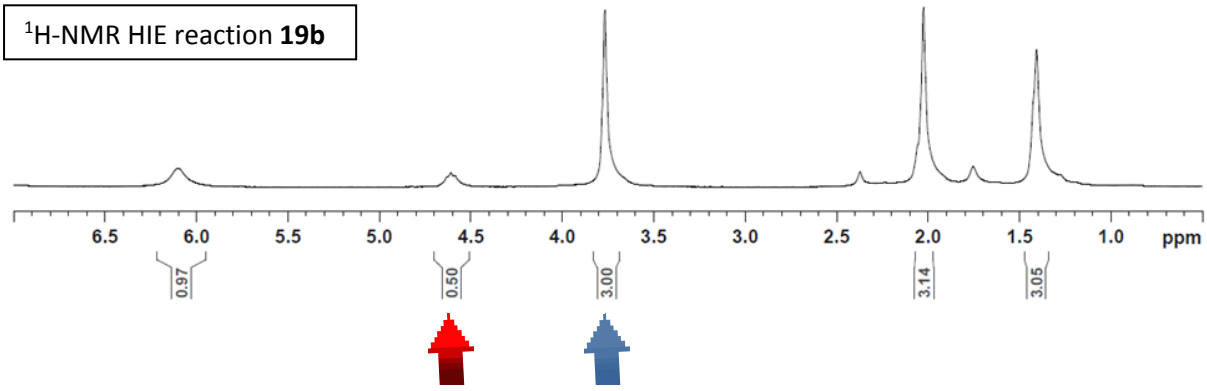

Enantioselective HPLC-Separation of L-Ac-Ala-OMe **19a** and D-Ac-Ala-OMe **19b**

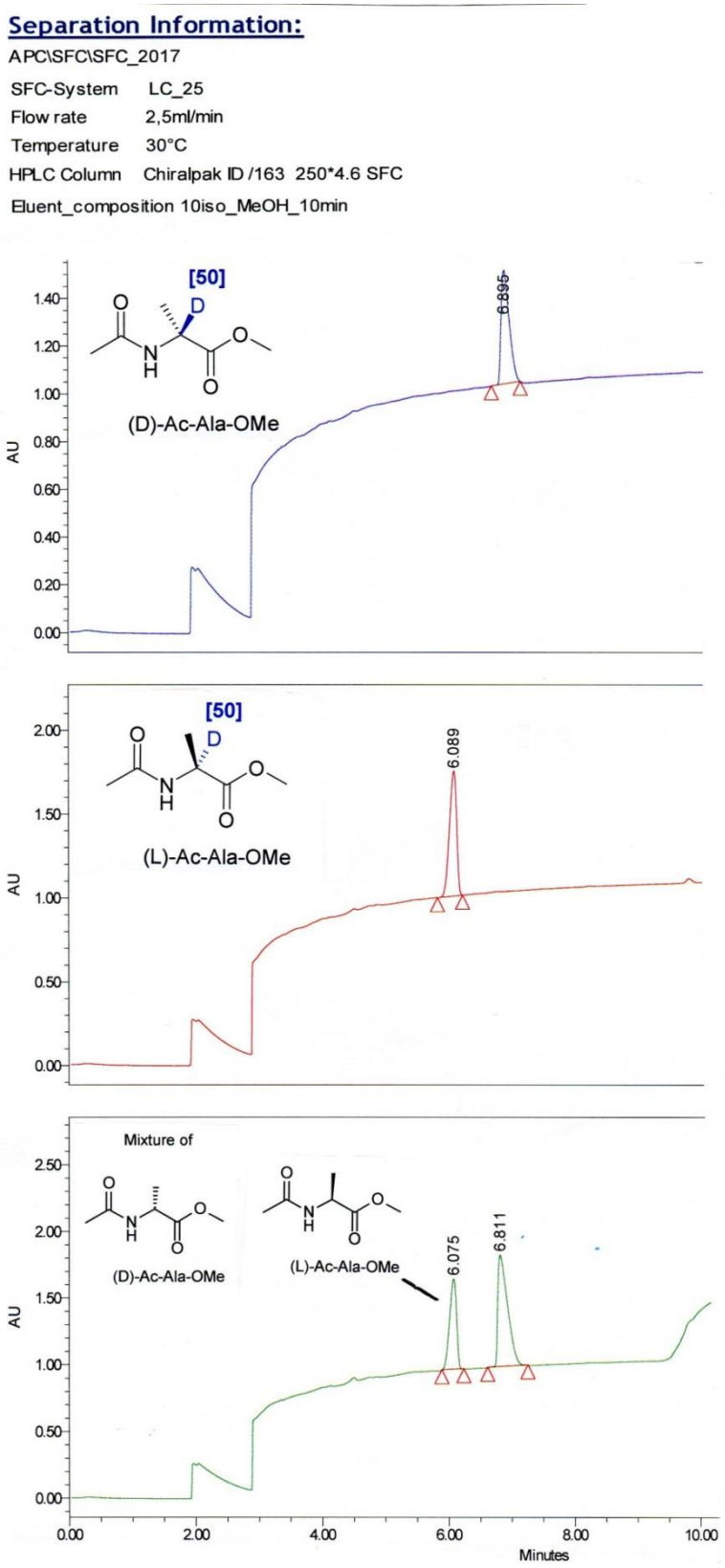

In all HIE reactions of **19a** and **19b** no isomerization of the stereocenter was observed.

Ac-beta-Ala-ethyl ester **22**

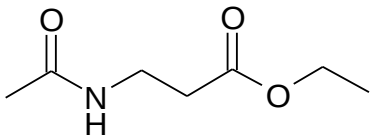

22

Ac-Beta-Ala-OEt

Molecular Weight =159,1866
Molecular Formula =C7H13NO3

^{1}H NMR (300 MHz, $CDCl_3$): δ 6.50 (br s, 1H, N*H*), 4.11 (dt, ^{3}J= 6.9 Hz, ^{3}J= 6.9 Hz, 2H), 3.46 (q, ^{3}J= 6.9 Hz, 2H, OCH_2CH_3), 2.48 (t, ^{3}J= 6.9 Hz, 2H), 1.94 (s, 3H, $COCH_3$), 1.21 (t, ^{3}J= 6.9 Hz, 3H, OCH_2CH_3) ppm. Incorporation expected at 3.46 δ (red arrow). Determined against integral at δ 1.89 (blue arrow).

Conditions: 10.0 mg (63.0 µmol) **22**; 11 mg (6.3 µmol) catalyst **B_b**, 8h.

Yield: 9.5 mg, 60.0 µmol, 95%; 91%D for δ 3.46.

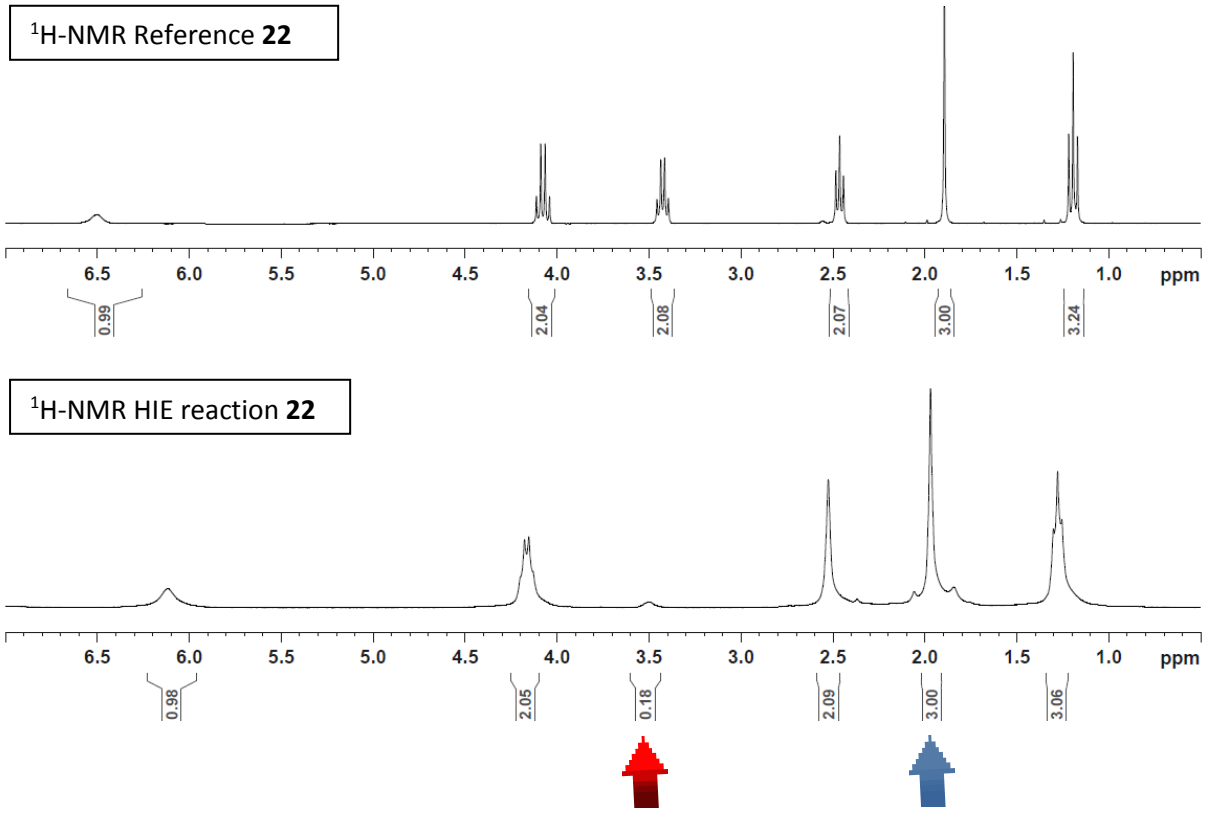

L-Ac-Gly-Phe-methyl ester **23**

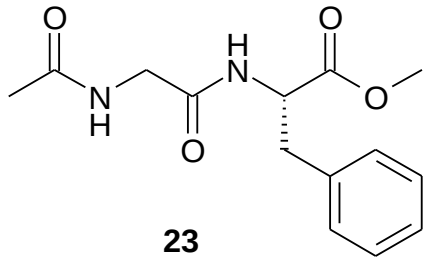

23

Molecular Weight =278,3106
Molecular Formula =C14H18N2O4

^{1}H NMR (300 MHz, $CDCl_3$): δ 7.32-7.05 (m, 5H, arom. CH), 6.51 (br s, 1H, N*H*), 6.28 (br s, 1H, N*H*), 4.88-4.83 (m, 1H), 3.95-3.88 (m, 2H), 3.74 (s, 3H, COOCH_3), 3.22-3.05 (m, 2H), 2.01 (s, 3H, COCH_3) ppm. Incorporation expected at δ 3.95-3.88 (red arrow). Determined against integral at δ 3.74 (blue arrow).

Conditions: 10.0 mg (36.0 µmol) **23**; 6.2 mg (3.6 µmol) catalyst **B_b**, 8h.

Yield: a) 9.0 mg, 32.0 µmol, 90%; 50%D for δ 3.95-3.88.
b) 8.7 mg, 31.0 µmol, 87%; 60% D for δ 3.95-3.88.

Average: y=89%, 55% D

^{1}H-NMR Reference **23**

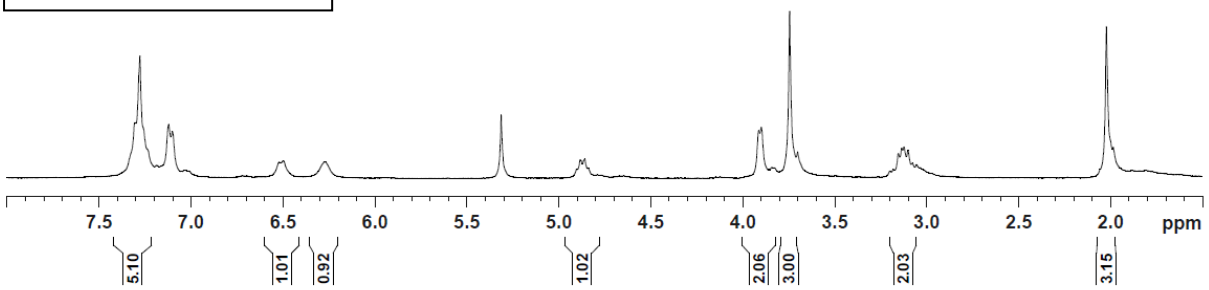

^{1}H-NMR HIE reaction **23**

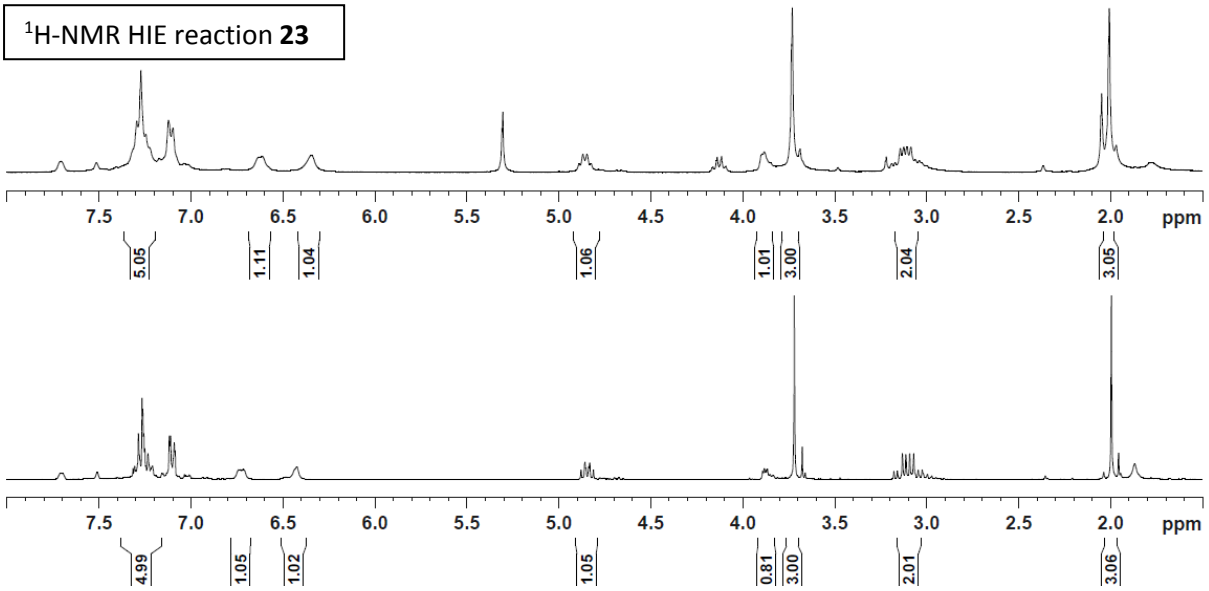

L-Cbz-Gly-Phe-methyl ester **24**

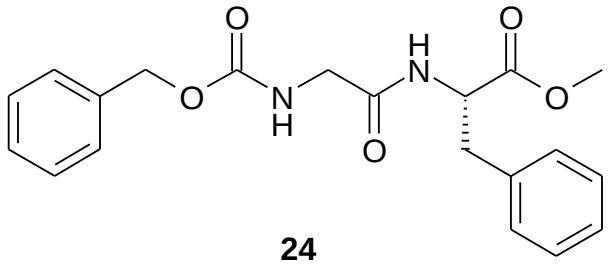

24

Molecular Weight =370.4087
Molecular Formula =C20H22N2O5

^{1}H NMR (300 MHz, $CDCl_3$): δ 7.39 (m, 5H, 5 CH Phe), 7.28 (m, 3H, 2 CH *meta* and 1 CH *para* Cbz), 7.10 (m, 2H, 2 CH *ortho* Cbz), 6.45 (br s, 1H, NH), 5.38 (br s, 1H, NH), 5.15 (s, 2H, CH_2 benzylic), 4.45 (m, 1H, CH Phe), 3.90 (m, 2H, CH_2 Gly), 3.75 (s, 3H, OCH_3), 3.15 (m, 2H, CH_2 Phe) ppm. Incorporation expected at δ 3.90 (red arrow). Determined against integral at δ 5.15 (blue arrow).

Conditions: 10.0 mg (27.0 µmol) **24**; 4.7 mg (2.7 µmol) catalyst **B_b**, 8h.

Yield: a) 8.4 mg, 23.0 µmol, 84%; 14%D for δ 3.90.

^{1}H-NMR Reference **24**

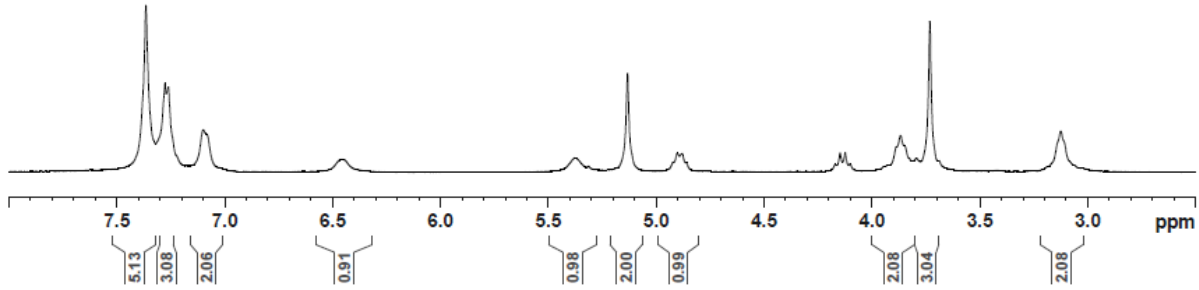

^{1}H-NMR HIE reaction **24**

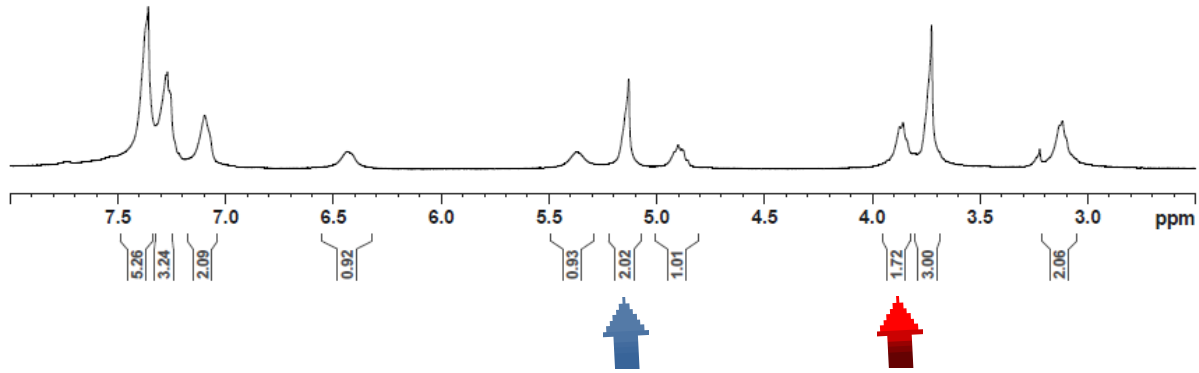

L-Ac-Gly-Tyr(OtBu)-tert-butyl ester **2527**

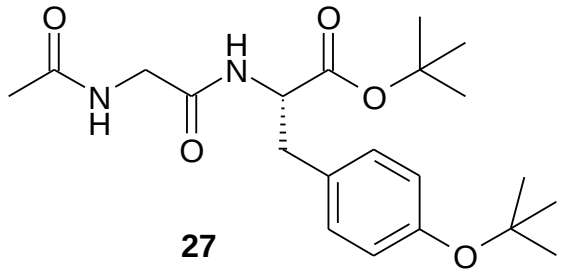

27

Molecular Weight =392,4996
Molecular Formula =C21H32N2O5

^{1}H NMR (300 MHz, $CDCl_3$): δ 7.06 (d, ^{3}J = 8.7 Hz, 2H), 6.93 (d, ^{3}J = 8.7 Hz, 2H), 6.26 (br s, 1H, N*H*), 6.12 (br s, 1H, N*H*), 4.75-4.68 (m, 1H), 3.94-3.91 (m, 2H), 3.06 (d, ^{3}J = 7.2 Hz, 2H), 2.03 (s, 3H, COCH_3), 1.52-1.35 (m, 18H, OtBu) ppm. Incorporation expected at δ 3.94-3.91 (red arrow). Determined against integral at δ 3.06 (blue arrow).

Conditions: 10.0 mg (26.0 µmol) **27**; 4.5 mg (2.6 µmol) catalyst **B_b**, 8h.

Yield: a) 7.4 mg, 19.0 µmol, 74%; 93% D for δ 3.94-3.91.
b) 6.6 mg, 17.0 µmol, 66%; 93% D for δ 3.94-3.91.

Average: y=70%, 93% D

^{1}H-NMR Reference **27**

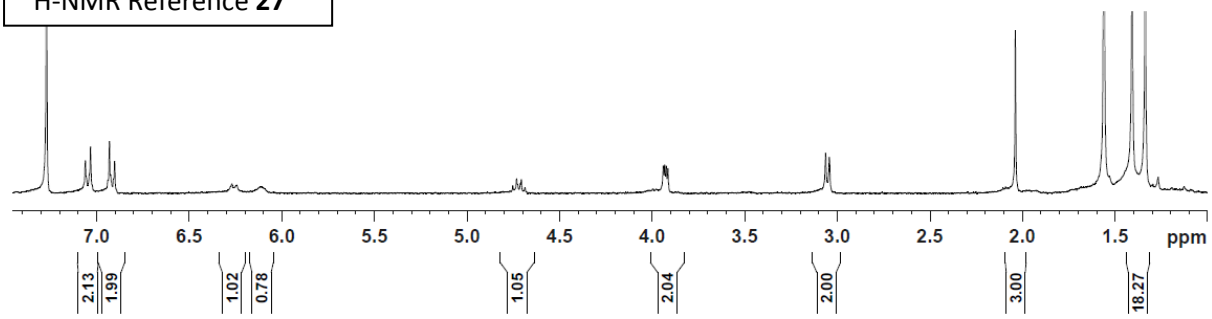

^{1}H-NMR HIE reaction **27**

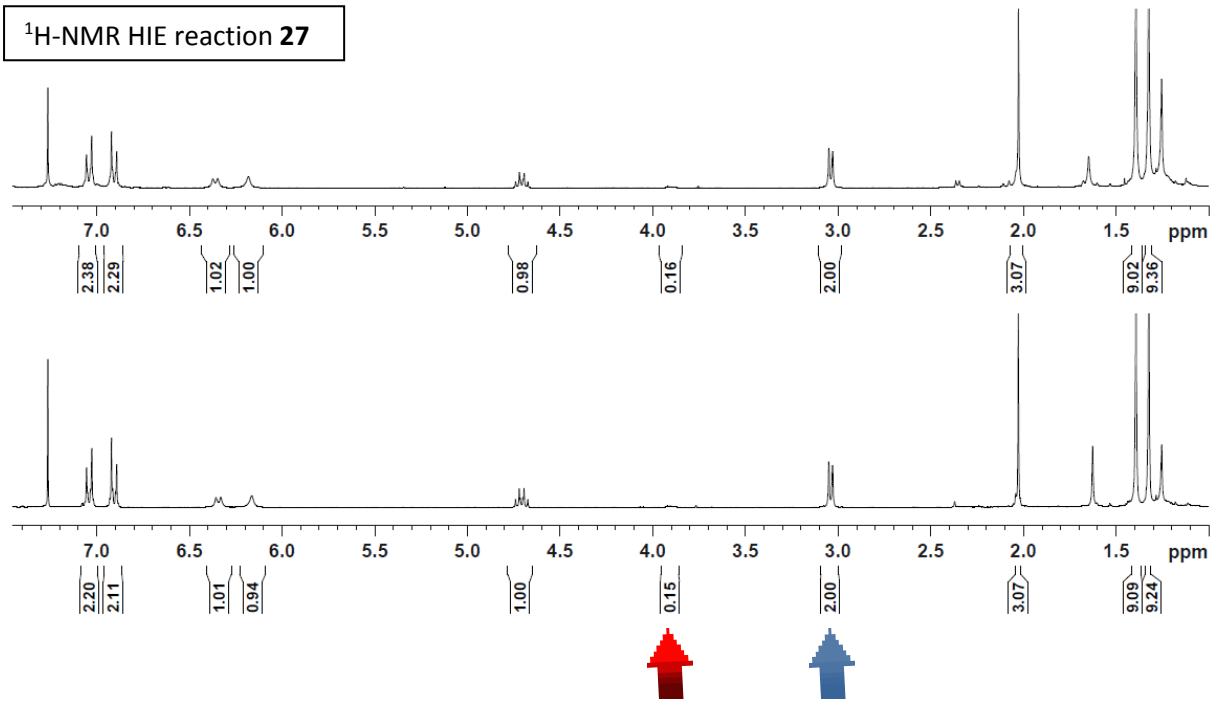

L-Ac-Gly-Gly-methyl ester **28**

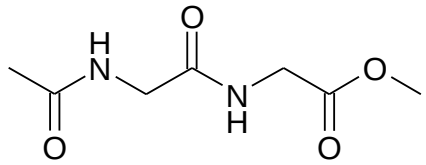

28

Molecular Weight =188,1847
Molecular Formula =C7H12N2O4

^{1}H NMR (300 MHz, $CDCl_3$): δ 6.45 (br s, 1H, N*H*), 6.17 (br s, 1H, N*H*), 4.00 (d, ^{3}J = 5.4 Hz, 2H), 3.93 (d, ^{3}J = 5.4 Hz, 2H), 3.70 (s, 3H, COOCH_3), 1.99 (s, 3H, COCH_3) ppm. Incorporation expected at δ 3.93 and 4.00 (red arrow). Determined against integral at δ 3.70 (blue arrow).

Conditions: 10.0 mg (53.0 µmol) **28**; 9.2 mg (5.3 µmol) catalyst **B_b**, 8h.

Yield: a) 9.7 mg, 52.0 µmol, 97%; 37% D for δ 4.00 and 55% D for δ 3.93.
b) 9.2 mg, 49.0 µmol, 92%; 37% D for δ 4.00 and 57% D for δ 3.93.

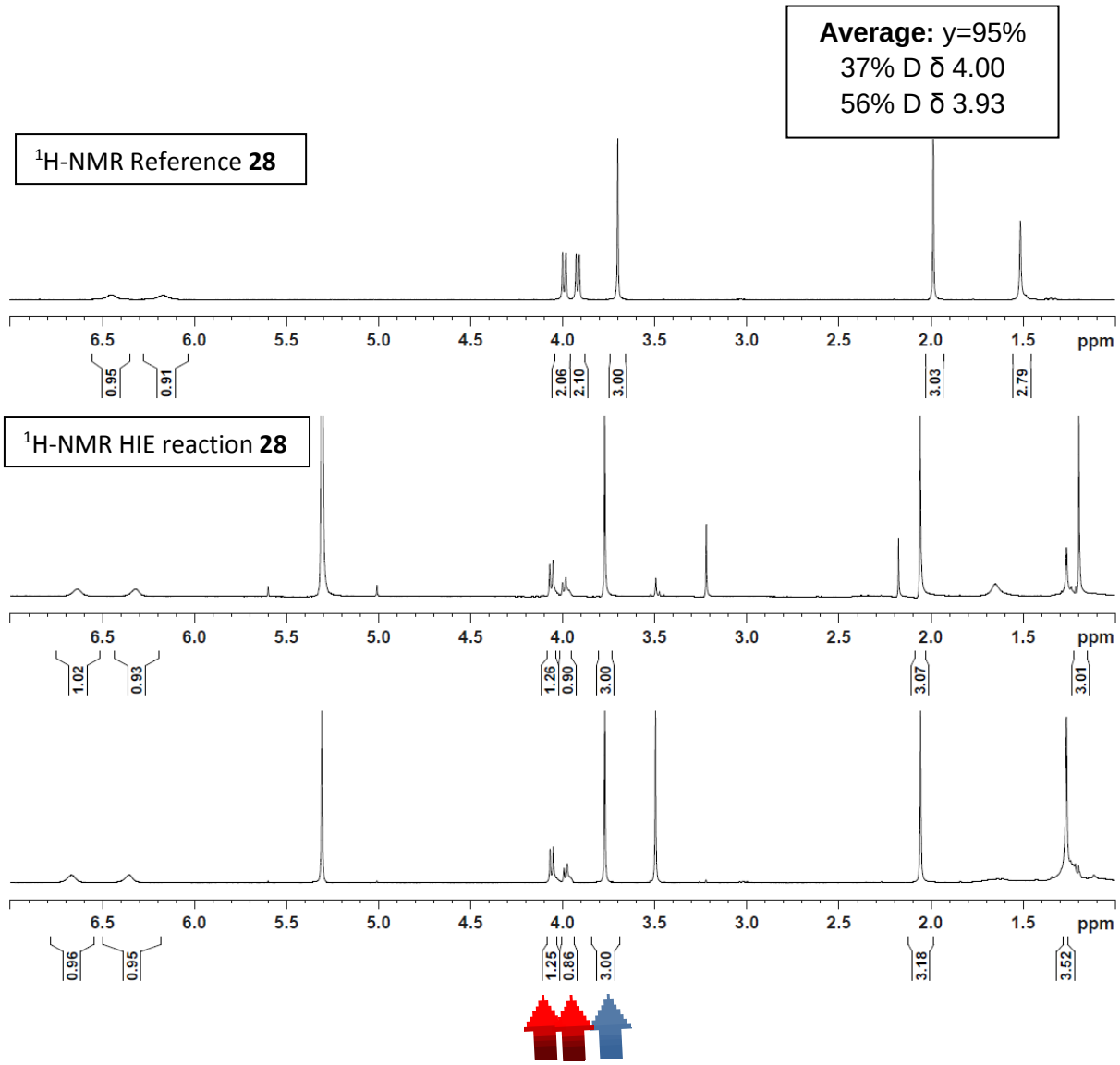

L-Boc-Gly-Gly-methyl ester **29**

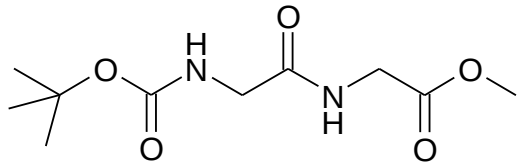

Molecular Weight =246,2654
Molecular Formula =C10H18N2O5

29

^{1}H NMR (300 MHz, $CDCl_3$): δ 6.55 (br s, 1H, N*H*), 5.06 (br s, 1H, N*H*), 4.01 (d, ^{3}J = 5.7 Hz, 2H), 3.80 (d, ^{3}J = 5.7 Hz, 2H), 3.70 (s, 3H, COOCH_3), 1.39 (s, 9H) ppm. Incorporation expected at δ 4.01 (red arrow). Determined against integral at δ 3.70 (blue arrow).

Conditions: 10.0 mg (41.0 µmol) **29**; 7.1 mg (4.1 µmol) catalyst **B_b**, 8h.

Yield: a) 7.8 mg, 32.0 µmol, 78%; 50% D for δ 4.01.
b) 8.9 mg, 36.0 µmol, 89%; 54% D for δ 4.01.

Average: y=84%, 52% D

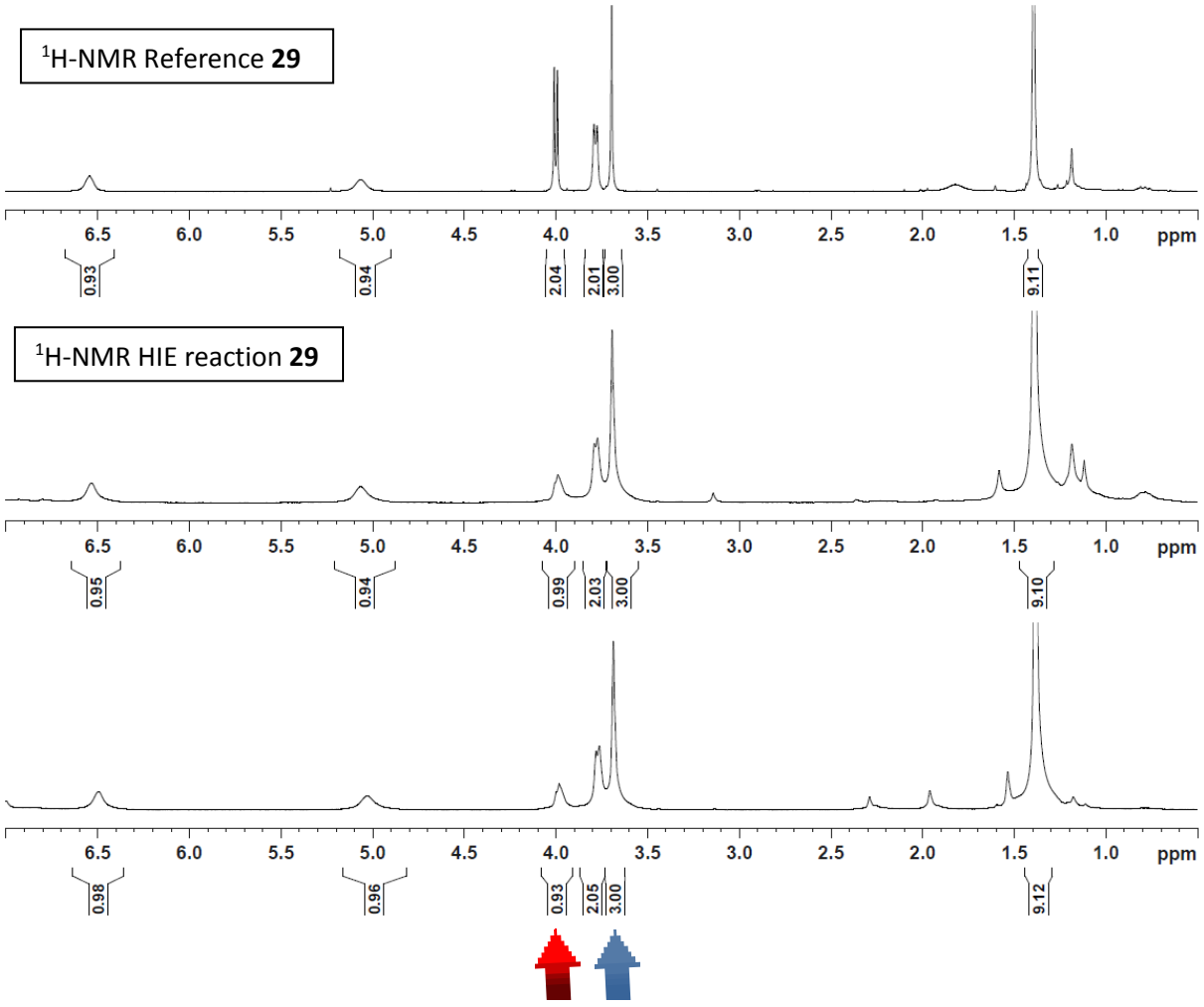

L-Boc-Ala-Gly-methyl ester **30**

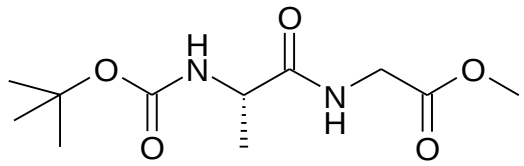

Molecular Weight =260,2925
Molecular Formula =C11H20N2O5

30

^{1}H NMR (300 MHz, $CDCl_3$): δ 6.56 (br s, 1H, N*H*), 4.87 (br s, 1H, N*H*), 4.21-4.09 (m, 1H), 3.98 (br s, 2H), 3.70 (s, 3H, $COOCH_3$), 1.39 (s, 9H) ppm. Incorporation expected at δ 3.98 (red arrow). Determined against integral at δ 3.70 (blue arrow).

Conditions: 10.0 mg (38.0 µmol) **30**; 6.6 mg (3.8 µmol) catalyst **B_b**, 8h.

Yields: a) 9.7 mg, 37.0 µmol, 97%; 59% D for δ 3.98.
b) 9.5 mg, 36.0 µmol, 95%; 60% D for δ 3.98.

Average: y=96%, 60% D

^{1}H-NMR Reference **30**

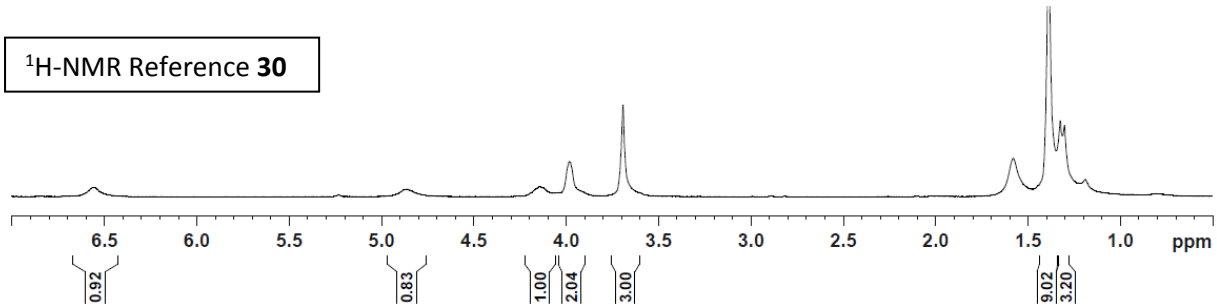

^{1}H-NMR HIE reaction **30**

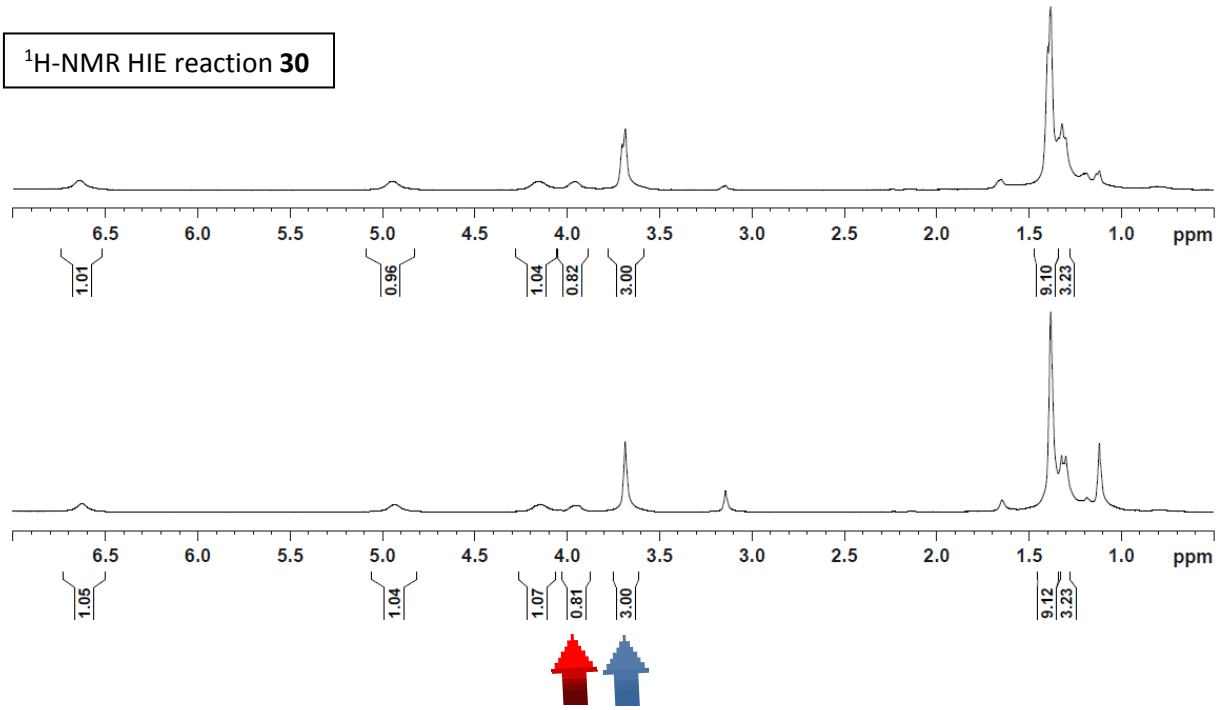

L-Boc-Leu-Gly-methyl ester **31**

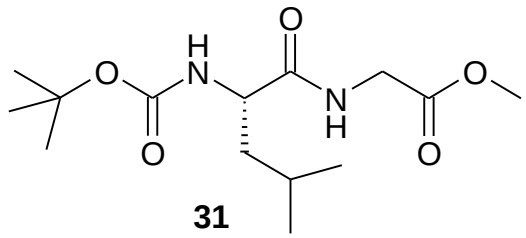

31

Molecular Weight =302,3737
Molecular Formula =C14H26N2O5

^{1}H NMR (300 MHz, $CDCl_3$): δ 6.63 (br s, 1H, N*H*), 4.85 (br s, 1H, N*H*), 4.21-4.11 (m, 1H), 4.06 (d, ^{3}J = 6.3 Hz, 2H), 3.77 (s, 3H, COOCH_3), 1.67-1.55 (m, 3H), 1.46 (s, 9H), 0.99-0.94 (m, 6H) ppm. Incorporation expected at δ 4.06 (red arrow). Determined against integral at δ 3.77 (blue arrow).

Conditions: 10.0 mg (33.0 µmol) **31**; 5.7 mg (3.3 µmol) catalyst **B_b**, 8h.

Yield: a) 7.1 mg, 23.0 µmol, 71%; 72% D for δ 4.06.
b) 7.3 mg, 24.0 µmol, 73%; 76% D for δ 4.06.

Average: y=72%, 74% D

^{1}H-NMR Reference **31**

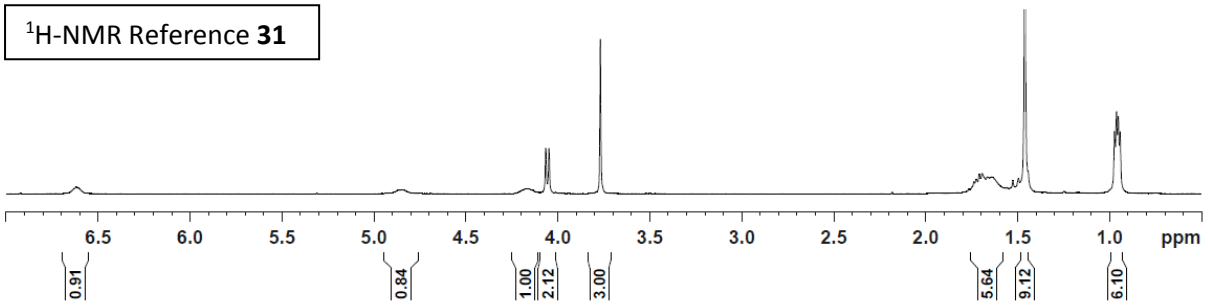

^{1}H-NMR HIE reaction **31**

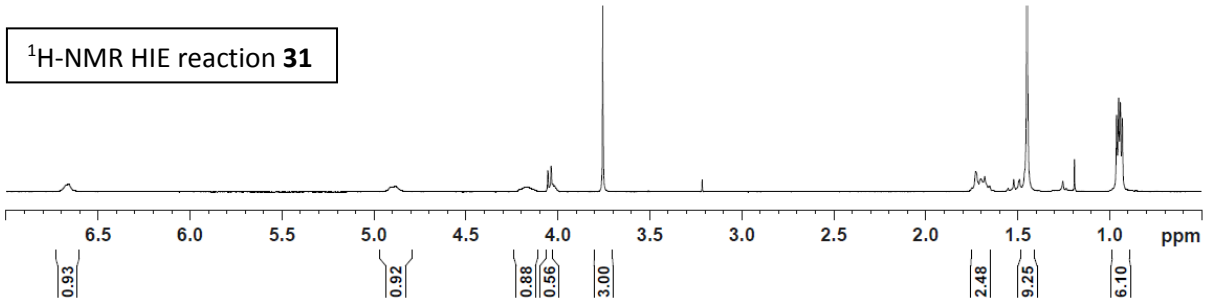

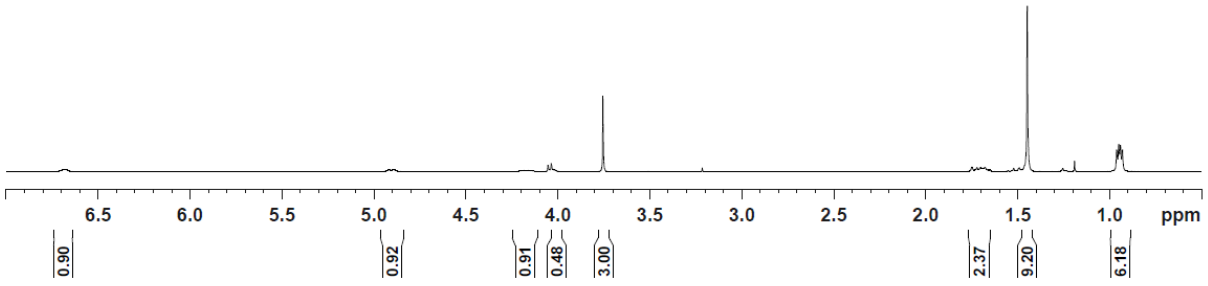

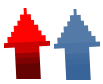

L-Boc-Phe-Gly-methyl ester **32**

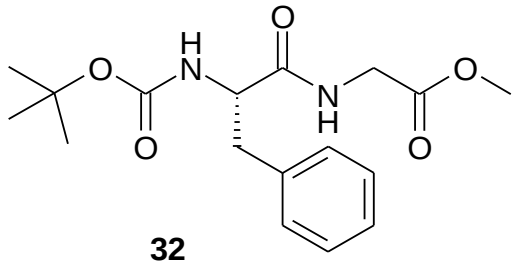

32

Molecular Weight =336,3912
Molecular Formula =C17H24N2O5

^{1}H NMR (300 MHz, $CDCl_3$): δ 7.36-7.21 (m, 5H, arom. CH), 6.35 (br s, 1H, N*H*), 4.95 (br s, 1H, N*H*), 4.45-4.37 (m, 1H), 4.09 (dd, ^2J = 15.6 Hz, ^3J = 5.7 Hz, 2H), 3.75 (s, 3H, COOCH_3), 3.11-3.05 (m, 2H), 1.42 (s, 9H) ppm. Incorporation expected at δ 4.09 (red arrow). Determined against integral at δ 3.75 (blue arrow).

Conditions: 12.0 mg (35.0 µmol) **32**; 6.0 mg (3.5 µmol) catalyst **B_b**, 8h.

Yield: a) 11.1 mg, 33.0 µmol, 93%; 95% D for δ 4.09.
b) 10.8 mg, 32.0 µmol, 90%; 89% D for δ 4.09.

Average: y=91%, 92% D

^{1}H-NMR Reference **32**

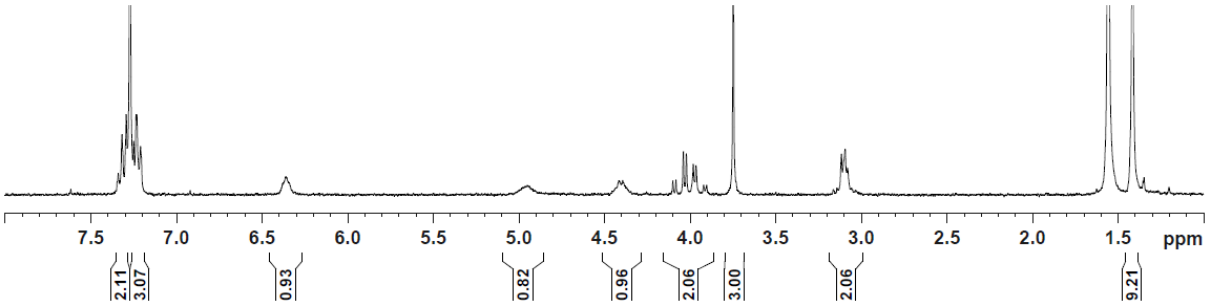

^{1}H-NMR HIE reaction **32**

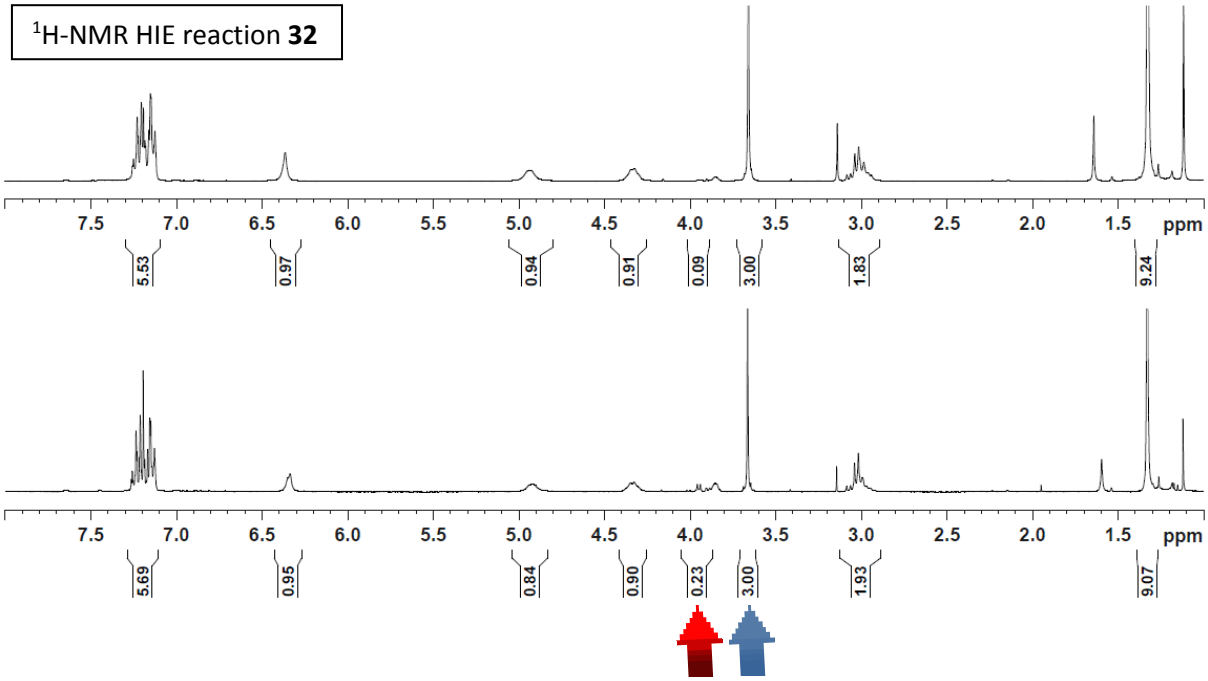

L-Boc-Gln(NEt)-Gly-methyl ester **33**

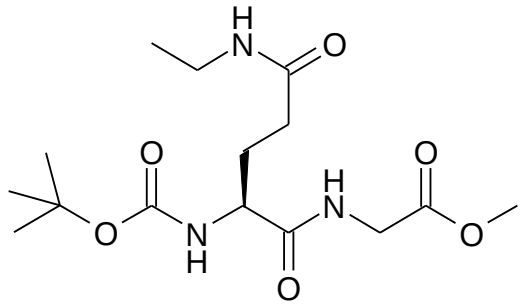

33

Molecular Weight =345,3989
Molecular Formula =C15H27N3O6

^{1}H NMR (300 MHz, $CDCl_3$): δ 7.69 (br s, 1H, N*H*), 6.61 (br s, 1H, N*H*), 5.91 (br s, 1H, N*H*), 4.28-4.16 (m, 1H), 4.15-3.88 (m, 2H), 3.72 (s, 3H, $COOCH_3$), 3.30-3.19 (m, 2H, NCH_2CH_3), 2.39-2.28 (m, 2H), 2.15-1.95 (m, 2H), 1.42 (s, 9H), 1.12 (t, ^3J = 7.2 Hz, NCH_2CH_3) ppm. Incorporation expected at δ 4.15-3.88 and 2.15-1.95 (red arrow). Determined against integral at δ 3.72 (blue arrow).

Conditions: 10.4 mg (30.0 µmol) **33**; 5.2 mg (3.0 µmol) catalyst **B_b**, 8h.

Yield: a) 8.7 mg, 25.0 µmol, 84%; 49% D for δ 4.15-3.88 and 69% D for δ 2.15-1.95.
b) 8.2 mg, 24.0 µmol, 79%; 54% D for δ 4.15-3.88 and 58% D for δ 2.15-1.95.

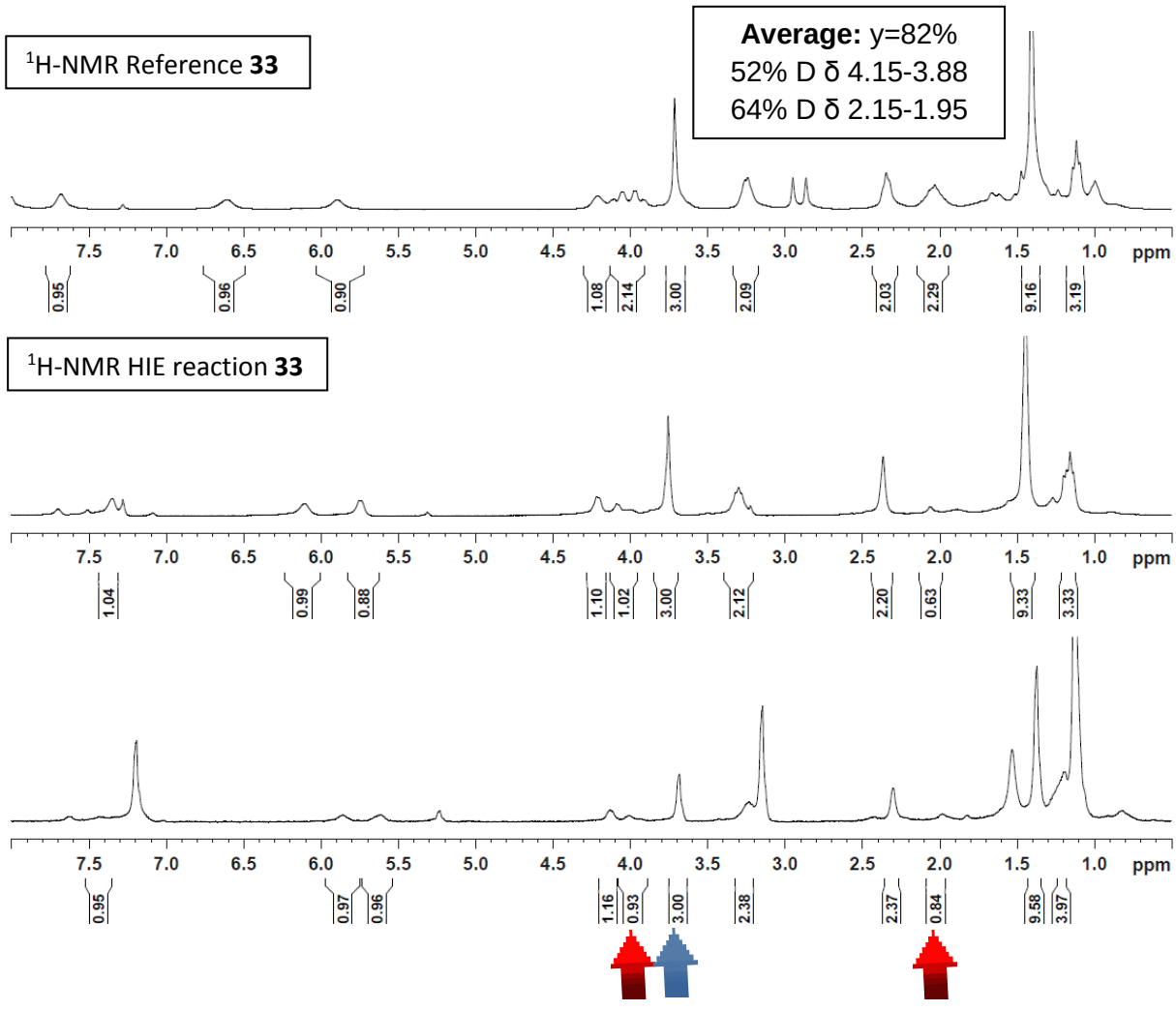

L-Boc-Pro-Gly-OMe **34**

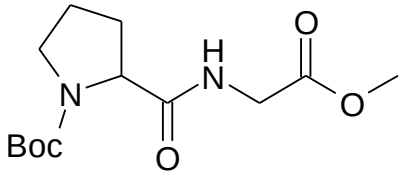

Molecular Weight =286.3307
Molecular Formula =C13H22N2O5

34

^{1}H NMR (300 MHz, $CDCl_3$): δ 4.32 (br s, 1H, CH *alpha* Pro), 4.08 (br s, 2H, CH_2 Gly), 3.75 (s, 3H, OCH_3), 3.48 (m, 3H, CH_2), 1.83 (m, 3H, CH_2), 1.40 (s, 9H, Boc) ppm. Incorporation expected at δ 4.32 and/or 4.08 (red arrow). Determined against integral at δ 3.75 (blue arrow).

Conditions: 10.0 mg (35.0 µmol) **34**; 6.0 mg (3.5 µmol) catalyst **B_b**, 8h.

LCMS (positive ESI): m/z 188.2 [M(1D)+H-Boc] (7%), 189.2 [M(2D)+H-Boc] (46%), 190.2 [M(3D)+H-Boc] (37%), 191.2 [M(4D)+H-Boc] (10%).

Yield: a) 10.3 mg, 36.0 µmol, quant.; 36% D for δ 4.32 and 93% D for δ 4.08.

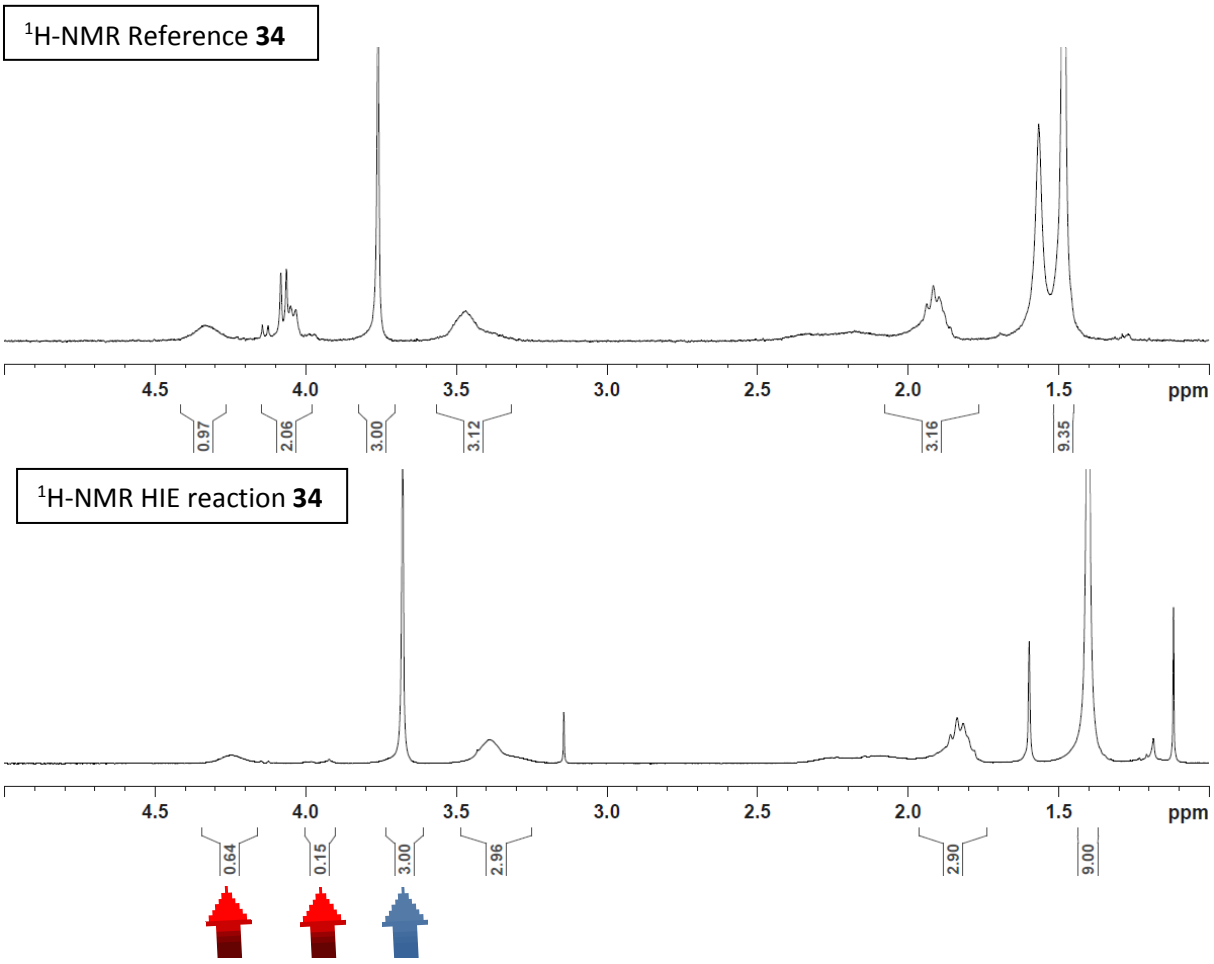

L-Cbz-Tyr(OtBu)-Gly-Leu-tert-butyl ester **35**

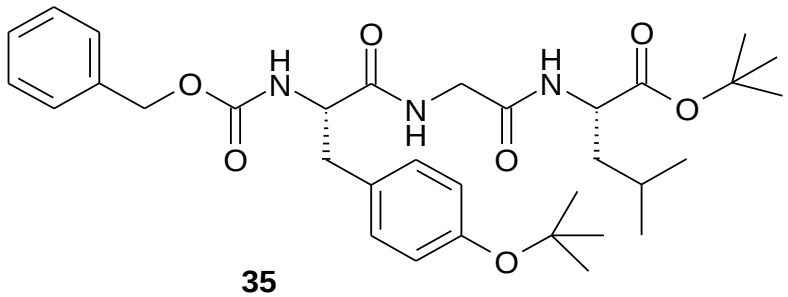

35

Molecular Weight =597,7584
Molecular Formula =C33H47N3O7

^{1}H NMR (300 MHz, $CDCl_3$): δ 7.39-7.24 (m, 5H), 7.04 (d, ^{3}J = 8.7 Hz, 2H), 6.89 (d, ^{3}J = 8.7 Hz, 2H), 6.64 (br s, 2H, N*H*), 5.45-5.32 (m, 1H), 5.11-4.95 (m, 2H), 4.52-4.42 (m, 1H), 4.39-4.28 (m, 1H), 4.11-3.96 (m, 1H), 3.79-3.68 (m, 1H), 3.13-2.91 (m, 2H), 1.71-1.50 (m, 3H), 1.44 (s, 9H), 1.31 (s, 9H), 0.96-0.88 (m, 6H) ppm. Incorporation expected at δ 4.11-3.96 (red arrow). Determined against integral at δ 5.11-4.95 (blue arrow).

Conditions: 12.0 mg (20.0 µmol) **35**; 3.5 mg (2.0 µmol) catalyst **B_b**, 8h.

Yield: a) 11.9 mg, 19.0 µmol, 99%; 98% D for δ 4.11-3.96 and 97% D for δ 3.79-3.68.
b) 11.7 mg, 19.0 µmol, 98%; 97% D for δ 4.11-3.96 and 82% D for δ 3.79-3.68.

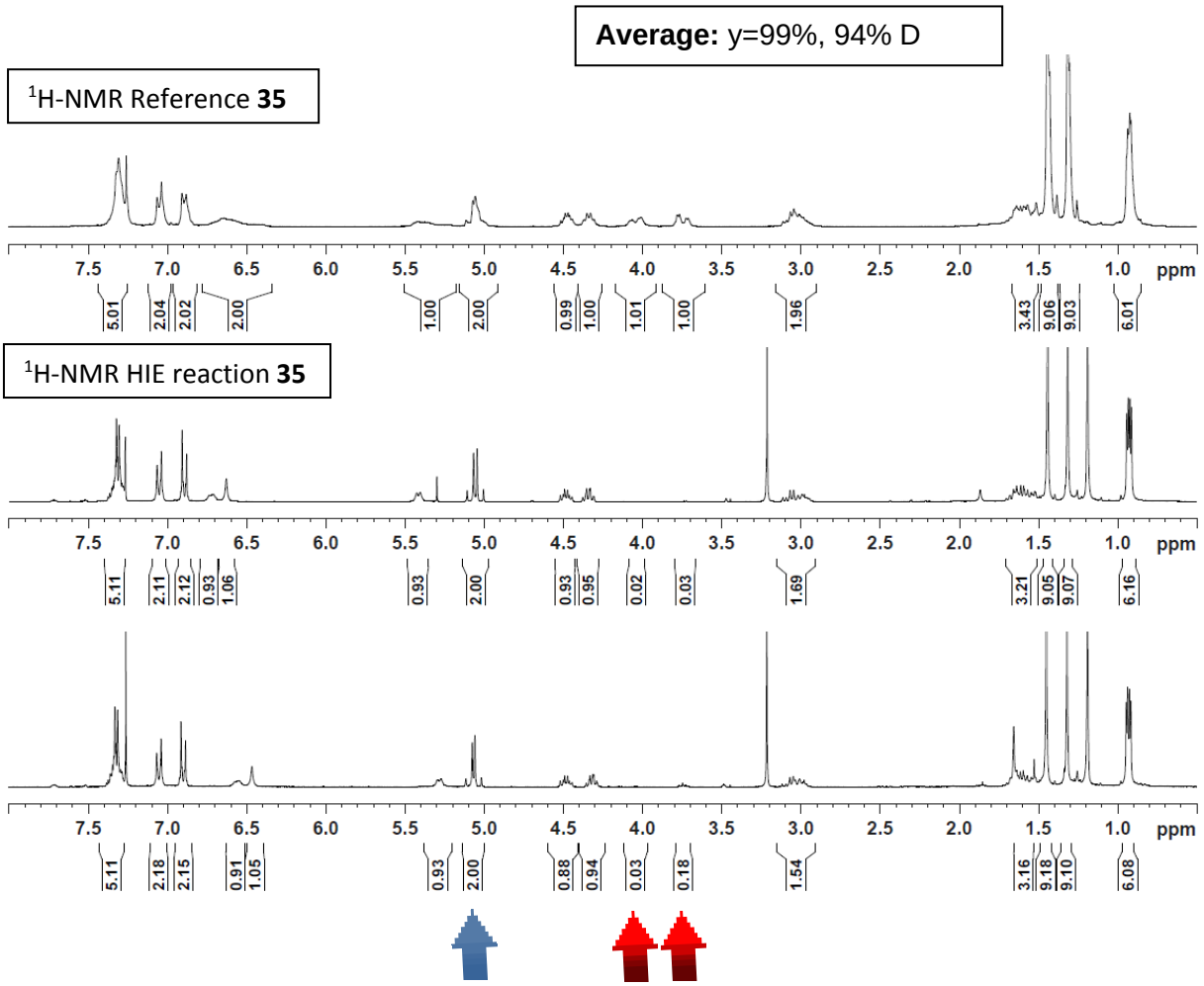

(L)-Boc-Tyr-Gly-Ala-Phe-methyl ester **36**

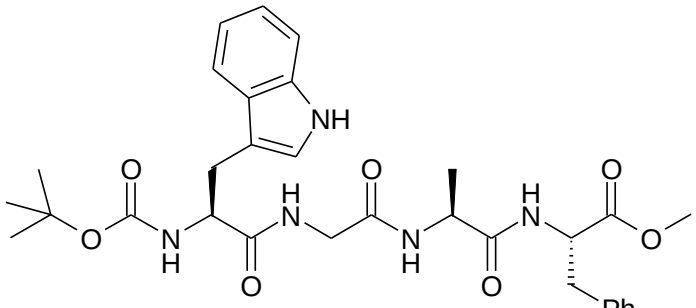

36

Molecular Weight =593,6858
Molecular Formula =C31H39N5O7

^{1}H NMR (300 MHz, $CDCl_3$): δ 8.50 (br s, 1H, N*H*), 7.62 (d, ^{3}J= 8.4 Hz, 1H), 7.36-7.08 (m, 8H), 7.00 (s, 1H), 6.84 (br s, 1H, N*H*), 6.63 (br s, 1H, N*H*), 6.52 (br s, 1H, N*H*), 5.22 (d, ^{3}J= 7.2 Hz, 1H, N*H*), 4.83-4.76 (m, 1H), 4.49-4.37 (m, 2H), 3.85-3.73 (m, 2H), 3.70 (s, 3H, COOCH_3), 3.33-3.17 (m, 2H), 3.15-3.02 (m, 2H), 1.41 (s, 9H), 1.23 (d, ^3J = 7.2 Hz, 3H) ppm. Incorporation expected at δ 3.85-3.73 and 3.33-3.17 (red arrow). Determined against integral at δ 3.70.

Conditions: 10.0 mg (17.0 µmol) **36**; 2.9 mg (1.7 µmol) catalyst **B_b**, 8h.

Yield: a) 9.6 mg, 16.0 µmol, 96%; 96% D for δ 3.85-3.73 and 50% D for δ 3.33-3.17.
b) 9.2 mg, 15.0 µmol, 92%; 94% D for δ 3.85-3.73 and 50% D for δ 3.33-3.17.

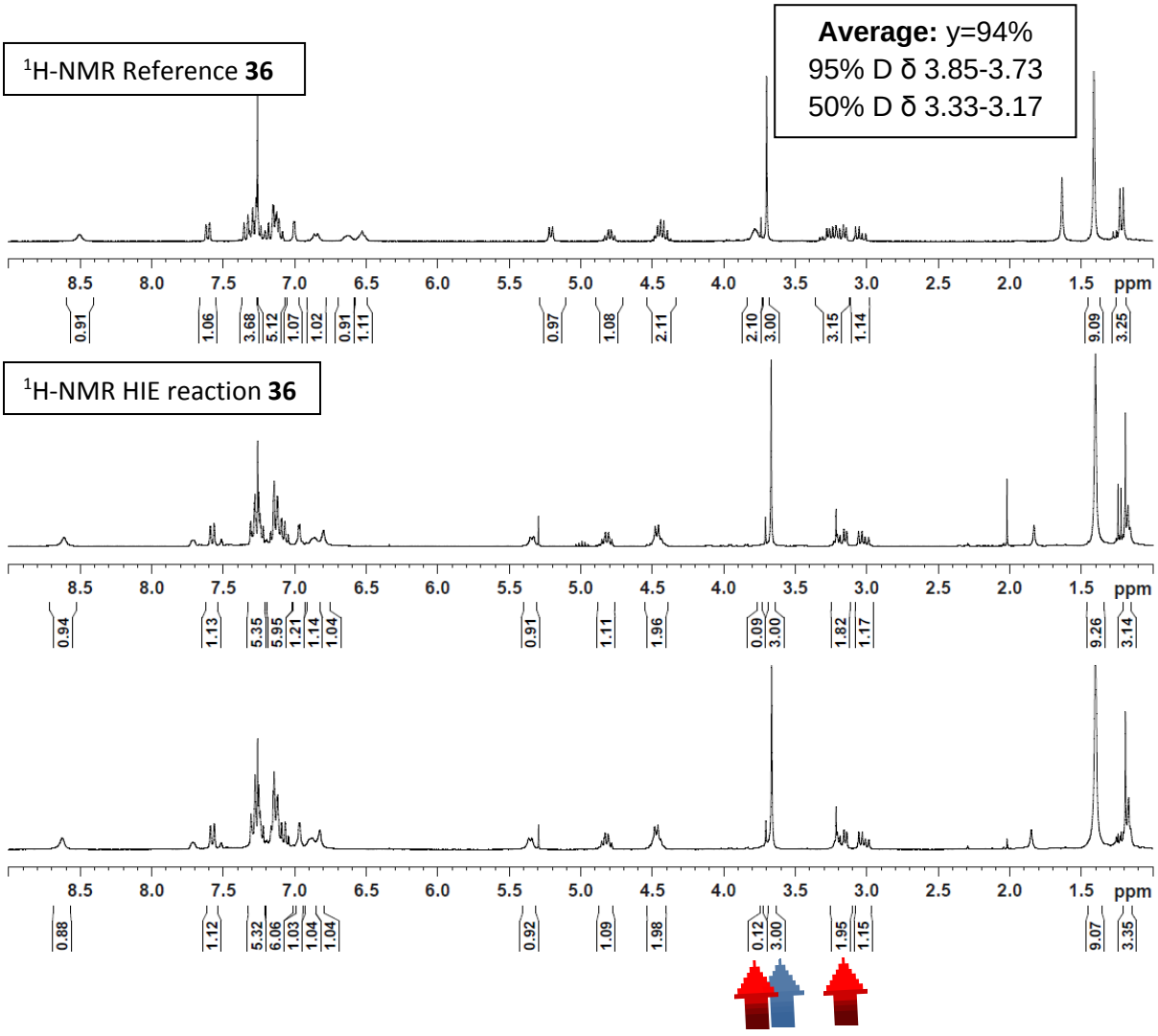

L-Fmoc-Gly-Phe-OMe **37**

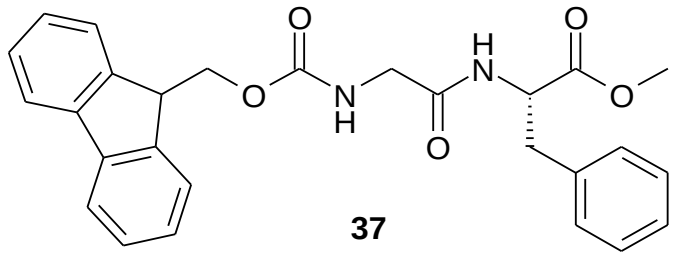

37

Molecular Weight =458.5187
Molecular Formula =C27H26N2O5

^{1}H NMR (300 MHz, $CDCl_3$): δ 7.80 (m, 2H, 2 CH aromatic), 7.60 (m, 2H, 2 CH aromatic), 7.30 (m, 8H, 8 CH aromatic), 7.10 (m, 2H, 2 CH aromatic), 6.45 (br s, 1H, NH), 5.45 (br s, 1H, NH), 4.90 (m, 2H, OCH_2), 4.25 (m, 1H, CH Fmoc), 3.90 (m, 2H, CH_2 Gly), 3.75 (s, 3H, OCH_3), 3.15 (m, 2H, CH_2 benzylic) ppm. Incorporation expected at δ 3.90. Determined against integral at δ 3.75.

Conditions: 10.0 mg (22.0 µmol) **37**; 2.2 mg (3.8 µmol) catalyst **B_b**, 8h.

LCMS (positive ESI): m/z 459.2 [M+H] (47%), 460.2 [M(1D)+H] (38%), 461.3 [M(2D)+H] (13%), 462.23 [M(3D)+H] (2%).

Yield: a) 8.6 mg, 19.0 µmol, 86%; 23% D for δ 3.90.

^{1}H-NMR Reference **37**

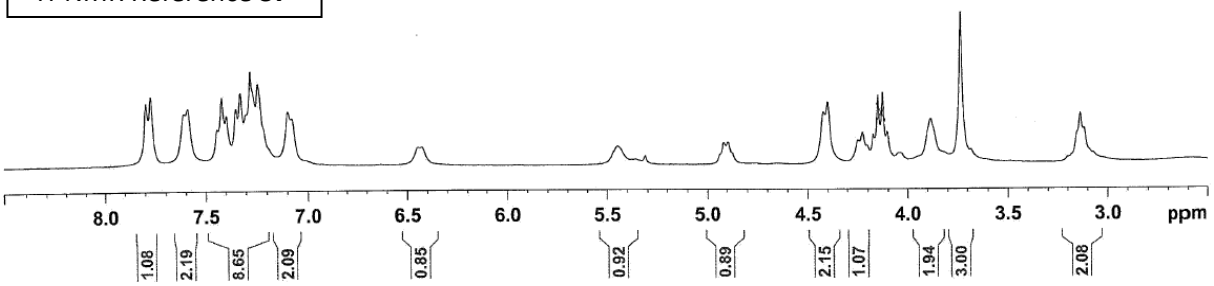

^{1}H-NMR HIE reaction **37**

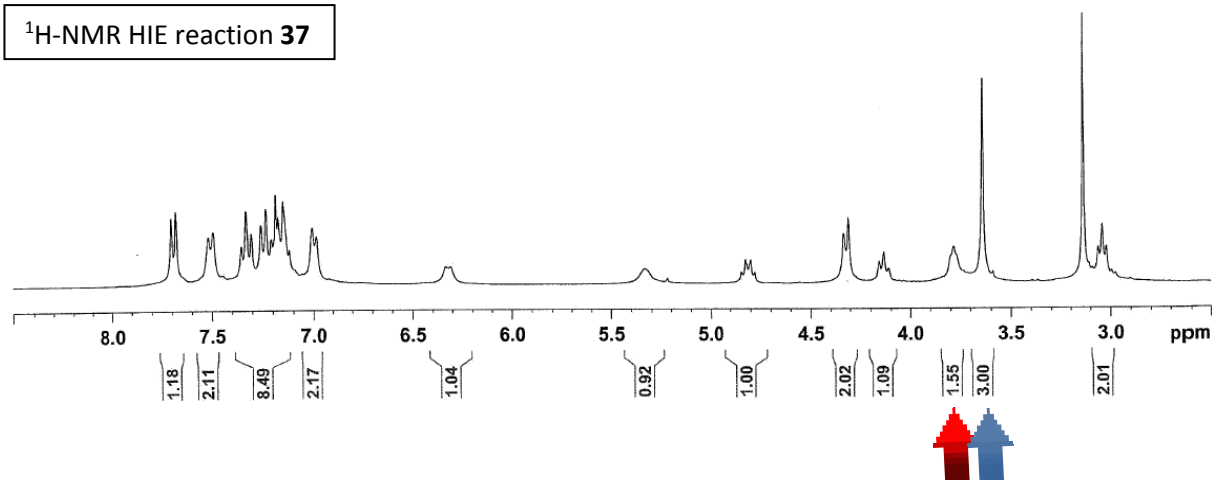

L-Boc-Lys(boc)-Met-methyl ester **38**

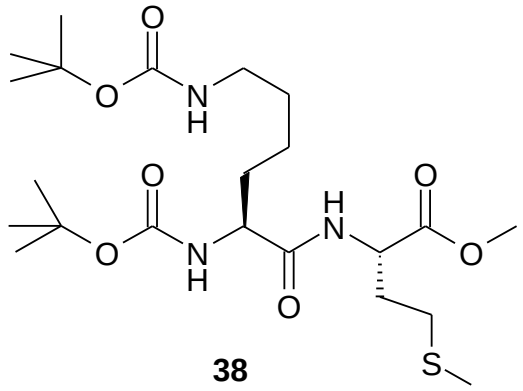

38

Molecular Weight =491,6520
Molecular Formula =C22H41N3O7S

^{1}H NMR (300 MHz, $CDCl_3$): δ 6.79 (br s, 1H, N*H*), 5.16 (br s, 1H, N*H*), 4.76-4.68 (m, 2H, N*H,CH*), 4.11-4.02 (m, 1H), 3.76 (s, 3H, COOCH_3), 3.18-3.05 (m, 2H), 2.53 (t, 3J=7.4 Hz, 2H), 2.24-2.11 (m, 1H), 2.09 (s, 3H, SCH_3), 2.05-1.93 (m, 2H), 1.90-1.55 (m, 2H), 1.54-1.35 (m, 20H) ppm. Incorporation expected at δ 4.76-4.68. Determined against integral at δ 3.76.

Conditions: 10.3 mg (21.0 µmol) **38**; 3.6 mg (2.1 µmol) catalyst **B_b**, 8h.

Yield: a) 10.0 mg, 21.0 µmol, 100%; 95% D for δ 4.76-4.68.
b) 9.8 mg, 20.0 µmol, 98%; 95% D for δ 4.76-4.68.

Average: y=99%, 95% D

^{1}H-NMR Reference **38**

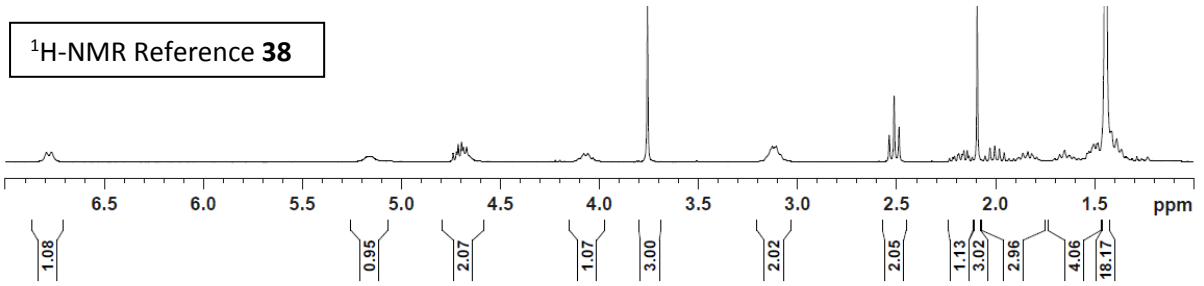

^{1}H-NMR HIE reaction **38**

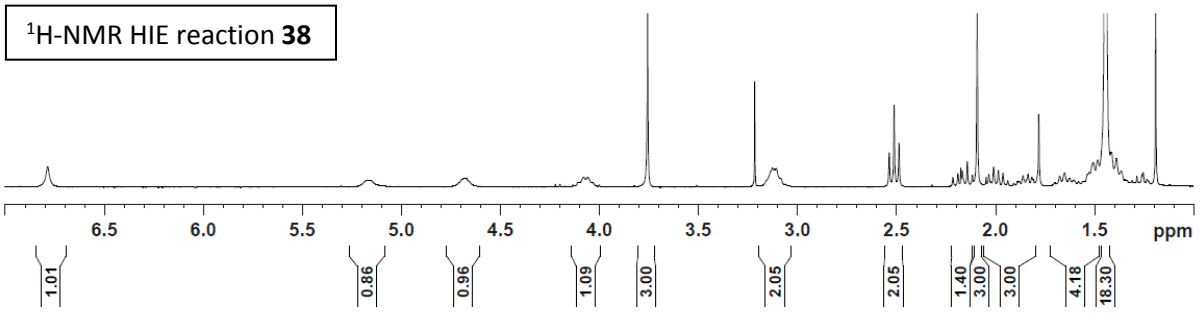

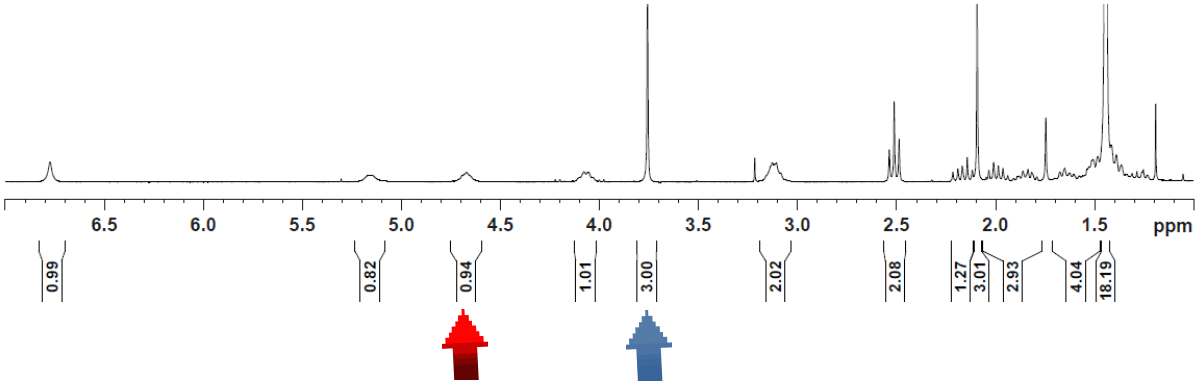

Computational Studies

Details of Computational Methods

DFT calculations (M06 functional) have been done by Dr. Stefan Güssregen from the Computational Drug Design group in Sanofi. DFT[1,2] have been employed to calculate gas-phase electronic structures and energies for all species in this paper. The hybrid meta-GGA exchange correlation functional M06[3] in combination with the 6-31G(d)[4] basis set for non-metal atoms and Stuttgart RSC[5] effective core potential for Iridium was used to optimize all structures, as this approach with validated by Kerr et al. Transition states were located at the same level of theory. Harmonic vibrational frequencies have been calculated at the same level of theory to characterize the respective minima (i.e.) and first order saddle points (TS). Thermal energies have been calculated at 353.15K corresponding to experimental conditions.

All calculations have been performed using the Gaussian 09 quantum chemistry program package. All coordinates provided are listed in Cartesian format, with charge and multiplicity of each system given at the top of the coordinate list (i.e. 0 1 = neutral singlet; 1 1 = 1+ charged singlet).

Calculation of the catalytic complex of catalyst 1

Following the approach published by Kerr et al. a catalytic complex was calculated assuming that two molecules isopropyl acetate are coordinated to the iridium center.

Conformational analysis of Ac-Gly-OMe 18a

The conformations were taken from the respective coordination products and optimized to the next local minimum. The conformation with the lowest energy was chosen for calculation of the reference point.

Calculation of the Potential Energy Surface (PES) for selective deuteration of Ac-Gly-OMe 18a with catalyst 1 (Figure 2)

Due to the pro-chiral environment of the Gly-alpha carbon and catalyst $\mathbf{B_b}$, four reaction pathways are conceivable: Two enter into the reaction by engaging the Ir-center with the Pro-R hydrogen while the Pro-S hydrogen is either facing towards the triphenylphosphine ligand (up, u) or towards the NHC ligand (down, d). All four pathways have been calculated up to the stage of the insertion product and the results are summarized in Figure S1.

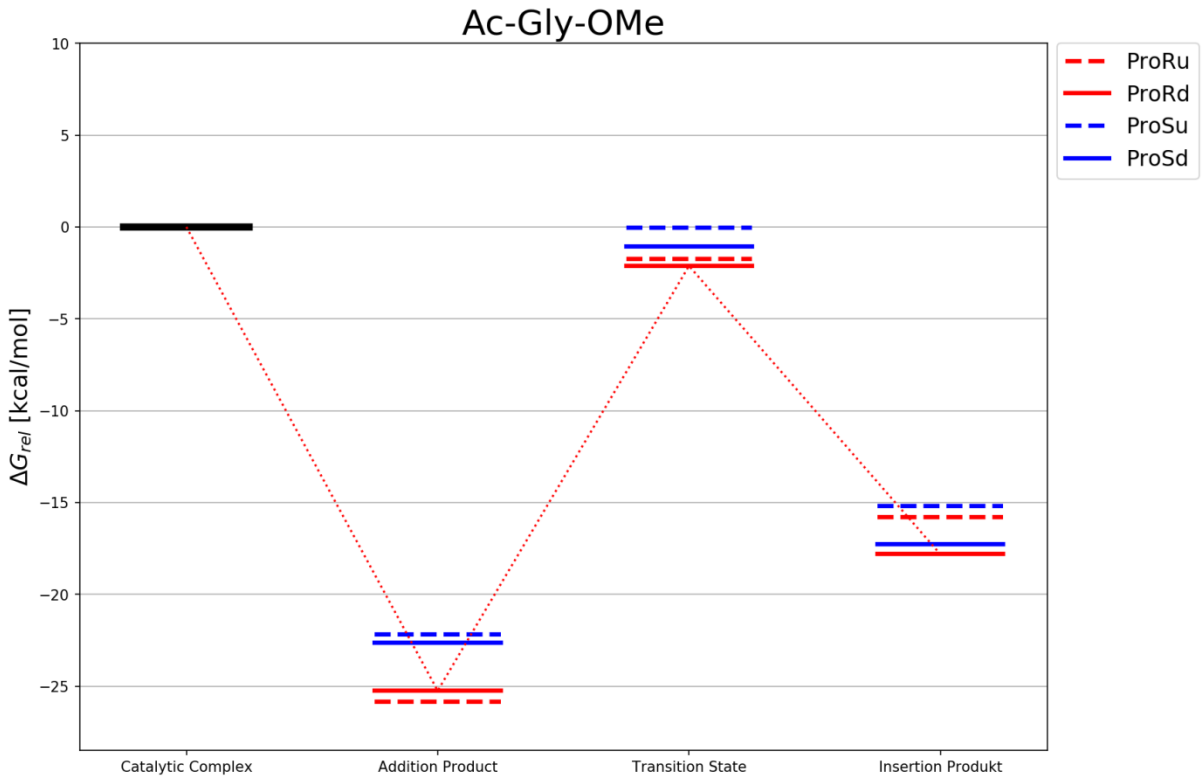

Figure S1

Calculation of the Potential Energy Surface (PES) for deuteration of (D/L) Ac-Ala-OMe 19a/b with catalyst B_b.

The PES for (D/L) Ac-Ala-OMe was calculated in the analogous to Ac-Gly-OMe. The results are summarized in Figure S2. Although the overall reaction enthalpy remains the same, the energies of the transition states increase compared to Gly. This is in line with the experimental finding that the reaction reaches a plateau.

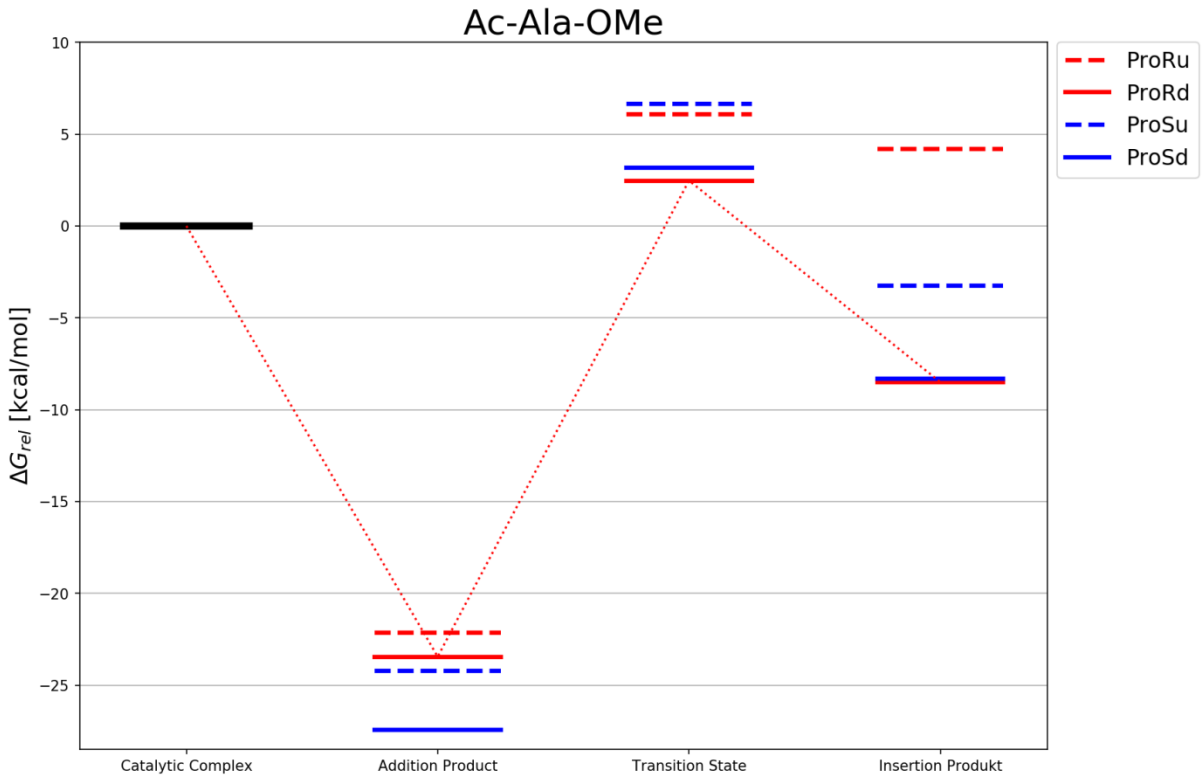

Figure S2

Calculation of the Potential Energy Surface (PES) for deuteration of Boc-Gly-OMe 18b with catalyst B_b.

The PES for (D/L) Boc-Gly-OMe was calculated in the analogous to Ac-Gly-OMe. The results are summarized in Figure S3. The energies of the transition states increase even more and the overall reaction is endergonic.

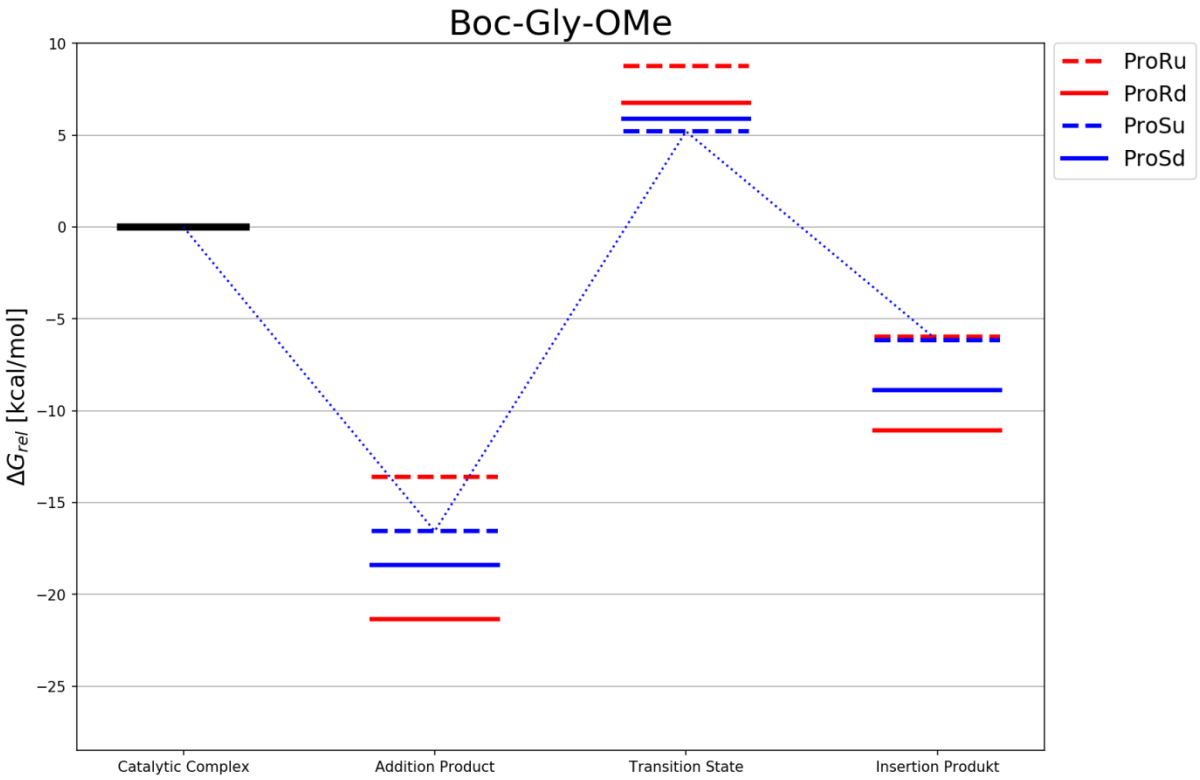

Figure S3

The details about the global DFT calculations are available in the supporting information of the online publication.[6]

References

(1) Kohn, W.; Sham, L., J., Phys. Rev. 1965, 140, 1133 - 1138.
(2) Parr, R. G.; Yang, W. T., Density Functional Theory of Atoms and Molecules, Oxford University Press, New York, 1989.
(3) Zhao, Y.; Truhlar, D. G., Theor. Chem. Acc. 2008, 120, 215 - 241.
(4) (a) Frisch, M. J.; Pople, J. A.; Binkley, J. S., J. Chem. Phys., 1984, 80, 3265 - 3269; (b) Ditchfield, R.; Hehre, W. J.; Pople, J. A., J. Chem. Phys. 1971, 54, 724 - 728.
(5) Andrae, D.; Haussermann, U.; Dolg, M.; Stoll, H.; Preuss, H., Theor. Chim. Acta 1990, 77, 123 - 141.
(6) M. Valero, R. Weck, S. Güssregen, J. Atzrodt, V. Derdau, *Angew. Chem. Int. Ed.* **2018**, *57*(*27*), 8159-8163.

Part V

Heterogeneous iridium catalysis on C(sp^2)-H centers

V.1. Heterogeneous iridium catalysis with nanoparticles

V.1.1. Nanoparticles: From homogeneous to heterogeneous catalysis

While we have focused on homogeneous catalysis for HIE reactions in Part II-IV, we were interested to outreach into the heterogenous iridium catalysis. In collaboration with Prof. Bruno Chaudret (LPCNO-INSA, Toulouse, France) and Dr. Grégory Pieters (LMT-CEA, Saclay, France) also part of the ISOTOPICS consortium, a method based on heterogeneous nanocatalysis for HIE was planned to be developed. Chaudret and Pieters *et al.* have already demonstrated the usefulness of metal nanocatalysts in HIE.[1] Nanoparticles (NPts) own unique physical and chemical properties being solid metal particles.[2] While a homogeneous catalyst (*figure V.1, left*) is solubilized in the solvent with the substrate in a single reaction phase, a heterogenous catalyst, like Ru/C (*figure V.1, right*) is present in the solvent as a suspension. These two different characteristics place the NPts (*figure V.1, middle*) in a borderline situation, as they are homogeneously distributed in the solvent like homogeneous catalyst, but they remain solid particles where the reaction is happening at the surface of the metal, like for heterogeneous catalysts.[2]

Figure V. 1: *Size comparison between homogeneous and heterogeneous catalysts*

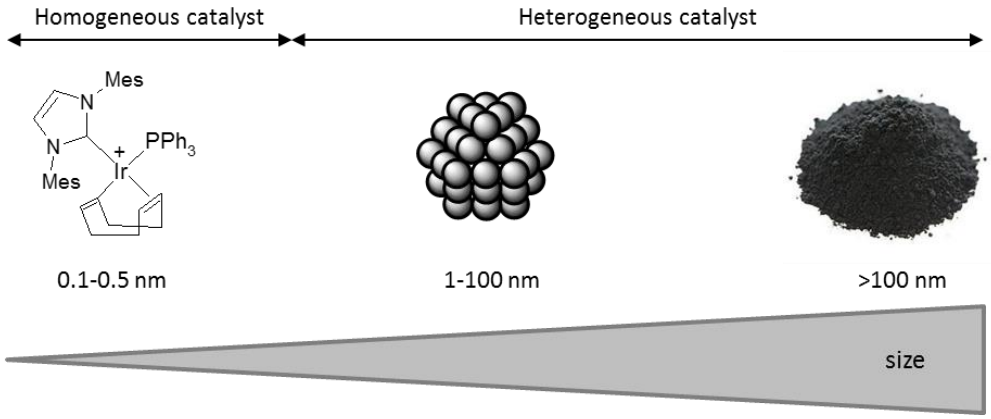

V.1.2. Development and synthesis of new iridium nanoparticles

These small metal catalysts have an extremely high specific surface and are therefore expected to exhibit new reactivities or selectivities related to their huge surface/volume ratio. I have done two secondments during my PhD. In my first secondment end of 2017 in Toulouse with Prof. Chaudret I worked with Donia Bouzouita, (another Isotopics PhD student) on the synthesis of nanoparticles. I was trained there on how to synthetize nanoparticles, how to characterize them and how to work in a glovebox. The first catalytic system envisioned was ruthenium nanoparticles (RuNps) as it has been demonstrated to be

very efficient for H/D exchange.[1] However, these particles are sometimes very efficacious for arene hydrogenation which is undesired in the HIE reaction. Indeed, our preliminary experiments showed that attempts at H/D exchange on few tested substrates using RuICyNps as catalyst lead to complete reduction of the aromatic ring. In order to circumvent this problem, we proposed that iridium could be a good substitute to ruthenium since iridium complexes are very efficient for H/D exchange, presumably because of a low barrier to C-H activation. However, they are generally less effective as hydrogenation catalysts than their ruthenium equivalents. Therefore, the project has focused on the synthesis of novel iridium nanoparticles, stabilized by N-heterocyclic carbenes (NHCs) as already done with RuNps. These ligands have demonstrated their strong binding to various transition metal like Au,[3] Pd,[4] Ni,[5] and Ru[6] nanoparticles. Also, to the best of our knowledge, there is only one report on the stabilization of Iridium NPs (IrNPs) using imidazolium-based ionic liquids.[7]

In our joined project, Donia has synthetized and characterized the nanoparticles we have used (*scheme V.1*). The precursor $[(COD)Ir(MeO)]_2$ **1** reacts with variable amounts of NHC ligands ICy **2** in the presence of H_2 (5 bars). Three different nanoparticles batches **3a-c** were prepared, containing different ratio of ligand **2**. These nanoparticles were characterized and showed to be very small, about 1.1 to 1.3 nm size as observed by Transmission Electron Microscopy (*figure V.2*). The IrNPs **3a-c** adopt the Face centered cubic (fcc) structure of bulk Ir as determines by X-ray diffraction (XRD) (for a detailed characterization of the IrNPs see supporting information). The IrNPs **3a-c** are isolated as a black powder which can be dissolved in organic solvents, e.g. THF. The metal content of the isolated powder depends upon the amount of initial ligand: metal ratio and was found between 70 and 91%.

Scheme V. 1: *Synthesis of N-heterocyclic carbene stabilized iridium nanoparticles IrICy* ***3a-c***

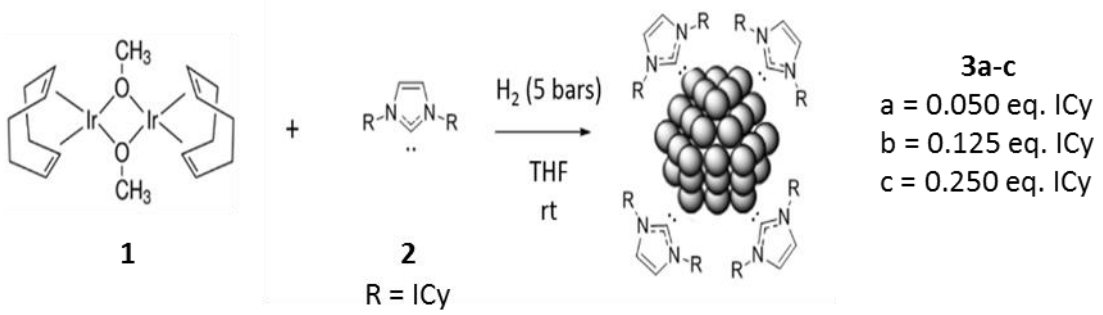

Figure V. 2: *TEM pictures and size distribution for NPs: (a) Ir@ICy (0.05 eq), (b) Ir@ICy (0.125 eq), (c) Ir@ICy (0.25 eq)*

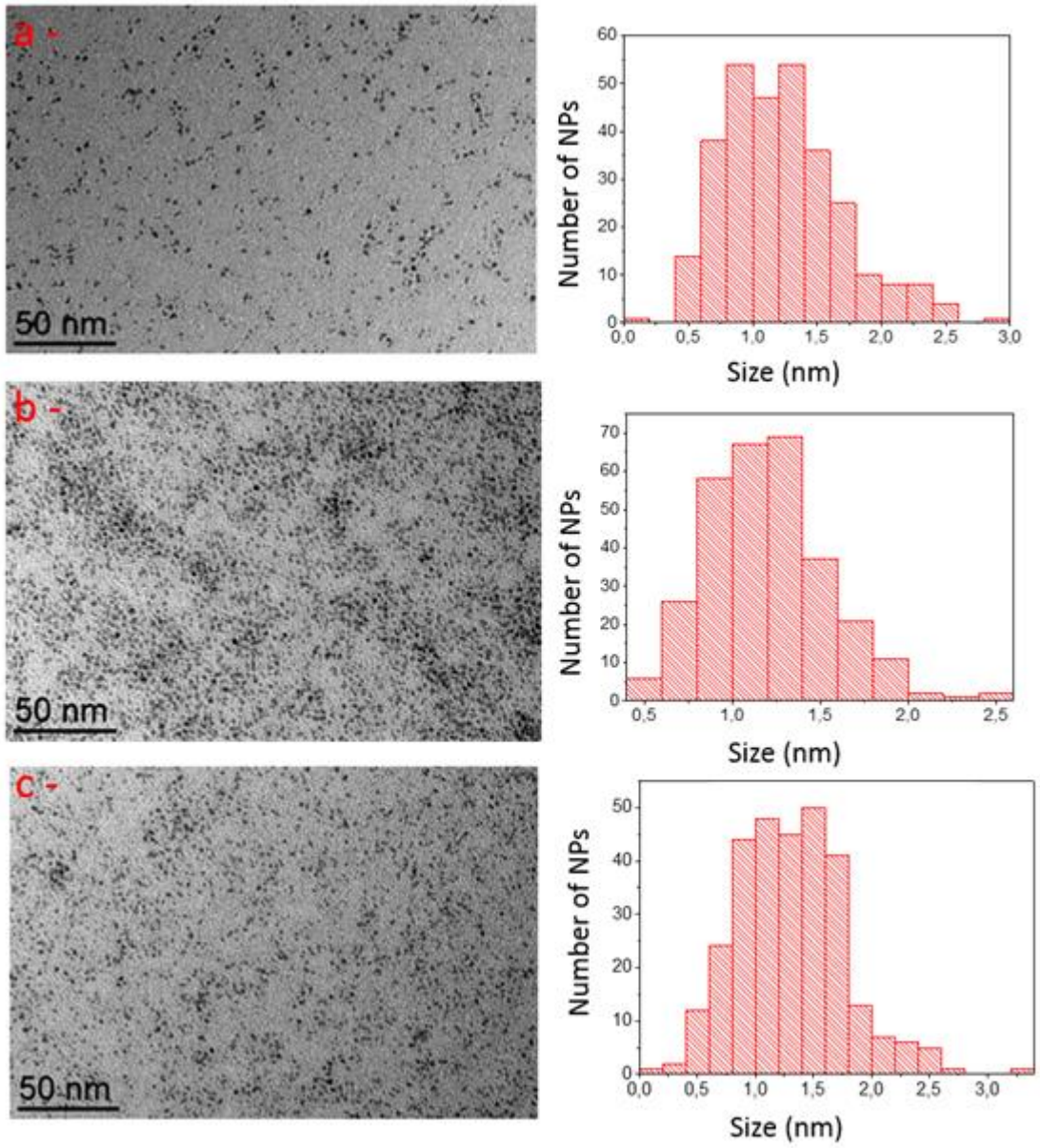

V.1.3. Identification of the new directing group of interest

Following on my first experience in Toulouse, I have made my second secondment end of 2018 with Dr. Pieters in Saclay, where I started applying the IrNPs **3b** in HIE reactions. After a general substrate screening, we have identified anilines as a potential new substrate class for HIE reactions with IrNPs. At this stage, there were two main reasons for developing more on the project described in this Part V: heterogeneous HIE applications with iridium are globally orphaned, and the isotope labelling of anilines as a directing group is still a challenge which wait to be overcome.

Aniline moieties are present in drug compounds like Darunavir **4**, Sulfadimethoxine **5**, Metoclopramide **6**, the B-galactosidase derivative **7**, DL-Aminoglutethimide **8**, Sulfaguanidine **9**, Sulfaxomole **10**, Menthyl anthranilate **11** *etc.* (*scheme V.2*).

Scheme V. 2: *Aniline drugs* ***4-11***

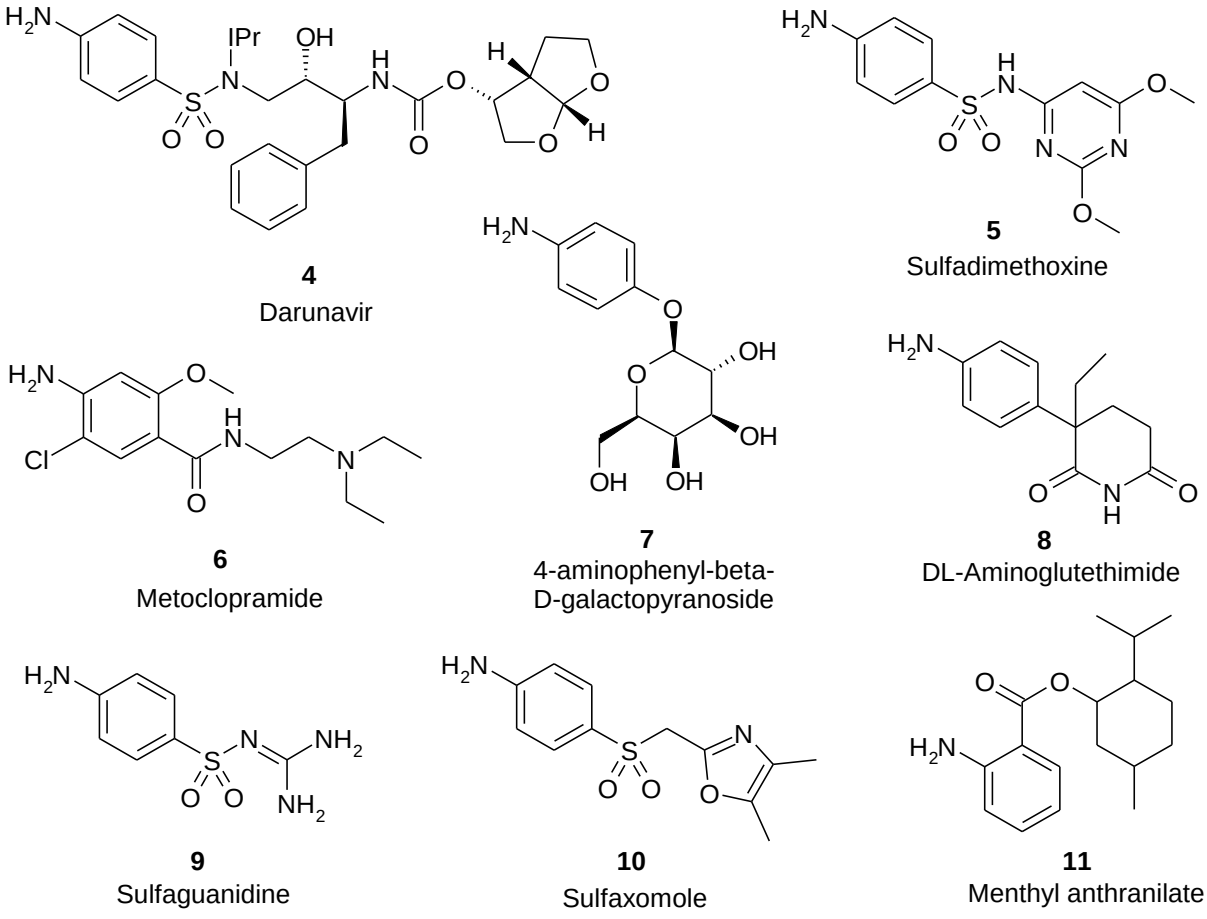

V.2. Literature background - HIE reactions of anilines in the past

Lautens *et al.* have described an unselective aniline labelling with deuterium (*scheme V.3, A*), utilizing strong acids like DCl in large excess at temperatures above 100°C giving access to 99%D incorporated (**12**).[8] Jung *et al.* have also developed a similar method, using in their case TFA instead of DCl.[9] Junk *et al.* described complete exchange (99%D) to generate [D_7]aniline **13** in D_2O/NaOD at 400°C (600 bar) over 10h (*scheme V.3, B*).[10] Recently Bagley reported an unselective deuteration of aniline and aminopyridines in neutral D_2O at 190°C (very high pressure) with up to 25%D for all CH-aniline positions in **14** (*scheme V.3, C*).[11] Another approach reported by Garnett *et al.* started from nitrobenzene **15**, which was reacted over raney-nickel (alternatively also platinum or palladium were applied) with D_2 or D_2O (or T_2 or HTO respectively) at 175°C over 4 days, to obtain the corresponding deuterated/tritiated anilines **16**, but with low D/T incorporation when the isotope source

was not used in large excess (*scheme V.3, D*).[12] Unfortunately, all these methods, with some others,[13] are difficult to transfer to tritium chemistry, yielding mainly a low specific activity.[14] Moreoever, only a few functional groups tolerate these harsh conditions.

Scheme V. 3: *Known aromatic HIE reactions on anilines* [8,10,11,12]

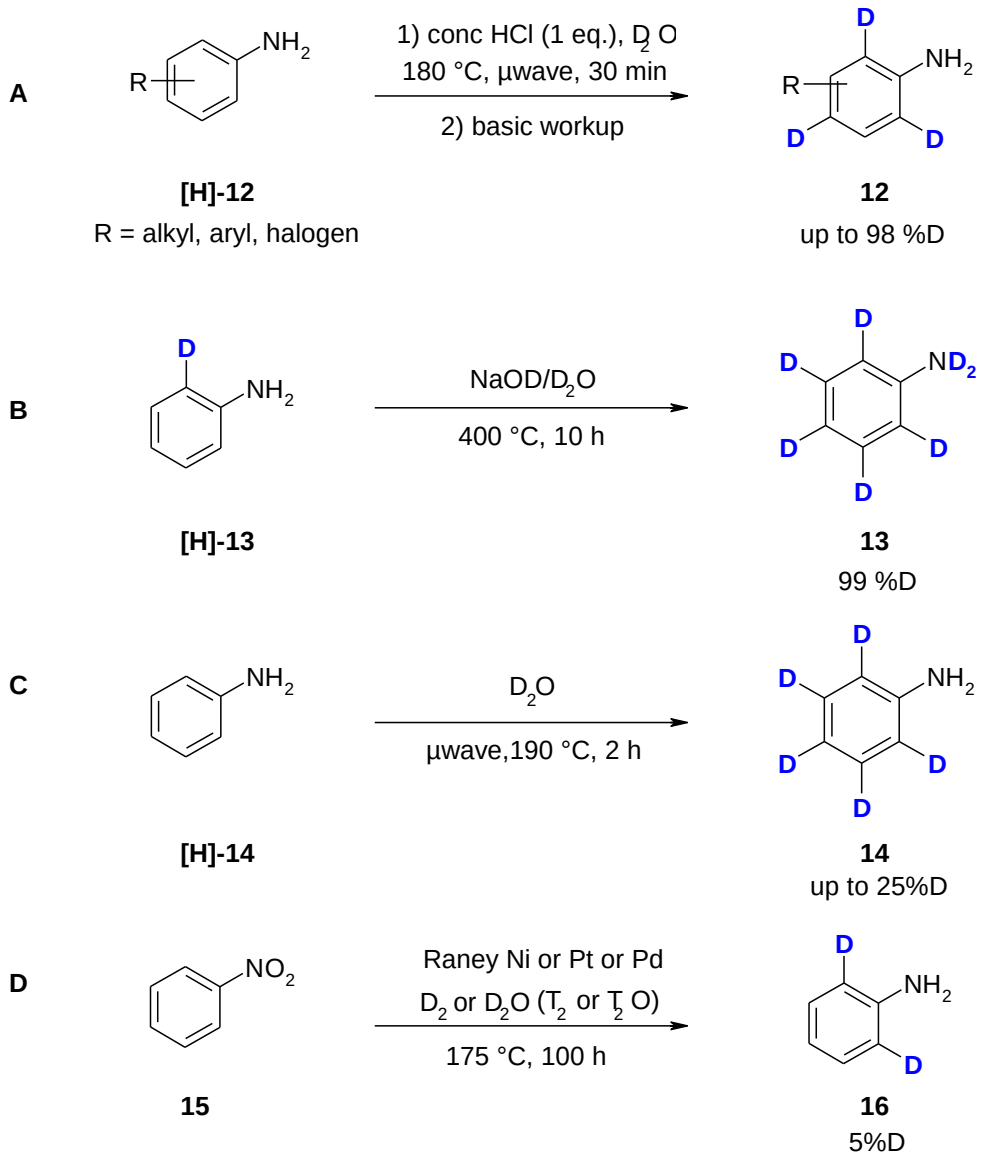

As showed above, even though there are already some examples published, there is still no simple and general method for the tritiation of complex anilines. This motivated us to search for an easy to handle, mild and generally applicable HIE method for isotope exchange on anilines, because mostly harsh conditions (**A-D**, *scheme V.4*) methods have been developed for over the past 50 years.

V.3. Evaluation of the iridium nanoparticles

The synthesis of IrNps has provided three different batches **3a-c**, with NHC-ligand ratios going from 0.05 to 0.25 equivalents of ligands regards to the metal iridium (*scheme V.1*). These nanoparticles have been evaluated in the HIE reaction of our model substrate 4-butylaniline **17**. A study of the deuterium incorporation versus time has been done for each of them (*figure V.3*). The IrICy **3b** provided the best result with incorporation of 1.85 D/molecule, in comparison with IrICy **3a** (1.79 D/molecule) and IrICy **3c** (1.72 D/molecule). Consequently, the IrICy **3b** was used for continuing the project.

Figure V. 3: *Comparison of the IrICy nanoparticles* ***3a-c*** *in the HIE reaction of aniline* ***17*** [a,b]

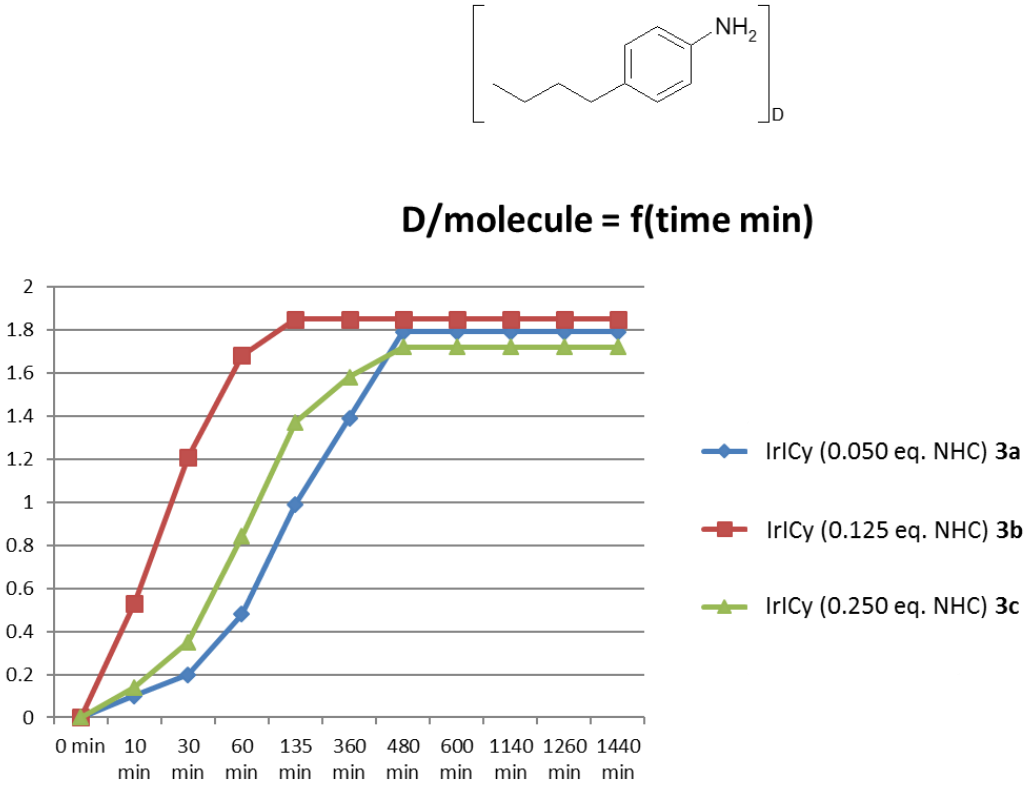

a) Conditions: substrate **17** (150 µmol), IrICy (4.0 mol%), THF (3 mL), D_2 (1 bar), 55°C, 24h. b) Deuterium incorporation analyzed by LC-MS.

An evaluation of the catalyst loading for IrICy **3b** was performed from a deuterium incorporation versus time study (*figure V.4*). We have observed that with a catalyst loading ranging from 4.0 to 8.0 mol%, the deuterium incorporation obtained in **17** was around 1.87 D/molecule, when it has reached 1.76 D/molecule with a catalyst loading of 2.5 mol%. For these reasons, the HIE reactions were performed using 4.0 mol% of IrICy **3b**.

Figure V. 4: *Evaluation of the catalyst loading of IrICy* ***3b*** *in the HIE reaction of aniline* ***17*** [a,b]

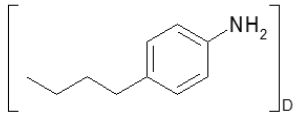

17

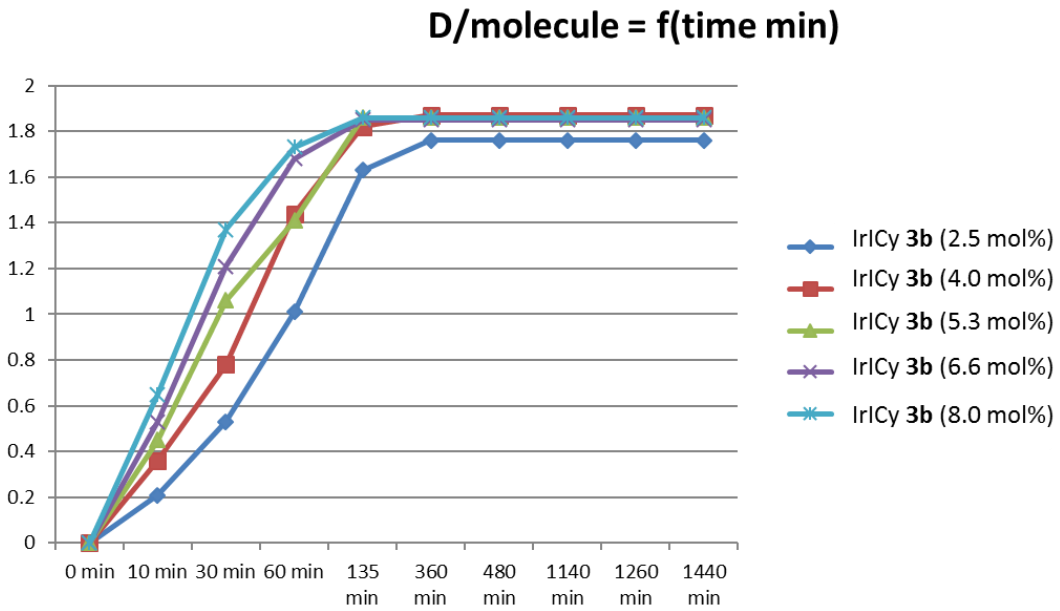

a) Conditions: substrate **17** (150 µmol), IrICy (2.5-8.0 mol%), THF (3 mL), D_2 (1 bar), 55°C, 24h. b) Deuterium incorporation analyzed by LC-MS.

Finally, the homogeneity between the different batches (*figure V.5)* appeared crucial to be evaluated, since nanoparticles **3b** have been synthetized in Toulouse throughout different synthesis. In total, five batches prepared at different dates were evaluated with our model substrate **17** before using them in HIE reactions with various anilines. Successfully, the synthesis of these nanoparticles was able to provide homogeneous batches of **3b,** with an HIE around 1.87 D/molecule in **17**. This demonstrates a sufficient homogeneity of the different IrCy **3b** batches.

It is important to state that these nanoparticles are air-stable since they were handled in the open-air without any precautions and used in HIE reactions without the need of a glovebox. This particularity suggests that it should be possible developing “easy to handle” methods for HIE reactions.

Figure V. 5: *Evaluation of the homogeneity between the different batches of IrICy* ***3b****.* [a,b]

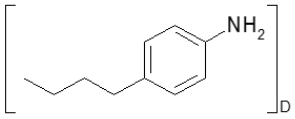

17

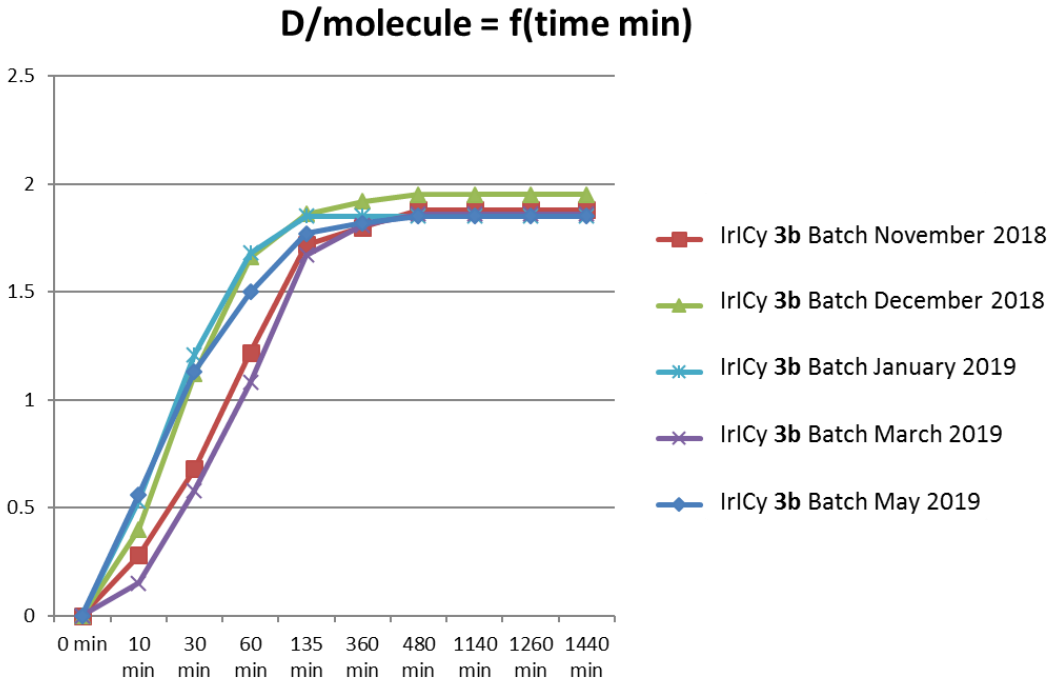

a) Conditions: substrate **17** (150 µmol), IrICy (4.0 mol%), THF (3 mL), D_2 (1 bar), 55°C, 24h. b) Deuterium incorporation analyzed by LC-MS.

V.4. Application of IrNPts in HIE of small aniline molecules

The IrICy nanoparticles **3b** have been applied to HIE on anilines **17-30** and gave good to excellent deuterium substitution (55-99%D) for simple anilines **17–21** (*scheme V.4*). Either electron-withdrawing functional groups (**18,20,21**) nor electron-donating ones (**17,19**) seemed to have a significant influence on the outcome of the HIE reaction. In contrast, steric interactions were identified as the major driver of the IrNPs-catalyzed HIE reactions. For example, no deuteration at all in ortho-position (**20**,**21**) of CF_3-groups were found. In the HIE reaction of naphthalenes **22-26**, different %D were observed for positions 2 and 8 in 1-amino-naphthalenes **22-24**. Interestingly, the C(sp^2)-H is significantly more reactive than the C(sp^3)-H as can be seen by comparison of 1-amino-naphthalenes **22** and **24**, probably due to a higher activation energy barrier. Furthermore, an evaluation of this HIE reaction with more complex anilines **26-30** containing other functional groups was done and deuterium incorporation was going from 26%D to 92%D. The reaction conditions tolerate halogens (**18**,**28**), phenols (**19**), ester (**26**,**30**) and ketones (**27**) without any influence on selectivity or

side-reactions. Up to now there is no scientific explanation for the decreased deuterium incorporation in aniline **30**. This observation needs to be investigated in the future.

Scheme V. 5: *HIE reaction with various anilines* ***17-30*** [a,b]

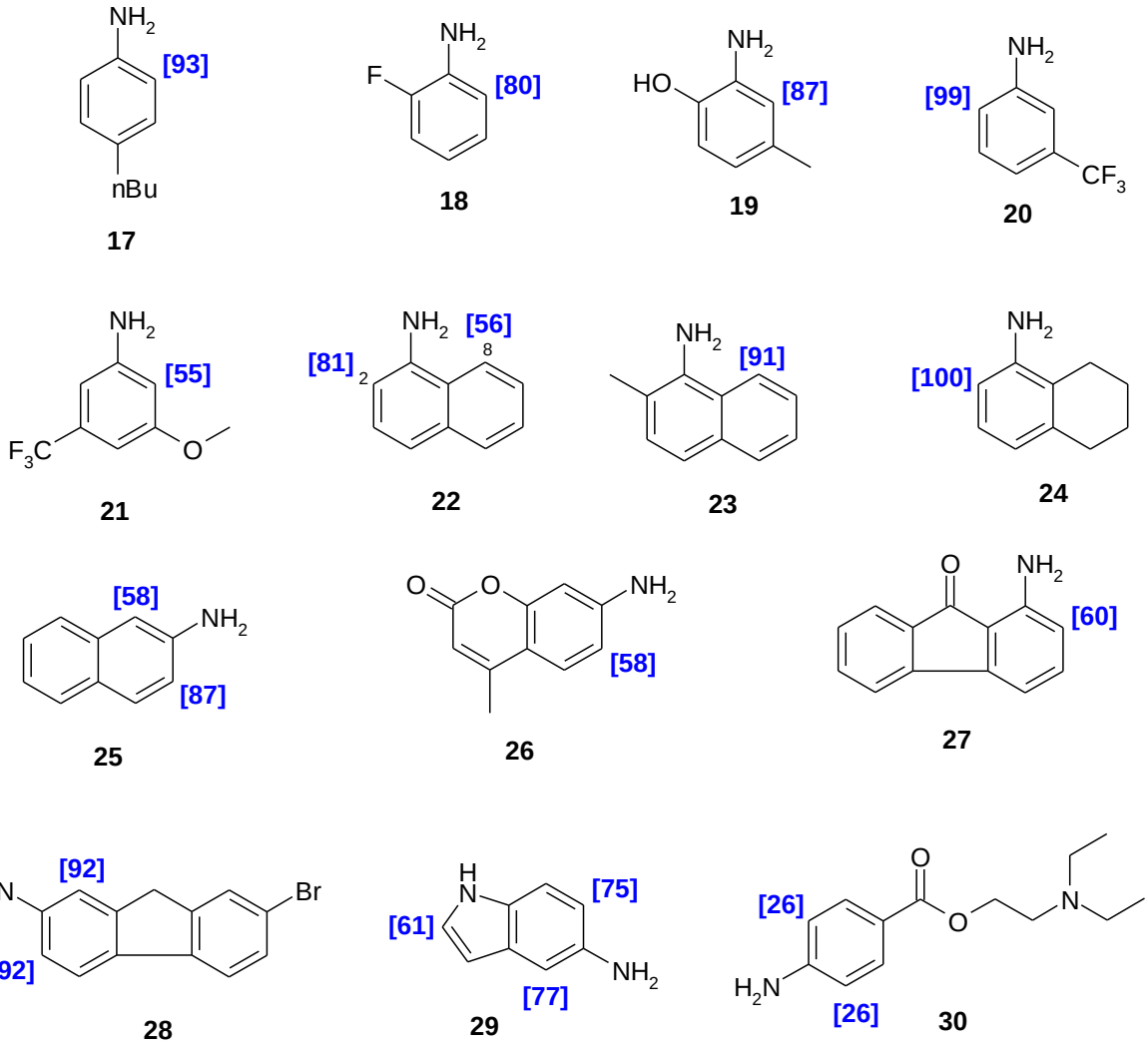

a) Conditions: substrate (1 eq.), IrICy **3b** (4.0 mol%), THF (3 mL), D_2 (1 bar), 3h, 55°C. b) Position and percentage of deuterium incorporation determined by ^{1}H NMR.

Nevertheless, we observed for a group of anilines **31**-**42** that the prior optimized conditions yield to low or nonexistent deuterium incorporation (*scheme V.5*). We postulated that due to the high polarity of the amino, a protic co-solvent like D_2O could be beneficial. Furthermore, as the boiling point of D_2O (101°C) is higher than for THF (66°C), we choose to use a 1:1 mixture of both, to be able to increase the reaction temperature.

Scheme V. 6: *HIE reaction with various anilines* ***21, 30*** *and* ***31-42*** [a,b,c]

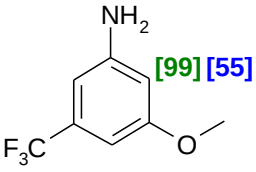

21

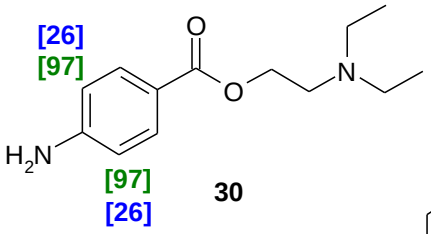

30

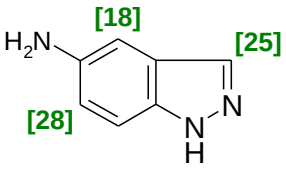

31 [0]

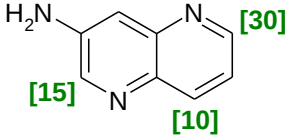

32 [0]

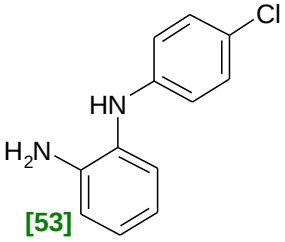

33 [0]

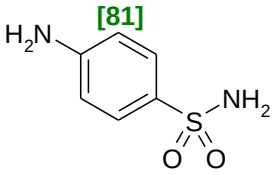

34 [0]

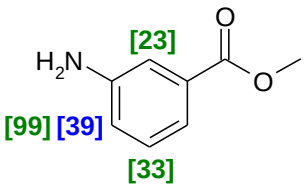

35

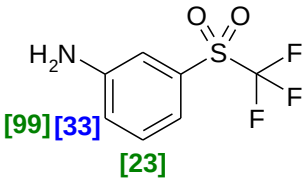

36

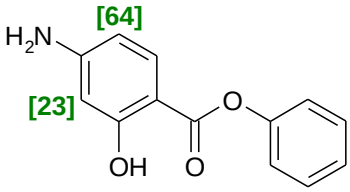

37

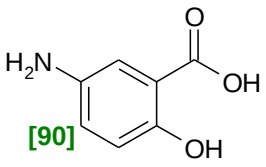

38

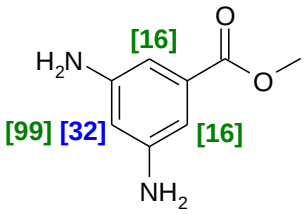

39

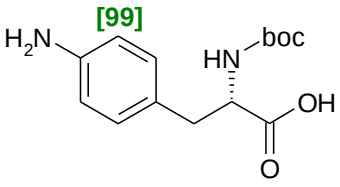

40

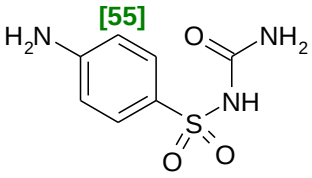

41 [0]

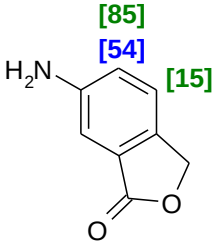

42

a)Conditions: substrate (1 eq.), IrICy **3b** (4.0 mol%), solvent (3 mL), D_2 (1 bar), 3h, Temp. (°C). b) **[%D with Method A]**: 55°C, THF. **[%D with Method B]**: 80°C, THF/D_2O (1:1). c) Position and percentage of deuterium incorporation determined by ^1H NMR.

Performing the HIE exchange with a THF/D_2O (1:1) solvent mixture (80°C) permitted to achieve successful HIE reactions with high deuterium uptake and regioselectivity. While in the HIE reaction of **30** there was only 26%D incorporation obtained with method A (THF, 55°C, blue bracket), with method B (THF/D_2O, 80°C, green bracket) the deuterium incorporation increased to 97%D. For **21** the deuterium incorporation increased from 55%D to 99%D. We observed similar improvements for anilines **35**, **36**, **39** and **42**. Whereas no deuteration at all was observed for anilines **31-34** and **41** with method A, conversely application of conditions B improved the HIE reaction outcome up to 81%D. While we obtained in most examples a high selectivity on the *ortho*-position relative to the aniline function, in the case of N-heterocycles an additional labelling was determined in *ortho*-position of the aromatic nitrogen atom (**29**, **31, 32**). Furthermore, we have observed the labelling in the *meta*-position of anilines **35, 36** and **42**. As the use of D_2O increased the deuterium incorporation, we were interested to understand its role in the HIE reaction.

V.5. The role of D_2O in IrNPts catalyzed HIE reactions

We investigated the influence of D_2O in the HIE reaction catalyzed with the IrNPs. For this purpose, deuteration of substrate **21** was performed for 3h, RT, 1 bar of gas (if any) as previously reported. If the reaction was carried out in THF under D_2 and in the absence of D_2O (*scheme V.6,* A), we observed 55% of isotopic enrichment, whereas if the reaction was performed in THF/D_2O in the absence of H_2 or D_2, no deuteration was found (*scheme V.6,* B).

Scheme V. 7**: Understanding the role of D_2O in the HIE reaction of aniline **21** with IrICy **3b [a,b,c]

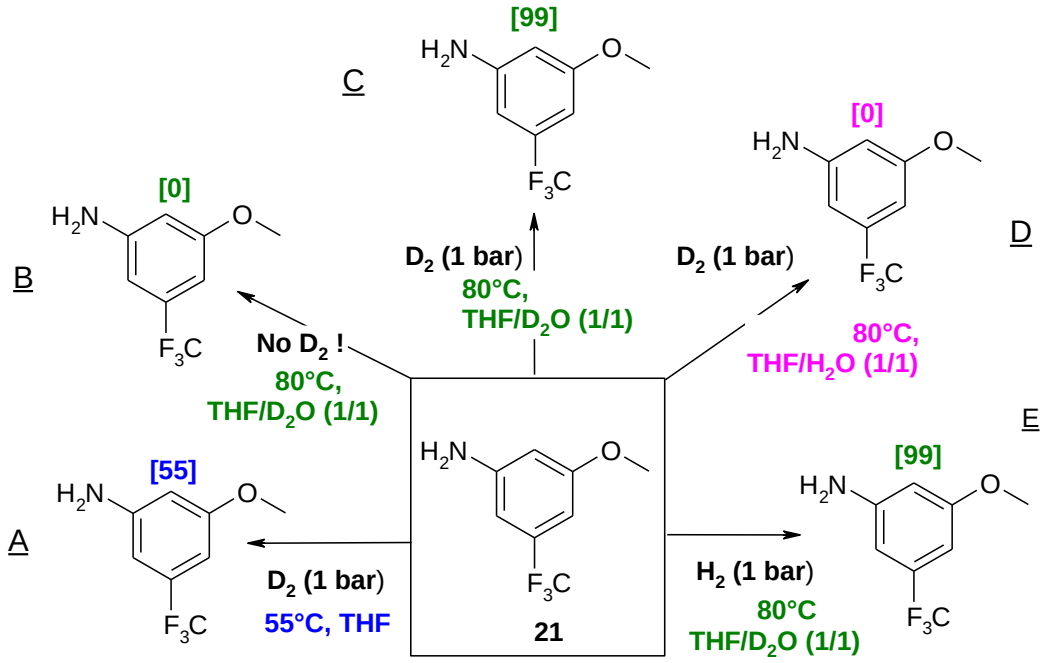

a) Conditions: substrate **21** (1 eq.), IrICy **3b** (4.0 mol%), solvent (3 mL), D_2 (1 bar), 3h, Temp. (°C). b) Method A (blue): 55°C, THF. Method B (green): 80°C, THF/D_2O (1:1). Method C (pink): 80°C, THF/H_2O (1:1). c) Position and percentage of deuterium incorporation determined by ^1H NMR or LC-MS.

However, if the deuteration was carried out in the presence of D_2 and in a THF/D_2O mixture (*scheme V.6,* C), the deuterium introduction jumped to 99%D. Thus, we hypothesized that upon fast equilibrium for HIE between gas and aqueous phase, D_2O may serve as kind of a reservoir to replenish the consumed D_2 in the gas phase. In order to verify this assumption, we planned two complementary experiments in THF/H_2O under D_2 (*scheme V.6,* D) and in THF/D_2O under H_2 (*scheme V.6,* E) where 0 and 99 %D deuteration were obtained, respectively.[15]

Interestingly these experiments demonstrate that this catalytic system does not require an additional supply of D_2 gas but can conveniently be carried out under H_2 in D_2O/THF mixtures. And it is likely to be extended to other D_2O organic solvent mixtures.

V.6. Applications of IrNPts in HIE reactions of complex molecules and drugs

The IrICy nanoparticles **3b** have been used for the HIE reaction on more complex structures, like the drugs sulfadimethoxine **5**, aminoglutethimide **8**, sulfamoxole **10**, methyl anthranilate **11** and the saccharose 4-aminophenyl-beta-D-galactopyranoside **7** (*scheme V.7*).

Scheme V. 8: *HIE reaction with aniline drugs* ***4-11*** [a,b]

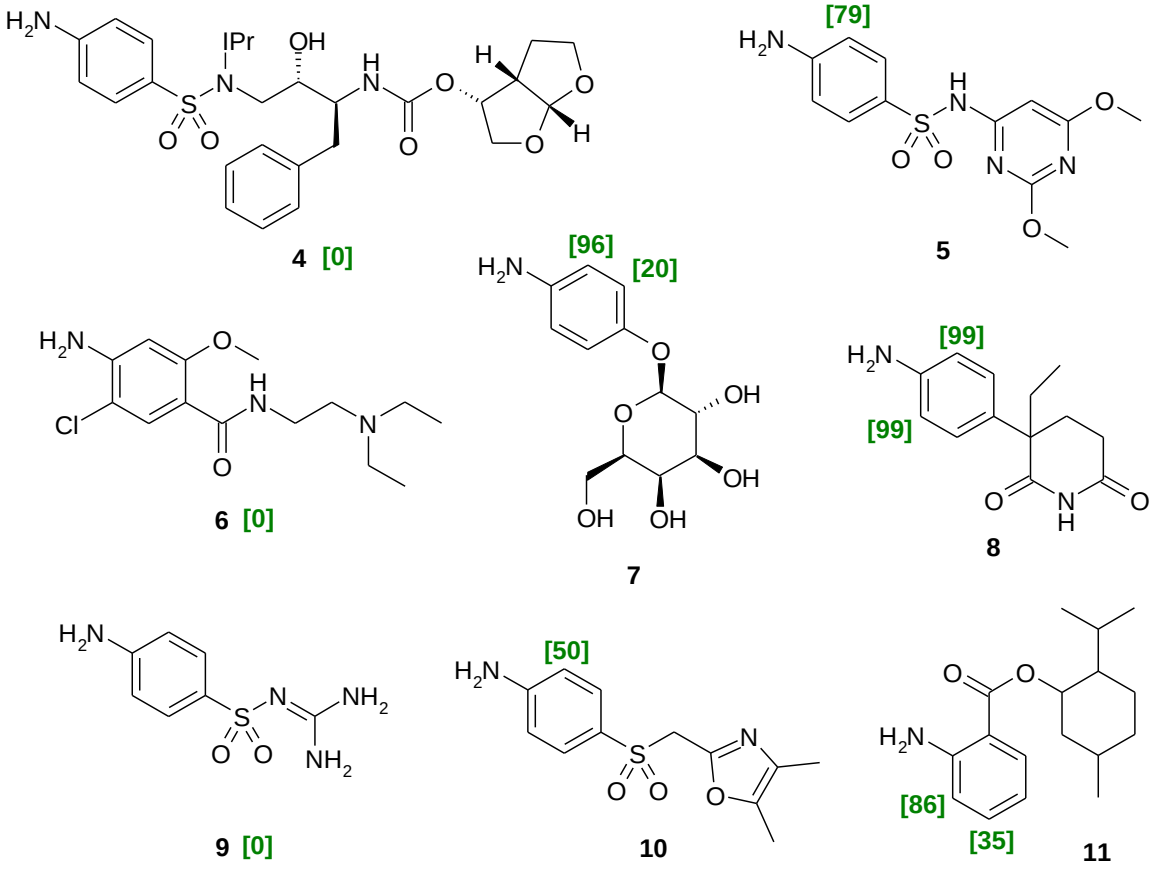

a) Conditions: substrate (1 eq.), IrICy **3b** (4.0 mol%), THF/D_2O (1:1) (3 mL), D_2 (1 bar), 3h, 80°C. b) Position and percentage of deuterium incorporation determined by ^1H NMR and LC-MS.

In all these examples, a good HIE efficacy was achieved providing deuterium incorporation from 50%D and up to 96%D. For the drug menthyl anthranilate **11** and the saccharose **7**, a side labelling in the *meta*-position with regards to the aniline DG has been observed, as this happened also for substrates **35**, **36** and **42**. Unfortunately, no deuteration was obtained for drugs **4**, **6** and **9**.

The late(last)-stage tritiation of a complex pharmaceutical, which was one of the major issues of this PhD work, has been realized on most target molecules using this novel iridium NPts. The deuterium and tritium HIE reaction conditions have been optimized using the aniline **43**, which is a pharmacophore of the drug Volixibat (*scheme V.8*).[16] This complex molecule is a medication under development as for cholestatic liver disease.

Scheme V. 9: *Deuteration and tritiation of Volixibat precursor* ***43*** [a,b,c]

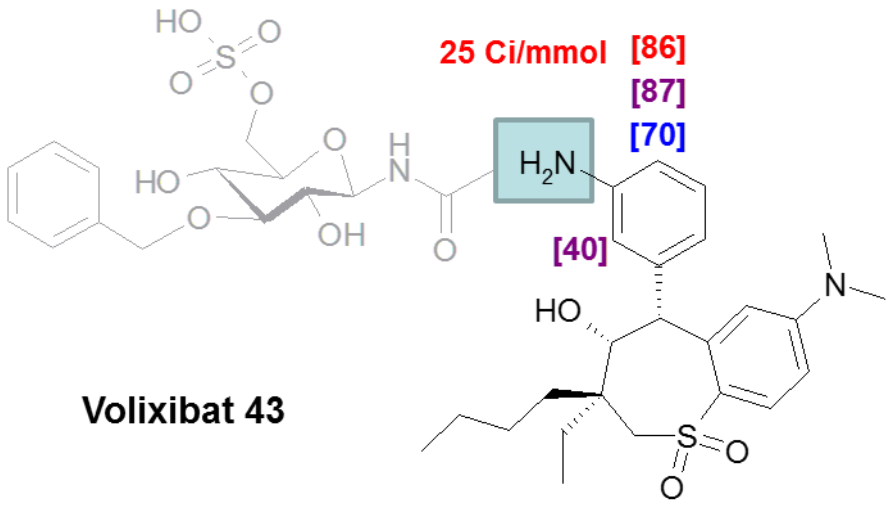

a) Conditions: volixibat pharmacophore **43** (1 eq.), IrICy **3b,** THF (3 mL), D_2 (1 bar), 3h, 55°C. b) IrICy **3b** (4 mol%) [%D blue bracket]; IrICy **3b** (80 mol%) [%D purple brackets] and [%T red brackets]. c) Position and percentage of deuterium incorporation determined by ^{1}H NMR, tritium NMR and LC-MS. d) In grey the connected side chain of the whole drug volixibat.

As the use of tritiated water T_2O was not practicable, an optimization of the reaction conditions in THF had to be done. The deuteration of **43** was done by using 4 mol% of the IrICy **3b**, in THF at 55°C (as used so far). These conditions led to a selective deuterium incorporation of **43** up to 70%D (*scheme V.8, blue bracket*). Nevertheless, as it is expected to get a lower tritium incorporation due the KIE between H, D and T, the conditions were further optimized to get more deuterium incorporated. Consequently, the reaction was run with a higher catalyst loading reaching 80 mol% of IrICy **3b**, still at 55°C in THF. In this case, both *ortho*-positions were deuterated with 41%D and 87%D in Volixibat precursor **43** (*scheme V.8, purple bracket*). Finally, the catalytic loading of 80 mol% of IrICy **3b** was used

for the tritiation of Volixibat pharmacophore **43**. The tritium reaction was run using subatmospheric pressure of tritium gas (p= 0.8 bar, 10 Ci) within a relatively short reaction time (3 h). In terms of regioselectivity, the labelling of the less sterically encumbered *ortho*-position of the NH_2 group was mainly observed in **43** with 86%T incorporated (*scheme V.8, red bracket*). Usually, a specific activity between 10–20 Ci/mmol is considered as suitable for the use of a tritiated molecules in the context of ADME studies. The high specific activity of 25 Ci/mmol obtained here clearly demonstrates the high potential of this novel method in the context of the late-stage labelling of complex pharmaceuticals containing aniline substructures.

V.7. Conclusion

For the first time air-stable and easy-to-handle iridium NHC-ligated nanoparticles can be used in HIE reactions. These catalysts showed a unique catalytic activity allowing a selective and efficient hydrogen isotope incorporation on anilines using D_2 or T_2 as isotopic source. The usefulness of this transformation has been demonstrated by the deuterium and tritium labelling of diverse complex pharmaceuticals. The method was fully adaptable to the specific requirements of tritium chemistry, which was demonstrated by direct tritium labelling of the volixibat pharmacophore **43** with high selectivity and specific radioactivity of 25 Ci/mmol (theoretical specific radioactivity of 29 Ci/mmol). This data is clearly fulfilling all requirements mentioned in the objectives of the thesis for the development of late-stage tritium labeling of drugable compounds.

[1] For selected examples: a) C. Taglang, L-M. Martínez-Prieto, I. del Rosal, L. Maron, R. Poteau, K. Philippot, B. Chaudret, S. Perato, A. Sam Lone, C. Puente, C. Dugave, B. Rousseau, G. Pieters, *Angewandte Chemie International Edition*, **2015**, *54(36)*, 10474-10477. b) L. Gao, S. Perato, S. Garcia-Argote, C. Taglang, L-M. Martinez-Prieto, C. Chollet, D-A. Buisson, V. Dauvois, P. Lesot, B. Chaudret, B. Rousseau, S. Feuillastre and G. Pieters, *Chemical Communications*, **2018**, *54(24)*, 2986-2989. c) A. Palazzolo, S. Feuillastre, V. Pfeifer, S. Garcia-Argote, D. Bouzouita, S. Tricard, C. Chollet, E. Marcon, D-A. Buisson, S. Cholet, F. Fenaille, G. Lippens, B. Chaudret and G. Pieters, *Angewandte Chemie International Edition*, **2019**, *58(15)*, 4891-4895.

[2] a) G. Schmid, Nanoparticles, From theory to applications, Weinheim, **2004**. b) A. Roucoux, J. Schulz and H. Patin, *Chem. Rev*. **2002**, *102*, 3757–3778.

[3] a) D. Canseco-Gonzalez, A. Petronilho, H. Mueller-Bunz, K. Ohmatsu, T. Ooi, M. Albrecht, *J. Am. Chem. Soc.* **2013**, *135*, 13193–13203; b) E. C. Hurst, K. Wilson, I. J. S. Fairlamb, V. Chechik, *New J. Chem*. **2009**, *33*, 1837–1840; c) A. V. Zhukhovitskiy, M. G. Mavros, T. Van Voorhis, J. A. Johnson*, J. Am. Chem. Soc*. **2013**, *135*, 7418–7421; d) G. Wang, A. Ruhling, S. Amirjalayer, M. Knor, J. B. Ernst, C. Richter, H.-J. Gao, A. Timmer, H.-Y. Gao, N. L. Doltsinis, F. Glorius, H. Fuchs, *Nat. Chem*. **2017**, *9*, 152–156.

[4] K. V. S. Ranganath, J. Kloesges, A. H. Schaefer, F. Glorius, *Angew. Chem., Int. Ed.* **2010**, *49*, 7786–7789.

[5] M. Diaz de los Bernardos, S. Perez-Rodrıguez, A. Gual, C. Claver, C. Godard *Chem. Commun*. **2017**, *53*, 7894-7897; b) J.-F. Soule, H. Miyamura, S. Kobayashi, *J. Am. Chem. Soc*. **2013**, *135*, 10602–10605.

[6] a) P. Lara, O. Rivada-Wheelaghan, S. Conejero, R. Poteau, K. Philippot, B. Chaudret, *Angew. Chem., Int. Ed*. **2011**, *50*, 12080–12084; b) L. M. Martinez-Prieto, A. Ferry, P. Lara, C. Richter, K. Philippot, F. Glorius, B. Chaudret, *Chem. Eur. J*. **2015**, *21*, 17495–17502.

[7] L. S. Ott, M. L. Cline, M. Deetlefs, K. R. Seddon and R. G. Finke, *J. Am. Chem. Soc*. **2005**, *127*, 5758–5759.

[8] A. Martens, M. Lautens Org. Lett. 2008, 10, 4351-4353.

[9] R. Giles, A. Lee, E. Jung, A. Kang, K. W. Jung, Tetrahedron Lett. 2015, 56, 747-749.

[10] T. Junk, WJ Catallo, LD Civils, J. Label Compd. Radiopharm. 1997

[11] Mark C. Bagley, Ayed Alnomsy, Hussein I. Sharhan, Synlett 2016, *27*, 2467–2472.

[12] John L. Garnett, Mervyn A. Long, Chit Than and Philip G. Williams, J. CHEM. SOC. FARADAY TRANS., 1990, 86(5), 875-879

[13] a) G. Ayrey and R.W. Dunlop, J. Label Compd. Radiopharm 1980, 17, 21-33. b) M. Tashiro, H. Tsuzuki, T. Tsukinoki, S. Mataka, K. Nakayama, T. Yonemitsu, J. Label Compd. Radiopharm. 1990, 28, 703-712. c) Calf, GE; Garnett, JL; Pickles, VA Aust. J. Chem., 1968, 21, 961-972. d) Hagiwara, Hiroshi; Echigoya, Etsuro Bull. Chem. Soc. Jp (1966), 39(8), 1683-1689. e) Macdonald, C. G.; Shannon, J. S. Tetrahedron Letters (1964), (45-46), 3351-3354.

[14] G. Ayrey and R.W. Dunlop, J. Label Compd. Radiopharm 1980, 17, 21-33.

[15] The deuterium molarity of 1.5 mL heavy water is 0.166 mol. The deuterium molarity of 20 mL D_2 gas is $1.78.10^{-3}$ mol.

[16] International Nonproprietary Names for Pharmaceutical Substances (INN). Recommended International Nonproprietary Names: List 75. World Health Organization. p. 166. Retrieved 21 January 2017.

Supporting information Part V

Materials: see Annex 1

General deuteration procedure (Annex 1):

- **Method A:** THF (3 mL), 55 °C. Deuterium incorporation showed in blue brackets.
- **Method B:** THF/D_2O (1:1) (3 mL), 80 °C. Deuterium incorporation showed in green brackets.

Hydrogen isotope exchange reactions data

Aniline **17**

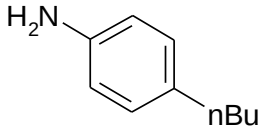

Molecular Weight =149.2378
Molecular Formula =C10H15N

17

^{1}H NMR (300 MHz, MeOD): δ 6.93 (d, ^3J = 8.1 Hz, 2H, 2 CH *meta*-NH_2), 6.66 (d, ^3J = 8.1Hz, 2H, 2 CH *ortho*-NH_2), 4.82 (br s, 2H, NH_2), 2.48 (t, ^3J = 7.0 Hz, 2H, CH_2 nBu), 1.54 (m, 2H, CH_2 nBu), 1.33 (m, 2H, CH_2 nBu), 0.92 (t, ^3J = 7.8 Hz, 3H, CH_3 nBu) ppm. Incorporation expected at δ 6.66 (red arrow). Determined against integral at δ 0.92 (blue arrow).

General method A: 22.5 mg (150. 0 µmol) **17**; 1.5 mg (6.0 µmol, 4 mol%) IrICy(0.125NHC) **3b**, THF (3 mL), 55 °C, 3h.

LC-MS (positive ESI): m/z 150.2 $[M+H]^+$ (2%), 151.1 $[M(1D)+H]^+$ (17%), 152.2 $[M(2D)+H]^+$ (76%), 153.1 $[M(3D)+H]^+$ (5%).

Yield: 22.1 mg, 148.0 µmol, 98%; 93% D for δ 6.66.

^{1}H-NMR Reference **17**

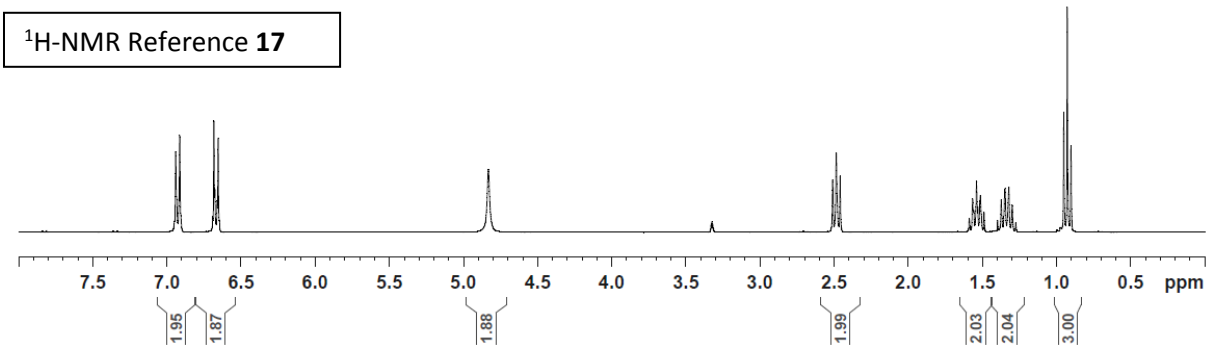

^{1}H-NMR HIE reaction **17**

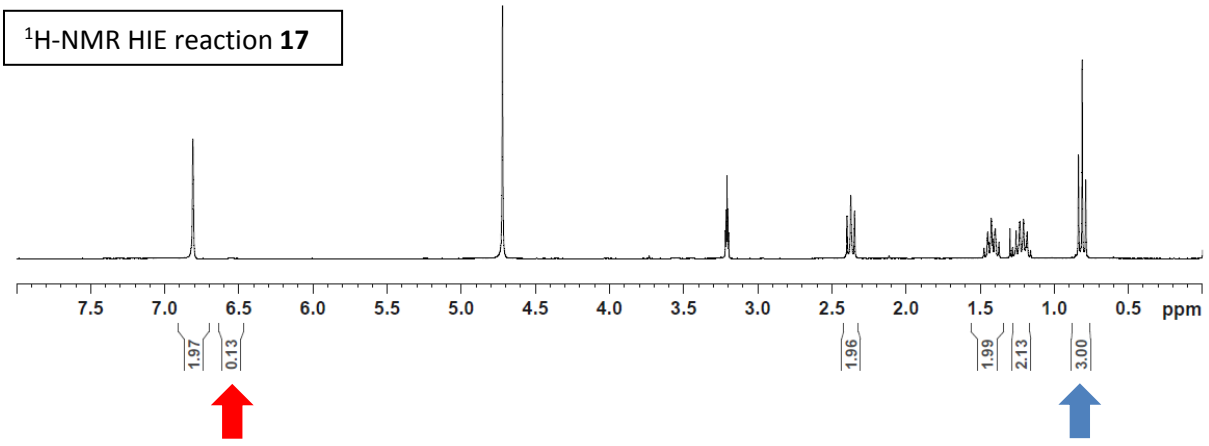

Aniline **18**

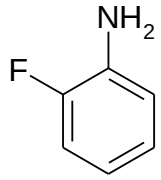

Molecular Weight =111.1198
Molecular Formula =C6H6FN

18

^{1}H NMR (300 MHz, MeOD): δ 6.99 (m, 2H, 2 CH phenyl), 6.76 (m, 2H, 2 CH phenyl), 3.69 (br s, 2H, NH_2) ppm. Incorporation expected at δ 6.76 (red arrow). Determined against integral at δ 6.99 (blue arrow).

General method A: 16.7 mg (150.0 µmol) **18**; 1.5 mg (6.0 µmol, 4 mol%) IrICy(0.125NHC) **3b**, THF (3 mL), 55 °C, 3h.

LC-MS (positive ESI): m/z 112.1 $[M+H]^+$ (21%), 113.1 $[M(1D)+H]^+$ (72%), 114.1 $[M(2D)+H]^+$ (7%).

Yield: 12.0 mg, 108.3 µmol, 72%; 80% D for δ 6.76.

^{1}H-NMR Reference **18**

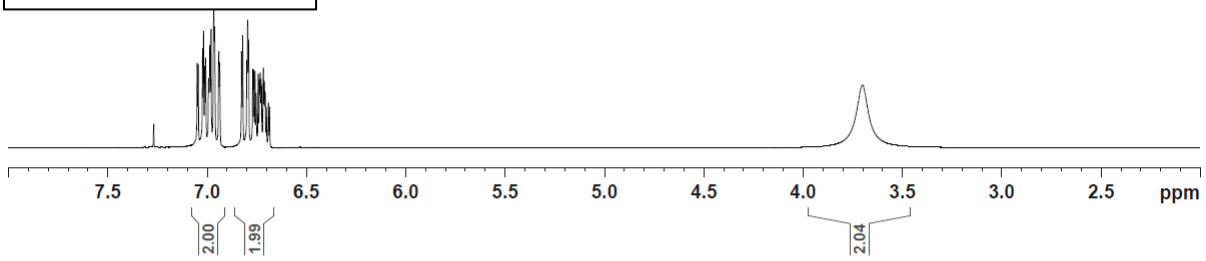

^{1}H-NMR HIE reaction **18**

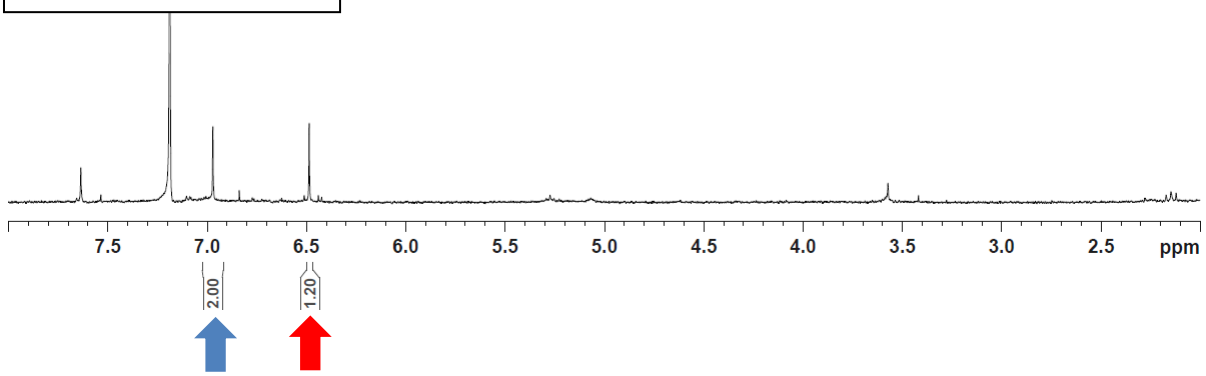

Aniline **19**

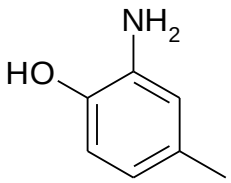

Molecular Weight =123.1559
Molecular Formula =C7H9NO

19

^{1}H NMR (300 MHz, MeOD): δ 6.59 (m, 2H, CH *ortho*-NH_2 and CH *ortho*-OH), 6.42 (dd, ^3J = 8.1 Hz and 1.7 Hz, 1H, CH *ortho*-methyl), 2.18 (s, 3H, CH_3) ppm. Incorporation expected at δ 6.59 (red arrow). Determined against integral at δ 2.18 (blue arrow).

General method A: 18.4 mg (150.0 µmol) **19**; 1.5 mg (6.0 µmol, 4 mol%) IrICy(0.125NHC) **3b**, THF (3 mL), 55 °C, 3h.

LC-MS (positive ESI): m/z 124.1 $[M+H]^+$ (18%), 125.1 $[M(1D)+H]^+$ (76%), 126.1 $[M(2D)+H]^+$ (6%).

Yield: 16.9 mg, 137.4 µmol, 92%; 87% D for δ 6.59.

^{1}H-NMR Reference **19**

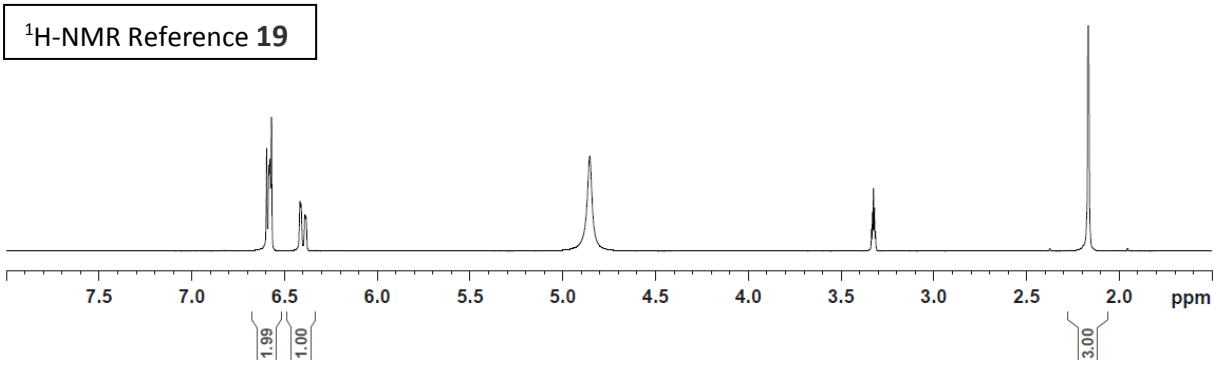

^{1}H-NMR HIE reaction **19**

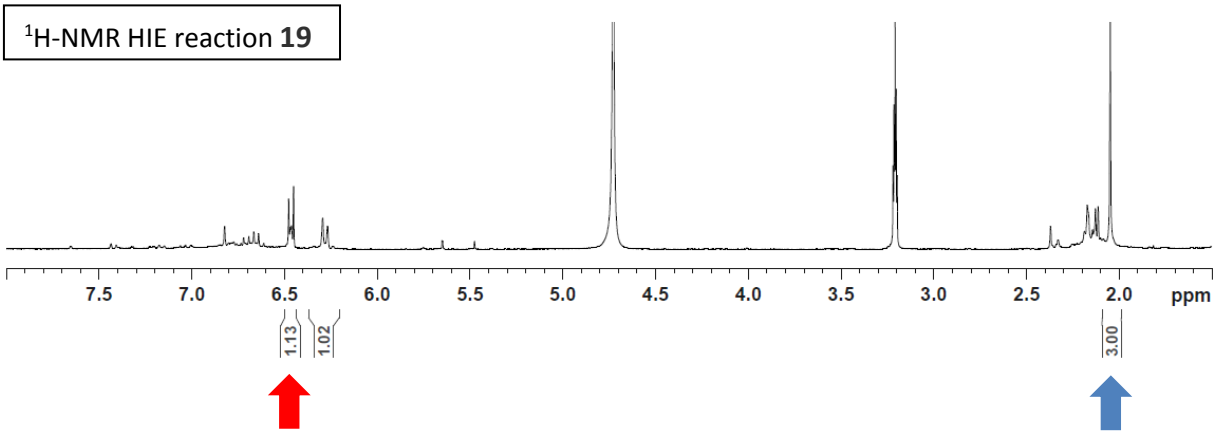

Aniline **20**

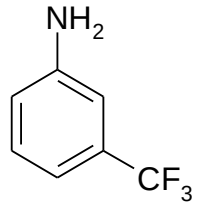

20

Molecular Weight =161.1278
Molecular Formula =C7H6F3N

^{1}H NMR (300 MHz, MeOD): δ 7.25 (t, ^{3}J = 7.6 Hz, 1H, CH *meta*-NH_2), 7.02 (d, ^{3}J = 7.6 Hz, 1H, CH *ortho*-NH_2), 6.92 (s, 1H, CH *ortho*-NH_2), 6.82 (dd, ^{3}J = 7.6 Hz and 2.3 Hz, 1H, CH *ortho*-CF_3) ppm. Incorporation expected at δ 7.02 (red arrow). Determined against integral at δ 7.25 (blue arrow).

General method A: 24.1 mg (150.0 µmol) **20**; 1.5 mg (6.0 µmol, 4 mol%) IrICy(0.125NHC) **3b**, THF (3 mL), 55 °C, 3h.

LC-MS (positive ESI): m/z 162.1 $[M+H]^+$ (1%), 163.1 $[M(1D)+H]^+$ (94%), 164.1 $[M(2D)+H]^+$ (5%).

Yield: 22.2 mg, 137.7 µmol, 92%; 99% D for δ 7.02.

^{1}H-NMR Reference **20**

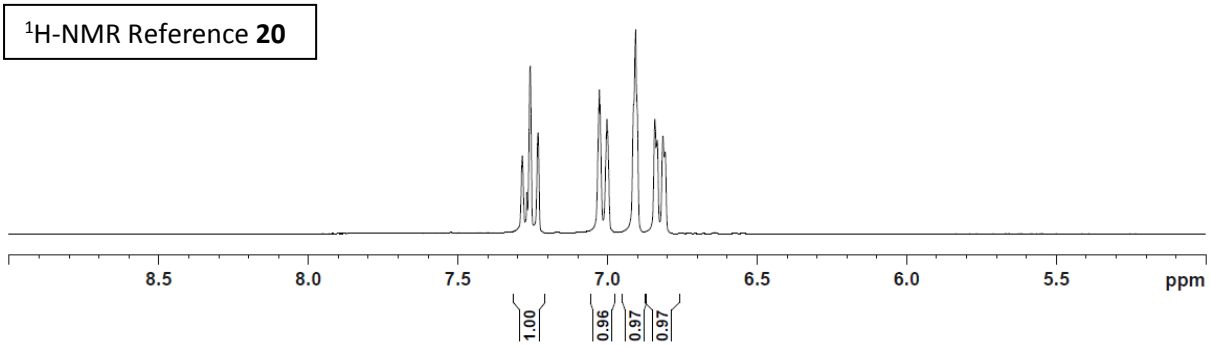

^{1}H-NMR HIE reaction **20**

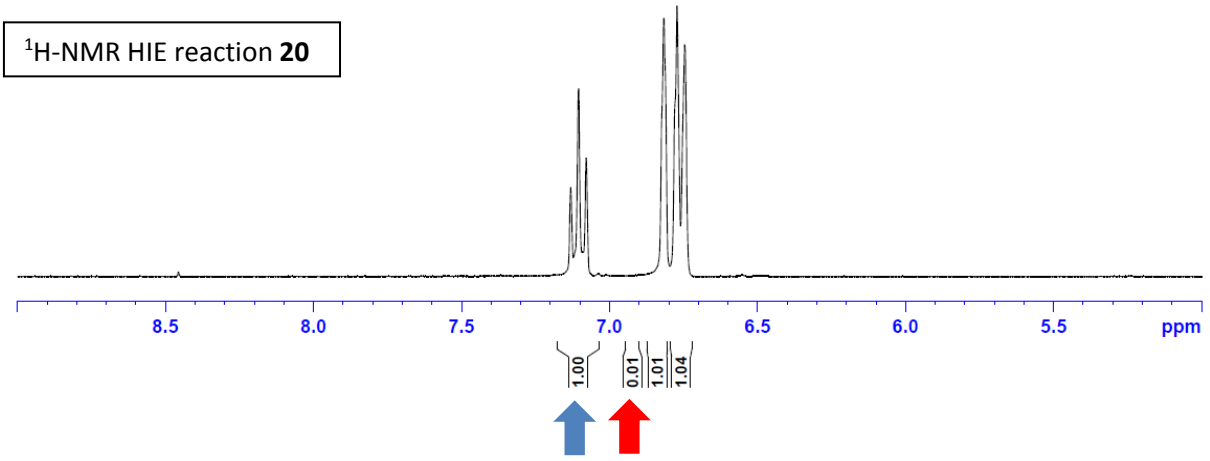

Aniline **21**

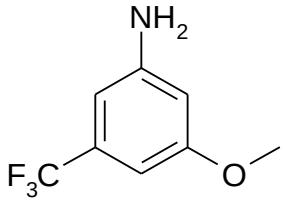

Molecular Weight =191.1543
Molecular Formula =C8H8F3NO

21

^{1}H NMR (300 MHz, MeOD): δ 6.52 (m, 2H, 2 CH *ortho*-CF_3), 6.35 (m, 1H, CH *ortho*-NH_2), 3.80 (s large and s, 5H, NH_2 and OCH_3) ppm. Incorporation expected at δ 6.35 (red arrow). Determined against integral at δ 3.80 (blue arrow).

General method A: 28.6 mg (150.0 µmol) **21**; 1.5 mg (6.0 µmol, 4 mol%) IrICy(0.125NHC) **3b**, THF (3 mL), 55 °C, 3h.

LC-MS (positive ESI): m/z 192.1 $[M+H]^+$ (46%), 193.1 $[M(1D)+H]^+$ (51%), 194.1 $[M(2D)+H]^+$ (3%).

Yield: 23.5 mg, 122.7 µmol, 82%; 55% D for δ 6.35.

^{1}H-NMR Reference **21**

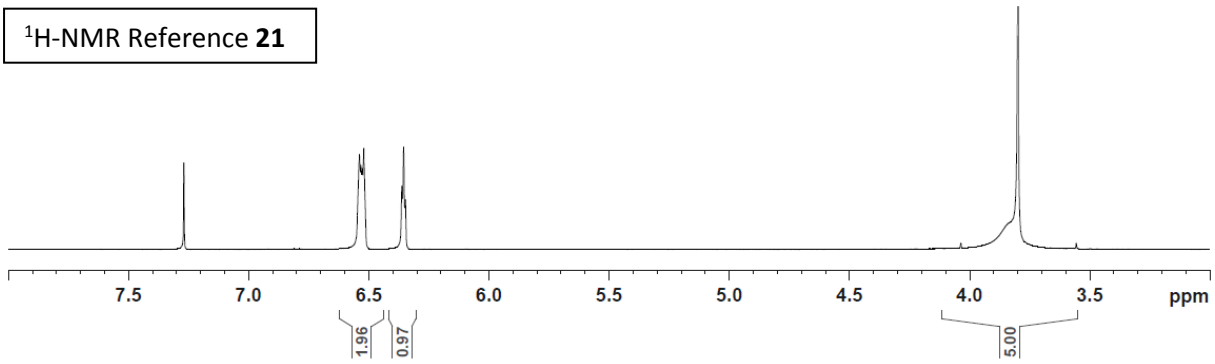

^{1}H-NMR HIE reaction **21**

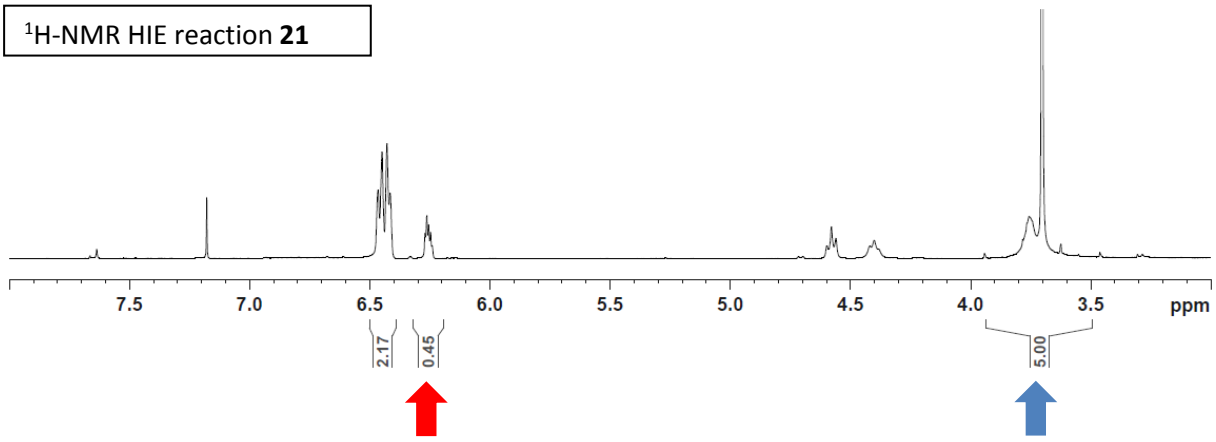

General method B: 28.6 mg (150.0 µmol) **21**; 1.5 mg (6.0 µmol, 4 mol%) IrICy(0.125NHC) **3b**, THF/D_2O (1:1) (3 mL), 80 °C, 3h.

LC-MS (positive ESI): m/z 192.1 $[M+H]^+$ (1%), 193.1 $[M(1D)+H]^+$ (95%), 194.1 $[M(2D)+H]^+$ (4%).

Yield: 22.3 mg, 116.8 µmol, 78%; 99% D for δ 6.35.

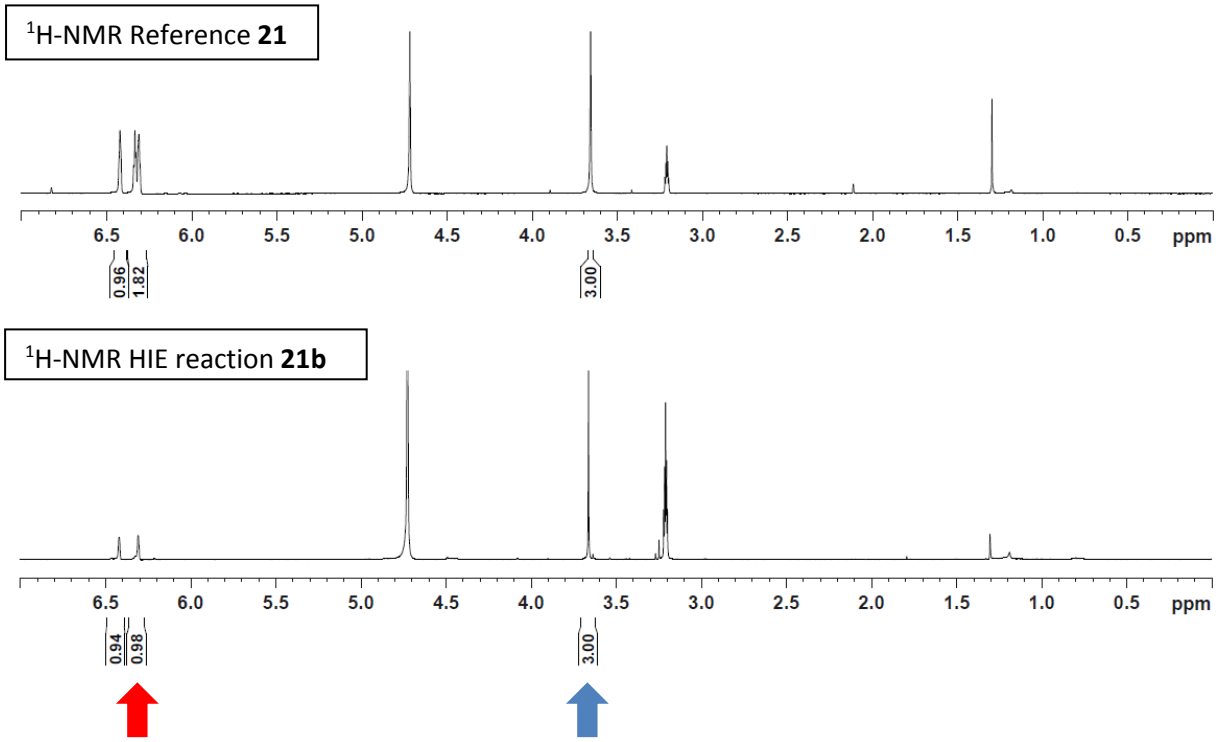

Other conditions (*Scheme V.6*):

- THF/H_2O (1:1) (3 mL), 80 °C, 3h: no deuterium incorporation.
- THF/D_2O (1:1) (3 mL), 80 °C, 3h, no gas: no deuterium incorporation.

Aniline **22**

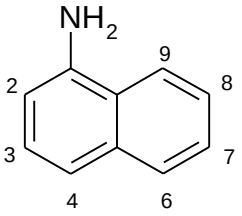

Molecular Weight =143.1899
Molecular Formula =C10H9N

22

^{1}H NMR (300 MHz, MeOD): δ 7.84 (m, 2H, $CH_{(9)}$ and $CH_{(7)}$), 7.48 (m, 2H, $CH_{(8)}$ and $CH_{(6)}$), 7.33 (m, 2H, $CH_{(3)}$ and $CH_{(4)}$), 6.80 (m, 1H, $CH_{(2)}$), 4.09 (br s, 2H, NH_2) ppm. Incorporation expected at δ 7.84 and 6.80 (red arrow). Determined against integral at δ 7.48 (blue arrow).

General method A: 21.4 mg (150.0 µmol) **22**; 1.5 mg (6.0 µmol, 4 mol%) IrICy(0.125NHC) **3b**, THF (3 mL), 55 °C, 3h.

LC-MS (positive ESI): m/z 144.1 $[M+H]^+$ (4%), 145.1 $[M(1D)+H]^+$ (30%), 146.1 $[M(2D)+H]^+$ (55%), 147.1 $[M(3D)+H]^+$ (9%), 148.1 $[M(4D)+H]^+$ (2%).

Yield: 18.8 mg, 131.4 µmol, 88%; 56% D for δ 7.84 and 81% D for δ 6.80.

^{1}H-NMR Reference **22**

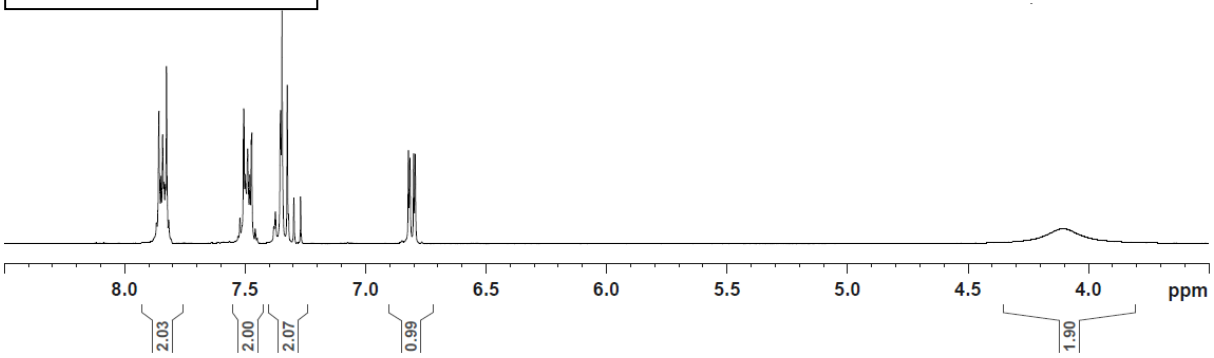

^{1}H-NMR HIE reaction **22**

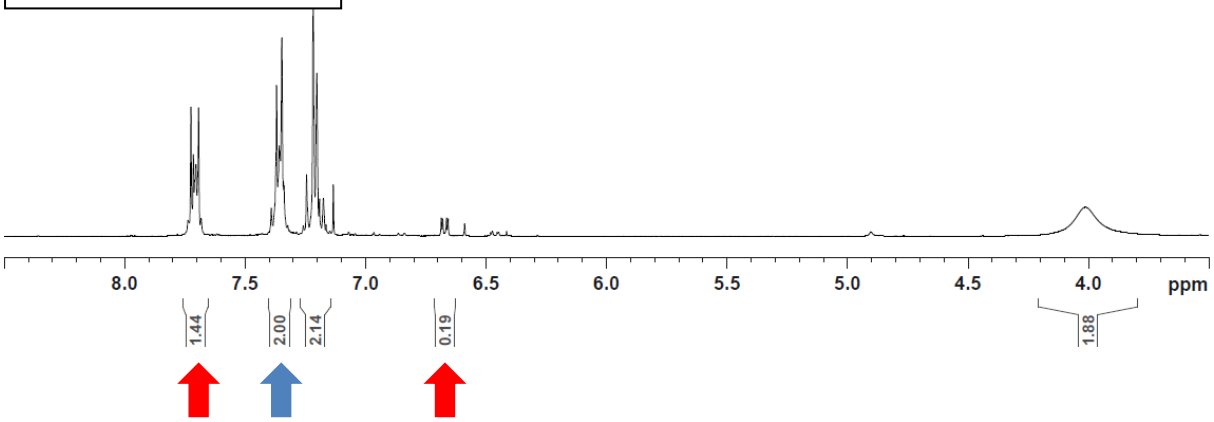

Aniline **23**

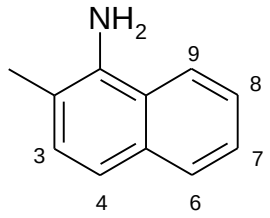

Molecular Weight =157.2170
Molecular Formula =C11H11N

23

^{1}H NMR (300 MHz, MeOD): δ 7.82 (m, 2H, $CH_{(9)}$ and $CH_{(7)}$), 7.46 (m, 2H, $CH_{(8)}$ and $CH_{(6)}$), 7.29 (m, 2H, $CH_{(3)}$ and $CH_{(4)}$), 4.11 (br s, 2H, NH_2), 2.40 (s, 3H, CH_3) ppm. Incorporation expected at δ 7.82 (red arrow). Determined against integral at δ 7.29 (blue arrow).

General method A: 23.5 mg (150.0 µmol) **23**; 1.5 mg (6.0 µmol, 4 mol%) IrICy(0.125NHC) **3b**, THF (3 mL), 55 °C, 3h.

LC-MS (positive ESI): m/z 158.2 $[M+H]^+$ (10%), 159.2 $[M(1D)+H]^+$ (85%), 160.2 $[M(2D)+H]^+$ (5%).

Yield: 23.1 mg, 146.7 µmol, 98%; 91% D for δ 7.82.

^{1}H-NMR Reference **23**

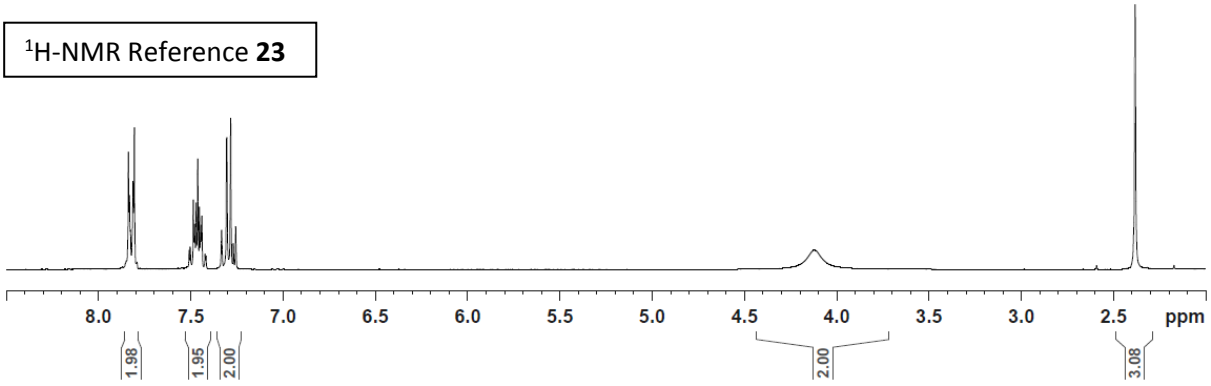

^{1}H-NMR HIE reaction **23**

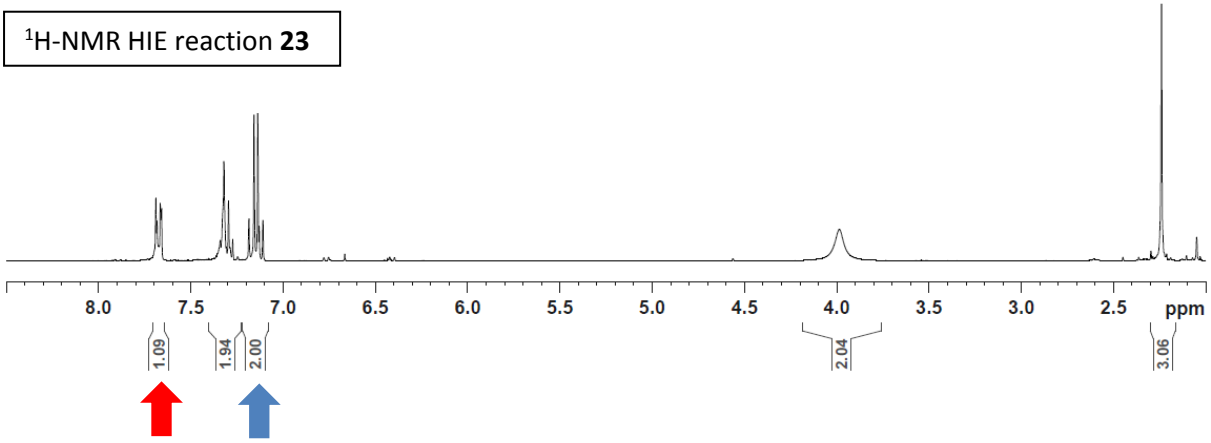

Aniline **24**

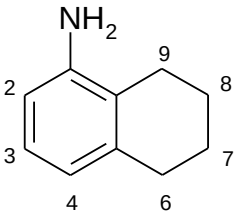

Molecular Weight =147.2218
Molecular Formula =C10H13N

24

^{1}H NMR (300 MHz, MeOD): δ 6.98 (m, 1H, $CH_{(3)}$), 6.56 (m, 2H, $CH_{(2)}$ and $CH_{(4)}$), 3.52 (br s, 2H, NH_2), 2.77 (m, 2H, $CH_{2(6)}$), 2.48 (m, 2H, $CH_{2(9)}$), 1.86 (m, 4H, $CH_{2(8)}$ and $CH_{2(7)}$) ppm. Incorporation expected at δ 6.56 (red arrow). Determined against integral at δ 2.48 (blue arrow).

General method A: 22.0 mg (150.0 µmol) **24**; 1.5 mg (6.0 µmol, 4 mol%) IrICy(0.125NHC) **3b**, THF (3 mL), 55 °C, 3h.

LC-MS (positive ESI): m/z 148.2 $[M+H]^+$ (2%), 149.2 $[M(1D)+H]^+$ (94%), 150.2 $[M(2D)+H]^+$ (4%).

Yield: 20.5 mg, 139.1 µmol, 93%; 99% D for δ 6.56.

^{1}H-NMR Reference **24**

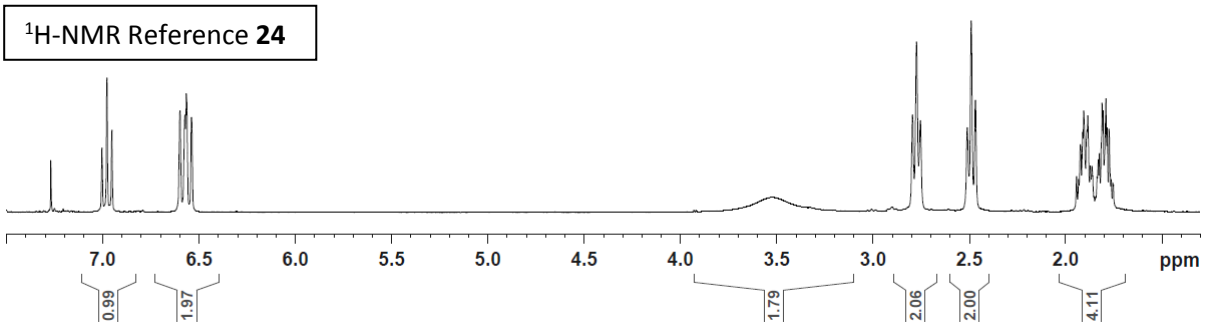

^{1}H-NMR HIE reaction **24**

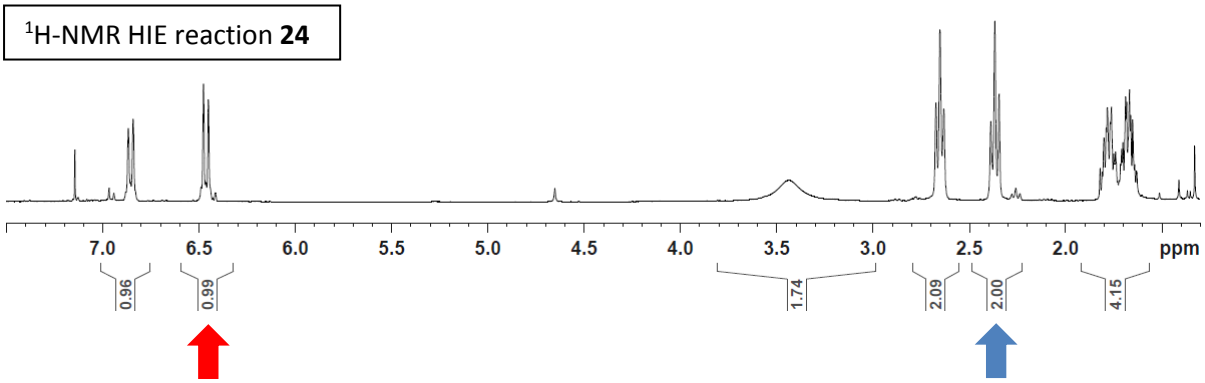

Aniline **25**

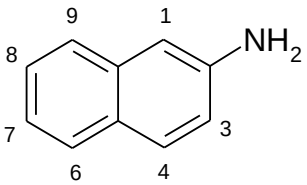

25

Molecular Weight =143.1899
Molecular Formula =C10H9N

^{1}H NMR (300 MHz, MeOD): δ 7.69 (m, 2H, $CH_{(4)}$ and CH phenyl), 7.61 (m, 1H, CH phenyl), 7.38 (m, 1H, CH phenyl), 7.22 (m, 1H, CH phenyl), 7.00 (s, 1H, $CH_{(1)}$), 6.96 (m, 1H, $CH_{(3)}$), 3.80 (br s, 2H, NH_2) ppm. Incorporation expected at δ 7.00 and 6.96 (red arrow). Determined against integral at δ 7.38 (blue arrow).

General method A: 21.4 mg (150.0 µmol) **25**; 1.5 mg (6.0 µmol, 4 mol%) IrICy(0.125NHC) **3b**, THF (3 mL), 55 °C, 3h.

LC-MS (positive ESI): m/z 144.1 $[M+H]^+$ (3%), 145.1 $[M(1D)+H]^+$ (38%), 146.1 $[M(2D)+H]^+$ (48%), 147.1 $[M(3D)+H]^+$ (9%), 148.1 $[M(4D)+H]^+$ (2%).

Yield: 20.3 mg, 142.2 µmol, 81%; 58% D for δ 7.00 and 87% D for δ 6.96.

^{1}H-NMR Reference **25**

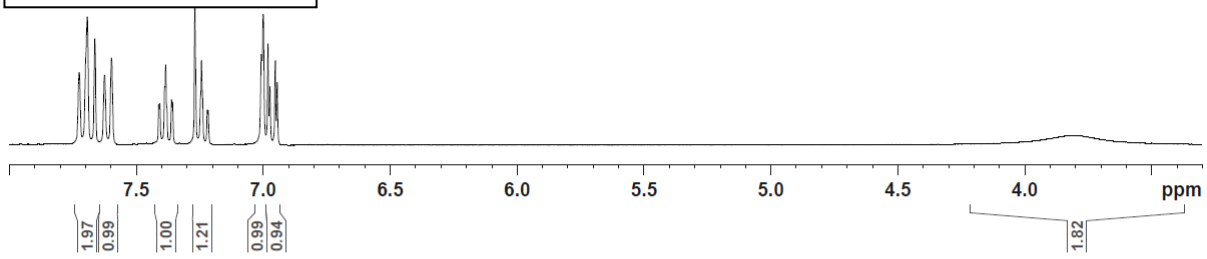

^{1}H-NMR HIE reaction **25**

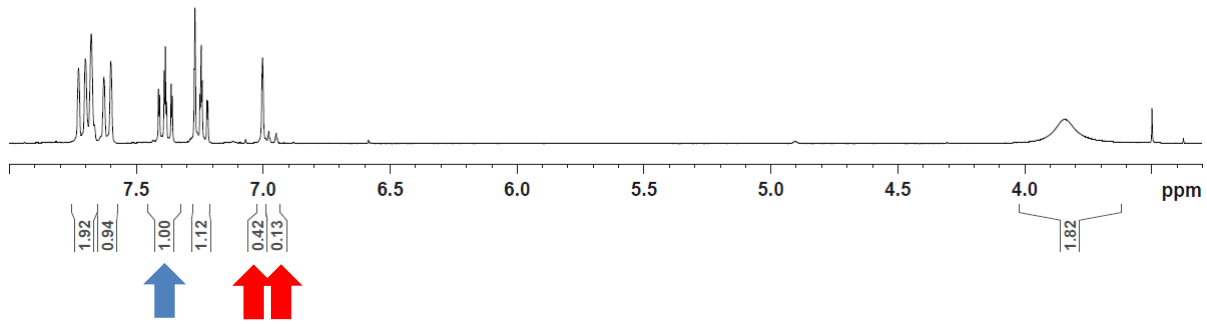

Aniline **26**

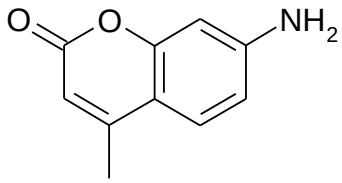

26

Molecular Weight =175.1887
Molecular Formula =C10H9NO2

^{1}H NMR (300 MHz, MeOD): δ 7.48 (d, ^3J = 8.7 Hz, 1H, CH *meta*-NH_2), 6.67 (dd, ^3J = 8.7 Hz and 2.5 Hz, 1H, CH *ortho*-NH_2), 6.51 (s, 1H, CH *ortho*-NH_2), 5.95 (s, 1H, CH alkene), 2.39 (s, 3H, CH_3) ppm. Incorporation expected at δ 6.67 (red arrow). Determined against integral at δ 5.95 (blue arrow).

General method A: 26.0 mg (150.0 µmol) **26**; 1.5 mg (6.0 µmol, 4 mol%) IrICy(0.125NHC) **3b**, THF (3 mL), 55 °C, 3h.

LC-MS (positive ESI): m/z 176.1 $[M+H]^+$ (42%), 177.1 $[M(1D)+H]^+$ (53%), 178.1 $[M(2D)+H]^+$ (5%).

Yield: 23.1 mg, 132.0 µmol, 89%; 58% D for δ 6.67.

^{1}H-NMR Reference **26**

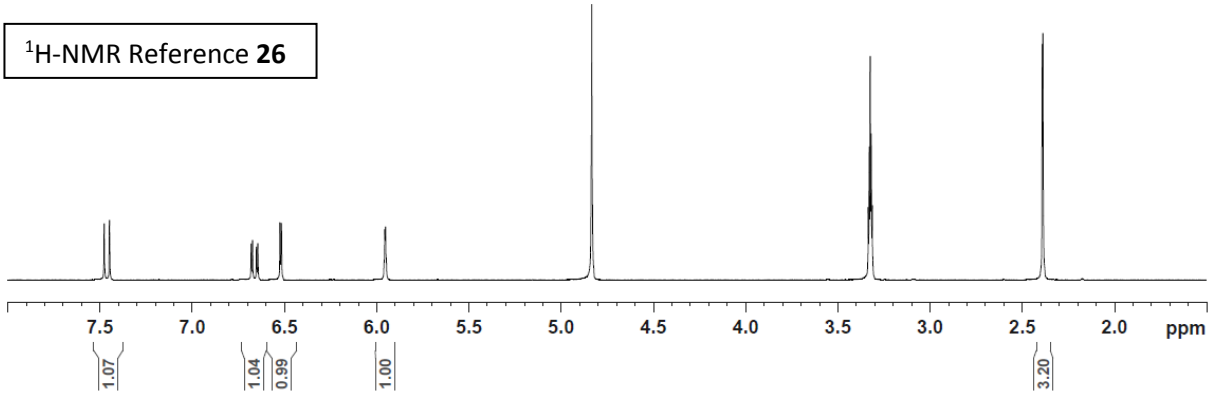

^{1}H-NMR HIE reaction **26**

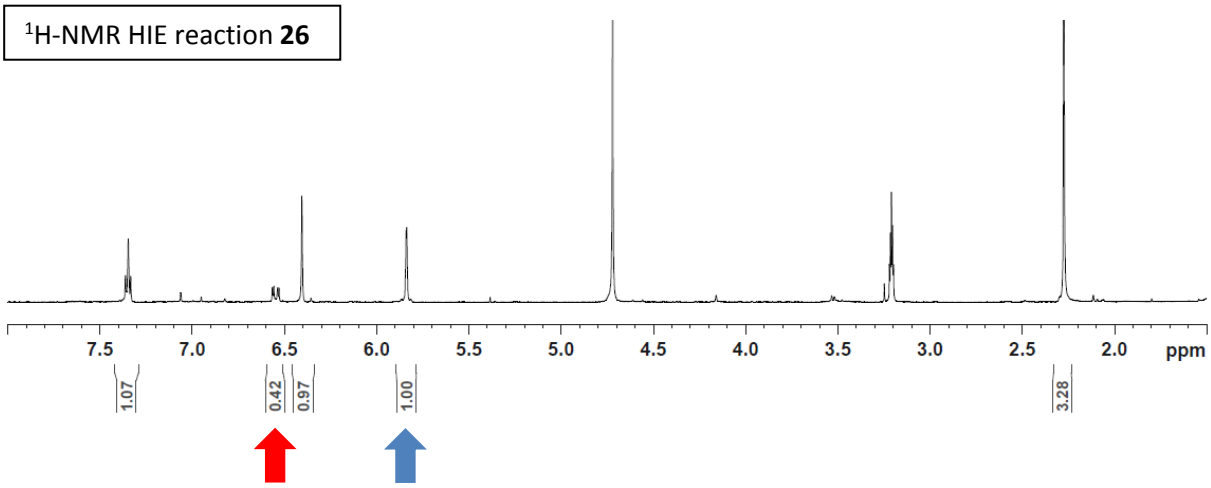

Aniline **27**

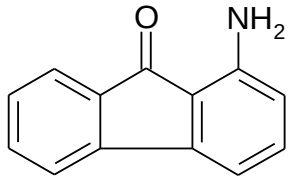

Molecular Weight =195.2228
Molecular Formula =C13H9NO

27

^{1}H NMR (300 MHz, MeOD): δ 7.63 (m, 1H, CH phenyl), 7.48 (m, 2H, 2 CH phenyl), 7.28 (m, 1H, CH phenyl), 7.23 (m, 1H, CH phenyl), 6.86 (d, ^3J = 8.6 Hz, 1H, CH *meta*-NH_2), 6.51 (d, ^3J = 8.6 Hz, 1H, CH *ortho*-NH_2), 5.51 (br s, 2H, NH_2) ppm. Incorporation expected at δ 6.51 (red arrow). Determined against integral at δ 5.51 (blue arrow).

General method A: 29.2 mg (150.0 µmol) **27**; 1.5 mg (6.0 µmol, 4 mol%) IrICy(0.125NHC) **3b**, THF (3 mL), 55 °C, 3h.

LC-MS (positive ESI): m/z 196.2 $[M+H]^+$ (39%), 197.2$[M(1D)+H]^+$ (55%), 198.2 $[M(2D)+H]^+$ (6%).

Yield: 28.9 mg, 148.2 µmol, 99%; 60% D for δ 6.51.

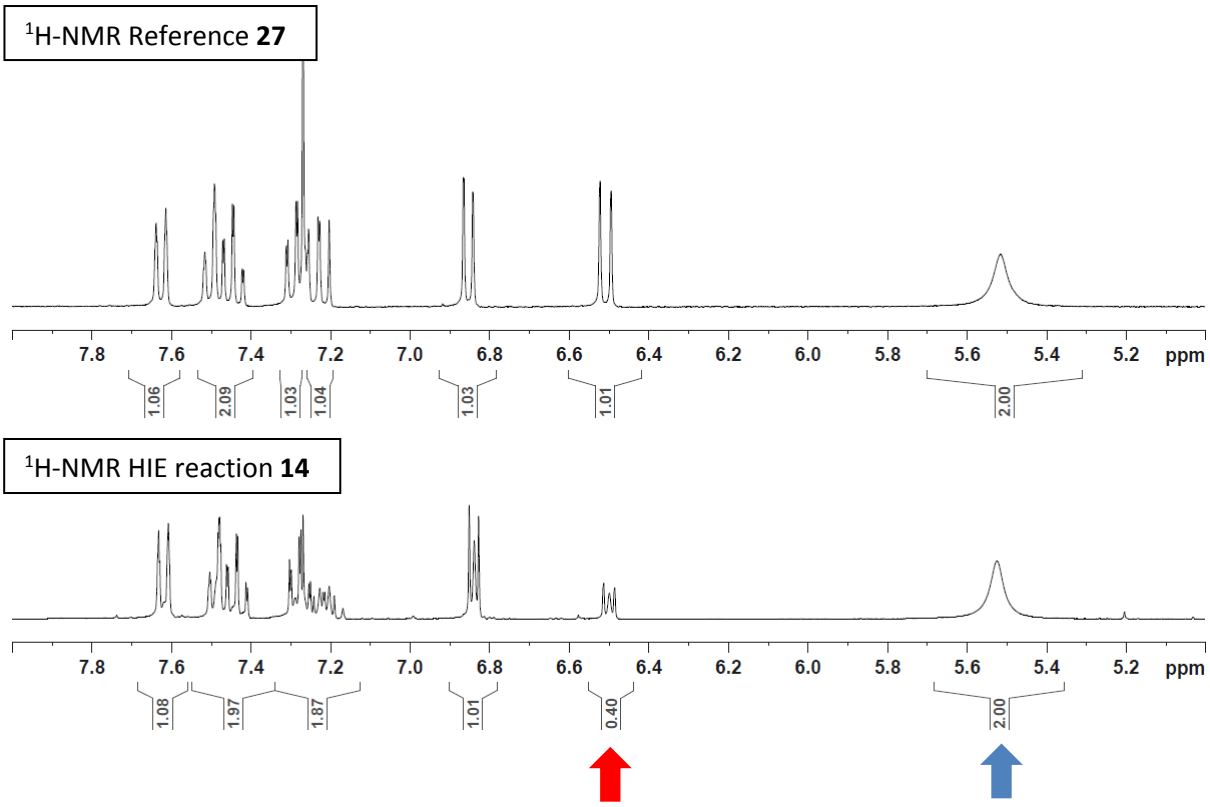

Aniline **28**

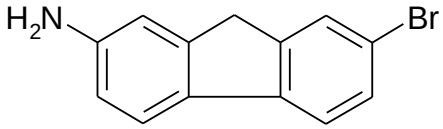

Molecular Weight =260.1354
Molecular Formula =C13H10BrN

28

^{1}H NMR (300 MHz, MeOD): δ 7.58 (s, 1H, CH phenyl), 7.53 (m, 1H, CH phenyl), 7.48 (m, 1H, CH phenyl), 7.43 (m, 1H, CH phenyl), 6.86 (s, 1H, CH *ortho*-NH_2), 6.71 (m, 1H, CH *ortho*-NH_2), 3.79 (br s, 4H, CH_2 and NH_2) ppm. Incorporation expected at δ 6.86 and 6.71 (red arrow). Determined against integral at δ 7.58 (blue arrow).

General method A: 39.0 mg (150.0 µmol) **28**; 1.5 mg (6.0 µmol, 4 mol%) IrICy(0.125NHC) **3b**, THF (3 mL), 55 °C, 3h.

LC-MS (positive ESI): no interpretation because of the natural isotopes of the Br.

Yield: 35.1 mg, 135 µmol, 90%; 92% D for δ 6.86 and 92% D for δ 6.71.

^{1}H-NMR Reference **28**

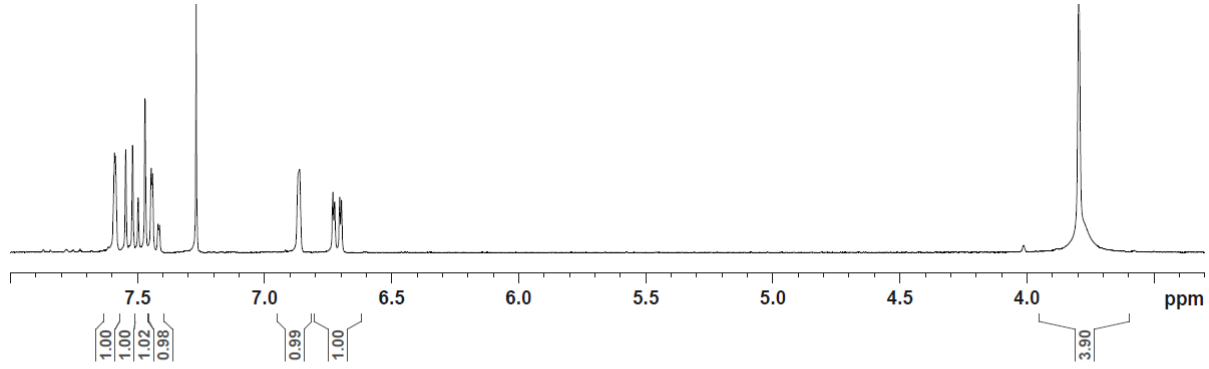

^{1}H-NMR HIE reaction **28**

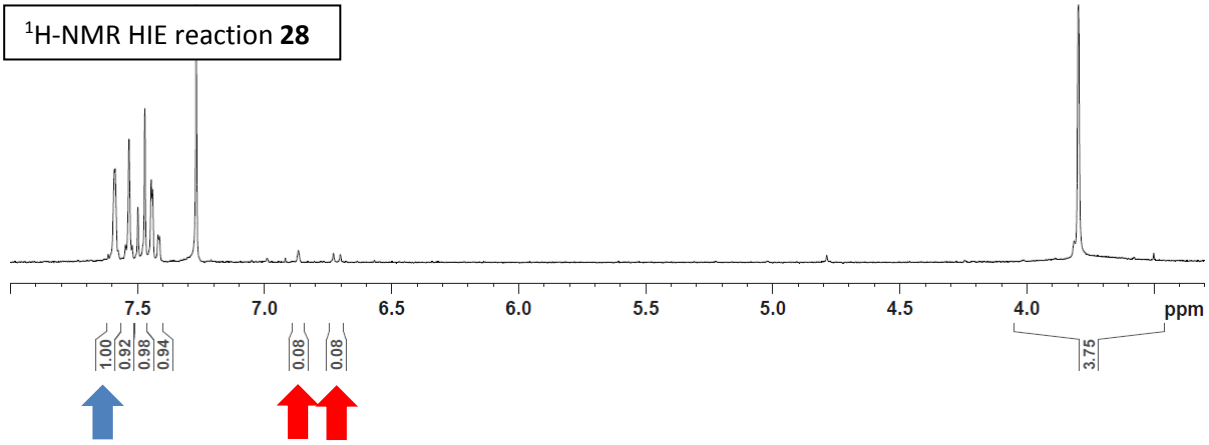

Aniline **29**

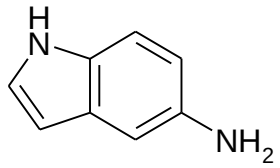

Molecular Weight =132.1664
Molecular Formula =C8H8N2

29

^{1}H NMR (300 MHz, MeOD): δ 7.99 (br s, 1H, NH), 7.21 (d, ^3J = 8.1 Hz, 1H, CH *meta*-NH_2), 7.14 (m, 1H, CH alkene *ortho*-NH), 6.96 (sd, ^3J = 1.1 Hz, 1H, CH *ortho*-NH_2), 6.68 (dd, ^3J = 8.1 Hz and 1.1 Hz, 1H, CH *ortho*-NH_2), 6.39 (m, 1H, CH alkene), 3.49 (br s, 2H, NH_2) ppm. Incorporation expected at δ 7.14, 6.96 and 6.68 (red arrow). Determined against integral at δ 6.39 (blue arrow).

General method A: 19.8 mg (150.0 µmol) **29**; 1.5 mg (6.0 µmol, 4 mol%) IrICy(0.125NHC) **3b**, THF (3 mL), 55 °C, 3h.

LC-MS (positive ESI): m/z 134.1 $[M(1D)+H]^+$ (24%), 135.1 $[M(2D)+H]^+$ (41%) 136.1 $[M(3D)+H]^+$ (29%), 137.1 $[M(4)+H]^+$ (6%).

Yield: 17.6 mg, 133.5 µmol, 89%; 61% D for δ 7.14, 77% D for δ 6.96 and 75% D for δ 6.68.

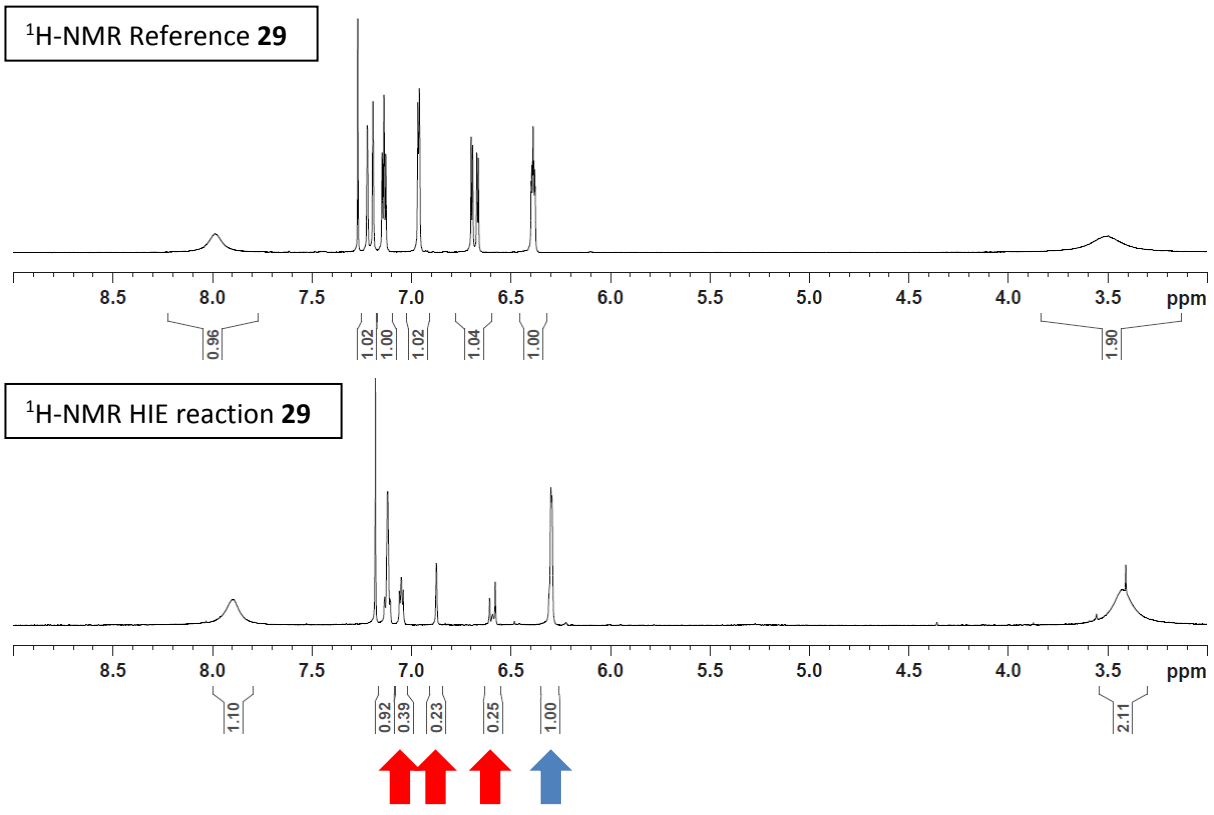

Aniline **30**

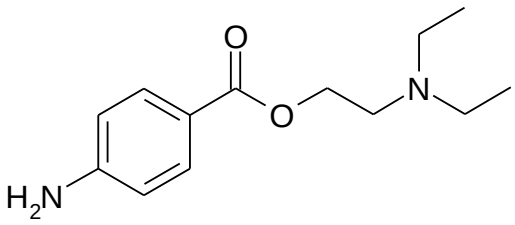

30

Molecular Weight =236.3165
Molecular Formula =C13H20N2O2

^{1}H NMR (300 MHz, MeOD): δ 7.85 (d, ^3J = 8.7 Hz, 2H, CH_2 *ortho*-ester), 6.64 (d, ^3J = 8.7 Hz, 2H, CH_2 *ortho*-NH_2), 4.34 (t, ^3J = 6.4 Hz, 2H, OCH_2), 4.04 (br s, 2H, NH_2), 2.83 (t, ^3J = 6.4 Hz, 2H, CH_2-N), 2.63 (q, ^3J = 7.1 Hz, 4H, 2xCH_2 Ethyl), 1.08 (t, ^3J = 7.1 Hz, 6H, 2xCH_3 Ethyl) ppm. Incorporation expected at δ 6.64 (red arrow). Determined against integral at δ 1.08 (blue arrow).

General method A: 35.4 mg (150.0 µmol) **30**; 1.5 mg (6.0 µmol, 4 mol%) IrICy(0.125NHC) **3b**, THF (3 mL), 55 °C, 3h.

LC-MS (positive ESI): m/z 237.2 $[M+H]^+$ (50%), 238.2 $[M(1D)+H]^+$ (33%), 239.1 $[M(2D)+H]^+$ (17%).

Yield: 34.3 mg, 145.5 µmol, 97%; 25% D for δ 6.64.

^{1}H-NMR Reference **30**

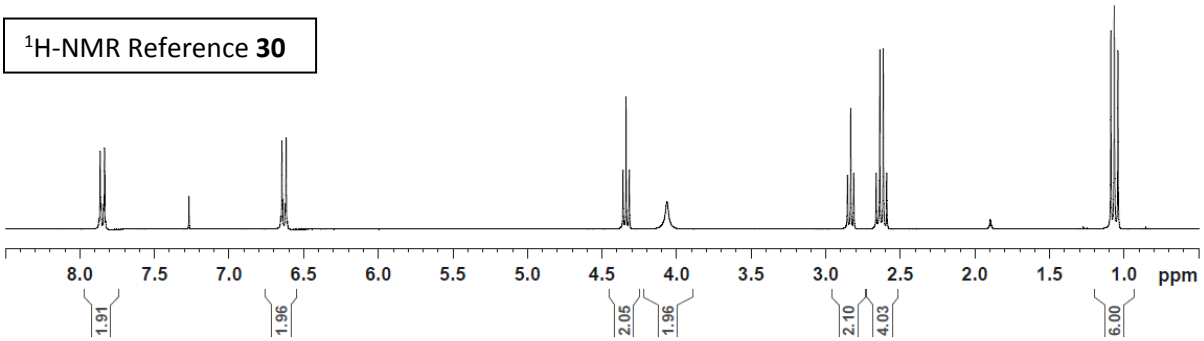

^{1}H-NMR HIE reaction **30**

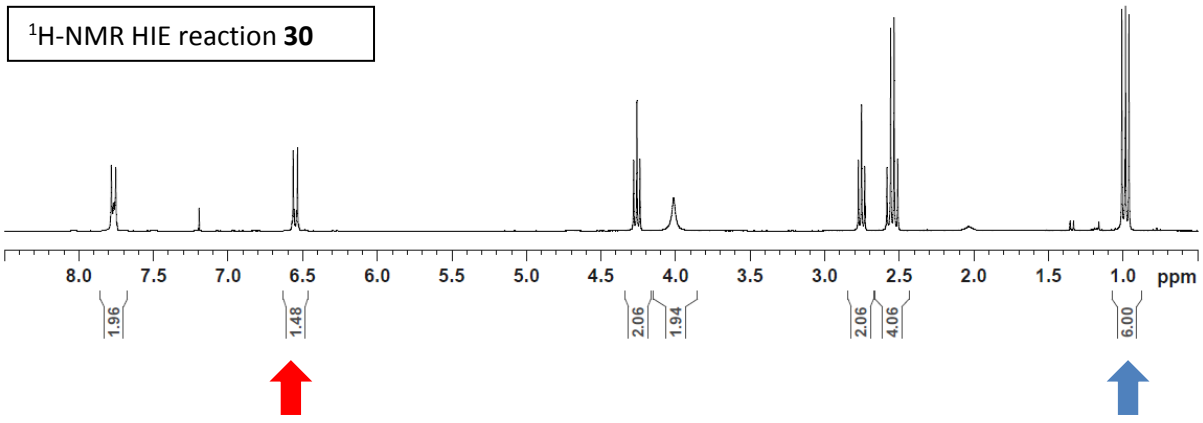

General method B: 35.4 mg (150.0 µmol) **30**; 1.5 mg (6.0 µmol, 4 mol%) IrICy(0.125NHC) **3b**, THF/D_2O (1:1) (3 mL), 80 °C, 3h.

LC-MS (positive ESI): m/z 239.1 $[M(2D)+H]^+$ (61%), 240.3 $[M(3D)+H]^+$ (26%), 241.2 $[M(4D)+H]^+$ (13%).

Yield: 32.5 mg, 138.0 µmol, 92%; 97% D for δ 6.64.

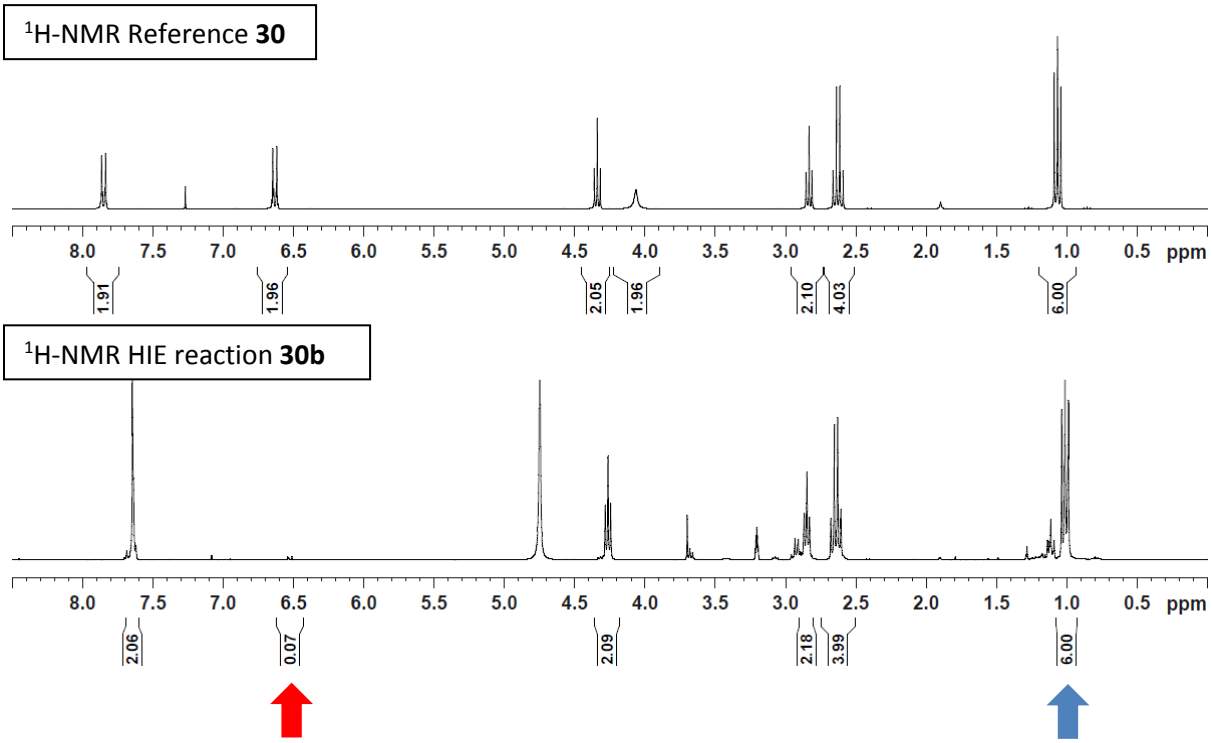

Aniline **31**

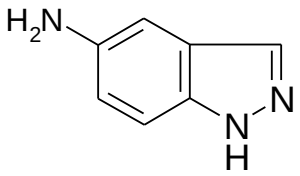

Molecular Weight =133.1539
Molecular Formula =C7H7N3

31

^{1}H NMR (300 MHz, MeOD): δ 7.80 (s, 1H, CH alkene), 7.34 (d, ^3J = 8.7 Hz, 1H, CH *meta*-NH_2), 7.03 (d, ^3J = 2.3 Hz, 1H, CH *ortho*-NH_2), 6.98 (dd, ^3J = 8.7 Hz and 2.3 Hz, 1H, CH *ortho*-NH_2) ppm. Incorporation expected at δ 7.80, 7.03 and 6.98 (red arrow). Determined against integral at δ 7.34 (blue arrow).

General method B: 20.0 mg (150.0 µmol) **31**; 1.5 mg (6.0 µmol, 4 mol%) IrICy(0.125NHC) **3b**, THF/D_2O (1:1) (3 mL), 80 °C, 3h.

LC-MS (positive ESI): m/z 134.1 $[M+H]^+$ (45%), 135.1 $[M(1D)+H]^+$ (37%), 136.1 $[M(2D)+H]^+$ (15%), 137.1 $[M(3D)+H]^+$ (3%).

Yield: 17.8 mg, 133.8 µmol, 89%; 25% D for δ 7.80, 18% D for δ 7.03 and 28% D for δ 6.98.

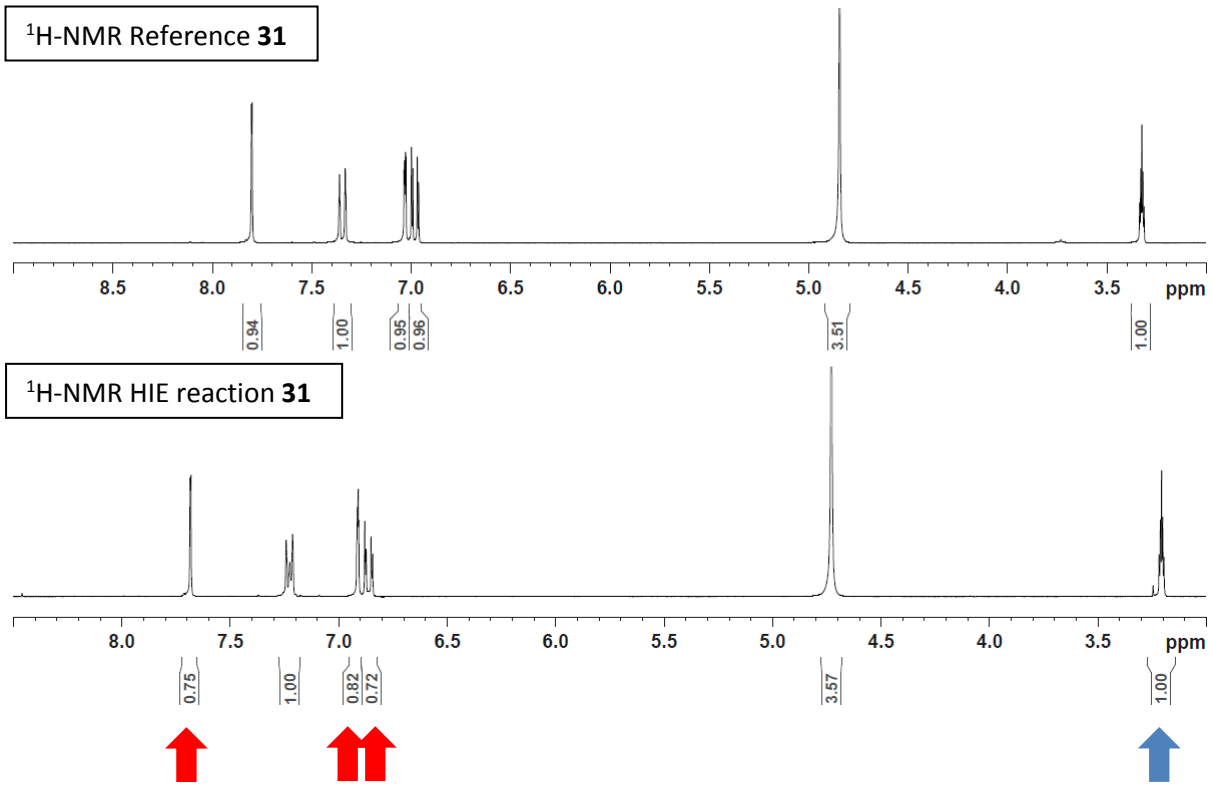

General method A: no deuterium incorporation.

Aniline **32**

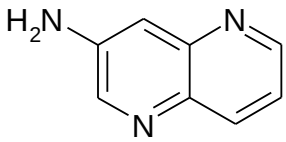

Molecular Weight =145.1651
Molecular Formula =C8H7N3

32

^{1}H NMR (300 MHz, MeOD): δ 8.83 (m, 1H, CH *ortho*-N), 8.55 (d, ^3J = 2.0 Hz, 1H, CH *ortho*-NH_2), 8.25 (dd, ^3J = 6.5 Hz and 1.8 Hz, 1H, CH *para*-N), 7.46 (d, ^3J = 2.0 Hz, 1H, CH *ortho*-NH_2), 7.38 (m, 1H, CH *meta*-NH_2), 4.16 (br s, 2H, NH_2) ppm. Incorporation expected at δ 8.83, 8.55 and 8.25 (red arrow). Determined against integral at δ 7.46 (blue arrow).

General method B: 21.8 mg (150.0 µmol) **32**, 1.5 mg (6.0 µmol, 4 mol%) IrICy(0.125NHC) **3b**, THF/D_2O (1:1) (3 mL), 80 °C, 3h.

LC-MS (positive ESI): m/z 146.1 $[M+H]^+$ (34%), 147.1 $[M(1D)+H]^+$ (39%), 148.1 $[M(2D)+H]^+$ (20%), 149.1 $[M(3D)+H]^+$ (7%).

Yield: 17.5 mg, 120.2 µmol, 80%; 30% D for δ 8.83, 15% D for δ 8.55 and 10% D for δ 8.25.

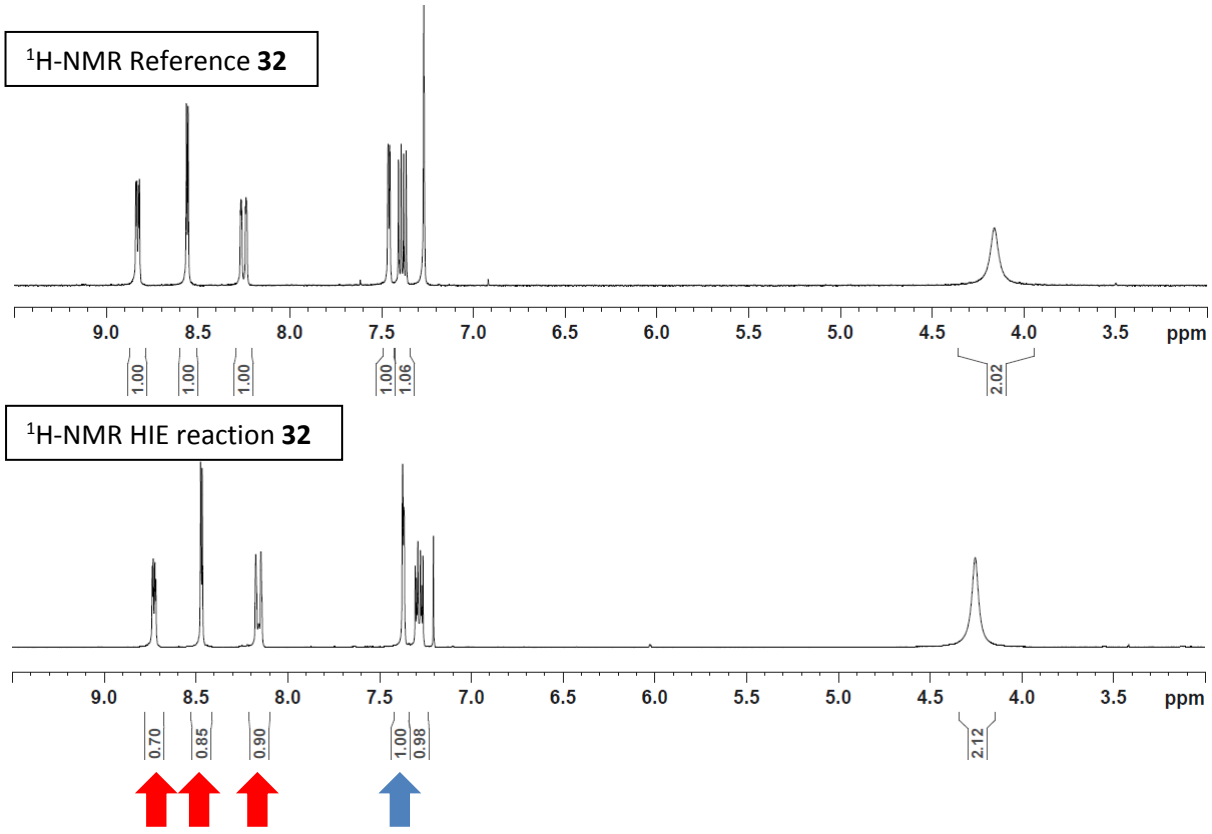

General method A: no deuterium incorporation.

Aniline **33**

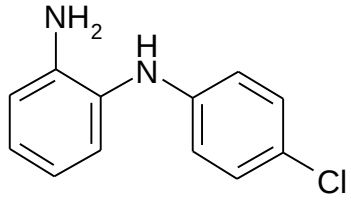

33

Molecular Weight =218.6879
Molecular Formula =C12H11ClN2

^{1}H NMR (300 MHz, MeOD): δ 7.18 (d, ^3J = 8.1 Hz, 2H, 2 CH *ortho*-Cl), 7.09 (m, 2H, CH *meta*-NH_2 and *para*-NH_2), 6.80 (m, 2H, CH *ortho*-NH_2 and *meta*-NH_2), 6.67 (d, ^3J = 8.1 Hz, 2H, 2 CH *ortho*-NH), 5.16 (br s, 1H, NH), 3.76 (br s, 2H, NH_2) ppm. Incorporation expected at δ 6.80 (red arrow). Determined against integral at δ 5.16 (blue arrow).

General method B: 32.8 mg (150.0 µmol) **33**; 1.5 mg (6.0 µmol, 4 mol%) IrICy(0.125NHC) **3b**, THF/D_2O (1:1) (3 mL), 80 °C, 3h.

LC-MS (positive ESI): no interpretation because of the natural isotopes of the Br.

Yield: 25.6 mg, 117.4 µmol, 78%; 53% D for δ 6.80.

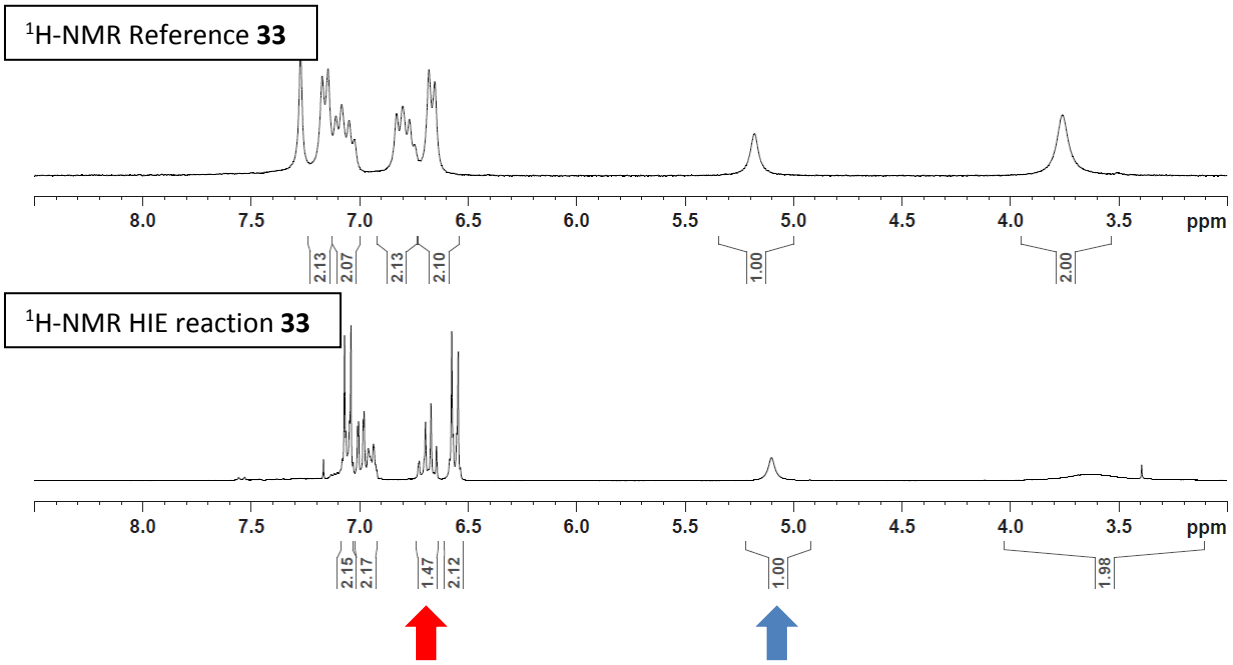

General method A: no deuterium incorporation.

Aniline **34**

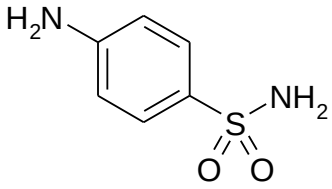

Molecular Weight =172.2069
Molecular Formula =C6H8N2O2S

34

^{1}H NMR (300 MHz, MeOD): δ 7.60 (d, ^3J = 8.7 Hz, 2H, 2 CH *ortho*-SO_2NH_2), 6.70 (d, ^3J = 8.7 Hz, 2H, 2 CH *ortho*-NH_2) ppm. Incorporation expected at δ 6.70 (red arrow). Determined against integral at δ 7.60 (blue arrow).

General method B: 25.8 mg (150.0 µmol) **34**; 1.5 mg (6.0 µmol, 4 mol%) IrICy(0.125NHC) **3b**, THF/D_2O (1:1) (3 mL), 80 °C, 3h.

LC-MS (positive ESI): m/z 174.1 $[M(1D)+H]^+$ (12%), 175.0 $[M(2D)+H]^+$ (82%), 176.1 $[M(3D)+H]^+$ (6%).

Yield: 21.9 mg, 127.5 µmol, 85%; 81% D for δ 6.70.

^{1}H-NMR Reference **34**

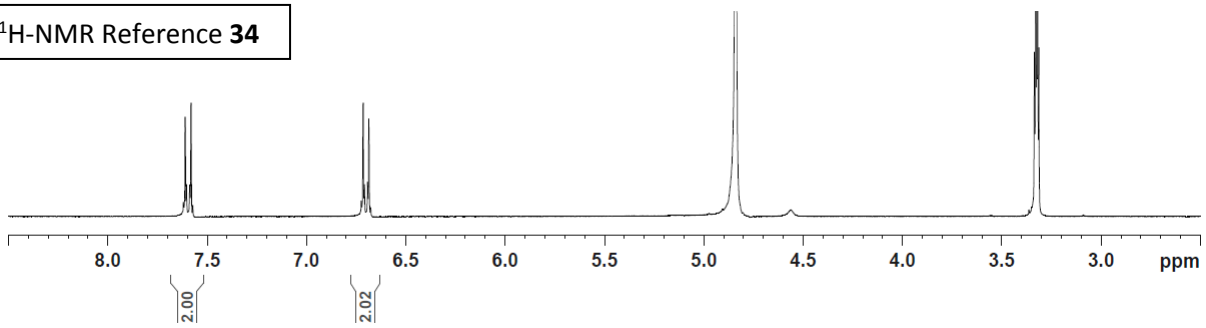

^{1}H-NMR HIE reaction **34**

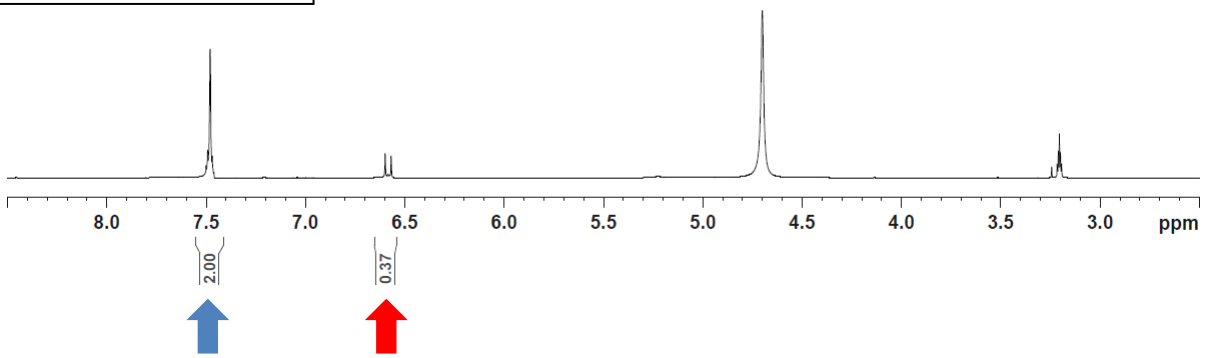

General method A: no deuterium incorporation.

Aniline **35**

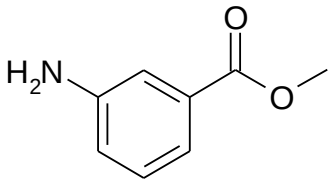

Molecular Weight =151.1664
Molecular Formula =C8H9NO2

35

^{1}H NMR (300 MHz, MeOD): δ 7.36 (m, 1H, CH *ortho*-NH_2), 7.31 (m, 1H,CH *ortho*-CO_2Me), 7.18 (m, 1H, CH *meta*-NH_2), 6.92 (m, 1H, CH *ortho*-NH_2), 3.88 (s, 3H, OCH_3) ppm. Incorporation expected at δ 6.92 (red arrow). Determined against integral at δ 3.88 (blue arrow).

General method A: 22.6 mg (150.0 µmol) **35**; 1.5 mg (6.0 µmol, 4 mol%) IrICy(0.125NHC) **3b**, THF (3 mL), 55 °C, 3h.

LC-MS (positive ESI): m/z 152.1 $[M+H]^+$ (60%), 153.1 $[M(1D)+H]^+$ (36%), 154.1 $[M(2D)+H]^+$ (4%).

Yield: 21.0 mg, 139.1 µmol, 93%; 39% D for δ 6.92.

^{1}H-NMR Reference **35**

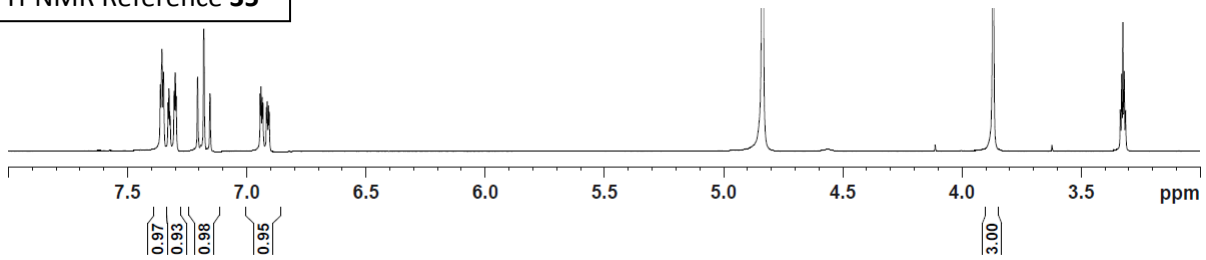

^{1}H-NMR HIE reaction **35**

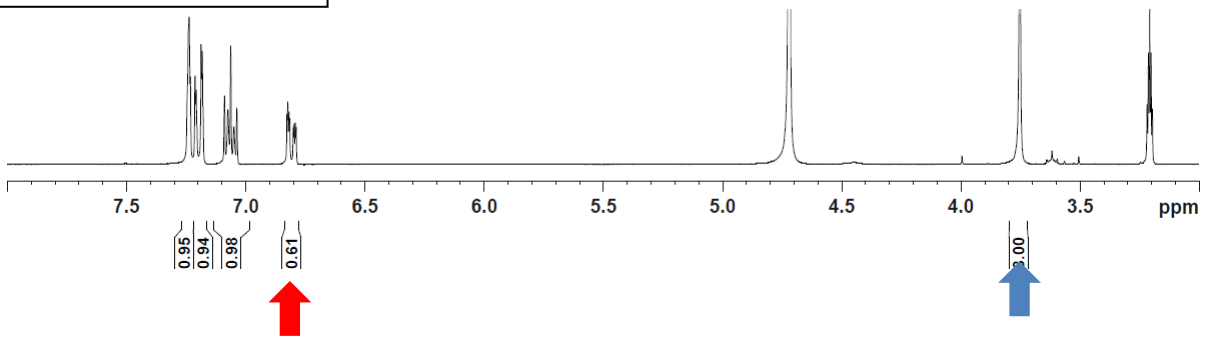

General method B: 22.6 mg (150.0 µmol) **35**; 1.5 mg (6.0 µmol, 4 mol%) IrICy(0.125NHC) **3b**, THF/D_2O (1:1) (3 mL), 80 °C, 3h.

LC-MS (positive ESI): m/z 153.1 $[M(1D)+H]^+$ (61%), 154.1 $[M(2D)+H]^+$ (34%), 155.1 $[M(3D)+H]^+$ (5%).

Yield: 19.9 mg, 131.7 µmol, 88%; 23% D for δ δ 7.36, 33% D for δ 7.18 and 99% D for δ 6.92.

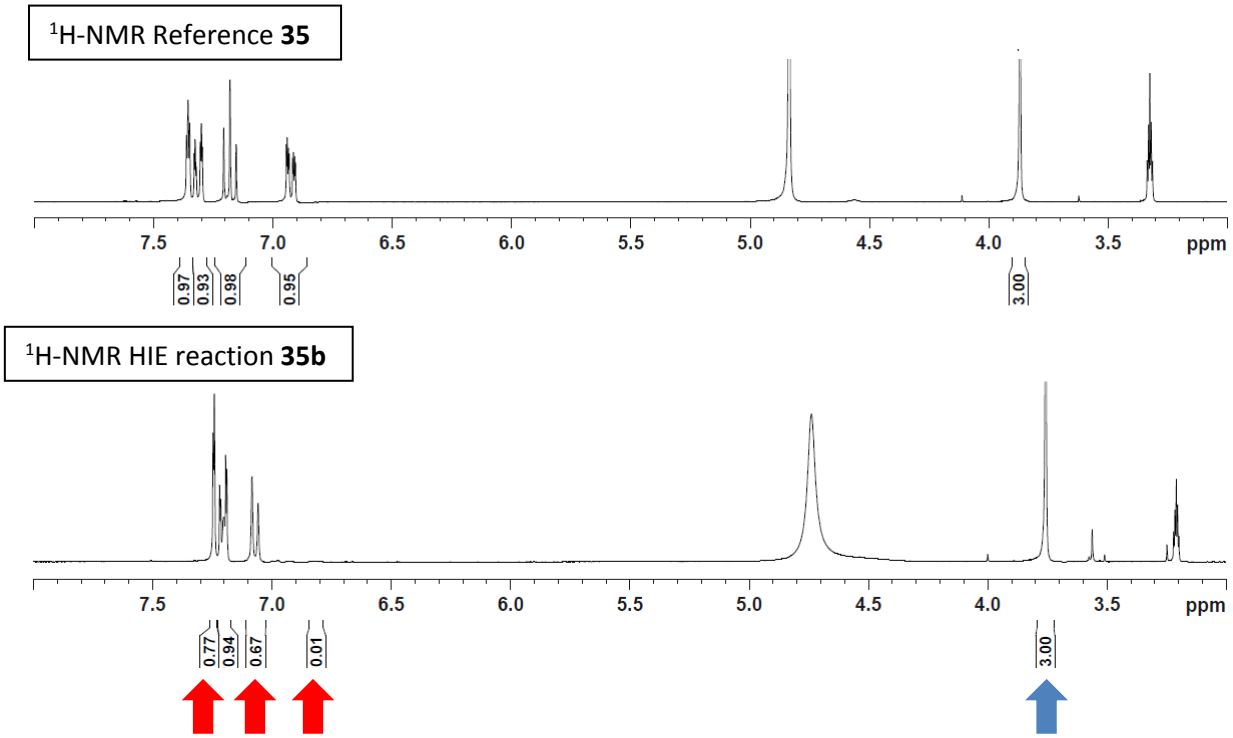

Aniline **36**

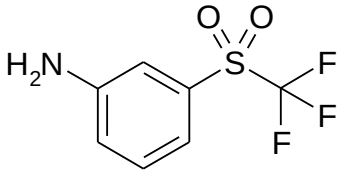

36

Molecular Weight =225.1906
Molecular Formula =C7H6F3NO2S

^{1}H NMR (300 MHz, MeOD): δ 7.41 (m, 1H, CH *meta*-NH_2), 7.27 (s, 1H, CH *ortho*-NH_2), 7.22 (m, 1H, CH *para*-NH_2), 7.13 (m, 1H, CH *ortho*-NH_2) ppm. Incorporation expected at δ 7.13 (red arrow). Determined against integral at δ 7.27 (blue arrow).

General method A: 33.7 mg (150.0 µmol) **36**; 1.5 mg (6.0 µmol, 4 mol%) IrICy(0.125NHC) **3b**, THF (3 mL), 55°C, 3h.

LC-MS (positive ESI): m/z 226.0 $[M+H]^+$ (61%), 227.1 $[M(1D)+H]^+$ (33%), 228.0 $[M(2D)+H]^+$ (6%).

Yield: 32.0 mg, 142.2 µmol, 95%; 33% D for δ 7.13.

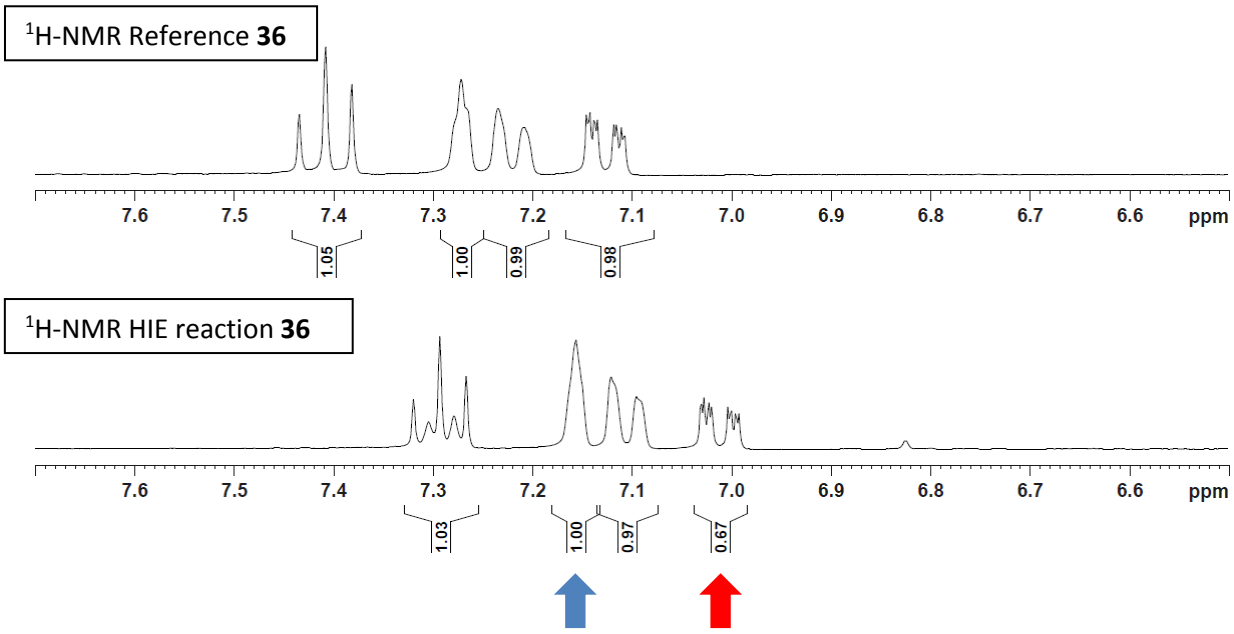

General method B: 33.7 mg (150.0 µmol) **36**; 1.5 mg (6.0 µmol, 4 mol%) IrICy(0.125NHC) **3b**, THF/D_2O (1:1) (3 mL), 80°C, 3h.

LC-MS (positive ESI): m/z 227.1 $[M(1D)+H]^+$ (67%), 228.0 $[M(2D)+H]^+$ (33%).

Yield: 29.3 mg, 130.3 µmol, 87%; 99% D for δ δ 7.13 and 23% D for δ 7.41.

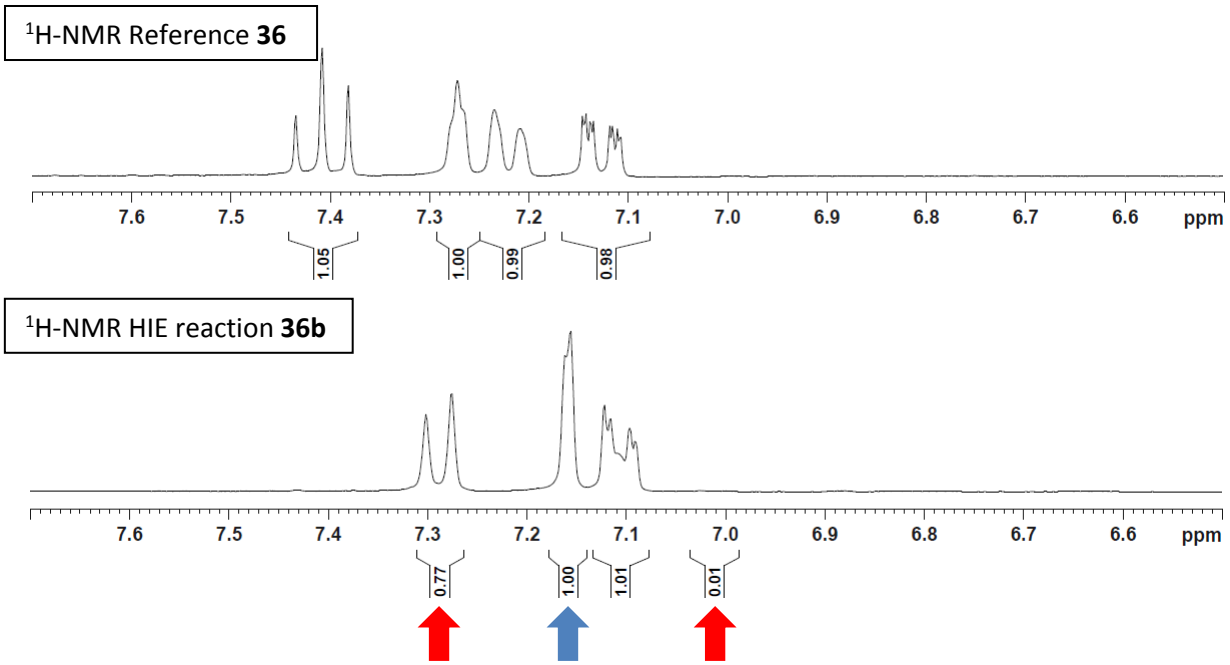

Aniline **37**

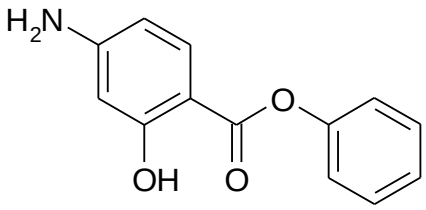

37

Molecular Weight =229.2375
Molecular Formula =C13H11NO3

^{1}H NMR (300 MHz, MeOD): δ 7.76 (d, ^3J = 9.1 Hz, 1H, CH *meta*-NH_2), 7.43 (m, 2H, CH_2 ester ring), 7.28 (m, 1H, CH ester ring), 7.19 (m, 2H, CH_2 ester ring), 6.26 (dd, ^3J = 9.1 Hz and 2.2 Hz, 1H, CH *ortho*-NH_2), 6.14 (d, ^3J = 2.2 Hz, 1H, CH *ortho*-OH) ppm. Incorporation expected at δ 6.26 and 6.14 (red arrow). Determined against integral at δ 7.76 (blue arrow).

General method B: 34.0 mg (150.0 µmol) **37**; 1.5 mg (6.0 µmol, 4 mol%) IrICy(0.125NHC) **3b**, THF/D_2O (1:1) (3 mL), 80°C, 3h.

LC-MS (positive ESI): m/z 230.2 $[M+H]^+$ (7%), 231.1 $[M(1D)+H]^+$ (57%), 232.1 $[M(2D)+H]^+$ (32%), 233.1 $[M(3D)+H]^+$ (4%).

Yield: 28.6 mg, 124.7 µmol, 84%; 64% D for δ 6.26 and 23% D for δ 6.14.

^{1}H-NMR Reference **37**

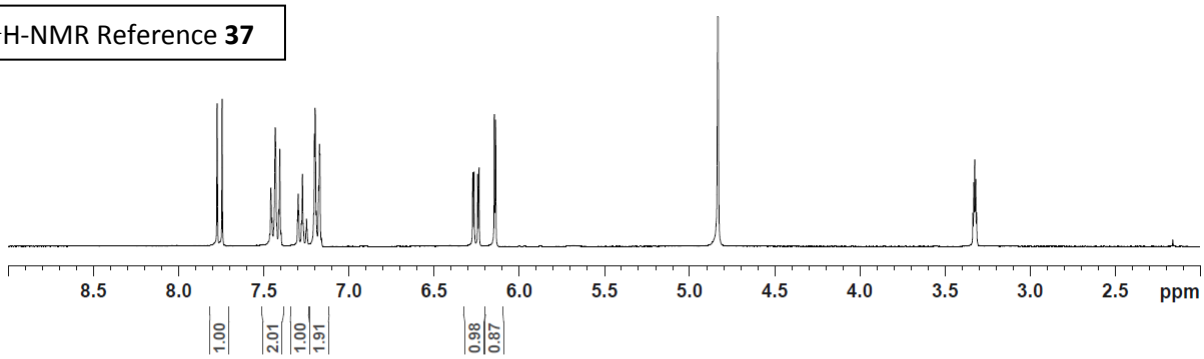

^{1}H-NMR HIE reaction **37**

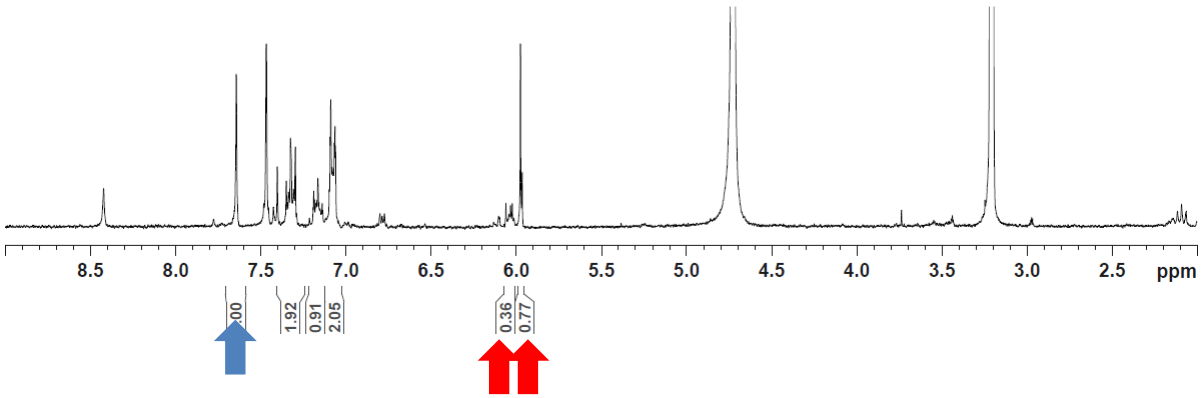

Aniline **38**

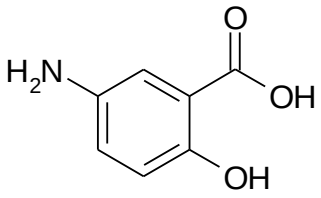

Molecular Weight =153.1387
Molecular Formula =C7H7NO3

38

^{1}H NMR (300 MHz, MeOD): δ 7.58 (d, ^3J = 3.1 Hz, 1H, CH *ortho*-COOH), 7.12 (dd, ^3J = 8.6 Hz and 3.1 Hz, 1H, CH *ortho*-NH_2), 6.84 (d, ^3J = 8.6 Hz, 1H, CH *meta*-NH_2) ppm. Incorporation expected at δ 7.12 (red arrow). Determined against integral at δ 6.84 (blue arrow).

General method B: 23.0 mg (150.0 µmol) **38**; 1.5 mg (6.0 µmol, 4 mol%) IrICy(0.125NHC) **3b**, THF/D_2O (1:1) (3 mL), 80°C, 3h.

LC-MS (positive ESI): m/z 154.1 $[M+H]^+$ (5%), 155.1 $[M(1D)+H]^+$ (91%), 156.1 $[M(2D)+H]^+$ (4%).

Yield: 17.7 mg, 116.0 µmol, 77%; 90% D for δ 7.12.

^{1}H-NMR Reference **38**

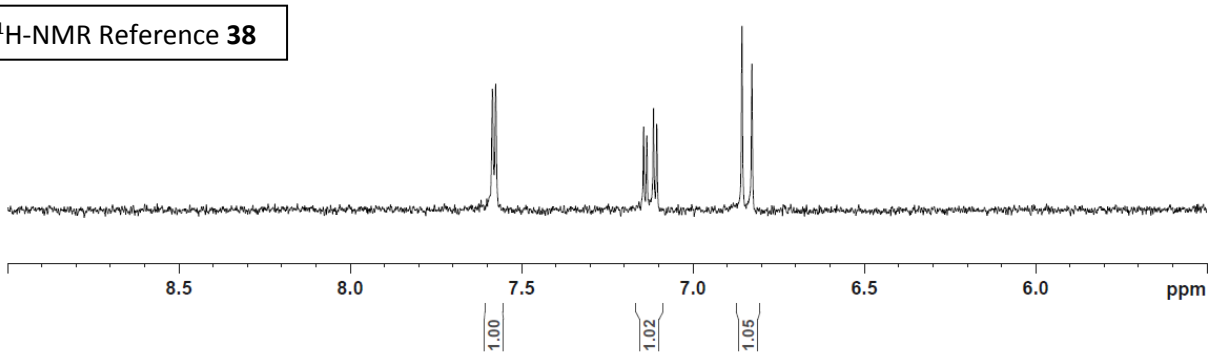

^{1}H-NMR HIE reaction **38**

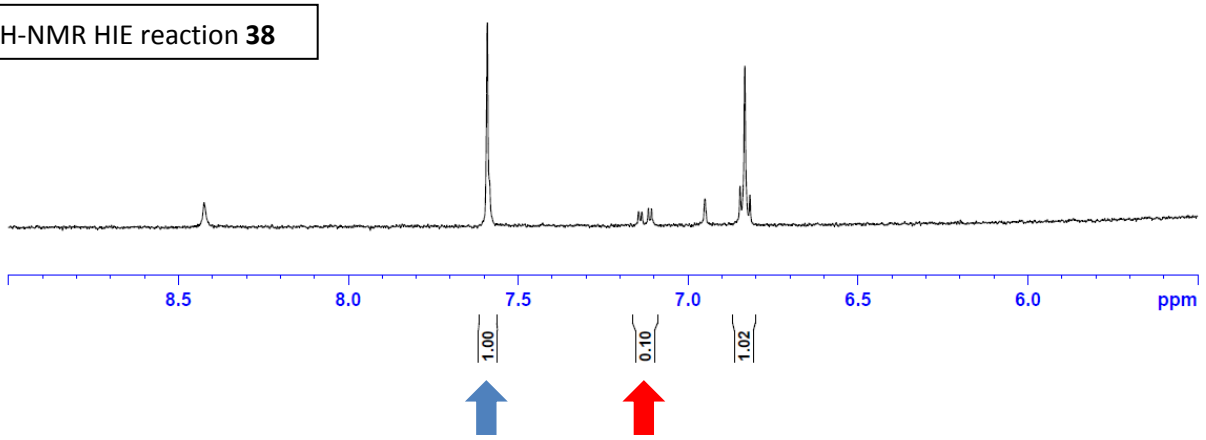

Aniline **39**

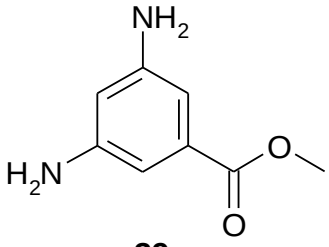

39

Molecular Weight =166.1811
Molecular Formula =C8H10N2O2

^{1}H NMR (300 MHz, MeOD): δ 6.76 (m, 2H, 2 CH *ortho*-COOMe), 6.33 (m, 1H, CH *ortho*-NH_2), 3.84 (s, 3H, CH_3) ppm. Incorporation expected at δ 6.33 (red arrow). Determined against integral at δ 3.84 (blue arrow).

General method A: 24.9 mg (150.0 µmol) **39**; 1.5 mg (6.0 µmol, 4 mol%) IrICy(0.125NHC) **3b**, THF (3 mL), 55°C, 3h.

LC-MS (positive ESI): m/z 167.1 $[M+H]^+$ (58%), 168.1 $[M(1D)+H]^+$ (32%), 169.1 $[M(2D)+H]^+$ (10%).

Yield: 21.4 mg, 129.0 µmol, 86%; 32% D for δ 6.33.

^{1}H-NMR Reference **39**

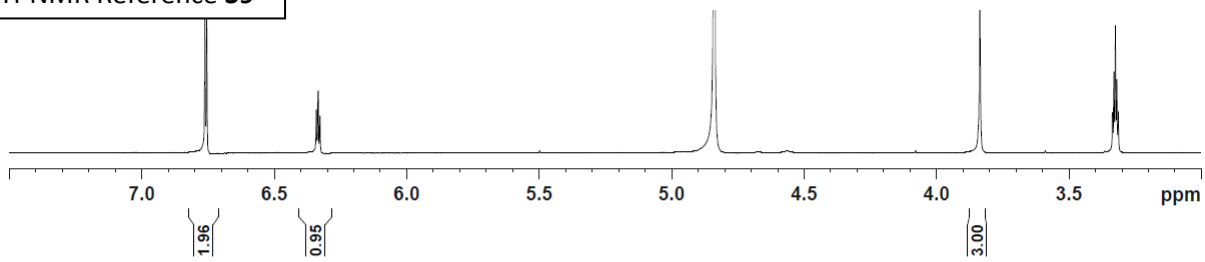

^{1}H-NMR HIE reaction **39**

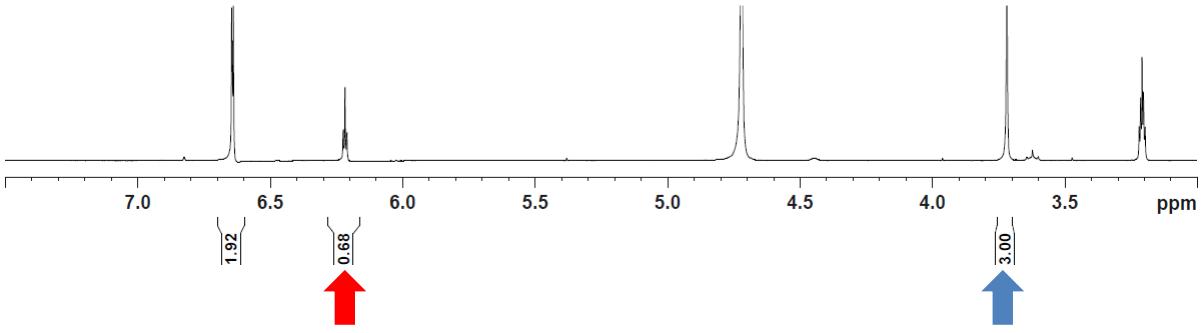

General method B: 24.9 mg (150.0 µmol) **39**; 1.5 mg (6.0 µmol, 4 mol%) IrICy(0.125NHC) **3b**, THF/D_2O (1:1) (3 mL), 80°C, 3h.

LC-MS (positive ESI): m/z 168.1 $[M(1D)+H]^+$ (73%), 169.1 $[M(2D)+H]^+$ (27%).

Yield: 18.7 mg, 112.6 µmol, 75%; 16% D for δ 6.76 and 99% D for δ 6.33.

^{1}H-NMR Reference **39**

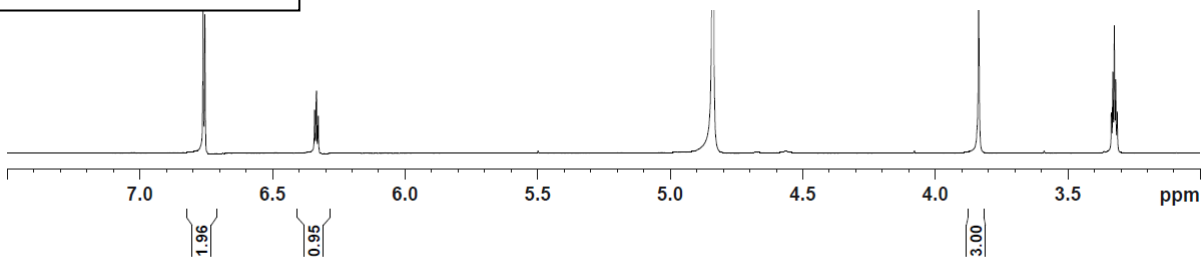

^{1}H-NMR HIE reaction **39b**

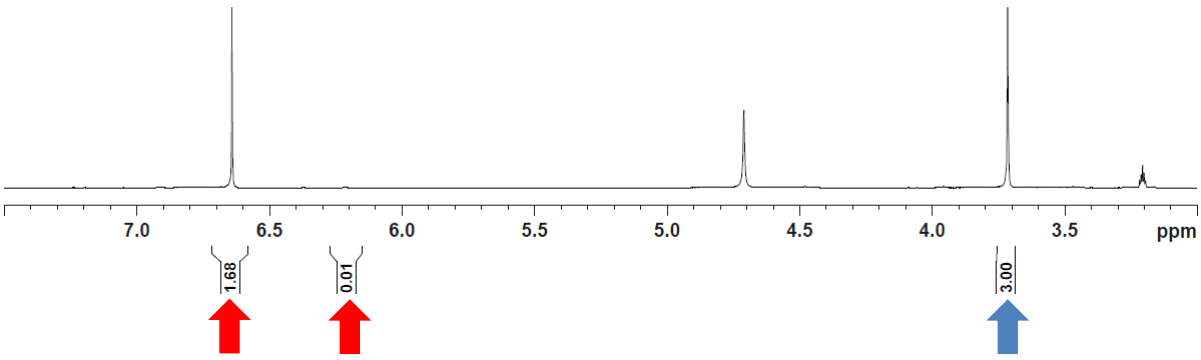

Aniline **40**

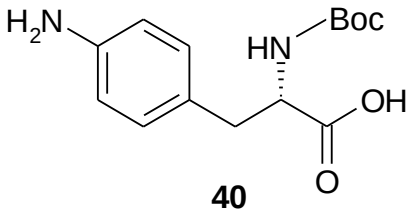

40

Molecular Weight =281.3345
Molecular Formula =C14H21N2O4

^{1}H NMR (300 MHz, MeOD): δ 6.97 (d, ^3J = 8.2 Hz, 2H, 2 CH *meta*-NH_2), 6.64 (d, ^3J = 8.2 Hz, 2H, 2 CH *ortho*-NH_2), 4.93 (br s, 1H, OH or NH), 4.50 (br s, 1H, CH), 3.66 (br s, 3H, NH_2 and OH or NH), 3.04 (m, 2H, CH_2), 1.43 (s, 9H, Boc) ppm. Incorporation expected at δ 6.64 (red arrow). Determined against integral at δ 1.43 (blue arrow).

General method B: 42.1 mg (150.0 µmol) **40**; 1.5 mg (6.0 µmol, 4 mol%) IrICy(0.125NHC) **3b**, THF/D_2O (1:1) (3 mL), 80°C, 3h.

LC-MS (positive ESI): m/z 182.1 $[M(1D)-Boc+H]^+$ (5%), 183.1 $[M(2D)-Boc+H]^+$ (90%), 184.1 $[M(3D)-Boc+H]^+$ (5%).

Yield: 35.4 mg, 125.9 µmol, 84%; 99% D for δ 6.64.

^{1}H-NMR Reference **40**

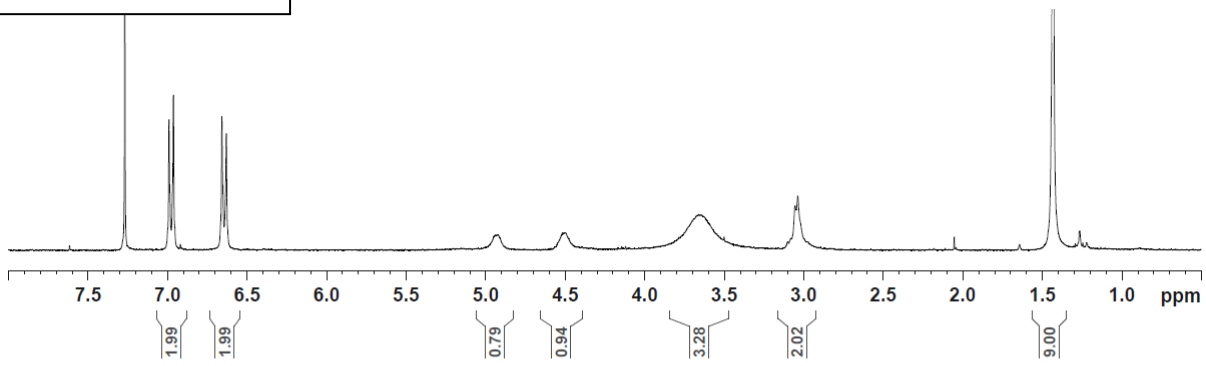

^{1}H-NMR HIE reaction **40**

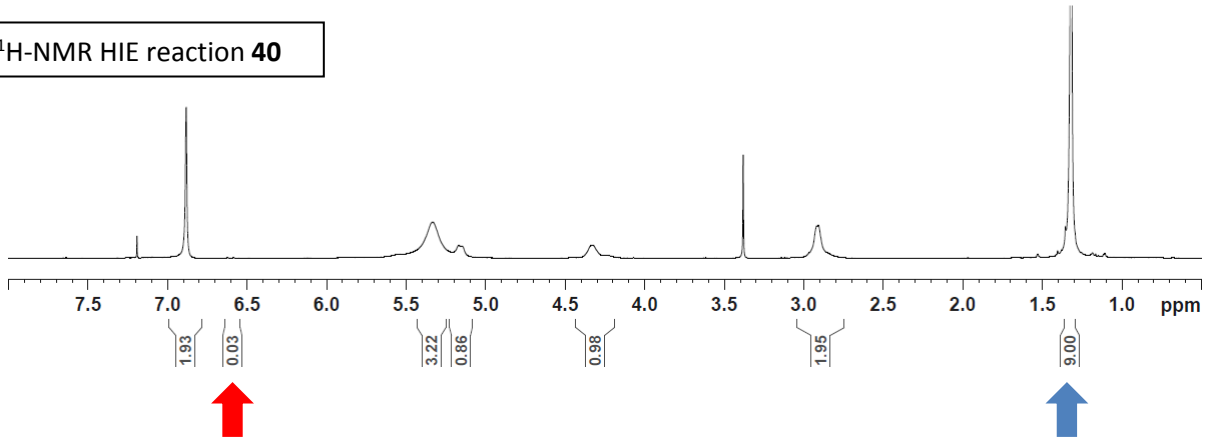

Aniline **41**

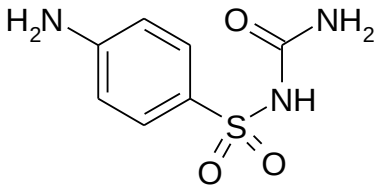

Molecular Weight =215.2321
Molecular Formula =C7H9N3O3S

41

^{1}H NMR (300 MHz, MeOD): δ 7.64 (d, ^3J = 8.8 Hz, 2H, 2 CH *meta*-NH_2), 6.69 (d, ^3J = 8.8 Hz, 2H, 2 CH *ortho*-NH_2) ppm. Incorporation expected at δ 6.69 (red arrow). Determined against integral at δ 7.64 (blue arrow).

General method B: 32.0 mg (150.0 µmol) **41**; 1.5 mg (6.0 µmol, 4 mol%) IrICy(0.125NHC) **3b**, THF/D_2O (1:1) (3 mL), 80°C, 3h.

LC-MS (positive ESI): m/z 216.1 $[M+H]^+$ (40%), 217.1 $[M(1D)+H]^+$ (55%), 218.0 $[M(2D)+H]^+$ (5%).

Yield: 25.6 mg, 119.0 µmol, 80%; 55% D for δ 6.69.

^{1}H-NMR Reference **41**

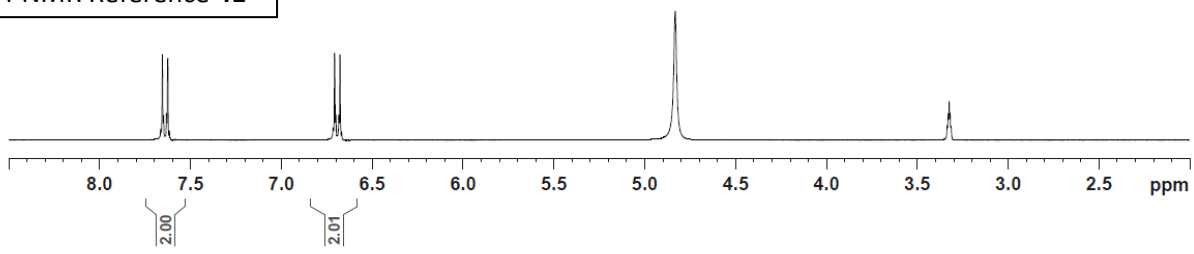

^{1}H-NMR HIE reaction **41**

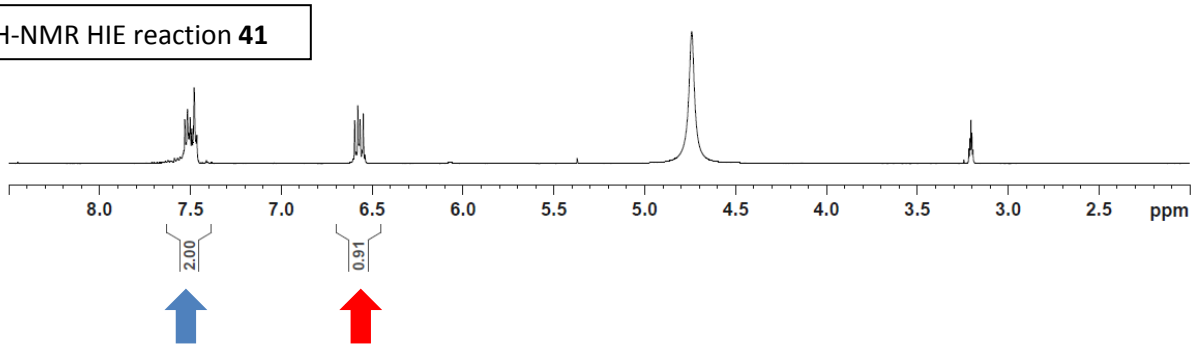

General method A: no deuterium incorporation.

Aniline **42**

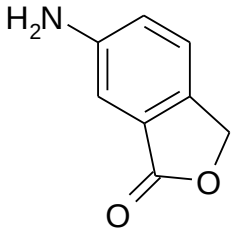

42

Molecular Weight =149.1505
Molecular Formula =C8H7NO2

^{1}H NMR (300 MHz, MeOD): δ 7.30 (m, 1H, CH *meta*-NH_2), 7.10 (m, 1H, CH *ortho*-NH_2), 7.07 (s, 1H, CH *ortho*-NH_2), 5.24 (s, 2H, CH_2) ppm. Incorporation expected at δ 7.10 (red arrow). Determined against integral at δ 5.24 (blue arrow).

General method A: 22.3 mg (150.0 µmol) **42**; 1.5 mg (6.0 µmol, 4 mol%) IrICy(0.125NHC) **3b**, THF (3 mL), 55°C, 3h.

LC-MS (positive ESI): m/z 150.1 $[M+H]^+$ (55%), 151.1 $[M(1D)+H]^+$ (45%), 152.0 $[M(2D)+H]^+$ (10%).

Yield: 21.9 mg, 147.0 µmol, 98%; 54% D for δ 7.10.

^{1}H-NMR Reference **42**

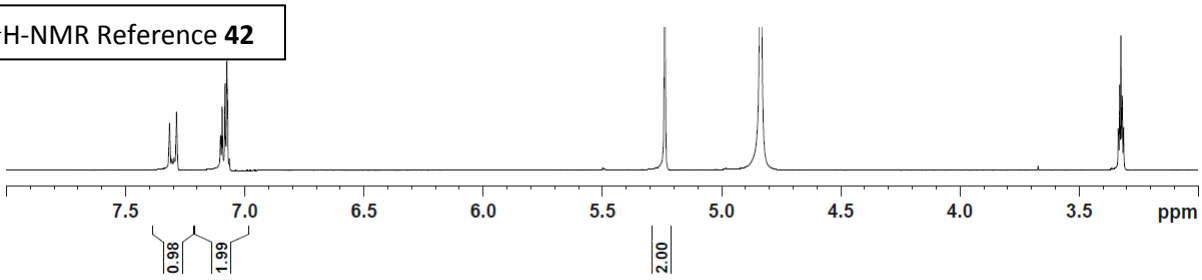

^{1}H-NMR HIE reaction **42**

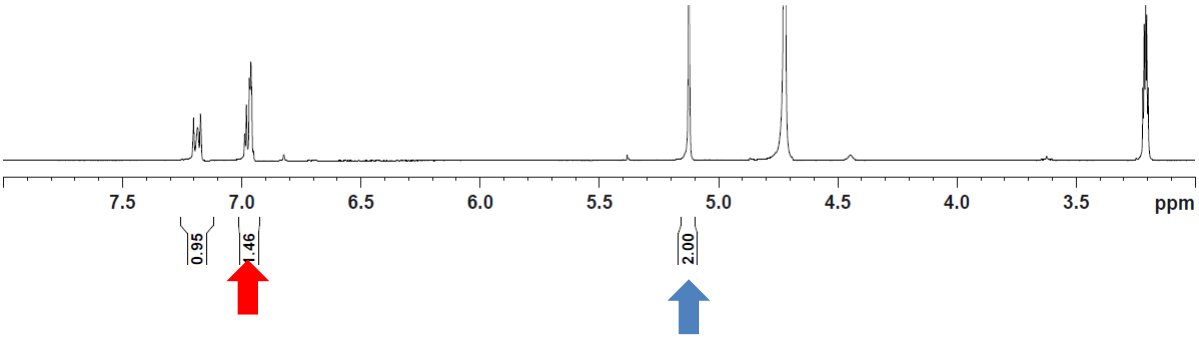

General method B: 22.3 mg (150.0 µmol) **42**; 1.5 mg (6.0 µmol, 4 mol%) IrICy(0.125NHC) **3b**, THF/D_2O (1:1) (3 mL), 80°C, 3h.

LC-MS (positive ESI): m/z 150.1 $[M+H]^+$ (25%), 151.1 $[M(1D)+H]^+$ (46%), 152.0 $[M(2D)+H]^+$ (29%).

Yield: 18.3 mg, 122.7 µmol, 82%; 15% D for δ 7.30 and 85% D for δ 7.10.

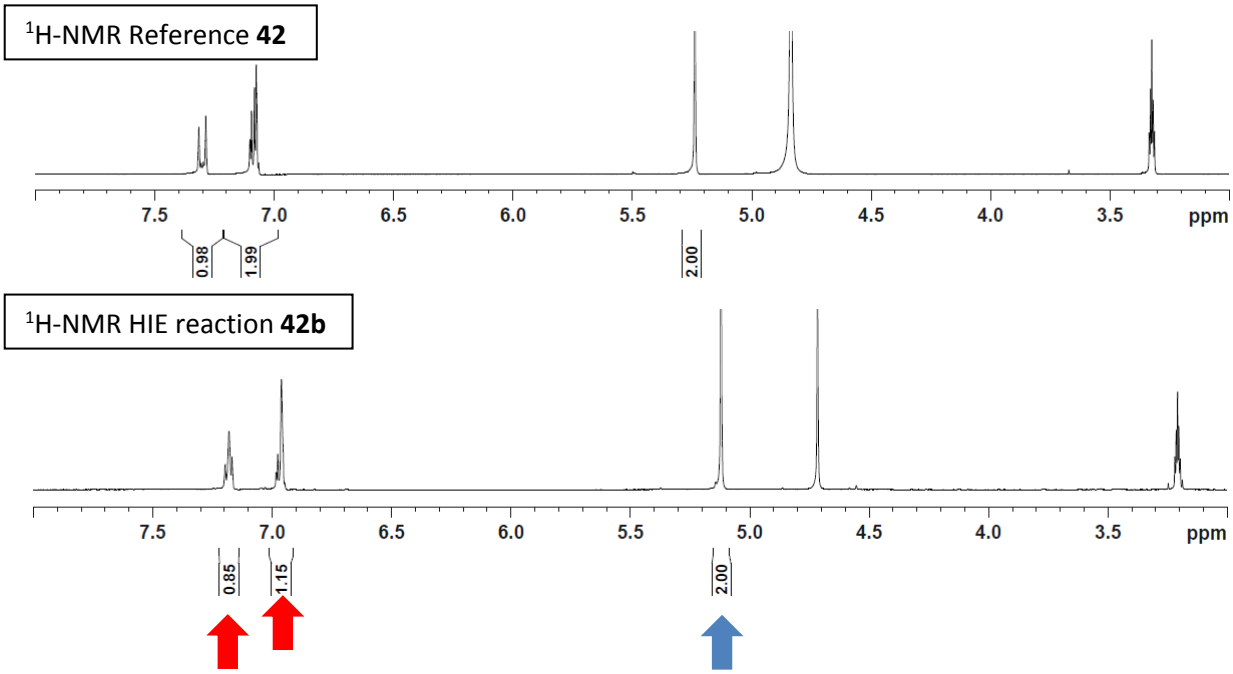

Aniline **5**

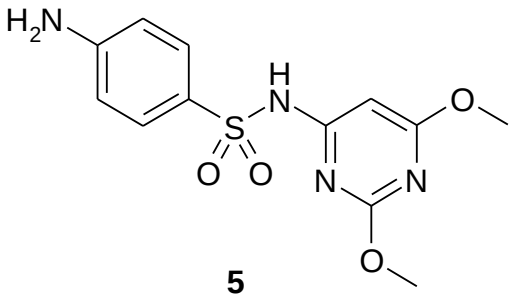

5

Molecular Weight =310.3338
Molecular Formula =C12H14N4O4S

^{1}H NMR (300 MHz, MeOD): δ 7.64 (d, ^3J = 8.2 Hz, 2H, 2 CH *meta*-NH_2), 6.67 (d, ^3J = 8.2 Hz, 2H, 2 CH *ortho*-NH_2), 6.05 (s, 1H, CH *ortho*-OMe), 3.87 (s, 6H, 2 OCH_3) ppm. Incorporation expected at δ 6.67 (red arrow). Determined against integral at δ 3.87 (blue arrow).

General method B: 46.5 mg (150.0 µmol) **5**; 1.5 mg (6.0 µmol, 4 mol%) IrICy(0.125NHC) **3b**, THF/D_2O (1:1) (3 mL), 80°C, 3h.

LC-MS (positive ESI): m/z 312.1 $[M(1D)+H]^+$ (11%), 313.0 $[M(2D)+H]^+$ (86%), 314.1 $[M(3D)+H]^+$ (3%).

Yield: 44.2 mg, 142.5 µmol, 95%; 79% D for δ 6.67.

^{1}H-NMR Reference **5**

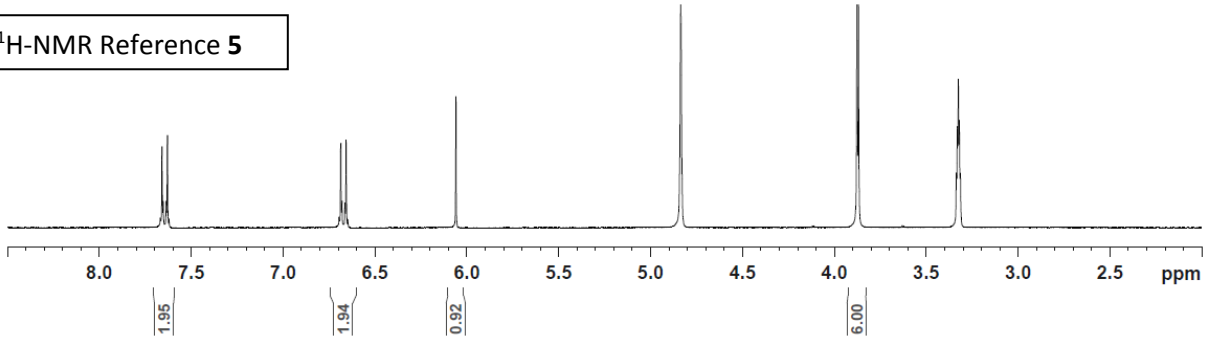

^{1}H-NMR HIE reaction **5**

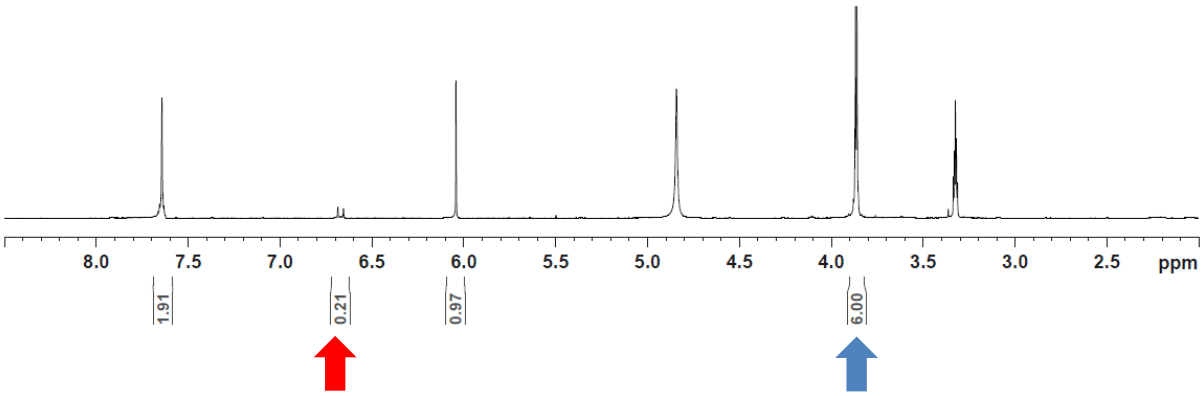

Aniline **7**

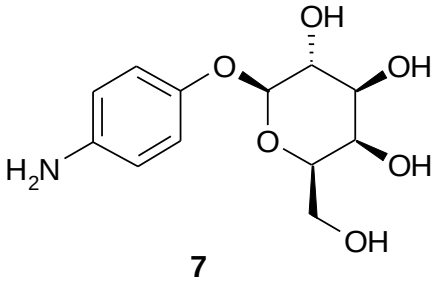

7

Molecular Weight =271.2724
Molecular Formula =C12H17NO6

^{1}H NMR (300 MHz, MeOD): δ 6.95 (d, ^3J = 8.0 Hz, 2H, 2 CH *meta*-NH_2), 6.70 (d, ^3J = 8.0 Hz, 2H, 2 CH *ortho*-NH_2), 4.69 (m, 1H, CH), 3.90 (m, 1H, CH), 3.77 (m, 3H, 3 CH), 3.59 (m, 2H, 2 CH) ppm. Incorporation expected at δ 6.70 (red arrow). Determined against integral at δ 6.95 (blue arrow).

General method B: 40.6mg (150.0 µmol) **7**; 1.5 mg (6.0 µmol, 4 mol%) IrICy(0.125NHC) **3b**, THF/D_2O (1:1) (3 mL), 80°C, 3h.

LC-MS (positive ESI): m/z 274.1 $[M(2D)+H]^+$ (95%), 275.1 $[M(3D)+H]^+$ (5%).

Yield: 36,4 mg, 134.3 µmol, 91%; 20% D for δ 6.95 and 96% D for δ 6.70.

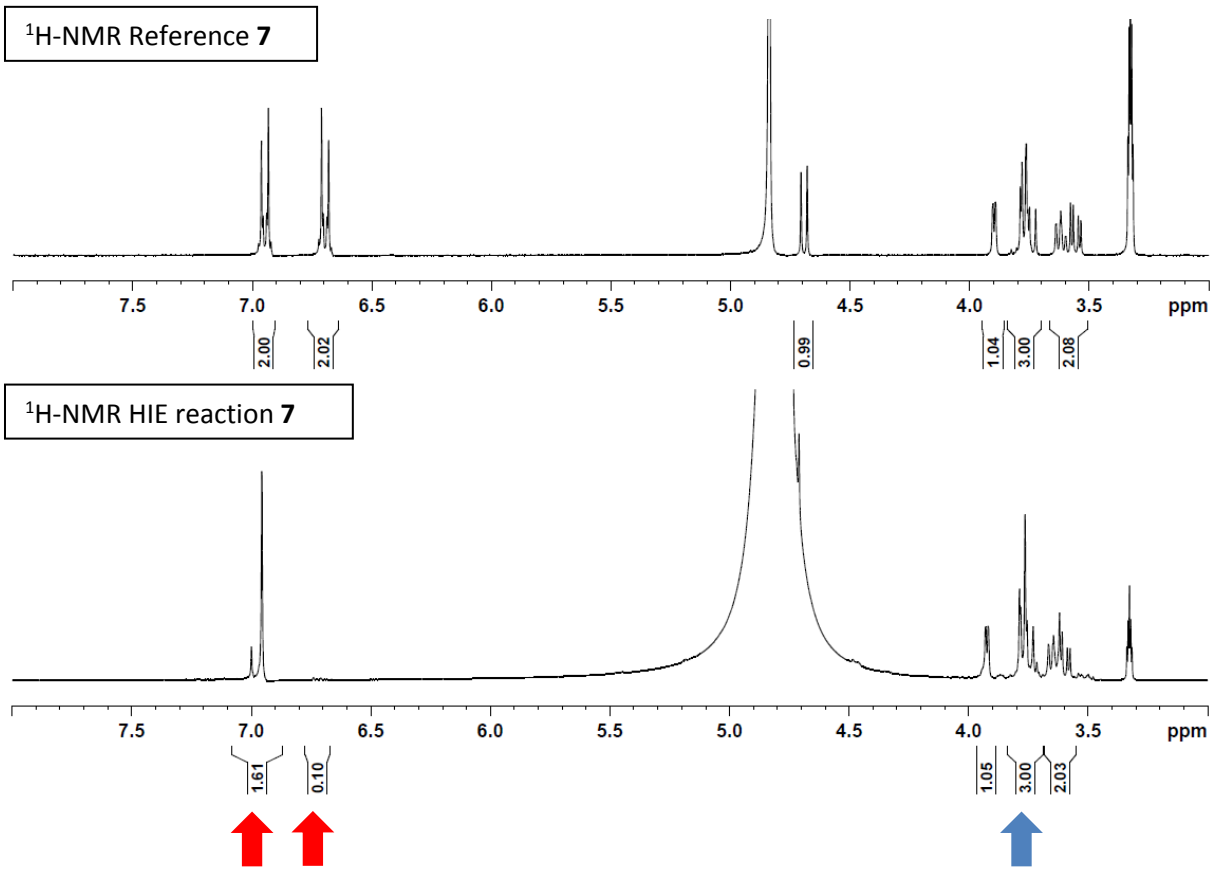

Aniline **8**

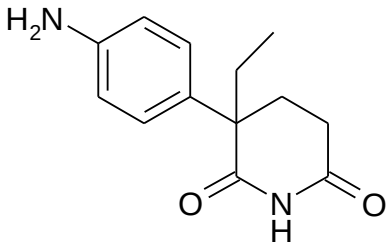

8

Molecular Weight =232.2847
Molecular Formula =C13H16N2O2

^{1}H NMR (300 MHz, MeOD): δ 7.05 (d, ^3J = 8.6 Hz, 2H, 2 CH *meta*-NH_2), 6.72 (d, ^3J = 8.6 Hz, 2H, 2 CH *ortho*-NH_2), 2.05 (m, 1H, CH aliphatic), 2.34 (m, 2H, CH_2 aliphatic), 2.19 (m, 1H, CH aliphatic), 1.90 (m, 2H, CH_2 aliphatic), 0.85 (m, 3H, CH_3 aliphatic) ppm. Incorporation expected at δ 7.10 (red arrow). Determined against integral at δ 0.85 (blue arrow).

General method B: 34.8 mg (150.0 µmol) **8**; 1.5 mg (6.0 µmol, 4 mol%) IrICy(0.125NHC) **3b**, THF/D_2O (1:1) (3 mL), 80°C, 3h.

LC-MS (positive ESI): m/z 234.2 $[M(1D)+H]^+$ (5%), 235.2$[M(2D)+H]^+$ (90%), 236.2$[M(3D)+H]^+$ (5%).

Yield: 28.5 mg, 12 3.0 µmol, 82%; 99% D for δ 6.72.

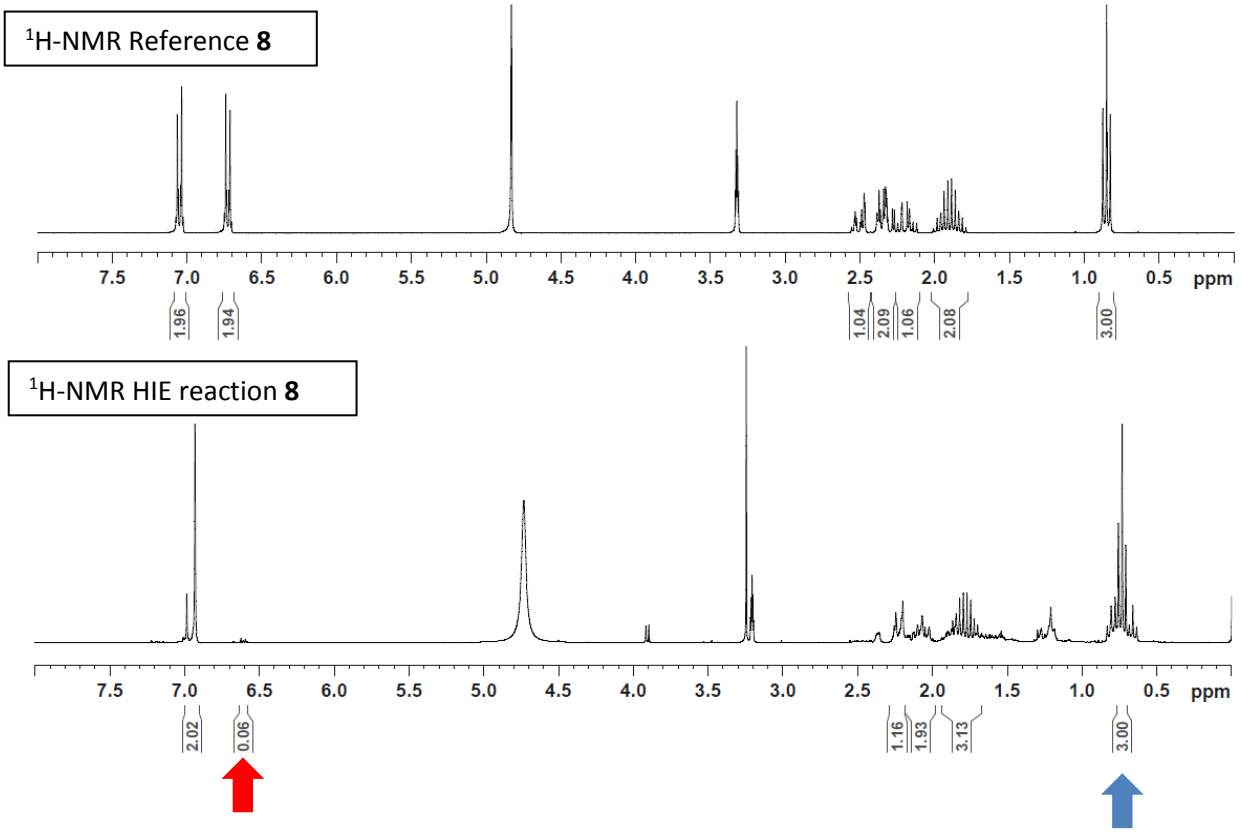

Aniline **10**

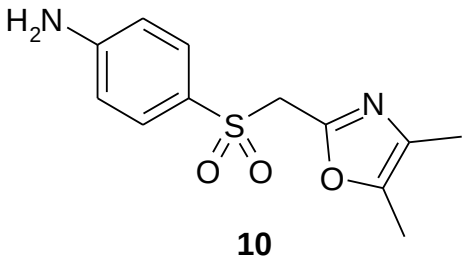

10

Molecular Weight =266.3210
Molecular Formula =C12H14N2O3S

^{1}H NMR (300 MHz, MeOD): δ 7.62 (d, ^3J = 8.5 Hz, 2H, 2 CH *meta*-NH_2), 6.66 (d, ^3J = 8.5 Hz, 2H, 2 CH *ortho*-NH_2), 2.08 (s, 3H, CH_3), 1.99 (s, 3H, CH_3) ppm. Incorporation expected at δ 6.66 (red arrow). Determined against integral at δ 2.08 (blue arrow).

General method B: 39.9 mg (150.0 µmol) **10**; 1.5 mg (6.0 µmol, 4 mol%) IrICy(0.125NHC) **3b**, THF/D_2O (1:1) (3 mL), 80°C, 3h.

LC-MS (positive ESI): m/z 267.3 $[M+H]^+$ (48%), 268.3 $[M(1D)+H]^+$ (47%), 269.3 $[M(2D)+H]^+$ (5%).

Yield: 30.3 mg, 114.0 µmol, 76%; 50% D for δ 6.66.

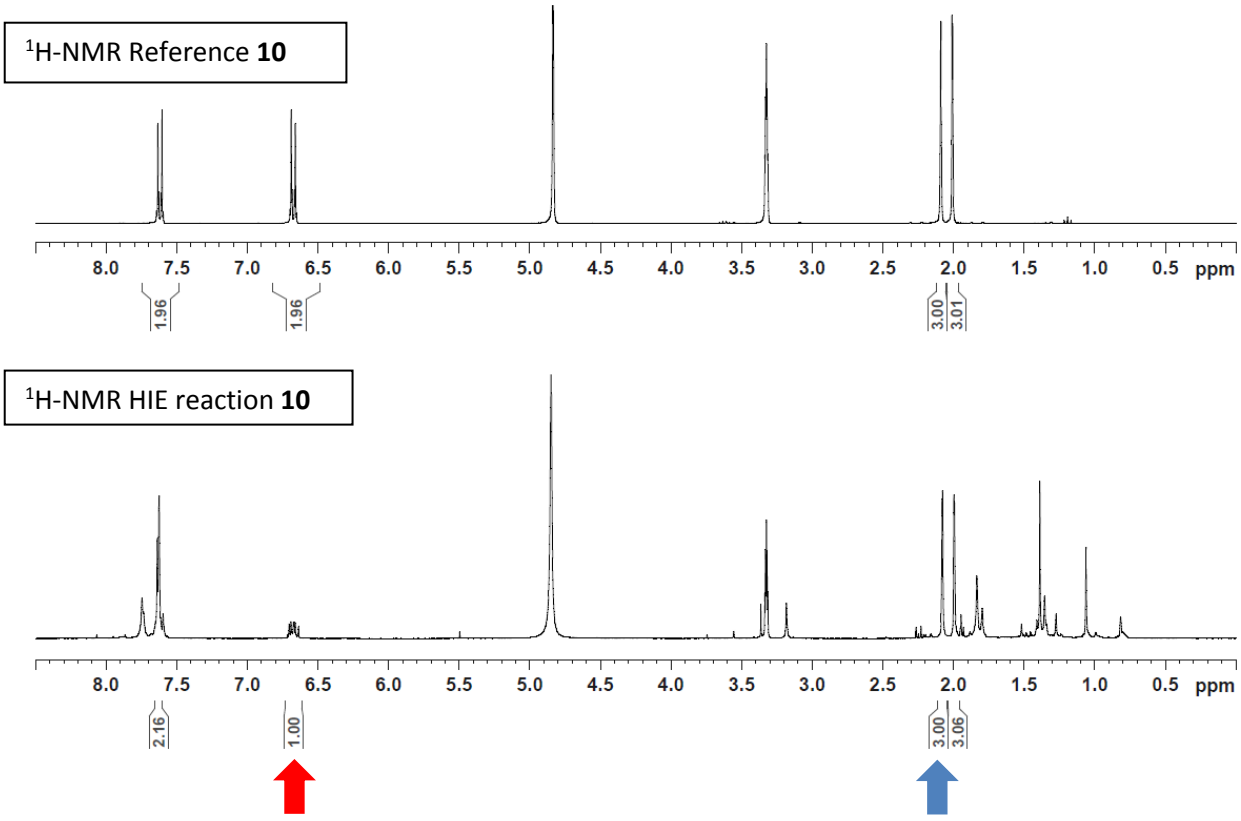

Aniline **11**

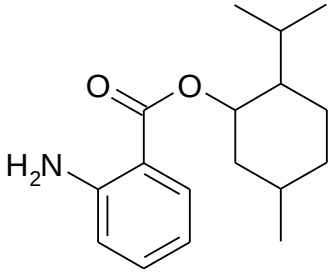

Molecular Weight =275.3943
Molecular Formula =C17H25NO2

11

^{1}H NMR (300 MHz, MeOD): δ 7.79 (dd, ^3J = 8.0 Hz and 1.6 Hz, 1H, CH *ortho*-COO), 7.24 (m, 1H, CH *meta*-NH_2), 6.75 (dd, ^3J = 8.5 Hz and 1.3 Hz, 1H, CH *ortho*-NH_2), 6.57 (m, 1H, CH *para*-NH_2), 4.91 (m, 1H, CH alpha IPr), 2.00 (m, 2H, CH aliphatic), 1.76 (m, 2H, CH aliphatic), 1.55 (m, 2H, CH aliphatic), 1.14 (m, 3H, CH aliphatic), 0.94 (m, 6H, CH IPr), 0.81 (m, 3H, CH_3) ppm. Incorporation expected at δ 7.24 and 6.75 (red arrow). Determined against integral at δ 7.79 (blue arrow).

General method B: 41.2 mg (150.0 µmol) **11**; 1.5 mg (6.0 µmol, 4 mol%) IrICy(0.125NHC) **3b**, THF/D_2O (1:1) (3 mL), 80°C, 3h.

LC-MS (positive ESI): m/z 276.2 $[M+H]^+$ (8%), 277.2 $[M(1D)+H]^+$ (47%), 278.3 $[M(2D)+H]^+$ (39%), 279.2 $[M(3D)+H]^+$ (6%).

Yield: 37.1 mg, 134.8 µmol, 90%; 35% D for δ 7.24 and 86% D for δ 6.75.

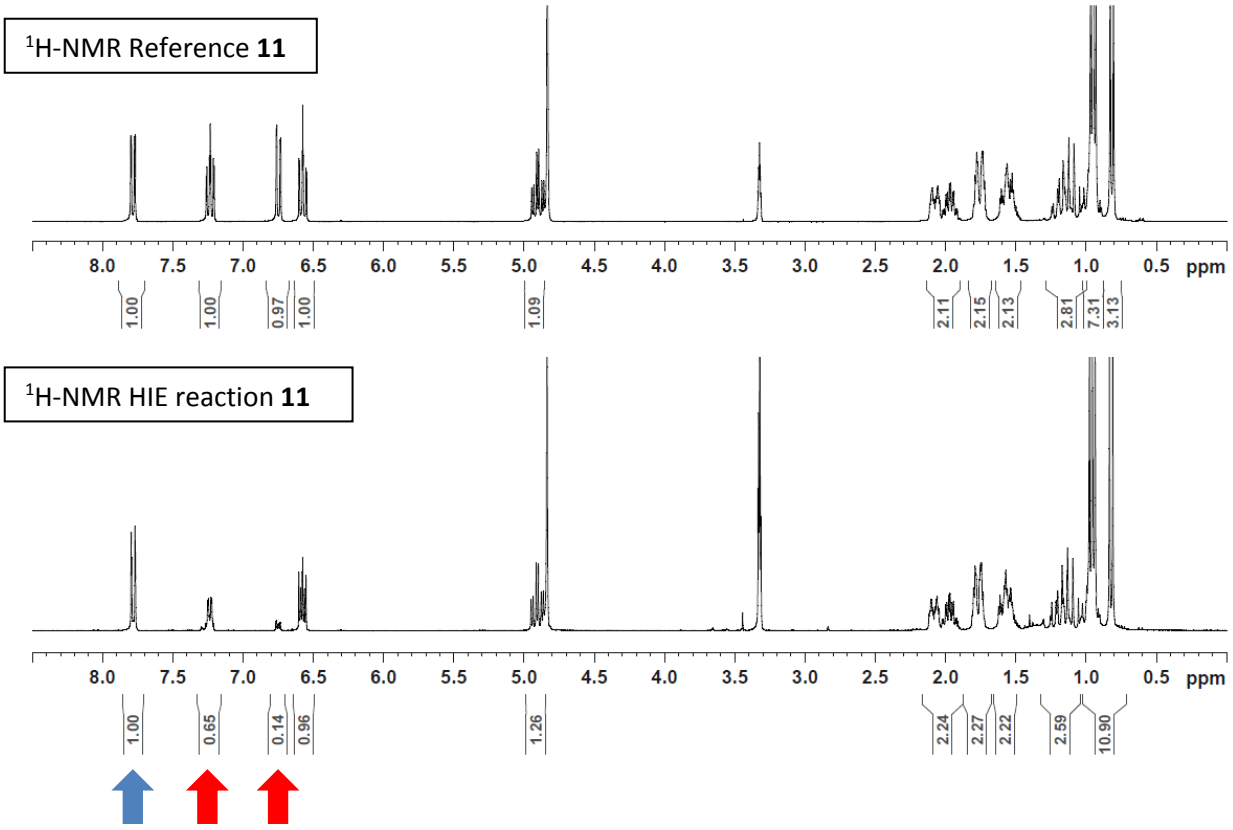

Aniline **43**

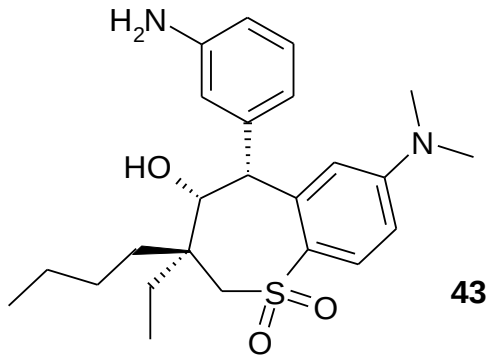

43

Molecular Weight =430.6142
Molecular Formula =C24H34N2O3S

^{1}H NMR (300 MHz, MeOD): δ 7.90 (d, ^3J = 8.7 Hz, 1H, CH *meta*-NMe_2), 7.20 (t, ^3J = 7.7 Hz, 1H, CH *meta*-NH_2), 6.94 (d, ^3J = 7.7 Hz, 1H, CH *para*-NH_2), 6.81 (s, 1H, CH *ortho*-NH_2), 6.65 (dd, ^3J = 7.7 Hz and 2.3 Hz, 1H, CH *ortho*-NH_2), 6.52 (dd, ^3J = 8.7 Hz and 2.5 Hz, 1H, CH *ortho*-NMe_2), 6.09 (d, ^3J = 2.5 Hz, 1H, CH *ortho*-NMe_2), 5.45 (s, 1H, CH aliphatic), 4.15 (d, ^3J = 6.9 Hz, 1H, CH aliphatic), 3.70 (br s, 2H, NH_2), 3.15 (d, ^3J = 15.0 Hz, 1H, CH *alpha*-SO_2), 2.99 (d, ^3J = 15.0 Hz, 1H, CH *alpha*-SO_2), 2.84 (s, 6H, 2 CH_3), 2.23 (m, 1H, CH aliphatic), 1.38 (m, 9H, CH aliphatic), 0.92 (t, ^3J = 7.1 Hz, 3H, CH_3), 0.85 (t, ^3J = 7.1 Hz, 3H, CH_3) ppm. Incorporation expected at δ 6.81 and 6.65 (red arrow). Determined against integral at δ 7.90 (blue arrow).

General method A: 64.5 mg (150.0 µmol) **43**; 1.5 mg (6.0 µmol, 4 mol%) IrICy (0.125NHC) **3b**, THF (3 mL), 55°C, 3h.

LC-MS (positive ESI): m/z 431.3$[M+H]^+$ (42%), 432.3 $[M(1D)+H]^+$ (38%), 433.3 $[M(2D)+H]^+$ (16%), 434.2 $[M(3D)+H]^+$ (4%).

Yield: 60.6 mg, 141.0 µmol, 94%; 70% D for δ 6.65.

^{1}H-NMR Reference **43**

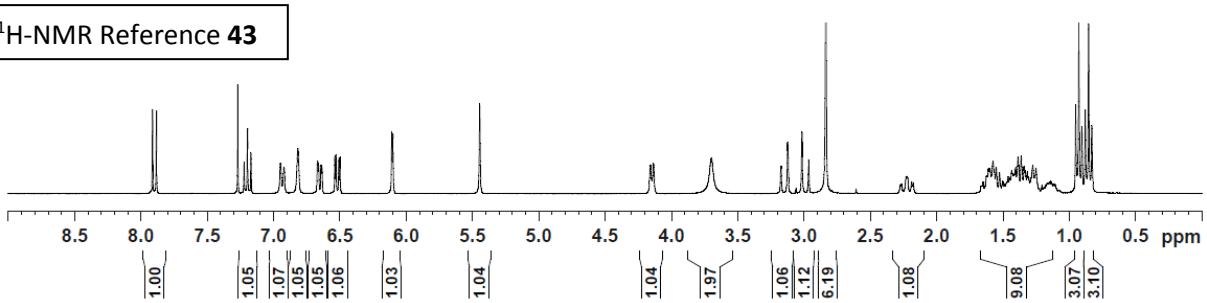

^{1}H-NMR HIE reaction **43**

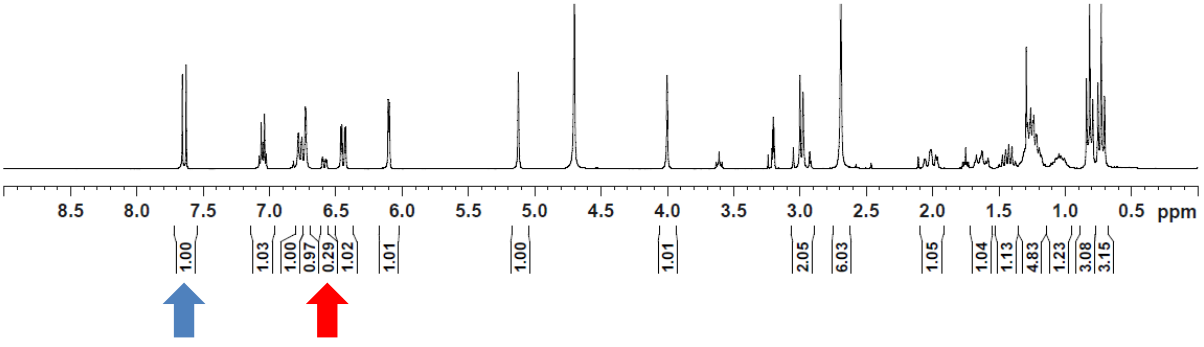

Conditions: 64.5 mg (150.0 µmol) **43**; 30.0 mg (120.0 µmol, 80 mol%) IrICy (0.125NHC) **3b**, THF (3 mL), 55°C, 3h.

LC-MS (positive ESI): m/z 431.3$[M+H]^+$ (9%), 432.3 $[M(1D)+H]^+$ (65%), 433.3 $[M(2D)+H]^+$ (19%), 434.2 $[M(3D)+H]^+$ (7%).

Yield: 56.1 mg, 130.5 µmol, 87%; 40% D for δ 6.81 and 87% D for δ 6.65.

^{1}H-NMR Reference **43**

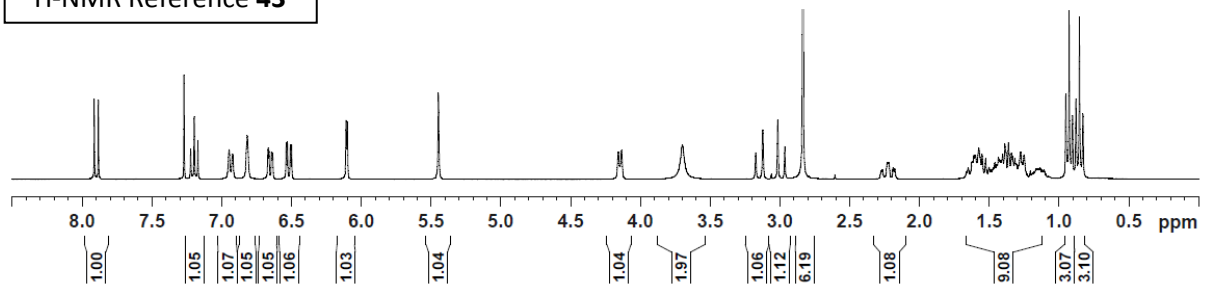

^{1}H-NMR HIE reaction **43**

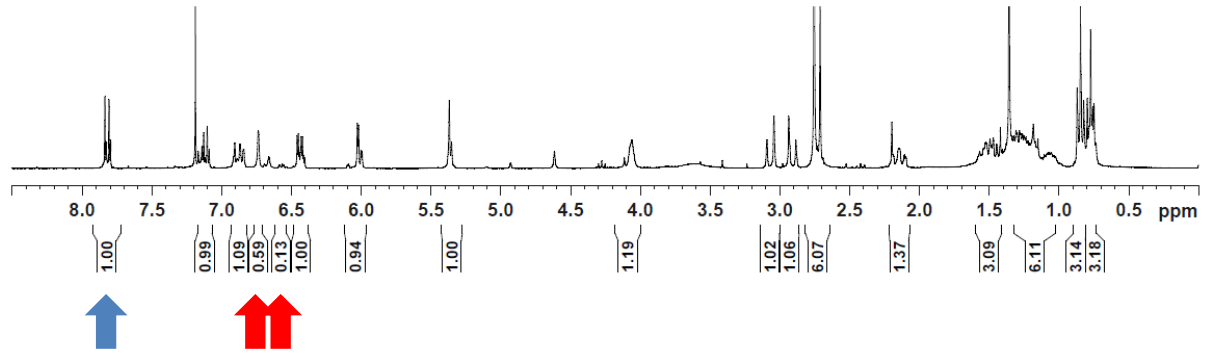

Tritium labelling of 43

This work was done in the LMT laboratory at CEA-Saclay (France), within our collaboration with Dr. Pieters, Dr. Feuillastre and Dr. Dugave.

A 5 mL Fischer–Porter bottle was equipped with a magnetic stir bar and charged with IrICy **3b** (8.8 µmol, 80 mol%) under air. Aniline **43** (5.0 mg, 11.0 µmol) was dissolved in THF (0.5 mL) and added to the Fischer–Porter bottle and the latter was then connected to the tritium manifold. The Fischer-Porter glassware was then frozen using a liquid nitrogen bath, left under vacuum for 5 min and then pressurized with T_2 gas (0.8 bar at room temperature, 10 Ci). The reaction mixture was magnetically stirred and heated at 55°C (sand bath) for 3 hours. The solution was then cooled down to room temperature, further cooled using a liquid nitrogen bath, the extra T2 gas was then removed. Then the solution was warmed to room temperature and 4 mL of methanol was added to precipitate the IrNp. The resulted suspension was filtred using Nylon filter membranes (0.45 µm) and the filtrate was evaporated under vacuum. The described procedure gave a crude total activity of 10.6 GBq (287 mCi). 25% of the crude was purified by preparative HPLC leading to a total activity of 1.4 GBq (38 mCi) with a molar activity of 962 GBq/mmol (26 Ci/mmol).

LC-MS (positive ESI): m/z 431.1 $[M+H]^+$ (13%), 432.1 $[M(1T)+H]^+$ (82%), 433.1 $[M(2T)+H]^+$ (5%).

^{3}H NMR (427MHz, Acetone-d_6 + TFA): δ 7.59 (s).

^{1}H-NMR Reference **43** in Acetone-*d_6 + TFA*

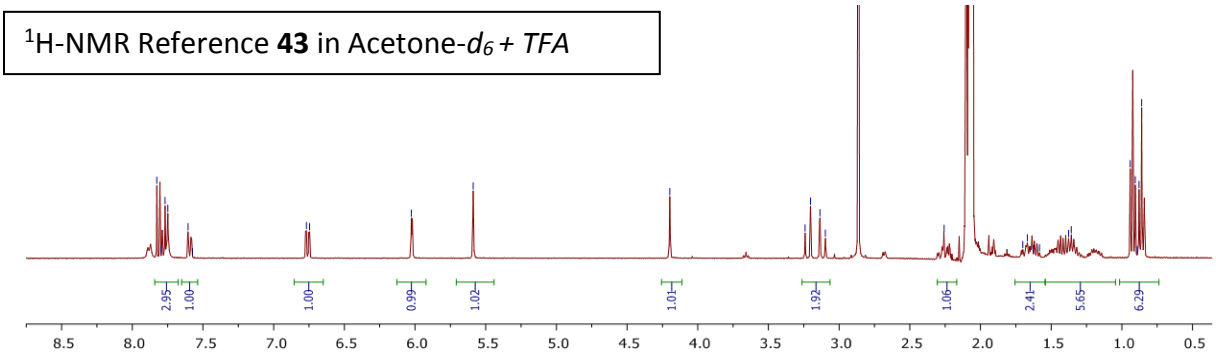

^{3}H-NMR tritiated-**43** in Acetone-*d_6 + TFA*

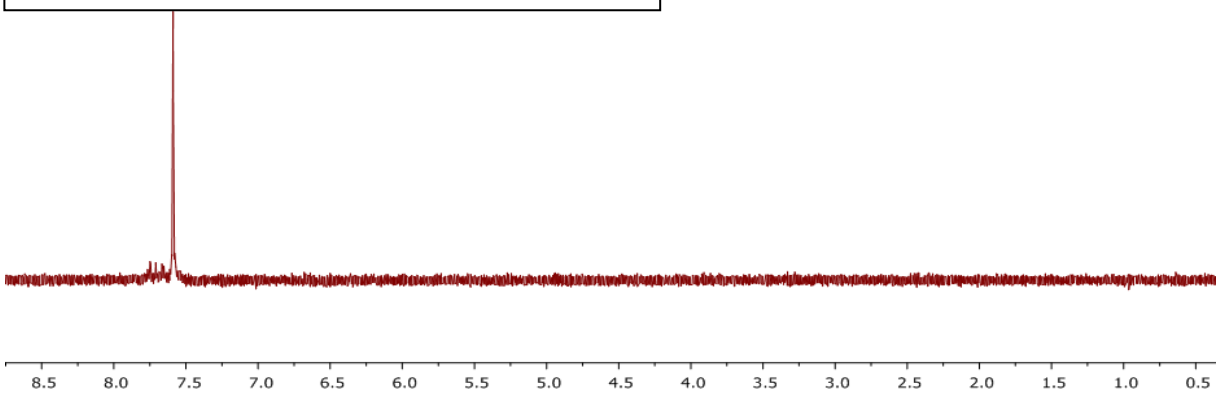

HPLC Chromatograms of purified tritiated aniline-43

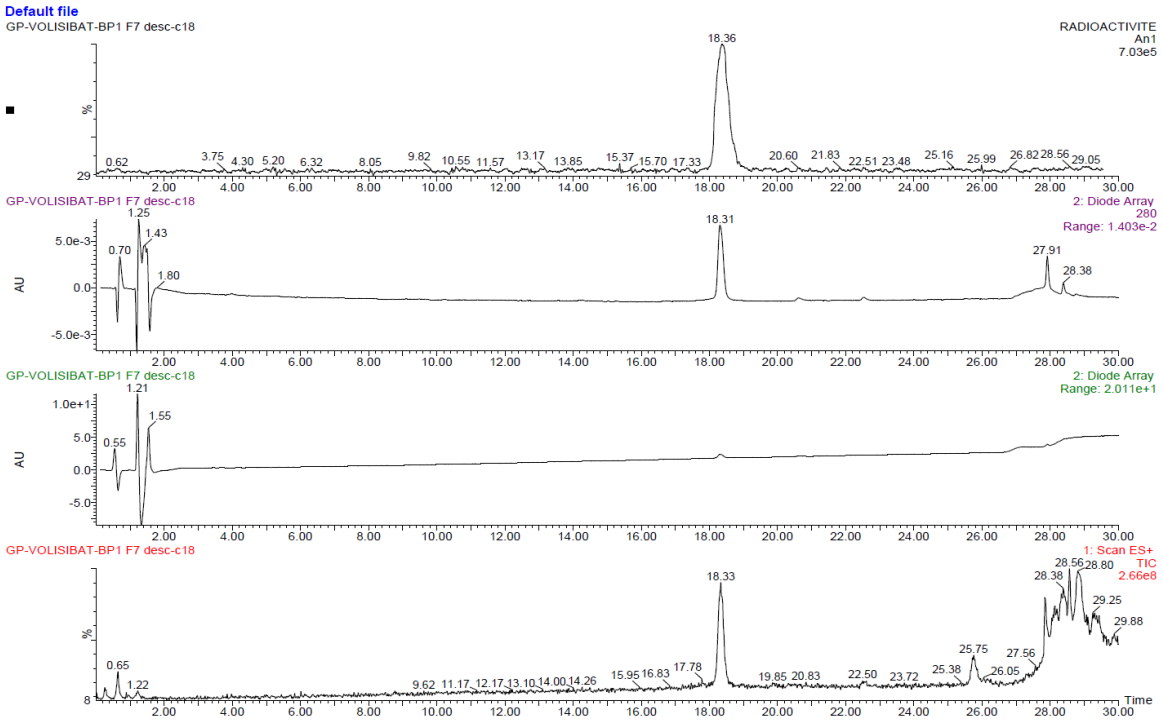

Mass spectrum of tritiated aniline-43

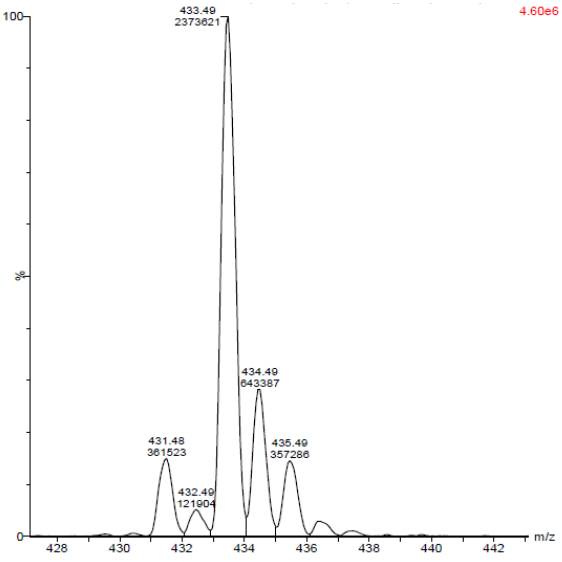

Iriridium nanoparticles data

This work was done by Donia Bouzouita in the LPCNO laboratory in Toulouse (France), within our collaboration with Prof. Chaudret et Dr. Tricard.

Synthesis of IrICy (0.05 eq) nanoparticles 3a

In the glove box, 10 mg of 1,3-dicyclohexylimidazolium chloride (0.037 mmol) and 5 mg KO^tBu (0.044 mmol) were dispersed in THF (15 mL) in a Schlenk flask. The mixture was let to stir at room temperature for 15 hours to give a yellowish solution containing the *free* carbene. Then, 200.0 mg of $[Ir(OMe)(COD)]_2$ (0.3 mmol) was dispersed in THF (15 mL) in a Fischer Porter bottle. The carbene solution was filtered through celite to remove the KCl formed during the deprotonation of the imidazolium salt and was transferred dropwise into the Fischer Porter containing the $[Ir(OMe)(COD)]_2$ solution. The mixture was pressurized with H_2 (5 bar) under stirring and heated at room temperature overnight. At the end of the reaction, the NPs were isolated as a brown solid after evaporation of the solvent under vacuum. TGA analysis: Ir, 91 wt%.

Synthesis of IrICy (0.125eq) nanoparticles 3b

In the glove box, 20 mg of 1,3-dicyclohexylimidazolium chloride (0.07 mmol) and 9 mg KO^tBu (0.077 mmol, 1.1 eg.) were dispersed in THF (15 mL) in a Schlenk flask. The mixture was let to stir at room temperature for 15 hours to give a yellowish solution containing the *free* carbene. Then, 200.0 mg of $[Ir(OMe)(COD)]_2$ (0.3 mmol) was dispersed in THF (15 mL) in a Fischer Porter bottle. The carbene solution was filtered through celite to remove the KCl formed during the deprotonation of the imidazolium salt and was transferred dropwise into the Fischer Porter containing the $[Ir(OMe)(COD)]_2$ solution. The mixture was pressurized with H_2 (5 bar) under stirring and heated at room temperature overnight. At the end of the reaction, the NPs were isolated as a brown solid after evaporation of the solvent under vacuum. Yield: 100 mg, 66%. TGA analysis: Ir, 77 wt%.

Synthesis of IrICy (0.25eq) nanoparticles 3c

In the glove box, 40 mg of 1,3-dicyclohexylimidazolium chloride (0.14 mmol) and 20 mg KO^tBu (0.18 mmol) were dispersed in THF (15 mL) in a Schlenk flask. The mixture was let to stir at room temperature for 15 hours to give a yellowish solution containing the *free* carbene. Then, 200.0 mg of $[Ir(OMe)(COD)]_2$ (0.3 mmol) was dispersed in THF (15 mL) in a Fischer Porter bottle. The carbene solution was filtered through celite to remove the KCl formed during the deprotonation of the imidazolium salt and was transferred dropwise into the Fischer Porter containing the $[Ir(OMe)(COD)]_2$ solution. The mixture was pressurized with H_2 (5 bar) under stirring and heated at room temperature overnight. At the end of the reaction, the NPs were isolated as a brown solid after evaporation of the solvent under vacuum. TGA analysis: Ir, 70 wt%.

Characterization of the Ir@INHC NPs

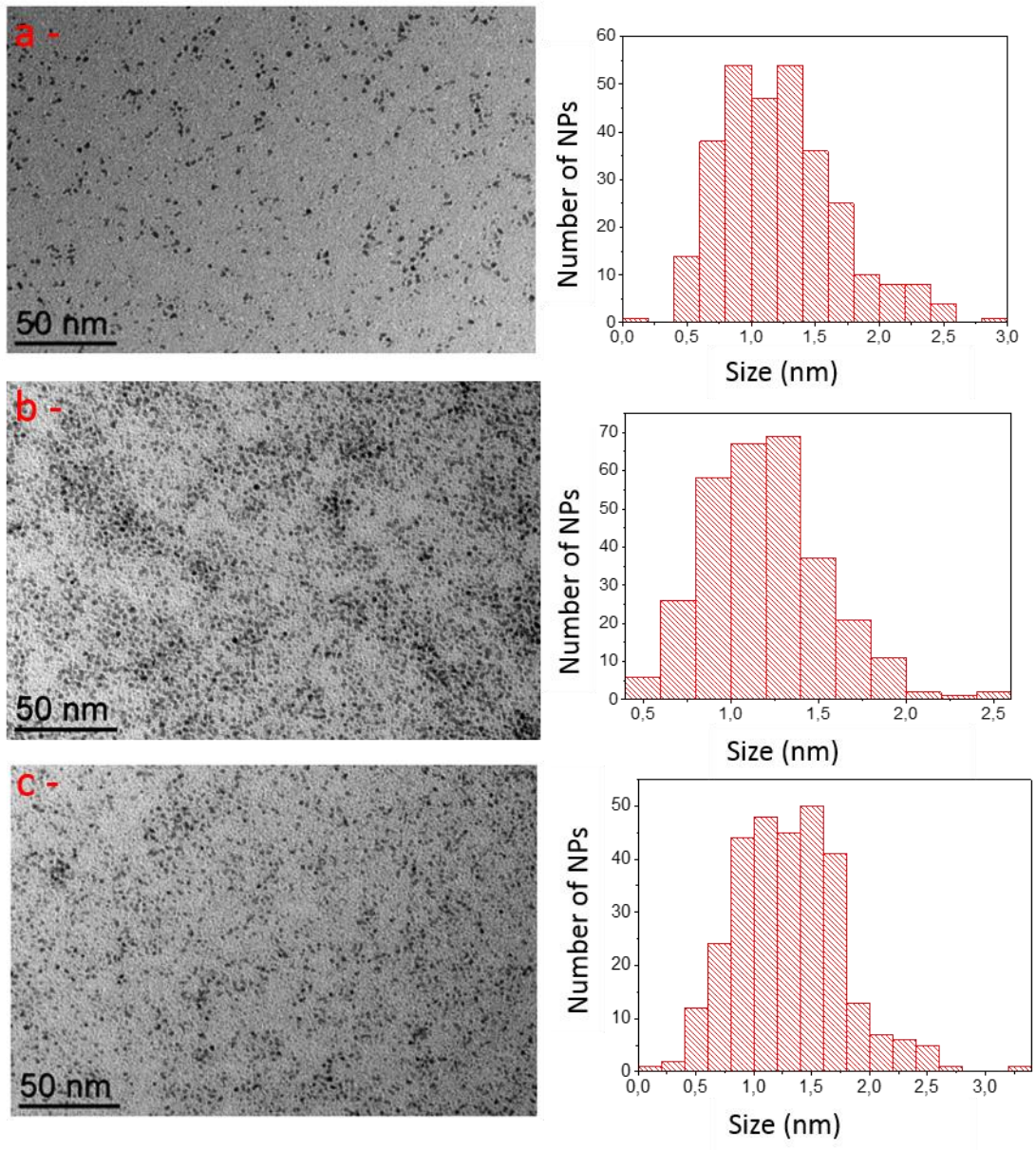

Figure 1 : TEM images and size distribution for NPs (a) Ir@ICy (0.05 eq) **3a**, (b) Ir@ICy (0.125 eq) **3b**, (c) Ir@ICy (0.25 eq) **3c**.

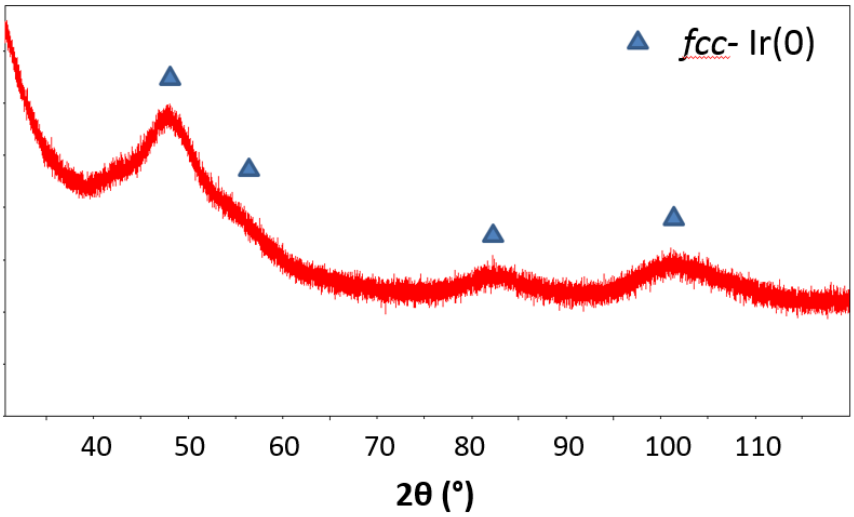

Figure 2 : XRD diffractograms for Ir@ICy NPs (0.125 eq) **3b**, showing the peaks corresponding to *fcc*-Ir(0).

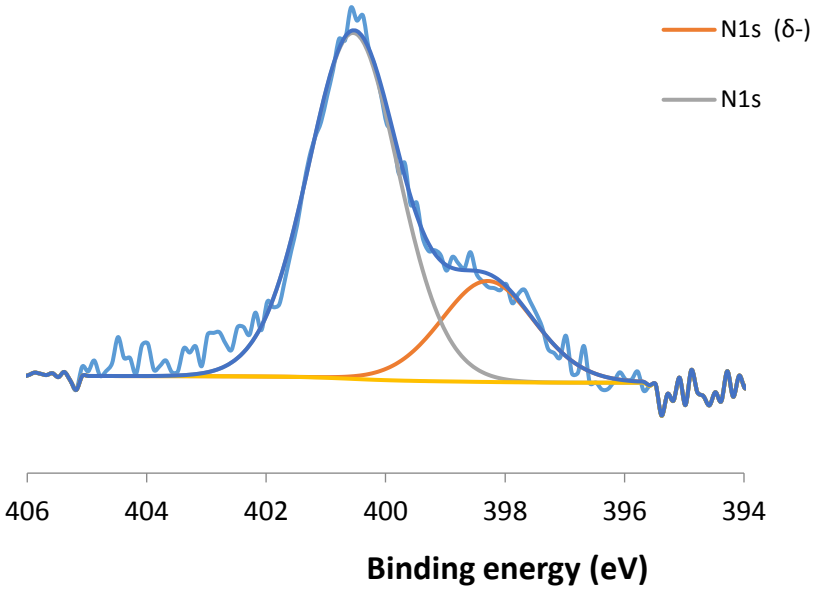

Figure 3 : X-ray photoelectron spectroscopy (XPS) of the N 1s signals of Ir@ICy (0.125 eq) **3b**.

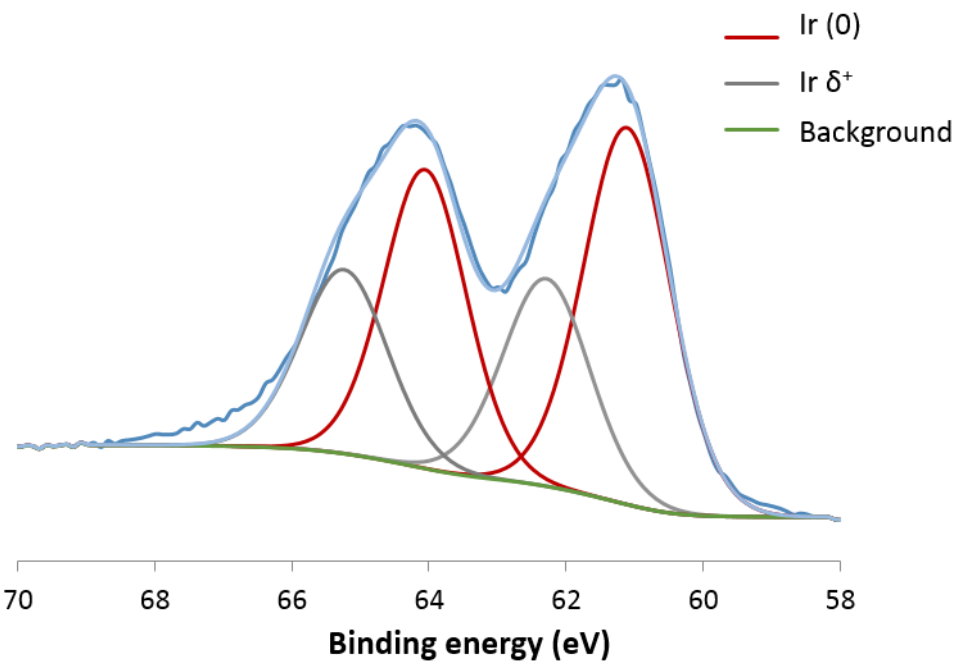

Figure 4 : X-ray photoelectron spectroscopy (XPS) Pt 4f5/2 and 4f7/2 signals of Ir@ICy (0.125 eq) **3b**.

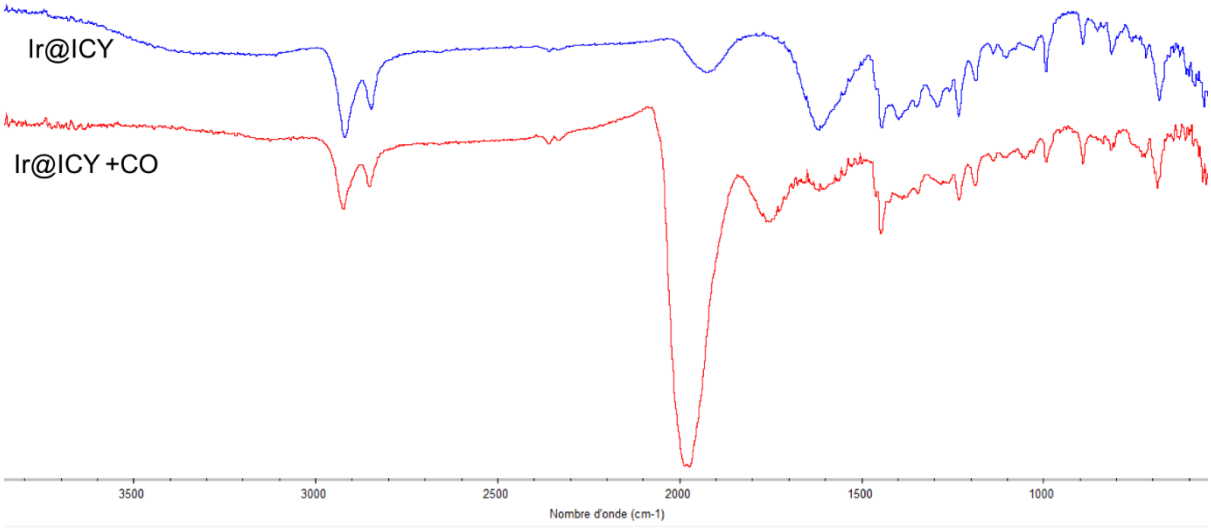

Figure 5 : ATR FT-IR spectra of Ir@ICy **3b** before and after CO adsorption.

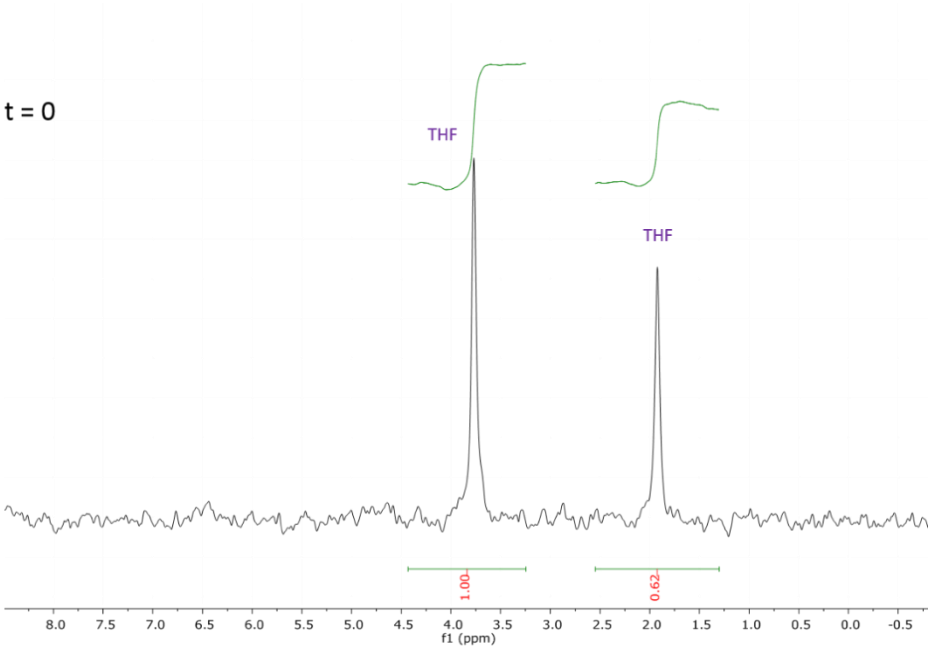

Figure 6 : ^{2}H NMR spectra of THF.

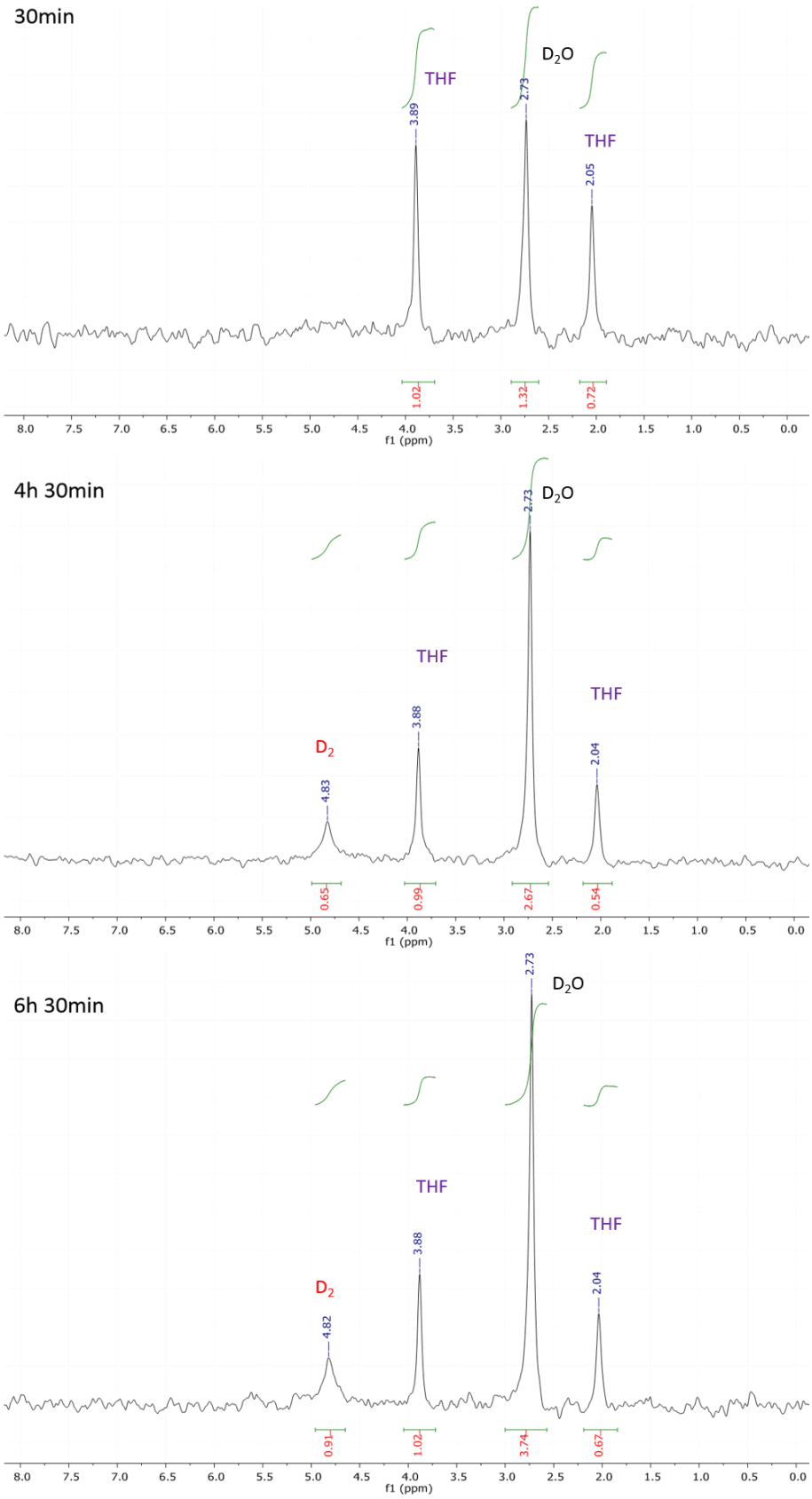

Figure 7 : ^{2}H NMR spectra of THF after reaction with Ir@ICy **3b** NPs under D_2 (5 bar) at different time (30 min, 4h 30min, 6h30min.

Part VI
Conclusion and future perspectives

<u>Part VI:</u> Conclusion and future perspectives

In this PhD project, it was aimed to develop new efficient, fast and easy-to-handle methods to label drug compounds with deuterium and tritium in one single step. These labelled compounds are an essential part in drug discovery and help to speed up the generation of the safety profile of a drug candidate. The development of new and efficient radioactive labelling methods can therefore lead to an improved attrition rate and a faster approval of necessary medications (*scheme VI.1*).

Scheme VI. 1: *Acceleration of the Drug Discovery Pathway by Isotope Chemistry*

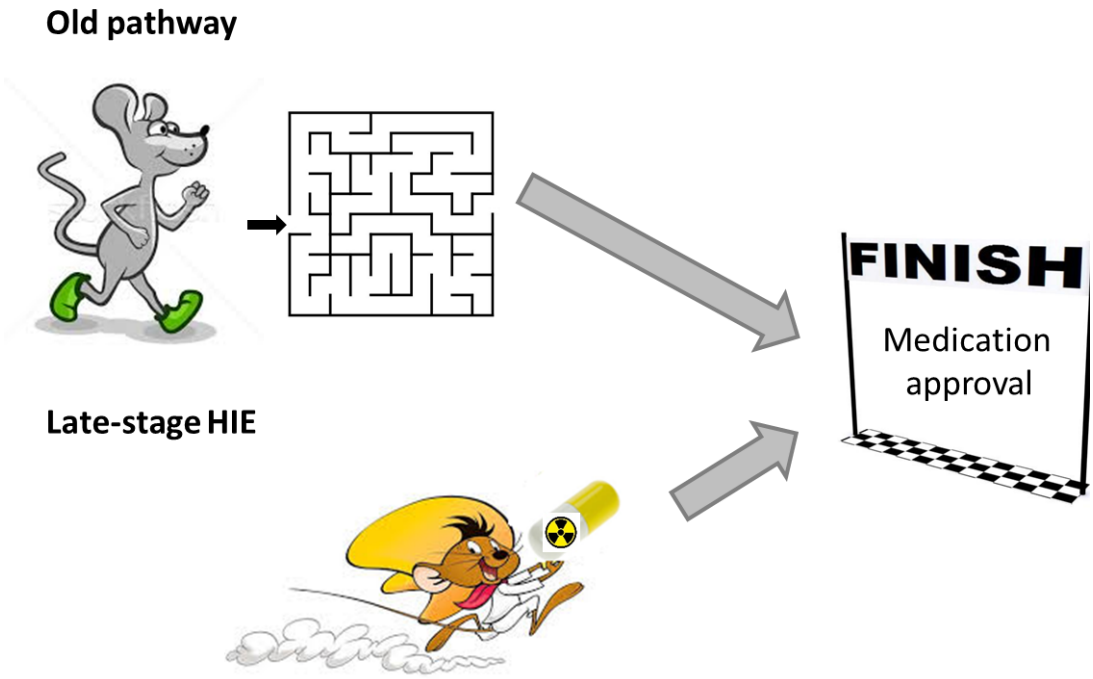

If working with radioactive material, the most convenient way to introduce the radioactive label is as late as possible to reduce waste, to increase the overall yield and to reduce the handling time with a potentially dangerous compound. In this regards, Isotope Chemistry can be considered as an ancestor of Late-Stage Functionalization. For deuterated compounds applied as internal MS standard, the selective introduction in very high percentages is essential to generate a suitable MS pattern. Therefore, the developed synthetic HIE methods need to be highly selective, highly efficient (>95%D) and should generally introduce 3-6 deuterium atoms in total.

In the Part II-Chapter 1, the use of a newly discovered Tamm catalyst (**F**) has been extended by evaluation of its activity in HIE reactions with sulfonamides (**1**), N-oxides (**2**) and phosphonamides (**3**). After optimization of the reaction conditions, the HIE reaction was able to be run under very mild conditions and provided very good deuterium incorporation in *ortho*-positions of sulphonamides DG_1 up to 92%D, phosphonamides DG_2 up to 99%D and N-oxides DG_3 up to 100%D (*scheme VI.2*).[1]

Scheme VI. 2: *Hydrogen Isotope Exchange reactions of Sulphonamides, Phoshonamides and N-oxides with iridium P,N-ligated catalyst* ***F*** *(Part II – Chapter 1)*

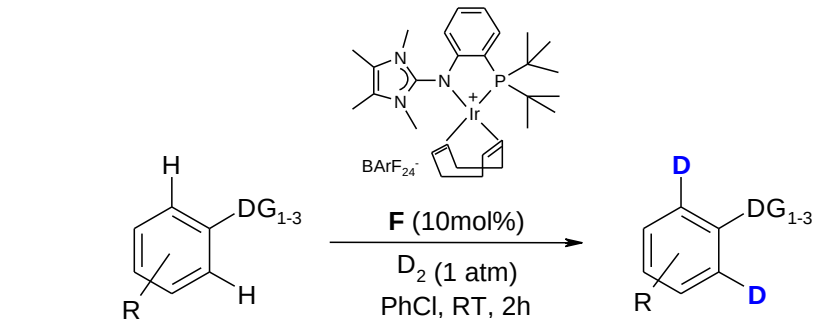

DG_1 = sulphonamides
DG_2 = phosphonamides
DG_3 = N-oxides

DG_1 : **43-92 %D**
DG_2 : **60-99 %D**
DG_3 : **45-100 %D**

Selected examples:

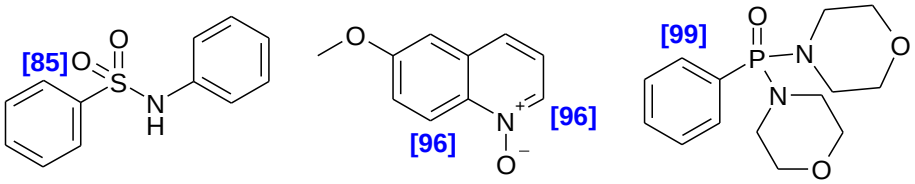

1 **2** **3**

In collaboration with the working group of Prof. Tamm, a long standing challenge in direct labelling of phenylacetic acid derivatives was solved (Part II-Chapter 2). While former methods have used non-catalytic reaction pathways or large excess of isotope source, the first efficient catalytic protocol for *ortho*-selective HIE of pharmacologically important phenylacetic acid esters and amides with D_2/T_2 gas under very mild reaction conditions was developed. The HIE reaction on 19 different phenylacetic esters has provided deuterium enrichment up to 91%D. The HIE reaction on 10 different phenylacetic amides has given deuterium incorporation up to 99%D. Furthermore, it was proven that the method was fully adaptable to the specific requirements of tritium chemistry mentioned in the thesis objectives. Indeed, a direct tritium labeling of Benalaxyl (25%T, 14 Ci/mmol) **5** and Camylofine (26%T, 32 Ci/mmol) **6** was achieved (*Scheme VI.3*).[2]

Scheme VI. 3: *Hydrogen Isotope Exchange reactions of Phenylacetic acid derivatives with iridium P,N-ligated catalyst* ***F*** *(Part II – Chapter 2)*

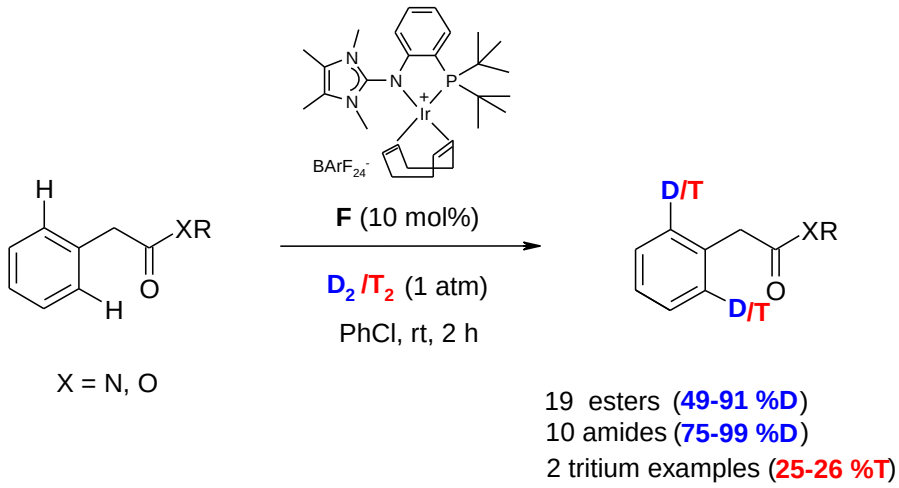

Selected examples:

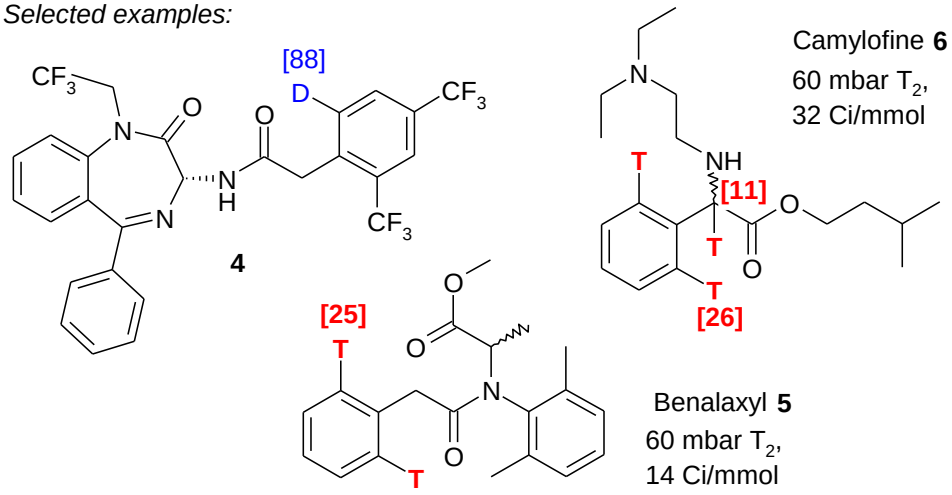

In Chapter 1 – Part III we have demonstrated that by applying the optimized combination of iridium catalysts **A-G** and reaction temperatures (-60 to 130°C), different HIE reaction outcomes in selectivity and reactivity can be achieved. Notably the temperature window for most studied iridium catalysts **A-G** were surprisingly broad. To use the right catalyst with the ideal reaction conditions is the trigger to either increase the selectivity and/or the deuterium incorporation (*scheme VI.4*). Based on our results, it is suggested to start the HIE optimization experiments with catalysts $\mathbf{B_a}$, **E** and **G** at room temperature and at 80°C in parallel. While rising the reaction temperature to a maximum prior catalyst decomposition is the key for maximum deuterium incorporation into the target molecule and was demonstarted for drugs like Celecoxib **7**, Vismodegib **8** and Glibenclamide **9**. We believe that evaluating selectivity and reactivity of different catalysts in a comparison study of a reaction class can make the prediction of CH-functionalization reaction more reliable and understandable. This could enable a greater probability of success with HIE reactions to

increase effectiveness and reduce the number of reactions needed and will therefore help to speed up drug discovery.[3]

Scheme VI. 4: *Temperature-mediated Hydrogen Isotope Exchange reactions with different iridium catalysts (Part III – Chapter 1)*

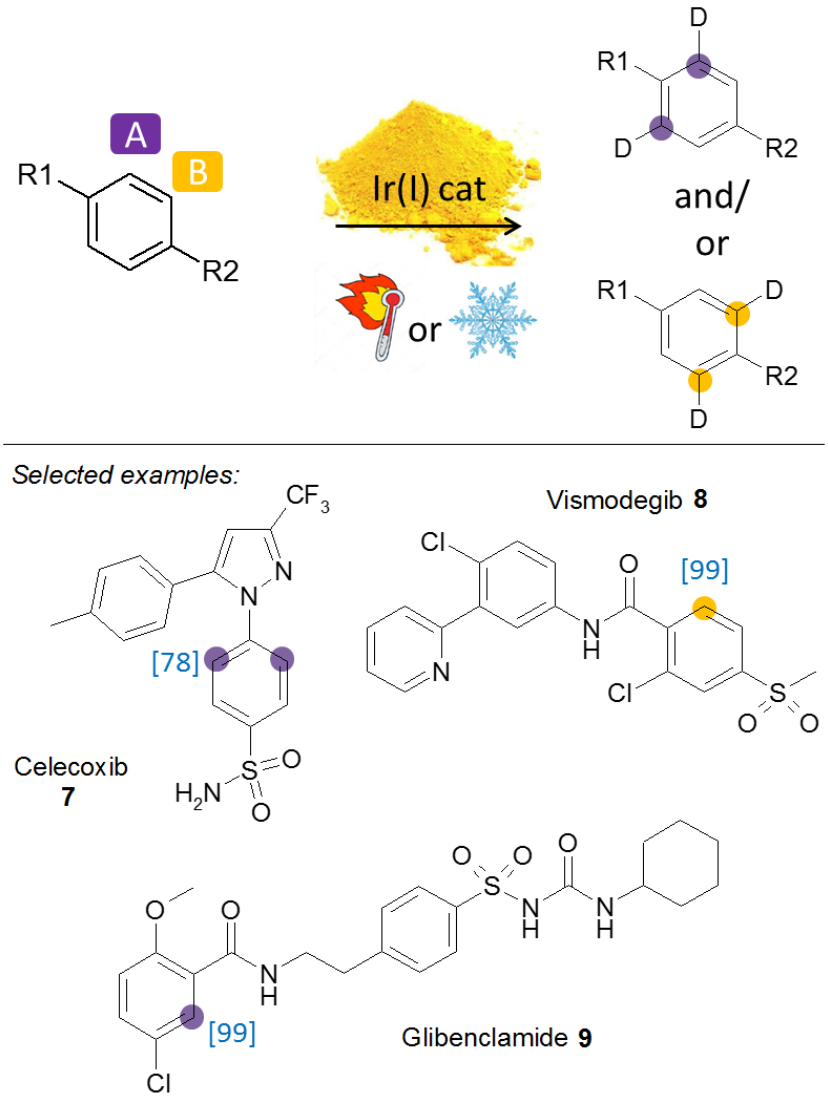

One of the key features in planning a synthesis is the predictivity and probability of success of the chosen approach. In Chapter 2-Part III, we described the result of experimental competition experiments to obtain an order of directing group influence in HIE reactions with catalyst $\mathbf{B_a}$. This was followed by DFT calculations, where we tried to get a theoretical understanding to explain the deuteration outcome (*scheme VI.5*). Interestingly, we have identified the iridium-substrate coordination complex to be the main trigger for reactivity and selectivity in the competition situation with two and more directing groups. This is remarkable as the general understanding of product formation is principally based on the

activation energy ΔH. Only if the energies of two competing coordination complexes are very similar, the formation of the CH activation transition-state became the most demanding parameter. These results are not only allowing predictions in regioselective HIE reactions of complex molecules as was shown for compounds **10-12**, they also give an outreach to develop the concept of directing group-induced late-stage functionalization in general. Understanding the influence of the directing groups could allow a much better planning and successful prediction of late-stage functionalization pathways. Such a prediction rule could save time and resources in drug discovery research or could even broaden the applications of tritiated molecules to new fields of the life sciences.[4]

Scheme VI. 5: *Prediction of Iridium catalysed Hydrogen Isotope Exchange reactions in competition situation (Part III – Chapter 2)*

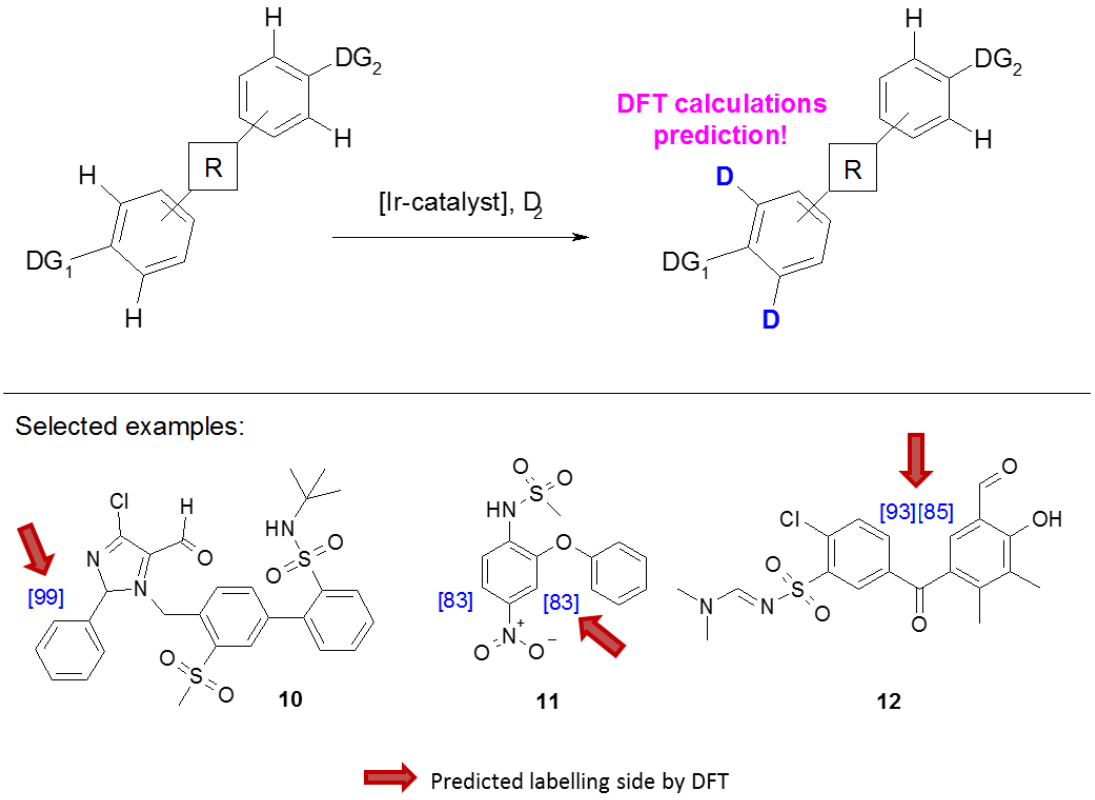

Meanwhile the Part II-III were focused on HIE on C(sp^2)-centers, the labelling of C(sp^3)-centers were still a challenge. Consequently, the Part IV focused on developing a new method for highly selective HIE of unactivated C(sp^3)-centers. Starting from a complex tritium labelling of the maytansine DM4 drug **13**, the HIE reaction on a series of common linker side-chains of antibody-drug-conjugates proceeded with high yields, high regioselectivity and with deuterium incorporations up to 99% (*scheme VI.6*). The scope of the method was further extended to amino acids, di- and tripeptides (**14-16**), with

deuterium incorporation up 95%D in the glycine moiety. Furthermore, DFT calculations gave insights into the mechanism and steric requirements of the HIE reaction, explaining the observed selectivities and the influence of the amino acid N-protecting groups.[5]

Scheme VI. 6: *Homogeneous iridium catalysis on C(sp3)-H centers (Part IV)*

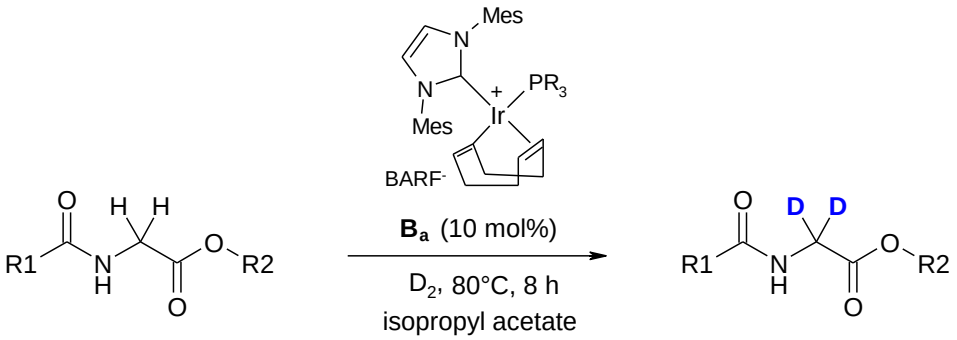

R1= N-protecting group or amino acid

R2= Me or amino acid

28 examples
1 complex tritium example
high selectivity
up to 99% D incorporation

Selected examples:

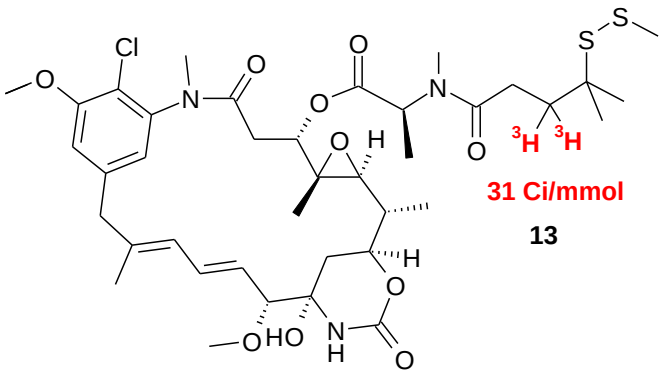

31 Ci/mmol

13

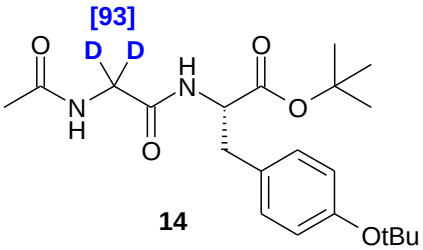

14

(L)-Ac-Gly-Tyr(OtBu)-OtBu

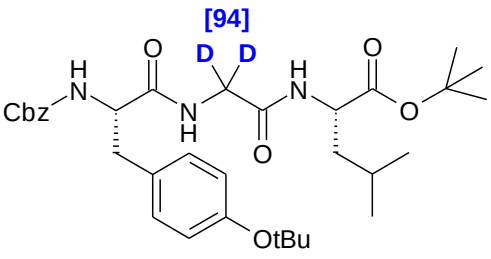

15

(L)-Cbz-Tyr(OtBu)-Gly-Leu-OtBu

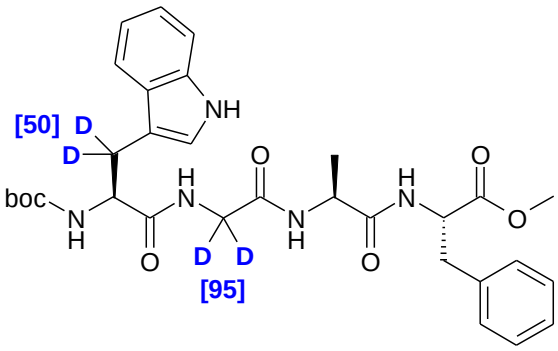

16

(L)-Boc-Trp-Gly-Ala-Phe-OMe

Finally, from homogeneous iridium catalysis we moved to heterogeneous iridium catalysis. In the Part V, air-stable and easy-to-handle iridium NHC-ligated nanoparticles were developed for the first time and used in HIE reactions. These nanocatalysts showed a unique catalytic activity allowing a selective and efficient hydrogen isotope incorporation on anilines **17-21**

using D_2 or T_2 as isotopic source (*scheme VI.7*). The application of the HIE reaction conditions was demonstrated by the deuterium and tritium labelling of diverse complex pharmaceuticals. Furthermore, the method was fully adaptable to the specific requirements of tritium chemistry, which was demonstrated by direct tritium labelling of the volixibat pharmacophore **21** with high selectivity and specific activity of 25 Ci/mmol.[6]

Scheme VI. 7: *Hydrogen Isotope Exchange reactions of anilines **17-21** with NHC-ligated iridium nanoparticles (Part V)*

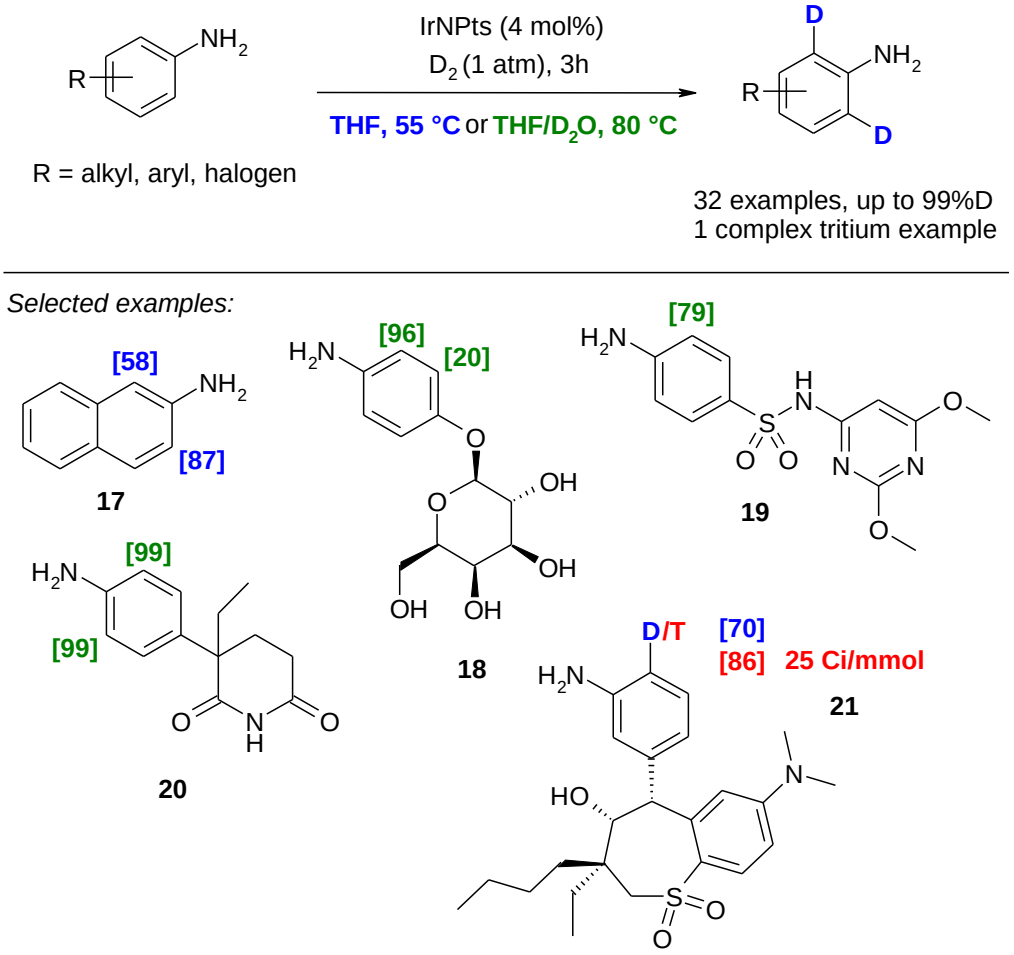

Introduction of deuterium or tritium into the final molecule has been done using homogeneous and heterogenous iridium catalysis and we have seen over the different Part II-V how these methods have been developed on small molecules first and successfully applied after on drug compounds.

Based on the work elaborated in the thesis, there are some challenges remaining and some scientific side projects which could not be followed due to limited time:

- In Part IV, we have developed a new method for C(sp^3)-labelling of small peptides (up to four amino acids). However, the method is only working with protecting groups on

the N,O-atoms. It would be highly needed to develop a selective method for bigger peptides without the need of any protecting groups. Therefore, new catalysts with a high stability and a better solubility in polar solvents are needed.

- In Part III - Chapter 2, we discovered a new way to predict the strength of different directing groups in HIE reactions in a competition situation. This is the normal case for a late-stage functionalization approach. It is therefore of great interest to bridge the obtained observations with other transition metal-catalyzed C-C and C-X coupling reactions.
- In Part V, we have studied IrNPts in HIE reactions. This has been the first time that these nanoparticles have been used in catalysis. It would be very interesting to follow a broader application scope and to study these IrNPts in further HIE reactions as in hydrogenations or reductions.
- The last topic necessary to address would be based on monoclonal antibody conjugates, like discussed in Part IV for the ADC. It would be of high value not only to be able to put a radioactive label on the drug, but also to develop methods that allow to visualize the pathway and distribution of the antibody.

Since the beginning of the PhD, highly interesting new HIE methods have been developed, especially from the ISOTOPICS groups. Pieters *et al.* reported the selective labelling of sulfur-ethers in the neighboring position of the sulfur-atom with Ru/C.[7] Furthermore, they reported the HIE with oligonucleotides[8] – a compound class never reported before. Audisio *et al.* developed a concept for carbon isotope exchange with [^{14}C]CO_2,[9] and a very fast approach to benzimidazolines and cyclic ureas with ^{14}C and ^{11}C carbonylation.[10] The PET chemistry was further improved by Genicot *et al.* reporting new activation methods of C-H bonds in order to introduce [^{18}F] into F,[11] CHF_2 or CF_3 moieties[12] to cite only a few.

---

1 M. Valero, A. Burhop, R. Weck, K. Jess, M. Tamm, V. Derdau, J. Atzrodt, *JLCR*, **2017**, *61*(*4*), 380-385.

2 M. Valero, D. Becker, K. Jess, R. Weck, J. Atzrodt, T. Bannenberg, V. Derdau, M. Tamm, *Chem. Eur. J.* **2019**, *25(26)*, 6517-6522.

3 M. Valero, A. Mishra, J. Blass, R. Weck, V. Derdau, *ChemistryOpen, **2019**, 8(9)*, 1183-1189.

4 M. Valero, T. Kruissink, J. Blass, R. Weck, S. Güssregen, A. T. Plowright, V. Derdau, *manuscript in preparation*.

5 M. Valero, R. Weck, S. Güssregen, J. Atzrodt, V. Derdau, *Angew. Chem. Int. Ed.* **2018**, *57*(*27*), 8159-8163.

6 M. Valero, D. Bouzouita, A. Palazzolo, J. Atzrodt, C. Dugave, S. Tricard, S. Feuillastre, G. Pieters, B. Chaudret, V. Derdau, *Angew. Chem. Int. Ed., manuscript in preparation.*

7 G. Pieters *et al. Chem. Commun*. **2018**, *54*, 2986-2989.

8 G. Pieters *et al. ACIE*, **2019**, *58*, 4891-4895.

9 D. Audisio *et al. JACS*, **2019**, *141*, 780-784.

10 D. Audisio *et al. ACIE*, **2018**, *57*, 9744-9748.

11 V. Gouverneur *et al. J. Am. Chem. Soc.,* **2019**, *141(7)*, 2878-2883 ; V. Gouverneur *et al. Science*, **2018**, *360(6389),* 638-642.

12 C. Genicot *et al. ACIE*, **2019**, 131, 13283-13288.

Appendix

Annex 1
Materials and General deuteration procedure

Materials:

- All substrates, catalysts and solvents were obtained from commercial suppliers and used without further purification, unless otherwise stated. Deuterium gas (99.9%D) was purchased in from Sigma Aldrich in 12 L bottles (CAS 7782-39-0).
- The degree and regioselectivity of deuterium incorporation in the substrates were determined by ^{1}H-NMR. ^{1}H (300, 500 MHz) and ^{13}C (75, 125 MHz) NMR spectra were obtained on Bruker spectrometers in the indicated solvents. Chemical shifts (δ) are reported in ppm. Coupling constants are reported in Hz and refer to ^{3}J H-H couplings, unless otherwise stated. NMR assignments were made using additional 2D NMR experiments. The listed ^{1}H-NMR spectra show sequential the substrate before reaction and the spectrum of the substrate after HIE reaction with the respective catalyst. Due to the automatic calibration from the Bruker instrument there is sometimes a small shift between the 2 compared spectra. The red arrow shows the position of the deuterium incorporation and the blue arrow shows the peak of calibration.
- The deuterium incorporation result of ^{1}H-NMR is calculated according to the following approach:
  [initial number of protons at carbon in reference] – [amount remaining, same position in HIE reaction] = X. Then: (X*100)/[initial number of proton] = % of D.
- Silica-gel column chromatography was carried out with SiO_2 (Merck, 0.063-0.200 mesh) with the indicated eluant.
- The distribution of hydrogen isotopes in the products was determined by a liquid chromatography-mass spectrometry (LC-MS) system with a Symmetry Shield RP18 column, 3.9 x 150 mm, with a gradient program. LC column conditions were as follows: mobile phase A: water (900 mL), acetonitrile (100 mL), TFA (1 mL); mobile phase B: water (100 mL), acetonitrile (900 mL), TFA (0.75 mL), Flow rate: 0.6 mL/min. Detection: UV 254 nm and UV 210 nm.
- The deuterium incorporation result of LC-MS is calculated according to the following approach: the area values of MS peaks M_0, M_0+1D, M_0+2D, M_0+3D, M_0+4D, etc. are added to a total sum.

  [D/molecule] = M1 area/total sum + M2 area/total sum*2 + M3 area/total sum*3 etc…

General deuteration procedure: To a carousel flask was added the substrate of choice (1 eq., unless otherwise stated) in solution (500 µL), unless otherwise stated, and iridium(I) catalyst (10 mol%, unless otherwise stated) in stock solution (500 µL), unless otherwise stated, under air. The desired solvent was added unless otherwise stated, rinsing the inner walls of the tube. The tube was sealed with the Teflon cap. The flask was evacuated and flushed with deuterium (1 atm) via a balloon three times. After sealing the flask, the reaction was started. The reaction mixture was stirred (500 rpm) for the indicated time at the indicated temperature. After the reaction, the mixture was analyzed by LC-MS. If the reaction was successful, the solvent was evaporated in vacuo. The residue was purified by chromatography with the indicated eluant. The product was analyzed by ^{1}H-NMR. The degree of deuterium incorporation and the regioselectivity of the labelling in the substrate were determined by ^{1}H-NMR. The integrals were calibrated against a peak corresponding to a position not expected to be labelled.

Annex 2
Detailed description of the HIE reaction process

The general reaction optimization process to establish a tritium method is structured into three main parts: the reactions in a parallel synthesizer with atmospheric deuterium gas (D_2), the optimization in the deuterium manifold with low D_2 pressure and finally the application on the tritium manifold (*figure 1*).

Figure 1: *General HIE reaction process and materials*

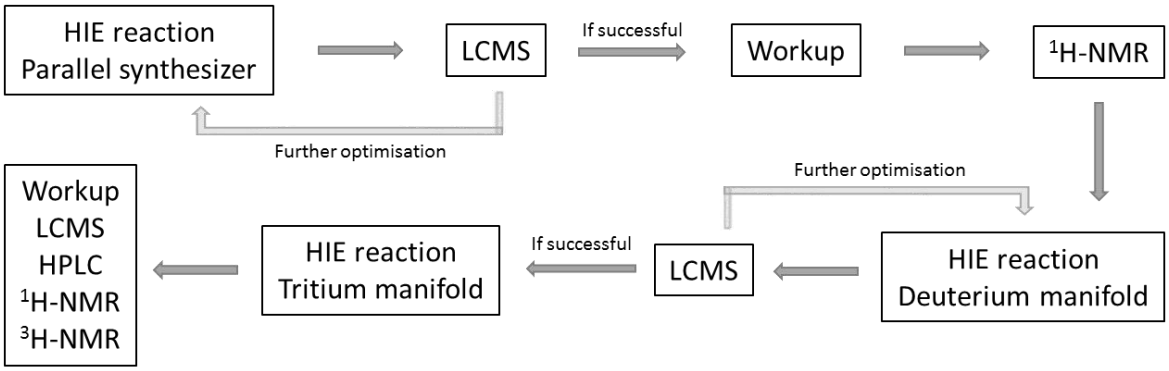

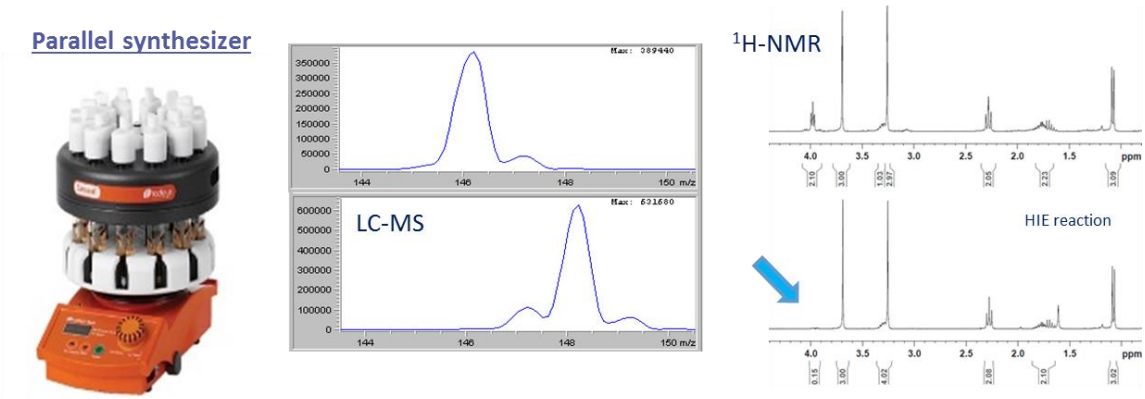

The first action is to choose an adapted model substrate which is, in plus of being related to the chosen topic, easy to get and easy to analyse. Also, the model compound must be ionisable and UV detectable to be easily seen in the mass spectrometry detector (LC-MS). In Sanofi there are automatic samplers connected with the LC-MS systems as standard analysis instruments, which provide a very quick and efficient analysis of the reaction, giving you immediately the answer if the HIE reaction was successful or not. In addition, the ^{1}H-NMR of the model compound needs to be clean enough to be analysed. In our case, ^{1}H-NMR was the only method to identify the labelling position. Therefore, it is important that there is no overlapping of the peaks characterising the molecule and the deuterated solvent. This is especially important when it comes to the evaluation of complex molecules.

- **The parallel synthesizer**

Having the model substrate chosen, the reaction was run on a Radley parallel synthesizer, in the following called "the carousel" (*figure 2*), under several conditions as different solvents, temperatures, times and catalyst ratios. However, the constant parameter on the carousel is the D_2 gas pressure, D_2 will always be 1013 mbar (= always set at 1 atm).

Figure 2: *The carousel Radleys®*

The carousel is composed of 12 glass flasks, which are tightened by locking the Teflon cap on top. The system is connected to a vacuum pump and to a balloon reservoir filled with D_2. The vacuum pump is evacuating the reaction flask before being filled with deuterium. This step is repeated at least three times. The vacuum pressure in the flask is the most critical parameter as any leakage in the system would cause false reaction outcomes due to the limited D_2 equivalents. There are other parameters which can negatively influence the reaction like decomposed catalyst or impurities in the solvent or substrates which can poison the catalyst. For this reason, it is always important to run a standard test reaction with the same conditions (solvent, temperature, time, catalyst) but with a substrate, which is known to work in the HIE reaction very well. Consequently, when 12 reactions are run on the carousel,

11 are test reactions and the last one is the control (blank) reaction. Finally, reactions are always run at least twice to ensure the reproducibility of the method. All values calculated are the mean (average) of at least two performed reactions.

- **The deuterium manifold**

After identification of the optimized deuteration conditions of a drug compound using the carousel with 1 bar D_2, the reaction needs to be adapted to the requirements of tritium chemistry. The deuterium manifold allows controlling the pressure of D_2, and thus the number of equivalents of D_2 in the reaction (*figure 3*). At 1 atm of D_2 gas on the carousel, a large excess of D_2 equivalent is used whereas 5 to 10 equivalents of tritium are generally used for the tritiation reaction. The pressure value depends of the molecular mass of the substrate and the number of equivalents used for the reaction. At the maximum we work in Sanofi with 500 mbar in our tritium manifold.

Figure 3: *The deuterium manifold*

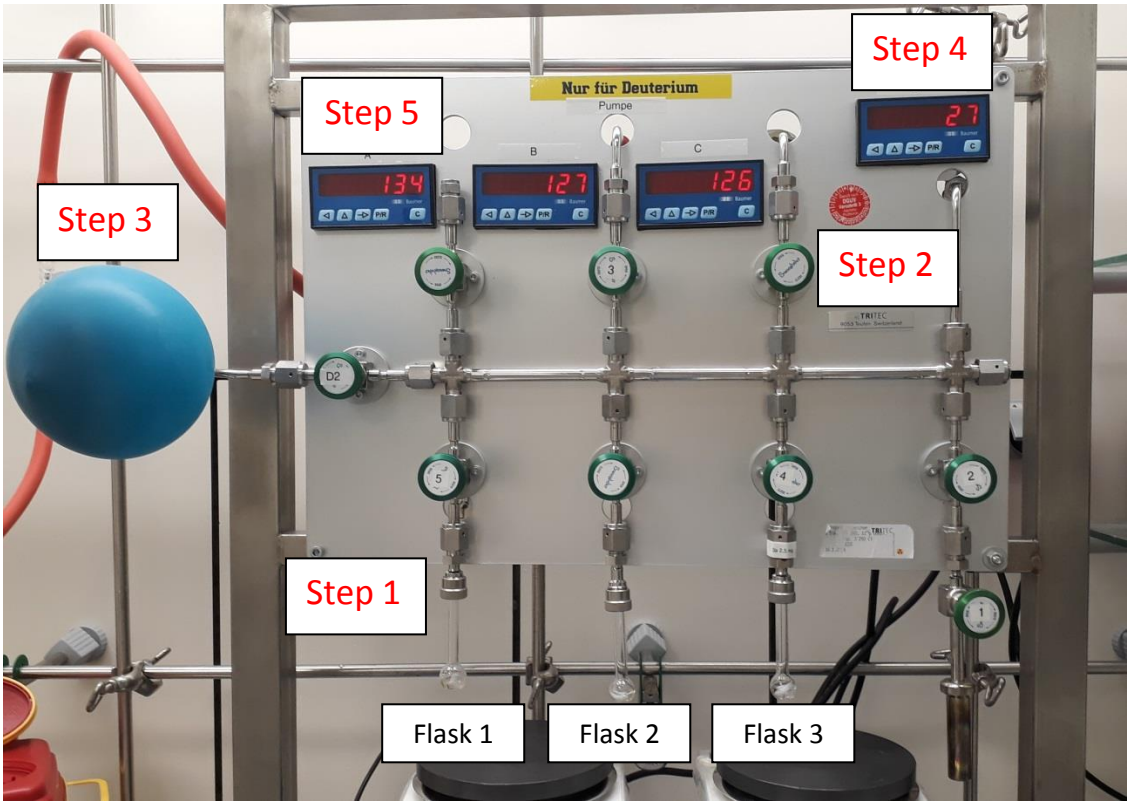

Three reactions can be run in parallel in our deuterium manifold with different equivalents of D_2. It is important to consider that the KIE (see Introduction section I.4.1.b) of tritium is much higher than for deuterium, so it is expected that the isotopic enrichment is lower with tritium than with deuterium. For this reason, the deuterium incorporation obtained on the

deuterium manifold should be significant (above 70%D) that even with transfer to the tritium chemistry it is still allowing a successful HIE reaction.

The deuterium manifold system consists of vacuum-lines made of stainless steel, which are leak tested down to less than 10^{-9} mbar l/s. The reaction flask 1 is connected at the bottom part and tightly attached (*figure 3*, step 1). The flask 1 is frozen in liquid nitrogen. The vacuum valve is opened to evacuate the flask but also the whole line system (*figure 3*, step 2). Then all valves are closed and the lines are filled with D_2 from the balloon (*figure 3*, step 3). As we want to control the number of equivalents, we carefully open the vacuum valve to evacuate D_2 until the wanted pressure value is reached. The pressure in the lines is seen on the blue screen on the top right of the manifold (*figure 3*, step 4). When we obtain the desired pressure, the vacuum valve is closed and the one controlling the opening of the reaction flask 1 is opened to let the gas get in. The diffusion of the D_2 between the flask 1 and the lines is made by equilibrium, the pressure in the flask 1 can be seen on the blue screen on top aligned with the respective flask and it must be noted carefully (*figure 3*, step 5). In the end, all valves are closed, the liquid nitrogen is removed and the reaction flask is enabled to warm up at room temperature within 15 min. The stirring and the reaction time are started. When the reaction is over, the flask is unplugged from the manifold and the reaction analysed by LC-MS.

- **The tritium manifold**

After a successful HIE reaction on the deuterium manifold, the same conditions are applied on the tritium manifold (*figure 4)*. The technology is similar than those of the deuterium manifold, however with a scrubber system attached to minimize tritium in the exhaust air after the reaction. The tritium gas is stored on unranium beds as uranium tritide (UT_3) and is released at the required pressure by heating up higher than 450°C. The biggest advantage of the manifold is the reversible formation of UT_3 after completion of the reaction.

The reaction flask is tightly connected to the manifold and frozen in liquid nitrogen. By opening and closing accordingly the different valves, the pipes are evacuated, and the flask is charged with tritium. The reaction mixture is then allowed to warm up to room temperature over 15 min and is run under the optimized deuterium conditions. In some cases, the reaction time is prolonged to take account of the KIE for tritium. After the reaction the solvent is evaporated. The flask is unplugged, methanol is added and the solvent mixture is evaporated again into a waste ampule. This procedure is repeated three times in total to get rid of volatile tritium atoms. The reaction mixture is then dissolved in methanol and filtered. A probe is transferred and analysed by LC-MS. If this was a success, purification and isolation *via* HPLC will be done and provide the tritiated product which will be analysed by ^{1}H and ^{3}H NMR.

Figure 4: The tritium manifold

General Work-up

After the HIE reaction, a probe is run in LC-MS. If the reaction was successful, the solvent is evaporated and the dry mixture is purified by chromatography on silica gel to separate the product from the catalyst. As the reactions were done on small scale (around 10 mg), the chromatography was done in a Pasteur pipette filled with cotton at the bottom and silica gel. In the ideal case, the product was eluted first and the catalyst was kept on the silica. When the substrate was too polar, the catalyst was eluted first with a medium polar solvent and then the polarity of the mobile phase was slightly increased to isolate the product. In these cases, the purity of the isolated compounds was always decreased which was seen in the ^{1}H-NMR spectra. After purification, the solution is evaporated and the dry product is diluted in the deuterated solvent. Degree of deuterium incorporation and position are identified by ^{1}H-NMR.

université PARIS-SACLAY

ECOLE DOCTORALE N°571
Sciences chimiques : molécules, matériaux, instrumentation et biosystèmes (2MIB)

Titre : Fonctionnalisation de liaisons C-H par catalyse à l'iridium: Développement de nouvelles méthodes pour l'échange d'isotopes d'hydrogène sur des petites molécules et des composés biothérapeutiques

Mots clés : fonctionnalisation-CH, échange d'isotopes d'hydrogène, catalyse, Drug Discovery

Résumé : Le développement de nouvelles méthodes, efficaces, rapides et facile à mettre en oeuvre pour le marquage avec du deutérium ou du tritium de composés organiques tels que des médicaments est indispensable dans le secteur industriel comme académique. Ces composés isotopiquement marqués sont essentiels lors des études précliniques. En effet, ces méthodes de marquages permettent d'obtenir plus rapidement les données nécessaires concernant la métabolisation et le profil de sécurité d'un candidat médicament, ce qui permet de réduire le temps investit dans cette recherche. Les méthodes classiques de marquages sont basées sur la synthèse d'un précurseur qui est ensuite marqué isotopiquement puis modifié jusqu'à l'obtention de la structure finale du candidat médicament. Ces anciennes méthodes, coûteuses en temps et en argent et génératrices d'effluents radioactifs, peuvent être évitées par fonctionnalisation sur la structure finale du composé d'intérêt, en particulier par échange d'isotope d'hydrogène. Au cours de ces travaux de thèse, nous avons développé la première méthode de marquage catalytique à l'iridium dans des conditions douces (température ambiante) sur les motifs dérivés d'acides phenylacetiques tels que esters et amides, motifs très présents dans les structures pharmacologiques. Cette méthode permet d'introduire du deutérium ou du tritium en position ortho du groupement directeur de façon sélective. Lors d'un autre projet, nous avons mis en évidence que la position de marquage au sein d'une molécule avec plusieurs groupements directeurs peut être modulée en fonction du catalyseur d'iridium utilisé ainsi que de la température réactionnelle (de -60°C à +130°C). L'utilisation de calculs de DFT nous a permis de postuler un ordre classifiant différents groupements directeurs par rapport à leur réactivité vis-à-vis de la réaction d'échange d'isotopes d'hydrogène en situation de compétition (deux substrats et un catalyseur d'iridium). Ces données théoriques ont été confirmées par les données expérimentales. Lors d'un autre projet, le marquage sélectif au tritium d'une structure complexe tel qu'un médicament cytotoxique (maytansine DM4) a débouché sur le marquage de différentes chaînes latérales employées dans des méthodes de conjugaison d'anticorps. Ces données ont permis d'étendre cette méthodologie au marquage au deutérium d'acides aminés et de di-tri et tétra-peptide, sélectivement sur le carbone alpha d'un résidu glycine. Finalement, en collaboration avec le CEASaclay et le CNRS, nous avons développé les premières nanoparticules d'iridium stable à l'air et actives vis-à-vis de l'échange d'isotopes d'hydrogène sur des anilines. L'ensemble des travaux réalisés pendant cette thèse a permis le marquage au tritium de composés médicamenteux tels que le DM4, le Benalaxyl, ou encore le pharmacophore du Volixibat.

Title : Iridium-Catalyzed CH-Functionalization: Development and Applications of Innovative Strategies for Hydrogen Isotope Exchange on Small Molecules and Biotherapeutic Drugs for Drug Discovery

Keywords : CH-functionalization, hydrogen isotope exchange, catalysis, Drug Discovery

Abstract : The development of new efficient, fast and easy to handle methods to label drug compounds with deuterium or tritium in one single step is of great importance in academia and industry. These labelled compounds are an essential part in drug discovery and help to speed up the generation of the safety profile of a drug candidate. Classical isotope labeling mainly relies on the transformation of precursors which require multistep synthesis, a drawback which may be overcome by late-stage functionalization. We reported the first efficient catalytic protocol for ortho-selective iridium(I)-catalyzed Hydrogen Isotope Exchange (HIE) reactions of pharmacologically important phenylacetic acid esters and amides with D2 or T2 under very mild reaction conditions (room temperature). We have demonstrated that by applying the optimized combination of different iridium catalysts and reaction temperatures (-60 to 130°C), different HIE reaction outcomes in selectivity and reactivity can be achieved. Together with DFT calculations, we have postulated a guideline for directing group strength of several functional groups, to predict the outcome of HIE reactions in the competition situation of complex molecules. Starting from a complex tritium labelling of the maytansine DM4 drug, the HIE reaction on a series of common linker side chains of antibody-drug-conjugates proceeded with high chemical yields, high regioselectivity and with deuterium incorporations up to 99%. The scope of the method was further extended to amino acids, di- and tripeptides, with deuterium incorporation up 95%D in the glycine moiety. Finally, in collaboration with CEA-Saclay and CNRS, airstable and easy-to-handle iridium NHC-ligated nanoparticles were developed for the first time and used in HIE reactions of complex anilines. The usefulness of the methods developed all along the PhD was demonstrated by tritiation of DM4, Camylofine, Benalaxyl and the Volixibat pharmacophore.

Université Paris-Saclay
Espace Technologique / Immeuble Discovery
Route de l'Orme aux Merisiers RD 128 / 91190 Saint-Aubin, France